

# An introduction to gauge theories and modern particle physics

Volume 1  
Electroweak interactions,  
the "new particles" and the parton model

ELLIOT LEADER  
ENRICO PREDAZZI

CAMBRIDGE MONOGRAPHS  
ON PARTICLE PHYSICS,  
NUCLEAR PHYSICS AND COSMOLOGY

The revolution in elementary particle physics sparked by the unearthing of the bizarre  $J/\Psi$  particle in 1974 and followed by the discovery of the equally mysterious  $\tau$  and  $\Upsilon$  particles, led to a beautiful interweaving of theory and experiment culminating in the Salam–Weinberg theory of electroweak interactions and the quantum chromodynamic (QCD) theory of strong interactions. The extraordinary prediction of the  $W$  and  $Z^0$  bosons was fulfilled in 1983, and it is now possible to produce  $Z^0$  in millions. The emphasis today is on refined testing of the detailed quantitative predictions of the theories, and, to match this, more sophisticated calculations are demanded. This book presents, in two volumes, a comprehensive and unified treatment of modern theoretical and experimental particle physics at a level accessible to beginning research students. The emphasis throughout is on presenting underlying physical principles in a simple and intuitive way, and the more sophisticated methods demanded by present-day research interests are introduced in a very gradual and gentle fashion.

Volume 1 covers electroweak interactions, the discovery and properties of the ‘new’ particles, the discovery of partons and the construction and predictions of the simple parton model. Volume 2 deals at some length with CP violation, but is mainly devoted to QCD and its application to ‘hard’ processes. A brief coverage of soft hadronic physics and of non-perturbative QCD is included.

This work will provide a comprehensive reference and textbook for all graduate students and researchers interested in modern particle physics.



CAMBRIDGE MONOGRAPHS ON  
PARTICLE PHYSICS,  
NUCLEAR PHYSICS AND COSMOLOGY  
3

General Editors: T. Ericson, P. V. Landshoff

AN INTRODUCTION TO GAUGE THEORIES AND  
MODERN PARTICLE PHYSICS, VOLUME 1

CAMBRIDGE MONOGRAPHS ON  
PARTICLE PHYSICS,  
NUCLEAR PHYSICS AND COSMOLOGY

1. K. Winter (ed.): *Neutrino Physics*
2. J. F. Donoghue, E. Golowich and B. R. Holstein: *Dynamics of the Standard Model*
3. E. Leader and E. Predazzi: *An Introduction to Gauge Theories and Modern Particle Physics, Volume 1: Electroweak interactions, the 'new particles' and the parton model*
4. E. Leader and E. Predazzi: *An Introduction to Gauge Theories and Modern Particle Physics, Volume 2: CP violation, QCD and hard processes*

**AN INTRODUCTION  
TO GAUGE THEORIES  
AND MODERN  
PARTICLE PHYSICS,  
VOLUME 1**

Electroweak interactions, the ‘new particles’ and the parton model

**ELLIOT LEADER**  
*Birkbeck College, University of London*

**ENRICO PREDAZZI**  
*University of Torino*



Published by the Press Syndicate of the University of Cambridge  
The Pitt Building, Trumpington Street, Cambridge CB2 1RP  
40 West 20th Street, New York, NY 10011-4211, USA  
10 Stamford Road, Oakleigh, Melbourne 3166, Australia

© Cambridge University Press 1996

First published 1996

*A catalogue record for this book is available from the British Library*

*Library of Congress cataloguing in publication data*

Leader, Elliot, 1935-

An introduction to gauge theories and modern particle physics /  
Elliot Leader, Enrico Predazzi.

p. cm. – (Cambridge monographs on particle physics,  
nuclear physics, and cosmology; 3–4)

Includes bibliographical references and index.

Contents: v. 1. Electroweak interactions, the “new particles”  
and the parton model – v. 2. CP-violation, QCD and hard processes.

ISBN 0 521 46468 4 (v. 1) – ISBN 0 521 46840 X (pbk. : v. 1.) –  
ISBN 0 521 49617 9 (v. 2). – ISBN 0 521 49951 8 (pbk. : v. 2)

1. Gauge fields (Physics) 2. Particles (Nuclear physics)

I. Predazzi, Enrico. II. Title. III. Series.

QC793.3.G38L43 1996

539.7'54-dc20 95-25233 CIP

Vol. 1 ISBN 0 521 46468 4 hardback

ISBN 0 521 46840 X paperback

Vol. 2 ISBN 0 521 49617 9 hardback

ISBN 0 521 49951 8 paperback

Set of two vols.

ISBN 0 521 57780 2 hardback

ISBN 0 521 57742 X paperback

Transferred to digital printing 2004

*Dedication*

To our children, Darian, Francesca, Imre, Irene and Valentina.

Perché si scrive?

... Per insegnare qualcosa a qualcuno. Farlo, e farlo bene, può essere prezioso per il lettore, ma ... l'intento didattico corrode la tela narrativa dal di sotto, la degrada e la inquina: il lettore che cerca il racconto deve trovare il racconto, e non una lezione che non desidera. Ma appunto, le eccezioni ci sono, e chi ha sangue di poeta sa trovare ed esprimere poesia anche parlando di stelle, di atomi, dell'allevamento del bestiame e dell'apicoltura...

Why does one write?

... To teach something to someone. To do this and do it well can be valuable for the reader but ... the didactic intention corrodes the narrative canvas from underneath, degrades it and contaminates it: the reader who looks for a story must find a story and not a lesson he does not want. But, of course, exceptions there are, and whoever has the blood of a poet will find and express poetry also when talking of stars, of atoms, of cattle breeding and of the raising of bees...

Primo Levi

# Contents: Volume 1

## Electroweak interactions, the ‘new particles’ and the parton model

<i>Preface</i>	xxi
<i>Acknowledgements</i>	xxiv
<i>Notational conventions</i>	xxv
Note added in proof: the discovery of the top quark (?)	xxxi
Note added in proof: the demise of the SSC	xxxiii
<b>1 Field theory and pre-gauge theory of weak interactions</b>	1
1.1 A brief introduction to field theory	1
1.2 Pre-gauge theory of weak interactions	6
1.3 The spin and isospin structure	15
1.3.1 The spin or helicity structure	16
1.3.2 Relation between particle and antiparticle matrix elements	17
1.3.3 The isospin structure	18
1.4 Tests of the $V-A$ structure and ‘lepton universality’	20
<b>2 The need for a gauge theory</b>	23
2.1 The intermediate vector boson	23
2.2 Towards a renormalizable theory	27
2.3 Gauge symmetry	29
2.3.1 Global gauge invariance—the Abelian case	30
2.3.2 Local gauge invariance—the Abelian case	31
2.3.3 Global gauge invariance—the non-Abelian case	33
2.3.4 Non-Abelian local gauge invariance—Yang–Mills theories	35
2.4 Freedom to choose the gauge	38
2.5 Summary	39
<b>3 Spontaneous symmetry breaking: the Goldstone theorem and the Higgs phenomenon</b>	40
3.1 Spontaneously broken symmetries in field theory: Goldstone’s theorem	41

3.2	The Higgs mechanism	45
3.3	Unitarity and renormalizability	47
3.4	Summary	48
<b>4</b>	<b>Construction of the standard model</b>	49
4.1	Model building (towards the standard model)	49
4.2	The standard model	50
4.2.1	Coupling of the gauge bosons to the Higgs scalars	52
4.2.2	Self-coupling of the gauge bosons	55
4.2.3	Coupling of the gauge bosons to the leptons	55
4.2.4	Coupling of the leptons to the Higgs	61
4.3	Discovery of $W$ and $Z^0$	63
4.3.1	Discovery of the $W$ boson(?)	63
<b>5</b>	<b>Lowest order tests of the SM in the leptonic sector</b>	67
5.1	Phenomenology of purely leptonic reactions	67
5.1.1	$\nu_{ee}$ and $\bar{\nu}_{ee}$ elastic scattering	69
5.1.2	$\nu_{\mu}e^-$ and $\bar{\nu}_{\mu}e$ elastic scattering	74
5.1.3	Inverse $\mu$ -decay	76
5.2	A check of the minimal Higgs mechanism	76
5.3	Support for the SM from hadronic collider data	77
5.3.1	$W$ production and decay in $\bar{p}p$ collisions	78
5.3.2	$\bar{p}p$ collider data	82
5.4	Concluding remarks	87
<b>6</b>	<b>The Higgs boson</b>	90
6.1	Introductory remarks	90
6.2	Higgs decay	91
6.3	Higgs production at the $Z^0$ mass	95
6.3.1	$Z^0 \rightarrow H f \bar{f}$	95
6.3.2	$Z^0 \rightarrow H \gamma$	96
6.4	Limits on the Higgs mass	97
6.5	Concluding comments	100
<b>7</b>	<b>The standard model beyond lowest order</b>	101
7.1	Radiative corrections	101
7.2	Renormalization and physical parameters	103
7.3	The effective fine structure constant	106
7.4	The muon lifetime revisited	107
7.5	Estimates of one loop corrections	109
7.6	Higher order corrections	110
7.7	Practical problems in testing radiative corrections	112
7.8	Strategies to overcome the imprecision in $M_W$	113
7.9	Testing the minimal Higgs mechanism	114
7.10	Beyond the standard model	115

<b>8 e<sup>+</sup>e<sup>-</sup> physics and the standard model</b>	118
8.1 Electron–positron storage rings	118
8.2 The new e <sup>+</sup> e <sup>-</sup> colliders: TRISTAN and LEP	121
8.3 e <sup>+</sup> e <sup>-</sup> physics at energies $\ll M_Z$	126
8.4 e <sup>+</sup> e <sup>-</sup> and the standard model	132
8.5 LEP data near the Z <sup>0</sup> peak	133
8.5.1 e <sup>+</sup> e <sup>-</sup> angular distributions	134
8.6 Determination of the SM parameters of the Z <sup>0</sup>	142
8.7 Neutrino counting	147
8.7.1 The invisible width method	147
8.7.2 The single photon method	148
8.8 Asymmetries and polarization measurements at the Z <sup>0</sup> peak	149
8.9 Conclusions	154
<b>9 Extension to the hadrons; quark–lepton universality</b>	157
9.1 Charm, bottom and top	157
9.2 Quark mixing	160
9.3 Electroweak interaction of the quarks	163
9.4 The GIM mechanism	164
9.5 Colour	166
9.5.1 The quark statistics	166
9.5.2 $\pi^0 \rightarrow 2\gamma$	168
9.5.3 Triangle anomalies	170
9.5.4 The cross-section for e <sup>+</sup> e <sup>-</sup> $\rightarrow$ <i>hadrons</i>	174
9.6 Summary of the quark sector of the standard model	176
9.7 Quark masses and the KM matrix	179
<b>10 Phenomenology of semi-leptonic reactions</b>	182
10.1 Model independent tests	184
10.2 Parity violation in electron–nucleus scattering	189
10.3 Optical rotation	193
10.4 Summary	201
<b>11 The discovery of the narrow vector resonances</b>	202
11.1 Introduction	202
11.2 The ‘new’ particles	204
11.3 Some qualitative features of QCD	206
11.4 Quark–lepton parallelism	208
11.5 Flavour classification of hadrons	209
11.6 The J/Ψ and the OZI rule	213
11.7 Experimental status of the J/Ψ spectroscopy	219
11.7.1 Mass determination of the J/Ψ	224
11.8 Properties of the J/Ψ(3097) and Ψ'(3685)	225
11.8.1 J/Ψ and Ψ' widths	225
11.8.2 J <sup>PC</sup> assignments	228
11.8.3 I <sup>G</sup> assignment	229
11.9 Baryonic decay of J/Ψ	232

11.10	The $\Upsilon$ family and its experimental status	234
<b>12</b>	<b>Hidden flavour bound states</b>	240
12.1	Quarkonium	240
12.1.1	The positronium analogy	241
12.1.2	The QCD potential	242
12.1.3	The strength of the potential	245
12.1.4	Spin dependence of the potential	248
12.1.5	Comparison with the data	249
12.2	$J/\Psi$ decays. Calculation of the widths	254
12.3	Determination of $\alpha_s$	260
12.4	Leptonic widths	262
12.5	Exotics: glueballs, hybrids, etc.	264
12.6	$\Psi' \rightarrow \varrho\pi$ : a puzzle	267
12.7	Conclusions	268
<b>13</b>	<b>Open heavy flavours</b>	269
13.1	Discovery and basic properties of charm and bottom particles	270
13.1.1	Detection of heavy flavours	276
13.1.2	Charge of the charm and bottom quarks	279
13.1.3	Heavy flavour masses	280
13.2	Charm decay	282
13.2.1	Heavy flavour lifetimes	284
13.2.2	Purely leptonic charm decays	286
13.2.3	Semi-leptonic and hadronic decays of charm mesons	287
13.3	$B$ physics	290
13.3.1	The decay $\bar{B}^0 \rightarrow D^{+*}\ell^-\bar{\nu}$	291
13.4	Production of heavy flavours	293
13.4.1	Theoretical estimates of heavy flavour production	293
13.5	Heavy flavours at LEP	295
13.5.1	Production of $c$ and $b$ quarks at the $Z^0$ pole	295
13.5.2	Production cross-section	296
13.5.3	Miscellaneous	297
13.6	Final comments	299
<b>14</b>	<b>The heavy lepton <math>\tau</math></b>	300
14.1	Introduction	300
14.2	Discovery of the $\tau$ lepton	301
14.3	Properties of the $\tau$ lepton	304
14.3.1	The $\tau$ mass	304
14.3.2	The $\tau$ lifetime	306
14.3.3	The spin of the $\tau$	307
14.3.4	Point-like structure	308
14.3.5	$\tau - e - \mu$ universality	309
14.4	$\tau$ decay	309
14.4.1	Semi-leptonic $\tau$ decays	310
14.4.2	QCD tests from $\tau$ decay	311
14.5	The $\tau$ neutrino	312

14.6	Rare $\tau$ decays	314
14.7	Miscellaneous and conclusions	314
<b>15</b>	<b>Towards the parton model—deep inelastic scattering</b>	316
15.1	Electron–muon scattering	317
15.2	Elastic electron–proton scattering	321
15.3	Inelastic electron–nucleon scattering	324
15.4	Inelastic neutrino–nucleon scattering	331
15.5	Deep inelastic scattering and scaling behaviour	335
15.6	Polarization effects in deep inelastic scattering	342
<b>16</b>	<b>The quark–parton model</b>	352
16.1	The introduction of partons	352
16.2	Antipartons	359
16.3	Partons as quarks	361
16.4	The detailed quark–parton model	364
16.4.1	The scaling functions for purely electromagnetic interactions	366
16.4.2	Charged current scaling functions	368
16.4.3	Neutrino and antineutrino neutral current scaling functions	373
16.5	Charged lepton induced reactions for $Q^2$ of order $M_Z^2$	374
16.6	Behaviour of the quark number densities as $x \rightarrow 0$	375
16.7	The missing constituents—gluons	377
16.8	The parton model in polarized deep inelastic scattering	378
16.9	Appendix to Chapter 16: The parton model as an impulse approximation	382
16.9.1	The parton model as an impulse approximation	382
16.9.2	The parton model including transverse motion	386
16.9.3	Current matrix elements in the quark–parton model	393
<b>17</b>	<b>Experimental tests of the quark–parton model</b>	396
17.1	Deep inelastic scaling functions for $Q^2 \ll M_Z^2$	396
17.1.1	Sum rules and their experimental tests	401
17.1.2	Polarized scattering sum rule and the ‘spin crisis’	405
17.1.3	The nuclear EMC effect	409
17.1.4	Experimental status of the scaling functions	416
17.2	Neutrino cross-sections in the quark–parton model for $Q^2 \ll M_Z^2$	416
17.3	Cross-sections in the quark–parton model for $Q^2$ comparable with $M_Z^2$	425
17.4	Application of the parton model to related processes	426
17.4.1	$e^+e^-$ annihilation into hadrons	427
17.4.2	The Drell–Yan process	428
17.4.3	Production of heavy mesons by Drell–Yan mechanism	440
	Note added in proof: polarized deep inelastic scattering	442

<b>Appendix 1: Elements of field theory</b>	443
A1.1 Fields and creation operators	443
A1.2 Parity, charge conjugation and $G$ -parity	447
A1.2.1 Parity	447
A1.2.2 Charge conjugation	447
A1.2.3 $G$ -parity	449
A1.3 The $S$ -matrix	449
<b>Appendix 2: Feynman rules for QED, QCD and the SM</b>	451
A2.1 Relation between $S$ -matrix and Feynman amplitude	451
A2.2 QCD and QED	452
A2.3 The SM	455
A2.4 Some examples of Feynman amplitudes	457
A2.5 Colour sums	459
A2.6 The Gell-Mann $SU(3)$ matrices	462
A2.7 The Fierz reshuffle theorem	463
A2.8 Dimension of matrix elements	464
<b>Appendix 3: Conserved vector currents and their charges</b>	465
<i>References</i>	470
<i>Analytic subject index for vols. 1 and 2</i>	482

# Contents: Volume 2

## CP Violation, QCD and hard processes

<i>Preface</i>	xix
<i>Acknowledgements</i>	xxii
<i>Notational conventions</i>	xxiii
Note added in proof: the discovery of the top quark (?)	xxix
Note added in proof: the demise of the SSC	xxxi
<b>18 Determination of the Kobayashi–Maskawa matrix</b>	1
18.1 KM matrix elements from $\beta$ -decay reactions	2
18.2 KM matrix elements from deep inelastic scattering	8
18.3 Summary	10
<b>19 Mixing and CP violation</b>	12
19.1 General phenomenology of mixing and CP violation	12
19.1.1 General formalism for mixing	12
19.1.2 General formalism for CP violation	15
19.1.3 Practical aspects of mixing and CP violation	17
19.2 Detailed phenomenology of CP violation in the $K^0-\bar{K}^0$ system	23
19.2.1 Formalism and summary of data	23
19.2.2 Relation between phenomenological parameters and the CP-violating Hamiltonian	28
19.3 Dynamics of mixing and CP violation	32
19.3.1 Connection with the SM (weak) Hamiltonian	32
19.3.2 Estimate for $\epsilon$ in the SM	35
19.3.3 Estimate of $\epsilon'/\epsilon$ in the SM	40
19.3.4 Summary on $\epsilon$ and $\epsilon'$ in the $K^0-\bar{K}^0$ system	44
19.4 Dynamics of $B^0-\bar{B}^0$ mixing	45
19.4.1 Mixing ignoring CP violation	46
19.4.2 CP violation in the $B^0-\bar{B}^0$ system	48
<b>20 Regularization, renormalization and introduction to the renormalization group</b>	53
20.1 Introduction	53
20.2 Parameters and physical observables in a field theory	54

20.3	The idea of renormalization	56
20.4	Choice of cut-off procedure—regularization	62
20.5	Choice of renormalization scheme	66
20.5.1	The momentum point subtraction (MPS) scheme	67
20.5.2	Renormalization schemes specifically linked to dimensional regularization (DR)	71
20.6	The renormalization group	73
20.7	A concrete example of different renormalization schemes	76
20.8	Consequences of the renormalization group equation	78
20.9	Scaling and asymptotic freedom	81
20.10	Appendix to Chapter 20	86
20.10.1	Definition of a $d$ -dimensional integral	86
20.10.2	Questions of convergence and analytic continuation	87
20.10.3	Some useful $d$ -dimensional integrals	91
20.10.4	Regularization of the 4-point vertex in $\phi^4$ theory	93
<b>21</b>	<b>Gauge theories, QCD and the renormalization group</b>	97
21.1	Introduction	97
21.2	Gauge theories: QED	98
21.2.1	Retaining Maxwell's equations for the field operators	101
21.2.2	Modifying Maxwell's equations for the field operators	103
21.3	Gauge theories: QCD	104
21.3.1	Differences between QCD and QED	107
21.4	Feynman rules for QCD	114
21.4.1	The propagators	114
21.4.2	The vertices	115
21.5	The renormalization group for QCD	116
21.5.1	Specification of the renormalization scheme in QCD	117
21.5.2	Consequences of the renormalization group in QCD	120
21.6	The effect of heavy quarks	121
21.7	The running coupling in QCD	124
21.7.1	Renormalization scheme dependence of $\alpha$ and $\Lambda$	127
21.8	Conclusion	127
<b>22</b>	<b>Applications of the QCD renormalization group</b>	128
22.1	$e^+e^- \rightarrow$ hadrons	128
22.2	Deep inelastic lepton scattering	135
22.2.1	The operator product expansion	136
22.2.2	Relating coefficient functions to moments of structure functions	137
22.2.3	Renormalization group analysis of coefficient functions	142
22.2.4	$q^2$ dependence of the moments in leading order	144
22.2.5	An interpretation of the $Q^2$ variation of parton distributions in leading logarithmic approximation	148
22.2.6	$q^2$ dependence of the moments in higher order	151
22.2.7	Conclusion	154
<b>23</b>	<b>The parton model in QCD</b>	155
23.1	Partons in a field theoretic context	155
23.1.1	Heuristic reinterpretation of simple Feynman diagrams	157
23.1.2	Application to QCD	160
23.1.3	The parton model in field theory	163
23.2	QCD corrections to the parton model	168
23.2.1	Redefinition of $f_{q/h}$	168

23.2.2	Collinear singularities—their physical origin	171
23.3	Structure of the leading logarithmic terms	174
23.4	$Q^2$ -dependent distribution functions	180
23.5	Summary of the evolution equations in LLA	186
23.6	Small $x$ behaviour of the $Q^2$ -dependent gluon distribution in LLA	189
23.7	Behaviour of distributions as $x \rightarrow 1$ in LLA	192
23.8	Beyond the LLA	195
23.9	Comparison with experiment in deep inelastic scattering	202
23.10	General form of the QCD-improved parton model	206
23.11	QCD corrections to Drell–Yan and $W$ production	209
23.11.1	Drell–Yan production	210
23.11.2	Transverse momentum distribution of Drell–Yan pairs	213
23.11.3	Hadronic production of $W$ and $Z^0$	216
23.11.4	Transverse momentum distribution of $W$ and $Z^0$	217
23.12	Summary	218
<b>24</b>	<b>Large <math>p_T</math> phenomena and jets in hadronic reactions</b>	219
24.1	Introduction	219
24.2	Historical survey. Hard $qq$ scattering	221
24.3	From quarks to hadrons	225
24.3.1	Inclusive reactions	225
24.3.2	Exclusive reactions	228
24.4	Comments on the QCD interpretation of large $p_T$ phenomena	232
24.4.1	Evidence for jets	233
24.4.2	Inclusive jet production	234
24.4.3	Transverse momentum distribution with respect to the jet axis	239
24.5	Two-jet production at large $p_T$	239
24.5.1	Jet angular distribution	241
24.5.2	Tests of the $Q^2$ evolution	242
24.5.3	Hadronic interactions at large $p_T$ revisited	244
24.6	Prompt photons	245
24.7	Two and more jets in the final state	249
24.8	Jet fragmentation	249
24.9	Comments on $O(\alpha_s^3)$ corrections and conclusions	250
<b>25</b>	<b>Jets and hadrons in <math>e^+e^-</math> physics</b>	253
25.1	Introduction	253
25.2	General outline of $e^+e^-$ jets	253
25.2.1	Angular distribution of hadrons produced in $e^+e^-$ collisions	255
25.3	SPEAR two-jet events	258
25.3.1	Sphericity	259
25.3.2	Jet axis	260
25.3.3	Corrections to $e^+e^- \rightarrow$ hadrons: multijets	262
25.4	Planar events: evidence for three jets	265
25.5	Tests of QCD up to LEP energies	268
25.6	The total hadronic width at the $Z^0$	269
25.7	Basic Monte Carlo formulations	270
25.8	QCD Monte Carlo programs	272
25.8.1	The perturbative phase	273
25.8.2	The hadronization phase	276
25.9	Multiplicity	277
25.10	Global event-shape analysis	278

25.11	Jet definition or recombination schemes	282
25.12	Particle flow patterns in 3-jet events	285
25.13	To what extent is QCD being tested?	285
<b>26</b>	<b>Low <math>p_T</math> or ‘soft’ hadronic physics</b>	289
26.1	The total and elastic cross-sections	289
26.2	The differential cross-section	292
26.3	The real to imaginary ratio	293
26.4	The inclusive $p_T$ distribution	295
26.5	Diffractive dissociation	295
26.6	The average multiplicity	296
26.7	The multiplicity distribution of charged particles	297
26.8	Conclusions Note added in proof: the real to imaginary ratio, $\varrho$ , in $p\bar{p}$ elastic scattering	298 300
<b>27</b>	<b>Some non-perturbative aspects of gauge theories</b>	301
27.1	QCD sum rules	302
27.2	Lattice approach to QCD	304
27.3	The vacuum in quantum mechanics and instantons 27.3.1 An example in one-dimensional motion	312 313
27.4	The QCD vacuum and instantons 27.4.1 Degenerate vacua in classical field theory 27.4.2 The $\theta$ -vacuum in QCD	318 318 326
27.5	Strong CP violation and the $U(1)$ problem	328
27.6	Baryon and lepton non-conservations: sphalerons 27.6.1 Degenerate vacua in the SM 27.6.2 Baryon and lepton numbers of the vacua 27.6.3 The sphaleron	332 333 334 336
<b>28</b>	<b>Beyond the standard model</b>	339
28.1	Introduction	339
28.2	The ‘missing links’ of the SM	340
28.3	Criticisms of the SM 28.3.1 The $U(1)$ and $\theta$ problems 28.3.2 Parameter counting	340 340 342
28.4	Grand unification theories (GUT)	342
28.5	Compositeness	347
28.6	Supersymmetry and supergravity	347
<b>Appendix 1: Elements of field theory</b>		351
A1.1	Fields and creation operators	351
A1.2	Parity, charge conjugation and $G$ -parity A1.2.1 Parity A1.2.2 Charge conjugation A1.2.3 $G$ -parity	355 355 355 357
A1.3	The $S$ -matrix	357

<b>Appendix 2: Feynman rules for QED, QCD and the SM</b>	359
A2.1 Relation between $S$ -matrix and Feynman amplitude	359
A2.2 QCD and QED	360
A2.3 The SM	363
A2.4 Some examples of Feynman amplitudes	365
A2.5 Colour sums	367
A2.6 The Gell-Mann $SU(3)$ matrices	370
A2.7 The Fierz reshuffle theorem	371
A2.8 Dimension of matrix elements	372
<b>Appendix 3: Conserved vector currents and their charges</b>	373
<b>Appendix 4: Operator form of Feynman amplitudes and effective Hamiltonians</b>	378
<b>Appendix 5: <math>S</math>-matrix, <math>T</math>-matrix and Feynman amplitude</b>	382
<b>Appendix 6: Consequences of CPT invariance for matrix elements</b>	384
<b>Appendix 7: Formulae for the basic partonic <math>2 \rightarrow 2</math> processes</b>	387
A7.1 Reactions with only quarks and gluons	387
A7.1.1 Comparison of parton cross-section at $90^\circ$	391
A7.2 Reactions with one photon	391
A7.3 Reactions with two photons	393
<b>Appendix 8: Euclidean space conventions</b>	395
<i>References</i>	397
<i>Analytic subject index for vols. 1 and 2</i>	405



## Preface

For a book of its genre, our previous book, *An introduction to gauge theories and the “new physics”* (1982) was a great success. It was not, alas, sold in airport lounges, but it did run to two additional printings (1983, 1985), and to extensively revised editions in Russian (1990), and in Polish (1991). More importantly, it seemed to achieve the principal goal which we had set ourselves, namely, to present a *pedagogical* account of modern particle physics with a balance of theory and experiment, which would be intelligible and stimulating for both theoretical and experimental graduate students. We did *not* try to write a profound book on field theory, *nor* a treatise on sophisticated experimental techniques. But we did wish to stress the deep, intimate and fruitful interaction between theoretical ideas and experimental results. Indeed, for us, it is just this aspect of physics which makes it seem so much more exciting than say pure mathematics. Our greatest pleasure came from the favourable reaction of students who were working through the book and from those reviewers who caught what we hoped was its essential flavour—‘the writing creates the feeling of an active progression of ideas arising from the repeated interaction of theoretical prejudice with experimental observation’, ‘unlike most textbooks, it is highly readable, and makes everything appear simple and obvious’. Well, the last comment is surely an exaggeration but that was our aim.

In thinking about a second edition we were faced with a serious conceptual problem. Ten years ago we were in a state of excited expectation. A beautiful theory had been created and led, via the simplest of calculations, to absolutely dramatic experimental predictions; principally the existence and basic properties of the heavy vector bosons  $W^\pm$  and  $Z^0$ . A host of interesting new phenomena could be studied with no more effort than the calculation of a lowest order Born diagram. Much of the new physics could be discussed and understood from rather qualitative arguments. That idyllic situation is much changed now.

After the few years during which the experimentalists were struggling to demonstrate the very existence of these new phenomena, when the world of physics was electrified by the discovery of *one single*  $W$  or  $Z$  event, we have moved into an era when LEP is mass-producing millions of  $Z^0$ s!

Consequently, and unavoidably, the physics emphasis has changed drastically. Now it is the fine quantitative detail, the precise width and line shape of the  $Z^0$ , precision measurements of forward-backward asymmetries and branching ratios etc. which are under scrutiny experimentally. And to match that, more sophisticated and vastly more complicated theoretical calculations are demanded. Thus we have passed from a simple heuristic era to one of demanding quantitative rigour.

One consequence is that instead of a second edition we have ended up with a large new two-volume book!

The above does not mean that the subject has become boring and moribund. On the contrary, great theoretical issues are at stake. For the earlier Born approximations did not really test the deeper *field-theoretic* aspects of the theory, whereas the present comparisons between theory and experiment *are* sensitive to these elements. They play a rôle almost like that of the Lamb shift in establishing the validity of quantum electrodynamics (QED).

Faced then with the need to introduce and discuss these more extensive calculations, and given that schoolchildren, so it seems, are taught about quarks and gluons, there was the temptation to abandon the long and leisurely historical introduction to partons, quarks and gluons that we had provided in the first edition.

We have not done so for the following reason. The introduction of the new level of ‘elementarity’, the quarks and gluons, beyond the level of mesons and baryons, is, we believe, of a fundamentally new kind, both physically and philosophically in the modern history of science. For in all previous cases the *ultimate* proof of the existence of a hypothesized constituent was to produce and identify that constituent in the laboratory, for example, via a track in a bubble-chamber; or, where a neutral particle was involved, like the  $\Lambda^0$ , to have very obvious and incontrovertible evidence of its propagation and decay into charged tracks.

Now, for the first time, we are postulating the existence of constituents which, according to the present interpretation of the theory, can never be truly freed, which can, *in principle*, never be seen as free particles in the laboratory. This means that we really must provide convincing evidence for these constituents and must examine very critically the steps that lead to our postulating their existence.

It is on these grounds we have decided to retain the detailed discussion of the historical process leading to the belief in the parton picture.

The major *new* features of this book are:

1. We give a detailed explanation of higher order electroweak effects (the so-called radiative corrections).
2. We provide a much expanded discussion of quark mixing (the Kobayashi–Maskawa matrix), of  $K^0$ – $\bar{K}^0$  and  $B^0$ – $\bar{B}^0$  mixing and new sections on both the phenomenology and dynamics of CP violation.
3. The sections on charm and beauty and on jet physics have been totally revised in order to take into account the mass of data that has accumulated over the past few years.
4. We have enlarged the treatment of deep inelastic lepton–hadron scattering in three directions. Catalyzed by the major discoveries of the European Muon Collaboration there is a more detailed treatment of both polarization effects and of nuclear effects. And in anticipation of HERA we discuss  $Z^0$ – $\gamma$  interference which will be important for large  $Q^2$  physics.
5. The treatment of QCD corrections to the simple parton model is presented in much more detail and a new chapter is devoted to the derivation of the parton model from field theory.
6. Also linked to the coming into operation of HERA we discuss in more detail the ‘low  $x$ ’ region in deep inelastic scattering. Here the usual evolution equations break down and one approaches the non-perturbative region of QCD, creating a tremendous challenge to theory.
7. A brief discussion of elastic and soft reactions is provided so as to give the reader at least an inkling of the remarkable  $\bar{p}p$  physics being carried out at the CERN collider and at the Fermilab Tevatron. In particular, we discuss the impact of the very unexpected result of the UA4 experiment at CERN.
8. An introduction is given to the many and varied attempts to deal with the non-perturbative or confinement region of QCD, especially to the lattice approach and to the sum rule method, and to the exciting new ideas about baryon and lepton number violations. Necessarily the treatment of these is rather brief and not very comprehensive. We seek to convey the basic ideas and methods.
9. The Appendix has been much enlarged. It now contains a more detailed specification of the Feynman rules for electroweak theory and QCD, and a discussion of the relations between  $S$ -matrix, transition

amplitudes and Feynman amplitudes. There are also sections on CPT invariance and on the operator form of Feynman amplitudes or effective Hamiltonians, both important for CP violation. The evaluation of matrix elements of conserved currents, much used in deep inelastic scattering and in the study of the Kobayashi-Maskawa matrix, is explained in some detail. Finally, a complete list of cross-section formulae for all  $2 \rightarrow 2$  partonic reactions is given.

It is fascinating to step back and to view what has been achieved in the past decade and where we now stand. Electroweak theory and quantum chromodynamics have been remarkably successful, even at the level of the detailed questions now being examined. But essential to their present formulation and to their success are two objects, two crucial ingredients, the top quark and the Higgs meson, which have not yet been found. The Higgs meson is central to the symmetry breaking mechanism which gives mass to the  $W$  and  $Z$  bosons. And the top quark plays a vital rôle in the cancellation of anomalies and in the higher order calculations of small but significant effects beyond the Born approximation. Indeed the success in comparing these small corrections with experiment has led to quite tight limits on what mass the top quark could have. Most recently, at the Dallas Conference on High Energy Physics in August 1992, the following remarkably narrow limits for  $m_t$  were reported:

$$\begin{aligned} 107 \leq m_t &\leq 143 \text{ GeV}/c^2 & \text{for } m_H = 60 \text{ GeV}/c^2, \\ 126 \leq m_t &\leq 162 \text{ GeV}/c^2 & \text{for } m_H = 300 \text{ GeV}/c^2, \\ 143 \leq m_t &\leq 179 \text{ GeV}/c^2 & \text{for } m_H = 1 \text{ TeV}/c^2. \end{aligned}$$

In a way the sense of expectation for the discovery of ‘top’ and the ‘Higgs’ is almost as strong as was the expectation of the  $W$  and  $Z$  a decade ago.

#### *Acknowledgements*

We are enormously indebted to Nora Leonard for her intelligent and skillful handling of a large part of the  $\text{LATEX}$  typesetting of our manuscript. We are grateful to Roy Abrahams for his preparation of many of the diagrams. Thanks are also due to Giuseppe Ferrante for help with the typing and to Nestor Patrikios for aid with computer generated figures.

Finally, there are many colleagues and friends, too many to mention individually, to whom we are indebted for providing data and comments and for drawing our attention to misprints and errors in the first edition.

# Notational conventions

## Units

Natural units  $\hbar = c = 1$  are used throughout.

For the basic unit of charge we use the *magnitude* of the charge of the electron:  $e > 0$ .

## Relativistic conventions

Our notation generally follows that of Bjorken and Drell (1964), in *Relativistic Quantum Mechanics*.

The metric tensor is

$$g_{\mu\nu} = g^{\mu\nu} = \begin{pmatrix} 1 & 0 & 0 & 0 \\ 0 & -1 & 0 & 0 \\ 0 & 0 & -1 & 0 \\ 0 & 0 & 0 & -1 \end{pmatrix}.$$

Space-time points are denoted by the contravariant four-vector  $x^\mu$  ( $\mu = 0, 1, 2, 3$ )

$$x^\mu = (t, \mathbf{x}) = (t, x, y, z),$$

and the four-momentum vector for a particle of mass  $m$  is

$$p^\mu = (E, \mathbf{p}) = (E, p_x, p_y, p_z),$$

where

$$E = \sqrt{\mathbf{p}^2 + m^2}.$$

Using the equation for the metric tensor, the scalar product of two four-vectors,  $A, B$ , is defined as

$$A \cdot B = A_\mu B^\mu = g_{\mu\nu} A^\mu B^\nu = A^0 B^0 - \mathbf{A} \cdot \mathbf{B}.$$

*$\gamma$ -matrices*

The  $\gamma$  matrices for spin-half particles satisfy

$$\gamma^\mu \gamma^\nu + \gamma^\nu \gamma^\mu = 2g^{\mu\nu}$$

and we use a representation in which

$$\gamma^0 = \begin{pmatrix} I & 0 \\ 0 & -I \end{pmatrix}, \quad \gamma^j = \begin{pmatrix} 0 & \sigma_j \\ -\sigma_j & 0 \end{pmatrix}, \quad j = 1, 2, 3,$$

where  $\sigma_j$  are the usual Pauli matrices. We define

$$\gamma^5 = \gamma_5 = i\gamma^0\gamma^1\gamma^2\gamma^3 = \begin{pmatrix} 0 & I \\ I & 0 \end{pmatrix}.$$

In this representation one has for the transpose T of the  $\gamma$  matrices:

$$\gamma^{jT} = \gamma^j \quad \text{for } j = 0, 2, 5,$$

but

$$\gamma^{jT} = -\gamma^j \quad \text{for } j = 1, 3.$$

For the Hermitian conjugates  $\dagger$  one has

$$\gamma^{0\dagger} = \gamma^0, \quad \gamma^{5\dagger} = \gamma^5,$$

but

$$\gamma^{j\dagger} = -\gamma^j \quad \text{for } j = 1, 2, 3.$$

The combination

$$\sigma^{\mu\nu} \equiv \frac{i}{2}[\gamma^\mu, \gamma^\nu]$$

is often used.

The scalar product of the  $\gamma$  matrices and any four-vector  $A$  is defined as

$$\mathcal{A} \equiv \gamma^\mu A_\mu = \gamma^0 A^0 - \gamma^1 A^1 - \gamma^2 A^2 - \gamma^3 A^3.$$

For further details and properties of the  $\gamma$  matrices see Appendix A of Bjorken and Drell (1964).

*Spinors and normalization*

The particle spinors  $u$  and the antiparticle spinors  $v$ , which satisfy the Dirac equations

$$\begin{aligned} (\not{p} - m)u(p) &= 0, \\ (\not{p} + m)v(p) &= 0, \end{aligned}$$

respectively, are related by

$$\begin{aligned} v &= i\gamma^2 u^*, \\ \bar{v} &= -iu^T \gamma^0 \gamma^2, \end{aligned}$$

where  $\bar{v} \equiv v^\dagger \gamma^0$  (similarly  $\bar{u} \equiv u^\dagger \gamma^0$ ).

Note that our spinor normalization differs from Bjorken and Drell. We utilize

$$u^\dagger u = 2E, \quad v^\dagger v = 2E,$$

the point being that the above can be used equally well for massive fermions and for neutrinos. For a massive fermion or antifermion the above implies

$$\bar{u}u = 2m, \quad \bar{v}v = -2m.$$

### Cross-sections

With this normalization the cross-section formula (B.1) of Appendix B in Bjorken and Drell (1964) holds for both mesons and fermions, massive or massless. This is discussed in our Appendix 2—see in particular eqn (A2.1.6).

### Fields

Often a field like  $\psi_\mu(x)$  for the muon is simply written  $\mu(x)$  or just  $\mu$  if there is no danger of confusion.

In fermion lines in Feynman diagrams the arrow indicates the direction of flow of *fermion number*. Thus incoming electrons or positrons are denoted as follows:



### Normal ordering

In quantum field theory the products of operators that appear in Lagrangians and Hamiltonians should really be *normal ordered* with all creation operators to the left of all annihilation operators. With the exception of Sections 5.1.1 and 19.4 this is irrelevant throughout this book, so the normal ordering symbol is never indicated.

### Group symbols and matrices

In dealing with the electroweak interactions and QCD the following symbols often occur:

- $n_f$  = number of flavours;
- $N$  which specifies the gauge group  $SU(N)$ —Note that  $N = 3$  for the colour gauge group QCD;
- the Pauli matrices are written either as  $\sigma_j$  or  $\tau_j$  ( $j = 1, 2, 3$ );
- the Gell-Mann  $SU(3)$  matrices are denoted by  $\lambda^a$  ( $a = 1 \dots 8$ );
- for a group  $(G)$  with structure constants  $f_{abc}$  one defines  $C_2(G)$  via

$$\delta_{ab}C_2(G) \equiv f_{acd}f_{bcd}$$

and one often writes

$$C_A \equiv C_2[SU(3)] = 3.$$

If there are  $n_f$  multiplets of particles, each multiplet transforming according to some representation  $R$  under the gauge group, wherein the group generators are represented by matrices  $t^a$ , then  $T(R)$  is defined by

$$\delta_{ab}T(R) \equiv n_f \text{Tr}(t^a t^b).$$

For  $SU(3)$  and the triplet (quark) representation one has  $t^a = \lambda^a/2$  and

$$T \equiv T[SU(3); \text{triplet}] = \frac{1}{2}n_f.$$

For the above representation  $R$  one defines  $C_2(R)$  analogously to  $C_2(G)$  via

$$\delta_{ij}C_2(R) \equiv t_{ik}^a t_{kj}^a.$$

For  $SU(3)$  and the triplet representation one has

$$C_F \equiv C_2[SU(3); \text{triplet}] = 4/3.$$

### The coupling in QCD

Finally, to conform with recent review articles, we have changed the sign convention for the coupling in QCD, i.e. our new  $g$  is minus the  $g$  used in the first edition. Since everything of physical interest in QCD depends upon  $g^2$  this is essentially irrelevant.

### Colour sums in weak and electromagnetic current

Since the weak and electromagnetic interactions are ‘colour-blind’ the colour label on a quark field is almost never shown explicitly when dealing with electroweak interactions. In currents involving quark field operators (e.g. in Sections 1.2 and 9.3) a *colour sum is always implied*. For example, the electromagnetic current of a quark of flavour  $f$  and charge  $Q_f$  (in units of  $e$ ) is written

$$J_{\text{em}}^\mu(x) = Q_f \bar{q}_f(x) \gamma^\mu q_f(x)$$

but if the colour of the quark is labelled  $j$  ( $j = 1, 2, 3$ ) then what is implied is

$$J_{\text{em}}^\mu(x) = Q_f \sum_{\substack{\text{colours} \\ j}} \bar{q}_{f_j}(x) \gamma^\mu q_{f_j}(x).$$



## Note added in proof: the discovery of the top quark (?)

On Tuesday 26 and Wednesday 27 April 1994 nearly simultaneous press conferences in the USA, Italy and Japan announced that evidence for the top quark had been found by the CDF collaboration at Fermilab. In fact most of the information had by then already appeared in a long article in *The New York Times* and rumours about the discovery had been circulating for some time.

The collaboration was at pains to insist that they were not claiming the *discovery* of top, but only some *evidence* for it. There are several reasons for their prudence. The main one is that the  $t\bar{t}$  cross-section measured,  $13.9^{+6.1}_{-4.8}$  pb, is a factor of three larger than the theoretical expectations. Also the other collaboration at Fermilab studying this question (the DO collaboration) is not yet willing to make any public statement, but it seems that their  $t\bar{t}$  cross-section would be considerably smaller. The calculated  $t\bar{t}$  cross-section at Fermilab energies is a sensitive function of  $m_t$ , varying from 20 pb for  $m_t = 120 \text{ GeV}/c^2$  to 4 pb for  $m_t = 180 \text{ GeV}/c^2$ .

Interestingly, the theoretical estimates of  $m_t$ , based on the calculation of radiative corrections to various high precision LEP electroweak measurements, have been moving towards higher and higher values. At the 1990 International High Energy Physics Conference at Singapore the best value was given as  $m_t = 137 \pm 40 \text{ GeV}/c^2$ , whereas recent studies suggest  $164 \pm 16 \pm 19 \text{ GeV}/c^2$ . The value for  $m_t$  given by CDF is compatible with these higher values, namely  $m_t = 174 \pm 13^{+13}_{-12} \text{ GeV}/c^2$ . Such a high value for  $m_t$  has significant implications for the radiative correction calculations and in particular for the theoretical understanding of CP violation, as discussed in Chapter 19.

The result reported by CDF is a 2.5 sigma effect, which becomes less than a 2 sigma effect when their data is combined with the DO data. Clearly, therefore, much better data are needed before a totally convincing picture can emerge. The evidence for top, if confirmed, would be one more

very strong factor in favour of the standard model. Ultimately, however, there will still remain the crucial question as to the existence or not of the Higgs boson. And it may be some time before we have a definitive answer to *that* question.

By May 1995 the evidence for the top quark is firmer. The new combined CDF and DO results have increased the significance of the signal to more than 4 sigma. The masses quoted are:

$$\text{CDF: } 176 \pm 8 \pm 10 \text{ GeV}/c^2$$

$$\text{DO: } 199_{-21}^{+19} \pm 22 \text{ GeV}/c^2.$$

## **Note added in proof: the demise of the SSC**

At various points in this book we have talked rather optimistically about future accelerators, in particular about the gigantic, 54 miles in circumference, Superconducting Super Collider (SSC) which was to be built at Waxahachie in Texas and which would have produced 20 TeV + 20 TeV proton–proton collisions. The energy densities attainable would have matched those found in the universe as close as  $10^{-13}$  seconds to the big bang, providing extraordinary possibilities for testing not just the standard model of elementary particle interactions, but the whole picture of the evolution of the universe.

Alas, on 22 October 1993, after a long and agonizing period of indecision, the US House of Representatives voted to end the funding of the SSC project. At this point, 2 billion US dollars had already been spent and about one-fifth of the tunnel completed.

In the words of Hazel O’Leary, the US Secretary of State for Energy, ‘this decision by Congress . . . is a devastating blow to basic research and to the technological and economic benefits that always flow from that research.’

There is still hope that the somewhat more modest European project for a Large Hadron Collider (LHC) with 8 TeV + 8 TeV proton–proton collision, will go ahead. A final decision was due during 1994. After much procrastination the CERN Council finally voted in favour of the project in December 1994. The construction will proceed in stages, with full-scale operation planned for 2008!



# 1

## Field theory and pre-gauge theory of weak interactions

Our principal aim in this chapter is to review briefly the basic ideas of field theory, which we shall illustrate with examples from quantum electrodynamics (QED) and the theory of strong interactions, quantum chromodynamics (QCD). Of necessity, we must assume that the reader has some knowledge of field theory and is conversant with the idea of Feynman diagrams and with the Dirac equation. We shall then give a resumé of the theory and phenomenology of the weak interactions as they stood at the time of the inception of the new ideas about quarks and gluons in the early 1970s. The chapter ends with some technical results which will be very useful in later chapters.

The detailed rules for the Feynman diagrams for the various field theories are given in Appendix 2.

### 1.1 A brief introduction to field theory

Processes in which particles can be created or annihilated are best treated in the language of quantum field theory, using field operators  $\phi(x)$  that are linear superpositions of operators  $a^\dagger(\mathbf{p})$  and  $a(\mathbf{p})$  which respectively *create* and *annihilate* particles of momentum  $\mathbf{p}$  when they act upon any state vector. If the state happens not to contain the relevant particle of momentum  $\mathbf{p}$  then  $a(\mathbf{p})$  acting on it just gives zero (the detailed mathematical relationship can be found in Appendix 1).

The field operators  $\phi(x)$  obey equations of motion that are derived from a Lagrangian  $L$  via a variational principle, in direct analogy to classical mechanics, and interactions between different fields are produced by adding to the free Lagrangian  $L_0$  an *interaction term*  $L'$  containing products of the various field operators that are to influence each other. The equations of motion thereby become coupled equations relating the different fields to each other. Usually  $L$  is written as an integral over all

space of  $\mathcal{L}(x, t)$ , the Lagrangian density, but we shall often refer to  $\mathcal{L}$  as simply ‘the Lagrangian’.

The techniques of field theory are highly sophisticated involving subtle questions of renormalization etc. (see e.g. Bjorken and Drell, 1964, 1965; Itzykson and Zuber, 1980). At this point we require only a simple heuristic appreciation of certain features.

If the interaction term is small, in the sense that it is proportional to a small coupling constant, a perturbative approach may work. The successive terms are usually shown graphically as Feynman diagrams—a line representing the free propagation of a particle, a vertex the interaction between particles, the structure of which is controlled by the form of the interaction term in the Lagrangian.

By far the best known field theory is quantum electrodynamics (QED) in which the coupling of the electron field  $\psi_e(x)$  to the electromagnetic vector potential  $A_\mu(x)$  is described in the Lagrangian by a term

$$e\bar{\psi}_e(x)\gamma^\mu\psi_e(x)A_\mu(x).$$

The appearance of  $\psi_e(x)$  signifies either annihilation of an electron or creation of a positron;  $\bar{\psi}_e(x)$  the creation of an electron or the annihilation of a positron;  $A_\mu(x)$  the creation or annihilation of a photon. Thus the vertex can give rise to the types of transition as seen in Fig. 1.1, where the arrow on a fermion line points in the direction of flow of fermion number ( $e^-$  is a fermion,  $e^+$  an antifermion).

Often we are not interested in the detailed space-time and spinorial structure of the fields, but simply in which particles occur at the vertices and in what combinations of charges, isotopic spins etc. When this is the case we shall simplify the notation, using the particle’s symbol to stand for its field operator, thus  $e$  for  $\psi_e(x)$ ,  $\bar{e}$  for  $\bar{\psi}_e(x)$ ,  $\mu$  for  $\psi_\mu(x)$  the field of the  $\mu$ -meson etc. (Since  $\mu, \nu$  will usually indicate  $\mu$  mesons and neutrinos, we shall often use  $\alpha$  or  $\beta$  to indicate Lorentz indices on vectors, tensors and  $\gamma$ -matrices.)

The expression for the QED vertex in the Lagrangian for any charged fermion is often written as

$$-eJ_{\text{em}}^\alpha(x)A_\alpha(x),$$

where  $e$  is the magnitude of the charge of the electron; the *electromagnetic current operator* for some particle,  $i$ , whose charge in units of  $e$  is  $Q_i$ , is

$$J_{\text{em}}^\alpha(x) = Q_i\bar{\psi}_i(x)\gamma^\alpha\psi_i(x). \quad (1.1.1)$$

The electromagnetic current is a *conserved current*. Mathematically this is expressed by the vanishing of the four-dimensional divergence of  $J_{\text{em}}^\alpha$ :

$$\partial_\alpha J_{\text{em}}^\alpha(x) = 0 \quad (1.1.2)$$

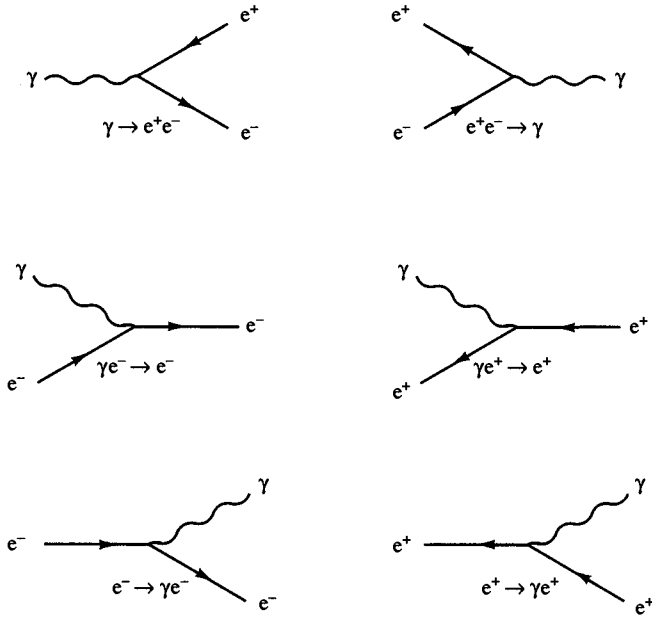


Fig. 1.1. Basic transitions (vertices) in QED.

where  $\partial_\alpha$  is short for  $\partial/\partial x^\alpha$ .

The conservation has a remarkable consequence for any matrix element of  $J_{\text{em}}$ . Just as in ordinary quantum mechanics, the momentum operators  $\hat{P}_j$  ( $j = x, y, z$ ) and the energy operator  $\hat{P}_0$  (the Hamiltonian) generate translations in space and time respectively. Thus for  $\hat{P}_\alpha = (\hat{P}_0, -\hat{\mathbf{P}})$  and any operator  $f(x)$  one has for the commutator

$$[\hat{P}_\alpha, f(x)] = i\partial_\alpha f(x). \quad (1.1.3)$$

If we take the matrix element of (1.1.2) between *arbitrary* states  $|A\rangle$  and  $|B\rangle$  and utilize (1.1.3), we have

$$\begin{aligned} 0 &= \langle B | \partial_\alpha J_{\text{em}}^\alpha(x) | A \rangle = -i \langle B | [\hat{P}_\alpha, J_{\text{em}}^\alpha(x)] | A \rangle \\ &= -i [p_\alpha(B) - p_\alpha(A)] \langle B | J_{\text{em}}^\alpha(x) | A \rangle \end{aligned}$$

where  $p_\alpha(A), p_\alpha(B)$  are the four-momenta of states  $|A\rangle$  and  $|B\rangle$ . Thus if  $q \equiv p(A) - p(B)$  is defined as the *momentum transfer vector* then the conservation of  $J_{\text{em}}$  has as a consequence that

$$q_\alpha \langle B | J_{\text{em}}^\alpha(x) | A \rangle = 0. \quad (1.1.4)$$

Eqn (1.1.4) is an example of a ‘Ward–Takahashi identity’, a relation that must be satisfied by the matrix elements of any operator that possesses

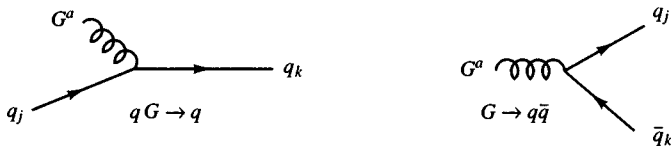


Fig. 1.2. Quark-gluon vertices in QCD.

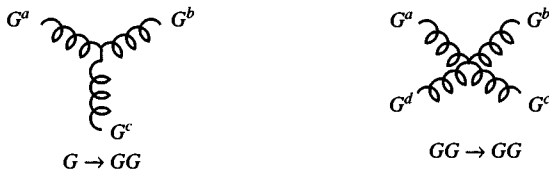


Fig. 1.3. Gluon-gluon vertices in QCD.

some conservation property. Relations of this type play a vital rôle in showing the renormalizability of a theory.

In QCD, which is to some extent similar to QED, the fundamental interactions are between spin  $\frac{1}{2}$  *quarks* and massless spin 1 *gluons*. The quarks and gluons carry a new quantum number somewhat misleadingly called *colour*. Each quark can exist in three different colour states and each gluon in eight colour states. Under an  $SU(3)$  group of transformations which mixes up colours the quarks and gluons are said to transform as a triplet and an octet respectively. No physical particle with the attribute of colour has ever been found so it is believed that all physical particles are ‘colour neutral’. By this, we mean that all physical states must be invariant, or *singlets* under colour transformations.

The transitions involving quarks, antiquarks and gluons are similar to those involving electrons and photons except for the added complication of the colour labels  $a, j, k$  (see Fig. 1.2).

However, whereas photons do not couple directly to each other, there exist both 3-gluon and 4-gluon couplings (Fig. 1.3) and these, as is discussed later, have a profound influence on the theory. Gauge transformations and gauge invariance are more complicated than in QED and the consequences of gauge invariance more subtle. In particular the colour current of quarks does not satisfy (1.1.2).

Later it will be important to define linear combinations of different fields. We wish to examine the conditions that ensure that the new fields are independent. Consider two boson fields  $\phi_1, \phi_2$ . The creation and annihilation operators (we ignore the momentum label for simplicity) must

satisfy the canonical commutation relations ( $i = 1, 2$ )

$$[a_i, a_i] = 0, \quad [a_i^\dagger, a_i^\dagger] = 0, \quad [a_i, a_i^\dagger] = 1,$$

but operators belonging to the independent fields  $\phi_1, \phi_2$  must commute. In particular

$$[a_1, a_2^\dagger] = 0$$

if  $\phi_1, \phi_2$  are independent. If now we define new fields

$$\begin{aligned} \phi'_1 &= \alpha_1 \phi_1 + \beta_1 \phi_2, \\ \phi'_2 &= \alpha_2 \phi_2 + \beta_2 \phi_1, \end{aligned} \quad \left. \right\} \quad (1.1.5)$$

and demand that they be independent, then their  $a'_1, a'_1^\dagger, a'_2, a'_2^\dagger$  must satisfy the above commutation conditions. A little algebra shows that one requires

$$\begin{aligned} |\alpha_1|^2 + |\beta_1|^2 &= |\alpha_2|^2 + |\beta_2|^2 = 1, \\ \alpha_1^* \alpha_2 + \beta_1^* \beta_2 &= 0. \end{aligned} \quad (1.1.6)$$

The transformation from  $\phi_1, \phi_2$  to  $\phi'_1, \phi'_2$  is ‘unitary’, i.e.

$$\begin{pmatrix} \phi'_1 \\ \phi'_2 \end{pmatrix} = U \begin{pmatrix} \phi_1 \\ \phi_2 \end{pmatrix},$$

where  $U$  is a unitary matrix. If, in particular, we take *real* linear combinations then (1.1.6) implies that they must be the orthogonal combinations

$$\begin{aligned} \phi'_1 &= \cos \theta \phi_1 + \sin \theta \phi_2, \\ \phi'_2 &= -\sin \theta \phi_1 + \cos \theta \phi_2. \end{aligned} \quad \left. \right\} \quad (1.1.7)$$

We end this section with a comment about dimensions. In natural units  $\hbar = c = 1$ , the Lagrangian  $L$  has dimensions of [M] and thus the Lagrangian density  $\mathcal{L}$ ,  $[M][L]^{-3} = [M]^4$ . From the form of the terms which occur in the *free* Lagrangian density, i.e. the kinetic energy terms, one can read off the dimensions of various fields:

spinor field

$$m\bar{\psi}\psi \rightarrow [\psi] = [M]^{3/2}$$

scalar and vector fields

$$m^2 \phi^\dagger \phi \rightarrow [\phi] = [M]$$

photon (or gluon)

$$F_{\mu\nu} F^{\mu\nu} \rightarrow [A_\mu] = [M]$$

This enables us to read off the dimensions of any coupling constant introduced in the interaction part of the Lagrangian.

Further details, in particular the rules for calculating Feynman diagrams in QED, QCD and in weak interactions, are given in Appendix 2. For a complete treatment the reader is referred to Bjorken and Drell (1964, 1965) and Itzykson and Zuber (1980).

## 1.2 Pre-gauge theory of weak interactions

After many years of effort, and many false starts, it was concluded in the mid-1950s that all of weak interaction phenomenology could be described by the Fermi Lagrangian

$$\mathcal{L}_F = \frac{G}{\sqrt{2}} J^\alpha(x) J_\alpha^\dagger(x), \quad (1.2.1)$$

where  $G$  (the  $\sqrt{2}$  is a historic convention) is the Fermi coupling constant, with dimensions  $[M]^{-2}$ , the value of which is [see also eqn (4.2.34)]

$$G \approx 1.03 \times 10^{-5} m_p^{-2}, \quad (1.2.2)$$

with  $m_p$  the proton mass. The *weak current*  $J^\alpha(x)$  is the analogue of the electromagnetic current, and is the sum of two parts, leptonic  $l^\alpha(x)$  and hadronic  $h^\alpha(x)$ :

$$J^\alpha(x) = l^\alpha(x) + h^\alpha(x). \quad (1.2.3)$$

The Fermi Lagrangian then gives rise to three types of weak process (all of a ‘point-like’ nature since interactions only take place when all the particles are at the same point):

(a) purely leptonic controlled by

$$\frac{G}{\sqrt{2}} l^\alpha(x) l_\alpha^\dagger(x),$$

e.g.  $\mu^- \rightarrow e^- + \bar{\nu}_e + \nu_\mu$ , i.e. muon  $\beta$ -decay;

(b) semi-leptonic determined by

$$\frac{G}{\sqrt{2}} [l^\alpha(x) h_\alpha^\dagger(x) + h^\alpha(x) l_\alpha^\dagger(x)],$$

e.g.  $n \rightarrow p + e^- + \bar{\nu}_e$ , i.e. neutron  $\beta$ -decay;

(c) purely hadronic controlled by

$$\frac{G}{\sqrt{2}} h^\alpha(x) h_\alpha^\dagger(x),$$

e.g.  $\Lambda \rightarrow p + \pi^-$ .

The vectorial and spin structure of the leptonic current is of the  $V - A$  form ( $V$  = vector,  $A$  = axial vector)

$$l^\alpha(x) = \bar{e}(x)\gamma^\alpha(1 - \gamma_5)\nu_e(x) + \bar{\mu}(x)\gamma^\alpha(1 - \gamma_5)\nu_\mu(x), \quad (1.2.4)$$

where  $e, \nu_e, \mu, \nu_\mu$  are the field operators for the electron  $e$ , its neutrino  $\nu_e$ , the muon  $\mu$  and its neutrino  $\nu_\mu$ . The spin structure is discussed further in Section 1.3.1.

When we take matrix elements of  $l^\alpha$  between a neutrino and electron state, then the field operators can be regarded as essentially free field operators so that, with the normalization given in Appendix 1,

$$\langle e | l^\alpha | \nu_e \rangle \rightarrow \bar{u}_e \gamma^\alpha(1 - \gamma_5) u_\nu, \quad (1.2.5)$$

where  $u_e, u_\nu$  are ordinary Dirac spinors.

Note that  $l^\alpha$  preserves the *electron number* and the *muon number* in the sense that it causes transitions  $e \rightarrow \nu_e$  and  $\mu \rightarrow \nu_\mu$  but not between  $e$  and  $\nu_\mu$  or  $\mu$  and  $\nu_e$ . Formally one states that  $(e^-, \nu_e)$  have *electron number* +1,  $(e^+, \bar{\nu}_e)$  have -1 and all other particles zero. Analogously  $(\mu^-, \nu_\mu)$  have *muon number* +1,  $(\mu^+, \bar{\nu}_\mu)$  have -1 and all other particles zero.

The validity of this structure is borne out by the absence of many reactions which would have been expected to be seen. Some examples are:

1. Absence of neutrinoless double  $\beta$ -decay

$$(Z, A) \not\rightarrow (Z + 2, A) + e^- + e^-$$

which would be kinematically favoured compared with the observed reaction

$$(Z, A) \rightarrow (Z + 2, A) + e^- + e^- + \bar{\nu}_e + \bar{\nu}_e$$

if it were possible to have the sequence, inside the nucleus

$$\begin{array}{c} n \rightarrow p + e^- + \bar{\nu}_e \\ \downarrow \\ \bar{\nu}_e + n \rightarrow p + e^- \end{array}$$

Typical half-lives for 2 neutrino double  $\beta$ -decay are  $10^{18}$ – $10^{20}$  years. The lower bound for neutrinoless  $\beta$ -decay is about  $10^{24}$  years.

2.  $\nu_\mu + (Z, A) \not\rightarrow (Z - 1, A) + \mu^+$   
but  $\nu_\mu + (Z, A) \rightarrow (Z + 1, A) + \mu^-$ .
3.  $\nu_\mu + (Z, A) \not\rightarrow (Z - 1, A) + e^+$   
 $\nu_\mu + (Z, A) \not\rightarrow (Z + 1, A) + e^-$ .

4. Perhaps the most remarkable of all is

$$\mu^+ \not\rightarrow e^+ + \gamma.$$

Here the branching ratio (BR), i.e. the fraction of decays into this channel, has been measured to fantastic accuracy (Bolton *et al.*, 1988):

$$\text{BR}(\mu \rightarrow e\gamma) < 4.9 \times 10^{-11}$$

and experiments are being planned which will test this to the level of  $10^{-13}$ .

Many further examples could be quoted in support of the selection rules implicit in (1.2.4) (see however Chapter 28). The structure of the hadronic part is more difficult to specify. Even if we had an *explicit* expression for  $h^\alpha(x)$  we could not, in general, compute matrix elements of  $h^\alpha$  between hadron states, because the hadrons, being severely affected by the strong interactions, are far from being like bare free particles. Nevertheless all aspects of classical  $\beta$ -decay including the neutron decay  $n \rightarrow p + e^- + \bar{\nu}_e$  are well described by matrix elements of a form very much like (1.2.5):

$$\langle p | h^\alpha | n \rangle \rightarrow \bar{u}_p \gamma^\alpha (G_V - G_A \gamma_5) u_n \quad (1.2.6)$$

with  $G_V$  very close to one in value and  $G_A \simeq 1.24$ .

The fact that  $G_V$  is so close to one in (1.2.6) is remarkable because that is the value of the coefficient of  $\gamma^\alpha$  in  $l^\alpha(x)$ . Yet one might have thought that the effect of the strong interactions in the hadrons would give a drastically different value. The result is explained by the ‘conserved vector current’ hypothesis (CVC) according to which the *vector part*  $V^\alpha(x)$  of  $h^\alpha(x)$  belongs to a triplet of *conserved* currents associated with the conservation of isospin in the hadronic reactions (Feynman and Gell-Mann, 1958). As we shall discuss in Section 2.3, conservation laws always imply the existence of conserved currents, e.g. charge conservation is linked to the conservation of  $J_{\text{em}}^\alpha(x)$ . The conservation of isospin then implies the existence of three currents:  $V_j^\alpha(x)$ ,  $j = 1, 2, 3$  all of which are conserved:

$$\partial_\alpha V_j^\alpha(x) = 0. \quad (1.2.7)$$

If we group p and n into an isospin doublet  $N = \begin{pmatrix} p \\ n \end{pmatrix}$  then for the nucleons

$$V_j^\alpha(x) = \bar{N}(x) \gamma^\alpha \left( \frac{\tau_j}{2} \right) N(x), \quad (1.2.8)$$

where the  $\tau_j$  are the Pauli matrices. But the electromagnetic current of the nucleons can also be written in this form:

$$J_{\text{em}}^\alpha(x) = \bar{N}(x) \gamma^\alpha \left( \frac{1 + \tau_3}{2} \right) N(x) \quad (1.2.9)$$

$$= J_{\text{em}}^\alpha(\text{isoscalar}) + J_{\text{em}}^\alpha(\text{isovector}), \quad (1.2.10)$$

showing that for the nucleons

$$V_3^\alpha(x) = J_{\text{em}}^\alpha(\text{isovector}). \quad (1.2.11)$$

In fact (1.2.11) holds for the full currents, not just for the nucleon contribution.

If now we *assume* that the *vector* part  $V^\alpha$  of  $h^\alpha$  is of the form

$$V^\alpha(x) = \bar{p}(x)\gamma^\alpha n(x) = \bar{N}(x)\gamma^\alpha \left( \frac{\tau_1 + i\tau_2}{2} \right) N(x)$$

then we have, by (1.2.8), for nucleons

$$V^\alpha = V_1^\alpha + iV_2^\alpha. \quad (1.2.12)$$

It is now postulated that (1.2.12) holds for the *entire* current, not just for the nucleon piece of it, and therefore  $V^\alpha$  is a conserved current. But precisely because it is conserved its matrix elements can be shown to be uninfluenced by the strong interactions, as is explained in some detail in Appendix 3, so that

$$\langle p | V^\alpha | n \rangle = \bar{u}_p \gamma^\alpha u_n, \quad (1.2.13)$$

which would explain the phenomenological result (1.2.6).

Notice that, whereas the electromagnetic current induces transitions between states of the same charge, both  $l^\alpha$  and  $h^\alpha$  cause transitions in which the charge is changed by one unit of  $e$ . It is customary to classify weak reactions according to what happens in the *hadronic* part of the transition. For example for neutron  $\beta$ -decay one has

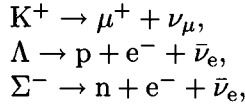
$$\begin{aligned} \Delta Q &= (\text{final hadron charge}) - (\text{initial hadron charge}) \\ &= +1 \end{aligned}$$

and, since there is no change of strangeness,

$$\Delta S = 0.$$

Now  $G_V$  in (1.2.6) has been measured very carefully and it is not exactly equal to 1. Indeed it differs significantly from one:  $1 - G_V \simeq 0.02$ . So (1.2.12) cannot be exact.

On the other hand, there are reactions, analogous to neutron  $\beta$ -decay, but involving strange particles. For example



which involve a change of strangeness  $\Delta S = 1$  at the hadronic vertex.

The amplitudes for these processes are considerably smaller than those of analogous  $\Delta S = 0$  reactions, e.g.  $\pi^+ \rightarrow \mu^+ + \nu_\mu$  and neutron  $\beta$ -decay.

Cabibbo (1963) noticed that if one writes, analogously to (1.2.6),

$$\langle p|h^\alpha|\Lambda\rangle = \bar{u}_p\gamma^\alpha \left( G_V^{\Delta S=1} - G_A^{\Delta S=1}\gamma_5 \right) u_\Lambda$$

then empirically

$$(G_V)^2 + (G_A^{\Delta S=1})^2 \approx 1. \quad (1.2.14)$$

He thus suggested that for the vector part of  $h^\alpha$  one should write

$$V^\alpha = \cos\theta_C V^\alpha(\Delta S = 0) + \sin\theta_C V^\alpha(\Delta S = 1), \quad (1.2.15)$$

where  $V^\alpha(\Delta S = 0)$  and  $V^\alpha(\Delta S = 1)$  are the conserved currents with properties like (1.2.13). Then

$$\begin{aligned} \langle p|V^\alpha|n\rangle &= \cos\theta_C \langle p|V^\alpha(\Delta S = 0)|n\rangle \rightarrow \cos\theta_C \bar{u}_p\gamma^\alpha u_n \\ \langle p|V^\alpha|\Lambda\rangle &= \sin\theta_C \langle p|V^\alpha(\Delta S = 1)|\Lambda\rangle \rightarrow \sin\theta_C \bar{u}_p\gamma^\alpha u_\Lambda \end{aligned}$$

so that  $G_V = \cos\theta_C$ ,  $G_V^{\Delta S=1} = \sin\theta_C$  and (1.2.14) is satisfied.  $\theta_C$  is known as the Cabibbo angle, and its value is

$$\sin\theta_C = 0.230 \pm 0.003.$$

(Since  $\cos\theta_C \gg \sin\theta_C$  some reactions, whose amplitudes are proportional to  $\cos\theta_C$ , will be much more probable than those whose amplitudes are proportional to  $\sin\theta_C$ . The two classes of reaction are often referred to as ‘Cabibbo allowed’ and ‘Cabibbo forbidden’.)

In fact Cabibbo went much further. The strong interactions are approximately invariant under the group of transformations  $SU(3)$  (Gell-Mann, 1962). Since  $SU(3)$  has eight generators (see, for example, Lichtenberg, 1978) there is an octet of conserved currents  $V_j^\alpha(x)(j = 1, \dots, 8)$  of which the first three are again the isospin triplet of currents introduced earlier. The current  $V_4^\alpha + iV_5^\alpha$  changes the strangeness by one unit and raises the charge by one unit, i.e. it causes  $\Delta Q = 1, \Delta S = 1$  transitions. Hence it is proposed to identify  $V^\alpha(\Delta S = 1)$  with these. We have then from (1.2.15)

$$V^\alpha = \cos\theta_C(V_1^\alpha + iV_2^\alpha) + \sin\theta_C(V_4^\alpha + iV_5^\alpha). \quad (1.2.16)$$

The electric current in terms of these is

$$J_{\text{em}}^\alpha = V_3^\alpha + \frac{1}{\sqrt{3}}V_8^\alpha. \quad (1.2.17)$$

Cabibbo also proposed the existence of an octet of axial-vector currents  $A_j^\alpha(j = 1, \dots, 8)$  in terms of which the axial-vector part  $A^\alpha$  of  $h^\alpha$  can be expressed. The  $A_j^\alpha$  cannot be exactly conserved since the symmetry of the Lagrangian that would be responsible, known as a *chiral* symmetry, could only hold if all particles were massless. (To the extent that the  $\pi$  and K mesons are *light* it is possible to give some meaning to the idea

of an *approximately* or partially conserved axial current (PCAC), but we shall not discuss that here.)

The main point is that the  $A_j^\alpha$  are supposed to behave under  $SU(3)$  transformations just like the  $V_j^\alpha$ . If  $T_j$  ( $j = 1, \dots, 8$ ) are the generators of  $SU(3)$  then one has

$$\left. \begin{aligned} [T_j, V_k^\alpha] &= i f^{jkl} V_l^\alpha, \\ [T_j, A_k^\alpha] &= i f^{jkl} A_l^\alpha, \end{aligned} \right\} \quad (1.2.18)$$

where the  $f^{jkl}$  are the structure constants of  $SU(3)$  (see Appendix 2.6). Eqn (1.2.18) simply states that the  $V_j^\alpha$  and  $A_j^\alpha$  transform as an octet of ‘vectors’ under  $SU(3)$  transformations.

It is interesting to note that whereas there are neutral currents amongst the  $J_j$  (e.g.  $J_3$  and  $J_8$  are both neutral) they play no rôle in the *weak* interactions in the Cabibbo theory. It will be seen later that there is now explicit evidence for neutral currents in weak interactions.

To summarize, we have, in Cabibbo theory,

$$h^\alpha(x) = V^\alpha(x) + A^\alpha(x), \quad (1.2.19)$$

with  $V^\alpha$  given by (1.2.16) and

$$A^\alpha(x) = \cos \theta_C (A_1^\alpha + i A_2^\alpha) + \sin \theta_C (A_4^\alpha + i A_5^\alpha). \quad (1.2.20)$$

It is important to note that  $V^\alpha$  and  $A^\alpha$  do not transform simply under isospin transformations. Only to the extent that  $\sin \theta_C \simeq 0$ ,  $\cos \theta_C \simeq 1$  do they behave simply.

Eqns (1.2.18) allow us to relate the matrix elements for particles belonging to the same  $SU(3)$  multiplet and thus to predict the details of many reactions in terms of just  $\theta_C$ ,  $G_A$  and one further constant, the so-called  $D/F$  ratio which enters because of  $SU(3)$  complications. [See Appendix 3; a more detailed treatment may be found in Lichtenberg (1978).]

The simplest way to implement the physical content of the above description of the weak interactions is to write the hadronic part of the current in terms of the fields of an  $SU(3)$  triplet of hypothetical *quarks*  $u$  ('up'),  $d$  ('down') and  $s$  ('strange'), which in the limit of exact  $SU(3)$  symmetry would all have the same mass. The quarks have rather peculiar properties. In particular, as can be seen in Table 1.1, their charges (in units of  $e$ ) and baryon numbers are fractional. No quark has even been seen experimentally despite many vigorous searches. There have been occasional claims for the discovery of a quark but none is really convincing. It is best therefore to think of the quarks as internal constituents of the hadrons, perhaps permanently bound therein, and much simplification follows from this. In fact the extension of these ideas to ‘hard’ processes, i.e. reactions at high energy *and* high momentum transfer, has led to

Charge $Q$	Strangeness $S$	Isospin $I$	$I_3$	Baryon number $B$	Hypercharge $Y = B + S$
$u$	$\frac{2}{3}$	0	$\frac{1}{2}$	$\frac{1}{2}$	$\frac{1}{3}$
$d$	$-\frac{1}{3}$	0	$\frac{1}{2}$	$-\frac{1}{2}$	$\frac{1}{3}$
$s$	$-\frac{1}{3}$	-1	0	0	$-\frac{2}{3}$

Table 1.1. Properties of quarks.

the very fruitful ‘quark–parton’ model that we shall examine at length in Chapters 15–17.

Note that the  $u$  and  $d$  quarks form an isospin doublet, and that  $s$  is an isosinglet.

If

$$q = \begin{pmatrix} u \\ d \\ s \end{pmatrix}$$

represents the triplet of quarks, then the octet of  $SU(3)$  currents can be written as

$$\left. \begin{aligned} V_j^\alpha(x) &= \bar{q}(x)\gamma^\alpha\left(\frac{\lambda_j}{2}\right)q(x), \\ A_j^\alpha(x) &= -\bar{q}(x)\gamma^\alpha\gamma_5\left(\frac{\lambda_j}{2}\right)q(x), \end{aligned} \right\} \quad (1.2.21)$$

the  $3 \times 3$  Hermitian, Gell-Mann matrices  $\lambda_j$  being the  $SU(3)$  analogues of the Pauli matrices, satisfying (see Appendix 2.6)

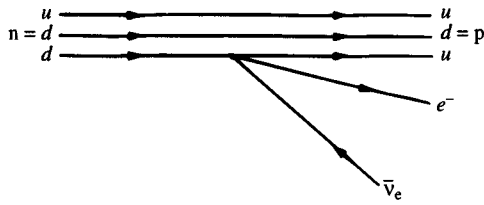
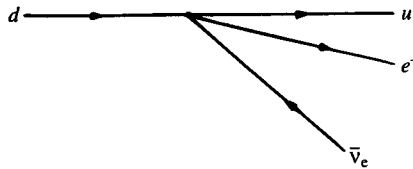
$$\left[ \frac{\lambda_j}{2}, \frac{\lambda_k}{2} \right] = i f^{jkl} \frac{\lambda_l}{2}. \quad (1.2.22)$$

(The above ignores the fact that each quark actually comes in three colours; the currents should be defined as a sum over the colours  $a$  of  $\bar{q}_a q_a$ .) Spelled out in detail, the hadronic current reduces to just

$$h^\alpha = \bar{u}\gamma^\alpha(1 - \gamma_5)(\cos\theta_C d + \sin\theta_C s). \quad (1.2.23)$$

In the quark picture the weak interaction processes of hadrons are regarded as originating in the interaction of their constituent quarks. Thus neutron  $\beta$ -decay is visualized as in Fig. 1.4 where the fundamental interaction is, at quark level, as in Fig. 1.5 and the amplitude for this is controlled by the weak current of the quarks, given in (1.2.23), and of the leptons.

Later, when we come to discuss intermediate vector mesons or gauge bosons which mediate the weak interactions, the picture will be altered to that in Fig. 1.6. It will often be convenient to visualize weak interaction

Fig. 1.4. Quark picture of neutron  $\beta$ -decay.Fig. 1.5. Quark level interaction responsible for  $\beta$ -decay in Cabibbo theory.

processes involving hadrons in these quark pictures, but it is best to think of them for the moment as a mnemonic for keeping track of quantum numbers and of the relative strengths of various reactions. They cannot be imbued with a really satisfactory dynamical content, though much progress has been made in trying to do so.

Notice that in Cabibbo theory it is only the combination

$$d_C \equiv \cos \theta_C d + \sin \theta_C s \quad (1.2.24)$$

that enters into the weak interactions. There appears then to be a formal similarity, a ‘universality’ between the doublets  $(\frac{\nu_e}{e^-}, \frac{\nu_\mu}{\mu^-})$ ,  $(\frac{u}{d_C})$  as regards the weak interactions. They are referred to as *weak-isospin* doublets. (Of course weak-isospin has nothing to do with the usual isospin. Indeed  $d_C$  does not even have a definite isospin, and leptons have zero isospin. It is, alas, an example of not unusual shoddy nomenclature in particle physics.) This formal similarity will play a very important rôle in the gauge theory formulation of the weak interactions.

The agreement between the predictions of Cabibbo theory and the data is generally very good for weak decays and for low energy scattering processes. A very detailed analysis of the situation can be found in Bailin (1982). Here we shall simply list some of the more spectacular successes of the theory.

1. The energy spectrum of the electron in

$$\mu^- \rightarrow e^- + \bar{\nu}_e + \nu_\mu$$

is in excellent agreement with predictions. The electron is predicted to be almost 100% polarized with helicity  $-\frac{1}{2}$ , i.e. it should be ‘left-handed’ as is found experimentally. The related reaction

$$\nu_\mu e^- \rightarrow \nu_e \mu^-$$

has also been studied (Section 4.4.3).

2. The rates for the pion decay reactions

$$\begin{aligned}\pi^- &\rightarrow e^- + \bar{\nu}_e \\ \pi^- &\rightarrow \mu^- + \bar{\nu}_\mu\end{aligned}$$

theoretically are in the ratio

$$\frac{\Gamma(\pi^- \rightarrow e^- \bar{\nu}_e)}{\Gamma(\pi^- \rightarrow \mu^- \bar{\nu}_\mu)} \propto \left(\frac{m_e}{m_\mu}\right)^2$$

as a result of the  $\gamma^\alpha(1 - \gamma_5)$  coupling. Explicit calculation yields a ratio of  $1.3 \times 10^{-4}$  which agrees perfectly with the experimental ratio—and this despite the fact that phase space alone would have favoured the mode  $\pi^- \rightarrow e^- + \bar{\nu}_e$ !

3. A beautiful test of CVC, i.e. of the relation between the weak and electromagnetic currents, is its prediction of ‘weak magnetism’, the analogue for weak transitions of electromagnetic transitions due to the anomalous magnetic moments. An excellent test was suggested by Gell-Mann (1958). The ground states of  $^{12}\text{B}$  and  $^{12}\text{N}$  and an excited state  $^{12}\text{C}^*$  of  $^{12}\text{C}$  are known to form an isotriplet with  $J^P = 1^+$  all of which decay to the ground state of  $^{12}\text{C}$  ( $J^P = 0^+$ ) (see Fig. 1.7). The decay  $^{12}\text{C}^* \rightarrow {}^{12}\text{C} + \gamma$  is of course electromagnetic and the weak decays are Gamow–Teller transitions. CVC predicts that the weak magnetism term will alter the energy spectrum of the  $e^-$  and  $e^+$ , and moreover that one can calculate the  $e^-$  and  $e^+$  spectra for the  $^{12}\text{B}$  and  $^{12}\text{N}$  decays directly in terms of the measured matrix element for the electromagnetic decay *without recourse to a nuclear model*. The results are in very good agreement with the data.
4. An even more dramatic prediction of CVC is simply that the  $\pi$  should undergo  $\beta$ -decay. Indeed the reaction

$$\pi^- \rightarrow \pi^0 + e^- + \bar{\nu}_e$$

is observed and its rate is in good agreement with the theory.

5. For strangeness-changing semileptonic processes  $h^\alpha(x)$  only allows  $\Delta S = +\Delta Q$  and  $|\Delta S| \leq 1$ . This is supported by the absence of the

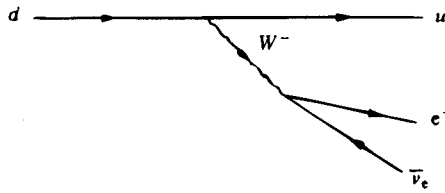


Fig. 1.6. Modern electroweak theory version of Fig. 1.5.

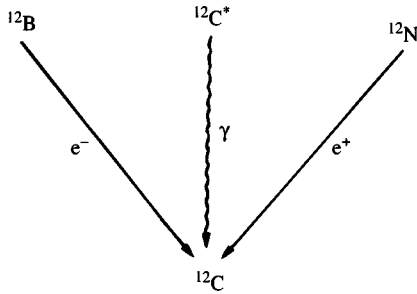


Fig. 1.7. Transitions involved in Gell-Mann's test of CVC.

following processes

$$\begin{aligned} \Xi^- &\not\rightarrow n + e^- + \bar{\nu}_e, & |\Delta S| &= 2, \\ K^+ &\not\rightarrow \pi^+ + \pi^+ + e^- + \nu_e, & \Delta S &= -\Delta Q = -1, \\ \Sigma^+ &\not\rightarrow n + e^+ + \nu_e, & \Delta S &= -\Delta Q = 1, \end{aligned}$$

whereas, for example, the following reactions are seen to occur

$$\begin{aligned} \Lambda &\rightarrow p + e^- + \bar{\nu}_e, & \Delta S &= \Delta Q = 1, \\ \Lambda &\rightarrow p + \mu^- + \bar{\nu}_\mu, & \Delta S &= \Delta Q = 1, \\ \Sigma^- &\rightarrow n + e^- + \bar{\nu}_e, & \Delta S &= \Delta Q = 1. \end{aligned}$$

For an excellent discussion of the physics of weak interactions see Wu and Moskowsky (1966). For a modern theoretical treatment and a critical analysis of the status of the theory see Bailin (1982).

### 1.3 The spin and isospin structure

We shall here derive some very useful technical properties of the structure of the classical weak interaction Lagrangian. These results will be utilized constantly in the following chapters.

### 1.3.1 The spin or helicity structure

When a Dirac particle is moving fast enough so that its energy  $E \gg m$  it can be shown that its spinor becomes an eigenstate of  $\gamma_5$  (see, for example, Section 7.10 of Bjorken and Drell, 1964). If  $u$  and  $v$  are spinors for particles and antiparticles respectively, and if we denote by R (right-handed) states with helicity  $+\frac{1}{2}$  and by L (left-handed) states with helicity  $-\frac{1}{2}$ , then one has

$$\begin{aligned} \gamma_5 u_R &= u_R, & \gamma_5 u_L &= -u_L, \\ \text{and } \gamma_5 v_R &= -v_R, & \gamma_5 v_L &= v_L \quad (E \gg m). \end{aligned} \quad (1.3.1)$$

These results are only true to the extent that  $E \gg m$ . For massless neutrinos they are, of course, exactly true.

It now follows that

$$\left( \frac{1 - \gamma_5}{2} \right) u_R = 0, \quad \left( \frac{1 - \gamma_5}{2} \right) u_L = u_L, \quad (1.3.2)$$

and thus we see that  $l^\alpha(x)$  in (1.2.4) only involves left-handed neutrinos.

To the extent that we can ignore the masses of the quarks, (1.2.23) tells us that only left-handed quarks participate in  $h^\alpha(x)$ .

Now the Hermitian conjugate of (1.3.2) when multiplied by  $\gamma^0$  yields

$$\bar{u}_R \left( \frac{1 + \gamma_5}{2} \right) = 0, \quad \bar{u}_L \left( \frac{1 + \gamma_5}{2} \right) = \bar{u}_L. \quad (1.3.3)$$

Then using the fact that

$$\left( \frac{1 - \gamma_5}{2} \right)^2 = \left( \frac{1 - \gamma_5}{2} \right)$$

we can write the typical term in the weak currents as

$$\begin{aligned} \bar{u}_A \gamma^\alpha (1 - \gamma_5) u_B &= 2\bar{u}_A \gamma^\alpha \left( \frac{1 - \gamma_5}{2} \right) u_B = 2\bar{u}_A \gamma^\alpha \left( \frac{1 - \gamma_5}{2} \right)^2 u_B \\ &= 2\bar{u}_A \left( \frac{1 + \gamma_5}{2} \right) \gamma^\alpha \left( \frac{1 - \gamma_5}{2} \right) u_B, \end{aligned} \quad (1.3.4)$$

which shows from (1.3.3) that in fact only the left-handed parts of all the particles actually play a rôle in the weak currents.

Note, incidentally, that we can *always* write

$$\begin{aligned} u &= \left( \frac{1 + \gamma_5}{2} \right) u + \left( \frac{1 - \gamma_5}{2} \right) u \\ &= u_R + u_L, \end{aligned} \quad (1.3.5)$$

but only when  $E \gg m$  does  $u_{R/L}$  really correspond to helicity  $\pm\frac{1}{2}$ .

Very similar manipulations give the following important results, all valid to the extent that  $E \gg m$ ; for spin  $\frac{1}{2}$  particles A, B:

## 1. In a scattering process

$$A + \dots \rightarrow B + \dots$$

if the particles A and B having helicities  $\lambda_A, \lambda_B$  come from the same vertex and if the coupling is vector or axial-vector, or some combination of both, then the helicity is preserved in the interaction, i.e.

$$\bar{u}_{\lambda_B} \gamma^\alpha (G_V - G_A \gamma_5) u_{\lambda_A} \propto \delta_{\lambda_B \lambda_A}. \quad (1.3.6)$$

## 2. In an annihilation process or in a creation process

$$A + \bar{B} \rightarrow \dots \quad \text{or} \quad \dots \rightarrow A + \bar{B}$$

if A and  $\bar{B}$  come from the same vertex which is some combination of vector and axial-vector coupling, then the reaction only proceeds if A and  $\bar{B}$  have *opposite* helicities, i.e.

$$\left. \begin{aligned} \bar{v}_{\lambda_B} \gamma^\alpha (G_V - G_A \gamma_5) u_{\lambda_A} &\propto \delta_{\lambda_B, -\lambda_A}, \\ \text{and} \quad \bar{u}_{\lambda_A} \gamma^\alpha (G_V - G_A \gamma_5) v_{\lambda_B} &\propto \delta_{\lambda_B, -\lambda_A}. \end{aligned} \right\} \quad (1.3.7)$$

## 1.3.2 Relation between particle and antiparticle matrix elements

Because the antiparticle spinors  $v$  are related to the particle spinors  $u$  by

$$\left. \begin{aligned} v &= i\gamma^2 u^*, \\ \bar{v} &= -iu^T \gamma^0 \gamma^2, \end{aligned} \right\} \quad (1.3.8)$$

we can relate the matrix element which occurs in the process

$$A(\mathbf{p}) + \dots \rightarrow B(\mathbf{p}') + \dots \quad (1)$$

to that which occurs in

$$\bar{A}(\mathbf{p}) + \dots \rightarrow \bar{B}(\mathbf{p}') + \dots \quad (2)$$

when A and B come from the same vertex. For (1) the AB vertex will involve calculating

$$\Gamma_{A \rightarrow B}(\mathbf{p}, \mathbf{p}') \equiv \bar{u}_B(\mathbf{p}') \gamma^\alpha (G_V - G_A \gamma_5) u_A(\mathbf{p}) \quad (1.3.9)$$

whereas for (2) one will need to evaluate

$$\Gamma_{\bar{A} \rightarrow \bar{B}}(\mathbf{p}, \mathbf{p}') \equiv \bar{v}_A(\mathbf{p}) \gamma^\alpha (G_V - G_A \gamma_5) v_B(\mathbf{p}'). \quad (1.3.10)$$

We then have from (1.3.8)

$$\Gamma_{\bar{A} \rightarrow \bar{B}}(\mathbf{p}, \mathbf{p}') = u_A^T(\mathbf{p}) \gamma^0 \gamma^2 \gamma^\alpha (G_V - G_A \gamma_5) \gamma^2 u_B^*(\mathbf{p}').$$

But this is a number, not a matrix, and hence equal to its transpose. Thus we can write

$$\Gamma_{\bar{A} \rightarrow \bar{B}}(\mathbf{p}, \mathbf{p}') = \bar{u}_B(\mathbf{p}') \gamma^0 \gamma^{2T} (G_V - G_A \gamma_5^T) \gamma^{\alpha T} \gamma^{2T} \gamma^{0T} u_A(\mathbf{p}).$$

Now  $\gamma_5^T = \gamma_5, \gamma^{0T} = \gamma^0, \gamma^{2T} = \gamma^2$ . Moreover  $(\gamma^0 \gamma^2) \gamma^{\alpha T} (\gamma^2 \gamma^0) = \gamma^\alpha$  for all  $\alpha$ . So finally

$$\Gamma_{\bar{A} \rightarrow \bar{B}}(\mathbf{p}, \mathbf{p}') = \bar{u}_B(\mathbf{p}') \gamma^\alpha (G_V + G_A \gamma_5) u_A(\mathbf{p}) \quad (1.3.11)$$

Comparing (1.3.11) with (1.3.9) we see that  $\Gamma_{\bar{A} \rightarrow \bar{B}}(\mathbf{p}, \mathbf{p}')$  is obtained from  $\Gamma_{A \rightarrow B}(\mathbf{p}, \mathbf{p}')$  simply by changing the sign of the axial-vector coupling. Since we inevitably deal with the modulus squared of matrix elements, this implies simply changing the sign of the vector–axial–vector interference term in the expression for physical observables.

This result will be useful, for example, in relating processes like

$$\begin{aligned} \nu_e + n &\rightarrow e^- + p \\ \bar{\nu}_e + p &\rightarrow e^+ + n. \end{aligned}$$

### 1.3.3 The isospin structure

The spin structure is irrelevant here, so let us simply denote by  $J_j$  a set of three Hermitian currents ( $j = 1, 2, 3$ ) which transform like an isospin triplet under isotopic spin rotations. Thus from (1.2.18), since for  $SU(2)$  the  $f^{jkl}$  are just the antisymmetric  $\epsilon_{jkl}$ , we have

$$[J_j, J_k] = i\epsilon_{jkl} J_l. \quad (1.3.12)$$

Use of (1.3.12) allows us to relate the matrix elements for transition between different members of an isospin multiplet. A similar approach works for  $SU(3)$ .

We shall illustrate the general idea by an example. Let

$$J_+ = J_1 + iJ_2 \quad (1.3.13)$$

be the charge-raising current. It will have non-zero matrix elements between states of isospin  $I$ , and third component  $I_3$  as follows:

$$M_+ = \langle I, I_3 + 1 | J_+ | I, I_3 \rangle. \quad (1.3.14)$$

Now consider the commutator of  $J_3$  with the isotopic spin ‘raising’ operator  $T_+ = T_1 + iT_2$  which, in the Condon–Shortley phase convention (Condon and Shortley, 1963) has the following effect:

$$T_+ |I, I_3\rangle = \sqrt{(I - I_3)(I + I_3 + 1)} |I, I_3 + 1\rangle. \quad (1.3.15)$$

From (1.3.12)

$$[J_3, T_+] = [J_3, T_1 + iT_2] = J_+. \quad (1.3.16)$$

Replacing  $J_+$  in (1.3.14) by the commutator gives

$$\begin{aligned} M_+ &= \langle I, I_3 + 1 | J_3 T_+ - T_+ J_3 | I, I_3 \rangle \\ &= \sqrt{(I - I_3)(I + I_3 + 1)} \{ \langle I, I_3 + 1 | J_3 | I, I_3 + 1 \rangle - \langle I, I_3 | J_3 | I, I_3 \rangle \}, \end{aligned} \quad (1.3.17)$$

where we have used

$$\langle I, I_3 + 1 | T_+ J_3 | I, I_3 \rangle = \langle I, I_3 | J_3 T_+^\dagger | I, I_3 + 1 \rangle^*$$

and  $T_+^\dagger = T_-$  and

$$T_- |I, I_3\rangle = \sqrt{(I + I_3)(I - I_3 + 1)} |I, I_3 - 1\rangle.$$

Eqn (1.3.17) thus relates matrix elements  $J_+$  to those of  $J_3$ .

An immediate application connects part of the neutron  $\beta$ -decay matrix element to the electromagnetic form factors of protons and neutrons. Taking for  $J_+$  the vector part of the hadronic weak current and using (1.2.11), (1.3.17) yields

$$\langle p | V^\alpha | n \rangle = \langle p | J_{\text{em}}^\alpha | p \rangle - \langle n | J_{\text{em}}^\alpha | n \rangle. \quad (1.3.18)$$

This relation, and many similar ones, are basically just applications of the Wigner–Eckart theorem (see, for example, Merzbacher, 1962), and can be obtained directly from it.

Further useful relations follow from making a rotation of  $\pi$  about the ‘l’ axis in isospace. This has the effect of making  $J_2 \rightarrow -J_2$  and  $J_3 \rightarrow -J_3$ . In particular therefore

$$J_+ \leftrightarrow J_-. \quad (1.3.19)$$

As an example, consider the matrix element  $M_+$  defined in (1.3.14) and let  $r_1$  be the operator causing the rotation of  $\pi$  about the ‘l’ axis in isospace, and which satisfies  $r_1^\dagger r_1 = I$ , i.e.  $r_1^\dagger = r_1^{-1}$ . Then

$$\begin{aligned} M_+ &= \langle I, I_3 + 1 | r_1^{-1} r_1 J_+ r_1^{-1} r_1 | I, I_3 \rangle \\ &= \langle I, I_3 + 1 | r_1^\dagger J_- r_1 | I, I_3 \rangle \\ &= \langle I, -(I_3 + 1) | J_- | I, -I_3 \rangle, \end{aligned} \quad (1.3.20)$$

where we have used

$$r_1 |I, I_3\rangle = e^{-i\pi I} |I, -I_3\rangle. \quad (1.3.21)$$

Thus we are able to relate matrix elements of  $J_+$  and  $J_-$  to each other.

If it happens that the current operators are Hermitian, i.e.  $J_i^\dagger = J_i$ , then we can also relate matrix elements of  $J_+$  and  $J_-$  via, for example,

$$\begin{aligned} M_+^* &= \langle I, I_3 + 1 | J_+ | I, I_3 \rangle^* \\ &= \langle I, I_3 | J_+^\dagger | I, I_3 + 1 \rangle \\ &= \langle I, I_3 | J_- | I, I_3 + 1 \rangle, \end{aligned} \quad (1.3.22)$$

but this property has nothing to do with the isospin structure of the currents.

### 1.4 Tests of the $V-A$ structure and ‘lepton universality’

Because of the powerful and beautiful unification of the weak and electromagnetic interactions to be discussed in the next few sections, it is largely taken for granted that the coupling involved in the weak currents is a mixture of vector and axial-vector. But it is important to try to verify this empirically with as few theoretical assumptions as possible. A very impressive experimental programme has been devoted to this question, particularly the validity of eqn (1.2.4), at SIN near Zurich for the past few years (see Fettscher, Gerber and Johnson, 1986). The most general Hamiltonian, consistent with deep theorems in field theory and allowing for parity violation, can be shown to be of the following form, involving ten independent complex coupling constants  $C_i, C'_i$  ( $i = 1, \dots, 5$ ):

$$H = \sum_i \left\{ C_i (\bar{\psi}_e \Gamma_i \psi_\mu) (\bar{\psi}_{\nu_\mu} \Gamma^i \psi_{\nu_e}) + C'_i (\bar{\psi}_e \Gamma_i \psi_\mu) (\bar{\psi}_{\nu_\mu} \Gamma^i \gamma_5 \psi_{\nu_e}) \right\} + \text{h.c.} \quad (1.4.1)$$

where the  $\Gamma^i$  are the five sets of Dirac matrix combinations discussed in Appendix 2.7: scalar I, vector  $\gamma^\mu$ , tensor  $\sigma^{\mu\nu}$ , axial-vector  $\gamma^\mu \gamma_5$ , pseudo-scalar  $\gamma_5$ . The lowest order matrix element for  $\mu^- \rightarrow e^- + \bar{\nu}_e + \nu_\mu$  can be rewritten, using the right- and left-handed spinors defined in (1.3.5) and the Fierz reshuffle theorem (see Appendix 2.7) in the form:

$$M \sim \sum_{\substack{i = S, V, T \\ \lambda' = \pm \lambda \text{ for } S, V \\ \lambda' = -\lambda \text{ for } T}} g_{\lambda' \lambda}^i (\bar{u}_{\lambda'}(e) \Gamma^i v_{\lambda'_i}(\nu_e)) (\bar{u}_{\lambda_i}(\nu_\mu) \Gamma_i u_\lambda(\mu)) \quad (1.4.2)$$

where  $\lambda, \lambda' = \pm 1$  correspond to R/L, and  $\lambda_i = \lambda$  for  $i = V$ ,  $\lambda_i = -\lambda$  for  $i = S, T$ , and  $\lambda'_i = -\lambda'$  for  $i = V$ ,  $\lambda'_i = \lambda'$  for  $i = S, T$  and the ten  $g_{\lambda' \lambda}^i$  are linear combinations of  $C_i, C'_i$ .

In a series of beautiful measurements of all sorts of spin correlations and distributions the SIN group have done a remarkable job of pinning down the values of the  $g_{\lambda' \lambda}^i$ . In a strictly  $V - A$  theory one expects

$$g_{LL}^V = 1; \text{ all other } g_{\lambda' \lambda}^i = 0. \quad (1.4.3)$$

The experimental limits (at the 90% confidence level) on the coupling constants are shown in Fig. 1.8. Note in particular the coupling  $g_{RR}^V$  which would correspond to a  $V + A$  interaction.

Later we shall encounter a third lepton, the  $\tau$ , discovered only in 1975. Its properties are discussed in detail in Chapter 14, but we note here that it is supposed to interact in exactly the same fashion as do the  $\mu$  and  $e$ . It can beta-decay into either a muon or an electron and a comparison of

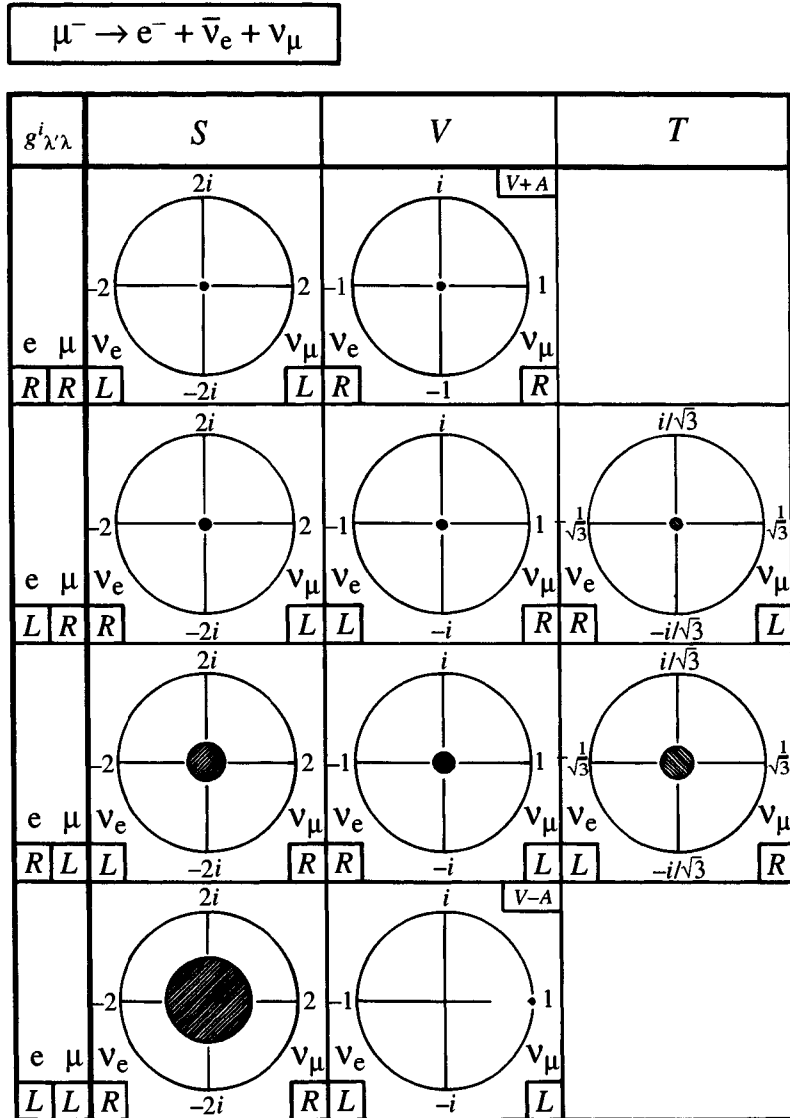


Fig. 1.8. 90% confidence level limits on the coupling constants  $g_{\lambda' \lambda}^i$  from the SIN experiments.

the rates (Gerber, 1987) yields

$$\frac{G_{\tau_\mu}}{G_{\tau_e}} = 1.00 \pm 0.02 \quad (1.4.4)$$

for the Fermi coupling constants involved. Thus the  $\tau$  couples to muons and electrons with the same strength. If, in addition, one uses the mea-

sured value of the  $\tau$  lifetime one obtains

$$\frac{G_{\tau_e}}{G_{\mu_e}} = 0.97 \pm 0.02 \quad (1.4.5)$$

showing that the  $\tau e$  coupling is essentially the same as the  $\mu e$  coupling. Thus there is good evidence for regarding  $e, \mu, \tau$  as interacting in a ‘universal’ fashion.

The evidence that the  $\tau$  coupling is of the  $V-A$  type is by now fairly conclusive (see Chapter 14). The shape of the energy spectrum of the emitted lepton in beta-decay contains a parameter  $\rho^M$  known as the ‘Michel parameter’, which is sensitive to the spin structure of the coupling (see Chapter 3 of Bailin, 1982). For example one has:

$$\rho^M = \frac{3}{4} \text{ for } V - A; \quad 0 \text{ for } V + A; \quad \frac{3}{8} \text{ for pure } V \text{ or } A. \quad (1.4.6)$$

The most recent data (see Section 14.4) yield

$$\rho_\tau^M = 0.734 \pm 0.055 \pm 0.026 \quad (1.4.7)$$

in good agreement with a  $V - A$  structure. One awaits with interest further experimental results. We shall generally assume that universality holds and that  $\tau, \mu, e$  behave identically in their weak interactions. Further tests will be discussed in later chapters.

# 2

## The need for a gauge theory

In this chapter we examine some of the problems inherent in the current-current form of the weak interaction Lagrangian, and are led to the idea of the weak force being mediated by the exchange of vector mesons. This picture too runs into difficulties which, however, can be alleviated in gauge-invariant theories. The latter are introduced and discussed at some length.

### 2.1 The intermediate vector boson

The trouble with (1.2.1) is that it cannot be correct, at least in the high energy domain. If, for instance, one evaluates the cross-section for the elastic reaction

$$\nu_e + e \rightarrow \nu_e + e$$

one immediately discovers (just by dimensional reasoning if one ignores the electron mass at high energies) that in lowest order  $\sigma$  grows with CM (centre of mass) momentum like  $G^2 k^2$ . More exactly, one finds in the CM

$$\frac{d\sigma}{d\Omega} = \frac{G^2 k^2}{\pi^2} \quad (2.1.1)$$

and

$$\sigma = \frac{4G^2 k^2}{\pi} \quad \text{for } k^2 \gg m_e^2. \quad (2.1.2)$$

Since the interaction is ‘point-like’ the scattering goes entirely via the s-wave, and partial wave unitarity then requires that

$$\sigma < \frac{\pi}{2k^2}. \quad (2.1.3)$$

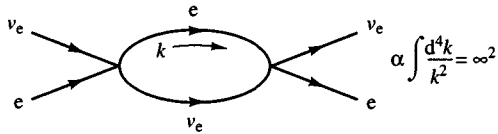


Fig. 2.1. Higher order graph which diverges.

Therefore above a certain energy,

$$k^4 \approx \frac{\pi^2}{8G^2}, \quad (2.1.4)$$

that is,

$$k \approx 300 \text{ GeV}/c,$$

the interaction (1.2.1) will violate unitarity.

Even worse, if one blames this on the lowest order approximation used and tries to evaluate higher order corrections, one immediately finds horrible divergences. Thus to order  $G^2$ , for the amplitude in Fig. 2.1, these divergences, unlike QED, cannot be eliminated by proper renormalization. To make the various matrix elements finite new arbitrary constants would have to be introduced in each order—the Fermi theory of weak interactions is non-renormalizable.

The first attempt to cure this disease is based upon the only working theory of elementary particles that we know of—QED. Just as the electromagnetic interactions are mediated by the exchange of photons, one postulates that the weak interactions too are mediated by a vector boson. But whereas the long range of the electromagnetic force comes from the *massless* photon, the short range weak interactions will require a rather heavy boson. We therefore replace (1.2.1) by a new weak Lagrangian

$$\mathcal{L}_W = -g_W J^\alpha(x) W_\alpha(x) + \text{h.c.}, \quad (2.1.5)$$

where  $W_\alpha(x)$  is the field of the vector boson which is to be the analogue of the photon field  $A_\alpha(x)$ , and h.c. is short for ‘Hermitian conjugate’. The coupling constant  $g_W$  is dimensionless.

Historically (see, for example, Lee and Wu, 1965) the vector boson was given the following properties:

1. two charge states ( $\pm$ ) since the familiar  $\beta$ -decay reactions require charge-changing currents;
2. a large mass to reproduce the almost point-like structure of weak interactions;
3. indefinite parity to allow for the  $V - A$  structure.

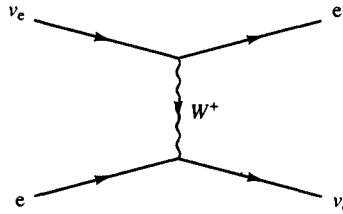


Fig. 2.2. Lowest order graph for  $\nu_e e \rightarrow \nu_e e$  with vector boson exchange.

The lowest order diagram for the reaction  $\nu_e + e \rightarrow \nu_e + e$  is shown in Fig. 2.2 which leads in the CM to

$$\frac{d\sigma}{d\Omega} = \frac{2g_W^4 k^2}{\pi^2 (q^2 - M_W^2)^2} \quad (k^2 \gg m_e^2) \quad (2.1.6)$$

where  $M_W$  is the mass of the  $W$  boson and  $q$  is the momentum transfer vector;

$$q^2 \simeq -2k^2(1 - \cos\theta). \quad (2.1.7)$$

Eqn (2.1.6) reduces to the Fermi result (2.1.1) as  $q^2 \rightarrow 0$  provided

$$\frac{g_W^2}{M_W^2} = \frac{G}{\sqrt{2}}. \quad (2.1.8)$$

However, the interaction is no longer point-like. The  $W$  exchange implies an interaction region of dimensions  $1/M_W$  and the angular dependence shows that more than just s-waves are participating.

The cross-section formula (2.1.2) is now replaced by

$$\sigma = \frac{4G^2 k^2}{\pi} \left(1 + \frac{4k^2}{M_W^2}\right)^{-1} \quad (2.1.9)$$

so that

$$\lim_{k \rightarrow \infty} \sigma = \frac{G^2 M_W^2}{\pi} = \text{constant}. \quad (2.1.10)$$

Despite this improved high energy behaviour, partial wave unitarity is still violated, albeit marginally. The s-wave amplitude is

$$a_0 = \frac{GM_W^2}{\sqrt{2}\pi} \log \left(1 + \frac{4k^2}{M_W^2}\right) \quad (2.1.11)$$

so that unitarity violation,  $a_0 > 1$ , occurs only at fantastically high ener-

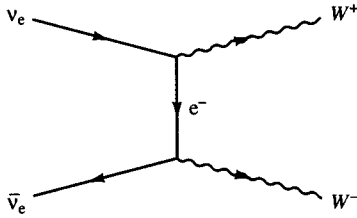


Fig. 2.3. Feynman diagram for  $\nu_e \bar{\nu}_e \rightarrow W^+ W^-$ .

gies for any reasonable mass  $M_W$ , i.e at

$$\begin{aligned} k &\simeq \frac{M_W}{2} \exp\left(\frac{\pi}{\sqrt{2G} M_W^2}\right) \\ &\simeq \frac{M_W}{2} \exp\left(\frac{\pi m_p^2}{2M_W^2} \times 10^5\right). \end{aligned} \quad (2.1.12)$$

This may not seem a serious problem but there are additional troubles arising from the existence of longitudinal states of polarization of the massive  $W$  in processes like that shown in Fig. 2.3 which, though the reaction is inconceivable in a practical experiment, ought to give a sensible result.

In the rest frame of the  $W$  its states of polarization are described by the vectors  $\epsilon_x = (0100)$  or  $\epsilon_y = (0010)$  which are the transverse states ( $\epsilon_T$ ), and  $\epsilon_z = (0001)$  which is longitudinal ( $\epsilon_L$ ). Applying a boost along the  $Z$ -axis, so that  $W$  has momentum  $k^\mu = (k^0, 0, 0, k)$ , these become

$$\begin{aligned} \epsilon_T(k) &= \epsilon_T(0), \\ \epsilon_L(k) &= \left(\frac{|k|}{M_W}, 0, 0, \frac{k^0}{M_W}\right) = \frac{k^\mu}{M_W} + 0\left(\frac{M_W}{k^0}\right). \end{aligned} \quad (2.1.13)$$

The above diagram then yields for the  $WW$  production cross-sections

$$\left. \begin{aligned} \sigma(\nu\bar{\nu} \rightarrow W_T^+ W_T^-) &\xrightarrow{k^2 \rightarrow \infty} \text{constant,} \\ \text{but } \sigma(\nu\bar{\nu} \rightarrow W_L^+ W_L^-) &\xrightarrow{k^2 \rightarrow \infty} (g_W/M_W)^4 k^2, \end{aligned} \right\} \quad (2.1.14)$$

which shows that unitarity is badly violated in the reaction  $\nu\bar{\nu} \rightarrow W^+ W^-$  when the  $Ws$  are produced in a state of longitudinal polarization.

An equivalent symptom shows up in the  $W$  propagator:

$$\frac{\sum_{\text{polarizations}} \epsilon_\mu^* \epsilon_\nu}{k^2 - M_W^2} = \frac{-g_{\mu\nu} + k_\mu k_\nu / M_W^2}{k^2 - M_W^2}, \quad (2.1.15)$$

which tends to a constant as  $k \rightarrow \infty$ , and will thus cause the divergence of integrals over closed loops in Feynman diagrams.

One may well wonder why longitudinal polarization states did not cause similar trouble in the case of virtual photons in QED. The reason is that gauge invariance, which implies that  $S$ -matrix elements are invariant under the replacement

$$\epsilon_\mu \rightarrow \epsilon_\mu + \Lambda k_\mu \quad (2.1.16)$$

for *any*  $\Lambda$ , ensures that the terms in  $\epsilon_\mu$  proportional to  $k_\mu$  [see (2.1.13)] are innocuous.

This suggests that it would be very interesting to extend gauge invariance to the present case of massive vector fields, perhaps resulting in a unification between weak and electromagnetic interactions. Note that we would then expect  $g_W \sim e$ . Use of this in (2.1.8) suggests that

$$M_W = \left( \frac{\sqrt{2}g_W^2}{G} \right)^{\frac{1}{2}} \sim \left( \frac{\sqrt{2}e^2}{G} \right)^{\frac{1}{2}} \sim 106 \text{ GeV}/c^2, \quad (2.1.17)$$

a very large mass! We shall see later that this estimate is close to what is suggested in the unified theory of weak and electromagnetic interactions.

When these ideas were first developed, there was no hint, experimentally, of the actual existence of  $W$  bosons. The situation has changed dramatically in the last few years and  $W$ s and their neutral counterparts  $Z^0$ s are produced copiously at CERN, in Geneva, and at Fermilab, near Chicago, in  $e^+e^-$ ,  $\bar{p}p$  and  $p\bar{p}$  collisions.

## 2.2 Towards a renormalizable theory

We have seen that the introduction of vector bosons goes in the right direction but does not remove all the diseases of the current-current form of the weak Lagrangian. The vector boson Lagrangian generates a theory that is still not renormalizable.

Aside from the possibility of developing a phenomenology of weak interactions outside the scheme of perturbation theory, we must aim to construct a renormalizable model. In that case the badly behaved contribution to the reaction  $\nu\bar{\nu} \rightarrow W^+W^-$ , discussed in Section 2.1, must be cancelled by other contributions which must operate in the same perturbative order, i.e. in lowest order.

We can invent new contributions to the  $\nu\bar{\nu} \rightarrow W^+W^-$  reaction such as those shown in Fig. 2.4. Diagram (b) requires the existence of a *neutral* vector boson in addition to the charged ones  $W^\pm$ . (This introduces ‘neutral currents’ and, as will be shown later, is a natural consequence of non-Abelian gauge theories.) Diagrams (c) and (d) would require the

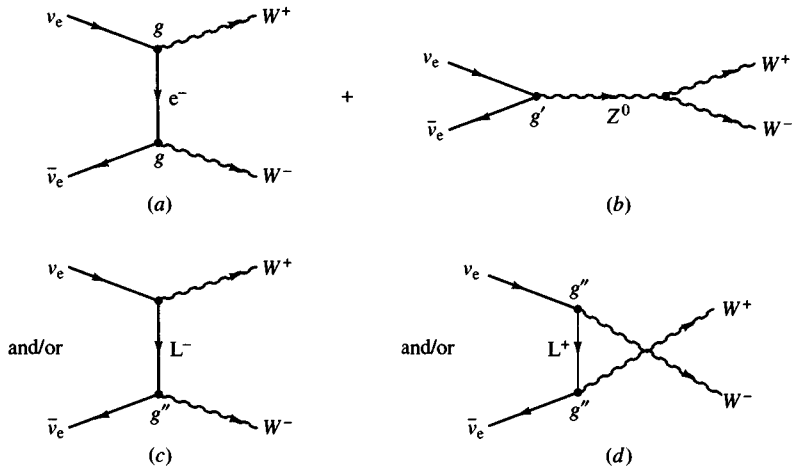


Fig. 2.4. Diagrams to cancel the bad behaviour of the graph in Fig. 2.3.

existence of new leptons which would need to be heavy to explain their non-discovery. Note that  $L^\pm$  cannot be a muon since we believe that lepton number is conserved. For the same reason it cannot be the newly discovered  $\tau$  lepton of mass  $\approx 1.8 \text{ GeV}/c^2$  (see Chapter 14) which could only communicate with its own neutrino  $\nu_\tau$ . However, heavy leptons can also occur quite naturally in a gauge theory. The couplings  $g, g', g''$  would have to be related to each other in a very specific way to ensure the sought-for cancellations.

In fact only (b) or (d) will work. Because of its similarity to (a), (c) will provide a term that *adds* to (a) and is thus no good for our purposes. For completeness we give a brief technical treatment which may be skipped without loss of continuity.

The badly behaved part of diagram (a) is obtained from

$$M(a) = g^2 \bar{v}(p_{\bar{\nu}}) \not{e}^-(1 - \gamma_5) \frac{1}{q - m_e} \not{e}^+(1 - \gamma_5) u(p_\nu).$$

Taking  $W^\pm$  both longitudinally polarized

$$\epsilon_\mu^+ \simeq \frac{k_\mu^+}{M_W}, \quad \epsilon_\mu^- \simeq \frac{k_\mu^-}{M_W},$$

neglecting  $m_e$  and using the Dirac equation, gives

$$M(a) \simeq \frac{-2g^2}{M_W^2} \bar{v}(p_{\bar{\nu}}) q(1 - \gamma_5) u(p_\nu).$$

To leading order, and if we neglect  $m_L$  compared with  $q^2$ , diagram (c) gives the same result with  $g^2$  replaced by  $(g'')^2$ . The two diagrams cannot cancel.

Diagram (d), on the other hand, yields

$$M(d) \simeq \frac{-2(g'')^2}{M_W^2} \bar{v}(p_{\bar{\nu}}) q'(1 - \gamma_5) u(p_{\nu}),$$

where  $q' = p_{\nu} - p_{\bar{\nu}} - q$ . Use of the Dirac equation gives

$$M(d) \simeq \frac{2(g'')^2}{M_W^2} \bar{v}(p_{\bar{\nu}}) q(1 - \gamma_5) u(p_{\nu}),$$

so that cancellation will occur if  $(g'')^2 = g^2$ .

A model based on this mode of cancellation has been developed by Georgi and Glashow (1972).

*The cancellation of the badly behaved part of diagram (a) forces the introduction of either neutral vector bosons or heavy leptons, or both.*

Note that most of the troubles that occur in other reactions, such as  $e^+e^- \rightarrow W^+W^-$  or  $\bar{\nu}_e e^- \rightarrow W^- \gamma$  can also be cured by the same sort of mechanism used above. These cancellation mechanisms are probably necessary but not sufficient for renormalizability.

To proceed further we must now study some of the essential features of gauge theories, wherein, it will be seen, this type of cancellation is automatic.

### 2.3 Gauge symmetry

As mentioned in Chapter 1, a basic object in field theory is the Lagrangian density  $\mathcal{L}$  which is a function of the fields  $\phi_j(x)$  and their gradients  $\partial_{\mu}\phi_j(x)$ :

$$\mathcal{L}(\mathbf{x}, t) = \mathcal{L}(\phi_j(x), \partial_{\mu}\phi_j(x)). \quad (2.3.1)$$

The space integral of  $\mathcal{L}$  is the Lagrangian  $L(t)$  and the four-dimensional integral over all time and space is the *action*  $S$ :

$$S = \int_{-\infty}^{\infty} L(t) dt = \int d^4x \mathcal{L}(\phi_j(x), \partial_{\mu}\phi_j(x)). \quad (2.3.2)$$

For the equations of motion to be covariant,  $\mathcal{L}$  must be a Lorentz scalar density. In this case the equations of motion, the Euler–Lagrange equations,

$$\frac{\delta\mathcal{L}}{\delta\phi_j} = \frac{\partial}{\partial x^{\mu}} \frac{\delta\mathcal{L}}{\delta(\partial_{\mu}\phi_j)}, \quad (2.3.3)$$

follow from Hamilton's variational principle

$$\delta \int_{t_1}^{t_2} L(t) dt = 0, \quad (2.3.4)$$

where  $t_1$  and  $t_2$  are arbitrary and the variations of the fields at  $t_1$  and  $t_2$  are chosen to be zero.

It is well known from classical mechanics that every continuous symmetry of the Lagrangian leads to a conservation law, and is associated with some quantity not being measurable. Thus the homogeneity of space, which implies that one cannot measure one's absolute position in space, is manifested by  $\mathcal{L}$  being translationally invariant, and this leads to the conservation of total linear momentum. Similar statements hold for energy and angular momentum conservation.

### 2.3.1 Global gauge invariance—the Abelian case

We now consider internal symmetries that do not involve space-time. Each such symmetry will be expressed by the fact that there exists a field transformation which leaves  $\mathcal{L}$  unaffected, and to each such symmetry there will correspond a conservation law and some quantity which is not measurable.

One such symmetry, which is associated with charge conservation, is *gauge invariance of the first kind* or *global gauge invariance*. The field transformation is a phase transformation

$$\phi_j(x) \rightarrow \phi'_j \equiv e^{-iq_j\theta} \phi_j(x), \quad (2.3.5)$$

where  $q_j$  is the charge in units of  $e$  ( $e$  is the *magnitude* of the electron's charge) and  $\theta$  is an arbitrary real number.

Now note that

- every term in  $\mathcal{L}$  is a product made up of fields  $\phi_1 \dots \phi_n$ , their Hermitian conjugates, and their gradients,
- since  $\theta$  is independent of  $x$ , the transformed gradients are multiples of the original gradients, i.e.

$$\partial_\mu \phi_j(x) \rightarrow e^{-iq_j\theta} \partial_\mu \phi_j(x), \quad (2.3.6)$$

- since charge is to be conserved every term in  $\mathcal{L}$  must be neutral. Thus every term involving a  $\phi$  must be multiplied by a term involving  $\phi^\dagger$ .

Clearly then  $\mathcal{L}$  is left invariant under (2.3.5). In other words  $\mathcal{L}$  does not depend on the phases of the  $\phi_j$ , which are therefore unmeasurable. If  $\theta$  is infinitesimal, then (2.3.5) becomes

$$\begin{aligned} \delta\phi_j(x) &\equiv \phi'_j(x) - \phi_j(x) \\ &= -i\theta q_j \phi_j(x). \end{aligned} \quad (2.3.7)$$

The global gauge invariance,  $\delta\mathcal{L} = 0$ , then implies

$$0 = \delta\mathcal{L} = \frac{\delta\mathcal{L}}{\delta\phi_j} \delta\phi_j + \frac{\delta\mathcal{L}}{\delta(\partial_\mu\phi_j)} \delta(\partial_\mu\phi_j),$$

which, using (2.3.7) and the equations of motion (2.3.3), yields

$$-\mathrm{i}\theta \frac{\partial}{\partial x^\mu} \left[ \frac{\delta \mathcal{L}}{\delta(\partial_\mu \phi_j)} q_j \phi_j \right] = 0. \quad (2.3.8)$$

If we define the current  $J^\mu$  associated with the gauge transformation by

$$J^\mu \equiv -\mathrm{i}q_j \frac{\delta \mathcal{L}}{\delta(\partial_\mu \phi_j)} \phi_j \quad (2.3.9)$$

then (2.3.8) shows that  $J^\mu$  is conserved, i.e.

$$\partial_\mu J^\mu = 0.$$

The fact that an invariance of  $\mathcal{L}$  leads to a conserved current is known as Noether's theorem and the currents are often called *Noether currents* (see, for example, Ramond, 1981).

The gauge transformations form a group. It is *Abelian*, i.e. different transformations of the group commute with each other, and it is *one-dimensional*, i.e. the transformations are specified by one parameter  $\theta$ . This group is  $U(1)$ , the group of unitary transformations in one dimension. We say that  $U(1)$  is a symmetry group of  $\mathcal{L}$ , and that the functions  $e^{-iq_j\theta}$  form a one-dimensional representation of  $U(1)$ .

The gauge group has a *charge operator*

$$\hat{Q} \equiv \int d^3x J_0(\mathbf{x}, t) \quad (2.3.10)$$

and one can show that the  $q_j$  are its eigenvalues. Moreover, the fact that  $J^\mu$  is conserved ensures that, despite appearances to the contrary,  $\hat{Q}$  does not depend on time.

Several generalizations of the above concepts are familiar in particle physics. The assumption that the proton and the neutron are two different states of the same particle, the *nucleon*, which transform into each other under isotopic spin rotations leads to invariance under the group  $SU(2)$  which is the simplest example of a *non-Abelian* group, i.e. one in which not all transformations commute with each other. In the 'eight-fold way' p, n,  $\Lambda$ ,  $\Sigma^+$ ,  $\Sigma^0$ ,  $\Sigma^-$ ,  $\Xi^0$ ,  $\Xi^-$  are all taken as states of a fundamental baryon and there results the symmetry  $SU(3)$ . When charm particles are included one has to deal with  $SU(4)$  etc.

### 2.3.2 Local gauge invariance—the Abelian case

In the case of global gauge invariance the phase  $\theta$  is not measurable and can be chosen arbitrarily, but once chosen it must be the same for all times everywhere in space. Could it happen that one can fix the phase locally and differently at different places? It turns out that in electrodynamics one can do this. It possesses a *local gauge symmetry* (or gauge

symmetry of the second kind) which is more powerful than the global invariance previously discussed. Now the transformations can depend upon the space-time point at which the field is acting.

Consider a transformation

$$\phi_j(x) \rightarrow \phi'_j(x) = e^{-iq_j\theta(x)}\phi_j(x), \quad (2.3.11)$$

where  $\theta(x)$  is an arbitrary function of  $x$ .

In infinitesimal form

$$\delta\phi_j(x) = -iq_j\theta(x)\phi_j(x). \quad (2.3.12)$$

Those terms of  $\mathcal{L}$  that contain only the fields and their Hermitian conjugates are invariant as before, but terms involving gradients must be handled with more care since, from (2.3.11), we have

$$\begin{aligned} \partial_\mu\phi_j(x) &\rightarrow \partial_\mu\phi'_j(x) \\ &= e^{-iq_j\theta(x)}\partial_\mu\phi_j(x) - iq_j[\partial_\mu\theta(x)]e^{-iq_j\theta(x)}\phi_j(x). \end{aligned} \quad (2.3.13)$$

The second term is new and did not occur for the global case. The main difficulty is that

$$\partial_\mu\phi_j(x) \not\rightarrow e^{-iq_j\theta(x)}\partial_\mu\phi_j(x).$$

Electrodynamics is locally gauge invariant because all derivatives occur in special combinations  $D_\mu$ , called ‘covariant derivatives’ which *do* have the property that

$$D_\mu\phi_j(x) \rightarrow e^{-iq_j\theta(x)}D_\mu\phi_j(x) \quad (2.3.14)$$

so that the gauge invariance of  $\mathcal{L}$  follows as it did in the global case. In QED

$$D_\mu^{(j)} \equiv \partial_\mu + ie q_j A_\mu, \quad (2.3.15)$$

where  $A_\mu(x)$  is the vector potential of the photon, the simplest example of a ‘gauge field’. (As usual  $e$  is the *magnitude* of the electron’s charge. As regards the gauge invariance,  $e$  could be any number, but (2.3.15) shows that  $eq_j$  must be the coupling constant linking  $A_\mu$  and  $\phi_j$ .) Thus in QED the coupling of photon and electron is contained in the terms in  $\mathcal{L}$  of the form

$$\bar{\psi}(x)[i\partial^\mu - eA^\mu - m]\psi(x) = -m\bar{\psi}\psi + i\bar{\psi}\gamma^\mu(\partial_\mu - ieA_\mu)\psi, \quad (2.3.16)$$

the latter term being of the form (2.3.15) since the electron has charge  $-e$ . The fact that only the combinations (2.3.15) occur is referred to as ‘minimal coupling’.

Now (2.3.15) will only satisfy (2.3.14) if  $A_\mu(x)$  is affected by the gauge

transformation in a particular way, viz

$$A_\mu(x) \rightarrow A'_\mu(x) \equiv A_\mu(x) + \frac{1}{e} \frac{\partial \theta(x)}{\partial x^\mu}. \quad (2.3.17)$$

It is then easy to show that

$$\begin{aligned} D_\mu^{(j)} \phi_j(x) &\rightarrow [D_\mu^{(j)} \phi_j(x)]' = D_\mu^{(j)\prime} \phi_j'(x) \\ &= [\partial_\mu + ie q_j A'_\mu(x)] e^{-iq_j \theta(x)} \phi_j(x) \\ &= e^{-iq_j \theta(x)} D_\mu^{(j)} \phi_j(x), \end{aligned}$$

the change in  $A_\mu$  in (2.3.17) being designed to cancel the unpleasant second term in (2.3.13).

The *local* gauge invariance is only attained because of the introduction of the ‘gauge boson’ field  $A_\mu$ , in this case associated with the photon. (This way of presenting the argument is of course the reverse of the usual one in elementary classical electrodynamics where one starts by noticing the gauge freedom in specifying the vector potential  $A_\mu$ .) Once  $A_\mu$  occurs in  $\mathcal{L}$  we will also need terms to describe the kinetic energy of the gauge boson, and, in general, a mass term. All these terms must themselves be gauge invariant.

The ‘field strength tensor’  $F_{\mu\nu}$  defined as

$$F_{\mu\nu} = \partial_\mu A_\nu - \partial_\nu A_\mu \quad (2.3.18)$$

is itself invariant under (2.3.17) and therefore the photon kinetic energy is gauge invariant if constructed with  $F_{\mu\nu}$ .

We have

$$\mathcal{L}_\gamma = -\frac{1}{4} F_{\mu\nu}(x) F^{\mu\nu}(x), \quad (2.3.19)$$

where the factor  $-\frac{1}{4}$  ensures that the Euler–Lagrange equations coincide with Maxwell’s equations. A mass term could only be of the form  $-\frac{1}{2} m_\gamma^2 A_\mu A^\mu$ , which is not gauge invariant unless  $m_\gamma = 0$ . To conclude: electrodynamics is locally gauge invariant provided the photon is massless.

It should be stressed that gauge invariance plays a vital rôle in proving that the theory is renormalizable. Technically, as mentioned in Section 1.1, it gives rise to the Ward–Takahashi identities amongst matrix elements (Ward, 1950; Takahashi, 1957).

### 2.3.3 Global gauge invariance—the non-Abelian case

The generalization to non-Abelian transformations is straightforward in the global case but is fairly complex in the local case.

As already mentioned the simplest non-Abelian invariance is isospin where the fields are assumed to come in multiplets

$$\phi = \begin{pmatrix} \phi_1 \\ \phi_2 \\ \vdots \\ \phi_n \end{pmatrix}$$

forming a basis for representations of the isospin group  $SU(2)$  involving rotations in isospin space. The gauge transformation is specified by three parameters  $\boldsymbol{\theta} = (\theta_1, \theta_2, \theta_3)$  and one has

$$\phi \rightarrow \phi' = e^{-i\mathbf{L}\cdot\boldsymbol{\theta}}\phi, \quad (2.3.20)$$

where the  $L_j$  ( $j = 1, 2, 3$ ) are  $n \times n$  matrices, representations of the generators of the  $SU(2)$  transformations. For instance, in the case of an isodoublet, say proton and neutron,  $n = 2$ , and  $\mathbf{L} = \frac{1}{2}\boldsymbol{\tau}$ , the  $\tau_j$  being the Pauli matrices, while for an isotriplet, say  $\pi^+, \pi^0, \pi^-$ ,  $(L_j)_{kl} = -i\epsilon_{jkl}$  etc. The group  $SU(2)$  has three generators  $T_j$ , corresponding to the fact that transformations are specified by the three parameters  $\theta_j$ , and they satisfy the commutation relations (we make no distinction between upper or lower indices for group structure constants)

$$[T_j, T_k] = i\epsilon^{jkl}T_l. \quad (2.3.21)$$

Naturally the  $L_j$ , representing the  $T_j$ , also satisfy this relation.

When the  $\theta_j$  are infinitesimal we have

$$\delta\phi = -i\mathbf{L} \cdot \boldsymbol{\theta}\phi. \quad (2.3.22)$$

For an isodoublet this reads

$$\delta\phi = -i\frac{\boldsymbol{\tau}}{2} \cdot \boldsymbol{\theta}\phi \quad (2.3.23)$$

and for an isotriplet

$$\delta\phi_j = \epsilon^{jkl}\theta_k\phi_l. \quad (2.3.24)$$

The formalism generalizes immediately to higher global non-Abelian gauge symmetries. Let  $T_j$  ( $j = 1, \dots, N$ ) be the generators of the group  $G$  of dimension  $N$  obeying the commutation relations

$$[T_j, T_k] = i\epsilon^{jkl}T_l. \quad (2.3.25)$$

The  $\epsilon^{jkl}$  are called the structure constants of the group and are anti-symmetric under interchange of any pair of indices. Given that the fields transform according to some representation of  $G$ , the generators  $T_j$  will be represented by matrices  $L_j$  satisfying (2.3.25). The gauge transformations, specified by  $N$  parameters  $\boldsymbol{\theta} = (\theta_1, \dots, \theta_N)$  are

$$\phi \rightarrow \phi' = e^{-i\mathbf{L}\cdot\boldsymbol{\theta}}\phi. \quad (2.3.26)$$

It is not difficult to construct Lagrangians invariant under global gauge transformations and there are no problems with gradient terms.

The number  $N$  of generators of  $G$  is 3 for  $SU(2)$ , 8 for  $SU(3)$  etc., and for each case of global gauge invariance of  $\mathcal{L}$  we can, as was done for the Abelian case in Section 2.3.1, show the existence of  $N$  conserved currents.

### 2.3.4 Non-Abelian local gauge invariance—Yang–Mills theories

We now turn to the much more subtle question of *local* non-Abelian gauge invariance. The first generalization of  $SU(2)$  to locally gauge invariant Lagrangians is due to Yang and Mills (1954) [a detailed account can be found in Taylor (1976)], but the treatment applies to any group with a finite number of generators [see Abers and Lee (1973)].

Let the group generators  $T_j$  obey

$$[T_j, T_k] = i\epsilon^{jkl}T_l \quad (2.3.27)$$

and let the set of fields

$$\phi = \begin{pmatrix} \phi_1 \\ \vdots \\ \phi_n \end{pmatrix}$$

transform according to

$$\begin{aligned} \phi(x) \rightarrow \phi'(x) &= e^{-i\mathbf{L}\cdot\boldsymbol{\theta}(x)}\phi(x) \\ &\equiv U(\boldsymbol{\theta})\phi(x), \end{aligned} \quad (2.3.28)$$

where the  $L_j$  ( $j = 1, \dots, N$ ) are  $n \times n$  matrices representing the group generators and  $\theta_j(x)$  ( $j = 1, \dots, N$ ) are arbitrary functions of space-time.

The aim is to introduce as many vector fields  $W_\mu^j(x)$ , gauge fields that are the analogue of the photon field  $A_\mu$ , as is necessary in order to construct a Lagrangian which is invariant under the local gauge transformations specified by  $\theta_j(x)$ .

From (2.3.28) we have

$$\partial_\mu\phi(x) \rightarrow U(\boldsymbol{\theta})\partial_\mu\phi(x) + [\partial_\mu U(\boldsymbol{\theta})]\phi(x). \quad (2.3.29)$$

By analogy with electrodynamics we seek a ‘covariant derivative’  $D_\mu$  such that

$$D_\mu\phi(x) \rightarrow D'_\mu\phi'(x) = U(\boldsymbol{\theta})D_\mu\phi(x) \quad (2.3.30)$$

and insist that the Lagrangian contain gradients only through the covariant derivative  $D_\mu$ . This will ensure invariance under the local, non-Abelian gauge transformations (2.3.28) for those pieces of  $\mathcal{L}$  that contain the fields  $\phi$  and their gradients.

If the group dimension is  $N$  we have to introduce one vector field  $W_\mu^j(x)$  for each dimension, and we can then define

$$D_\mu \phi(x) \equiv [\partial_\mu + ig\mathbf{L} \cdot \mathbf{W}_\mu(x)]\phi(x), \quad (2.3.31)$$

where  $g$  will play the rôle of a coupling constant and we use the shorthand

$$\mathbf{W}_\mu = (W_\mu^1(x), W_\mu^2(x), \dots, W_\mu^N(x)).$$

We now seek the analogue of (2.3.17), i.e. the rule for the effect of the gauge transformations upon the  $W_\mu^j(x)$ .

From (2.3.31),

$$\begin{aligned} D'_\mu \phi'(x) &= \partial_\mu \phi'(x) + ig\mathbf{L} \cdot \mathbf{W}'_\mu \phi'(x) \\ &= U(\theta) \partial_\mu \phi(x) + [\partial_\mu U(\theta)]\phi(x) + ig\mathbf{L} \cdot \mathbf{W}'_\mu U(\theta)\phi(x). \end{aligned} \quad (2.3.32)$$

This, from (2.3.30), should equal

$$U(\theta) D_\mu \phi(x) = U(\theta) [\partial_\mu + ig\mathbf{L} \cdot \mathbf{W}_\mu] \phi(x), \quad (2.3.33)$$

so that, comparing (2.3.32) and (2.3.33), we require

$$\mathbf{L} \cdot \mathbf{W}'_\mu U(\theta)\phi(x) = U(\theta) \mathbf{L} \cdot \mathbf{W}_\mu \phi(x) + \frac{i}{g} [\partial_\mu U(\theta)]\phi(x).$$

Now this relation must be true for all  $\phi(x)$ , so we get, after a little manipulation, the requirement

$$\mathbf{L} \cdot \mathbf{W}'_\mu = U(\theta) \left[ \mathbf{L} \cdot \mathbf{W}_\mu + \frac{i}{g} U^{-1}(\theta) \partial_\mu U(\theta) \right] U^{-1}(\theta). \quad (2.3.34)$$

This specifies, in a rather complicated way, how the  $W_\mu^j$  must transform.

(It is straightforward, incidentally, to show that the above transformations form a group. For example a second transformation using functions  $\theta'_j(x)$  will yield  $\mathbf{W}''_\mu$  related to the original  $\mathbf{W}_\mu$  by a relation like (2.3.34) involving  $U(\theta'') \equiv U(\theta')U(\theta)$ .)

To see more directly the effect of the transformation on the  $W_\mu^j$  we take an infinitesimal transformation

$$U(\theta) \simeq I - i\mathbf{L} \cdot \boldsymbol{\theta}$$

and get, to first order in  $\theta_j$ ,

$$\begin{aligned} \mathbf{L} \cdot \delta \mathbf{W}_\mu &\equiv \mathbf{L} \cdot (\mathbf{W}'_\mu - \mathbf{W}_\mu) \\ &= iL_k W_\mu^k L_j \theta_j - iL_j \theta_j L_k W_\mu^k + \frac{1}{g} L_j \partial_\mu \theta_j \\ &= i\theta_j W_\mu^k [L_k, L_j] + \frac{1}{g} L_j \partial_\mu \theta_j. \end{aligned}$$

The commutator is given by (2.3.27) so that

$$L_k \delta W_\mu^k = \frac{1}{g} L_k \partial_\mu \theta_k + c_{klm} \theta_l W_\mu^m L_k.$$

Finally, using  $c_{klm} = -c_{mlk}$  and the fact that the  $L_k$  are linearly independent, we get the transformation rule for  $W_\mu^j$ :

$$\delta W_\mu^j(x) = \frac{1}{g} \partial_\mu \theta_j(x) + c_{jkl} \theta_k(x) W_\mu^l(x). \quad (2.3.35)$$

This is the generalization of (2.3.17) for the photon field, to the non-Abelian case. Note that for the group  $U(1)$ ,  $c_{jkl} \equiv 0$  so only the first term of (2.3.35) appears in (2.3.17). Contrary to what one might have feared from (2.3.34), the transformation rule for the vector fields  $W_\mu^j$  does not depend upon the representation matrices  $L_j$ .

In summary, if the Lagrangian is constructed from products of fields and their Hermitian conjugates, and if all derivatives appear only in the form

$$D_\mu = \partial_\mu + ig \mathbf{L} \cdot \mathbf{W}_\mu,$$

we can ensure that  $\mathcal{L}$  is gauge invariant.

We must now ask about the kinetic energy and mass terms associated with the gauge fields  $W^j$ . It is not difficult to see that the combination (2.3.18) is no longer gauge invariant. It is much more laborious to show that a new combination, a generalized field tensor

$$G_{\mu\nu}^j = \partial_\mu W_\nu^j - \partial_\nu W_\mu^j + gc_{jkl} W_\mu^k W_\nu^l \quad (2.3.36)$$

transforms in such a way that

$$\mathcal{L}_0 = -\frac{1}{4} G_{\mu\nu}^j G^{j,\mu\nu} \quad (2.3.37)$$

is gauge invariant,  $\delta \mathcal{L}_0 = 0$ .

For an infinitesimal transformation (2.3.35), using the fact that the  $c_{jkl}$  can be regarded as the  $kl$  element of a set of matrices  $c_j$ , i.e.

$$c_{jkl} = (c_j)_{kl}$$

satisfying  $[c_j, c_k] = c_{jkl} c_l$ , one can show that

$$\delta G_{\mu\nu}^j = c_{jkl} \theta_k G_{\mu\nu}^l$$

from which the invariance of (2.3.37) follows.

A major new feature is that, unlike the photon case, the non-Abelian gauge fields  $\mathbf{W}_\mu$  are self-coupled through the term  $G_{\mu\nu}^j G^{j,\mu\nu}$  which appears in  $\mathcal{L}_0$ . As in the photon case, however, mass terms for the  $W^j$  cannot be tolerated since  $\mathbf{W}_\mu \cdot \mathbf{W}^\mu$  is not gauge invariant.

In the above we have not specified what the label  $k$  on  $W_\mu^k$  refers to. We have simply assumed a multiplet of fields transforming according to some representation of the symmetry group with  $k$  labelling the different members of the multiplet. For electroweak theory, where the non-Abelian part of the group is  $SU(2)$  the  $W^k$  will form a triplet with  $k$  essentially labelling the charge. For QCD where the non-Abelian group is  $SU(3)$ ,  $k$  will be a colour label. The self-coupling of gluons, mentioned in Section 1.1, is a direct consequence of the non-linear form of  $G_{\mu\nu}^j$  in (2.3.36) and (2.3.37). This is discussed in Chapter 21. In both electroweak theory and QCD the formal structure is the same as above.

Finally, then, a Lagrangian  $\mathcal{L}$  will be invariant under the local non-Abelian gauge transformation

$$U(\theta) = e^{-i\mathbf{L}\cdot\boldsymbol{\theta}} = e^{-i\mathbf{L}_j\theta_j} \quad (j = 1, \dots, N)$$

connected with a group  $G$  with  $N$  generators  $T_j$  of which the  $L_j$  are matrix representatives provided it is of the form

$$\mathcal{L} = \mathcal{L}_0 + \mathcal{L}_{\text{int}}[\phi^j, (\partial_\mu + ig\mathbf{L}\cdot\mathbf{W}_\mu)\phi^j]. \quad (2.3.38)$$

As there is a one-to-one correspondence between the dimension of the group and the number of massless gauge fields  $W_\mu^j$  that are necessary to attain gauge invariance, and, since the only known massless vector boson is the photon, it might appear that non-Abelian gauge symmetries just define an elegant formalism that has very little to do with physics.

## 2.4 Freedom to choose the gauge

In theories that are gauge invariant we are free either to try to work in a manifestly gauge-invariant fashion, or, since it cannot affect the final physical results, to choose a convenient gauge in which to work. In classical electrodynamics one often uses the *Lorentz* gauge in which

$$\partial_\mu A^\mu = 0. \quad (2.4.1)$$

This makes Maxwell's equations look simple. In quantum field theory things are more complicated because equations like (2.4.1), if interpreted literally as equations for the field *operators*, sometimes contradict the fundamental commutation relations that the fields must satisfy. Another common choice in QED is to have

$$\nabla \cdot \mathbf{A} = 0, \quad (2.4.2)$$

which is known as the ‘Coloumb gauge’. Since this is not a relativistically covariant equation when  $A_\mu$  as usual is thought of as a four-vector, it is necessary to modify the Lorentz transformation properties of  $A_\mu$ . Other gauges will be discussed in Chapter 21. In general any gauge may be

chosen classically, but some care must be exercised in fixing the gauge when using a canonical quantization formalism in a quantum field theory.

## 2.5 Summary

Starting from the Fermi current-current form of the weak interaction Lagrangian we tried progressively to eliminate the difficulties, divergences, unitarity violations etc. of the model. First we were led to introduce charged massive vector bosons and this led to the need for neutral bosons as well. Secondly, we tried to extend to weak interactions the property, gauge invariance, that makes QED a well-behaved, renormalizable theory. This led to Yang–Mills theories with non-Abelian gauge invariance, which, having a high degree of symmetry, may be renormalizable. The apparently incurable ailment of such theories is the need for a large number of massless gauge vector bosons which are not found in nature. Indeed  $M_W = 0$  is also ruled out by everything we know about the nearly point-like structure of weak interactions. The miraculous solution to this trouble will be discussed in the next chapter.

# 3

## Spontaneous symmetry breaking: the Goldstone theorem and the Higgs phenomenon

We here discuss dynamical systems in which the ground state does not possess the same symmetry properties as the Lagrangian. When this happens in certain field theories one finds that there inevitably exist massless scalar bosons, the so-called Goldstone bosons. Remarkably, however, when this happens in a local gauge theory involving massless vector fields and scalar fields, the would-be Goldstone bosons disappear, but contrive to re-emerge disguised as the *longitudinal* mode of the vector fields, which thereupon behave like massive vector bosons with three spin degrees of freedom. In this way the unwanted massless vector bosons of the gauge theory are replaced by heavy vector mesons as demanded by the phenomenology of the weak interactions.

It is well known that a considerable simplification obtains in a problem whenever the interaction possesses some symmetry. Exact symmetries, such as electric charge conservation, are, however, fairly rare in nature, and the usual way of representing the situation is to assume that a *small* piece of the Lagrangian violates a particular symmetry whereas the rest of  $\mathcal{L}$  is invariant. Thus strong interactions conserve parity, isospin and strangeness, whereas electromagnetic interactions violate isospin, and weak interactions violate isospin, strangeness and parity, so that a hierarchy of forces results. A very interesting situation occurs when the *solutions* of a problem are not symmetric in spite of the Lagrangian being exactly symmetric—in particular if this is so for the ground state of the system. One then talks, somewhat inappropriately, of a ‘spontaneously broken symmetry’. The most celebrated classical example is a ferromagnet. Although the Hamiltonian is rotationally invariant, the ground state is not, since in it the spins are all aligned along a definite, albeit arbitrary, direction. There thus exist infinitely many vacua, i.e. ground states. Another example is the buckling of a rod under axial pressure. The equations are symmetric under rotations about the axis of the

rod, yet it buckles in one particular, albeit arbitrary, direction. Again there are infinitely many states for the buckled rod.

In both these examples the non-symmetric states correspond to a lower energy than the symmetric ones. The original symmetry of the equations of motion is hidden. It is evident only in our inability to predict in which direction the spins will align or the rod bend and in the fact that all the non-symmetric solutions are equivalent and can be obtained from one another by a symmetry operation.

In both examples there exists a critical point, i.e. a critical value of some quantity, either temperature or external force, which will determine whether spontaneous symmetry breaking will occur. Beyond the critical point the vacuum becomes degenerate and the symmetric solution unstable. These properties are typical of all examples of spontaneous symmetry breaking.

### 3.1 Spontaneously broken symmetries in field theory: Goldstone's theorem

Remarkably, we shall find that the above phenomenon allows the construction of a gauge theory in which the underlying symmetry is spontaneously broken, and as a result masses for the  $W$ s as well as for the leptons are ‘spontaneously generated’.

Consider the following (classical) Lagrangian

$$\mathcal{L} = (\partial_\mu \phi)(\partial^\mu \phi^*) - \mu^2 \phi \phi^* - \lambda(\phi \phi^*)^2, \quad (3.1.1)$$

where  $\phi(x)$  is a *complex* scalar field. (Note that for a real field,  $\phi$ , the mass term and the kinetic energy term would each have an extra factor  $\frac{1}{2}$ .) In a quantum theory  $\mu^2$  would normally be regarded as the (bare) mass of the field quanta and the  $\lambda$  term as a form of self-interaction.  $\mathcal{L}$  is invariant under the group  $U(1)$  of *global* transformations

$$\phi(x) \rightarrow \phi'(x) = e^{-i\theta} \phi(x), \quad (3.1.2)$$

where  $\theta$  is an arbitrary constant.

The kinetic energy term is positive and can vanish only if  $\phi = \text{constant}$ . The ground state of the system will be obtained when the value of the constant corresponds to the minimum of the ‘potential’:

$$V(\phi) \equiv \mu^2 \phi \phi^* + \lambda(\phi \phi^*)^2. \quad (3.1.3)$$

Since  $V$  depends only on  $\phi$  and  $\phi^*$  in the combination  $\phi \phi^*$  let us define

$$\rho \equiv \phi \phi^* \quad (3.1.4)$$

so that

$$V(\rho) = \mu^2 \rho + \lambda \rho^2. \quad (3.1.5)$$

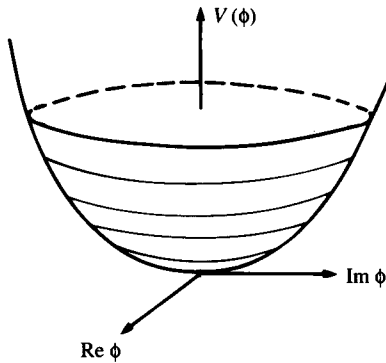


Fig. 3.1. The potential for  $\mu^2 > 0$ .

In fact  $V$  only has a minimum when  $\lambda > 0$ , which we take to be so. Let us, however, not insist on interpreting  $\mu$  as a mass and let us consider what happens for  $\mu^2$  both  $> 0$  and  $< 0$ .

For  $\mu^2 > 0$ ,  $V$  is as shown in Fig. 3.1 and the minimum of  $V$  is at the origin  $\rho = 0$ , i.e. at  $\phi = 0$ , and we have a symmetric ground state configuration, i.e. the ground state  $\phi = 0$  is unique and is invariant under (3.1.2). If however  $\mu^2 < 0$  the minimum is at

$$\rho = -\frac{\mu^2}{2\lambda}, \quad (3.1.6)$$

which means that there is a whole ring of radius

$$|\phi| \equiv \frac{v}{\sqrt{2}} = \sqrt{\frac{-\mu^2}{2\lambda}} \quad (3.1.7)$$

in the complex  $\phi$  plane at each of whose points  $V$  is at its minimum value, as shown in Fig. 3.2.

In this case  $\phi = 0$  is an unstable point and any value of  $\phi$  satisfying (3.1.7) will give a true ground state. There are infinitely many ground states and each is not symmetric in the sense that it is altered by (3.1.2). Indeed (3.1.2) takes one from one ground state to another since each is clearly of the form

$$\phi_{\text{vac}} = \frac{v}{\sqrt{2}} e^{i\Lambda},$$

with  $\Lambda$  real but otherwise arbitrary.

We see that  $\mu^2 = 0$  is the critical transition point between the symmetric solution and the degenerate ground state case. From now on we consider only the case  $\mu^2 < 0$ . Any point on the ring of minima is equivalent since they can all be obtained from any one point by applying the

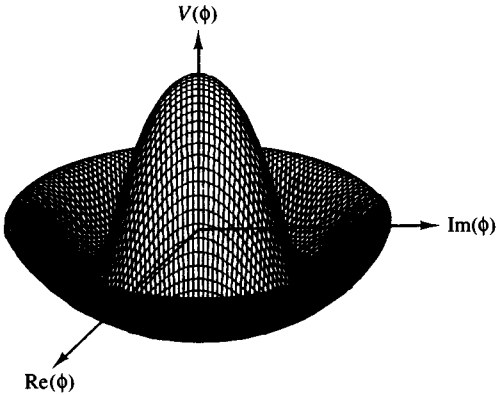


Fig. 3.2. The potential for  $\mu^2 < 0$ .

transformation (3.1.2). If we choose this point on the real axis we can write

$$\phi(x) = \frac{1}{\sqrt{2}} [v + \xi(x) + i\chi(x)], \quad (3.1.8)$$

with  $\xi, \chi$  real and  $\xi = \chi = 0$  in the ground state. Substituting in (3.1.1), and ignoring unimportant constant terms, one has

$$\begin{aligned} \mathcal{L} = & \frac{1}{2}(\partial_\mu \xi)^2 + \frac{1}{2}(\partial_\mu \chi)^2 - \lambda v^2 \xi^2 \\ & - \lambda v \xi (\xi^2 + \chi^2) - \frac{1}{4}\lambda (\xi^2 + \chi^2)^2. \end{aligned} \quad (3.1.9)$$

If we were to consider  $\mathcal{L}$  as a quantum theory Lagrangian, with  $\xi$  and  $\chi$  as the basic fields, then it would contain no mass terms for the  $\chi$  field but a normal mass term  $-\frac{1}{2}m_\xi^2 \xi^2$  for the  $\xi$  field with

$$m_\xi^2 = 2\lambda v^2. \quad (3.1.10)$$

Presumably the change of variables (3.1.8) cannot alter the physics if the problem is solved exactly. However, if perturbation methods are used in the quantum theory, this need not be true. For example, while in (3.1.9) it might be sensible to take the kinetic energy and mass terms as the unperturbed Lagrangian  $\mathcal{L}_0$ , it would be disastrous to do so in (3.1.1) because of the negative mass squared terms.

In the above example we started with an  $\mathcal{L}$  invariant under  $U(1)$ , constructed from a complex scalar field  $\phi(x)$ , and in the case  $\mu^2 < 0$  (so that  $\mu$  cannot be considered as the mass of  $\phi$ ) we have ended up with a massless field  $\chi$  and a field  $\xi$  whose mass  $m_\xi$  has been ‘spontaneously’ generated.

If we consider a generalization of (3.1.1) with  $n$  real scalar fields  $\phi_j$ :

$$\mathcal{L} = \frac{1}{2}(\partial_\mu \phi^j)(\partial^\mu \phi^j) - \frac{1}{2}\mu^2 \phi^j \phi^j - \lambda(\phi^j \phi^j)^2 \quad (3.1.11)$$

( $j$  is summed over) the invariance group of  $\mathcal{L}$  is now the orthogonal group in  $n$  dimensions  $O(n)$  which mixes up the fields with each other, and which possesses  $\frac{1}{2}n(n - 1)$  generators. Again we find a ‘ring’ of minima now at  $\sum_j \phi^j \phi^j = -\mu^2/4\lambda$  provided that  $\mu^2 < 0$ . If one thinks of the  $\phi^j$  as the components of a vector  $\phi$ , then the minimum fixes the length of the vector, but leaves its direction arbitrary. In this case we can choose just one of the  $\phi^j$ , say  $\phi^n$ , to be the one that is non-zero in the vacuum state, while all the others are zero, and all the other vacuum configurations can be obtained from this via  $O(n)$  transformations. A major difference as compared with our earlier example is that our choice of vacuum state

$$\phi_{\text{vac}} = \begin{pmatrix} 0 \\ 0 \\ \vdots \\ 0 \\ v \end{pmatrix}$$

is invariant under a non-trivial subgroup of  $O(n)$ , namely the  $O(n - 1)$  that does not mix the  $n$ th field with the others. Now  $O(n - 1)$  has  $\frac{1}{2}(n - 1)(n - 2)$  generators, so that the difference between the number of generators of the *original* group  $O(n)$  and of the *residual* group  $O(n - 1)$  is exactly  $n - 1$ . We say that there are  $n - 1$  ‘broken generators’.

The same calculation as before shows that still only one field acquires a genuine mass whereas the other  $n - 1$  scalar fields remain massless. These massless bosons are usually called ‘Goldstone bosons’.

The above are examples of a general theorem due to Goldstone (1961; see also Jona-Lasinio and Nambu, 1961 a, b; Goldstone, Salam and Weinberg, 1962) and are not linked specifically to the particular group  $O(n)$ : *for every broken generator in a spontaneous symmetry breaking there exists a massless scalar boson.*

Physically, the various equivalent ground states differ according to the number of Goldstone bosons of zero energy and momentum that they contain. It can be shown that the *physical scattering amplitudes* do not show any zero-mass pole terms.

Having set out to see whether spontaneous symmetry breaking can cure the disease of unwanted massless vector bosons in gauge theories, we seem to have reached the conclusion that spontaneous symmetry breaking introduces its own massless bosons, so that there appear to be two diseases instead of one. The extraordinary thing is, that, taken together, these two problems mutually compensate.

### 3.2 The Higgs mechanism

We now consider the earlier model (3.1.1) for a charged scalar field but impose invariance under *local*  $U(1)$  gauge transformations (Higgs, 1964 a, b, 1966).

According to our previous discussion (Section 2.3.2) we must replace the derivative  $\partial_\mu$  by the covariant derivative  $D_\mu = \partial_\mu + ieA_\mu$  and add the kinetic term  $-\frac{1}{4}F_{\mu\nu}F^{\mu\nu}$  so that  $\mathcal{L}$  of (3.1.1) becomes

$$\begin{aligned}\mathcal{L} = & -\frac{1}{4}F_{\mu\nu}F^{\mu\nu} + [(\partial_\mu - ieA_\mu)\phi^*][(\partial_\mu + ieA_\mu)\phi] \\ & -\mu^2\phi\phi^* - \lambda(\phi\phi^*)^2,\end{aligned}\quad (3.2.1)$$

which is invariant under the local Abelian gauge transformation

$$U(\theta) = e^{-i\theta(x)}, \quad (3.2.2)$$

where

$$\left. \begin{aligned}\phi(x) &\rightarrow \phi'(x) = e^{-i\theta(x)}\phi(x), \\ \phi^*(x) &\rightarrow \phi^{*\prime}(x) = e^{i\theta(x)}\phi^*(x), \\ A_\mu(x) &\rightarrow A'_\mu(x) = A_\mu(x) + \frac{1}{e}\partial_\mu\theta(x).\end{aligned}\right\} \quad (3.2.3)$$

$A_\mu$ , according to (3.2.1), is a massless gauge boson.

We can once again look for a minimum in the potential, and we find one if  $\lambda > 0$ . If  $\mu^2 < 0$  there is again a ring of degenerate ground states, whereas the symmetric ground state  $\phi = 0$  obtains if  $\mu^2 > 0$ .

The interesting case is  $\mu^2 < 0$ , and, proceeding as before, we set

$$\phi(x) = \frac{1}{\sqrt{2}}[v + \xi(x) + i\chi(x)] \quad (3.2.4)$$

with

$$v = \sqrt{\frac{-\mu^2}{\lambda}} \quad (3.2.5)$$

so that  $\phi_{vac} = v/\sqrt{2}$ , and, substituting in (3.2.1), find

$$\begin{aligned}\mathcal{L} = & -\frac{1}{4}F_{\mu\nu}F^{\mu\nu} + \frac{e^2v^2}{2}A_\mu A^\mu + \frac{1}{2}(\partial_\mu\xi)^2 + \frac{1}{2}(\partial_\mu\chi)^2 \\ & -\frac{1}{2}(2\lambda v^2)\xi^2 - evA_\mu\partial^\mu\chi + \dots\end{aligned}\quad (3.2.6)$$

The term involving  $A_\mu A^\mu$  is a great surprise since in a quantum picture it looks as if the gauge vector field  $A_\mu$  has acquired a mass. Gauge invariance is, of course, still there since (3.2.6) must be equivalent to (3.2.1). However, the gauge transformations look a little more complicated in terms

of  $\xi$  and  $\chi$ . From (3.2.4) and (3.2.3) one obtains

$$\left. \begin{aligned} \xi(x) &\rightarrow \xi'(x) = [v + \xi(x)] \cos \theta(x) + \chi(x) \sin \theta(x) - v, \\ \chi(x) &\rightarrow \chi'(x) = \chi(x) \cos \theta(x) - [v + \xi(x)] \sin \theta(x), \\ A_\mu(x) &\rightarrow A'_\mu(x) = A_\mu(x) + \frac{1}{e} \partial_\mu \theta(x). \end{aligned} \right\} \quad (3.2.7)$$

If we look at the structure of  $\mathcal{L}$  in (3.2.6) it now seems to describe the interaction of a massive vector field  $A_\mu$  and two scalars, the massive  $\xi$  field and the massless  $\chi$  field. It is instructive to count the ‘degrees of freedom’ in the two versions of  $\mathcal{L}$ . In (3.2.1) there is one massless vector field (two degrees of freedom corresponding to the two independent transverse modes) and one complex scalar field (two degrees). In (3.2.6) we have one massive vector field (three degrees of freedom—the longitudinal mode is now allowed) and two real scalar fields (two degrees), so we seem to have gained an extra degree of freedom. This, however, is only apparent, and we shall see that we can utilize the gauge invariance to choose a particular gauge in which  $\chi$  simply does not appear.

Since the theory does not change with any choice of the transformation function  $\theta(x)$  in (3.2.2) let us choose  $\theta(x)$  at each space-time point to equal the phase of  $\phi(x)$ . Then in this gauge

$$\phi'(x) = e^{-i\theta(x)} \phi(x)$$

is real, and equal to

$$\frac{1}{\sqrt{2}}[v + \eta(x)], \quad (3.2.8)$$

say, with  $\eta$  real, and

$$A'_\mu(x) = A_\mu(x) + \frac{1}{e} \frac{\partial \theta(x)}{\partial x^\mu}.$$

The Lagrangian in (3.2.1) now becomes, instead of (3.2.6),

$$\begin{aligned} \mathcal{L} = & -\frac{1}{4} F'_{\mu\nu} F'^{\mu\nu} + \frac{1}{2} e^2 v^2 A'_\mu A'^\mu + \frac{1}{2} (\partial_\mu \eta)^2 \\ & - \frac{1}{2} (2\lambda v^2) \eta^2 - \frac{1}{4} \lambda \eta^4 + \frac{1}{2} e^2 (A'_\mu)^2 (2v\eta + \eta^2), \end{aligned} \quad (3.2.9)$$

where

$$F'_{\mu\nu} = \partial_\mu A'_\nu - \partial_\nu A'_\mu,$$

and where we have now written all the terms in  $\mathcal{L}$ .

In this form  $\mathcal{L}$  describes the interaction of the massive vector boson  $A'_\mu$  with the massive, real, scalar field  $\eta$  (called the ‘Higgs boson’), whose mass squared is given by

$$2\lambda v^2 = -2\mu^2. \quad (3.2.10)$$

All massless particles have completely disappeared and the number of degrees of freedom is back to four, as it ought to be.

We started from a Lagrangian (3.2.1) which was gauge invariant but which contained a parameter that looked like a negative squared mass. We went to a new form of  $\mathcal{L}$  (3.2.6) which was still gauge invariant, but under a more complicated type of transformation law and which had an unphysical degree of freedom. Finally we chose a particular gauge (often called the ‘ $U$  gauge’) where the unphysical field has been ‘gauged away’ and we then had a form for  $\mathcal{L}$  (3.2.9) which was no longer invariant under any gauge transformation (we had fixed the gauge) but which had a sensible looking physical spectrum of massive particles, one vector, one scalar.

What has happened is that in the spontaneously broken symmetry the gauge boson has acquired mass at the expense of the would-be Goldstone boson, which simply disappears. For each vector gauge field that gets massive we need one complex scalar field, one piece of which becomes unphysical and disappears (it reappears as the longitudinal mode of the vector field) leaving one real scalar physical field, the Higgs boson.

The whole of the above analysis can be adapted to any non-Abelian gauge theory.

### 3.3 Unitarity and renormalizability

If we take the form of  $\mathcal{L}$  given in (3.2.9) as our quantum Lagrangian and we attempt to do perturbation theory, all propagators will look sensible, with poles corresponding only to the physical particles. For this reason the chosen gauge is called a ‘unitary’ gauge ( $U$  gauge).

However, the high momentum limit of the propagators will be dominated by the term [see (2.1.15)]

$$\frac{k_\mu k_\nu / m^2}{k^2 - m^2}$$

which tends to a constant as  $k \rightarrow \infty$ , and which, as discussed in Section 2.1, seems to lead to unpleasant divergences. In the present case, however, because of the underlying gauge invariance of the theory, it can be shown that the divergences cancel out and the theory is renormalizable. The actual proof of renormalizability is a major achievement ('tHooft and Veltman, 1974).

To actually prove renormalizability it is convenient not to use the  $U$  gauge, but to introduce a family of gauges called ‘ $R$  gauges’ labelled by a parameter  $\alpha$ . In these gauges the vector boson propagator has the form

$$\frac{-g_{\mu\nu} + (k_\mu k_\nu (1 - \alpha)) / (m^2 - \alpha k^2)}{k^2 - m^2}, \quad (3.3.1)$$

which tends to 0 as  $1/k^2$  if  $\alpha \neq 0$  as  $k^2 \rightarrow \infty$ , so that divergence problems disappear. However, there is a pole in the propagator at  $k^2 = m^2/\alpha$ , and it has to be, and can be, shown that the spurious pole cancels out, leaving the physics independent of  $\alpha$ .

Although it is seldom emphasized, this kind of dependence of the form of the propagator on the choice of gauge is already present in QED. The often used form  $-g_{\mu\nu}/k^2$  for the photon propagator corresponds to  $\alpha = 1$  in (3.3.1) and is very convenient for proving renormalizability.

### 3.4 Summary

For any Lagrangian invariant under Abelian or non-Abelian local gauge transformations, it can be shown that, if spontaneous symmetry breaking takes place, then the would-be massless Goldstone bosons associated with each broken generator become associated with the originally massless vector bosons, turning the latter into massive vector bosons and materializing as the longitudinal component of these bosons. The number of degrees of freedom remains the same. In other words there is a perfect matching between the number of gauge fields that acquire mass and the number of broken generators, and the remaining vector mesons remain massless corresponding to the surviving unbroken symmetry of the ground state. It appears that in nature only one such unbroken symmetry generator exists, in that only one massless vector field, the photon, exists. This exact symmetry law is, as we discussed in Section 2.3.1, associated with charge conservation.

# 4

## Construction of the standard model

The developments of the previous chapters provide the ingredients that one can use to construct models of spontaneously broken non-Abelian gauge theories. In Chapters 21–23 we shall discuss quantum chromodynamics (QCD) which is proposed as a model for strong interactions. Here we shall concentrate on models which attempt to unify the weak and electromagnetic interactions into a unique renormalisable theory.

We first give the general rules to be followed for model building. Then we apply them to the most successful of these models—in fact, the only one that has so far passed all experimental tests—the electroweak standard model (SM) and show how its structure arises.

In the literature, the term *standard model* sometimes refers to the combination of the electroweak sector with the colour  $SU(3)$  theory of strong interaction mentioned above (QCD). In this and in the following chapters, we shall use the term standard model for the purely electroweak part of the theory. The SM is due to various authors (Glashow, 1961; Weinberg, 1967; Salam, 1968) and its predictions are in good agreement with the data.

With the recent coming into operation of the electron–positron collider (LEP) at CERN, where over  $10^6 Z^0$ s are collected in a year of operation, it becomes possible to test the predictions of the SM to a fantastic accuracy. So far, all the evidence is that the SM works incredibly well.

### 4.1 Model building (towards the standard model)

The general principles to be followed in constructing models are:

- (a) Choose a gauge group  $G$  and as many vector fields as there are generators of  $G$ .

- (b) Choose the fields of the *elementary particles* one wants to describe and their representations, i.e. how they transform under the operations of  $G$ . If a certain number of the gauge vector fields are to become massive then there must be at least this number plus one of independent scalar fields present.
- (c) Write down the most general renormalizable Lagrangian invariant under the group  $G$  which couples all the fields so far introduced. At this stage  $\mathcal{L}$  is still gauge invariant and all vector bosons are still massless.
- (d) Choose the coupling parameters of the scalar fields so that at the minimum of the potential the fields do not have the value zero (in practice this means taking  $\mu^2 < 0$ ).
- (e) Introduce new scalar fields whose value at the minimum is zero.
- (f) Choose a convenient gauge, interpret the Lagrangian as a quantum Lagrangian and apply the usual techniques of quantum field theory.
- (g) Verify that the theory is renormalizable.

There are, in addition, one or two technical constraints to which we shall return later.

We now illustrate these rules by constructing the simplest, and indeed the most successful, gauge theory that unifies the weak and electromagnetic interactions—the standard model.

## 4.2 The standard model

For many decades it was believed that the only leptons were the electron and the muon and their respective neutrinos. But in 1975 a new spin-half particle called  $\tau$  was discovered, which despite its huge mass on the scale of  $m_e$  or  $m_\mu$ , i.e.  $m_\tau \approx 1.8 \text{ GeV}/c^2$ , was found to behave in all respects like a lepton. (A detailed discussion of the properties of the  $\tau$  is given in Chapter 14.) All the present evidence seems to indicate that the  $\tau$  interacts exactly like an  $e$  or  $\mu$  and that it possesses a neutrino partner  $\nu_\tau$  though this has not yet been identified experimentally.

Prior to going into the details of building the SM, we have, therefore, to agree that there are three generations of leptons  $(\nu_e^-)$ ,  $(\nu_\mu^-)$  and  $(\nu_\tau^-)$  and that the neutrinos are treated as massless. Clearly, this is an input which must be injected by hand in the model.

In what follows we shall usually refer to just electrons and their neutrinos. It should be understood that identical terms involving muons, heavy electrons ( $\tau$ ) and their respective neutrinos are always implied.

From the phenomenology of the weak interactions we know that we require both charge changing leptonic currents as well as neutral currents. It is by now reasonably certain that the neutral currents have exactly the same  $V - A$  structure as the charged ones, and we will assume this to be so. Given that the weak interactions are to be mediated by our gauge vector bosons, we thus require three vector mesons  $W_\mu^j$  ( $j = 1, 2, 3$ ), at this stage all massless. The simplest group that contains the required three generators is  $SU(2)$ . However, it is clear that this is not enough if we wish to include electromagnetic interactions as well. For all the  $W_\mu^j$  couple in a parity-violating fashion only to the left-handed parts of the leptons, as required for the weak interactions, whereas the electromagnetic interaction conserves parity and involves both left and right parts of the leptons. For example, using  $e = e_R + e_L$  we can write the electromagnetic current of the leptons as

$$\begin{aligned} -l_{\text{em}}^\mu &= \bar{e}\gamma^\mu e + \dots \\ &= \bar{e}_R\gamma^\mu e_R + \bar{e}_L\gamma^\mu e_L + (\mu, \tau \text{ terms}) \end{aligned} \quad (4.2.1)$$

(the cross-terms vanish). Thus we need one further gauge vector meson, call it  $B_\mu$ , and correspondingly a group with one generator,  $U(1)$ . The overall gauge group is then  $U(1) \otimes SU(2)$  with a total of four generators.

We now consider the choice of the scalar fields. Since we desire to end up with three heavy vector bosons associated with the weak interactions and a massless vector boson, the photon, we require  $3+1 = 4$  independent scalar fields. The simplest choice (sometimes referred to as the *minimal SM*) is a doublet of complex scalar fields, one charged, one neutral:

$$\phi = \begin{pmatrix} \phi^+ \\ \phi^0 \end{pmatrix}. \quad (4.2.2)$$

More complex schemes with several Higgs doublets have been considered in the literature. The  $2 \times 2$  matrices representing the generators of  $U(1)$  and  $SU(2)$  are just the unit matrix  $I$  and the Pauli matrices divided by two  $\frac{1}{2}\tau_j$ , so  $\phi$  will transform under the local gauge transformations as follows:

$$\left. \begin{array}{ll} SU(2) & : \phi \rightarrow \phi' = e^{-i\tau \cdot \theta(x)/2} \phi, \\ U(1) & : \phi \rightarrow \phi' = e^{-iI\theta(x)/2} \phi, \end{array} \right\} \quad (4.2.3)$$

where the functions  $\theta(x)$ ,  $\theta(x)$  are independent. (The factor  $\frac{1}{2}$  in  $U(1)$  is for later convenience.)

### 4.2.1 Coupling of the gauge bosons to the Higgs scalars

According to Section 2.3 the locally gauge invariant Lagrangian for the coupling of the gauge bosons ( $GB$ ) to the scalars ( $S$ ) is

$$\mathcal{L}_{GB-S} = \left\{ (\partial_\mu + i\frac{1}{2}g\mathbf{W}_\mu \cdot \boldsymbol{\tau} + i\frac{1}{2}g'IB_\mu)\phi \right\}^\dagger \times \left\{ \dots \right\} - V(\phi^\dagger\phi). \quad (4.2.4)$$

The potential is

$$V(\phi^\dagger\phi) = \mu^2\phi^\dagger\phi + \lambda(\phi^\dagger\phi)^2 \quad (4.2.5)$$

as earlier; we adjust it so as to produce spontaneous symmetry breaking.

Note that the invariance of (4.2.4) requires (see (2.3.17) and (2.3.35)) that under infinitesimal gauge transformations

$$\begin{aligned} \delta B_\mu &= \frac{1}{g'}\partial_\mu\theta(x), \\ \delta W_\mu^j &= \frac{1}{g}\partial_\mu\theta^j(x) + \epsilon^{jkl}\theta^k(x)W_\mu^l(x), \end{aligned} \quad \left. \right\} \quad (4.2.6)$$

since for  $SU(2)$  the structure constants  $\epsilon^{jkl} = \epsilon^{jkl}$  the anti-symmetric tensor.

We choose  $\phi^0$  to have the non-zero value  $(1/\sqrt{2})v$  in the vacuum state, so that, in the vacuum state,

$$\phi = \phi_{\text{vac}} = \begin{pmatrix} 0 \\ \frac{v}{\sqrt{2}} \end{pmatrix}. \quad (4.2.7)$$

None of the original transformations  $I - (\boldsymbol{\tau} \cdot \boldsymbol{\theta}/2) \dots$  or  $I(1 - \boldsymbol{\theta} \dots)$  leaves  $\phi_{\text{vac}}$  unchanged. But the combination  $\frac{1}{2}(I + \tau_3) = \begin{pmatrix} 1 & 0 \\ 0 & 0 \end{pmatrix}$ , and any transformations based upon it as generator, will certainly have no effect on  $\phi_{\text{vac}}$ . We must therefore rearrange (4.2.4) so that we can identify the field that multiplies  $\frac{1}{2}(I + \tau_3)$  as the gauge boson that remains massless, i.e. as the photon. To this end put

$$\begin{aligned} B_\mu &= \cos\theta_W A_\mu + \sin\theta_W Z_\mu, \\ W_\mu^3 &= \sin\theta_W A_\mu - \cos\theta_W Z_\mu. \end{aligned} \quad \left. \right\} \quad (4.2.8)$$

This is an orthogonal transformation and the new free fields  $A_\mu, Z_\mu$  will thus be independent, as discussed in Section 1.1.

$\theta_W$  is called the Weinberg angle and we shall adjust its value so that  $A_\mu$  turns out to be the photon field.  $Z_\mu$  will then be the massive neutral boson. The terms involving  $W_\mu^3$  and  $B_\mu$  in (4.2.4) become, using (4.2.8),

$$\begin{aligned} &i\left(\frac{g}{2}W_\mu^3\tau_3 + \frac{g'}{2}IB_\mu\right)\phi \\ &= i\left[A_\mu \frac{1}{2}(\tau_3 g \sin\theta_W + g' I \cos\theta_W) \right. \\ &\quad \left. + Z_\mu \frac{1}{2}(g' I \sin\theta_W - g \tau_3 \cos\theta_W)\right]\phi. \end{aligned} \quad (4.2.9)$$

We see that  $A_\mu$  will be coupled through the unbroken generator  $\frac{1}{2}(I + \tau_3)$  if

$$g \sin \theta_W = g' \cos \theta_W$$

or

$$\tan \theta_W = g'/g \quad (4.2.10)$$

and will thus remain massless.

Substituting (4.2.10) into (4.2.9) gives

$$ig \sin \theta_W \left[ A_\mu \frac{1}{2}(I + \tau_3) + \frac{1}{2}Z_\mu(\tan \theta_W I - \cot \theta_W \tau_3) \right] \phi. \quad (4.2.11)$$

Note that the generator  $\frac{1}{2}(I + \tau_3)$  just measures the charge of  $\phi$  in units of  $e$  in the sense that

$$\begin{aligned} \frac{1}{2}(I + \tau_3) \begin{pmatrix} \phi^+ \\ 0 \end{pmatrix} &= \begin{pmatrix} \phi^+ \\ 0 \end{pmatrix}, \\ \frac{1}{2}(I + \tau_3) \begin{pmatrix} 0 \\ \phi^0 \end{pmatrix} &= 0. \end{aligned}$$

So the coupling of  $A_\mu$  is proportional to the charge, as it must be if we are to identify  $A_\mu$  as the photon, and in order to have the correct strength of electromagnetic coupling of  $\phi^+$  we must have the important relation

$$g \sin \theta_W = e. \quad (4.2.12)$$

Since  $g$  will clearly play the rôle of the coupling involved in the weak interactions, (4.2.12) provides a unification of the weak and electromagnetic interactions.

The part of  $\mathcal{L}_{GB-S}$  (4.2.4) that gives rise to non-zero masses for  $W_\mu^1$ ,  $W_\mu^2$  and  $Z_\mu$  is

$$\begin{aligned} &\left\{ \left[ \frac{g}{2} \begin{pmatrix} 0 & W_\mu^1 - iW_\mu^2 \\ W_\mu^1 + iW_\mu^2 & 0 \end{pmatrix} + \frac{g \sin \theta_W}{2} \right. \right. \\ &\quad \times \left( \begin{pmatrix} (\tan \theta_W - \cot \theta_W)Z_\mu & 0 \\ 0 & (\tan \theta_W + \cot \theta_W)Z_\mu \end{pmatrix} \right] \left( v \cdot 2^{-\frac{1}{2}} \right) \Big\} \\ &\quad \times \left\{ \dots \right\}^\dagger = \frac{g^2 v^2}{4} \left( W_\mu^+ W^{\mu+\dagger} + \frac{1}{2 \cos^2 \theta_W} Z_\mu Z^{\mu\dagger} \right) \quad (4.2.13) \end{aligned}$$

where

$$W_\mu^\pm = \frac{1}{\sqrt{2}} \left( W_\mu^1 \mp iW_\mu^2 \right) \quad (4.2.14)$$

are the fields of the charged vector bosons.

Since  $W_\mu^+$  is a complex field, its mass must be

$$M_W = \frac{gv}{2}. \quad (4.2.15)$$

For the neutral field  $Z_\mu$  the mass is

$$M_Z = \frac{gv}{2 \cos \theta_W}. \quad (4.2.16)$$

Thus we have the interesting relation

$$\frac{M_W}{M_Z} = \cos \theta_W. \quad (4.2.17)$$

It is perhaps important to bear in mind that there is a qualitative difference between the equations (4.2.12) and (4.2.17).

The first is a direct consequence of  $\gamma - Z^0$  mixing in constructing a unified gauge theory of the electromagnetic and weak interactions. (A sharper version of this statement will be presented in Section 5.1). The second reflects the choice of the simplest Higgs mechanism to give mass to the vector bosons. Because the Higgs meson has not yet been discovered it is sometimes felt that the *minimal Higgs mechanism* may not be the correct way to generate mass. In that case eqn (4.2.17) would cease to be true, whereas (4.2.12) would continue to hold. In Section 5.2 we mention a rather direct way to test the mutual consistency of (4.2.12) and (4.2.17). In this book we always deal with the SM in its *minimal* form except when expressly considering extensions to it.

The relation (4.2.17) follows directly from the Lagrangian, and is therefore true in lowest order perturbation theory. It could get altered in higher order perturbation theory, especially as a consequence of renormalization effects. As regards the Higgs scalar  $H$  which survives and becomes massive, it will as usual have a mass (3.2.10)

$$m_H = \sqrt{-2\mu^2}, \quad (4.2.18)$$

which is a free parameter in the theory. Since no such scalar particles have so far been seen, its mass is presumably quite large.

If one chooses a gauge so that

$$\phi = \begin{pmatrix} 0 \\ \frac{1}{\sqrt{2}}(v + H) \end{pmatrix},$$

with  $H$  a real Higgs scalar field then it is clear from the form of (4.2.13) that there is the following interaction between  $H$  and the massive bosons:

$$\mathcal{L}_{H-GB} = \frac{g^2}{4}(2vH + H^2) \left( W^{\mu+}W_\mu^{+\dagger} + \frac{1}{2 \cos^2 \theta_W} Z_\mu Z^{\mu\dagger} \right), \quad (4.2.19)$$

i.e. both tri-linear and quadri-linear couplings occur. We shall return to discuss the strength of the coupling later.

### 4.2.2 Self-coupling of the gauge bosons

Up to this point we have considered only that part of  $\mathcal{L}$  that contains the Higgs scalars and their coupling to the gauge bosons.

For the gauge bosons themselves we have the expected gauge invariant terms (see (2.3.19) and (2.3.37))

$$\mathcal{L}_{GB} = -\frac{1}{4}G_{\mu\nu}^j G^{j\mu\nu} - \frac{1}{4}B_{\mu\nu} B^{\mu\nu}, \quad (4.2.20)$$

where

$$B_{\mu\nu} = \partial_\mu B_\nu - \partial_\nu B_\mu \quad (4.2.21)$$

and

$$G_{\mu\nu}^j = \partial_\mu W_\nu^j - \partial_\nu W_\mu^j + g\epsilon^{jkl}W_\mu^k W_\nu^l. \quad (4.2.22)$$

The photon was chosen so that the theory remained invariant under transformations generated by  $\frac{1}{2}(I + \tau_3)$  which for  $\phi^+, \phi^0$  would be the usual electromagnetic gauge transformations. To check what happens to the photon under this transformation we must set  $\theta^1(x) = \theta^2(x) = 0$  and  $\theta^3(x) = \theta(x)$  in (4.2.3).

For the infinitesimal case, from (4.2.6),

$$\begin{aligned} \delta B_\mu &= \frac{1}{g'} \partial_\mu \theta(x) \\ \delta W_\mu^3 &= \frac{1}{g} \partial_\mu \theta(x) \end{aligned}$$

which via (4.2.8), gives for the photon field

$$\delta A_\mu = \left( \frac{\cos \theta_W}{g'} + \frac{\sin \theta_W}{g} \right) \partial_\mu \theta(x).$$

Using (4.2.10) and (4.2.12) we then have

$$\delta A_\mu = \frac{1}{e} \partial_\mu \theta(x) \quad (4.2.23)$$

as desired.

### 4.2.3 Coupling of the gauge bosons to the leptons

We consider now that part of the Lagrangian containing the leptons and their interactions with the gauge fields. We consider just the electron  $e$  and its neutrino  $\nu_e$ . Analogous statements hold for the muon  $\mu$  and its neutrino  $\nu_\mu$  and for the heavy electron  $\tau$  and its neutrino  $\nu_\tau$ .

In so far as the weak interactions are concerned, we believe that only the left-handed parts  $e_L$  and  $\nu_{e_L}$  are involved. The simplest way to get

the correct coupling structure for the gauge bosons is to take the doublet of fields

$$\mathbf{L} \equiv \begin{pmatrix} \nu_e \\ e \end{pmatrix}_{\text{left-hand part}}$$

and assume that it transforms under our  $SU(2)$  gauge transformations as

$$\mathbf{L} \rightarrow \mathbf{L}' = e^{-i\tau \cdot \theta(x)/2} \mathbf{L}. \quad (4.2.24)$$

Under  $U(1)$ , however, we take

$$\mathbf{L} \rightarrow \mathbf{L}' = e^{i\theta(x)/2} \mathbf{L}, \quad (4.2.25)$$

i.e. with opposite phase to the  $\phi$  case. If we don't, we end up with the photon coupled to neutrinos.

Since we have already determined how  $W_\mu$  and  $B_\mu$  transform under these gauge transformations, the gauge invariant coupling to the left-handed leptons is now fixed. One must have

$$\mathcal{L}_{GB-L} = \bar{\mathbf{L}} i \gamma^\mu \left( \partial_\mu - \frac{1}{2} i g' B_\mu + \frac{1}{2} i g \boldsymbol{\tau} \cdot \mathbf{W}_\mu \right) \mathbf{L}. \quad (4.2.26)$$

The structure involving  $B_\mu$  and  $W_\mu$  is like it was in  $\mathcal{L}_{GB-S}$  except for  $g' \rightarrow -g'$  and can be rewritten in terms of  $W_\mu^\pm$ ,  $Z_\mu$  and  $A_\mu$  as

$$\begin{aligned} & -e \bar{\mathbf{L}} \gamma^\mu \left[ \frac{1}{2} (\tau_3 - I) A_\mu - \frac{1}{2} (\tan \theta_W I + \cot \theta_W \tau_3) Z_\mu \right] \mathbf{L} \\ & - \frac{g}{\sqrt{2}} \bar{\mathbf{L}} \gamma^\mu (W_\mu^+ \tau_+ + W_\mu^- \tau_-) \mathbf{L} \end{aligned} \quad (4.2.27)$$

where

$$\tau_\pm = \frac{1}{2} (\tau_1 \pm i \tau_2). \quad (4.2.28)$$

Consider first the term involving the charged  $W$ . It is of the form

$$- \frac{g}{2\sqrt{2}} \ell^\mu W_\mu^- + \text{h.c.}, \quad (4.2.29)$$

where  $\ell^\mu$  is the weak leptonic current discussed in Section 1.2. (The extra factor of 2 in the denominator emerges because (4.2.27) is written in terms of  $\mathbf{L}$  and  $\bar{\mathbf{L}}$ .)

Comparing (4.2.29) with (2.1.5) we see that  $g/2\sqrt{2} = g_W$  and, therefore, from (2.1.8), follows the important relation

$$\frac{g^2}{8M_W^2} = \frac{G}{\sqrt{2}} \quad (4.2.30)$$

which connects the low energy content of the SM to the old Fermi theory, at least to lowest order.

Note that (4.2.15) now gives for the vacuum value of  $\phi^0$ :

$$v^2 = \frac{1}{\sqrt{2}G}. \quad (4.2.31)$$

If we now express everything in terms of  $\sin \theta_W$  and the fine structure constant  $\alpha = e^2/4\pi$ , we have from (4.2.30)

$$M_W = \frac{e}{2 \sin \theta_W} \frac{1}{(\sqrt{2}G)^{\frac{1}{2}}} = \left( \frac{\pi \alpha}{\sqrt{2}G} \right)^{\frac{1}{2}} \frac{1}{\sin \theta_W} \equiv \frac{A}{\sin \theta_W}. \quad (4.2.32)$$

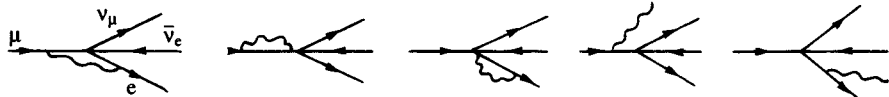
Later, when we come to consider more refined tests of the SM, it will be important to have a precise value for  $G$  (or  $A$ ).

To this end,  $G$  is *defined* from the very accurate measurement of the muon lifetime ( $\mu^- \rightarrow e^- + \bar{\nu}_e + \nu_\mu$ ; for this reason it is sometimes labelled  $G_\mu$ ) by taking into account the electromagnetic corrections to muon decay, in the Fermi model, using the formula (Behrends *et al.*, 1956; Kinoshita and Sirlin 1959):

$$\frac{1}{\tau_\mu} \equiv \frac{G^2 m_\mu^5}{192\pi^3} f \left( \frac{m_e^2}{m_\mu^2} \right) \left[ 1 + \frac{\alpha(m_\mu^2)}{2\pi} \left( \frac{25}{4} - \pi^2 \right) \right] \quad (4.2.33)$$

where  $f(x) = 1 - 8x + 8x^3 - x^4 - 12x^2 \ln x$  comes from integration over phase space and would vanish if  $m_e$  were equal to  $m_\mu$ .

If we limit ourselves to just the lowest order QED corrections to the Fermi four-point interaction



the result is

$$\frac{1}{\tau_\mu} = \frac{G^2 m_\mu^5}{192\pi^3} f(x) \left[ 1 + \frac{\alpha}{2\pi} \left( \frac{25}{4} - \pi^2 \right) \right]$$

The leading second order correction is obtained by replacing  $\alpha$  by  $\alpha(m_\mu^2)$  to get (4.2.33) where

$$\alpha(m_\mu^2) = \alpha \left[ 1 + \frac{2\alpha}{3\pi} \ln \left( \frac{m_\mu}{m_e} \right) \right] \simeq \frac{1}{136}.$$

Differently stated, the fine structure constant is altered by radiative corrections and  $\alpha(m_\mu^2)$  is the effective electromagnetic coupling at the  $\mu$  mass.

This concept is explained in detail in Chapters 20 and 21.

Eqn (4.2.33) is used as the defining equation for  $G$ , in terms of the experimental  $\mu$  lifetime.

The very precise measurement of the muon lifetime (Particle Data Group, 1992) gives

$$G = 1.166389 \text{ (22)} \times 10^{-5} \text{ GeV}^{-2}. \quad (4.2.34)$$

From (4.2.32, 34) we have

$$A \equiv \left( \frac{\pi\alpha}{\sqrt{2}G} \right)^{\frac{1}{2}} = (37.2802 \pm 0.0003) \text{ GeV}. \quad (4.2.35)$$

If in eqn (4.2.32) we use the minimal Higgs relation (4.2.17)  $\cos\theta_W = M_W/M_Z$  to eliminate  $M_W$  we see that after  $M_Z$  has been specified,  $M_W$  and  $\sin^2\theta_W$  are also fixed, by the muon lifetime, i.e.

$$\sin^2\theta_W = \frac{1}{2} \left[ 1 - \left( 1 - \frac{4A^2}{M_Z^2} \right)^{\frac{1}{2}} \right] \quad (4.2.36)$$

and

$$M_W^2 = \frac{M_Z^2}{2} \left[ 1 + \left( 1 - \frac{4A^2}{M_Z^2} \right)^{\frac{1}{2}} \right]. \quad (4.2.37)$$

The interpretation of these equations when higher order electroweak perturbative effects are included is rather subtle and will be discussed in Section 7.1.

From (4.2.31) and (4.2.34), incidentally, we have the Higgs vacuum expectation value

$$v = (\sqrt{2}G)^{-\frac{1}{2}} = 246.2186 \text{ (16)} \text{ GeV}. \quad (4.2.38)$$

From (4.2.32) we see that the mass of the  $W$  must be very large, at least  $37 \text{ GeV}/c^2$ , and via (4.2.17) that the  $Z^0$  must be even heavier

$$M_Z \simeq \frac{37}{\sin\theta_W \cos\theta_W} = \frac{74}{\sin 2\theta_W}, \quad (4.2.39)$$

i.e.  $M_Z \geq 74 \text{ GeV}/c^2$ . All this is in nice agreement with the phenomenology of the weak interactions, where, it should be remembered, we could only reproduce the Fermi point-like interaction if the intermediate  $W$  boson had very large mass.

As will be discussed later, the best estimate for  $\theta_W$  obtained by comparing experiment with lowest order calculations

$$\sin^2\theta_W \approx 0.223$$

gives

$$M_W \simeq 80 \text{ GeV}/c^2, \quad M_Z \simeq 90 \text{ GeV}/c^2,$$

which is in extraordinary agreement with what is now observed experimentally.

The SM gauge theory has now reproduced exactly the previous form of the charge changing leptonic weak interaction Lagrangian involving charged vector bosons  $W^\pm$ . But most beautifully, it has provided a relationship between the  $W$  and  $Z^0$  masses and between these and the fine structure constant in terms of the one parameter,  $\theta_W$ .

We turn now to the neutral parts of (4.2.27). Writing out the photon piece in detail gives

$$-e\bar{L}\gamma^\mu \frac{1}{2}(\tau_3 - I)\mathbf{L}A_\mu = e\bar{e}_L\gamma^\mu e_L A_\mu.$$

We see from (1.1.1) that this is *not* the correct electromagnetic coupling. There is a piece missing involving the right-hand part of the electrons, namely,

$$e\bar{e}_R\gamma^\mu e_R A_\mu. \quad (4.2.40)$$

The simplest way to get such a term in  $\mathcal{L}$  is to allow a coupling of just  $B_\mu$  with  $R \equiv e_R$ , i.e. to utilize a singlet under the  $SU(2)$  gauge transformations for the right-hand part of the electron.

Let us thus add a term

$$\mathcal{L}_{GB-R} = \bar{R}i\gamma^\mu(\partial_\mu - ig''B_\mu)R \quad (4.2.41)$$

and adjust  $g''$  to give the correct term (4.2.40). Note that we cannot simply make a doublet out of  $e_R$  since to the best of our knowledge there is no neutrino (as distinct from antineutrino) that is right-handed.

Substituting for  $B_\mu$  from (4.2.8) and comparing with (4.2.40) we see that we need  $g''\cos\theta_W = e$  and thus  $g'' = g'$ .

In order for (4.2.41) to be gauge invariant we are forced to take the transformation of  $R$  as

$$R \rightarrow R' = e^{i\theta(x)}R. \quad (4.2.42)$$

Note the factor of 2 in the exponent, compared with  $\mathbf{L}$  in (4.2.25). The complete interaction of the photon is

$$(\mathcal{L}_{GB-L} + \mathcal{L}_{GB-R})_{\substack{\text{photon} \\ \text{part}}} = \bar{e}i\gamma^\mu(\partial_\mu - ieA_\mu)e \quad (4.2.43)$$

as it ought to be.

One can regard the  $U(1)$  transformations as generated by *weak hypercharge*  $Y_W$

$$\psi \rightarrow \psi' = e^{-i(Y_W/2)\theta(x)}\psi$$

and the  $SU(2)$  transformations by weak isospin  $I_W$ . The particle assignments are then as shown in Table 4.1, and similarly for  $\mu^-$ ,  $\nu_\mu$ ,  $\tau^-$ ,  $\nu_\tau$ .

Table 4.1.

	$Y_W$	$I_W$	$I_{3W}$	$I_{3W} + \frac{1}{2}Y_W$
$\mathbf{L}$	-1	$\frac{1}{2}$	$\begin{cases} \nu_L & \frac{1}{2} \\ e_L^- & -\frac{1}{2} \end{cases}$	0 -1
$R$	-2	0	$e_R^-$	0 -1
$\phi$	-1	$\frac{1}{2}$	$\begin{cases} \phi^+ & \frac{1}{2} \\ \phi^0 & -\frac{1}{2} \end{cases}$	1 0

Note that the electric charge is given by

$$Q = I_{3W} + \frac{1}{2}Y_W.$$

Finally we examine the *new weak neutral current* interaction which arises as a consequence of the existence of the  $Z^0$  boson.

From (4.2.27) and (4.2.41) the complete interaction terms for the  $Z$  field contained in  $\mathcal{L}_{GB-L} + \mathcal{L}_{GB-R}$  are

$$\begin{aligned} & \frac{e}{2} \bar{\mathbf{L}} \gamma^\mu (\tan \theta_W I + \cot \theta_W \tau_3) \mathbf{L} Z_\mu - g'' \sin \theta_W \bar{R} \gamma^\mu R Z_\mu \\ &= e \tan \theta_W \left[ \frac{1}{2} \text{cosec}^2 \theta_W (\bar{\nu}_L \gamma^\mu \nu_L - \bar{e}_L \gamma^\mu e_L) + \bar{e} \gamma^\mu e \right] Z_\mu. \end{aligned}$$

It is convenient to write this as

$$\frac{e}{2 \sin \theta_W \cos \theta_W} \left\{ l_3^\mu - 2 \sin^2 \theta_W l_{\text{em}}^\mu \right\} Z_\mu, \quad (4.2.44)$$

where  $l_{\text{em}}^\mu$  is the electromagnetic current of the leptons and  $l_3^\mu$  is the third component of a triplet of leptonic weak-isospin currents (of which only the charged pieces  $l_1^\mu \pm i l_2^\mu$  played a rôle in the Fermi or Cabibbo theories):

$$\begin{aligned} l_3^\mu &= \frac{1}{2} \bar{\nu} \gamma^\mu (1 - \gamma_5) \nu - \frac{1}{2} \bar{e} \gamma^\mu (1 - \gamma_5) e \\ &= \bar{\mathbf{L}} \gamma^\mu \tau_3 \mathbf{L}. \end{aligned}$$

We can also write (4.2.44) in the useful form

$$\left( \frac{2G}{\sqrt{2}} \right)^{\frac{1}{2}} M_Z l_Z^\mu Z_\mu, \quad (4.2.45)$$

where

$$l_Z^\mu \equiv l_3^\mu - 2 \sin^2 \theta_W l_{\text{em}}^\mu. \quad (4.2.46)$$

Note the important fact that  $Z^0$  couples to the electromagnetic current of the leptons. It will thus contribute to processes like  $e^- e^- \rightarrow e^- e^-$  or

$e^- e^+ \rightarrow e^- e^+$  which were previously thought of as purely electromagnetic. There are two kinds of new contribution. The first, from the direct coupling to  $l_{em}^\mu$ , will look like heavy photon exchange and will be less important than  $\gamma$  exchange by a factor  $q^2 \tan^2 \theta_W / M_Z^2$ , where  $q$  is the momentum transfer.

For values of  $q$  in pre-LEP weak or electromagnetic interactions this is a huge suppression factor. This will no longer be so at LEP energies.

The second is more interesting since it is a parity-violating term. The theory thus predicts parity violation in processes normally thought of as electromagnetic. This term, in amplitude, is down on  $\gamma$  exchange by a factor

$$\frac{q^2}{\sin^2 \theta_W \cos^2 \theta_W} \frac{1}{M_Z^2} \simeq \left( \frac{q}{37 \text{ GeV}/c} \right)^2. \quad (4.2.47)$$

Effects arising from this have been detected and will be discussed in Chapter 10.

#### 4.2.4 Coupling of the leptons to the Higgs

We have now examined all the terms in  $\mathcal{L}$  involving the gauge bosons. But  $\mathcal{L}$  is not yet as general as it can be with the fields we are using. There cannot be any lepton mass terms to begin with since  $\bar{e}e = \bar{e}_L e_R + \bar{e}_R e_L$  is not gauge invariant (recall that  $e_R$  and  $e_L$  transform differently). However, one can have a gauge invariant interaction between the scalars and the leptons ( $L$ ):

$$\mathcal{L}_{S-L} = -G_e \left[ (\bar{L}\phi)R + \bar{R}(\phi^\dagger L) \right]. \quad (4.2.48)$$

The non-zero vacuum value of  $\phi$  which spontaneously breaks the gauge symmetry gives terms

$$\begin{aligned} & -G_e \left[ \bar{L} \begin{pmatrix} 0 \\ v/\sqrt{2} \end{pmatrix} R + \bar{R} \begin{pmatrix} 0, v/\sqrt{2} \end{pmatrix} L \right] \\ &= -\frac{G_e v}{\sqrt{2}} (\bar{e}_L e_R + \bar{e}_R e_L) \\ &= -\frac{G_e v}{\sqrt{2}} \bar{e}e, \end{aligned} \quad (4.2.49)$$

implying that the electron has acquired a mass. Thus

$$m_e = \frac{G_e v}{\sqrt{2}}. \quad (4.2.50)$$

The neutrino, because it has no  $R$  part, has remained massless.

Since  $v$  is determined (4.2.31) we see that

$$\begin{aligned} G_e &= \frac{\sqrt{2}m_e}{v} = \sqrt{2}m_e(\sqrt{2}G)^{\frac{1}{2}} \\ &\simeq 5.3 \frac{m_e}{m_p} \times 10^{-3}. \end{aligned} \quad (4.2.51)$$

If we choose our gauge so that

$$\phi = \begin{pmatrix} 0 \\ \frac{1}{\sqrt{2}}(v + H) \end{pmatrix},$$

where  $H$  is a real scalar Higgs field, then (4.2.48) gives rise to an interaction term in  $\mathcal{L}$  between the Higgs meson and the leptons:

$$-\frac{G_e}{\sqrt{2}}\bar{e}eH. \quad (4.2.52)$$

Thus the coupling is

$$\begin{aligned} g_{eH} &= \frac{G_e}{\sqrt{2}} \simeq 3.8 \frac{m_e}{m_p} \times 10^{-3} \\ &\simeq 2 \times 10^{-6}, \end{aligned} \quad (4.2.53)$$

with a similar result for muons. This coupling is extremely weak compared with the coupling of  $W$ ,  $Z^0$  or  $\gamma$  to the leptons.

Finally, let us return to the Higgs scalar coupling to the vector bosons (4.2.19) and substitute for  $v$  and  $g$ :

$$\begin{aligned} L_{H-GB} &= \frac{e^2}{4\sin^2\theta_W} \left[ \left( \frac{2\sqrt{2}}{G} \right)^{\frac{1}{2}} H + H^2 \right] \\ &\times \left( W_\mu^+ W^{\mu+\dagger} + \frac{1}{2\cos^2\theta_W} Z_\mu Z^{\mu\dagger} \right) \end{aligned} \quad (4.2.54)$$

showing that the coupling is determined once  $\theta_W$  is known.

The above exhausts our discussion of the various couplings in the SM which will enable us to calculate amplitudes at the *Born* approximation level. Going to higher order in perturbation theory involves severe complications. These so-called radiative corrections will be taken up in Chapter 7 after discussing the present evidence in favour of the SM.

In Chapter 5 we shall look at the phenomenological consequences of the model in the lepton sector and its confrontation with experiment. The extension to hadrons will be dealt with in Chapter 9.

We should mention that strictly speaking the theory as presented is *not* renormalizable, despite our pretending it was so, because of a technical complication known as a *triangle anomaly*. It will turn out, surprisingly,

that the inclusion of hadrons can eliminate this difficulty, as is discussed in Section 9.5.3.

### 4.3 Discovery of $W$ and $Z^0$

Clearly, the beautiful theoretical construction that led us to the SM is poised upon the existence in nature of the  $W^\pm$  and  $Z^0$  bosons (and the Higgs, we should add). The discovery of  $W^\pm$  and  $Z^0$  in fact occurred soon after the CERN  $p\bar{p}$  collider came into operation in 1982. In order to convey the excitement that accompanied the experimental discovery of the  $W$  boson, we include here more or less verbatim the ‘Note added’ which appeared in the second printing of the first edition of the present book.

#### 4.3.1 Discovery of the $W$ boson(?)

In an almost unprecedented outburst of publicity on 20 January 1983, and for a few days thereafter, press, radio and television in many countries reported the discovery of the remarkable  $W$  particle. What they were responding to, in fact, were seminars given at CERN on Thursday 20 and Friday 21 January by the spokesman for the UA1 and UA2 experimental groups which were beginning to identify events which looked convincingly as if they had arisen from the production of a  $W$  followed by its almost instantaneous decay into an  $e\nu$  pair. The submitted title-pages of the publications from these groups, announcing their results, are nice examples of scientific reticence/integrity in the face of the temptation for the spectacular, and are worthy of reproduction, as shown in Figs. 4.1 and 4.2.

In a sense the discovery of the  $W$  was quite expected, and its existence has been taken for granted throughout this book [the first edition]. Nonetheless the present luminosity of the CERN  $\bar{p}p$  collider is still well below its design specification of  $10^{30} \text{ cm}^{-2} \text{ s}^{-1}$ , and the events that have been interpreted as  $Ws$  have emerged from some  $10^9 \bar{p}p$  collisions collected in a 30 day data-taking period between November and December 1982—a formidable achievement.

Without going into detail, the experimental technique consists of (i) detecting events which contain a very high energy electron moving more or less transversely to the axis of the colliding  $p\bar{p}$  beams, (ii) searching for events where there is no observed flow of energy transversely, to balance the momentum of the fast

EUROPEAN ORGANIZATION FOR NUCLEAR RESEARCH

CERN-EP/83-13  
21 January 1983EXPERIMENTAL OBSERVATION OF ISOLATED LARGE TRANSVERSE ENERGY ELECTRONSWITH ASSOCIATED MISSING ENERGY AT  $\sqrt{s} = 540 \text{ GeV}$ UA1 Collaboration, CERN, Geneva, Switzerland

Aachen<sup>1</sup>-Annecy (LAPP)<sup>2</sup>-Birmingham<sup>3</sup>-CERN<sup>4</sup>-Helsinki<sup>5</sup>-Queen Mary College, London<sup>6</sup>-Paris<sup>7</sup>  
 (Coll. de France<sup>7</sup>-Riverside<sup>8</sup>-Roma<sup>9</sup>-Rutherford Appleton Lab.<sup>10</sup>-Saclay (CEN)<sup>11</sup>  
 Vienna<sup>12</sup> Collaboration

G. Arnison<sup>10</sup>, A. Astbury<sup>10</sup>, B. Aubert<sup>2</sup>, C. Bacci<sup>9</sup>, G. Bauer<sup>\*\*</sup>, A. Bézeguet<sup>4</sup>,  
 R. Böck<sup>4</sup>, T.J.V. Bowcock<sup>3</sup>, M. Calvetti<sup>4</sup>, T. Carroll<sup>4</sup>, P. Catz<sup>2</sup>, P. Cennini<sup>4</sup>  
 S. Centro<sup>4</sup>, F. Ceradini<sup>4</sup>, S. Cittolin<sup>4</sup>, D. Cline<sup>\*\*</sup>, C. Cochet<sup>11</sup>, J. Coles<sup>2</sup>  
 M. Corden<sup>2</sup>, D. Dallman<sup>4</sup>, M. DeBeer<sup>11</sup>, M. Della Negra<sup>2</sup>, M. Demoulin<sup>4</sup>  
 D Denegr<sup>11</sup>, A. Di Ciaccio<sup>9</sup>, D. DiBitonto<sup>4</sup>, L. Dobrzynski<sup>7</sup>, J.D. Dowell<sup>3</sup>, M. Edwards<sup>5</sup>,  
 K. Eggert<sup>1</sup>, E. Eisenhandler<sup>6</sup>, N. Ellis<sup>4</sup>, P. Erhard<sup>1</sup>, H. Faissner<sup>1</sup>, G. Fontaine<sup>7</sup>,  
 R. Frey<sup>8</sup>, R. Früwirth<sup>12</sup>, J. Garvey<sup>3</sup>, S. Geer<sup>7</sup>, C. Chesquiére<sup>7</sup>,  
 P. Chez<sup>2</sup>, K.L. Giboni<sup>1</sup>, W.K. Gibson<sup>6</sup>, Y. Giraud-Héraud<sup>7</sup>, A. Givernaud<sup>11</sup>  
 A. Gonidec<sup>3</sup>, G. Grayer<sup>10</sup>, P. Gutierrez<sup>8</sup>, T. Hansl-Kozanecka<sup>1</sup>,  
 W.J. Haynes<sup>10</sup>, L.O. Hertzberger<sup>\*</sup>, C. Hodges<sup>8</sup>, D. Hoffmann<sup>1</sup>, H. Hoffmann<sup>4</sup>,  
 D.J. Holthuizen<sup>\*</sup>, R.J. Homer<sup>3</sup>, A. Honma<sup>6</sup>, W. Jenk<sup>6</sup>, G. Jorat<sup>4</sup>, P.I.P. Kalmus<sup>6</sup>,  
 V. Karimski<sup>5</sup>, R. Keeler<sup>6</sup>, I. Kenyon<sup>3</sup>, A. Kernan<sup>8</sup>, R. Kinnunen<sup>8</sup>, H. Kowalski<sup>4</sup>,  
 W. Kozanecki<sup>6</sup>, D. Kryz<sup>4</sup>, F. Lacava<sup>4</sup>, J.-P. Laugier<sup>11</sup>, J.-P. Lees<sup>6</sup>, H. Lehmann<sup>1</sup>,  
 K. Leuchs<sup>1</sup>, A. Lévéque<sup>11</sup>, D. Linglin<sup>2</sup>, E. Locci<sup>11</sup>, J.-J. Melosse<sup>11</sup>,  
 T. Markiewicz<sup>4</sup>, G. Maurin<sup>4</sup>, T. McMahon<sup>3</sup>, J.-P. Mendiburu<sup>7</sup>, M.-N. Minard<sup>2</sup>,  
 M. Moricca<sup>8</sup>, H. Muirhead, F. Muller<sup>4</sup>, A.K. Nandi<sup>10</sup>, L. Naumann<sup>9</sup>, A. Norton<sup>4</sup>  
 A. Orkin-Lecourtois<sup>7</sup>, L. Paoluzi<sup>9</sup>, G. Petrucci<sup>9</sup>, G. Piano Mortari<sup>9</sup>, M. Pimiä<sup>5</sup>  
 A. Placci<sup>4</sup>, E. Radermacher<sup>1</sup>, J. Ransdell<sup>8</sup>, H. Reithler<sup>1</sup>, J.-P. Revol<sup>4</sup>, J. Rich<sup>11</sup>,  
 M. Rijssenbeek<sup>4</sup>, C. Roberts<sup>10</sup>, J. Rohlf<sup>4</sup>, P. Kossi<sup>9</sup>, C. Rubbia<sup>4</sup>, B. Sadoulet<sup>4</sup>,  
 G. Sajot<sup>6</sup>, G. Salvi<sup>6</sup>, G. Salvini<sup>9</sup>, J. Sass<sup>11</sup>, J. Saudraix<sup>11</sup>, A. Savoy-Bavarro<sup>11</sup>,  
 D. Schinzel<sup>2</sup>, W. Scott<sup>10</sup>, T.P. Shah<sup>10</sup>, M. Spiro<sup>11</sup>, J. Strauss<sup>11</sup>, K. Sumorok<sup>9</sup>,  
 F. Szoncs<sup>11</sup>, D. Smith<sup>6</sup>, C. Tao<sup>4</sup>, G. Thompson<sup>6</sup>, J. Timmer<sup>4</sup>, E. Tscheslog<sup>1</sup>,  
 J. Tuominen<sup>8</sup>, S. Van der Meer<sup>4</sup>, J.-P. Vielle<sup>4</sup>, J. Vrama<sup>7</sup>, V. Vuillemin<sup>4</sup>,  
 H.D. Wahl<sup>12</sup>, P. Watkins<sup>2</sup>, J. Wilson<sup>2</sup>, G.Y. Xie<sup>4</sup>, M. Yvert<sup>2</sup>, E. Zurtluh<sup>4</sup>

Submitted to Physics Letters B

<sup>\*</sup> NIKHEF, Amsterdam, The Netherlands<sup>\*\*</sup> University of Wisconsin Madison, Wisconsin, USAABSTRACT

We report the results of two searches made on data recorded at the CERN SPS Proton-Antiproton Collider: one for isolated large- $E_T$  electrons, the other for large- $E_T$  neutrinos using the technique of missing transverse energy. Both searches converge to the same events, which have the signature of a two-body decay of a particle of mass  $\sim 80 \text{ GeV}/c^2$ . The topology as well as the number of events fits well the hypothesis that they are produced by the process  $\bar{p} + p \rightarrow W^\pm + X$ , with  $W^\pm \rightarrow e^\pm + \nu$ ; where  $W^\pm$  is the Intermediate Vector Boson postulated by the unified theory of weak and electromagnetic interactions.

Fig. 4.1. UA1 (1983), 'Experimental observation of isolated larger transverse energy electrons with associated missing energy at  $\sqrt{s} = 540 \text{ GeV}$ '.

EUROPEAN ORGANIZATION FOR NUCLEAR RESEARCH

CERN-EP/83-25  
February 15th 1983OBSERVATION OF SINGLE ISOLATED ELECTRONS  
OF HIGH TRANSVERSE MOMENTUM IN EVENTS WITH  
MISSING TRANSVERSE ENERGY AT THE CERN $\bar{p}p$  COLLIDER

The UA2 Collaboration.

M. Banner<sup>(f)</sup>, R. Battiston<sup>\*;f</sup>, Ph. Bloch<sup>(f)</sup>, F. Bonaudi<sup>(b)</sup>, K. Borer<sup>(a)</sup>  
 M. Borghini<sup>(b)</sup>, J.-C. Chollet<sup>(d)</sup>, A.G. Clark<sup>(b)</sup>, C. Conta<sup>(a)</sup>, P. Darriulat<sup>(b)</sup>,  
 L. Di Lella<sup>(b)</sup>, J. Dines-Hansen<sup>(c)</sup>, P.-A. Dorsaz<sup>(d)</sup>, L. Fayard<sup>(d)</sup>, M. Frernali<sup>(e)</sup>,  
 D. Froidevaux<sup>(b)</sup>, J.-M. Gaillard<sup>(d)</sup>, O. Gildemeister<sup>(b)</sup>, V.G. Goggi<sup>(e)</sup>, H. Grote<sup>(b)</sup>,  
 B. Hahn<sup>(a)</sup>, H. Hänni<sup>(a)</sup>, J.R. Hansen<sup>(b)</sup>, P. Hansen<sup>(c)</sup>, T. Himel<sup>(b)</sup>, V. Hungerbühler<sup>(b)</sup>,  
 P. Jenni<sup>(b)</sup>, O. Kofoed-Hansen<sup>(c)</sup>, E. Lancon<sup>(f)</sup>, M. Livan<sup>(b;e)</sup>, S. Loucas<sup>(f)</sup>,  
 B. Madsen<sup>(c)</sup>, P. Mani<sup>(a)</sup>, B. Mansoulié<sup>(f)</sup>, G.C. Mantovani<sup>\*</sup>, L. Mapelli<sup>(b)</sup>,  
 B. Merkel<sup>(d)</sup>, M. Mermikides<sup>(b)</sup>, R. Møllerud<sup>(c)</sup>, B. Nilsson<sup>(c)</sup>, C. Onions<sup>(b)</sup>,  
 G. Parrou<sup>(b;d)</sup>, F. Pastore<sup>(b;e)</sup>, H. Plotnow-Besch<sup>(b;d)</sup>, M. Polverel<sup>(f)</sup>,  
 J-P. Repellin<sup>(d)</sup>, A. Rothenberg<sup>(b)</sup>, A. Roussarie<sup>(f)</sup>, G. Sauvage<sup>(d)</sup>, J. Schacher<sup>(a)</sup>,  
 J.L. Siegrist<sup>(b)</sup>, H.M. Steiner<sup>(b)</sup>, G. Stimpfl<sup>(b)</sup>, F. Stocker<sup>(a)</sup>, J. Teiger<sup>(f)</sup>,  
 V. Vercesi<sup>(e)</sup>, A. Weidberg<sup>(b)</sup>, H. Zaccone<sup>(f)</sup> and W. Zeller<sup>(a)</sup>.

a) Laboratorium für Hochenergie Physik, Universität Bern, Sidlerstrasse 5, Bern, Switzerland.

b) CERN, 1211 Geneva 23, Switzerland.

c) Niels Bohr Institute, Blegdamsvej 17, Copenhagen, Denmark.

d) Laboratoire de l'Accélérateur Linéaire, Université de Paris-Sud, Orsay, France.

e) Dipartimento di Fisica Nuclare e Teorica, Università di Pavia and INFN,

Sezione di Pavia, Via Bassi 6, Pavia, Italy.

f) Centre d'Etudes Nucléaires de Saclay.

\* Gruppo INFN del Dipartimento di Fisica dell'Università di Perugia (Italy),

† On leave from Dept. of Physics, University of California, Berkeley.

f Also at Scuola Normale Superiore, Pisa, Italy.

Submitted to Physics Letters B

ABSTRACT

We report the results of a search for single isolated electrons of high transverse momentum at the CERN  $\bar{p}p$  collider. Above 15 GeV/c, four events are found having large missing transverse energy along a direction opposite in azimuth to that of the high  $p_T$  electron. Both the configuration of the events and their number are consistent with the expectations from the process  $\bar{p} + p \rightarrow W^\pm + \text{anything}$ , with  $W \rightarrow e + \nu$ , where  $W^\pm$  is the charged Intermediate Vector Boson postulated by the unified electroweak theory.

Fig. 4.2. UA2 (1983), 'Observation of single isolated electrons of high transverse momentum in events with missing transverse energy at the CERN  $\bar{p}p$  collider'.

electron. The imbalance of momentum flow is then attributed to an (unseen) neutrino coming from the decay  $W \rightarrow e\nu$ . At the time of writing a total of some ten events have been seen, in rough agreement with the cross-section estimates.

Analysis of muon events is under way and many more candidates for  $W$  production are expected within the next few months.

There is now an air of excitement about the possibility of seeing the  $Z^0$  boson as well. The  $Z^0$  decay into  $e^+e^-$  or  $\mu^+\mu^-$  will be dramatic, with a quite unequivocal signal.

Using the couplings listed and allowing for the different probabilities for finding the combinations of quark–antiquark pairs in the proton and antiproton needed to form  $Ws$ , and  $Z^0s$ , one arrives at the estimate that roughly one  $Z^0$  should be produced for every ten  $Ws$  in the above experiments. There will be a long experimental run during March–May 1983, so expectations are high that the  $Z^0$  will soon reveal itself.

The discovery of these massive (one is almost tempted to say unnatural!) particles, whose whole existence is tied to the beautiful unification of the weak and electromagnetic interactions, must rank as one of the most remarkable discoveries in twentieth-century science. Indeed there is a striking parallel between this and the experimental discovery by Hertz, a century ago, of electromagnetic radiation—the last step in validating Maxwell's brilliant unification of electricity and magnetism.

As will appear in the following (see Chapter 11 for the discoveries of the  $J/\Psi$  and of the  $\Upsilon$ ), there is a certain trend in the discovery of new particles. Several, in recent years, were first found at hadronic machines and then their accurate study was carried out at  $e^+e^-$  colliders. Thus, soon after the  $W^\pm$ , the  $Z^0$  was discovered at the CERN  $p\bar{p}$  collider by the UA1 and UA2 collaborations. Subsequently, these particles were also studied by CDF at the Tevatron  $p\bar{p}$  collider (Fermilab). More recently, the coming into operation of the new  $e^+e^-$  machines, SLC (SLAC) and, most especially, LEP 1 (CERN) have given the  $Z^0$  parameters with a precision conceivable only at  $e^+e^-$  machines (see Chapter 8).

# 5

## Lowest order tests of the SM in the leptonic sector

In order to avoid complications due to the strong interactions we shall at first study the phenomenological consequences of the SM in the leptonic sector. We work to lowest order (Born approximation) and seek to test the theory by comparing its predictions with as many different reactions as possible.

### 5.1 Phenomenology of purely leptonic reactions

The standard model, the simple and beautiful gauge theory that unites weak and electromagnetic interactions, was developed in Section 4.2 only as far as the inclusion of leptons was concerned. Even in the limited realm of purely leptonic reactions it has a rich and predictive structure which we shall here confront with experiment.

Let us write out in detail the relevant parts of the Lagrangian for these reactions. From (4.2.27) and (4.2.44) we have

- Charged weak leptonic interaction:

$$-\frac{e}{2\sqrt{2}\sin\theta_W} \left\{ \bar{\nu}_e \gamma^\mu (1 - \gamma_5) e W_\mu^+ + \bar{e} \gamma^\mu (1 - \gamma_5) \nu_e W_\mu^- \right. \\ \left. + \mu \text{ terms} + \tau \text{ terms} \right\} \quad (5.1.1)$$

It will be useful to remember that in order to yield the correct  $\mu$  lifetime in lowest order one requires [see (4.2.30)]

$$\frac{e}{2\sqrt{2}\sin\theta_W} = M_W \left( \frac{G}{\sqrt{2}} \right)^{\frac{1}{2}}. \quad (5.1.2)$$

- Neutral weak leptonic interaction:

$$e \left\{ \bar{e} \gamma^\mu (v_e - a_e \gamma_5) e + \frac{1}{2} \bar{\nu}_e \gamma^\mu (v_{\nu_e} - a_{\nu_e} \gamma_5) \nu_e \right. \\ \left. + \mu \text{ terms} + \tau \text{ terms} \right\} Z_\mu \quad (5.1.3)$$

where for each left-handed fermion doublet  $f_L$

$$v_f = \frac{I_{W3}^{f_L} - 2Q_f \sin^2 \theta_W}{2 \sin \theta_W \cos \theta_W} \equiv \frac{g_V^f}{2 \sin \theta_W \cos \theta_W}, \quad (5.1.4)$$

$$a_f = \frac{I_{W3}^{f_L}}{2 \sin \theta_W \cos \theta_W} \equiv \frac{g_A^f}{2 \sin \theta_W \cos \theta_W}, \quad (5.1.5)$$

where  $I_{W3}^{f_L}$  is the third component of weak isospin of the fermion left-handed doublet and  $Q_f$  the charge of the fermion  $f$ . Thus, we have

$$v_e = \frac{-1 + 4 \sin^2 \theta_W}{4 \sin \theta_W \cos \theta_W}, \quad (5.1.6)$$

$$a_e = -\frac{1}{4 \sin \theta_W \cos \theta_W}, \quad (5.1.7)$$

and

$$v_{\nu_e} = a_{\nu_e} = \frac{1}{4 \sin \theta_W \cos \theta_W}. \quad (5.1.8)$$

Because the SM has exact lepton universality, we have also

$$v_e = v_\mu = v_\tau \quad \text{and} \quad a_e = a_\mu = a_\tau. \quad (5.1.9)$$

It is sometimes more convenient to write (5.1.3) in the equivalent form

$$\begin{aligned} & \frac{e}{2 \sin \theta_W \cos \theta_W} \{ \bar{e} \gamma^\mu (g_V - g_A \gamma_5) e + \frac{1}{2} \bar{\nu}_e \gamma^\mu (1 - \gamma_5) \nu_e \\ & + \mu \text{ terms} + \tau \text{ terms} \} Z_\mu \end{aligned} \quad (5.1.10)$$

where

$$g_V \equiv g_V^e = 2 \sin^2 \theta_W - \frac{1}{2}, \quad g_A \equiv g_A^e = -\frac{1}{2}. \quad (5.1.11)$$

The reader is warned that some authors use  $v, a$  and  $g_V, g_A$  which are twice our convention which follows the standard works on the subject.

The expressions (5.1.1) and (5.1.10, 11) highlight the rôle of  $\theta_W$  in both determining the relative strengths of charged versus neutral current reactions, and in fixing the ratio of vector to axial-vector coupling of the  $Z^0$  to leptons. This rôle reflects the  $\gamma-Z^0$  mixing inherent in the electroweak unification and does not depend on choosing the minimal Higgs' mechanism to generate mass.

The above interaction Lagrangians give rise to the following Feynman diagram vertices:

(5.1.12)

$$\frac{-ie}{2\sqrt{2} \sin \theta_W} \gamma_\mu (1 - \gamma_5)$$

(5.1.13)

$$ie\gamma_\mu (v_f - a_f \gamma_5) = \frac{ie}{2 \sin \theta_W \cos \theta_W} \gamma_\mu (g_V - g_A \gamma_5)$$

(5.1.14)

$$-ieQ_f \gamma_\mu$$

The propagators are standard and are listed in Appendix 2.3. By convention all topologically similar vertices are given the same sign in a Feynman diagram. The overall sign of the diagram has to be determined by comparing the order of the fermion operators in the diagram with their normal order in the  $S$  operator. An example is worked out in Section 5.1.1.

We ignore the coupling to the Higgs meson  $H$ . The coupling is very weak, so  $H$  exchange could only be important if  $m_H$  was extremely small.

The coupling of the  $W_\mu^\pm$  was designed to agree exactly with the intermediate vector boson description of the weak interactions which in turn was designed to reproduce the highly successful four-fermion Fermi description, at least for momentum transfers such that  $q^2 \ll M_W^2$ . This implies immediately that the classical leptonic weak interaction processes such as  $\mu^- \rightarrow e^- + \bar{\nu}_e + \nu_\mu$  will be correctly described by the SM. Until very large momentum transfers are obtained, all details of the spectra, helicities etc. will agree with the Fermi result except for corrections of order  $m_\mu^2/M_W^2$ .

### 5.1.1 $\nu_e e^-$ and $\bar{\nu}_e e^-$ elastic scattering

Certain processes, which are possible in the old theory with only charged currents, will be modified by neutral current effects. The most accessible of these, although still remarkably difficult to study in practice, are:

$$\nu_e + e^- \rightarrow \nu_e + e^- \quad (A)$$

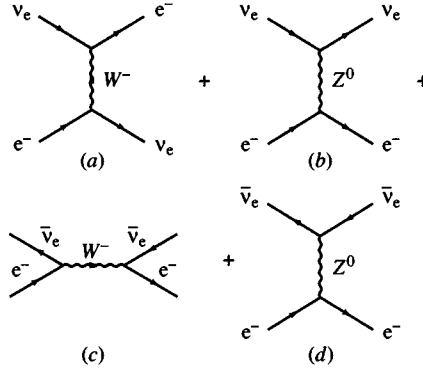


Fig. 5.1. Lowest order Feynman diagrams for neutrino–electron scattering.

and

$$\bar{\nu}_e + e^- \rightarrow \bar{\nu}_e + e^- \quad (B)$$

The lowest order Feynman diagrams for the two processes are shown in Fig. 5.1. This implies that each process gets contributions from two diagrams so that interference effects can be sought. The Feynman amplitudes are written down following the rules in Appendix 2. We label the initial and final electrons and neutrinos as  $e, e', \nu, \nu'$  respectively.

For  $\nu_e e^- \rightarrow \nu_e e^-$  we have

$$\begin{aligned} M_W^{\nu_e e^-} = & -\frac{ie^2}{8\sin^2\theta_W} [\bar{u}(e')\gamma^\mu(1-\gamma_5)u(\nu)] \\ & \times \frac{g_{\mu\nu} - q'_\mu q'_\nu/M_W^2}{(q')^2 - M_W^2} \times [\bar{u}(\nu')\gamma^\nu(1-\gamma_5)u(e)] \end{aligned} \quad (5.1.15)$$

where the momentum transfer is

$$q' = p(\nu) - p(e'). \quad (5.1.16)$$

Use of the Dirac equation shows that the  $q'_\mu q'_\nu$  term in the propagator is of order  $m_e^2/M_W^2$  and is thus completely negligible. For present-day experiments  $q'^2 \ll M_W^2$  so that

$$M_W^{\nu_e e^-} = \frac{ie^2}{8M_W^2 \sin^2\theta_W} [\bar{u}(e')\gamma^\mu(1-\gamma_5)u(\nu)][\bar{u}(\nu')\gamma_\mu(1-\gamma_5)u(e)]. \quad (5.1.17)$$

In the new generation of experiments now being planned it may be necessary to retain the  $q^2$  dependence in the denominator of the  $W$  propagator.

For later convenience we rearrange (5.1.17) using the Fierz reshuffle theorem on direct products of  $\gamma$ -matrices (see Appendix 2.7). Then

$$M_W^{\nu_e e^-} = \frac{-ie^2}{8M_W^2 \sin^2 \theta_W} [\bar{u}(e')\gamma^\mu(1 - \gamma_5)u(e)][\bar{u}(\nu')\gamma_\mu(1 - \gamma_5)u(\nu)]. \quad (5.1.18)$$

For the  $Z^0$  exchange diagram we must be careful of relative signs coming from the order of the anticommuting fermion operators, compared with the  $W$  exchange case.

Schematically, when one calculates the  $S$  matrix to second order using the SM Lagrangians, the fermion operators occur in the following order:

$$Z^0 \text{ exchange : } (\bar{\nu}_e \nu_e)(\bar{e}e) \quad (1)$$

$$W \text{ exchange : } (\bar{e}\nu_e)(\bar{\nu}_e e) \quad (2)$$

However, in order to match creation and annihilation operators in the above with those involved in the definition of the initial and final state vectors in terms of the vacuum state, i.e.

$$|\nu_e e^- \rangle \equiv a_{\nu_e}^\dagger a_e^\dagger |0\rangle$$

the order of the field operators in (1) and (2) has to be changed to  $\bar{e}\bar{\nu}_e\nu_e e$ . For  $Z^0$  exchange this involves two interchanges whereas for  $W$  exchange only one is required. Thus there is a relative minus sign and we have

$$\begin{aligned} M_Z^{\nu_e e^-} &= \frac{ie^2}{8 \sin^2 \theta_W \cos^2 \theta_W} [\bar{u}(e')\gamma^\mu(g_V - g_A \gamma_5)u(e)] \\ &\times \frac{g_{\mu\nu} - q_\mu q_\nu/M_Z^2}{q^2 - M_Z^2} [\bar{u}(\nu')\gamma^\nu(1 - \gamma_5)u(\nu)], \end{aligned} \quad (5.1.19)$$

where  $q = p(\nu) - p(\nu')$ .

Note that, neglecting the electron mass, one has

$$q^2 = -\frac{s}{2}(1 - \cos \theta), \quad q'^2 = -\frac{s}{2}(1 + \cos \theta) \quad (5.1.20)$$

where  $\sqrt{s}$  is the total CM energy and  $\theta$  is the CM scattering angle between incoming  $\nu_e$  and outgoing  $\nu'_e$ .

For  $\sqrt{s} \ll M_Z$  we combine (5.1.18) and (5.1.19) using (5.1.2) and the minimal Higgs relation (4.2.17) to get:

$$\begin{aligned} M^{\nu_e e^-} &\simeq -\frac{iG}{\sqrt{2}} [\bar{u}(e')\gamma^\mu(c_V - c_A \gamma_5)u(e)] \\ &\times [\bar{u}(\nu')\gamma_\mu(1 - \gamma_5)u(\nu)] \end{aligned} \quad (5.1.21)$$

where

$$\left. \begin{array}{l} c_V = 1 + g_V \\ c_A = 1 + g_A \end{array} \right\} \quad (5.1.22)$$

If  $c_V, c_A$  are regarded as arbitrary parameters then (5.1.21) is the matrix element for the most general mixture of  $V$  and  $A$  type coupling. In the SM  $c_V$  and  $c_A$  are fixed by (5.1.22) and (5.1.11). We have deliberately kept separate in (5.1.22) the contributions  $g_V, g_A$  coming from  $Z^0$  exchange. The old theory, without neutral currents, would have  $g_V = g_A = 0$ , i.e.  $c_V = c_A = 1$ .

Phenomenologically, it is convenient to use as variables,  $E$ , the LAB energy of the incoming neutrino, and

$$y = \frac{[p(\nu) - p(\nu')] \cdot p(e)}{p(\nu) \cdot p(e)}. \quad (5.1.23)$$

In the LAB, neglecting  $m_e/E$

$$y = \frac{E - E'}{E} = \frac{E'_R}{E}, \quad (5.1.24)$$

where  $E'_R$  is energy of the recoil electron, and thus  $y$  measures the fraction of the neutrino energy transferred to the recoil electron.

In the CM, again neglecting  $m_e/E$

$$y = \frac{1}{2}(1 - \cos\theta), \quad (5.1.25)$$

where  $\theta$  is the CM scattering angle. Note the range of  $y$ :

$$0 \leq y \leq 1.$$

Using the matrix element (5.1.21) one finds

$$\begin{aligned} \frac{d\sigma}{dy}(\nu_e e^- \rightarrow \nu_e e^-) &= \frac{2G^2 m_e E}{\pi} \left[ \left( \frac{c_V + c_A}{2} \right)^2 \right. \\ &\quad \left. + \left( \frac{c_V - c_A}{2} \right)^2 (1 - y)^2 \right], \end{aligned} \quad (5.1.26)$$

where the first term alone would survive if only charged bosons existed, and the cross-section would then be independent of  $y$ . The total cross-section is

$$\sigma(\nu_e e^- \rightarrow \nu_e e^-) = \frac{2G^2 m_e E}{\pi} \left[ \left( \frac{c_V + c_A}{2} \right)^2 + \frac{1}{3} \left( \frac{c_V - c_A}{2} \right)^2 \right]. \quad (5.1.27)$$

To get a feeling for the minute size of the cross-section note that

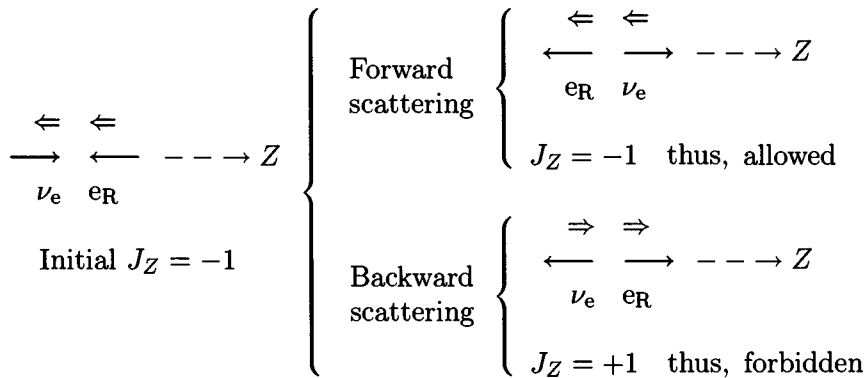
$$\frac{2G^2 m_e E}{\pi} = 1.72 \times 10^{-14} E (\text{GeV}) \text{ mb.}$$

The  $y$  dependence in (5.1.26) can be understood in simple physical terms. We can always write

$$c_V - c_A \gamma_5 = \left( \frac{c_V + c_A}{2} \right) (1 - \gamma_5) + \left( \frac{c_V - c_A}{2} \right) (1 + \gamma_5). \quad (5.1.28)$$

For a fast electron the factors  $(1 \pm \gamma_5)$  just pick out right-handed or left-handed electrons (see Section 1.3), and their contributions add incoherently in the cross-section. For  $\nu_e + e_L^- \rightarrow \nu_e + e_L^-$  we have initially helicities  $\lambda_\nu = -\frac{1}{2}, \lambda_{e_L} = -\frac{1}{2}$  and thus  $\lambda \equiv \lambda_\nu - \lambda_{e_L} = 0$ ; and finally also  $\mu \equiv \lambda_\nu - \lambda_{e'_L} = 0$ . The Jacob-Wick partial wave expansion thus involves angular functions  $d_{\lambda\mu}^J = d_{00}^J = P_J(\cos \theta)$  and there are no forward or backward angular suppression factors. On the contrary for  $\nu_e + e_R^- \rightarrow \nu_e + e_R^-$ ,  $\lambda_{e_R} = +\frac{1}{2}$ ; we have  $\lambda = -1, \mu = -1$  and thus a backward suppression factor  $\frac{1}{2}(1 + \cos \theta) = 1 - y$  in the amplitude.

The CM picture below shows how conservation of  $J_Z$  forbids backward scattering in  $\nu_e + e_R^- \rightarrow \nu_e + e_R^-$  (spin direction shown by  $\Rightarrow$  or  $\Leftarrow$ ).



For the reaction  $\bar{\nu}_e + e^- \rightarrow \bar{\nu}_e + e^-$ , since  $\lambda_{\bar{\nu}} = +\frac{1}{2}$ , there is a reversal of what is allowed or forbidden, and one finds similarly

$$\begin{aligned} \frac{d\sigma}{dy}(\bar{\nu}_e + e^- \rightarrow \bar{\nu}_e + e^-) &= \frac{2G^2 m_e E}{\pi} \left[ \left( \frac{c_V + c_A}{2} \right)^2 (1 - y)^2 \right. \\ &\quad \left. + \left( \frac{c_V - c_A}{2} \right)^2 \right] \end{aligned} \quad (5.1.29)$$

and for the total cross-section

$$\sigma(\bar{\nu}_e e^- \rightarrow \bar{\nu}_e e^-) = \frac{2G^2 m_e E}{\pi} \left[ \frac{1}{3} \left( \frac{c_V + c_A}{2} \right)^2 + \left( \frac{c_V - c_A}{2} \right)^2 \right]. \quad (5.1.30)$$

Note the important fact that if only charged  $W$ s contribute  $c_V = c_A = 1$  and we have

$$\sigma(\bar{\nu}_e e^- \rightarrow \bar{\nu}_e e^-) = \frac{1}{3} \sigma(\nu_e e^- \rightarrow \nu_e e^-). \quad (5.1.31)$$

Note also that all the above cross-sections depend on one parameter,  $\theta_W$ , only for the minimal Higgs case.

Experiments of this type are exceedingly difficult and the early data from the Savannah River detector by Reines and collaborators (see Baltay,

1978) for  $\bar{\nu}_e$  energies of a few MeV, for two ranges of electron recoil energy  $1.5 \text{ MeV} < E'_R < 3.0 \text{ MeV}$  and  $3.0 \text{ MeV} < E'_R < 4.5 \text{ MeV}$  had a large estimated error ( $\sim 30\%$ ). These data were just good enough to check that no large discrepancies existed between the old  $V - A$  charged current theory ( $c_V = c_A = 1$ )

$$\sigma^{V-A}(\bar{\nu}_e e^- \rightarrow \bar{\nu}_e e^-) = \frac{1}{3} \frac{2G^2 m_e E}{\pi} \quad (5.1.32)$$

and the lowest order SM predictions. From (5.1.30), (5.1.22) and (5.1.11) we have

$$\sigma(\bar{\nu}_e e^- \rightarrow \bar{\nu}_e e^-) = \frac{1}{3} \left( \frac{1}{4} + \sin^2 \theta_W + 4 \sin^4 \theta_W \right) \frac{2G^2 m_e E}{\pi} \quad (5.1.33)$$

which led to an early determination of  $\sin^2 \theta_W \simeq 0.29 \pm 0.05$ .

New data have in the meantime accumulated and the first direct cross-section measurement of  $\nu_e e^- \rightarrow \nu_e e^-$  was made with neutrinos of energy less than 53 MeV (Allen *et al.*, 1985). The resulting cross-section

$$\sigma(\nu_e e^-) = [8.9 \pm 3.2 \text{ (stat)} \pm 1.5 \text{ (syst)}] 10^{-42} \text{cm}^2 \cdot E_\nu(\text{GeV}) \quad (5.1.34)$$

was found to agree with the SM prediction.

Recently (Allen *et al.*, 1990) the same reaction was studied more precisely at the Meson Physics Facility (LAMPF) of the Los Alamos National Laboratory, using a beam-stop source of  $\nu_e$ . (Stopped  $\pi^+$  mesons decay into  $\mu^+$  and  $\nu_\mu$ . The  $\mu^+$  leptons are stopped and decay into  $\bar{\nu}_\mu$  and  $\nu_e$  with end-point energies of 53 MeV; the mean  $\nu_e$  energy is 31.7 MeV.)

The result is

$$\sigma(\nu_e e^-) = [9.9 \pm 1.5 \text{ (stat)} \pm 1.0 \text{ (syst)}] 10^{-42} \text{cm}^2 \cdot E_\nu(\text{GeV}) \quad (5.1.35)$$

or

$$\sigma(\nu_e e^-) = (1.15 \pm 0.21) G^2 m_e E_\nu / \pi. \quad (5.1.36)$$

We shall not compare this result directly with eqn (5.1.27) as there is a more interesting method involving combining the above with data on  $\nu_\mu e^- \rightarrow \nu_\mu e^-$ , which will be dealt with in the next section. We note in the meantime that from (5.1.27) the contribution to (5.1.36) from the charged current interaction alone is

$$\sigma(\nu_e e^-)|_{CC} = \frac{2G^2 m_e E_\nu}{\pi}. \quad (5.1.37)$$

### 5.1.2 $\nu_\mu e^-$ and $\bar{\nu}_\mu e$ elastic scattering

We now consider the interesting reactions

$$\nu_\mu + e^- \rightarrow \nu_\mu + e^-, \quad (C)$$

$$\bar{\nu}_\mu + e^- \rightarrow \bar{\nu}_\mu + e^-, \quad (D)$$

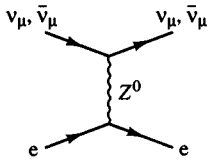


Fig. 5.2. Feynman diagram for  $\nu_\mu$  or  $\bar{\nu}_\mu$  scattering on electrons.

which are *forbidden* in the old theory since there is no charged current interaction that turns a  $\nu_\mu$  into an electron. With neutral currents both reactions can occur, via  $Z^0$  exchange (Fig. 5.2). Experiments with  $\nu_\mu$  and  $\bar{\nu}_\mu$  at accelerators are much easier than with  $\nu_e$ ,  $\bar{\nu}_e$  since the fluxes coming from the decays  $\pi$  or  $K \rightarrow \mu + \nu_\mu$  are about one hundred times larger than for  $\nu_e$ .

For this reason, much more abundant data exist on  $\nu_\mu e$  elastic scattering. We will report here the data from the CHARM detector exposed to neutrino and antineutrino wide-band beams at the CERN SPS.

The same formulae for  $d\sigma/dy$  and  $\sigma$  hold as in (5.1.26, 27, 29 and 30) with the replacement

$$c_V \rightarrow g_V; \quad c_A \rightarrow g_A \quad (5.1.38)$$

yielding to lowest order and with the minimal Higgs mechanism

$$\sigma(\nu_\mu e^-) = \frac{m_e E}{2\pi} G^2 \left[ \frac{4}{3} \sin^4 \theta_W + (-1 + 2 \sin^2 \theta_W)^2 \right], \quad (5.1.39)$$

$$\sigma(\bar{\nu}_\mu e^-) = \frac{m_e E}{2\pi} G^2 \left[ 4 \sin^4 \theta_W + \frac{1}{3} (-1 + 2 \sin^2 \theta_W)^2 \right]. \quad (5.1.40)$$

The measurements give (CHARM, 1989)

$$\sigma(\nu_\mu e^-)/E = [2.2 \pm 0.4(\text{stat}) \pm 0.4(\text{syst})] 10^{-42} \text{cm}^2/\text{GeV} \quad (5.1.41)$$

$$= [0.22 \pm 0.01] G^2 m_e / \pi$$

$$\sigma(\bar{\nu}_\mu e^-)/E = [1.6 \pm 0.3(\text{stat}) \pm 0.3(\text{syst})] 10^{-42} \text{cm}^2/\text{GeV}. \quad (5.1.42)$$

In the same paper a comparison shows consistency with all other experimental results.

A challenging test of the SM is the comparison of the results for  $\sigma(\nu_\mu e)$  above with those for  $\sigma(\nu_e e)$  given in (5.1.36). If we form the expression

$$I \equiv \frac{\pi}{G^2 m_e E} \left\{ \sigma(\nu_e e^-) - 2G^2 m_e E / \pi - \sigma(\nu_\mu e^-) \right\} \quad (5.1.43)$$

then it should be non-zero solely on account of the interference term in  $\sigma(\nu_e e)$  between the  $W$  and  $Z$  exchange diagrams in Fig. 5.1.

From (5.1.27) and (5.1.38) we find, in the SM

$$\begin{aligned} I_{\text{SM}} &= 2(g_V + g_A) \\ &= 2(2 \sin^2 \theta_W - 1). \end{aligned} \quad (5.1.44)$$

Experimentally, from (5.1.36) and (5.1.41) one obtains (Allen *et al.*, 1990)

$$I_{\text{EXPT}} = -1.07 \pm 0.15$$

yielding

$$\sin^2 \theta_W = 0.23 \pm 0.04. \quad (5.1.45)$$

We shall utilize the  $\bar{\nu}_\mu e$  data in Section 5.2.

### 5.1.3 Inverse $\mu$ -decay

Also noteworthy is the charged current  $\nu_\mu e$  interaction (or inverse  $\mu$ -decay)

$$\nu_\mu e^- \rightarrow \mu^- \nu_e \quad (5.1.46)$$

which has been measured for  $E_\nu > m_\mu^2/m_e$  (CHARM, 1989) to obtain

$$\sigma(\nu_\mu e^- \rightarrow \mu^- \nu_e)/E_\nu = [1.693 \pm 0.085(\text{stat}) \pm 0.041(\text{syst})] 10^{-41} \text{cm}^2/\text{GeV} \quad (5.1.47)$$

The cross-section is calculated from a diagram analogous to the  $W$ -exchange part of Fig. 5.1(a) and aside from tiny mass corrections yields, via (5.1.37)

$$\begin{aligned} \sigma(\nu_\mu e^- \rightarrow \mu^- \nu_e) &= \sigma(\nu_e e^- \rightarrow \nu_e e^-)|_{CC} = \frac{2G^2 m_e E_\nu}{\pi} \\ &= 1.72 \times 10^{-41} E_\nu (\text{GeV}) \text{cm}^2 \end{aligned} \quad (5.1.48)$$

in beautiful agreement with (5.1.47).

## 5.2 A check of the minimal Higgs mechanism

Up to the present we have worked purely in a theory with mass generation by the minimal Higgs mechanism, i.e. in which (4.2.17) holds:

$$\frac{M_W}{M_Z} = \cos \theta_W. \quad (5.2.1)$$

Can we check the validity of (5.2.1)?

Let us suppose that the mass generation arises from a *non-minimal* Higgs mechanism and let us define (Ross and Veltman, 1975)

$$\rho_0 \equiv \frac{M_W^2}{M_Z^2} \frac{1}{\cos^2 \theta_W}. \quad (5.2.2)$$

To lowest order accuracy a non-minimal mechanism would be signalled by finding  $\rho_0 \neq 1$ . We can, in principle, utilize the  $\nu_\mu e^- \rightarrow \nu_\mu e^-$  and  $\bar{\nu}_\mu e^- \rightarrow \bar{\nu}_\mu e^-$  reactions to test this. The formulae (5.1.39, 40) for these purely neutral current (NC) reactions utilized the relations (5.1.2) and (5.2.1). We can avoid use of these equations to write

$$\sigma(\nu_\mu e^-) = \frac{m_e E}{\pi} \left( \frac{e^2}{8 \sin^2 \theta_W \cos^2 \theta_W M_Z^2} \right)^2 \left( 1 - 4 \sin^2 \theta_W + \frac{16}{3} \sin^4 \theta_W \right), \quad (5.2.3)$$

$$\sigma(\bar{\nu}_\mu e^-) = \frac{m_e E}{3\pi} \left( \frac{e^2}{8 \sin^2 \theta_W \cos^2 \theta_W M_Z^2} \right)^2 \left( 1 - 4 \sin^2 \theta_W + 16 \sin^4 \theta_W \right). \quad (5.2.4)$$

Either by comparing these with the experimental cross-sections, using the by now accurate value of  $M_Z$ , or by taking the ratio of these cross-sections which is independent of  $M_Z$ , one measures  $\sin^2 \theta_W$  in its essential rôle as the  $\gamma-Z^0$  mixing parameter linked to the electroweak unification.

Let us call  $\sin^2 \theta_W$  measured this way  $(\sin^2 \theta_W)_{\nu_\mu e}$ . We can now check (5.2.1) by computing  $\rho_0$  using the measured boson masses and taking

$$\cos^2 \theta_W = 1 - (\sin^2 \theta_W)_{\nu_\mu e}. \quad (5.2.5)$$

Results of the CHARM II collaboration at CERN (CHARM II, 1991) yield

$$(\sin^2 \theta_W)_{\nu_\mu e} = 0.239 \pm 0.009 \pm 0.007 \quad (5.2.6)$$

from which we find

$$\rho_0 = 1.009 \pm 0.049 \quad (5.2.7)$$

perfectly consistent with the SM value  $\rho_0 = 1$ . Later, in Section 7.9, we shall see that higher order corrections alter eqns (5.2.3, 4) in such a way that  $(\cos^2 \theta_W)_{\nu_\mu e}$  is not quite equal to  $M_W^2/M_Z^2$ , thereby complicating the interpretation of the value of  $\rho_0$ .

### 5.3 Support for the SM from hadronic collider data

Historically, hadronic colliders have played a leading rôle in opening new territory. More precise exploration then follows with  $e^+e^-$  machines. The latter are considered in Chapter 8. Here, we study some of the major results that emerge from the CERN  $\bar{p}p$  Collider and the FNAL  $\bar{p}p$  Tevatron. The pioneering rôle of hadronic colliders in discovering the gauge vector mesons was mentioned in Section 4.3 and will be analysed in more detail here.

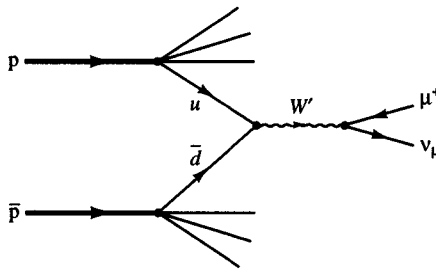


Fig. 5.3. Quark model picture of  $W^+$  production in  $\bar{p}p$  collision.

As for the future, the  $p\bar{p}$  machines presently under discussion (LHC in Europe, SSC in the USA and UNK in the former USSR) could lead to a new qualitative advancement, e.g. the testing of the gauge structure, the discovery of the Higgses and of the precise mechanism of symmetry breaking. Possibly, a new generation of  $e^+e^-$  machines (CLIC?) will then refine these findings.

### 5.3.1 $W$ production and decay in $\bar{p}p$ collisions

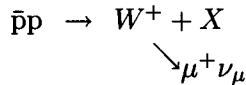
We begin by considering  $W$  production and decay in  $\bar{p}p$  collisions.

The main  $W^+$  production mechanism and its subsequent decay say into  $\mu^+\nu_\mu$  can be visualized in the quark-parton model as in Fig. 5.3. Let  $\sqrt{s}$  be the CM energy of the  $\bar{p}p$  collision. The cross-section  $\sigma^\mu(s, \hat{s})$  to produce a  $\mu^+\nu_\mu$  of invariant mass  $\sqrt{\hat{s}}$  will depend upon the elementary cross-section for  $u\bar{d} \rightarrow \mu^+\nu_\mu$ ,  $\hat{\sigma}^\mu(\hat{s})$ , multiplied by the flux of  $u$  and  $\bar{d}$  quarks per unit flux in the  $\bar{p}p$  collision. The elementary cross-section is easy to write down for  $\hat{s}$  close to  $M_W^2$  and yields a Breit-Wigner like description:

$$\hat{\sigma}^\mu(\hat{s}) = \frac{12\pi\hat{s}}{M_W^2} \frac{\Gamma_W(\mu\nu)\Gamma_W(u\bar{d})}{(\hat{s} - M_W^2)^2 + \hat{s}^2\Gamma_W^2/M_W^2} \quad (5.3.1)$$

where  $\Gamma_W$  is the total  $W$  width and  $\Gamma_W(\mu\nu)$ ,  $\Gamma_W(u\bar{d})$  the partial width for  $W^+ \rightarrow \mu^+\nu$ ,  $W^+ \rightarrow u\bar{d}$  respectively.

The cross-section  $\sigma_W^\mu(s)$  for the reaction



can be defined by integrating over all  $\mu\nu$  events with energy  $\sqrt{\hat{s}}$  lying inside the Breit-Wigner peak. However, the flux of  $u\bar{d}$  requires a knowledge of the number densities of quarks in hadrons, a subject we shall only

encounter in Chapter 16. Let us here make a very simplistic estimate of the cross-section. Let the total  $u\bar{d}$  flux be  $F$  per unit  $\bar{p}p$  flux, taken as constant across the resonance region. Then counting the number of events under the peak leads to the approximate form for the cross-section:

$$\sigma_W^\mu(s) = F \int \hat{\sigma}^\mu(\hat{s}) d\hat{s}/M_W^2.$$

Using (5.3.1) one finds

$$\begin{aligned} \sigma_W^\mu(s) &\simeq 12\pi\Gamma_W(u\bar{d})\Gamma_W(\mu\nu)\left(\frac{F}{2M_W\Gamma_W}\right)\left(\frac{\pi}{M_W^2}\right) \\ &= F \frac{6\pi^2}{M_W^3} BR(u\bar{d})BR(\mu\nu)\Gamma_W. \end{aligned} \quad (5.3.2)$$

By definition this should equal the  $W$  production cross-section  $\sigma_W(s)$  times the branching fraction for  $W^+ \rightarrow \mu^+\nu_\mu$ . Thus we obtain

$$\sigma_W(s) = F \frac{6\pi^2}{M_W^2} BR(u\bar{d}) \left(\frac{\Gamma_W}{M_W}\right). \quad (5.3.3)$$

To obtain an estimate for the branching fraction we require the partial width  $\Gamma(W \rightarrow u\bar{d})$ . As will be discussed in Chapter 9 quarks are assumed to couple to the  $W$  like the leptons (aside from the complication of Cabibbo mixing and its generalization, which we here ignore). To be precise we shall go through the calculation of  $\Gamma(W^+ \rightarrow \mu^+\nu_\mu)$  in full detail in lowest order.

Let us label the four-momenta as follows:

$$p(W) = K, p(\mu) = p \text{ with } p^2 = m_\mu^2, p(\nu) = q \text{ with } q^2 = 0.$$

The decay rate for  $W^+ \rightarrow \mu^+\nu_\mu$  in its rest frame is then given by

$$\begin{aligned} \Gamma(W^+ \rightarrow \mu^+\nu_\mu) &= \frac{1}{2M_W} \int \frac{d^3p}{(2\pi)^3 2E_\mu} \frac{d^3q}{(2\pi)^3 2E_\nu} (2\pi)^4 \\ &\times \delta(K - p - q) \overline{|M|^2}, \end{aligned} \quad (5.3.4)$$

where  $\overline{|M|^2}$  is the spin summed and averaged square of the Feynman amplitude [see (5.1.12)]

$$M = \frac{-ig}{2\sqrt{2}} \bar{u}(q)\gamma^\alpha(1 - \gamma_5)v(p)\epsilon_\alpha, \quad (5.3.5)$$

where we are abbreviating  $e/\sin\theta_W$  by  $g$  (4.2.12) and where  $\epsilon_\alpha$  is the polarization vector of the  $W$  [see (2.1.13)] and the spinor normalization is  $u^\dagger u = 2E$ .

Summing over the spins of  $\mu$  and  $\nu$  involves

$$\begin{aligned}\sum_{\text{spins}} |M|^2 &= \frac{g^2}{8} \epsilon_\alpha \epsilon_\beta^* \text{Tr} \left\{ (\not{p} + m_\mu) \gamma^\alpha (1 - \gamma_5) \not{q} \gamma^\beta (1 - \gamma_5) \right\} \\ &= \frac{g^2}{8} \epsilon_\alpha \epsilon_\beta^* \text{Tr} \left\{ \not{p} \gamma^\alpha \not{q} \gamma^\beta - \not{p} \gamma^\alpha \not{q} \gamma^\beta \gamma_5 \right\}. \end{aligned} \quad (5.3.6)$$

Averaging over the  $W$  spin involves

$$\frac{1}{3} \sum_\lambda \epsilon_\alpha^{(\lambda)} \epsilon_\beta^{(\lambda)*} = \frac{1}{3} \left( -g_{\alpha\beta} + \frac{K_\alpha K_\beta}{M_W^2} \right), \quad (5.3.7)$$

which is symmetric in  $\alpha, \beta$  (for traces consult Bjorken and Drell, 1964, Appendix A). The second term in the trace in (5.3.6) is antisymmetric in  $\alpha, \beta$ , so does not contribute. The first term yields

$$\overline{|M|^2} = \frac{g^2}{3} \left\{ p \cdot q + \frac{2(p \cdot K)(q \cdot K)}{M_W^2} \right\}. \quad (5.3.8)$$

The  $\delta$ -function in (5.3.4) ensures energy-momentum conservation, so that  $K = p + q$ . Then remembering that  $q^2 = 0$  we have

$$\left. \begin{aligned} p \cdot q &= \frac{1}{2}[(p+q)^2 - p^2] = \frac{1}{2}(M_W^2 - m_\mu^2), \\ p \cdot K &= m_\mu^2 + p \cdot q = \frac{1}{2}(M_W^2 + m_\mu^2), \\ q \cdot K &= q \cdot p. \end{aligned} \right\} \quad (5.3.9)$$

So

$$\begin{aligned}\overline{|M|^2} &= \frac{1}{3} g^2 \frac{1}{2} (M_W^2 - m_\mu^2) \left( 1 + \frac{M_W^2 + m_\mu^2}{M_W^2} \right) \\ &= \frac{1}{3} g^2 (M_W^2 - m_\mu^2) \left( 1 + \frac{m_\mu^2}{2M_W^2} \right).\end{aligned} \quad (5.3.10)$$

The integrations and other kinematic variables in (5.3.4) give a factor

$$\frac{1}{4\pi^2} \times \frac{1}{2M_W} \times \frac{1}{2} \times \frac{1}{2} \times 4\pi \times \frac{E_\nu}{M_W} = \frac{1}{16\pi M_W} \left( 1 - \frac{m_\mu^2}{M_W^2} \right).$$

Putting all this together,

$$\Gamma(W^+ \rightarrow \mu^+ \nu_\mu) = \frac{g^2}{48\pi} M_W \left( 1 - \frac{m_\mu^2}{M_W^2} \right)^2 \left( 1 + \frac{m_\mu^2}{M_W^2} \right)$$

and using  $g^2/8M_W^2 = G/\sqrt{2}$  we have finally

$$\Gamma(W^+ \rightarrow \mu^+ \nu_\mu) = \frac{G}{6\pi\sqrt{2}} M_W^3 \left( 1 - \frac{m_\mu^2}{M_W^2} \right)^2 \left( 1 + \frac{m_\mu^2}{M_W^2} \right). \quad (5.3.11)$$

Since  $M_W \gg m_\ell$  for *any* of the known leptons, we see that for any leptonic decay

$$W^+ \rightarrow \ell^+ + \nu_\ell$$

we will have

$$\begin{aligned} \Gamma(W^+ \rightarrow \ell^+ \nu_\ell) &\sim \frac{GM_W^3}{6\pi\sqrt{2}} \\ &\sim \frac{10^{-5}}{6\pi\sqrt{2}} \left(\frac{M_W}{m_p}\right)^3 m_p. \end{aligned} \quad (5.3.12)$$

For  $M_W \sim 80$  GeV/ $c^2$  this gives  $\approx 223$  MeV.

If there are many decay channels the total width  $\Gamma_W$  will satisfy

$$\Gamma_W \gg \Gamma(W^+ \rightarrow \mu^+ \nu_\mu)$$

and will therefore be very large by comparison with widths of typical hadronic resonances.

For the lifetime  $\tau_W$  we have

$$\begin{aligned} \tau_W = \frac{1}{\Gamma_W} &\ll \frac{1}{\Gamma(W^+ \rightarrow \mu\nu)} \\ &\ll 2 \times 10^{-18} \left(\frac{m_p}{M_W}\right)^3 \text{ seconds.} \end{aligned} \quad (5.3.13)$$

With  $M_W \sim 80m_p$  we see that  $\tau_W$  is exceedingly short,  $\sim 4 \times 10^{-24}$  s! So there is no possibility of seeing the track of a  $W^\pm$ .

It is believed that all decay channels of the  $W$  are analogous to the  $\mu\nu$  one, and comprise three leptonic channels and  $u\bar{d}, u\bar{s}, u\bar{b}, c\bar{d}, c\bar{s}, c\bar{b}$  (each of the latter coming in three colours). As discussed in Chapter 9 the quark couplings are flavour dependent with, for example, the sum of  $u\bar{d} + u\bar{s} + u\bar{b}$  for each colour being equal in weight to one leptonic channel. Thus we expect, aside from small effects due to phase space

$$\begin{aligned} \Gamma_W &\simeq (3 + 3 \times 2)\Gamma_W(\mu\nu) = 9\Gamma_W(\mu\nu) \\ &\simeq 2 \text{ GeV} \end{aligned} \quad (5.3.14)$$

which is not far from more accurate estimates. The  $W$  width is extremely difficult to measure and the only datum at present seems to be from  $UA(1)$ :

$$\Gamma_W = (2.8 \pm 1.4 \pm 1.3) \text{ GeV} \quad (5.3.15)$$

manifestly compatible with (5.3.14).

Returning now to our estimate of the  $W$  production cross-section, in (5.3.3) we may take  $BR(u\bar{d}) \approx \frac{1}{9}$ . For the flux  $F$  we make an extremely rough approximation: assume the proton is made up of two  $u$  quarks

and one  $d$  quark each carrying  $\frac{1}{3}$  of the proton's momentum. In that case  $\hat{s} = s/9$  so that only for  $s \approx 9M_W^2$  would there be a significant production of  $W$ s. The quarks come in three colours and only quarks of the same colour can annihilate. The probability that a particular  $\bar{q}q$  collision involves the correct colours is then  $\frac{1}{9}$  and we must sum over the colour which yields a factor of 3. Also there are two  $u$  quarks in the proton and one  $\bar{d}$  in the antiproton. Thus, very crudely, the effective flux is  $3 \times \frac{1}{9} \times 2 = \frac{2}{3}$ . Hence, using (5.3.12) in (5.3.3), we obtain

$$\sigma_W(s \approx M_W^2) \approx \frac{\pi}{3} \sqrt{2} G \approx 6 \times 10^{-33} \text{cm}^2 \quad (5.3.16)$$

which is an overestimate since, in fact, there is a considerable spread in the momentum carried by the quarks. Shown in Fig. 5.4 are results of a study of the total inclusive  $W$  production cross-section  $\sigma_W$  in  $\bar{p}p$  and  $p\bar{p}$  collisions using a more realistic assessment of the parton fluxes, as explained in Section 17.4.3 (Quigg, 1977). Note that in fact  $\sigma_W$  depends only upon the ratio  $M_W/\sqrt{s}$ . The vertical arrow corresponds to  $M_W = 80 \text{ GeV}/c^2$  and  $\sqrt{s} = 540 \text{ GeV}$  (CERN collider). Results of calculations for higher energies, relevant for LHC or SSC, are shown in Fig. 5.5 (Eichten *et al.*, 1984, 1986). The growth with  $\sqrt{s}$  comes from the increasing rôle played by the so-called ‘sea quarks’, i.e.  $\bar{q}q$  pairs moving with a very small fraction of the proton’s momentum. The larger  $\sqrt{s}$  is, the smaller this fraction can be while still making  $\sqrt{\hat{s}} \approx M_W$ . This also explains why the proton–proton and proton–antiproton cross-sections tend to become equal—the ‘sea’ is supposed to be the same in protons and antiprotons.

### 5.3.2 $\bar{p}p$ collider data

Data taken at the CERN  $\bar{p}p$  collider in the period 1981–85 were used by the *UA*(1) and *UA*(2) collaborations to determine the production cross-sections of the  $W$  and  $Z$  bosons. Later a data sample corresponding to an integrated luminosity of  $\sim 7.8 \text{ pb}^{-1}$  at  $\sqrt{s} = 630 \text{ GeV}$  was, for example, collected by the upgraded *UA*(2) detector during the 1988 and 1989 runs at peak luminosities of up to  $3 \times 10^{30} \text{ cm}^{-2} \text{s}^{-1}$ . This gave more precise values of  $W$  and  $Z$  production cross-section times branching ratios  $\sigma_W^e \equiv \sigma(\bar{p}p \rightarrow W + X) \cdot BR(W \rightarrow e\nu)$  and  $\sigma_Z^e \equiv \sigma(\bar{p}p \rightarrow Z + X) \cdot BR(Z \rightarrow e^+e^-)$  leading to meaningful comparisons with theoretical predictions [full QCD corrections to order  $O(\alpha_s)$  (Altarelli *et al.*, 1985) and partial  $O(\alpha_s^2)$  (Matsuura *et al.*, 1988a and b, 1989)].

Typical results from *UA*(1) and *UA*(2) are shown in Table 5.1 and Table 5.2. The significance of  $\rho_0$  was explained in Section 5.2, and it is expected to equal 1 for the minimal SM. It is seen that  $\rho_0$  is nicely compatible with the SM value 1.

$\sqrt{s}$ GeV	$\sigma_W^\ell$ (nb)			Mass	$\rho_0$
	546	630	$\sigma_W^\ell(630)/\sigma_W^\ell(546)$	$M_W$ (GeV)	
UA1	$\ell = e$	$0.55 \pm 0.08 \pm 0.09$	$0.63 \pm 0.04 \pm 0.09$	$1.15 \pm 0.19$	$82.7 \pm 1.0 \pm 2.7$
	$\ell = \mu$	$0.56 \pm 0.18 \pm 0.12$	$0.64 \pm 0.09 \pm 0.11$		$81.8^{+6.0}_{-5.3} \pm 2.6$
	$\ell = \tau$	$0.63 \pm 0.13 \pm 0.12$			$89 \pm 3 \pm 6$
UA2	$\ell = e$	$0.61 \pm 0.10 \pm 0.07$	$0.57 \pm 0.04 \pm 0.07$	$0.93 \pm 0.17$	$80.2 \pm 0.6 \pm 0.5 \pm 1.3$
					$1.001 \pm 0.028 \pm 0.006$

Table 5.1. Properties of the W meson [Note that  $\sigma_W^\ell = \sigma_W \cdot BR(W \rightarrow \ell\nu)$ ].

$\sqrt{s}$ GeV	$\sigma_Z^{\ell^+\ell^-}$ (nb)			Mass	Width
	546	630	$\sigma_Z(630)/\sigma_Z(546)$	$M_Z$ (GeV)	$\Gamma_Z$ (GeV)
UA1	$\ell = e$	$41^{+25}_{-17} \pm 6$	$74 \pm 14 \pm 11$	$1.8 \pm 0.9$	$93.1 \pm 1.0 \pm 3.11$
	$\ell = \mu$	$100 \pm 50 \pm 20$	$67 \pm 17 \pm 10$		$2.7^{+1.2}_{-1.0} \pm 1.3$
UA2	$\ell = e$	$116 \pm 39 \pm 11$	$73 \pm 14 \pm 7$	$0.6 \pm 0.3$	$91.5 \pm 1.2 \pm 1.7$
					$2.7 \pm 2.0 \pm 1.0$

Table 5.2. Properties of the  $Z^0$  meson [Note that  $\sigma_Z^\ell = \sigma_Z \cdot BR(Z \rightarrow \ell^+\ell^-)$ ].

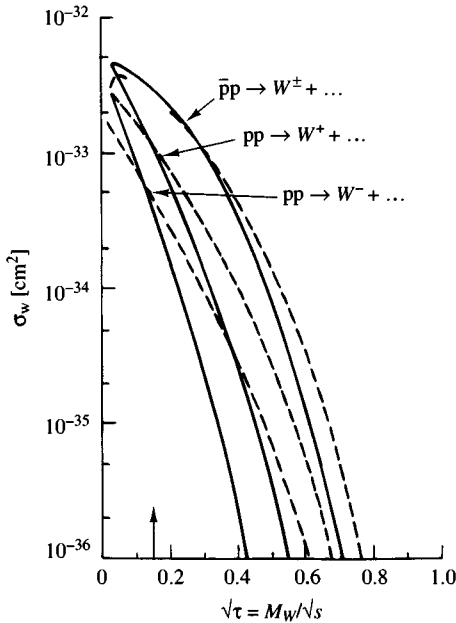


Fig. 5.4. Calculated parton model cross-sections for the production of  $W$  bosons in  $pp$  and  $\bar{p}p$  collisions. Solid and dashed lines correspond to different assumed parton distribution functions. (From Quigg, 1977.)

As for the Tevatron, in the first run (1987) with proton–antiproton beams colliding at 1.8 TeV, during a five month period, the peak luminosity reached  $1.3 \times 10^{29} \text{ cm}^{-2}\text{s}^{-1}$  and about  $70 \text{ nb}^{-1}$  of integrated luminosity was delivered to the CDF experiment. In the second run of almost a year (June 1988 to June 1989) the total integrated luminosity was  $\sim 9.6 \text{ pb}^{-1}$  with a peak luminosity of  $\sim 2 \times 10^{30} \text{ cm}^{-2}\text{s}^{-1}$ .

To reduce systematic errors (both theoretical and experimental), the ratio  $\sigma_W^e/\sigma_Z^e$  is often considered since it can be expressed in terms of simpler quantities that can be evaluated within the SM

$$\frac{\sigma_W^e}{\sigma_Z^e} = \frac{\sigma_W}{\sigma_Z} \frac{\Gamma(W \rightarrow e\nu)}{\Gamma(W)} \frac{\Gamma(Z)}{\Gamma(Z \rightarrow e^+e^-)}. \quad (5.3.17)$$

[ $\Gamma(W \rightarrow e\nu)$  was given above and  $\Gamma(Z \rightarrow e^+e^-)$  is calculated in Section 8.5.] All quantities are calculable knowing the SM parameters, the parton number densities (from which the major uncertainties arise) and the vector boson masses.

Recently the above information has been used to place limits on the number  $N_\nu$  of light neutrino generations. The  $e^+e^-$  measurements discussed in Chapter 8 have fixed the total width  $\Gamma_Z$  of the  $Z^0$  with high

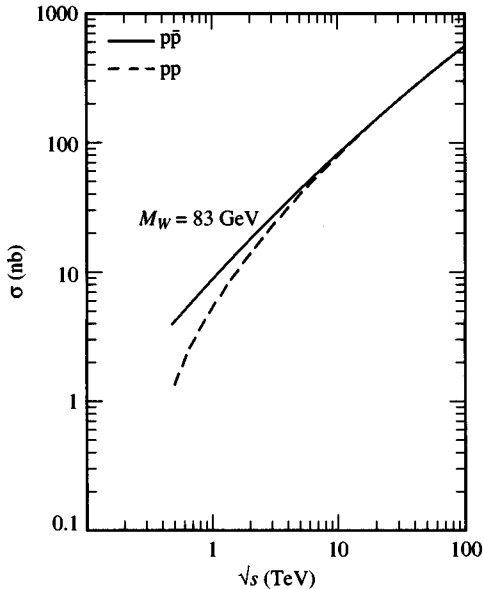


Fig. 5.5. Total cross-section for the production of  $W^+$  and  $W^-$  (for  $M_W = 83 \text{ GeV}/c^2$ ) versus centre of mass energy. The solid line is for  $\bar{p}p$  collisions and the dashed line is for  $pp$  collisions.

$M_Z(\text{GeV}/c^2)$	$M_W(\text{GeV}/c^2)$	$\Gamma_W^*(\text{GeV})$	$\sigma_W^e/\sigma_Z^e$
$Z \rightarrow e^+e^-$	$91.1 \pm 0.3 \pm 0.4$		
$Z \rightarrow \mu^+\mu^-$	$90.7 \pm 0.4 \pm 0.2$	$79.78 \pm 0.50$	$2.19 \pm 0.20$

\* This is obtained from  $\sigma_W^e/\sigma_Z^e$  using the predicted value of  $\sigma_W/\sigma_Z = 3.23 \pm 0.03$  (Martin *et al.*, 1989),  $\Gamma(W \rightarrow e\nu)/\Gamma(Z \rightarrow e^+e^-) = 2.70 \pm 0.02$  (Hollik, 1990a) and the value  $\Gamma_Z = 2.57 \pm 0.07$  measured from  $e^+e^-$  (see Chapter 8).

Table 5.3. Some Tevatron data on  $W$  and  $Z$  bosons.

precision. Thus all quantities on the right-hand side of (5.3.17) are known or calculable except  $\Gamma_W$  whose value depends upon  $N_\nu$ . Thus one evaluates the right-hand side of (5.3.17) for various assumptions about  $N_\nu$  and compares with the experimental ratio  $\sigma_W^e/\sigma_Z^e$ .

The quality of information that can be typically attained is shown in Fig. 5.6, where the measured ratio  $\sigma_W^e/\sigma_Z^e$  is compared with standard model predictions as a function of  $m_{\text{top}}$ . The predictions are very sensitive to  $m_t$  since its value will determine whether the decay channel  $W \rightarrow t\bar{b}$  is open or not. The shaded band represents the  $1\sigma$  confidence interval; the hatched region is excluded at 90% confidence level. The

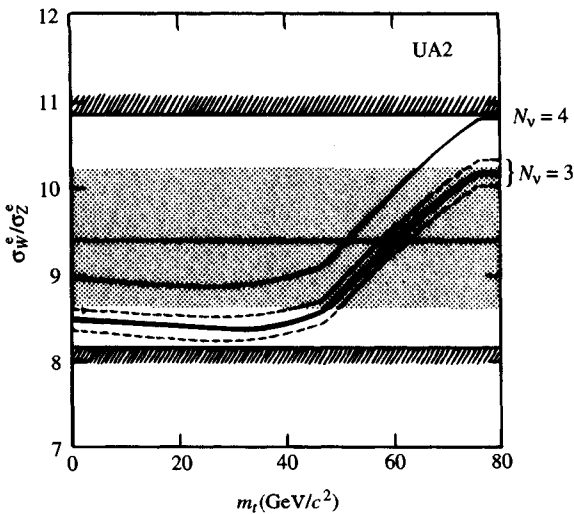


Fig. 5.6. Comparison between measured value of  $\sigma_W^e/\sigma_Z^e$  at CERN and SM predictions as function of the top mass for 3 and 4 species of neutrino. (From Eichten *et al.*, 1986.)

lower solid curve corresponds to the predicted value using the DFLM parton distribution functions by Diemoz *et al.* (1988) and assuming three light neutrinos. The thickness of this line represents the variation observed between the Born,  $o(\alpha_s)$  and  $O(\alpha_s^2)$  calculations. The upper dashed curve uses the parametrizations by Martin *et al.* (1988), while the lower dashed curve uses the parametrizations by Martin *et al.* (1989). The upper solid curve corresponds to four light neutrinos using parametrizations by Diemoz *et al.* (1988).

An analogous sample of results obtained by CDF at the Tevatron at  $\sqrt{s} = 1.8$  TeV is displayed in Table 5.3 (Kamon, 1989). In Table 5.3 the first error is statistical, the second systematic. The value for  $\Gamma_W$  is to be compared with the SM prediction  $\Gamma_W = 2.07$  GeV [obtained with  $M_W = 80$  GeV,  $\alpha_s = 0.13$  and  $m_t > M_W - m_b$ ; see also our naive estimate (5.3.14)].

Fig. 5.7 shows the CDF measurement and the relationship between the top mass and the number  $N_\nu$  of light neutrino generations. More stringent evidence that  $N_\nu = 3$  will be discussed in Chapter 8.

#### 5.4 Concluding remarks

The minimal standard model, a gauge theory with broken symmetry, constructed according to the rules studied in the previous chapters, provides a

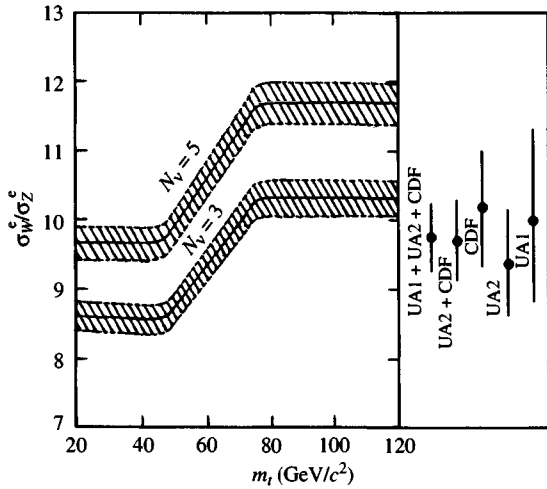


Fig. 5.7. Comparison between measured value of  $\sigma_W^e/\sigma_Z^e$  at Fermilab and SM predictions as function of the top mass for 3 and 4 species of neutrino.

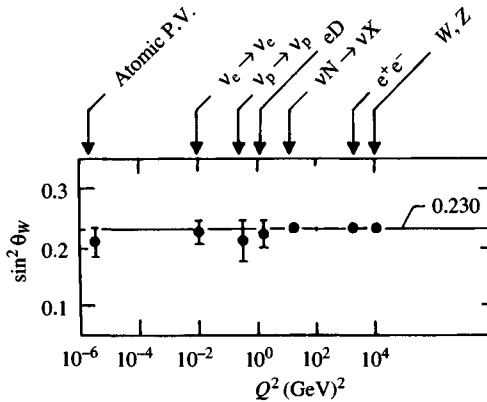


Fig. 5.8. Values of  $\sin^2 \theta_W$  from many different reactions. The relevant  $Q^2$  is indicated.

beautiful unification of the electromagnetic and weak interactions. Lowest order calculations in the leptonic sector are in excellent agreement with experiment.

If we write the various cross-section formulae (5.1.27, 30, 39 and 40) in terms of  $g_V$  and  $g_A$ , and compare with experiment we get the allowed regions for  $g_{V,A}$  shown in Fig. 8.21. This figure also shows data from LEP to be discussed in Chapter 8. Note the beautiful overlap in the region expected from electroweak theory. Using the relation (5.1.11) between

$g_V$  and  $\sin^2 \theta_W$  leads to nicely compatible values of  $\sin^2 \theta_W$  as shown in Fig. 5.8 (Langacker, 1989). (Some of the reactions indicated have not yet been discussed.)

The question of more refined tests to higher order, and of extending the theory to the hadronic sector, are dealt with in the next few chapters. The interplay between electroweak and strong forces (QCD) is discussed in Chapters 22 and 23.

# 6

## The Higgs boson

Another consequence of the standard model (SM), at least in its minimal form, is the existence of a doublet of scalar bosons  $H$ , the Higgs particles whose field was written as  $H(x)$  in earlier chapters. It is possible to have larger schemes with more than one Higgs or, alternatively, to try to produce the spontaneous symmetry breaking that gives the particles their masses by dynamical means (Weinberg, 1976a) and thus to avoid the need for the  $H$ .

It should be stressed that despite its great successes, the SM will not be proved until the Higgs boson is discovered and the symmetry breaking mechanism tested.

### 6.1 Introductory remarks

Let us recall (Section 4.2) that one of the parameters of the Higgs interaction, the coupling constant to fermions, is fixed. One has [see (4.2.52) and (4.2.53)]

$$g_{f\bar{f}H} \bar{\Psi}_f \Psi_f H \quad (6.1.1)$$

with

$$g_{f\bar{f}H} = (\sqrt{2}G)^{1/2} m_f \quad (6.1.2)$$

where the remarkable property is the proportionality to the mass of the fermion.

The Higgs mass, on the other hand, is completely arbitrary within the paradigm of the SM. In fact, there are arguments suggesting that the SM with fundamental Higgs fields cannot be the full story and that some new kind of physics must appear at a high energy scale. This is linked to the so-called ‘hierarchy problem’ and will be briefly mentioned in the next section.

The complete arbitrariness of the Higgs meson mass has many consequences. Having some idea of its mass would be instrumental in devising the proper experiment to find it, and its value influences some theoretical estimates.

In what follows we consider briefly three aspects of Higgs searches: (i) Higgs decay, (ii) Higgs production at the  $Z^0$  mass, and (iii) limits on the Higgs mass.

## 6.2 Higgs decay

The fundamental vertices for the Higgs coupling to fermions and to the weak gauge bosons are

$$\left. \begin{aligned} f &\quad \text{---} H \quad g_{f\bar{f}H} = \frac{e m_f}{2M_W \sin \theta_W}, \\ \bar{f} & \\ W^+ &\quad \text{---} H \quad g_{WWH} = \frac{e M_W}{\sin \theta_W}, \\ W^- & \\ Z^0 &\quad \text{---} H \quad g_{ZZH} = \frac{e M_Z}{\sin \theta_W \cos \theta_W}. \end{aligned} \right\} \quad (6.2.1)$$

From (5.1.2), we can rewrite  $g_{WWH} = 2(\sqrt{2}G)^{1/2}M_W^2$ . This shows that the Higgs coupling to the  $W$  is proportional to the square of the boson mass as compared with the linear dependence on the fermion mass [eqn (6.1.2)].

Because of its simple coupling, the calculation of its decay width into a fermion–antifermion pair can be carried out in an analogous fashion to the treatment of the  $W$  in Section 5.3.1; we have (Ellis *et al.*, 1976)

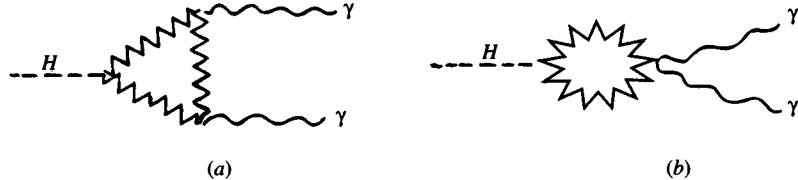
$$\Gamma(H \rightarrow f\bar{f}) = N_{cf} \frac{Gm_f^2 m_H}{4\pi\sqrt{2}} \left(1 - \frac{4m_f^2}{m_H^2}\right)^{3/2}, \quad (6.2.2)$$

where  $N_{cf}$  counts colour (3 for quarks and 1 for leptons). We also have

$$\begin{aligned} \Gamma(H \rightarrow W^+W^-) &= \frac{Gm_H^3}{8\pi\sqrt{2}} \left(1 - \frac{4M_W^2}{m_H^2}\right)^{3/2} \\ &\times \left(1 - \frac{4M_W^2}{m_H^2} + 12\frac{M_W^4}{m_H^4}\right), \end{aligned} \quad (6.2.3)$$

$$\Gamma(H \rightarrow Z^0Z^0) = \frac{1}{2}\Gamma(H \rightarrow W^+W^-)\Big|_{M_W \rightarrow M_Z}. \quad (6.2.4)$$

Another decay mode, especially relevant at LEP energies for light Higgs, is  $H \rightarrow 2\gamma$  which goes via one-loop diagrams involving  $W$  bosons, quarks and leptons:



In the above diagrams the intermediate particles in the loops will be spin 0,  $\frac{1}{2}$  and 1 in (a) and 0 and 1 in (b).

We skip the lengthy calculations and simply give the results. The  $H \rightarrow \gamma\gamma$  width is given by (Franzini *et al.*, 1989):

$$\Gamma(H \rightarrow \gamma\gamma) = \frac{G}{\sqrt{2}} \frac{m_H^3}{8\pi} \left( \frac{\alpha}{4\pi} \right)^2 \left| \sum_j e_j^2 N_{cj} F_j \right|^2 \quad (6.2.5)$$

where

$$\frac{G}{\sqrt{2}} \frac{m_H^3}{8\pi} \left( \frac{\alpha}{4\pi} \right)^2 \text{ (in GeV)} \simeq 1.0 \times 10^{-13} (m_H \text{ in GeV}/c^2)^3. \quad (6.2.6)$$

In (6.2.5) the spin 0, spin  $\frac{1}{2}$  and spin 1 contributions are

$$\left. \begin{aligned} F_0 &= \tau \left[ 1 - \tau f(\tau) \right], \\ F_{\frac{1}{2}} &= -2\tau \left[ 1 + (1-\tau)f(\tau) \right], \\ F_1 &= 2 + 3\tau + 3\tau(2-\tau)f(\tau), \end{aligned} \right\} \quad (6.2.7)$$

where  $\tau = 4m_j^2/m_H^2$  (under the assumption that the coupling of a particle to the Higgs is proportional to its mass; this is not always true for scalars in extended models).  $f(\tau)$  in (6.2.7) is a complex function given by

$$\begin{aligned} f(\tau) &= \left[ \arcsin \left( \frac{1}{\sqrt{\tau}} \right) \right]^2, \quad \tau \geq 1 \\ f(\tau) &= -\frac{1}{4} \left[ \ln \frac{1 + \sqrt{1-\tau}}{1 - \sqrt{1-\tau}} - i\pi \right]^2, \quad \tau < 1. \end{aligned}$$

In the large  $\tau$  limit

$$F_0 \rightarrow -\frac{1}{3}, \quad F_{\frac{1}{2}} \rightarrow -\frac{4}{3}, \quad F_1 \rightarrow 7 \quad (6.2.8)$$

which shows that  $W$  and fermions have opposite contributions and scalars have little relevance.

If the Higgs is light (i.e. lighter than the  $\mu$  or the  $s$  quark) the contribution of the ‘heavy’ fermions (i.e. all quarks and leptons except  $e, u$

and  $d$ ) is  $-7.11$  times (6.2.6), that is it almost exactly cancels the  $W$  contribution [7 times (6.2.6)]. In this case, the  $H \rightarrow \gamma\gamma$  channel is highly suppressed.

The Higgs decay into two gluons can be obtained from the above formulae (6.2.5–6.2.8) keeping just the quark loop contributions and replacing  $\alpha^2 e_j^4 N_{Cj}^2$  by  $2\alpha_s^2$  (note, however, that the one-loop calculation can only be trusted in this case if the Higgs is sufficiently heavy, say above  $\sim 1$  GeV, so that  $\alpha_s$  is sufficiently small). Keeping only the main contribution (coming from heavy quarks), a reasonable estimate for  $\Gamma(H \rightarrow GG)$  is then

$$\Gamma(H \rightarrow GG) \text{ (in GeV)} \simeq 1.5 \times 10^{-10} \left( m_H \text{ in } \frac{\text{GeV}}{c^2} \right)^3 (\alpha_s/0.15)^2 n_h^2 \quad (6.2.9)$$

where  $n_h$  is the number of quarks heavier than the Higgs.

A summary of all two-body (leptonic, photonic, gluonic and partonic) Higgs decay widths is shown in Fig. 6.1 (from Franzini *et al.*, 1989) where one has taken

$$\begin{aligned} m_u &= 5 \text{ MeV}/c^2, \\ m_d &= 10 \text{ MeV}/c^2, \\ m_s &= 150 \text{ MeV}/c^2, \\ m_c &= 1.5 \text{ GeV}/c^2, \\ m_b &= 5 \text{ GeV}/c^2 \quad \text{and} \quad m_t = 60 \text{ GeV}/c^2. \end{aligned}$$

For gluons (dot-dashed upper curve) the constant value  $\alpha_s = 0.15$  is used. Note that present estimates of  $m_t$  are much higher,  $\approx 130$  GeV/ $c^2$ .

In Fig. 6.2 the lifetime and full width of the Higgs versus its mass (based on the partial widths of Fig. 6.1) are shown.

It should be stressed, however, that the conversion of the partonic and gluonic widths into hadronic ones is not unambiguous and the results below 1–2 GeV/ $c^2$  are not very meaningful.

If  $m_H < 2m_\mu$  one finds for the  $H$  lifetime  $\tau_H > 10^{-12}$ s, so it would leave a detectable gap between its point of production and the point where its decay vertex is seen. For higher values of  $m_H$ ,  $\tau_H$  decreases rapidly, and no gap would be detected.

The factor  $m_f^2$  in (6.2.2) implies that decays into heavier particles would be favoured and  $H$  would appear as a small peak in the mass distribution of the pair. But the tiny production cross-section implies that a very high statistics experiment would be required.

If the  $H$  is truly very massive then the decays  $H \rightarrow W^+W^-$  or  $Z^0Z^0$  will dominate as eqns. (6.2.2)–(6.2.4) show.

QCD corrections to the previous estimates have been calculated, as they are particularly relevant in the large Higgs mass range where hadr-

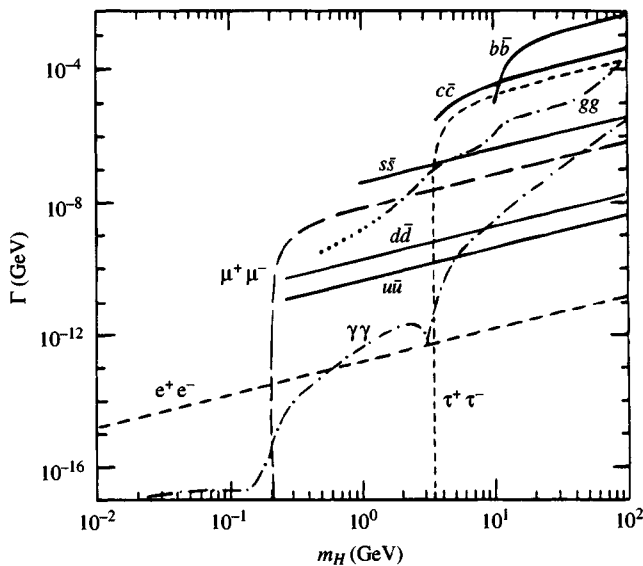


Fig. 6.1. The approximate partial decay widths of  $H$  to all two-body partonic decay modes. The dashed curves show decays to charged leptons, the solid curves the decay into hadrons as computed from the contributions to each quark separately. The dot-dashed curves illustrate the two-gluon and two-photon decays. See text.

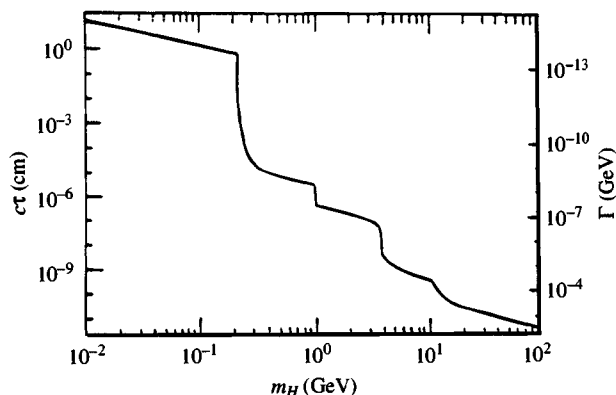


Fig. 6.2. The lifetime and width of the Higgs versus its mass taking into account the decays displayed in Fig. 6.1. The ‘jumps’ come from the imperfect treatment of the threshold, i.e. cutting off  $q\bar{q}$  decays at the quarkonium mass.

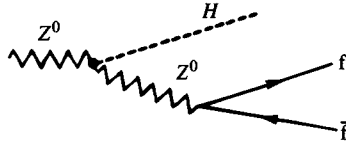
onic decays are very sizable or even dominant (Fig. 6.1; Franzini *et al.*, 1989).

### 6.3 Higgs production at the $Z^0$ mass

Assuming that  $m_H < M_Z$  a number of ‘rare’  $Z^0$  decays into Higgs particles are possible such as  $Z^0 \rightarrow H f\bar{f}$ ,  $Z^0 \rightarrow H\gamma$  or, if the Higgs is sufficiently low in mass, even  $Z^0 \rightarrow HH f\bar{f}$  etc. The rates for these decays may be rather low as compared with the dominant  $Z^0$  decays (i.e.  $Z^0 \rightarrow \ell^+\ell^-$ ,  $Z^0 \rightarrow \nu_e\bar{\nu}_e$ ,  $Z^0 \rightarrow q\bar{q}$ ) but if some  $10^7$   $Z^0$  events were collected, branching ratios as low as  $10^{-6}$  could be measured.

#### 6.3.1 $Z^0 \rightarrow H f\bar{f}$

This process is especially interesting due to the relatively large  $Z^0 Z^0 H$  coupling. The process goes via



so that detection and mass reconstruction of the Higgs may be obtained from studying the outgoing fermions and the Higgs decay products.

The differential decay rate, normalized to the decay rate  $Z^0 \rightarrow f\bar{f}$  is (Glover *et al.*, 1989)

$$\frac{1}{\Gamma(Z^0 \rightarrow f\bar{f})} \frac{d\Gamma(Z^0 \rightarrow H f\bar{f})}{dE} = \frac{\alpha M_Z^2}{\pi s_W^2 c_W^2} \times \left[ 1 - \frac{2E}{M_Z} + \frac{E^2}{3M_Z^2} + \frac{2m_H^2}{3M_Z^2} \right] \times \frac{(E^2 - m_H^2)^{\frac{1}{2}}}{(2EM_Z - m_H^2)^2 + M_Z^2 \Gamma_Z^2} \quad (6.3.1)$$

where the Higg boson energy  $E$  in the  $Z^0$  rest frame is related to the  $f\bar{f}$  invariant mass by

$$E = (M_Z^2 + m_H^2 - M_{f\bar{f}}^2)/2M_Z. \quad (6.3.2)$$

The total event rate is obtained by integrating eqn. (6.3.1) (see Berends and Kleiss, 1985).

The production rate for the Bjorken process (Bjorken, 1977)  $Z^0 \rightarrow H\mu^+\mu^-$  compared with  $Z^0 \rightarrow \mu^+\mu^-$  is shown in Fig. 6.3. This is expected to be the cleanest reaction. The corresponding number of events is shown on the right of Fig. 6.3 assuming, conservatively,  $10^6 Z^0$ s. The contributions of  $Z^0 \rightarrow H\mu^+\mu^- \rightarrow b\bar{b}\mu^+\mu^-$  (dashed curve),  $Z^0 \rightarrow H\mu^+\mu^- \rightarrow$

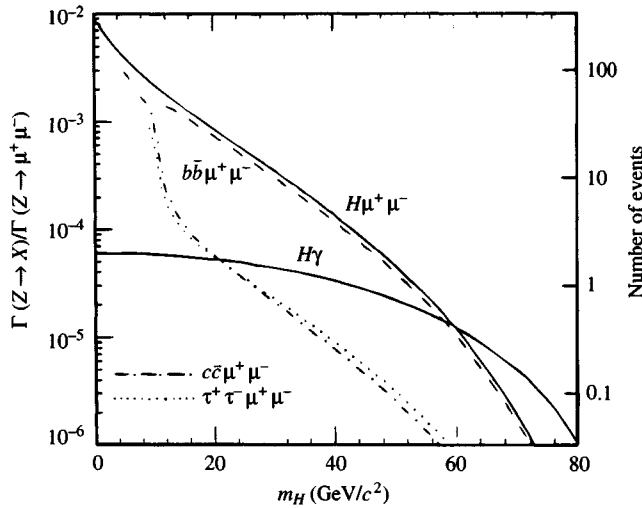


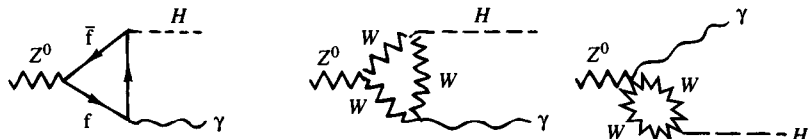
Fig. 6.3. Branching ratios for  $Z \rightarrow H\mu^+\mu^-$  and  $Z \rightarrow H\gamma$ , relative to that for  $Z \rightarrow \mu^+\mu^-$ . For  $Z \rightarrow H\mu^+\mu^-$  we give the breakdown for three two-fermion decays of the  $H$ :  $Z \rightarrow H\mu^+\mu^- \rightarrow b\bar{b}\mu^+\mu^-$  (dashed),  $Z \rightarrow H\mu^+\mu^- \rightarrow c\bar{c}\mu^+\mu^-$  (dotdashed), and  $Z \rightarrow H\mu^+\mu^- \rightarrow \tau^+\tau^-\mu^+\mu^-$  (dotted). On the right-hand axis we translate branching ratio to number of events, given  $10^6 Z^0$ s. See text.

$c\bar{c}\mu^+\mu^-$  (dot-dashed curve) and  $Z^0 \rightarrow H\mu^+\mu^- \rightarrow \tau^+\tau^-\mu^+\mu^-$  (dotted curve) are shown separately. The branching ratio  $Z^0 \rightarrow H\gamma$  is also given in Fig. 6.3 where the following parameters are used:  $\alpha(M_Z) = 1/128$ ,  $\sin^2 \theta_W = 0.23$ ,  $M_Z = 92$  GeV/ $c^2$ ,  $\Gamma_Z = 2.55$  GeV,  $\text{BR}(Z^0 \rightarrow \mu^+\mu^-) = 3.3\%$  and  $m_t = 60$  GeV/ $c^2$  (but the dependence on  $m_t$  is quite negligible).

If  $m_H$  is close to zero, the relative rate for  $Z^0 \rightarrow H\mu^+\mu^-$  can be as high as  $\sim 1\%$  of  $Z^0 \rightarrow \mu^+\mu^-$ . In order to obtain about 10 events, we need some  $10^6 Z^0$ s if  $m_H \simeq 40$  GeV/ $c^2$  or  $\sim 10^7 Z^0$ s if  $m_H \simeq 60$  GeV/ $c^2$ . For details and references see Glover *et al.* (1989).

### 6.3.2 $Z^0 \rightarrow H\gamma$

Another clean signature is expected from this reaction thanks to its outgoing monochromatic photon. The process, however, occurs only through loop diagrams of the kind



and is similar to the process  $H \rightarrow \gamma\gamma$  discussed previously in this section.

As it turns out, in this case the largest contribution comes from the  $W$  loop.

The decay rate relative to  $Z^0 \rightarrow \mu^+ \mu^-$  has been analysed by several authors (see Franzini *et al.*, 1989 for details) and can be approximately written as

$$\frac{\Gamma(Z^0 \rightarrow H\gamma)}{\Gamma(Z^0 \rightarrow \mu\mu)} \simeq 6.94 \times 10^{-5} \left(1 - \frac{m_H^2}{M_Z^2}\right)^3 \left(1 + 0.07 \frac{m_H^2}{M_Z^2}\right). \quad (6.3.3)$$

The exact result, given in Fig. 6.3, shows that even with  $10^7 Z^0$ s one ends up with about 10–20 events for light  $m_H (\lesssim 40 \text{ GeV}/c^2)$ . The process becomes comparable to  $Z^0 \rightarrow H f \bar{f}$  for  $m_H > 60 \text{ GeV}/c^2$  but is also rather hopeless at LEP.

The above resumé should at least give the reader some flavour of the difficulties to be faced by a prospective Higgs hunter [Dawson *et al.* (1989)].

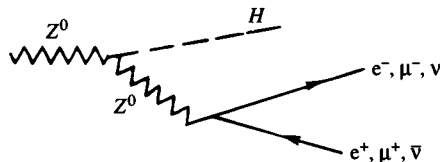
#### 6.4 Limits on the Higgs mass

In the discussion of radiative corrections in Chapter 7 it will be seen that the results depend upon the unknown masses  $m_t$  and  $m_H$ . While the dependence upon  $m_t$  is very sensitive, this is not so for  $m_H$  (see Figure 7.1). Theory alone, therefore, does not place very stringent limits upon  $m_H$ .

Prior to the functioning of LEP there were several experiments which claimed to exclude various regions for  $m_H$ , but all of these had loopholes [Rabi *et al.* (1989)]. The situation has changed dramatically since the commissioning of LEP. As reported by Dydak at the 25th International High Energy Conference (Dydak, 1990) the mass range

$$0 \leq m_H \lesssim 40 \text{ GeV}/c^2$$

is rigorously excluded by the complete absence of any signal, for the process



which was discussed in detail in Section 6.3.

There are also theoretical arguments which place some constraints on  $m_H$ . In Section 3.1 we discussed the Higgs potential  $V(\rho) = \mu^2\rho + \lambda\rho^2$  for the case  $\mu^2 < 0$ . We found that  $V$  had a minimum when  $\rho \equiv \phi^* \phi = -\mu^2/2\lambda \equiv v^2/2$ . Let us rewrite  $V$  as

$$V(\rho) = -|\mu^2|\rho + |\mu^2|\rho^2/v^2. \quad (6.4.1)$$

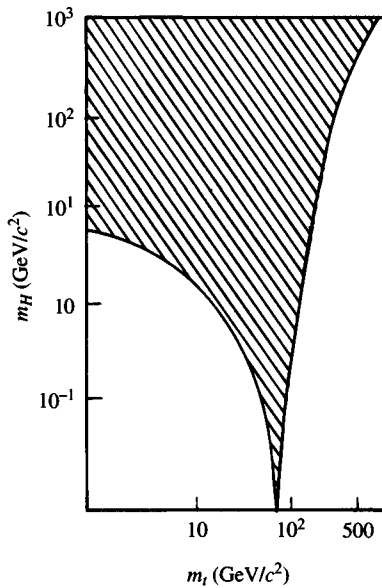


Fig. 6.4. The shaded area shows the permitted range of  $m_H$  vs  $m_t$  in order that the Higgs potential has an acceptable shape (see text).

As a consequence of one loop quantum correction the effective Higgs potential is modified to

$$V(\rho) = -|\mu^2|\rho + \frac{|\mu^2|}{v^2}\rho^2 + \gamma\rho^2 \left[ \ln\left(2\rho/v^2\right) - \frac{1}{2} \right] \quad (6.4.2)$$

where, in the SM with three fermion families,

$$\gamma \approx [3M_Z^4 + 6M_W^4 + m_H^4 - 12m_t^4]/16\pi^2 v^2. \quad (6.4.3)$$

The condition that  $V(\rho)$  again has the required shape (see Fig. 3.2) yields the lower bound constraint relating  $m_H$  to  $m_t$  shown in Fig. 6.4 (Linde, 1976; Weinberg, 1976a).

On the other hand we saw in (4.2.18) that  $m_H^2 = -2\mu^2$  so that for given  $v^2$  the coefficient of  $\rho^2$  in (6.4.2) increases with  $m_H$ . It can be argued that problems arise if the quartic term in the Higgs potential becomes too strong. (These problems concern questions relating to unitarity and also to the fact that the  $\phi^4$  field theory is now believed to be a ‘trivial’ field theory.) Requiring that the theory remains non-trivial up to some energy scale  $\Lambda$  imposes an upper limit on  $m_H$  for given  $m_t$ . The results are summarized in Fig. 6.5 for various choices of  $\Lambda$ . The allowed regions for  $m_H$  are inside the closed boundaries (Lindner, 1986).

For higher Higgs masses (say  $m_H \sim 70 - 80 \text{ GeV}/c^2$ ), i.e. at LEP2, the best signal is expected to come from

$$e^+ e^- \rightarrow ZH \begin{array}{l} \\ \searrow b\bar{b} \end{array} \quad (6.4.4)$$

as shown in Figure 6.1 but the situation becomes hopelessly confusing as  $m_H$  approaches  $M_Z$ .

Only supercolliders, either hadronic such as SSC ( $\sqrt{s} \simeq 40 \text{ TeV}$ ), LHC ( $\sqrt{s} \sim 16 - 20 \text{ TeV}$ ) or  $e^+ e^-$ , such as CLIC ( $\sqrt{s} \simeq 2 \text{ TeV}$ ) could pursue the hunt for Higgs particles of mass higher than the  $Z^0$ . Up to  $2M_W$  or, roughly, up to  $\sim 200 \text{ GeV}/c^2$  the main decay mode would still be that into the heaviest pair of quarks allowed by phase space whereas for  $m_H > 2M_W$ , or  $m_H \gtrsim 200 \text{ GeV}/c^2$ , the Higgs will decay predominantly into  $W^+ W^-$  or  $Z^0 Z^0$  as we have already mentioned.

As discussed in Mulvey (1987), the intermediate mass domain of heavy Higgs particles ( $M_Z < m_H \lesssim 200 \text{ GeV}$ ) would be best accessible in an  $e^+ e^-$  machine of  $\sqrt{s} \sim 1 - 2 \text{ TeV}$  provided  $\mathcal{L} \gtrsim 10^{33} \text{ cm}^{-2} \text{s}^{-1}$ . No such machine, however, is presently under consideration and at these masses, searches with hadronic supercolliders will have severe QCD background problems both for inclusive Higgs production ( $pp \rightarrow HX$ ) as well as for  $HW$  production ( $pp \rightarrow HWX$ ). However, with hadronic supercolliders, due to the large intermediate-Higgs production cross-section (coming, mainly, from gluon fusion)  $\sigma \simeq 10^2 \text{ pb}$  for  $m_H \simeq 150 \text{ GeV}/c^2$  at  $\sqrt{s} = 40 \text{ TeV}$  and a few times smaller at  $\sqrt{s} \simeq 16 \text{ TeV}$ , one can actually hope to be able to see some of the rarer Higgs decays such as  $H \rightarrow \gamma\gamma$ ,  $H \rightarrow \tau^+ \tau^-$  or  $H \rightarrow f\bar{f}f\bar{f}$ . This is true so long as  $m_H < 2m_t$ ; in this case  $H \rightarrow b\bar{b}$  is the main decay mode; its width is not too large and rare decay modes are enhanced.

If, finally, the Higgs is very heavy and  $m_H > 2m_t$ , the most promising channel appears to be  $H \rightarrow Z^0 Z^0 \rightarrow f\bar{f}\nu\bar{\nu}$  with  $f = e$  or  $\mu$ . This avoids all QCD background problems and has no additional difficulties in the event that  $m_t > M_W$  (as we now expect) since the main  $t$ -quark decay mode would then be  $t \rightarrow Wb$  and each  $t\bar{t}$  pair produced would just increase the  $H \rightarrow W^+ W^-$  background. Because of the small branching ratio ( $\sim 8 \times 10^{-3}$ ) of the reaction  $H \rightarrow Z^0 Z^0 \rightarrow f\bar{f}\nu\bar{\nu}$ , the estimate is that LHC ( $\sqrt{s} \sim 16 \text{ TeV}$ ) could detect the Higgs only if  $m_H \lesssim 0.6 \text{ TeV}/c^2$ . A similar estimate holds for  $H \rightarrow f\bar{f}f\bar{f}$  ( $f = e, \mu$ ) if  $\mathcal{L} \sim 5 \times 10^{33} \text{ cm}^{-2} \text{s}^{-1}$  whereas it could detect up to  $m_H \lesssim 0.8 \text{ TeV}/c^2$  in  $Z \rightarrow f\bar{f}f\bar{f}$  ( $f = e, \mu$ ) if the luminosity is increased up to  $\mathcal{L} \sim 5 \times 10^{34} \text{ cm}^{-2} \text{s}^{-1}$ . Concerning SSC a Higgs of up to  $m_H \simeq 0.8 \text{ TeV}/c^2$  could be detected from  $H \rightarrow f\bar{f}f\bar{f}$ .

From all these considerations, it is clear that only high luminosity hadronic supercolliders have a real chance of detecting large mass Higgs

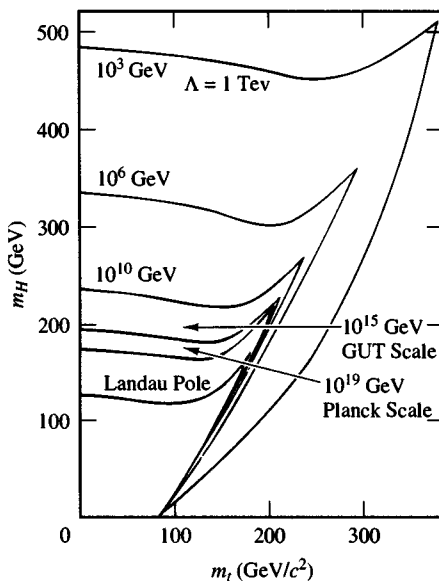


Fig. 6.5. Allowed regions for  $m_H$  vs  $m_t$  from the requirement that the theory remains non-trivial up to various energy scales  $\Lambda$ .

particles. It is also clear that unless spectacular improvements are made in  $e^+e^-$  supercolliders to increase their luminosity and/or their energy, a detailed analysis of the properties of very heavy Higgs particles will remain an extremely difficult task.

### 6.5 Concluding comments

The actual discovery of the  $W$  and  $Z$  bosons at the expected masses is, no doubt, the best support for the SM. Thus, even though the missing link of the Higgs meson is a serious one, one feels that even in its lowest order, the electroweak model gives a reasonably correct description of nature (at least down to distances of  $\sim 10^{-16}$  cm). Higher order corrections and the precision tests from LEP1 will be discussed in the next chapters. As we have already stated, however, unless the Higgs mesons are found and the symmetry breaking mechanism is fully tested, no definite conclusion can be drawn as to whether or not a more refined theory is needed to replace the SM and whether or not some of the (too many) free parameters of the SM might become calculable.

# 7

## The standard model beyond lowest order

In the previous chapters we have discussed the construction of the Born approximation to the standard model (SM). Here we tackle the extremely complicated issue of bringing radiative (both photonic and electroweak) corrections into the model. This is a crucial step towards a more profound testing of the SM.

We then proceed to enumerate the ideas that have been put forward to go beyond the SM.

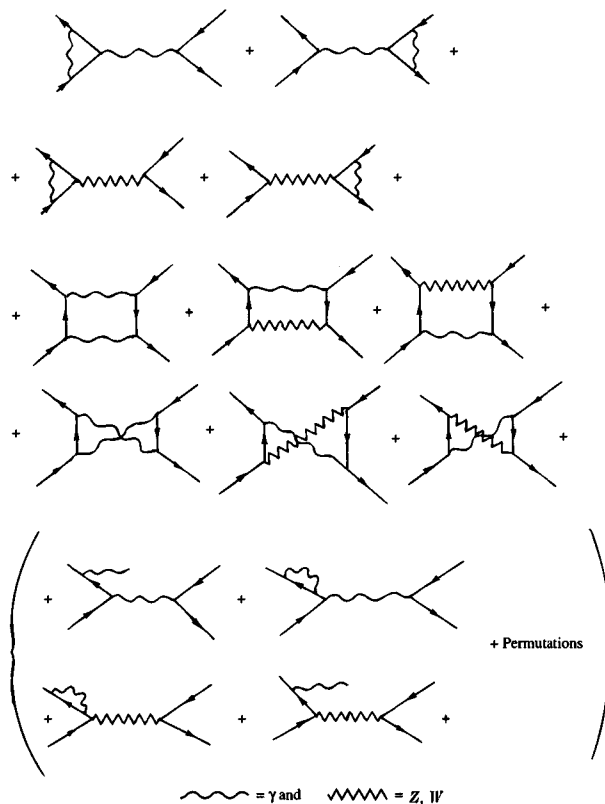
### 7.1 Radiative corrections

The importance of radiative corrections in testing the true field-theoretic structure of the SM has long been recognised. The calculations are laborious and difficult and the literature has grown enormously in recent years. We shall only give some of the most important modifications due to radiative corrections. For details, see Altarelli *et al.*, (1989) and Peccei (1988), where references to the extensive literature can be found.

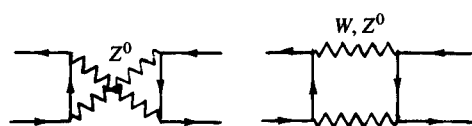
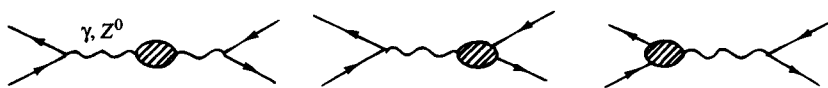
Radiative corrections can be either of QED (photonic) or of electroweak origin.

To get some feeling for what is involved we show below the set of second order diagrams for the important reaction  $e^+e^- \rightarrow f\bar{f}$  ( $f$  any charged fermion) whose lowest order cross-section will be calculated explicitly in Section 8.6. These can be divided naturally into two classes:

1. QED corrections consisting of an extra photon (a real bremsstrahlung photon or a virtual photon loop) added to the Born terms. These corrections are quite substantial at LEP energies.



2. Weak corrections to the vector boson propagators, the vertices and box diagrams.



$\sim \sim \sim = \gamma$  and  $\backslash \backslash \backslash \backslash \backslash = Z, W$

We will return to the latter diagrams when discussing in detail the effect of weak radiative corrections in muon decay.

Quantitatively, the most important contributions arise either from ‘large’ logarithms (e.g. terms of the form  $\left(\frac{\alpha}{\pi} \ln \frac{M_Z}{m_f}\right)^n$  where  $f$  is a light fermion) or from terms quadratic in the top mass.

## 7.2 Renormalization and physical parameters

Even non-theoretical readers are urged to peruse the introductory part of Chapter 20 where the *idea* of renormalization is explained without any detailed mathematical calculations. Nonetheless we feel it important to make some comments here on this question.

If higher order perturbative effects are calculated using the Lagrangian couplings given in (5.1.1) and (5.1.3) in which the parameters  $e$  and  $\sin^2 \theta_W$  are considered as *fixed numbers*, many diagrams yield infinite answers and the theory has to be renormalized.

In books on field theory one starts with the Lagrangian in which all the parameters, coupling and masses are called ‘bare parameters’ and are labelled  $e_0, g_0, m_0$  etc. These bare parameters are not what one measures; to make the theory finite they have to be allowed to depend on a cut-off  $\lambda$  temporarily introduced into the theory and most of them become infinite when at the end one lets  $\lambda \rightarrow \infty$ . What  $\lambda$  is depends upon the *method* of ‘regularization’. Thus  $\lambda$  may literally be a cut-off, i.e. the upper limit of some loop integration, or it may be  $1/\epsilon$  where one uses dimensional regularization to work in  $4 - \epsilon$  dimensions and at the end lets  $\epsilon \rightarrow 0$ .

Each bare parameter (let us generically call it  $g_0$ ) is replaced by a power series expansion in a finite parameter  $g$ , schematically of the form

$$g_0(\lambda) = g \left[ 1 + g a_1(\lambda) + \dots \right] \quad (7.2.1)$$

where  $a_1(\lambda)$  can be split into two pieces

$$a_1(\lambda) = a_1^{\text{inf}}(\lambda) + a_1^{\text{finite}}(\lambda) \quad (7.2.2)$$

in which

$$a_1^{\text{inf}}(\lambda) \rightarrow \infty \quad \text{as} \quad \lambda \rightarrow \infty \quad (7.2.3)$$

but

$$a_1^{\text{finite}}(\lambda) \rightarrow \text{finite result } a_1^F \quad \text{as} \quad \lambda \rightarrow \infty.$$

In a *renormalizable* theory the  $a_1^{\text{inf}}$  cancel out in the calculation of any physical observable, so that the results depend on  $g[1 + g a_1^F + \dots]$ . When we work to lowest order we neglect the terms  $g a_1^F + \dots$ . For all lowest order calculations this is equivalent to simply replacing  $g_0$  by  $g$  in the

Lagrangian, and the numerical value of  $g$  is then found by comparing some lowest order calculation with an experimental observable. It is for this reason that we did not introduce bare parameters in Chapters 1–4.

When we measure several different quantities and compare with lowest order calculations of these quantities, each comparison will yield a value of  $g$ . If the theory is a true description of nature we should find that all these determinations of the value of  $g$  are compatible.

A classic example in electroweak theory is the many determinations of  $\sin^2 \theta_W$  from different reactions.

The above is subtle but gives the false impression of being unique. Alas, this is not so. The process of splitting  $a_1(\lambda)$  into an infinite and a finite part can be done in many ways. Each way defines a different renormalization scheme with different finite pieces, say  $a_1^{\text{SMITH}}$ ,  $a_1^{\text{ROSSI}}$  etc. and correspondingly different renormalized parameters  $g^{\text{SMITH}}$ ,  $g^{\text{ROSSI}}$  etc. In lowest order these are all equal, but with the inclusion of higher order corrections they will differ

$$g^{\text{SMITH}} = g^{\text{ROSSI}} + \Delta g \quad (7.2.4)$$

where  $\Delta g$  is of order  $g^2$ .

Many possible schemes may *a priori* be equally good and there is then no problem provided the parameters are labelled carefully, so that we don't confuse  $g^{\text{SMITH}}$  with  $g^{\text{ROSSI}}$ .

But some schemes may be better than others in practice. This raises the question of the best way to define the physical parameters. For pure QED there is an obvious and simple choice. One can show that the *exact* formula for Thomson scattering becomes

$$\frac{d\sigma}{d\Omega} = \frac{\alpha^2}{m_e^2} (\boldsymbol{\epsilon}' \cdot \boldsymbol{\epsilon})^2 \quad (7.2.5)$$

as the kinetic energy tends to zero.

Comparison of (7.2.5) with experiment *defines* the usual fine structure constant  $\alpha$  which is then used as the (renormalised) coupling parameter in the Lagrangian. This is the universally accepted procedure.

There is no clear-cut analogue of (7.2.5) for the electroweak couplings  $g$  and  $g'$  that appear in (4.2.4) and (4.2.26) and several rival schemes exist (see Peskin, 1990; Passarino and Veltman, 1990). Each has merits and defects. It does not matter very much which scheme is used provided that the notation indicates clearly *what the parameters mean* and formulae can be given relating the parameters in the different schemes to each other. Of course to lowest order in perturbation theory the various schemes will be identical.

In discussing true radiative corrections we shall work strictly within the minimal SM in which the minimal Higgs mechanism generates the

masses. Thus at lowest order we have the relation (4.2.17)

$$\sin^2 \theta_W = 1 - \frac{M_W^2}{M_Z^2}. \quad (7.2.6)$$

All the lowest order relations will be modified by the radiative corrections, the modifications depending on the scheme adopted.

We shall only discuss the ‘on shell’ scheme (Sirlin, 1980) in which (7.2.6) holds exactly. To emphasize this we shall use the symbols  $s_W^2$  and  $c_W^2$  where, *by definition*,

$$s_W^2 = 1 - \frac{M_W^2}{M_Z^2}. \quad (7.2.7)$$

Returning to our original electroweak Lagrangian, but now with couplings and masses labelled ‘0’ for bare, we have, from (4.2.12),

$$g_0 = \frac{e_0}{\sin \theta_W^0} = \frac{e_0}{\sqrt{1 - \frac{M_W^{02}}{M_Z^{02}}}}. \quad (7.2.8)$$

and from (4.2.10)

$$g'_0 = g_0 \tan \theta_W^0 = e_0 \frac{M_Z^0}{M_W^0}. \quad (7.2.9)$$

These equations *define* the minimal standard model and the fundamental parameters are taken to be  $e_0$ ,  $M_Z^0$  and  $M_W^0$ .

Analogous to (7.2.1), the renormalization is carried out by putting

$$\left. \begin{aligned} e_0 &= e \left( 1 + \frac{\delta e}{e} \right) \\ M_W^{02} &= M_W^2 \left( 1 + \frac{\delta M_W^2}{M_W^2} \right) \\ M_Z^{02} &= M_Z^2 \left( 1 + \frac{\delta M_Z^2}{M_Z^2} \right) \end{aligned} \right\} \quad (7.2.10)$$

wherein we have suppressed the dependence on the cut-off  $\lambda$ . The ‘on-shell’ scheme is defined by demanding that

$$\frac{e^2}{4\pi\hbar c} = \text{usual fine structure constant}, \quad (7.2.11)$$

$$M_W, M_Z = \text{physical masses of } W \text{ and } Z^0. \quad (7.2.12)$$

These demands are sufficient to fix  $\delta e$ ,  $\delta M_W^2$ ,  $\delta M_Z^2$ , i.e. to remove the ambiguity in the  $a_1^F$  discussed in connection with (7.2.1) and (7.2.2). Technically (7.2.12) is a statement about where the poles in the boson propagators occur.

Because of (7.2.8) and (7.2.9) it is not necessary to renormalize  $g_0$  and  $g'_0$  independently. Using (7.2.10) defines the renormalized couplings as

$$\left. \begin{aligned} g &= \frac{e}{s_W}, \\ g' &= \frac{e}{c_W}. \end{aligned} \right\} \quad (7.2.13)$$

Thus all calculations are done using the Lagrangians (5.1.1) and (5.1.3) in which  $\sin^2 \theta_W$  is replaced by  $s_W^2$  etc.

The above is deceptively simple for two reasons.

Firstly, because  $W$  and  $Z^0$  are unstable particles what we mean by their masses is not unambiguous. Later in Section 8.6 we shall see that  $M_Z$  is determined from fits to the shape of the cross-section for  $e^+e^- \rightarrow X$  in the region of the  $Z^0$  peak as measured at LEP 1. But the formulae for these cross-sections are modified by radiative corrections which involve the very parameters  $M_Z$ ,  $M_W$  that we are trying to determine, as well as others, such as the top mass, which are unknown. However these corrections have a negligible effect upon the determination of  $M_Z$  from the fit to the  $e^+e^- \rightarrow X$  cross-sections. Thus we can adopt this as a practical method to find  $M_Z$ . Note however, that the peak in the cross-section does not occur at  $s = M_Z^2$ , as will be explained in Section 8.5. A similar argument can be made for  $M_W$ . In conclusion the first difficulty concerning this scheme can probably be ignored.

The second and more important problem in practice is that we do not have a really accurate determination of  $M_W$  at present, (though the situation will improve greatly when LEP 2 is built) so that we cannot use eqn (7.2.7) to get an accurate *numerical value* for  $s_W^2$ . A strategy to get around this difficulty is discussed in Section 7.8.

### 7.3 The effective fine structure constant

The simplest radiative correction is due to  $f\bar{f}$  self-energy loops in the photon propagator. Their effect can be taken into account by defining a ‘running’ or ‘effective’ coupling constant  $\alpha(q^2)$  which depends upon the  $q^2$  carried by the photon line when it couples to a charged fermion. (This concept is treated in Section 21.7.) Thus one should use

$$\alpha(q^2) = \frac{\alpha}{1 - \Delta\alpha(q^2)} \quad (7.3.1)$$

where  $\alpha$  is the usual fine structure constant defined in (7.2.5), which corresponds to a real photon ( $q^2 = 0$ ) coupling to a physical electron.

It will turn out that the most important scale for us is  $q^2 = M_Z^2$  and we shall abbreviate  $\Delta\alpha(M_Z^2)$  by  $\Delta\alpha$ . The present best estimate for  $\Delta\alpha$

(Consoli *et al.*, 1989) is

$$\Delta\alpha = 0.0601 + \frac{40}{9} \frac{\alpha}{\pi} \ln \left( \frac{M_Z}{91 \text{ GeV}} \right) \pm 0.0009 \quad (7.3.2)$$

which yields  $\alpha(M_Z^2) \approx 1.064\alpha$ .

It is of interest to note that ‘heavy’ fermions, i.e. whose mass satisfies  $m_f^2 \gg q^2$ , yield a negligible contribution to  $\Delta\alpha(q^2)$  of order  $\frac{\alpha}{3\pi} \cdot \frac{q^2}{5m_f^2}$ . This feature is referred to as the ‘decoupling of heavy fermions’. This is *not* the case when dealing with corrections to the  $W$  and  $Z$  propagators and one obtains contributions of order  $m_f^2/q^2$  even for  $m_f^2 \gg q^2$ .

## 7.4 The muon lifetime revisited

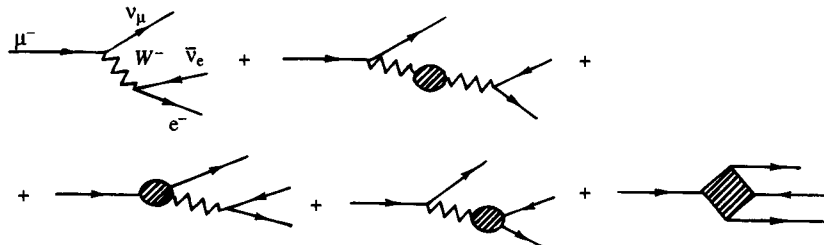
Let us now consider the SM corrections to the lowest order relation between  $G$ ,  $\alpha$  and  $M_W$  given in (4.2.32).

Historically,  $G$  was defined from the muon lifetime as calculated in the Fermi current-current model together with photonic radiative corrections, so that the amplitude is given by the Feynman diagrams following eqn (4.2.33).

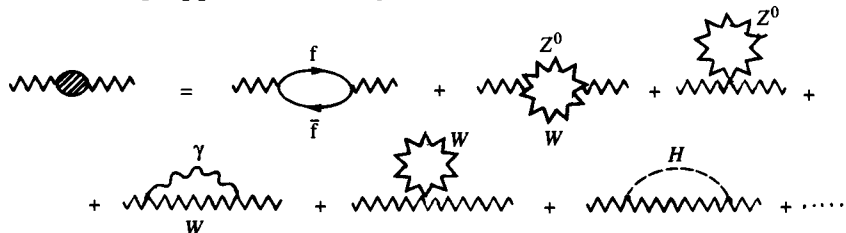
Schematically, the amplitude is proportional to

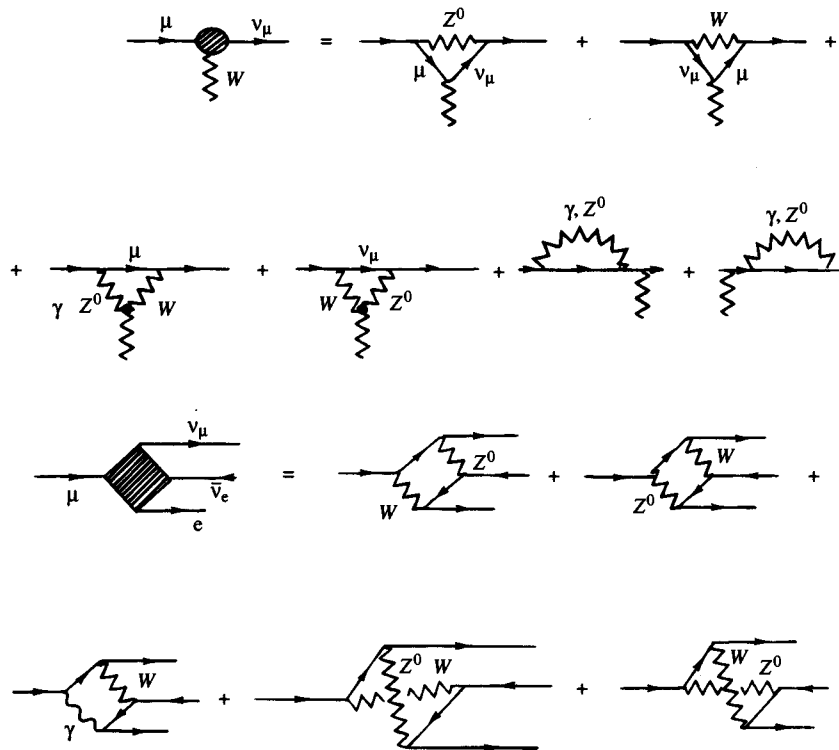
$$\frac{G}{\sqrt{2}} \left[ 1 + \text{photonic corrections to Fermi amplitude} \right] \quad (A)$$

In the SM calculations of the muon lifetime we have the diagrams



In the above, the ‘propagator’, ‘vertex’ and ‘box’ corrections are given in the one-loop approximation by





The amplitude in the SM calculation is proportional to

$$\frac{e^2}{8s_W^2 c_W^2 M_Z^2} \left[ (1 + \text{photonic corrections}) + \text{propagator} + \text{vertex} + \text{box terms} \right] \quad (B)$$

Equating (A) and (B) yields

$$\frac{G}{\sqrt{2}} = \frac{e^2}{8s_W^2 c_W^2 M_Z^2} \left[ 1 + \text{photonic corrections} + \text{propagator} + \text{vertex} + \text{box terms} - \text{photonic corrections to the Fermi amplitude} \right] \quad (7.4.1)$$

In fact because of the tiny momentum transfer compared with  $M_W$ , the photonic corrections to the two models effectively cancel in (7.4.1).

Eqn (7.4.1.) is written

$$\frac{G}{\sqrt{2}} = \frac{e^2}{8s_W^2 c_W^2 M_Z^2} (1 + \Delta r) \quad (7.4.2)$$

Even to one loop order, the detailed calculation of the radiative correction  $\Delta r$  is very complicated and the interested reader is referred to the

specialised literature (see, e.g., Hollik, 1990b, and Peskin, 1990). We shall discuss the result for  $\Delta r$  in the next section.

## 7.5 Estimates of one loop corrections

$\Delta r$  as defined in (7.4.2) involves vacuum polarization effects and other weak corrections which depend on all the parameters of the model, including the (so far unknown) Higgs and top masses  $m_H$  and  $m_t$ .

The most important diagrams are expected to be



The complete expression for  $\Delta r$  can be written as

$$\Delta r = \Delta\alpha - \frac{c_W^2}{s_W^2} \Delta\rho + \Delta r_{\text{rem}}. \quad (7.5.1)$$

where  $\Delta\alpha$  is given in (7.3.2).

The term  $\Delta\rho$  in eqn (7.5.1) is given, to one loop, by

$$\Delta\rho = \frac{e^2}{64\pi^2 s_W^2 c_W^2 M_Z^2} \sum_f N_{cf} \left| m_{f_1}^2 - m_{f_2}^2 \right|^2 \quad (7.5.2)$$

where  $N_{cf} = 1$  for leptons,  $= 3$  for quarks, and  $m_{f_{1,2}}$  are the masses of the fermions in each fermion doublet. The sum extends over all fermion doublets (Veltman, 1977). The largest contribution to (7.5.2) comes from the  $(^t_b)$  doublet due to the large  $m_t - m_b$  mass difference. Thus

$$\Delta\rho \approx \frac{3e^2}{64\pi^2 s_W^2 c_W^2 M_Z^2} m_t^2. \quad (7.5.3)$$

In  $\Delta r_{\text{rem}}$  are included all the ‘remainder’ contributions, i.e. all non-leading corrections including the Higgs contribution and other logarithmic contributions due to top.

For heavy Higgs particles ( $m_H \gg M_W$ ), the principal contribution is logarithmic:

$$\Delta r_{\text{rem}}^{\text{Higgs}} = \frac{e^2}{64\pi^2 s_W^2} \cdot \frac{11}{3} \left[ \ln \left( \frac{m_H^2}{c_W^2 M_Z^2} \right) - \frac{5}{6} \right]. \quad (7.5.4)$$

The leading contribution to the remainder comes from top and is also logarithmic:

$$\Delta r_{\text{rem}}^{\text{top}} = \frac{e^2}{64\pi^2 s_W^2} \cdot 2 \left( \frac{c_W^2}{s_W^2} - \frac{1}{3} \right) \ln \left( \frac{m_t^2}{c_W^2 M_Z^2} \right). \quad (7.5.5)$$

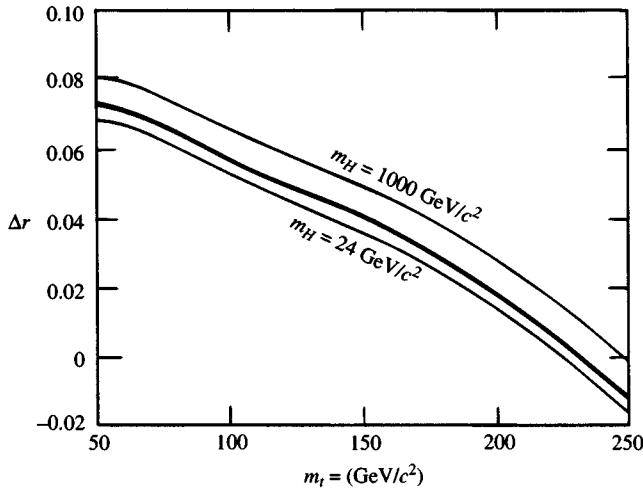


Fig. 7.1.  $\Delta r$  as calculated from eqn (7.5.1) as function of  $m_t$  for few choices of  $m_H$  (from Hollik, 1990b).

Note that  $\Delta\alpha$  does not depend on unknown parameters whereas  $\Delta\rho$  and  $\Delta r_{\text{rem}}$  do.

Typical estimates of the size of  $\Delta r$  are shown in Fig. 7.1 where  $\Delta r$  is plotted as a function of  $m_t$  for three values of the Higgs mass,  $m_H = 24, 100$  and  $1000 \text{ GeV}/c^2$ .

## 7.6 Higher order corrections

Higher order effects can be evaluated by using renormalization group arguments (Marciano, 1979) which lead to the replacement  $1 + \Delta r \rightarrow 1/(1 - \Delta r)$  so that (7.4.2) for the muon lifetime becomes

$$G = \frac{\pi\alpha}{\sqrt{2}M_Z^2 s_W^2 c_W^2} \frac{1}{1 - \Delta r}. \quad (7.6.1)$$

It can be shown that this takes into account all terms in  $(\Delta\alpha)^n$ . Thus, it gives a reliable result if  $\Delta\alpha$  is a good approximation to  $\Delta r$ , which will be the case for reasonable top masses ( $\lesssim 120 \text{ GeV}/c^2$ ). Note that using our definition of  $s_W^2$  (7.2.7), we can turn (7.6.1) into a formula for  $M_W^2$ , i.e.

$$M_W^2 = \frac{M_Z^2}{2} \left[ 1 + \left( 1 - \frac{4A^2}{M_Z^2} \frac{1}{1 - \Delta r} \right)^{\frac{1}{2}} \right] \quad (7.6.2)$$

where  $A^2 = \pi\alpha/\sqrt{2}G$  was introduced in (4.2.32). Note also that (7.6.2) is a radiatively corrected version of (4.2.37) in the on-shell scheme.

If on the other hand it turns out that the top mass is very large  $\Delta\alpha$  will no longer be a good approximation to  $\Delta r$  and the above treatment (7.6.1) is inadequate. For example if  $m_t = 230 \text{ GeV}/c^2$  one finds for the terms in  $\Delta r$  (7.5.1)

$$\left. \begin{aligned} \left( \frac{c_W^2}{s_W^2} \Delta\rho \right)^2 &\simeq 3.9 \times 10^{-3}, \\ \left( \Delta\alpha \right)^2 &\simeq 3.6 \times 10^{-3}, \\ \left( \Delta\alpha \right) \frac{c_W^2}{s_W^2} (\Delta\rho) &\simeq 3.7 \times 10^{-3}. \end{aligned} \right\} \quad (7.6.3)$$

In this situation it can be shown that, correct to  $O(\alpha^2)$ , (7.6.1) should be replaced by (Consoli *et al.*, 1989)

$$G = \frac{\pi\alpha}{\sqrt{2}M_Z^2 s_W^2 c_W^2} \cdot \left[ \frac{1}{1 - \Delta\alpha} \cdot \frac{1}{1 + c_W^2 \Delta\rho_i / s_W^2} + \Delta r_{\text{rem}} \right] \quad (7.6.4)$$

where  $\Delta\rho_i$  is an improved, more accurate estimate of  $\Delta\rho$  including the higher order ‘irreducible’ contribution coming from irreducible diagrams such as



The leading term in  $\Delta\rho_i$  is (van der Bij and Hoogeveen, 1987)

$$\Delta\rho_i = \frac{e^2}{64\pi^2 s_W^2 c_W^2} \cdot 3 \left( \frac{m_t^2}{M_Z^2} \right) \left\{ 1 + \frac{e^2}{64\pi^2 c_W^2 s_W^2} \left( \frac{m_t^2}{M_Z^2} \right) (19 - 2\pi^2) \right\}. \quad (7.6.5)$$

Often one writes

$$\rho \equiv \frac{1}{1 - \Delta\rho_i} \quad (7.6.6)$$

and eqn (7.6.4) is then written as

$$G = \rho \frac{\pi\alpha}{\sqrt{2}c_W^2 M_Z^2} \cdot \left[ \frac{1}{\rho - c_W^2} \cdot \frac{1}{1 - \Delta\alpha} + \Delta r_{\text{rem}} \right]. \quad (7.6.7)$$

Just as we did before, we can turn (7.6.7) into an equation for  $M_W$  upon using the on-shell definition of  $s_W^2$  (7.2.7).

Thus, we obtain instead of (7.6.2)

$$M_W^2 = \rho \frac{M_Z^2}{2} \left\{ 1 + \sqrt{1 - \frac{4A^2}{\rho M_Z^2} \left[ \frac{1}{1 - \Delta\alpha} + \Delta r_{\text{rem}} \right]} \right\}. \quad (7.6.8)$$

One often introduces the definition

$$\cos^2 \bar{\theta}_W \equiv \frac{1}{2} \left\{ 1 + \sqrt{1 - \frac{4A^2}{\rho M_Z^2} \frac{1}{1 - \Delta\alpha}} \right\} \quad (7.6.9)$$

useful when  $\Delta r_{\text{rem}}$  is negligible, as it is expected to be, and whose significance will be discussed in Section 8.6, in which case (7.6.8) can be written

$$c_W^2 = \rho \cos^2 \bar{\theta}_W \quad (7.6.10)$$

When eventually  $M_W$  is accurately known from experiments at LEP 2, it will be possible to use (7.6.1) or (7.6.7) to measure  $\Delta r$  or  $\rho$  and thus to check the validity of the standard model at a fundamental level or to put constraints on the top mass if it has not been discovered by then. Of course, even with the present imprecise value of  $M_W$ , one can still use (7.6.1) or (7.6.7) to put constraints on  $m_t$  as discussed below.

## 7.7 Practical problems in testing radiative corrections

As we have already seen for the leptonic sector and, as we shall see later for the hadronic sector, the SM in lowest order provides a wonderfully successful description of a huge range of experimental phenomena. But to test the theory more profoundly requires the comparison of precise higher order calculations with precise experimental data. In the on shell renormalization scheme, all calculations are expressed in terms of the parameters  $M_Z$  and  $s_W^2$ . The former is known to great accuracy and we would clearly like to have an equally precise value for the latter. Unfortunately, this is precluded by the limited precision in our measurements of  $M_W$ . Thus, taking e.g. the UA2 value (Table 5.1)  $M_W = (80.2 \pm 1.5) \text{ GeV}/c^2$  and (Table 8.3)  $M_Z = (91.177 \pm 0.006) \text{ GeV}/c^2$ , we obtain the rather imprecise estimate  $s_W^2 = 0.226 \pm 0.029$ .

It therefore seems advisable for the present to adopt a procedure similar to the one used in comparing the SM with experiment in lowest order (as was done even before the discovery of the  $W$  and  $Z^0$ ). Thus we fit as many higher order calculations, containing the now ‘unknown’ parameter  $s_W^2$ , to experiment and examine the compatibility of the various determinations. This programme is complicated by the fact that the higher order formulae involve the unknown top and Higgs masses as is explained in Section 7.8.

Given that the top mass is not expected to be exceedingly large, i.e. one expects  $m_t = (130 \pm 40) \text{ GeV}/c^2$  (see Section 8.6), we shall base the following discussion on eqn (7.6.2).

Since the calculated value of  $\Delta r$  reflects the fundamental structure of the SM it is important to ask to what accuracy it can be deduced experimentally from a knowledge of  $M_W$  and  $M_Z$ .

Given that the uncertainties in  $G$  (4.1.34) and in  $\alpha = 1/(137.0359895(61))$  are negligibly small, from (7.6.2) the uncertainties in

$\Delta r$  will be dominated by

$$\delta(\Delta r) \simeq \frac{2A^2}{M_Z^2 s_W^4} \left\{ \left( \frac{\delta M_Z}{M_Z} \right)^2 + \left( 1 - \frac{s_W^2}{c_W^2} \right) \left( \frac{\delta M_W}{M_W} \right)^2 \right\}^{\frac{1}{2}}. \quad (7.7.1)$$

While the precision in the measurement of  $M_Z$  will improve greatly as LEP statistics increase, the best limit on  $\delta M_W$  from hadron colliders is expected to approach  $\simeq 190$  MeV, giving an uncertainty  $\delta(\Delta r) = 0.018$  compared with the present measured value  $\Delta r = 0.061 \pm 0.081$ . The precision in  $M_W$  will improve to  $\sim 100$  MeV when ultimately LEP 2 collects data on  $W^+W^-$  pair production. By then we expect the uncertainties on  $\Delta r$  to approach the value  $\delta(\Delta r) \simeq 0.0056$ . Referring to Fig. 7.1 we see that such an evaluation of  $\Delta r$  would be quite useful in pinning down the unknown parameters of the theory.

## 7.8 Strategies to overcome the imprecision in $M_W$

Suppose we evaluate  $\Delta r$  from (7.6.2) using say the CDF value  $M_W = 79.78 \pm 0.5$  GeV/c $^2$ .  $\Delta r$  depends sensitively upon  $m_t$  and insensitively on  $m_H$  (see Fig. 7.1). Thus choosing say  $m_H = 100$  GeV/c $^2$  one can solve for  $m_t$  and find (Halzen and Morris, 1991)

$$m_t = 143 \pm 38 \text{ GeV/c}^2. \quad (7.8.1)$$

An alternative strategy is the following. Consider (7.6.2) as containing three unknown parameters  $M_W$ ,  $m_t$  and  $m_H$ . Fix  $m_t$  and  $m_H$  and solve (7.6.2) numerically for  $M_W$  (or equivalently for  $s_W^2$  since  $M_Z$  is known to high precision) using the theoretical formula (7.5.1) for  $\Delta r$ . Then change  $m_t$ ,  $m_H$ . In this way one obtains a series of values  $M_W(m_t, m_H)$  or  $s_W^2(m_t, m_H)$  based upon assuming that the SM correctly describes muon decay.

One can now repeat this exercise for other experimental quantities  $E_1, E_2, \dots$ . Each will yield a numerical function  $s_W^2|_{E_1}, s_W^2|_{E_2}, \dots$  of  $m_t$ ,  $m_H$ . If the SM is correct all these experimental ' $s_W^2$ ' should be equal for some  $m_t$  and  $m_H$ . We can then search for the values of  $m_t$ ,  $m_H$  that yield a best fit to these differently determined ' $s_W^2$ '.

A comprehensive analysis is due to Ellis and Fogli (1990). It takes into account all the purely leptonic data discussed in Chapter 5, the semi-leptonic data to be presented in Chapter 10 and the LEP results which will be examined in detail in Chapter 8. They find

$$m_t = 127^{+24}_{-30} \text{ GeV/c}^2 \quad (7.8.2)$$

for  $m_H = M_W$ .

Moreover there are non-trivial bounds on  $m_H$ :

$$1.8 \text{ GeV}/c^2 < m_H < 6 \text{ TeV}/c^2 \quad (68\% \text{ CL}) \quad (7.8.3)$$

with the preferred value of  $m_H$  being less than  $M_Z$ .

### 7.9 Testing the minimal Higgs mechanism

We mentioned in Section 5.2 that the minimal Higgs mechanism can be tested, at Born level, by checking whether

$$\rho_0 = \left( \frac{M_W}{M_Z} \right)^2 \frac{1}{(\cos^2 \theta_W)_{\nu_\mu e}} \quad (7.9.1)$$

is equal to 1. In a non-minimal model eqn (4.2.17) would be replaced by

$$\frac{M_W}{M_Z} = \sqrt{\rho_0} \cos \theta_W \quad (7.9.2)$$

with  $\rho_0 \neq 1$  an additional parameter of the theory. However the most important effect of the higher order corrections for reactions involving  $Z^0$  exchange is the replacement [see (5.1.4), and (5.1.5)]

$$g_V^f \rightarrow \bar{g}_V^f = \sqrt{\rho} \left( I_{W_3}^{f_L} - 2Q_f \sin^2 \bar{\theta}_W \right) \quad (7.9.3)$$

$$g_A^f \rightarrow \bar{g}_A^f = \sqrt{\rho} I_{W_3}^{f_L} \quad (7.9.4)$$

where  $\rho$  was defined in (7.6.6) and  $\bar{\theta}_W$  in (7.6.10). The cross-section for  $\nu_\mu e^- \rightarrow \nu_\mu e^-$  and  $\bar{\nu}_\mu e^- \rightarrow \bar{\nu}_\mu e^-$  then becomes, instead of (5.2.3) and (5.2.4)

$$\begin{aligned} \sigma(\nu_\mu e) &= \frac{m_e E}{\pi} \left( \frac{e^2(1 + \Delta r)}{8s_W^2 c_W^2 M_Z^2} \right)^2 \rho \left( 1 - 4 \sin^2 \bar{\theta}_W + \frac{16}{3} \sin^4 \bar{\theta}_W \right) \\ \sigma(\bar{\nu}_\mu e) &= \frac{m_e E}{3\pi} \left( \frac{e^2(1 + \Delta r)}{8s_W^2 c_W^2 M_Z^2} \right)^2 \rho \left( 1 - 4 \sin^2 \bar{\theta}_W + 16 \sin^4 \bar{\theta}_W \right) \end{aligned} \quad (7.9.5)$$

where  $\Delta r$  was given in (7.5.1). Use of (7.4.2) allows us to replace

$$\frac{e^2(1 + \Delta R)}{8s_W^2 c_W^2 M_Z^2} \text{ by } \frac{G}{\sqrt{2}}$$

in (7.9.5) if we are interested in the individual cross-sections. We can, however, as in Section 5.2, take the ratio of the cross-sections and measure  $\sin^2 \bar{\theta}_W$ ; call it  $(\sin^2 \bar{\theta}_W)_{\nu_\mu e}$ . From (7.6.10) we see that we should find, in the minimal model,

$$\frac{M_W^2}{M_Z^2} \frac{1}{(\cos^2 \bar{\theta}_W)_{\nu_\mu e}} = \frac{c_W^2}{(\cos^2 \bar{\theta}_W)_{\nu_\mu e}} = \rho \neq 1. \quad (7.9.6)$$

Thus higher order corrections spoil the simplicity of the test for a non-minimal mechanism. On the other hand  $\rho_0$  in (5.2.2) is a free parameter whereas  $\rho$  in (7.9.6) is a calculable quantity once we know  $m_t$  and have some control of  $m_H$ , and will be very close to 1 in value.

Returning to our discussion in Section 5.2 we see that what we called  $(\sin^2 \theta_W)_{\nu_\mu e}$  in a lowest order treatment should more correctly be interpreted as  $(\sin^2 \bar{\theta}_W)_{\nu_\mu e}$  and the experimentally determined parameter  $\rho_0$  (5.2.7) can be taken as the value of  $\rho$  in the higher order *minimal* SM.

However the error on  $\rho$  is then too large to deduce any useful information on  $m_t$  from (7.6.5).

A similar phenomenon occurs in a non-minimal model when considering the muon lifetime. Consistency with the Fermi theory will lead once again to (4.2.32)

$$G = \frac{\pi\alpha}{\sqrt{2}} \frac{1}{M_W^2 \sin^2 \theta_W} \quad (7.9.7)$$

which via (7.9.2) becomes

$$G = \frac{\pi\alpha\rho_0}{\sqrt{2}M_W^2} \cdot \frac{1}{\rho_0 - M_W^2/M_Z^2}. \quad (7.9.8)$$

Photonic corrections will alter this to

$$G = \frac{\pi\rho_0}{\sqrt{2}M_W^2} \cdot \frac{\alpha}{1 - \Delta\alpha} \cdot \frac{1}{\rho_0 - M_W^2/M_Z^2}. \quad (7.9.9)$$

Unfortunately the radiative corrections to the *minimal* SM give precisely this kind of result. For if  $\Delta r_{\text{rem}}$  in (7.6.7) is negligible as expected, then (7.6.7) can be written

$$G = \frac{\pi\rho}{\sqrt{2}M_W^2} \cdot \frac{\alpha}{1 - \Delta\alpha} \cdot \frac{1}{\rho - M_W^2/M_Z^2} \quad (7.9.10)$$

which is of the form (7.9.9). Thus finding  $\rho^0 \neq 1$  from (7.9.9) is not in itself proof of a non-minimal Higgs mechanism.

Again, the difference between the two cases is the fact that the value of  $\rho$ , in the minimal model, is calculable in principle.

## 7.10 Beyond the standard model

We cannot end this chapter without mentioning the large variety of options possible if the SM is not the final word. There are in fact arguments indicating that the minimal SM with fundamental Higgs fields cannot be the full story and new physics must appear beyond some high energy scale.

As we have seen, the Higgs mechanism is a clever way of putting together separate gauge groups and couplings for each interaction while allowing the existence of massive vector bosons; this leaves open the possibility that all observed interactions derive from a unified theory at some more fundamental level. The grand unified theories (see Chapter 28) set the scale for this unification around  $10^{15}\text{--}10^{16}\text{ GeV}/c^2$  but the inclusion of gravity would suggest a scale of the order of the Planck energy  $E_P \sim 10^{19}\text{ GeV}$ .

If for no other reasons, the mere fact that gravity is outside the SM tells us that new physics must emerge at some large energy scale  $\Lambda$  (i.e. equivalently at some small distance). The question (one of many questions, actually!) is: what this scale  $\Lambda$  is, and how one can explain the huge value of  $E_P/M_W$ , i.e. the ratio between the Planck scale and the electroweak scale.

Recall that, in the SM, a natural scale is set by the vacuum expectation value of the Higgs field  $v$ , related to the parameters of the Higgs potential, and it has a rather precise value (4.2.38)

$$v = \frac{\mu}{\sqrt{\lambda}} = (\sqrt{2}G)^{-\frac{1}{2}} \simeq 246 \text{ GeV}. \quad (7.10.1)$$

If  $\Lambda \sim 10^{15}\text{--}10^{16}\text{ GeV}/c^2$ , the problem arises of explaining the presence of two such enormously different energy scales in the theory: the so-called hierarchy problem. For a very pedagogical introduction, see Altarelli (1989).

Many unanswered questions in the SM may hint at how to go beyond it. Some of these are:

1. What is the origin of the electroweak symmetry breaking? This is directly related to the hierarchy problem.
2. What is the origin of CP violation (see Chapter 19)?
3. What determines the mass spectrum of the ‘fundamental’ ingredients of the SM and how many of its parameters are really fundamental?
4. Is the observed gauge group unified at a larger scale and does this unification include gravity?
5. Is there a theory of ‘everything’?

No discussion of the many theoretical ideas proposed is even vaguely possible here. We merely list the principal categories:

- (a) *compositeness* of some or all of the ‘elementary’ constituents of the SM (i.e. of its fermions and/or of the Higgs);

- (b) *technicolour*, i.e. compositeness only of the Higgs sector (Weinberg, 1976b; Susskind, 1977);
- (c) *supersymmetry*, i.e. the symmetry relating bosons and fermions (Wess and Zumino, 1974; see, e.g., Van Nieuwenhuizen, 1981, and Haber and Kane, 1985, for references);
- (d) *theories of ‘everything’* as, for example, superstring theories (Green and Schwarz, 1984) of which, for instance, the so-called heterotic string has enjoyed considerable popularity (Gross *et al.*, 1985).

For the time being, no evidence for any of these mechanisms has been found.

From the CERN  $S\bar{p}pS$  colliders we have a limit on a possible second generation of gauge vector bosons (CHARM, 1989)  $M_{Z'} > 280$  GeV. No squark or gaugino (i.e. the supersymmetric partners of quarks and gauge vectors) below  $\sim 100$  GeV have been found nor have any heavy stable charged particles been seen at the 1.8 Tevatron by CDF (CDF, 1989). No fourth quark generation (i.e. no  $b'$ ) is found by DELPHI at LEP 1 below 44 GeV in the decay of the  $Z$  (DELPHI, 1990). A summary of the situation can be found in Dydak (1991).

# 8

## e<sup>+</sup>e<sup>-</sup> physics and the standard model

The recent story of narrow resonance discoveries (see Chapter 11) has shown how the properties of systems with quantum numbers of the photon ( $1^{--}$ ) can best be studied with e<sup>+</sup>e<sup>-</sup> colliders. In this chapter we review some of the information that has come from e<sup>+</sup>e<sup>-</sup> machines. In particular, we shall see what support they provide for the SM. We also discuss the perspective for future e<sup>+</sup>e<sup>-</sup> colliders.

### 8.1 Electron–positron storage rings

The ideal tools for studying the spectroscopy of the new vector meson particles have undoubtedly been the various e<sup>+</sup>e<sup>-</sup> colliding beam machines: SPEAR at SLAC, DORIS at DESY (Deutsches Elektronen Synchrotron), PETRA at DESY and, more recently, SLC at Stanford and LEP 1 at CERN though the actual discovery (Aubert *et al.*, 1974; Herb *et al.*, 1977; UA1, 1983; UA2, 1983) of some of these particles occurred on the proton machines (Brookhaven, Fermilab and CERN).

The reason for the latter lies in the narrowness of these particles; one can simply miss them as one varies the energy. On the other hand, once discovered, the fact that  $J/\Psi(3097)$ ,  $\Upsilon(9.46)$  and the  $Z$  are vector particles  $1^{--}$ , and thus couple naturally to a virtual photon, makes an e<sup>+</sup>e<sup>-</sup> machine particularly efficacious since the main channel of e<sup>+</sup>e<sup>-</sup> annihilation is into a virtual photon.

Thus, it is rather difficult in an e<sup>+</sup>e<sup>-</sup> machine to sit right on top of one of these very narrow resonances whose width may be much smaller than the energy resolution of the machine itself. On the other hand, once the mass of a narrow resonance is known, an e<sup>+</sup>e<sup>-</sup> machine can be tuned to the right energy to obtain an extremely large number of events.

In a hadronic machine, the reaction not only does not proceed uniquely through the  $1^{--}$  channel, but the  $1^{--}$  states are produced together with a

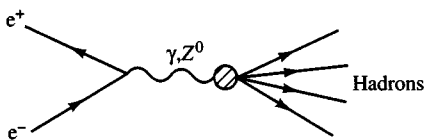
lot of other particles. Thus, once a particular decay channel (like  $e^+e^-$  or  $\mu^+\mu^-$ ) is selected, and the centre-of-mass energy is above the production threshold, the resonance is produced over all the available phase space and a narrow peak gets smeared out into a broader bump.

The rôle of  $e^+e^-$  machines has been so important in the development of the new narrow resonance spectroscopy as to merit a short digression on their origin, their kinematics, some of their properties and some of their achievements.

Colliding-beam  $e^+e^-$  machines were first advocated by B. Touschek in the late fifties, but not even the greatest optimist could have foreseen the development that took place after the early days of the single ring device ADA (Anello Di Accumulazione) whose operation began in 1960.

In an  $e^+e^-$  machine there is no distinction between ‘beam’ and ‘target’ particles, and each beam has about the same density of particles (typically,  $10^8\text{--}10^{12}$  particles per beam depending on the kind of particle). In a fixed-target machine, the density of particles in the target is of course much higher. Thus, to have a comparable rate of events, in an  $e^+e^-$  machine particles must be accumulated for hours (which corresponds to billions of revolutions) and this is the reason for the ‘storage ring’ approach.

One of the greatest advantages of colliding-beam devices as compared with conventional fixed-target accelerators is, of course, the enormous gain in energy that one obtains. A further advantage of  $e^+e^-$  machines, in particular, is that for hadronic production at least at the leptonic vertex, the reaction is supposed to be understood since at lower energies one virtual photon exchange, and at higher energies, photon and  $Z^0$  exchanges dominate so that a reaction proceeds essentially as shown:



Furthermore, at low energies the quantum numbers  $J^{PC}$  of the final state are well defined being those of the photon  $1^{--}$ . In this case, the analysis of the final state is not obscured by the need to separate the various contributions that would be present in channels involving hadrons (as, for instance, in  $pp$  or  $p\bar{p}$  colliders). At higher energies the final state still has  $J = 1$  but its parity is not determined on account of  $Z^0$  exchange.

When the final state is simply a hadron-antihadron pair,  $h\bar{h}$ , one has a direct measurement of the hadron’s electromagnetic form factor in the time-like region.

Let  $m_i$ ,  $\mathbf{p}_i$  and  $E_i$  ( $i = 1, 2$ ) be the masses, momenta and energies of the initial particles in the LAB. Since the LAB and CM essentially coincide,

the total CM energy is given by

$$E_{\text{CM}}^2 = (E_1 + E_2)^2 - (\mathbf{p}_1 + \mathbf{p}_2)^2 = m_1^2 + m_2^2 + 2(E_1 E_2 - \mathbf{p}_1 \cdot \mathbf{p}_2). \quad (8.1.1)$$

For head-on collisions ( $\mathbf{p}_1 = -\mathbf{p}_2, E_1 = E_2 = E$ ) we have

$$E_{\text{CM}} = 2E. \quad (8.1.2)$$

Compare this with a fixed-target collision ( $\mathbf{p}_2 = 0, E_2 = m_2$ ) where we would have, at high energy,

$$E_{\text{CM}}^2 = m_1^2 + m_2^2 + 2m_2 E \simeq 2m_2 E. \quad (8.1.3)$$

Thus, as an example, to attain the equivalent maximum CM energy of  $\simeq 100$  GeV at which the  $e^+e^-$  machine LEP 1 operates, one would need an  $e^+$  beam striking a stationary target at an energy of approximately  $10^7$  GeV!

As already mentioned, the shortcoming of a collider as compared with a fixed-target accelerator lies in the intensity, whose measure in a storage ring is given by the *luminosity*. For a given reaction, this is defined as the rate of interactions per unit cross-section

$$\text{Rate} = L\sigma \equiv N. \quad (8.1.4)$$

If  $n_i$  ( $i = 1, 2$ ) are the number of particles per bunch,  $f$  is the frequency of revolution,  $b$  the number of bunches per beam and  $A$  the transverse area of the beam, the event rate is given by

$$N = \frac{n_1 n_2}{A} b \sigma f = L\sigma. \quad (8.1.5)$$

For a Gaussian density distribution with transverse r.m.s. radii  $\sigma_x, \sigma_y$  we have  $A = 4\pi\sigma_x\sigma_y$ . If we introduce the beam currents  $I_i = n_i e f b$  ( $e$  being the magnitude of the electron charge) we finally have

$$L = \frac{I_1 I_2}{e^2 b f A}. \quad (8.1.6)$$

Typical parameters for an electron-positron storage ring are  $f \simeq 10^6 \text{ s}^{-1}$ ,  $I_i \simeq 50 \text{ mA} \simeq 3 \times 10^{17} e/\text{s}$ ,  $b = 1$ ,  $\sigma_x \simeq \sigma_y \simeq 0.03 \text{ cm}$ , yielding a luminosity of about  $L \simeq \frac{1}{4} \times 10^{32} \text{ cm}^{-2}\text{s}^{-1}$ . With a cross-section  $\sigma \simeq 1\mu\text{b} = 10^{-30} \text{ cm}^2$ , (8.1.5) leads to a (somewhat optimistic) counting rate of about  $N = 25$  collisions per second.

In practice  $e^+e^-$  machines operate at luminosities between  $10^{29}\text{--}10^{31} \text{ cm}^{-2}\text{s}^{-1}$  although the new generation of such devices has been planned for a maximum luminosity of  $10^{32} \text{ cm}^{-2}\text{s}^{-1}$ .

It is instructive to compare the previous estimate ( $N \lesssim 100$  events per second for  $\sigma \simeq 1\mu\text{b}$ ) with the corresponding rate expected for a conventional fixed-target accelerator, where

$$N = n \varrho \sigma, \quad (8.1.7)$$

$n$  being the number of particles per second in the beam (typically  $n \simeq 10^{12} \text{ s}^{-1}$ ),  $\varrho$  the density of nucleons in the target and  $l$  the target length (typically  $\varrho l \simeq 10^{23} \text{ cm}^{-2}$ ). For a cross-section  $\sigma = 1\mu\text{b}$  one thus gets an estimate of  $N \simeq 10^5$  events per second which would only be matched by a luminosity  $L \simeq 10^{35} \text{ cm}^{-2}\text{s}^{-1}$ ! Design luminosities for the SSC (Superconducting Super Collider) in the USA and for LHC (Large Hadron Collider) at CERN are  $10^{33} \text{ cm}^{-2}\text{s}^{-1}$  and  $\sim 10^{34} \text{ cm}^{-2}\text{s}^{-1}$  respectively.

In  $e^+e^-$  colliders, the maximum luminosity is severely limited by the electromagnetic forces acting between: (i) the particles of the same beam; (ii) the particles in different beams; (iii) the particles and the ring. The luminosity varies with the beam energy  $E$  in a way which may be very different for machines of comparable energy. Typically, however, it increases with a power law between  $E^2$  and  $E^4$  up to a maximum energy and then decreases very steeply ( $\sim E^{-10}$ ).

The rich physics harvest which emerged from the study of the spectroscopy of the narrow resonances owed everything to a series of gigantic detectors whose acronymic names have become part of the physics heritage (see Chapters 11 and 12).

Another important feature of  $e^+e^-$  machines is that the magnetic guide field together with the synchrotron radiation lead to transverse polarizations of the beams, with electron (positron) polarization antiparallel (parallel) to the magnetic field. The polarization arises because the synchrotron radiation induces up-down spin transitions which, for the positron, say, are larger for down $\rightarrow$ up than for up $\rightarrow$ down, where ‘up’ means along the guide field  $B$ .

If we start from unpolarized beams, the increase of polarization with time goes as

$$P(t) = P_0(1 - e^{-t/\tau}), \quad (8.1.8)$$

where the proportionality factor is  $P_0 = 8\sqrt{3}/15 = 0.92$ . The  $\tau$  parameter depends on the machine parameters and on energy. The above formula is an idealization and the polarization is destroyed when the operating energy is close to so-called ‘depolarizing’ resonances.

## 8.2 The new $e^+e^-$ colliders: TRISTAN and LEP

TRISTAN, the Japanese  $e^+e^-$  collider at KEK, has been in operation since the autumn of 1986. It began functioning with an energy of 25 GeV per beam and was upgraded reaching a CM energy  $\sqrt{s} = 61.4 \text{ GeV}$  in the spring of 1989. There are three general purpose detectors, AMY, TOPAZ and VENUS, and one detector, SHIP, specially designed to search for highly ionizing particles. The parameters of the collider are given in Table 8.1.

	Design parameters	Achieved
Beam energy	30 GeV	30.4 GeV
Injection energy	8 GeV	8.0 GeV
Single bunch current	5 mA	4.8 mA
$2e^+ + 2e^-$ beam current	15 mA	13.6 mA
Filling time	15~20 min	20~30 min
Beam life	4~5 hr	4 hr with $\sim 8$ mA
Beam emittance	$1.6 \times 10^{-7}$ m rad	$1.0 \times 10^{-7}$ m rad
Emittance ratio, $V/H$	2~6%	0.5~1%
$\beta_V^*/\beta_H^*$	0.1 m/1.6 m	0.1 m/1.8~2 m
Peak luminosity	$1.6 \times 10^{31}$ cm $^{-2}$ s $^{-1}$	$\sim 2 \times 10^{31}$ cm $^{-2}$ s $^{-1}$
Integrated luminosity/day		300~400 nb $^{-1}$

Table 8.1. Machine parameters for the TRISTAN  $e^+e^-$  collider.

LEP (Large Electron Positron collider) at CERN came into operation in August 1989 with a CM design energy of  $\sim 110$  GeV in phase 1.

At the time of writing, LEP 1 is the great focus of excitement in the field. It was constructed to study the intermediate vector boson  $Z^0$  which was expected to dominate  $e^+e^-$  collisions in the energy region around 90 GeV (Fig. 8.1).

A preliminary indication of this dominance is seen in the TRISTAN data on  $R = \sigma(e^+e^- \rightarrow \text{hadrons})/\sigma(e^+e^- \rightarrow \mu^+\mu^-)_{QED}$  (Fig. 8.2) where  $\sigma(e^+e^- \rightarrow \mu^+\mu^-)_{QED} \equiv 4\pi\alpha^2/3s$  is evaluated in (8.3.5). The final, dramatic, indication of this expectation is seen in the beautiful LEP cross-section in the  $Z^0$  mass region in Fig. 8.2(b) (DELPHI, 1990).

The layout for LEP is shown schematically in Fig. 8.3. Note the circumference of the ring, nearly 27 km! (By comparison with the tunnel planned for SSC, however, nearly 84 km, this appears quite modest.)

LEP hosts four huge experimental detectors ALEPH, DELPHI, L3 and OPAL run by large international collaborations. (It is a sobering thought that the number of physicists, e.g. in the L3 collaboration, is 581 from 38 institutions from 13 countries at the time of writing.)

Each detector is equipped with a solenoidal magnet, central tracking chamber, electromagnetic and hadron calorimeters, muon detectors, luminosity monitor and a high degree of hermeticity. The complementary aspects of the four detectors make the whole system rather complete for a wide ranging physics programme [for a comparative analysis of the four detectors, see Thresher (1988)].

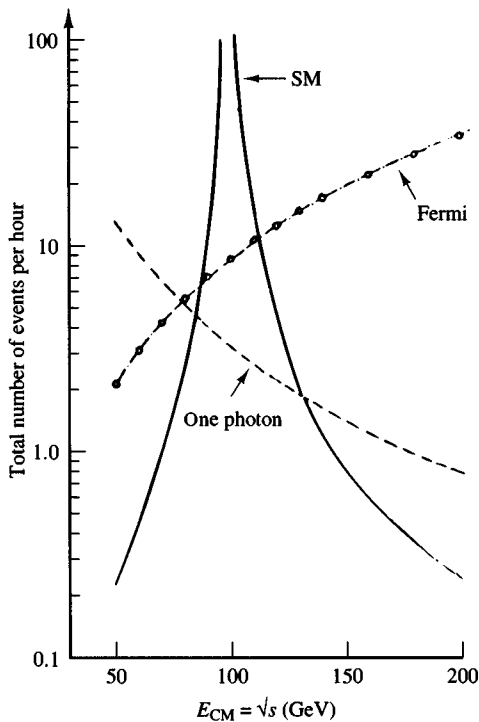


Fig. 8.1. Qualitative prediction of cross-sections for  $e^+e^-$  annihilation as a function of CM energy in the SM, the old Fermi theory and for purely electromagnetic annihilation (From Richter, 1976).

Table 8.2 gives the LEP design parameters. These correspond to between 1 and  $(3\text{--}4)\times 10^6$   $Z^0$ 's per year at LEP 1. In the first year of operation,  $4.2 \times 10^5$   $Z^0$ 's were produced and a maximum luminosity of  $6 \times 10^{30} \text{cm}^{-2}\text{s}^{-1}$  achieved. Increases of both energy (up to  $\sqrt{s} \sim 190$  GeV) and intensity is planned in LEP 2.

Concerning polarized beams, in addition to the natural transverse polarization, spin rotation at LEP will also yield longitudinal polarization and this could prove extremely useful in allowing measurements of the weak couplings at the  $Z^0$  peak with a precision otherwise unattainable. The most promising points, in this context, are the left-right asymmetry and the longitudinal polarization predictions which will be discussed in Section 8.8 and which could be the key to a substantial reduction of the experimental error on several parameters of the SM. As an example,  $\sin^2 \theta_W$  could be measured at LEP, without polarization, to an accuracy of 0.00033 in a  $200 \text{ pb}^{-1}$  exposure at the  $Z^0$  peak, whereas it becomes  $\sim 0.00013$  with 50% polarization and  $30 \text{ pb}^{-1}$ !

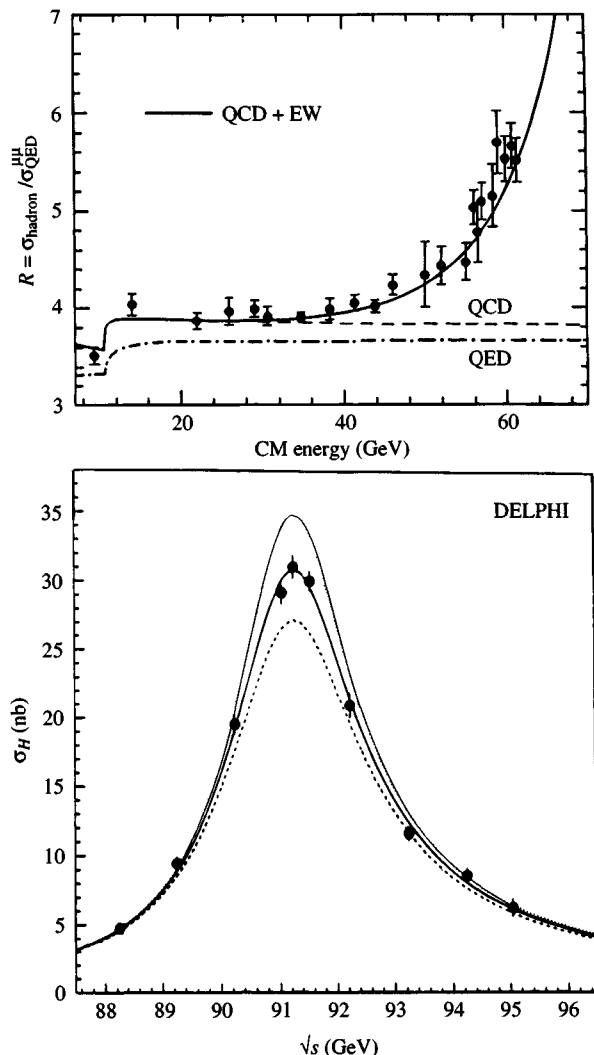


Fig. 8.2. (a) The prediction for the  $e^+e^-$  cross-section in the SM compared with the data from TRISTAN. The full contributions: electroweak (EW) plus QCD is shown by the continuous line. The QCD and the QED contributions are shown by dashed and dot-dashed lines respectively. (b) The cross-section for  $e^+e^- \rightarrow$  hadrons around the  $Z^0$  mass (DELPHI, 1990). The dotted, continuous and dashed lines are the predictions of the SM assuming two, three and four massless neutrino species respectively. (From Abe, 1991.)

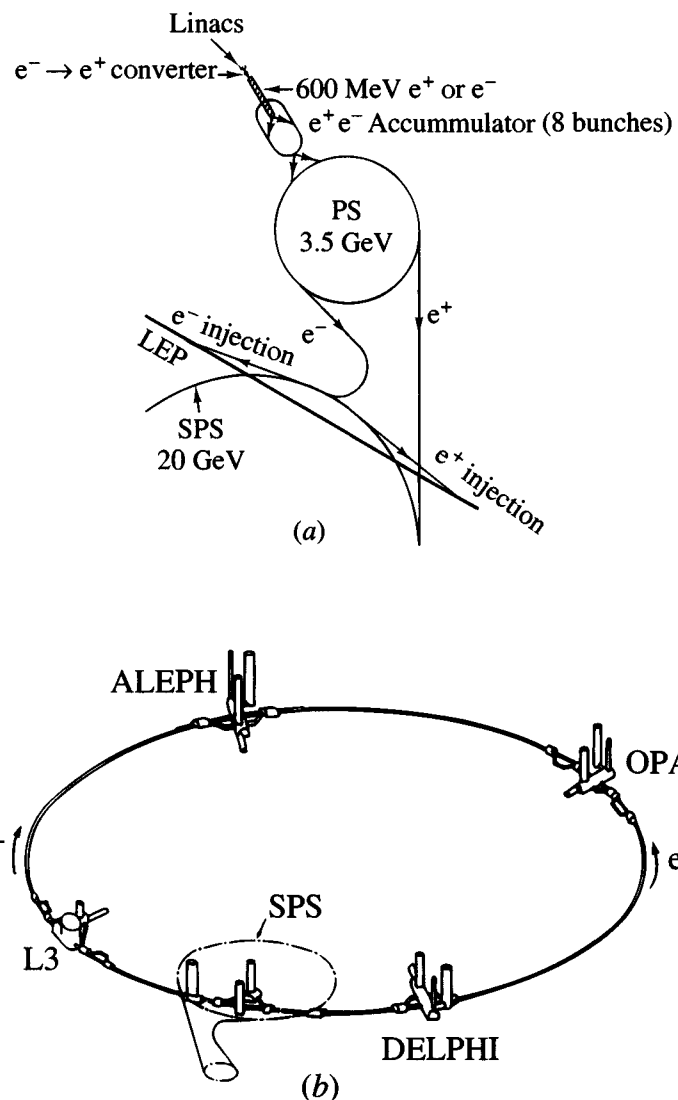


Fig. 8.3. Schematic layout of LEP (see text).

Finally, we wish to mention the Stanford Linear Collider (SLC) operating at about 100 GeV CM energy, whose first  $Z^0$  was recorded on April 12, 1989. SLC is a single pass collider which consists of the old 3 km Stanford linac that now accelerates electrons (and positrons) to 50 GeV and two new collider arcs that bring them into head-on collision at the detector. Every other electron bunch from the injector is diverted onto a positron producing target. The low energy positron bunch is reinjected into the

	Phase 1	Phase 2
Beam energy (GeV)	55	95
Circumference (km)	26.66	26.66
Dipole field (T)	0.0645	0.1114
Injection energy (GeV)	20	20
R.F. frequency (MHz)	352	352
Dist. between supercond. quads (m)	$\pm 3.5$	$\pm 3.5$
r.m.s. bunch length (mm)	17.2	13.9
r.m.s. beam radii:		
$\sigma_x$ ( $\mu\text{m}$ )	255	209
$\sigma_y$ ( $\mu\text{m}$ )	15.3	10.8
Bunch spacing ( $\mu\text{s}$ )	22	22
Nom. luminosity ( $\text{cm}^{-2}\text{s}^{-1}$ )	$1.6 \times 10^{31}$	$2.7 \times 10^{31}$
Beam lifetime (h)	6	5
r.m.s. energy spread	$0.92 \times 10^{-3}$	$2.06 \times 10^{-3}$
Current (4 bunches) (mA)	3	3
Synchr. rad. loss per turn (GeV)	0.263	2.303

Table 8.2. LEP design parameters.

linac via a return line. Both electron and positron beams are very diffuse and are cooled radiatively in damping rings. The positron beam is then accelerated to 50 GeV by the linac and reaches the collision point just in time to collide with the next 50 GeV electron bunch. Notice that subsequent phases of the same accelerating field are used here to accelerate both  $e^+$  and  $e^-$  bunches. The layout of SLC is shown in Fig. 8.4.

### 8.3 $e^+e^-$ physics at energies $\ll M_Z$

The physics involved in  $e^+e^-$  collisions depends very much on the energy range under consideration. The current ‘last word’ is presently being written at LEP 1 where the effects induced by working at the  $Z^0$  mass are under study. In this section, we shall deal with lower energies where only electromagnetic interactions need to be taken into account.

If we assume that only electromagnetic interactions are relevant, to lowest order  $\alpha^2$  the only allowed processes are Bhabha scattering (Fig. 8.5 (a, b)), muon production (Fig. 8.5b) and  $2\gamma$  annihilation (Fig. 8.6(c)).

Although only of order  $\alpha^3$  (or higher) (Fig. 8.6) radiative corrections may be rather important and have usually to be removed before giving

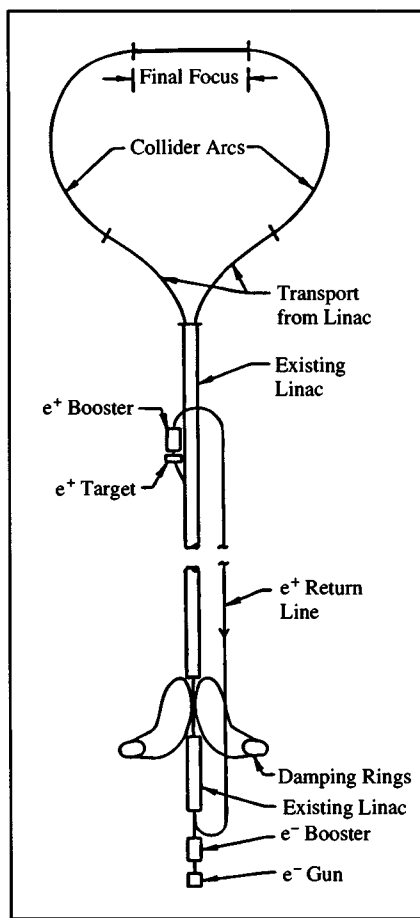
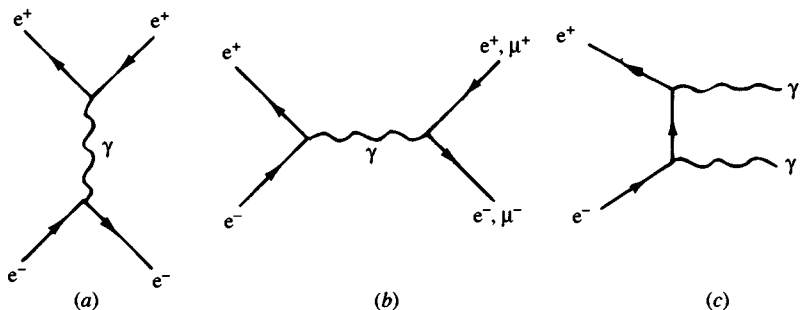
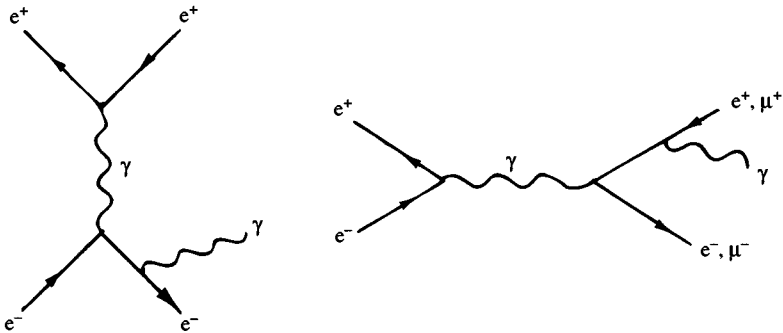
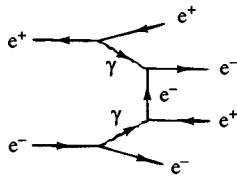


Fig. 8.4. Schematic layout of SLC (see text).

Fig. 8.5. Feynman diagrams for Bhabha scattering ( $e^+e^- \rightarrow e^+e^-$ ), muon production ( $e^+e^- \rightarrow \mu^+\mu^-$ ) and two-photon annihilation.

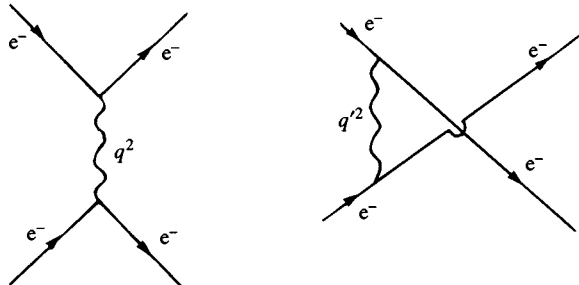
Fig. 8.6. Radiative corrections to  $e^+e^- \rightarrow e^+e^-, \mu^+\mu^-$ .Fig. 8.7. Order  $\alpha^4$  diagram for  $e^+e^- \rightarrow e^+e^+e^-e^-$ .

an experimental result. These corrections play an increasingly important rôle with increasing energy (see Caffo *et al.*, 1989).

In order  $\alpha^4$  we find a new class of phenomena described by  $2\gamma$  scattering. An example is shown in Fig. 8.7. After integrating over the photon spectra one obtains a cross-section proportional to  $\alpha^4 \ln^2(E/m_e)$ . In the GeV region,  $\ln(E/m_e) \simeq 10$  so that one factor of  $\alpha$  is practically cancelled by the integration.

Since all these processes can be calculated in QED, their experimental analysis provides a direct test of QED, to the extent that one may neglect electroweak effects.

In the case of  $e^-e^- \rightarrow e^-e^-$  scattering (Möller scattering)



where only space-like photons contribute the CM cross-section to produce

an  $e^-$  at angle  $\theta$  (as can be derived from the rules in Appendix 2) is

$$\frac{d\sigma}{d\Omega} = \frac{\alpha^2}{2s} \left( \frac{q'^4 + s^2}{q^4} + \frac{s^2}{q^2 q'^2} + \frac{q^4 + s^2}{q'^4} \right), \quad (8.3.1)$$

where if we neglect the electron mass,  $q^2 = -s \cos^2 \frac{1}{2}\theta$ ,  $q'^2 = -s \sin^2 \frac{1}{2}\theta$ ;  $s = (p_{e_1} + p_{e_2})^2$  is the square of the total energy.

The cross-section (8.3.1) is forward–backward symmetrically peaked. The tests on the validity of QED consist in studying the shape of the angular distribution. Deviations are expected to be more prominent in the central region ( $\cos \theta \simeq 0$ ) corresponding to the largest values of  $q^2$  and  $q'^2$ .

The cross-section for Bhabha scattering with the final  $e^+$  emerging at angle  $\theta$  to the initial  $e^+$  beam proceeds via the diagrams (a) and (b) of Fig. 8.5 involving both time-like and space-like photons, and is given by

$$\frac{d\sigma}{d\Omega} = \frac{\alpha^2}{2s} \left( \frac{q'^4 + s^2}{q^4} + \frac{2q'^4}{q^2 s} + \frac{q'^4 + q^4}{s^2} \right). \quad (8.3.2)$$

This angular distribution presents a strong forward peak only (coming from the first term).

The data are shown in Fig. 8.8 and compared with the QED calculation.

Of great interest is the reaction  $e^+e^- \rightarrow \mu^+\mu^-$  which, electromagnetically, proceeds via time-like photon exchange (Fig. 8.5(b)) *only*. At high energies, however, we can have interference between the pure photon exchange and the  $Z^0$ . This opens new possibilities that will be discussed in detail in Section 8.8.

Restricting ourselves to energies  $\sqrt{s} \ll M_Z$ , the electromagnetic cross-section for  $e^+e^- \rightarrow \mu^+\mu^-$  from Fig. 8.5(b) is

$$\frac{d\sigma}{d\Omega} = \frac{\alpha^2}{4s} \frac{p_\mu}{E_\mu} \left[ (1 + \cos^2 \theta) + \left( 1 - \frac{p_\mu^2}{E_\mu^2} \right) \sin^2 \theta \right]. \quad (8.3.3)$$

For  $p_\mu \simeq E_\mu$ , i.e. for  $\sqrt{s} \gg m_\mu$ ,

$$\frac{d\sigma}{d\Omega} = \frac{\alpha^2}{4s} (1 + \cos^2 \theta). \quad (8.3.4)$$

Integrating over angles gives

$$\sigma(e^+e^- \rightarrow \mu^+\mu^-)_{\text{QED}} \equiv \frac{\alpha^2}{s} \frac{4\pi}{3} \simeq \frac{22 \text{nb}}{E^2} \quad (E \text{ in GeV}). \quad (8.3.5)$$

The possible deviations from QED will depend on  $s$  and can be detected by measuring the magnitude of the cross-section.

Also the reaction  $e^+e^- \rightarrow \tau^+\tau^-$  is expected to proceed according to (8.3.3)!

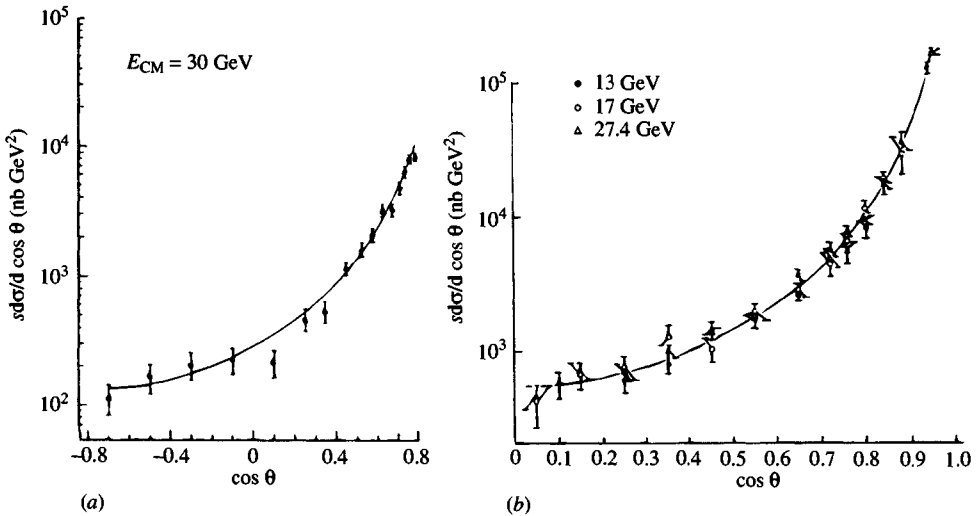


Fig. 8.8. Comparison of data with QED calculation for angular dependence in Bhabha scattering: (a) 30 GeV energy data over wide range of  $\theta$ , (b) several energies over smaller range of  $\theta$ . (From Berger *et al.*, 1980.)

The comparison between QED for the two reactions  $e^+e^- \rightarrow \mu^+\mu^-$ ,  $\tau^+\tau^-$  and experiment (Kinoshita, 1978; Barber *et al.*, 1979; Berger *et al.*, 1980) is given in Fig. 8.9, where the energy goes up to  $\simeq 30$  GeV.

The reaction  $e^+e^- \rightarrow 2\gamma$  proceeds via electron exchange (see Fig. 8.10) and the CM cross-section is given by

$$\frac{d\sigma}{d\Omega} = \frac{\alpha^2}{2s} \left( \frac{q^2}{q'^2} + \frac{q'^2}{q^2} \right). \quad (8.3.6)$$

Deviations from QED will necessitate the introduction of a form factor which in this case is usually parametrized as

$$F(q^2) = 1 \pm q^4/\Lambda_\pm^4 \quad (8.3.7)$$

and one finds (Kinoshita, 1978; Barber *et al.*, 1979; Berger *et al.*, 1980)  $\Lambda_+ \simeq 10.7$  GeV/c,  $\Lambda_- \simeq 9$  GeV/c from the data at  $\sqrt{s} \ll M_Z$ .

In fact, this reaction provides interesting tests of QED and the SM also at high energies  $\sqrt{s} \sim M_Z$ , since there are no weak interaction corrections to this process to lowest order in the SM. There are two ways to interpret the high energy data. (i) Assuming the  $Z^0$  does not contribute we can, as before, introduce the form factor  $F(q^2)$  and find (OPAL, 1990; L3, 1990a)  $\Lambda_+ > 103$  GeV/c,  $\Lambda_- > 118$  GeV/c. (ii) Allowing for a breakdown of the SM in which  $Z^0$  could couple directly to photon, the data puts upper limits on the branching ratios for  $Z^0$  into various channels:  $\gamma\gamma <$

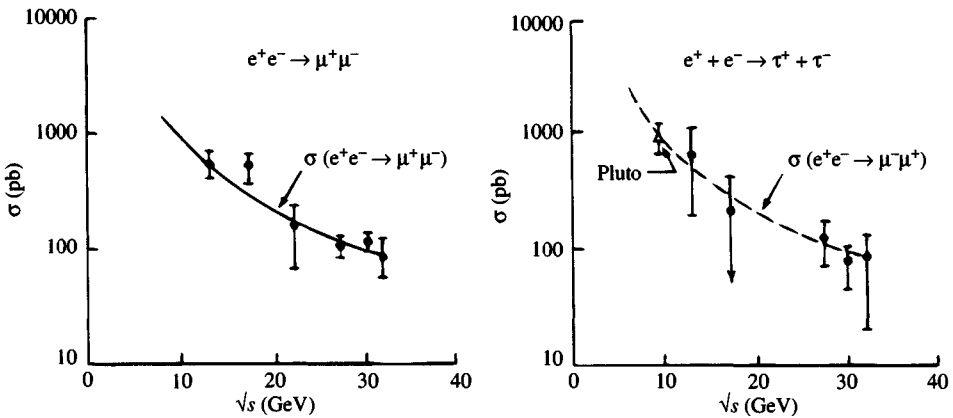


Fig. 8.9. Comparison of cross-section data for  $e^+e^- \rightarrow \mu^+\mu^-$  and  $\tau^+\tau^-$  with QED calculations as function of CM energy. (From Berger *et al.*, 1980.)

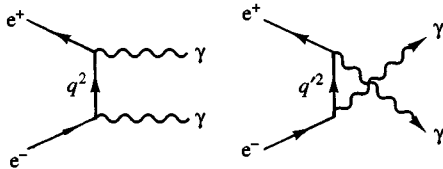


Fig. 8.10. Feynman diagrams for  $e^+e^- \rightarrow 2\gamma$ .

$2.9 \times 10^{-4}$ ,  $\pi^0\gamma < 2.9 \times 10^{-4}$ ,  $\eta\gamma < 4.1 \times 10^{-4}$ ,  $\gamma\gamma\gamma < 1.2 \times 10^{-4}$  at the 95% CL.

The purely electromagnetic angular distributions and relative magnitudes of the four processes ( $e^-e^- \rightarrow e^-e^-$ ,  $e^+e^- \rightarrow e^+e^-$ ,  $e^+e^- \rightarrow \mu^+\mu^-$ ,  $e^+e^- \rightarrow \gamma\gamma$ ) for a beam energy of 1 GeV are shown in Fig. 8.11. As can be seen, for  $e^+e^-$  collisions, Bhabha scattering gives the highest cross-section.

For this reason, small angle Bhabha scattering is used to measure the luminosity, so that in a sense the ‘absolute’ measurements are really a comparison with the magnitude of small angle Bhabha scattering.

As we have seen, from both low and high energy  $e^+e^-$  data we get good support for the validity of QED.

It will be one of the main aims of the next chapters to discuss the phenomenology of hadron production in  $e^+e^-$  collisions in the *high energy* region. This, as we have already pointed out, is the natural source of information on the new narrow vector meson resonances.

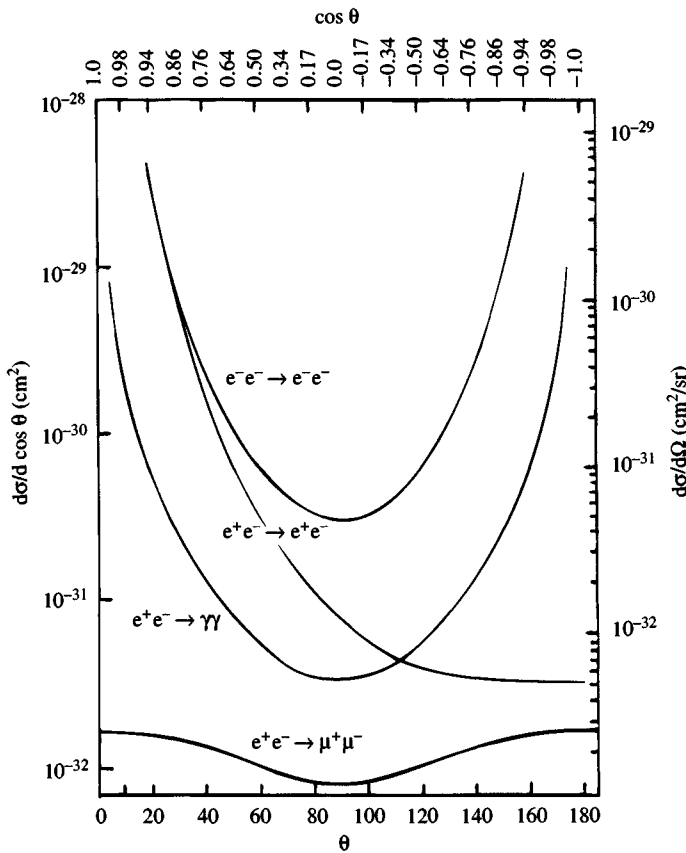


Fig. 8.11. Comparison of the QED differential cross-section for  $e^+e^- \rightarrow e^+e^-$ ,  $\mu^+\mu^-$ ,  $2\gamma$  and  $e^-e^- \rightarrow e^-e^-$  at a beam energy of 1 GeV. (From Wiik and Wolf, 1978.)

For a detailed discussion of *low energy* hadron phenomenology in  $e^+e^-$  colliders, see Wiik and Wolf (1978).

#### 8.4 $e^+e^-$ and the standard model

The comparative high precision (relative to hadronic machines) attainable at  $e^+e^-$  colliders, has made it possible to perform at SLC (SLAC) and LEP (CERN) many checks of the SM predictions and to obtain much information on the SM parameters. In what follows, we concentrate on the results obtained at LEP 1.

As we have emphasized, in the SM the electroweak interactions are mediated by the exchange of photons,  $Z^0$ s and  $W$ s whose couplings to

the basic fermions (leptons and quarks) are a mixture of vector and axial vector as summarized in (5.1.1) and (5.1.3) to (5.1.5).

In addition, the theory requires the neutral scalar particle called the Higgs meson  $H$  whose mass is left undetermined by the theory.

As pointed out in Chapter 4, the most dramatic confirmation of the SM comes, of course, from the actual discovery of the gauge vector boson. More importantly, the experimental masses are very near the values anticipated by the SM. The ultimate confirmation of the theory will come from detecting the Higgs meson. For the time being this is the most serious missing link in the theory. In every other respect the theory has been remarkably well confirmed by the data.

An early indication of success was the astounding closeness of the many determinations of the Weinberg angle from different reactions.

As already mentioned, the SM has been extended to accommodate the three known generations of leptons  $\begin{pmatrix} \nu_e \\ e^- \end{pmatrix}$ ,  $\begin{pmatrix} \nu_\mu \\ \mu^- \end{pmatrix}$  and  $\begin{pmatrix} \nu_\tau \\ \tau^- \end{pmatrix}$ , where the neutrinos are treated as massless (though they need not be massless and possibly are not). All these particles interact like  $\begin{pmatrix} \nu_e \\ e^- \end{pmatrix}$  in the SM as discussed in Sections 4.2 and 8.6.

The correspondence between the three lepton families and the three generations of quarks  $\begin{pmatrix} u \\ d \end{pmatrix}$ ,  $\begin{pmatrix} c \\ s \end{pmatrix}$  and  $\begin{pmatrix} t \\ b \end{pmatrix}$  is discussed in many chapters throughout the book.

In what follows we present a summary of tests of the SM and of high precision experiments planned to provide the final word on this subject. In particular, spin dependent tests at LEP appear quite promising and will be discussed in some detail.

We focus on four major topics: (i) the angular distributions; (ii) determination of the parameters of the  $Z^0$ ; (iii) neutrino counting and (iv) asymmetries and polarisation measurements. The major source of information comes from the reactions:

$$e^+e^- \rightarrow \mu^+\mu^- \text{ or } \tau^+\tau^-, \quad (8.4.1)$$

$$e^+e^- \rightarrow \nu\bar{\nu}, \quad (8.4.2)$$

$$e^+e^- \rightarrow \text{hadrons}. \quad (8.4.3)$$

## 8.5 LEP data near the $Z^0$ peak

Information on the  $Z^0$  mass, its total and partial widths, on the number of neutrino species  $N_\nu$ , and on the couplings  $g_V$  and  $g_A$  have been extracted from the data in the region where the  $Z^0$  pole dominates. An

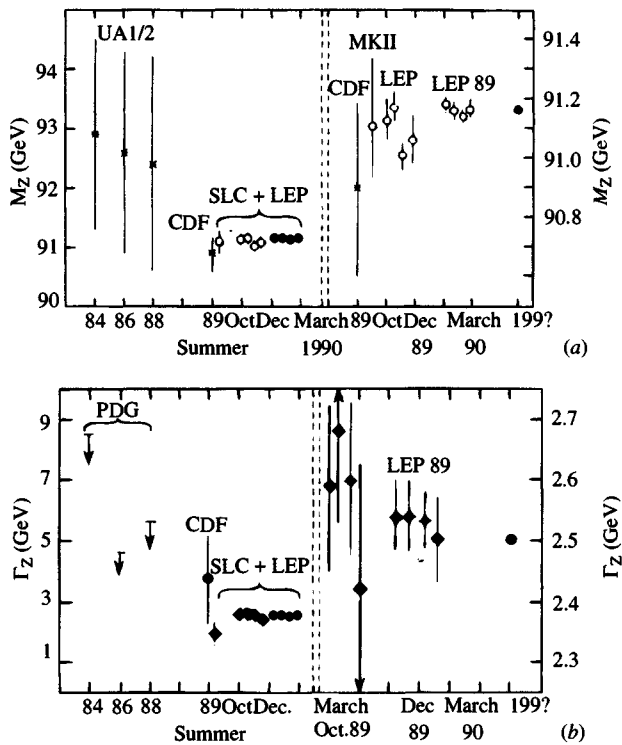


Fig. 8.12. ‘History’ of the  $Z^0$  (a) mass and (b) width measurements during the past few years (from Dittmar, 1990).

indication of the quality of the data at the time of the 25th International Conference on High Energy Physics can be seen in Fig. 8.12 (Dittmar, 1990) and Fig. 8.13 (Dydak, 1991). Note the absolutely extraordinary improvement in the accuracy of the measurements in Fig. 8.12! In some cases, the experimental uncertainty is smaller than the theoretical one. The numerical results, which we discuss below in some detail, are given in Table 8.3 (Dydak, 1991). For an updated summary, see Zumerle (1992) (the data in the latter review differ very slightly from those reported in Table 8.3).

### 8.5.1 $e^+e^-$ angular distributions

Consider reactions

$$e^+e^- \rightarrow X$$

for  $\sqrt{s} \approx M_Z$ , which, in lowest order, can take place via the annihilation diagrams in Fig. 8.14.

	ALEPH	DELPHI	L3	OPAL	AVERAGE	$\chi^2/DOF$	SM
$M_Z$ ( $\text{GeV}/c^2$ )	$91.186 \pm 0.013$	$91.188 \pm 0.013$	$91.161 \pm 0.013$	$91.174 \pm 0.011$	$91.177 \pm 0.006$	0.93	
$\Gamma_Z$ ( $\text{GeV}/c^2$ )	$2.506 \pm 0.026$	$2.476 \pm 0.026$	$2.492 \pm 0.025$	$2.505 \pm 0.020$	$2.496 \pm 0.012$	0.32	$2.500 \pm 0.042$
$\sigma_{\text{had}}$ (nb)	$41.78 \pm 0.55$	$42.38 \pm 0.96$	$41.38 \pm 0.65$	$41.88 \pm 0.62$	$41.78 \pm 0.33$	0.27	$41.30 \pm 0.10$
$\Gamma_{\text{had}}$ (MeV)	$1764 \pm 23$	$1756 \pm 31$	$1748 \pm 35$	$1778 \pm 24$	$1764 \pm 14$	0.28	$1747 \pm 34$
$\Gamma_{ee}$ (MeV)	$84.9 \pm 1.1$	$82.0 \pm 1.7$	$84.3 \pm 1.4$	$82.7 \pm 1.0$	$83.6 \pm 0.6$	1.06	$83.8 \pm 0.9$
$\Gamma_{\mu\mu}$ (MeV)	$80.7 \pm 2.2$	$87.2 \pm 3.4$	$83.5 \pm 1.3$	$85.9 \pm 2.0$	$84.1 \pm 1.3$	2.08	$83.8 \pm 0.9$
$\Gamma_{\tau\tau}$ (MeV)	$81.8 \pm 2.2$	$86.0 \pm 3.9$	$83.5 \pm 1.4$	$83.9 \pm 2.3$	$83.2 \pm 1.5$	0.52	$83.8 \pm 0.9$
$\Gamma_l$ (MeV)	$84.2 \pm 1.0$	$83.7 \pm 1.4$	$83.7 \pm 1.1$	$83.6 \pm 0.9$	$83.7 \pm 0.5$	0.13	$83.8 \pm 0.9$
$\Gamma_{\text{had}}/\Gamma_l$	$20.95 \pm 0.30$	$21.00 \pm 0.47$	$21.02 \pm 0.62$	$21.26 \pm 0.31$	$21.08 \pm 0.19$	0.19	$20.86 \pm 0.20$
$g_V(M_Z^2)$	$-0.044 \pm 0.008$	$-0.056 \pm 0.021$	$-0.062 \pm 0.018$	$-0.031 \pm 0.0015$	$-0.045 \pm 0.006$	0.69	
$g_A(M_Z^2)$	$-0.502 \pm 0.003$	$-0.502 \pm 0.003$	$-0.497 \pm 0.005$	$-0.501 \pm 0.003$	$-0.501 \pm 0.002$	0.30	
$\sin^2 \bar{\theta}_W(M_Z^2)$	$0.2288 \pm 0.0023$	$0.2309 \pm 0.0047$	$0.2272 \pm 0.0033$	$0.2315 \pm 0.0024$	$0.2302 \pm 0.0015$	0.23	
$\Gamma_{\text{inv}}$ (MeV)	$489 \pm 20$	$469 \pm 27$	$494 \pm 30$	$476 \pm 23$	$482 \pm 12$	0.19	$502 \pm 5$

Table 8.3.  $Z^0$  parameters at LEP1 (Dydak, 1991). The relation between  $\theta_W$  and  $\bar{\theta}_W$  is discussed in Section 7.6.  $\Gamma_{\text{inv}}$  is explained in Section 8.7. The last column gives the standard model prediction.

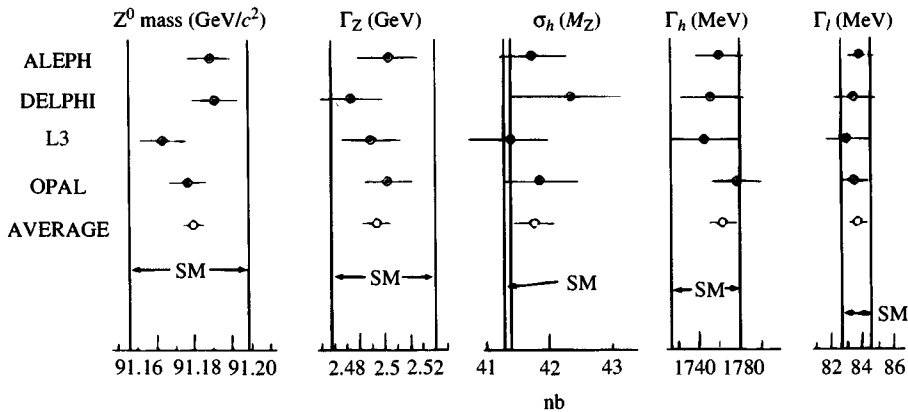


Fig. 8.13. Graphical summary of LEP data at the  $Z^0$  mass six months after the commissioning of LEP, compared with SM predictions (from Dydak, 1991).

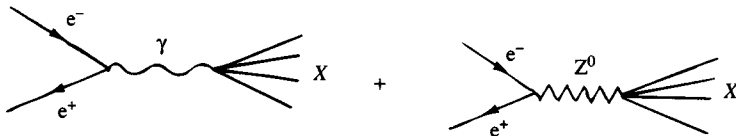


Fig. 8.14. Direct channel diagrams for  $e^+e^- \rightarrow X$  to leading electromagnetic and electroweak order.

Note that for the elastic reaction  $e^+e^- \rightarrow e^+e^-$  there are in addition the exchange diagrams shown in Fig. 8.15.

Compared with the pure QED case we now have interference between  $\gamma$  and  $Z^0$  exchange. (The Higgs particle could also contribute, but as discussed in Section 6.1 its coupling should be very small for the reactions we shall consider).

To be specific consider the simple case

$$e^+e^- \rightarrow \mu^+\mu^-$$

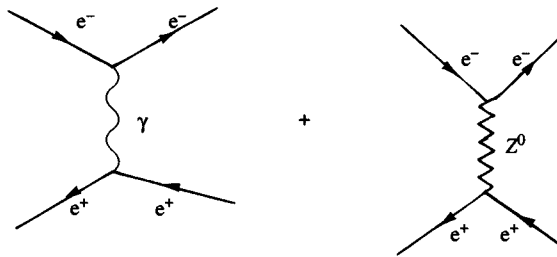
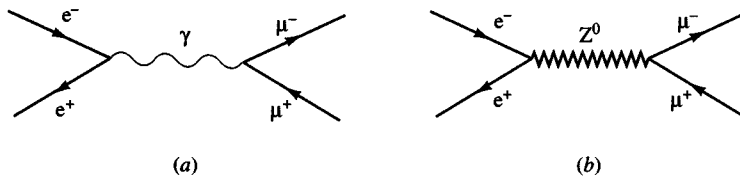
The relevant diagrams are shown in Fig. 8.16.

For the photon diagram, for  $\sqrt{s} \gg m_\mu$ , one has the well known result (easily derived from the rules in Appendix 2):

$$\sigma(e^+e^- \rightarrow \mu^+\mu^-)_{\text{QED}} = \frac{4\pi\alpha^2}{3s}, \quad (8.5.1)$$

where  $s$  = square of CM energy, and the angular distribution in the CM is

$$\left(\frac{d\sigma}{d\Omega}\right)_{\text{QED}} = \frac{\alpha^2}{4s}(1 + \cos^2\theta). \quad (8.5.2)$$

Fig. 8.15. Leading order exchange diagrams for  $e^+e^- \rightarrow e^+e^-$ .Fig. 8.16. Leading order direct diagrams for  $e^+e^- \rightarrow \mu^+\mu^-$ .

The angular distribution can be understood as follows. At high energies the vector coupling  $\gamma^\mu$  will only permit electrons and positrons of opposite helicity to annihilate. (See Section 1.3. This is true also of the axial-vector coupling  $\gamma^\mu\gamma_5$ .) The helicity amplitudes are of the form

$$H_{\mu^+\mu^-;e^+e^-} = M_{\mu^+\mu^-} - M_{e^+e^-} d_{\lambda\mu}^1(\theta) e^{i(\mu-\lambda)\phi}, \quad (8.5.3)$$

where, for simplicity, we use particle labels to indicate helicities, and where  $\lambda = e^+ - e^-$  and  $\mu = \mu^+ - \mu^-$ . From parity invariance

$$M_{-e^+,-e^-} = \pm M_{e^+e^-} \quad (8.5.4)$$

for  $\begin{pmatrix} \text{vector} \\ \text{axial-vector} \end{pmatrix}$  coupling. The differential cross-section then involves

$$|H_{+-;+-}|^2 + |H_{+-;-+}|^2 + |H_{-+;-+}|^2 + |H_{-+;+-}|^2, \quad (8.5.5)$$

which leads to the angular function

$$\begin{aligned} (d_{11}^1)^2 + (d_{-1-1}^1)^2 &= \frac{1}{4}(1 + \cos\theta)^2 + (1 - \cos\theta)^2 \\ &= \frac{1}{2}(1 + \cos^2\theta). \end{aligned} \quad (8.5.6)$$

The matrix element for  $Z$  exchange for  $s \gg m_\mu^2$  will look like  $\gamma$  exchange except that  $e^2/s$  is replaced by

$$\left(\frac{e}{2s_W c_W}\right)^2 \frac{1}{s - M_Z^2 + iM_Z\Gamma_Z} \quad (8.5.7)$$

multiplied by various combinations of  $g_V$  and  $g_A$ , depending on the helicity amplitude involved, which should be of order one. Because  $s$  can equal  $M_Z^2$ , it is essential to include the term depending on the width of the  $Z$  in the propagator.

For  $m_\mu^2 \ll s \ll M_Z^2$ , the new term should cause a small departure from the QED result. Here one has, for the amplitudes

$$\begin{aligned} \frac{\text{Z exchange}}{\text{QED}} &\simeq \frac{1}{4s_W^2 c_W^2} \left( \frac{s}{M_Z^2} \right) \\ &\simeq 2 \times 10^{-4} (s/\text{GeV}^2). \end{aligned} \quad (8.5.8)$$

Thus at energies  $\ll M_Z$  the largest term will arise from interference, and one finds a fractional change

$$\frac{\Delta\sigma}{\sigma_{\text{QED}}} \simeq 2v_e v_\mu (s/M_Z^2). \quad (8.5.9)$$

Given that  $\sin^2 \theta_W$  is close to the value 0.25 that makes  $v_e = 0, v_\mu = 0$ , the effect is exceedingly small. However, the angular dependence of the differential cross-section is sensitive to the axial-vector coupling of the  $Z^0$  and gives rise to a forward-backward asymmetry in the angular distribution

$$A(\theta) \equiv \frac{d\sigma(\theta) - d\sigma(\pi - \theta)}{d\sigma(\theta) + d\sigma(\pi - \theta)}. \quad (8.5.10)$$

For  $\sqrt{s} \ll M_Z$  it is given by

$$A(\theta) \approx -2a_e a_\mu (s/M_Z^2) \frac{2 \cos \theta}{1 + \cos^2 \theta} \quad (8.5.11)$$

which amounts to a few per cent at PETRA energies. (An exact formula for  $A(\theta)$  will be derived shortly.) Fig. 8.17 shows the asymmetry measured at  $\sqrt{s} = 34.5$  GeV, in good agreement with the SM curve labelled ‘QED+WEAK’.

The situation is reversed when we look at energies around the  $Z^0$  peak. Here one may effectively neglect the photon exchange in Fig. 8.14.

Consider the process

$$e^+ e^- \rightarrow f\bar{f} \quad (f \neq e^-)$$

for  $\sqrt{s} \approx M_Z$  with longitudinally polarized electrons and positrons and where  $f$  is a fermion for which  $\frac{m_f}{M_Z} \ll 1$ . At the huge energies involved, helicity and chirality are indistinguishable (see Section 1.3.1). The relevant diagrams are identical to Fig. 8.16.

Because the energy is close to the  $Z^0$  mass it is not adequate to use the propagator given in (A2.3.1) of Appendix 2 and a more realistic version

which takes into account the finite total width  $\Gamma_Z$  of the  $Z$  must be used, i.e.

$$\mu \overbrace{\text{~~~~~}}_k^{Z^0} \nu = \frac{i(-g_{\mu\nu} + k_\mu k_\nu / M_Z^2)}{k^2 - M_Z^2 + ik^2 \Gamma_Z / M_Z} \quad (k^2 \approx M_Z^2). \quad (8.5.12)$$

The contribution from  $\gamma$  exchange is of order  $\Gamma_Z/M_Z$  compared with  $Z^0$  exchange, so will be neglected in our qualitative discussion. It can easily be included. In fact, we will not actually evaluate the Feynman diagrams but derive the results in a fashion which highlights the physical ingredients. Thus, we shall view the process as a physical process of resonance formation and decay

$$e^+ e^- \rightarrow Z^0 \rightarrow f \bar{f}. \quad (8.5.13)$$

To simplify the notation, let us use the particle symbols to indicate their helicity. The helicity amplitudes are then a slight generalization of the form (8.5.3) (we take  $\phi = 0$ )

$$\begin{aligned} H_{f\bar{f},ee}(\theta) &= M_{f\bar{f}} M_{e\bar{e}} d_{\lambda\mu}^1(\theta) \\ \lambda &= e - \bar{e}, \mu = f - \bar{f} \end{aligned} \quad (8.5.14)$$

where now parity is not conserved at the vertices, and we have left out a function of energy related to the behaviour of the  $Z$  propagator.

We know from Section 1.3.1 that the fermions and antifermions must have opposite helicity, so only two decay amplitudes occur,  $M_{+-}$  and  $M_{-+}$ . Moreover if in (5.1.3) we write

$$v - a\gamma_5 = \frac{1}{2}(v + a)(1 - \gamma_5) + \frac{1}{2}(v - a)(1 + \gamma_5) \quad (8.5.15)$$

we see that apart from irrelevant normalization we can take

$$\begin{aligned} M_{+-} &= v - a \\ M_{-+} &= v + a. \end{aligned} \quad (8.5.16)$$

The only helicity amplitudes are then

$$\left. \begin{aligned} H_{+-;+-} &= (v_f - a_f)(v_e - a_e) d_{1,1}^1(\theta) \\ H_{-+;-+} &= (v_f + a_f)(v_e + a_e) d_{-1,-1}^1(\theta) \\ H_{+-;-+} &= (v_f - a_f)(v_e + a_e) d_{-1,1}^1(\theta) \\ H_{-+;+-} &= (v_f + a_f)(v_e - a_e) d_{1,-1}^1(\theta) \end{aligned} \right\}, \quad (8.5.17)$$

where

$$\left. \begin{aligned} d_{1,1}(\theta) &= d_{-1,-1}(\theta) = \frac{1}{2}(1 + \cos \theta) \\ d_{1,-1}(\theta) &= d_{-1,1}(\theta) = \frac{1}{2}(1 - \cos \theta) \end{aligned} \right\}. \quad (8.5.18)$$

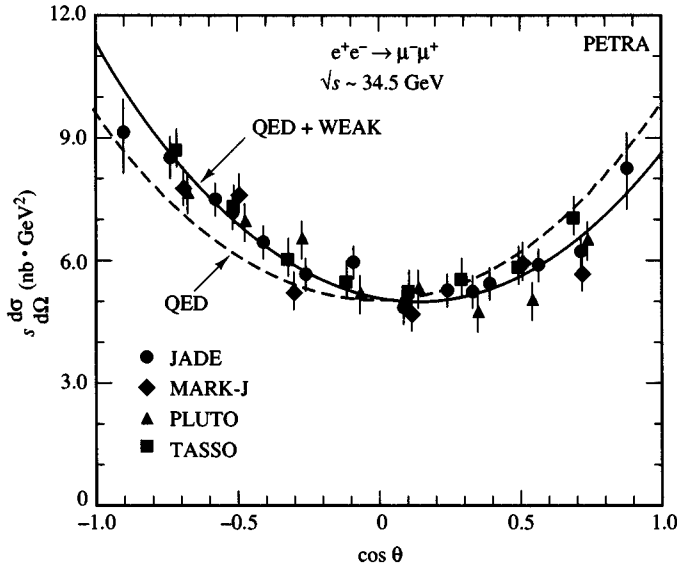


Fig. 8.17. The asymmetry in  $e^+e^- \rightarrow \mu^+\mu^-$  as measured at PETRA energies (from Stirling and Wu, 1984).

Adding the moduli squared of the amplitudes to form the unpolarized differential cross-section, and restoring the normalization, we find

$$\frac{d\sigma(s, \theta)}{d\Omega} = \frac{3}{16\pi} \sigma_{e^+e^- \rightarrow f\bar{f}}(s) \left\{ 1 + \cos^2 \theta + 2A_e A_f \cos \theta \right\}, \quad (8.5.19)$$

where

$$A_e \equiv \frac{2v_e a_e}{v_e^2 + a_e^2} = \frac{2g_V^e g_A^e}{(g_V^e)^2 + (g_A^e)^2};$$

$$A_f \equiv \frac{2v_f a_f}{v_f^2 + a_f^2} = \frac{2g_V^f g_A^f}{(g_V^f)^2 + (g_A^f)^2}. \quad (8.5.20)$$

The forward-backward asymmetry evident in eqn (8.5.19) will be discussed in connection with the possibility of polarized  $e^+e^-$  collisions in Section 8.8.

The total cross-section for  $e^+e^- \rightarrow f\bar{f}$  ( $f \neq e^-$ ) in eqn (8.5.19) is for  $s \approx M_Z^2$  given by the modified Breit-Wigner form (Blatt and Weisskopf, 1979)

$$\sigma_{e^+e^- \rightarrow f\bar{f}}(s) = \frac{s}{M_Z^2} \frac{12\pi\Gamma_{ee}\Gamma_{ff}}{(s - M_Z^2)^2 + s^2\Gamma_Z^2/M_Z^2}, \quad (8.5.21)$$

where  $\Gamma_{ee}, \Gamma_{ff}$  are the partial widths for  $Z^0 \rightarrow e^+e^-$  and  $Z^0 \rightarrow f\bar{f}$  respectively. For the reaction  $e^+e^- \rightarrow X$  one simply replaces  $\Gamma_{ff}$  by  $\Gamma_X$  in (8.5.21).

For very accurate work, or for the region outside the  $Z^0$  peak, we must take into account both  $\gamma$  and  $Z^0$  exchange using the propagator (8.5.12) for the  $Z^0$ . It is a simple matter to redo the previous analysis for the general case. One finds for  $e^+e^- \rightarrow f\bar{f}$

$$\begin{aligned} \frac{d\sigma}{d\Omega} = \frac{\alpha^2}{4s} & \left\{ Q_f^2 (1 + \cos^2 \theta) - \right. \\ & - 2Q_f [\text{Re}\chi(s)] [v_f v_e (1 + \cos^2 \theta) + 2a_f a_e \cos \theta] \\ & \left. + |\chi(s)|^2 (v_e^2 + a_e^2) (v_f^2 + a_f^2) [1 + \cos^2 \theta + 2 \cos \theta A_e A_f] \right\}, \end{aligned}$$

where

$$\chi(s) \equiv \frac{s}{s - M_Z^2 + is\Gamma_Z/M_Z}. \quad (8.5.22)$$

(The reader is warned of a profusion of different notations in the literature. Some groups use  $g_V, g_A$  for twice our  $g_V, g_A$  (5.1.4) and (5.1.5). Others use  $v$  and  $a$  for  $2g_V, 2g_A$ . In consequence  $\chi(s)$  is sometimes defined with  $c_W^2 s_W^2$  or  $4c_W^2 s_W^2$  in its denominator.)

It should be noted that even for pure  $Z^0$  exchange, the peak in (8.5.21) is not at  $s = M_Z^2$  owing to the use of the improved  $q^2$  dependent form of the  $Z^0$  propagator denominator in (8.5.12). Thus, the peak is essentially at

$$s = \frac{M_Z^2}{1 + \Gamma_Z^2/M_Z^2}. \quad (8.5.23)$$

Aside from the improved propagator, (8.5.21) and (8.5.22) are still lowest order calculations. But since experimental accuracies of  $\sim 1\%$  are feasible, one should take into account higher order corrections since they are at the level of a few per cent. The most important corrections to (8.5.22) have the following effect:

$$\begin{aligned} \frac{d\sigma}{d\Omega} = \frac{\alpha^2}{4s} & \left\{ \frac{Q_f^2}{(1 - \Delta\alpha)^2} (1 + \cos^2 \theta) - \frac{2Q_f(1 + \Delta r)}{1 - \Delta\alpha} [\text{Re}\chi(s)] \right. \\ & \times [v_f v_e (1 + \cos^2 \theta) + 2\bar{a}_f \bar{a}_e \cos \theta] + (1 + \Delta r)^2 |\chi(s)|^2 \\ & \left. \times (\bar{v}_e^2 + \bar{a}_e^2) (\bar{v}_f^2 + \bar{a}_f^2) [1 + \cos^2 \theta + 2 \cos \theta \bar{A}_e \bar{A}_f] \right\}, \quad (8.5.24) \end{aligned}$$

where

$$\begin{aligned} \bar{v}_f & \equiv \frac{\bar{g}_V^f}{2s_W c_W} = \frac{\sqrt{\varrho}}{2s_W c_W} (I_{W3}^{f_L} - 2Q_f \sin^2 \bar{\theta}_W) \\ \bar{a}_f & \equiv \frac{\bar{g}_A^f}{2s_W c_W} = \frac{\sqrt{\varrho}}{2s_W c_W} I_{W3}^{f_L} \end{aligned} \quad (8.5.25)$$

and  $\bar{A}_{e,f}$  are  $A_{e,f}$  of (8.5.20) written in terms of  $\bar{v}_{e,f}$  and  $\bar{a}_{e,f}$ . As to the

correction terms,  $\Delta\alpha$  was given in (7.3.2),  $\varrho$  in (7.6.6),  $\bar{\theta}_W$  was defined in (7.6.10) and  $\Delta r$  is given by (7.5.1) in which  $\Delta r_{\text{rem}}$  is neglected.

There are, in addition, very small effects which replace  $\sin^2 \bar{\theta}_W$  in (8.5.25) by an effective mixing angle  $\sin^2 \theta_{\text{eff}}^f$ , which depends upon the fermion  $f$ . But the difference ( $\sin^2 \bar{\theta}_W - \sin^2 \theta_{\text{eff}}^f$ ) is only a few times  $10^{-4}$ . Numerical tables are given in Hollik (1990). Incidentally  $\sin^2 \bar{\theta}_W$  is essentially equal to the quantity  $\sin^2 \theta_{\overline{\text{MS}}}(M_Z^2)$  used in the so-called  $\overline{\text{MS}}$  renormalization scheme (see Chapter 20).

Finally, there are very tiny corrections to the coupling of the photon, including an induced  $\gamma_\mu \gamma_5$  coupling, but these are totally negligible at LEP energies.

Given the uncertainties in  $M_W$  and  $\Delta r$  it may be preferable, at present, if we assume the correctness of the SM description of muon decay and use (7.4.2) to replace, in (8.5.24),

$$(1 + \Delta r)\alpha \rightarrow \frac{\sqrt{2}G}{\pi} M_Z^2 s_W^2 c_W^2 \quad (8.5.26)$$

in which case (8.5.24) becomes [see (7.3.2)]

$$\begin{aligned} \frac{d\sigma}{d\Omega} = & \frac{1}{4s} \left\{ \alpha^2(M_Z^2) Q_f^2 (1 + \cos^2 \theta) - \frac{G\alpha(M_Z^2) Q_f M_Z^2}{\sqrt{2}\pi} [\text{Re}\chi(s)] \times \right. \\ & \times [\bar{g}_V^f \bar{g}_V^e (1 + \cos^2 \theta) + 2\bar{g}_A^f \bar{g}_A^e \cos \theta] + \left( \frac{GM_Z^2}{2\sqrt{2}\pi} \right)^2 |\chi(s)|^2 (\bar{g}_V^e + \bar{g}_A^e) \\ & \times (\bar{g}_V^{f^2} + \bar{g}_A^{f^2}) [1 + \cos^2 \theta + 2\cos \theta \bar{A}_f \bar{A}_e] \Big\}. \end{aligned} \quad (8.5.27)$$

## 8.6 Determination of the SM parameters of the $Z^0$

The first aim is to derive values for  $M_Z$ ,  $\Gamma_Z$  and the various partial widths by fitting (8.5.21) to the cross-section data near the  $Z^0$  peak, after correcting for soft photon radiation using a Monte Carlo approach. A fit to the  $s$  dependence of  $\sigma$  for many channels, but principally for  $\sigma(e^+e^- \rightarrow \text{hadrons})$ , yields the values of  $M_Z$  and  $\Gamma_Z$  given in Table 8.3.

Next a fit is made to the data on  $e^+e^- \rightarrow e^+e^-$  using a cross-section formula that includes the effects of the diagrams in both Fig. 8.15 and Fig. 8.16. This permits the determination of  $\Gamma_{ee}$ .

For any channel  $e^+e^- \rightarrow f\bar{f}$  the only unknown in (8.5.21) is now  $\Gamma_{ff}$  which can thus be determined from the data. In this way one fixes  $\Gamma_{\mu\mu}$ .

Any other partial width  $\Gamma_X$  can then be found from the ratio

$$\frac{\Gamma_X}{\Gamma_{\mu\mu}} = \frac{\sigma_{e^+e^- \rightarrow X}}{\sigma_{e^+e^- \rightarrow \mu^+\mu^-}}. \quad (8.6.1)$$

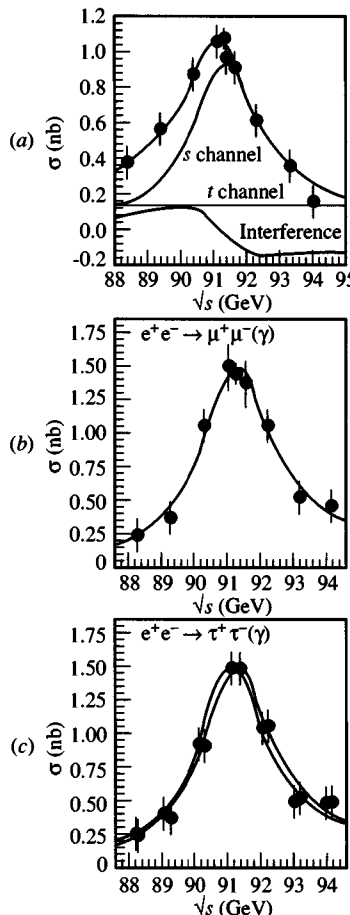


Fig. 8.18. An example of a fit around the  $Z^0$  peak (from L3, 1990b).

This leads to the entries  $\Gamma_{\tau\tau}$  and  $\Gamma_{\text{had}}$  in Table 8.3.

As an example of the above procedures, Fig. 8.18 shows the fit made by the L3 group to their data (L3, 1990b).

Let us turn now to the theoretical calculation of the leptonic widths in the SM in lowest order.

Let us label the four-momentum as follows:

$$p(Z) = K, p(\bar{f}) = p \text{ with } p^2 = m_f^2, p(\bar{f}) = q \text{ with } q^2 = m_f^2.$$

The decay rate for  $Z \rightarrow f\bar{f}$  in its rest frame is then given by [see (A2.1.7) of Appendix 2]

$$\Gamma(Z \rightarrow f\bar{f}) = \frac{1}{2M_Z} \int \frac{d^3p}{(2\pi)^3 2E_f} \frac{d^3q}{(2\pi)^3 2E_{\bar{f}}} (2\pi)^4 \delta(K - p - q) \overline{|M|^2}, \quad (8.6.2)$$

where  $\overline{|M|^2}$  is the spin summed and averaged square of the Feynman amplitude

$$M = ie\bar{u}(q)\gamma^\alpha(v_f - a_f\gamma_5)v(p)\varepsilon_\alpha. \quad (8.6.3)$$

$\varepsilon_\alpha$  is the polarization vector of the  $Z$  (see (2.1.13)) and the spinor normalization is  $u^\dagger u = 2E$ .

Summing over the spins of  $f$  and  $\bar{f}$  involves

$$\begin{aligned} \sum_{\text{spins}} |M|^2 &= e^2 \varepsilon_\alpha \varepsilon_\beta^* T_r \{ (\not{p} + m_f) \gamma^\alpha (v_f - a_f \gamma_5) (\not{q} - m_f) \gamma^\beta (v_f - a_f \gamma_5) \} \\ &= e^2 \varepsilon_\alpha \varepsilon_\beta^* T_r \{ (v_f^2 + a_f^2) \not{p} \gamma^\alpha \not{q} \gamma^\beta - m_f^2 (v_f^2 - a_f^2) \gamma^\alpha \gamma^\beta \\ &\quad - 2v_f a_f \not{p} \gamma^\alpha \not{q} \gamma^\beta \gamma_5 \}. \end{aligned} \quad (8.6.4)$$

Averaging over the  $Z$  spin gives

$$\frac{1}{3} \sum_\lambda \varepsilon_\alpha^{(\lambda)} \varepsilon_\beta^{(\lambda)*} = \frac{1}{3} \left( -g_{\alpha\beta} + \frac{K_\alpha K_\beta}{M_Z^2} \right), \quad (8.6.5)$$

which is symmetric in  $\alpha, \beta$ . (For reference to Dirac traces, see end of Appendix 2.1.) The last term in the trace in (8.6.4) is antisymmetric in  $\alpha, \beta$ , so does not contribute. The first terms yield

$$\overline{|M|^2} = \frac{4e^2}{3} \left\{ (v_f^2 + a_f^2) \left( p \cdot q + \frac{2K \cdot p \cdot K \cdot q}{M_Z^2} \right) + 3m_f^2 (v_f^2 - a_f^2) \right\}. \quad (8.6.6)$$

The  $\delta$ -function in (8.6.2) ensures energy-momentum conservation, so that  $K = p + q$ . Then we have

$$\begin{aligned} p \cdot q &= \frac{1}{2} [(p + q)^2 - p^2 - q^2] = \frac{M_Z^2}{2} - m_f^2 \\ p \cdot K &= p \cdot (p + q) = \frac{M_Z^2}{2} = q \cdot K. \end{aligned} \quad (8.6.7)$$

So, finally,

$$\overline{|M|^2} = \frac{4e^2 M_Z^2}{3} \left\{ a_f^2 \left( 1 - \frac{4m_f^2}{M_Z^2} \right) + v_f^2 \left( 1 + \frac{2m_f^2}{M_Z^2} \right) \right\}. \quad (8.6.8)$$

The integration and other kinematic variables in (8.6.2) yield a factor  $\frac{1}{16\pi M_Z} \sqrt{1 - \frac{4m_f^2}{M_Z^2}}$ . Multiplying by the number  $N_{C_f}$  of colours that  $f$  can have, we end up with

$$\Gamma_{Z \rightarrow f\bar{f}} = \frac{N_{C_f} M_Z \alpha}{3} \sqrt{1 - \frac{4m_f^2}{M_Z^2}} \left\{ a_f^2 \left( 1 - \frac{4m_f^2}{M_Z^2} \right) + v_f^2 \left( 1 + \frac{2m_f^2}{M_Z^2} \right) \right\}. \quad (8.6.9)$$

(See also Niclosini and Trentadue, 1987, 1988.)

For all the leptons the terms  $m_f^2/M_Z^2$  are negligible, so, to lowest order, we have

$$\Gamma_{Z \rightarrow l\bar{l}} = \frac{M_Z \alpha}{3} (a_l^2 + v_l^2). \quad (8.6.10)$$

Substituting for  $a_l, v_l$  from (5.1.4) and (5.1.5) gives

$$\Gamma_{ee} = \Gamma_{\mu\mu} = \Gamma_{\tau\tau} = \frac{M_Z \alpha}{24 s_W^2 c_W^2} [1 - 4s_W^2 + 8s_W^4]. \quad (8.6.11)$$

To match the accuracy of the data (8.6.9) and (8.6.10) should be corrected for higher order effects using the substitutions for  $v_f$  and  $a_f$  as in (8.5.5) and (8.5.6). Thus

$$\begin{aligned} \Gamma_{Z \rightarrow l\bar{l}} &= \frac{M_Z \alpha (1 + \Delta r)}{3} (\bar{a}_l^2 + \bar{v}_l^2) \\ &= \frac{M_Z \alpha (1 + \Delta r) \varrho}{12 s_W^2 c_W^2} \{(I_{W3}^l)^2 + (I_{W3}^l - 2Q_l \sin^2 \bar{\theta}_W)^2\}. \end{aligned} \quad (8.6.12)$$

Again, at present, it may be better to use the relation (8.5.26) coming from muon decay, so that

$$\Gamma_{Z \rightarrow l\bar{l}} = \frac{\sqrt{2} G M_Z^3 \varrho}{12\pi} \{(I_{W3}^l)^2 + (I_{W3}^l - 2Q_l \sin^2 \bar{\theta}_W)^2\}. \quad (8.6.13)$$

When the fermion  $f$  in (8.6.9) is a quark (8.6.12) must be multiplied by  $N_{C_f}$ , but account must also be taken of important QCD corrections which amount to multiplying (8.6.12) by a factor  $(1 + \delta_{\text{QCD}})$ . For example, for light quarks, this is a factor  $1.040 \pm 0.007$  (Hollik, 1990).

Returning to (7.6.8) and assuming that  $\Delta r_{\text{rem}}$  is negligible, we can compute  $\varrho$  from the measured masses  $M_W, M_Z$  and  $G$ :

$$\varrho = \frac{c_W^2}{1 - \frac{A^2}{M_W^2(1 - \Delta\alpha)}}. \quad (8.6.14)$$

We recall that  $\Delta\alpha$  is independent of  $m_f$  and  $m_H$ , so that  $\varrho$  is determined given  $M_W$ . One finds, using  $M_W = 80.15 \pm 0.25 \text{ GeV}/c^2$ ,

$$\varrho = 1.004 \pm 0.008. \quad (8.6.15)$$

Once  $\varrho$  is determined in this fashion, eqn (8.6.13) really can be used to measure  $\sin^2 \bar{\theta}_W$ .

Using the above value of  $\varrho$  one obtains a best estimate for  $\sin^2 \bar{\theta}_W$  from the experimental widths in Table 8.3:

$$\sin^2 \bar{\theta}_W = 0.2302 \pm 0.0015 \quad (8.6.16)$$

which leads to

$$\sin^2 \theta_W = 0.227 \pm 0.010 \quad (8.6.17)$$

in beautiful agreement with the value of  $M_W$  used above.

Clearly the difference between  $\sin^2 \theta_W$  and  $\sin^2 \bar{\theta}_W$  is extremely small. Also  $\varrho$  is very nearly equal to 1. Hence,  $\bar{v}, \bar{a}$  will differ from  $v, a$  by a very small amount.

Note also that the measurements of the different leptonic channels are nicely compatible with the universality implied by (8.6.11) or (8.6.12).

If one *assumes* lepton universality by putting

$$\Gamma_{ee} = \Gamma_{\mu\mu} = \Gamma_{\tau\tau} \equiv \Gamma_l \quad (8.6.18)$$

in (8.5.21) and makes a global fit to all the leptonic data one obtains the values of  $\Gamma_l$  in Table 8.3. This quantity will be useful when trying to determine how many species of neutrinos exist.

We shall not attempt to derive  $\Gamma_{had}$  in the SM but note that it is calculated by summing over all quark–antiquark pairs and modified by strong interaction effects such as gluon radiation.

Assuming  $m_H < 1000$  GeV and letting  $m_t$  and  $\alpha_s$  vary within the present experimental limitations, the theoretical uncertainty on  $\Gamma_{had}$  can be shown to be about 30 MeV. This is of the same order of magnitude as the experimental error (Table 8.3).

Finally, if we use the theoretical calculation (7.6.5) for  $\Delta\varrho_i$  to compute  $\varrho$  as a function of  $m_t$  and if we now fit the LEP partial widths using (8.6.13) with  $\sin^2 \bar{\theta}_W$  replaced by

$$\sin^2 \bar{\theta}_W = s_W^2 + \Delta\varrho_i c_W^2 \quad (8.6.19)$$

which follows from (7.6.10), we obtain a relation between the leptonic widths and  $m_t$ . Using the value of  $M_W$  above, the LEP data then leads to

$$m_t = 137 \pm 40 \text{ GeV}/c^2, \quad (8.6.20)$$

where allowance has been made in the error for the unknown Higgs mass (Dydak, 1991).

Finally we consider the question of testing the minimal Higgs mechanism using data at the  $Z^0$  peak. In a non-minimal model eqns. (5.2.2) and (7.9.7) hold. It is easy to see that the *lowest order* non-minimal formula for the  $e^+e^- \rightarrow f\bar{f}$  differential cross-section can be obtained from the higher order minimal formula (8.5.27) by the following replacement:

$$\begin{aligned} \bar{g}_V^f &\rightarrow \sqrt{\varrho_0}(I_{W3}^{f_L} - 2Q_f \sin^2 \theta_W) \\ \bar{g}_A^f &\rightarrow \sqrt{\varrho_0} I_{W3}^{f_L}. \end{aligned} \quad (8.6.21)$$

Similarly, the lowest order non-minimal formula for the partial width  $\Gamma(Z \rightarrow l\bar{l})$  can be obtained from the higher order minimal result (8.6.13)

by the replacements:

$$\begin{aligned}\varrho &\rightarrow \varrho_0 \\ \sin^2 \bar{\theta}_W &\rightarrow \sin^2 \theta_W.\end{aligned}\quad (8.6.22)$$

But in the minimal model we have, from (7.6.10),

$$\cos^2 \bar{\theta}_W = \frac{c_W^2}{\varrho} = \frac{1}{\varrho} \frac{M_W^2}{M_Z^2}, \quad (8.6.23)$$

whereas in the non-minimal case

$$\cos^2 \theta_W = \frac{1}{\varrho_0} \frac{M_W^2}{M_Z^2}. \quad (8.6.24)$$

We thus see that the non-minimal model in lowest order gives precisely the results of the higher order corrections to the minimal model with  $\varrho \rightarrow \varrho_0$ . Thus, once again (see Section 7.9) the interpretation of a measurement that finds  $\varrho \neq 1$  is not absolutely straightforward.

## 8.7 Neutrino counting

'Light' neutrinos, i.e. those with  $m_\nu < \frac{1}{2}M_Z$ , will contribute to the  $Z^0$ , width via  $Z^0 \rightarrow \nu\bar{\nu}$  and thus one can estimate the number of such neutrinos  $N_\nu$  (i.e. the number of leptonic doublet generations) from consideration of the total and partial  $Z^0$  widths. We shall discuss two rather different approaches.

### 8.7.1 The invisible width method

We write

$$\Gamma_Z = \Gamma_{\text{had}} + \Gamma_{ee} + \Gamma_{\mu\mu} + \Gamma_{\tau\tau} + \Gamma_{\text{inv}}, \quad (8.7.1)$$

where we assume that the invisible width is given by

$$\Gamma_{\text{inv}} = N_\nu \Gamma_\nu. \quad (8.7.2)$$

Further we approximate

$$\Gamma_{ee} + \Gamma_{\mu\mu} + \Gamma_{\tau\tau} = 3\Gamma_l,$$

where the latter was explained in (8.6.18).

Then

$$\begin{aligned}N_\nu &= \frac{\Gamma_{\text{inv}}}{\Gamma_\nu} = \frac{1}{\Gamma_\nu} (\Gamma_Z - \Gamma_{\text{had}} - 3\Gamma_l) \\ &= \frac{\Gamma_l}{\Gamma_\nu} \left( \frac{\Gamma_Z}{\Gamma_l} - \frac{\Gamma_{\text{had}}}{\Gamma_l} - 3 \right).\end{aligned}\quad (8.7.3)$$

Now from (8.5.21) for  $\sigma_{\text{had}} \equiv \sigma_{e^+e^- \rightarrow \text{hadrons}}$  evaluated at  $s = M_Z^2$ , one has

$$\left(\frac{\Gamma_Z}{\Gamma_l}\right)^2 = \frac{12\pi}{M_Z^2 \sigma_h} \frac{\Gamma_{\text{had}}}{\Gamma_l}. \quad (8.7.4)$$

Thus (8.7.3) can be written

$$N_\nu = \frac{\Gamma_l}{\Gamma_\nu} \left\{ \left( \frac{12\pi}{M_Z^2 \sigma_h} \frac{\Gamma_{\text{had}}}{\Gamma_l} \right)^{1/2} - \frac{\Gamma_{\text{had}}}{\Gamma_l} - 3 \right\}, \quad (8.7.5)$$

a form which is practically useful since it can be shown that the ratio  $\frac{\Gamma_l}{\Gamma_\nu}$  as calculated to higher order in the SM is almost independent of  $m_t$ .

Using the calculated SM value for  $\Gamma_\nu$  and the measured  $\Gamma_l$  gives

$$\frac{\Gamma_l}{\Gamma_\nu} = 0.5010 \pm 0.0005$$

and hence

$$N_\nu = 2.89 \pm 0.10. \quad (8.7.6)$$

While not an absolute proof this is, nonetheless, remarkable evidence in favour of just three generations.

### 8.7.2 The single photon method

Consider events of the type

$$e^+e^- \rightarrow \text{single isolated photon}.$$

It is assumed that these are either due to the reaction

$$e^+e^- \rightarrow \nu\bar{\nu}\gamma \quad (8.7.7)$$

or to other reactions like  $e^+e^- \rightarrow \nu\bar{\nu}\gamma\gamma$ ,  $e^+e^- \rightarrow \gamma\gamma\gamma$  or  $e^+e^- \rightarrow e^+e^-\gamma$  etc., where limited detector acceptance is responsible for the failure to detect the other particles. If this background can be controlled then the rate for (8.7.7) provides a nice measure of  $N_\nu$ .

To lowest order the relevant diagrams are shown in Fig. 8.19 (a) and (b) for

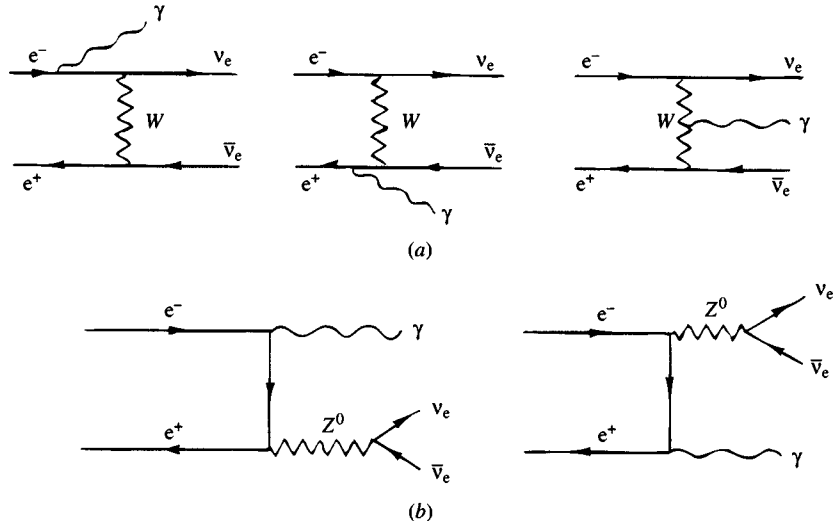
$$e^+e^- \rightarrow \nu_e\bar{\nu}_e\gamma. \quad (8.7.8)$$

For any other species of neutrino the diagrams of type (a) are absent.

The formula for the cross-section is rather complicated and can be found in Berends *et al.* (1988b). We note simply that the amplitudes for a given neutrino species  $j$ , i.e. production of a given  $\nu_j\bar{\nu}_j$  pair is of the form:

$$A_{\nu_e} = A + B$$

$$A_{\nu_j} = B, \quad j \neq e,$$

Fig. 8.19. Relevant diagrams for  $e^+e^- \rightarrow \nu_e\bar{\nu}_e\gamma$ .

where  $A$  and  $B$  come from the diagrams in Fig. 8.19 (a) and (b) respectively and the value of  $B$  is independent of the type of neutrino. The total rate for (8.7.7) is then proportional to

$$|A + B|^2 + (N_\nu - 1)|B|^2$$

and could thus yield a determination of  $N_\nu$ . At the time of writing no results of this approach have yet appeared.

## 8.8 Asymmetries and polarization measurements at the $Z^0$ peak

In many ways one of the most characteristic features of the SM is the parity-violating coupling of the  $Z^0$  to fermions [(see eqns (5.1.3)–(5.1.9)]. It is thus of great importance to have an accurate measurement of  $v$  and  $a$ . As is clear from (8.6.10) or (8.6.12) the  $Z^0$  leptonic partial widths, or equivalently  $e^+e^- \rightarrow l\bar{l}$  cross-sections, only yield information on the combination  $(v_l^2 + a_l^2)$  or  $(\bar{v}_l^2 + \bar{a}_l^2)$  if one uses the higher order result (8.5.24).

From (8.5.19) the forward–backward asymmetry  $A_{FB}$  defined by

$$A_{FB} \equiv \frac{n_F - n_B}{n_F + n_B}, \quad (8.8.1)$$

where  $n_{F,B}$  are the numbers of events in the forward and backward hemi-

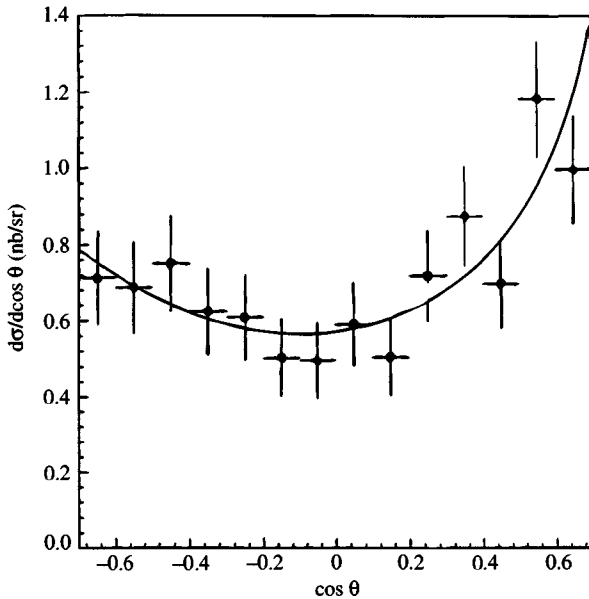


Fig. 8.20. The asymmetry in  $e^+e^- \rightarrow \mu^+\mu^-$  as measured at LEP (from L3, 1990c).

spheres respectively, is given for  $e^+e^- \rightarrow f\bar{f}$ , by

$$A_{FB} = \frac{3}{4} A_f A_e, \quad (8.8.2)$$

where  $A_{e,f}$ , defined in (8.5.20), are proportional to the product of vector and axial-vector couplings. Including one loop corrections (8.5.20) must be replaced by

$$\bar{A}_f = \frac{2\bar{g}_{V_f}\bar{g}_{A_f}}{\bar{g}_{V_f}^2 + \bar{g}_{A_f}^2} = \frac{2\bar{v}_f\bar{a}_f}{\bar{v}_f^2 + \bar{a}_f^2}. \quad (8.8.3)$$

Recall that from (5.1.6) the vector coupling  $v_e$  and  $\bar{v}_e$  of the leptons is very small, so that also the  $A_l$  are very small. For  $\sin^2 \theta_W = 0.23$  we estimate  $A_e = A_\mu \simeq 0.16$  implying a tiny asymmetry  $A_{FB} \approx 1.9\%$ . This is borne out in the data of Fig. 8.20 (L3, 1990c) which corresponds to  $A_{FB} = (2.52 \pm 0.06)\%$ .

The values for  $g_V, g_A$  given in Table 8.3 are obtained from fitting (8.8.2), (8.8.3) and (8.6.3) to the data and then converting from  $\bar{g}_{V,A}$  to  $g_{V,A}$  via (8.5.25) and (8.6.19). For an average of all LEP data,

$$\begin{aligned} g_A &= -0.501 \pm 0.002 \\ g_V &= -0.045 \pm 0.006 \end{aligned} \quad (8.8.4)$$

(the signs are not determined, but chosen to agree with the SM). Com-

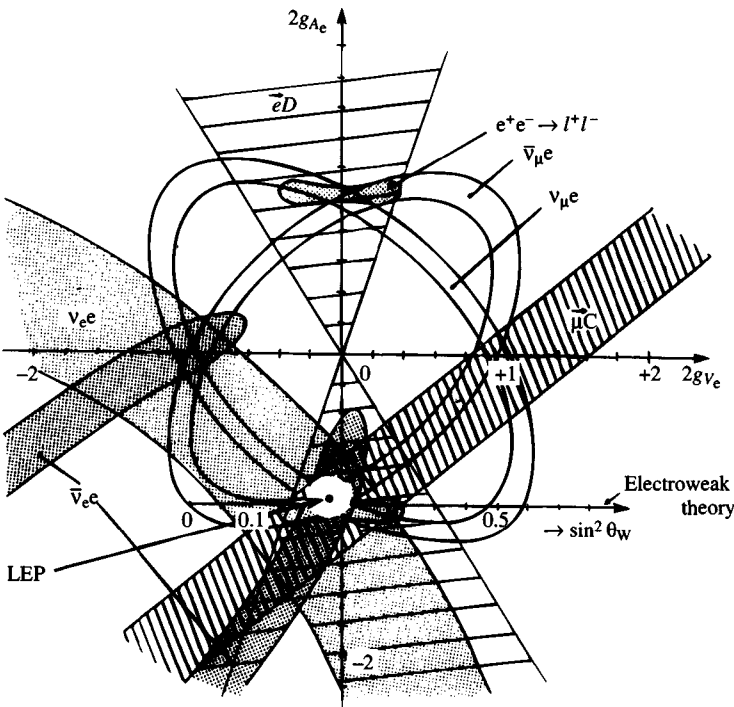


Fig. 8.21. Allowed domain in the  $g_{A_e}$ – $g_{V_e}$  plane from various reactions:  $\nu e$  scattering,  $e^+e^-$ ,  $\bar{e}D$  scattering and  $\bar{\mu}C$  scattering;  $e^-\mu^-\tau$  universality is assumed. (From Dydak, 1991.)

pared with all previous determinations the LEP result is spectacular, as shown in Fig. 8.21. The error is barely visible. Nonetheless, the above accuracy is not sufficient for a refined test of the theory with higher order corrections.

Now for a given experimental error  $\delta A_{FB}$  in the measured asymmetry we have from (8.8.2)

$$\delta A_f \approx \frac{1}{A_e} \delta A_{FB} \gg \delta A_{FB} \quad (8.8.5)$$

leading to a loss of accuracy in the determination of  $g_V$  and  $g_A$ .

We shall now demonstrate how experiments with longitudinally polarized  $e^\pm$  beams could lead to a much more accurate measurement of  $g_{V,A}$ . For simplicity we deal just with  $Z^0$  exchange.

Let  $\mathcal{P}_e$  and  $\mathcal{P}_{\bar{e}}$  be the degree of longitudinal polarization of the  $e^+$  and  $e^-$  beams. Then the relative numbers of right- and left-handed particles

present, since

$$\mathcal{P} = \frac{n_R - n_L}{n_R + n_L}, \quad (8.8.6)$$

is

$$n_{R/L} = \frac{1}{2}(1 \pm \mathcal{P})n, \quad (8.8.7)$$

where  $n = n_R + n_L$ .

In terms of the helicity amplitudes (8.5.17) the cross-section to produce the final  $f\bar{f}$  state with definite helicity  $(+-)$  is then

$$\begin{aligned} \sigma_{+-}(\theta; \mathcal{P}_e, \mathcal{P}_{\bar{e}}) &= (1 + \mathcal{P}_e)(1 - \mathcal{P}_{\bar{e}})|H_{+-,+-}|^2 \\ &\quad + (1 - \mathcal{P}_e)(1 + \mathcal{P}_{\bar{e}})|H_{+-,-+}|^2 \\ &= (v_f - a_f)^2 \{(1 + \mathcal{P}_e)(1 - \mathcal{P}_{\bar{e}})(v_e - a_e)^2(1 + \cos \theta)^2 \\ &\quad + (1 - \mathcal{P}_e)(1 + \mathcal{P}_{\bar{e}})(v_e + a_e)^2(1 - \cos \theta)^2\} \\ &= 2(v_f - a_f)^2(v_e^2 + a_e^2)\{[(1 - \mathcal{P}_e\mathcal{P}_{\bar{e}}) - \\ &\quad - A_e(\mathcal{P}_e - \mathcal{P}_{\bar{e}})](1 + \cos^2 \theta) + \\ &\quad + [(\mathcal{P}_e - \mathcal{P}_{\bar{e}}) - A_e(1 - \mathcal{P}_e\mathcal{P}_{\bar{e}})]2 \cos \theta\}. \end{aligned} \quad (8.8.8)$$

Similarly, one obtains

$$\begin{aligned} \sigma_{-+}(\theta; \mathcal{P}_e, \mathcal{P}_{\bar{e}}) &= 2(v_f + a_f)^2(v_e^2 + a_e^2)\{[(1 - \mathcal{P}_e\mathcal{P}_{\bar{e}}) - \\ &\quad - A_e(\mathcal{P}_e - \mathcal{P}_{\bar{e}})](1 + \cos^2 \theta) - \\ &\quad - [(\mathcal{P}_e - \mathcal{P}_{\bar{e}}) - A_e(1 - \mathcal{P}_e\mathcal{P}_{\bar{e}})]2 \cos \theta\} \end{aligned}$$

On adding these and restoring the normalization we get for the differential cross-section

$$\begin{aligned} \frac{d\sigma}{d\Omega} \Big|_{e^+e^- \rightarrow f\bar{f}} (\theta; \mathcal{P}_e, \mathcal{P}_{\bar{e}}) &= \\ \frac{3}{16\pi} \sigma_{e^+e^- \rightarrow f\bar{f}} \{ &[1 - \mathcal{P}_e\mathcal{P}_{\bar{e}} + A_e(\mathcal{P}_{\bar{e}} - \mathcal{P}_e)](1 + \cos^2 \theta) + \\ &+ A_f[\mathcal{P}_{\bar{e}} - \mathcal{P}_e + A_e(1 - \mathcal{P}_e\mathcal{P}_{\bar{e}})]2 \cos \theta \}, \end{aligned} \quad (8.8.9)$$

where  $\sigma_{e^+e^- \rightarrow f\bar{f}}$  is given in (8.5.21).

The forward-backward asymmetry in the polarised case is thus given by

$$A_{FB}(\mathcal{P}_e, \mathcal{P}_{\bar{e}}) = \frac{3}{4} \frac{A_f[\mathcal{P}_{\bar{e}} - \mathcal{P}_e + A_e(1 - \mathcal{P}_e\mathcal{P}_{\bar{e}})]}{1 - \mathcal{P}_e\mathcal{P}_{\bar{e}} + A_e(\mathcal{P}_{\bar{e}} - \mathcal{P}_e)} \quad (8.8.10)$$

to be compared with eqn (8.8.2) for the unpolarized case.

This is a fundamental result and will illustrate the power of utilizing polarized beams in leading to a more accurate determination of  $A_f$ .

Consider, for example, the case  $\mathcal{P}_{\bar{e}} = 0$  but  $\mathcal{P}_e$  large. Then from (8.8.10)

$$A_{FB}(\mathcal{P}_e) = -\frac{3}{4} \frac{A_f(\mathcal{P}_e - A_e)}{1 + \mathcal{P}_e A_e} \quad (8.8.11)$$

$$\approx -\frac{3}{4} A_f \mathcal{P}_e. \quad (8.8.12)$$

In this case the error in  $\delta A_f$  will be comparable to that in  $A_{FB}$  i.e.

$$\delta A_f \approx \delta A_{FB}. \quad (8.8.13)$$

It is believed that by this method  $\sin^2 \theta_W$  can be measured to an accuracy of  $\pm 0.00013$  with  $\mathcal{P}_e \approx 50\%$  in a  $30 \text{ pb}^{-1}$  exposure.

Consider now the degree of longitudinal polarization  $\mathcal{P}_f(\theta)$  of the produced fermion  $f$ . It will be given by

$$\mathcal{P}_f(\theta) = \frac{\sigma_{+-}(\theta) - \sigma_{-+}(\theta)}{\sigma_{+-}(\theta) + \sigma_{-+}(\theta)}. \quad (8.8.14)$$

From (8.8.8) and (8.8.9) one obtains

$$\mathcal{P}_f(\theta, \mathcal{P}_e, \mathcal{P}_{\bar{e}}) = -\frac{A_f \alpha(1 + \cos^2 \theta) + \beta(2 \cos \theta)}{\alpha(1 + \cos^2 \theta) + A_f \beta(2 \cos \theta)}, \quad (8.8.15)$$

where

$$\begin{aligned} \alpha &\equiv 1 - \mathcal{P}_e \mathcal{P}_{\bar{e}} + A_e (\mathcal{P}_{\bar{e}} - \mathcal{P}_e) \\ \beta &\equiv \mathcal{P}_{\bar{e}} - \mathcal{P}_e + A_e (1 - \mathcal{P}_e \mathcal{P}_{\bar{e}}). \end{aligned} \quad (8.8.16)$$

It is perfectly adequate here to use unpolarized beams,  $\mathcal{P}_e = \mathcal{P}_{\bar{e}} = 0$ , in which case

$$\mathcal{P}_f(\theta) = -\frac{A_f(1 + \cos^2 \theta) + A_e 2 \cos \theta}{1 + \cos^2 \theta + A_f A_e 2 \cos \theta} \quad (8.8.17)$$

which in principle allows a determination of  $A_f$  and  $A_e$  if the longitudinal polarization of the final fermion can be measured.

If we assume lepton universality and take  $A_e = A_f \approx 0.16$  corresponding to  $\sin^2 \theta_W = 0.23$  then we see that  $\mathcal{P}_f(\theta)$  varies from 0 at  $\theta = \pi$  to about  $-30\%$  at  $\theta = 0$ .

However, the measurement of  $\mathcal{P}_f(\theta)$  requires an analysis of the angular distribution of the decay products of  $f$  which is a non-trivial matter.

It may therefore be better, from the point of view of statistics, to deal with an integrated quantity. Thus define

$$\bar{\mathcal{P}}_f \equiv \frac{\int \mathcal{P}_f(\theta) \frac{d\sigma}{d\Omega}}{\int \frac{d\sigma}{d\Omega}}. \quad (8.8.18)$$

From the definition of  $\mathcal{P}_f(\theta)$  in terms of relative numbers of R and L handed  $f$  particles produced at angle  $\theta$ , it is clear that

$$\bar{\mathcal{P}}_f = \frac{\sigma(f_R) - \sigma(f_L)}{\sigma(f_R) + \sigma(f_L)}, \quad (8.8.19)$$

where  $\sigma(f_{R|L})$  are the total cross-sections to produce R or L handed  $f$ s in  $e^+e^- \rightarrow f\bar{f}$ .

From (8.5.19) and (8.8.17) we see that

$$\bar{\mathcal{P}}_f = -A_f, \quad (8.8.20)$$

a beautiful and simple result.

In practice it appears that the most accurate results will come from  $e^+e^- \rightarrow \tau^-\tau^+$  since the  $\tau$  polarization can be studied via various decays, e.g.  $\tau \rightarrow \mu\nu, \tau \rightarrow \rho\nu, \tau \rightarrow a_1\nu$ .

For a detailed discussion of all sources of uncertainties in the measurements involving polarized  $\tau$ s, see Jadach *et al.* (1989). See also Blondel (1990) for a description of tests of the SM using longitudinal polarization and asymmetry measurements.

## 8.9 Conclusions

LEP and SLC should provide further understanding of the underlying physics in the next few years. But if the Higgs is not found at LEP 2 it is not easy to foresee the future for  $e^+e^-$  machines. If the Higgs mass is beyond LEP 2 one hopes it will be discovered at the hadronic colliders LHC and SSC as discussed in Section 6.4. But only an  $e^+e^-$  machine could allow a detailed study of its properties.

It seems that the linear collider technique is the only way to reach CM energies in the  $e^+e^-$  system much higher than those of LEP 2. In an electron storage ring intense synchrotron radiation is emitted as the beam circulates with an energy loss proportional to the fourth power of the energy divided by the bending radius. The optimized size and cost for such a machine are proportional to the square of the beam energy (Richter, 1976). Thus, to achieve an energy ten times that of LEP 2 one would have to increase the circumference by a factor of 100 to 2700 km with a cost of about  $10^{11}$  US dollars!

An example of a future linear collider is the CLIC proposal of a 2 TeV  $e^+e^-$  machine. For the conceptual difficulties connected with such an accelerator, e.g. beamsstrahlung, see the specialized literature (Jacob and Wu, 1987).

Fig. 8.22 taken from Amaldi (1990) gives an ‘artist’s impression’ of the  $e^+e^-$  cross-section as a function of the total CM energy based on a

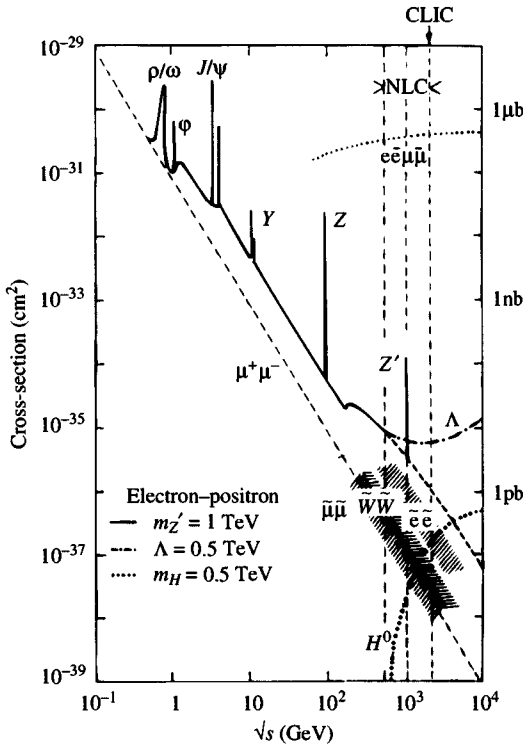


Fig. 8.22. An ‘artist’s impression’ of the  $e^+e^-$  cross-section up to very high CM energies; see text for details. (From Amaldi, 1990.)

number of theoretical scenarios. The light dashed line is the QED cross-section. The continuous line is what is seen up to 100 GeV and what one expects according to the SM above 100 GeV. Notice that the  $Z$  peak is not only higher but also different in character compared with the other (lower energy) peaks, due to its elementary nature.

At 2 TeV the rate for producing  $W$  pairs (thick dashed line) in a  $4\pi$  detector is  $\sim 50$  times larger than for  $\mu$  pairs. This may be useful for physics but is also the source of a considerable background.

Various ‘new’ possible physics effects are also shown in Fig. 8.22. First, there is a  $Z'$  drawn at 1 TeV. Such a particle is required in superstring theories (but its localisation at 1 TeV is just for the purpose of illustration). A Higgs of 0.5 TeV is shown by the thick-dotted curve and corresponds to  $> 10^3$  events per year at  $\sqrt{s} = 2$  TeV with a luminosity

$$L \simeq 10^{33} \text{ cm}^{-2} \text{ s}^{-1}. \quad (8.9.1)$$

Compositeness would show up as a flattening of the cross-section; this is simulated by the dot-dashed line, where it is assumed that the composite-

ness scale is  $\Lambda \simeq 0.5$  TeV (corresponding to a distance of  $\sim 4 \times 10^{-17}$  cm).

Finally, supersymmetric particles such as selectron pairs ( $\tilde{e}\tilde{e}$ ), wino pairs ( $\tilde{W}\tilde{W}$ ) or smuons ( $\tilde{\mu}\tilde{\mu}$ ) could be detected. The exact prediction of the production rates for these sparticles depends on many model-dependent parameters, so this effect is indicated simply by the shaded areas.

# 9

## Extension to the hadrons; quark–lepton universality

We here enlarge the standard model to include the weak and electromagnetic interactions of hadrons. We encounter serious technical problems if we try to restrict ourselves to the original three quarks,  $u, d, s$ . In particular we find unwanted neutral strangeness-changing currents in the theory. These difficulties are eliminated by the introduction of a new ‘charm’ quark  $c$ . There is then a very attractive universality between the two lepton doublets  $(\nu_e^-), (\nu_\mu^-)$  and two quark doublets formed from  $u, d, s, c$ .

The discovery of a third generation lepton, the  $\tau$ , recreates technical problems which are resolved by the discovery of a third generation quark, the  $b$  (for ‘bottom’). Assuming that the hitherto unobserved partners  $\nu_\tau$  and the ‘top’ quark  $t$  really exist, we have an enlarged lepton–quark universality between three generations of leptons and three generations of quarks.

We further find that it is necessary to endow each quark with a completely new, internal degree of freedom called ‘colour’. Each quark can exist in three different colour states. Several technical problems—the statistics of quarks, the  $\pi^0$  decay rate, and the existence of triangle anomalies—are thereby resolved. The implications of colour for the famous ratio

$$R = \frac{\sigma(e^+e^- \rightarrow \text{hadrons})}{\sigma(e^+e^- \rightarrow \mu^+\mu^-)}$$

are discussed. Finally we summarise the structure of the quark sector of the standard model by giving the form of the Feynman graph vertices that occur.

### 9.1 Charm, bottom and top

Not so long ago it seemed clear that the underlying symmetry group of strong interactions was  $SU(3)$  and that all hadrons could be constructed

from three fundamental building blocks, the quarks, which one would wish to utilize in making a renormalizable model of semi-leptonic and non-leptonic weak interactions.

The most natural way to enlarge  $\mathcal{L}$  to include hadrons is to extend the gauge invariance plus spontaneous symmetry breaking prescription to include quark fields  $q = (u, d, s)$  in an analogous fashion to the leptons but taking account of the Cabibbo mixing of  $d$  and  $s$ .

One of the most interesting outcomes of gauge theory is the impossibility of making a reasonable model using just three quarks within the conventional Cabibbo current approach. Gauge theories require a larger group than  $SU(3)$  for hadrons. At the simplest level we require one new quark, the ‘charm’ quark  $c$ .

The original motivation for charm (Bjorken and Glashow, 1964; Hara, 1964) was principally based upon the aesthetic considerations of establishing a lepton–hadron parallelism, but it became an operative concept only when it was shown how its introduction could solve the problem of eliminating unwanted strangeness-changing neutral currents, and could alleviate certain other difficulties encountered in higher orders, including the technical problem of ‘triangle anomalies’.

Already at a phenomenological level, in the language of an effective current-current Lagrangian, one can see the need for a fourth quark.

In the current-current approach we have a parallelism between the leptonic doublets  $(\nu_e)_L, (\nu_\mu)_L$  and the quark doublet  $(d_C)_L$  involving the Cabibbo mixture

$$d_C = d \cos \theta_C + s \sin \theta_C \quad (9.1.1)$$

The data, as already mentioned, require the presence of neutral currents. If only  $u$  and  $d_C$  appear we would expect to find neutral current terms in the effective Lagrangian of the form

$$G[\bar{d}_C \gamma_\mu (1 - \gamma_5) d_C][\bar{\mu} \gamma^\mu (1 - \gamma_5) \mu] \quad (9.1.2)$$

and

$$G[\bar{d}_C \gamma_\mu (1 - \gamma_5) d_C][\bar{d}_C \gamma^\mu (1 - \gamma_5) d_C]. \quad (9.1.3)$$

There are terms in these of the form

$$\cos \theta_C \sin \theta_C (\bar{d} s + s \bar{d})$$

which will generate transitions with  $|\Delta S| = 1, 2$  and  $\Delta Q = 0$ , processes that are known to be totally absent, or at least very highly suppressed. For example (9.1.2) would predict the occurrence of the decay  $K_L \rightarrow \mu^+ \mu^-$  or  $e^+ e^-$  at a rate comparable with  $K^+ \rightarrow \mu^+ \nu_\mu$  whereas experimentally

(Particle Data Group, 1992)

$$\frac{\Gamma(K_L \rightarrow e^+ e^-)}{\Gamma_{\text{tot}}} < 1.6 \times 10^{-10}$$

and from (9.1.3) one will have a term giving rise to the virtual transitions with  $|\Delta S| = 2$

$$K^0 = d\bar{s} \rightarrow s\bar{d} = \bar{K}^0 \quad (9.1.4)$$

to first order in  $G$ , which would imply a  $K_L - K_S$  mass difference hundreds of times larger than found by experiment.

If we introduce  $s_C$  the combination of  $d$  and  $s$  orthogonal to Cabibbo's  $d_C$

$$s_C = s \cos \theta_C - d \sin \theta_C \quad (9.1.5)$$

and if the weak neutral current is symmetric under  $d_C \leftrightarrow s_C$ , i.e. contains also a term  $\bar{s}_C \gamma_\mu (1 - \gamma_5) s_C$ , one will find that the sum of the  $d_C$  and  $s_C$  terms is just

$$\bar{d} \gamma_\mu (1 - \gamma_5) d + \bar{s} \gamma_\mu (1 - \gamma_5) s, \quad (9.1.6)$$

i.e. the strangeness-changing cross-terms have cancelled out and there are no  $\Delta S \neq 0$  neutral currents.

However, as discussed earlier, in order to have a renormalizable theory we are forced to work with a gauge theory in which the weak and electromagnetic currents are coupled to the gauge vector bosons. It turns out to be impossible to simply add an extra piece to  $\mathcal{L}$  involving  $s_C$ . The simplest scheme which will eliminate the unwanted strangeness-changing neutral currents is that of Glashow, Iliopoulos and Maiani (1970) (GIM) in which a new quark, the charm quark  $c$ , is introduced. Since the usual hadrons are well described using just  $u, d, s$  as building blocks one has to explain why the effects of  $c$  are not seen. This is done by giving it a new quantum number, charm ( $C$ ), which is conserved in strong and electromagnetic interactions. The usual quarks, and indeed all the 'old' particles, have  $C = 0$  whereas  $c$  has  $C = +1$ . The mass of  $c$  is postulated to be larger than the masses of the usual quarks and one therefore expects to find a new species of hadrons, charm hadrons, with masses somewhat higher than the usual hadrons. All this was put forward as an hypothesis in 1970!

Today charm particles are produced in abundance and their properties are discussed in Chapters 11–13. It is by now an experimentally well established fact that the charm quark has charge  $2/3$ . This leads to a second quark doublet  $\begin{pmatrix} c \\ s_C \end{pmatrix}$ .

The discovery of the third generation lepton  $\tau$  and a third generation quark  $b$  (for 'bottom') complicates the above picture, but, as will be seen,

	$I$	$I_3$	$Q$	B	$S$	$C$	B	T
$u$	1/2	1/2	2/3	1/3	0	0	0	0
$d$	1/2	-1/2	-1/3	1/3	0	0	0	0
$c$	0	0	2/3	1/3	0	1	0	0
$s$	0	0	-1/3	1/3	-1	0	0	0
$t$	0	0	2/3	1/3	0	0	0	1
$b$	0	0	-1/3	1/3	0	0	-1	0

Table 9.1. Quantum numbers of the quarks.

enriches it too.

Although neither the  $\tau$ -neutrino  $\nu_\tau$  nor the partner of the  $b$  quark, named  $t$  (for ‘top’), have yet been discovered, it is assumed that they do exist, so that we are dealing with two extra doublets  $(\begin{smallmatrix} \nu_\tau \\ \tau^- \end{smallmatrix})$  and  $(\begin{smallmatrix} t \\ b \end{smallmatrix})$ .

The quantum number which distinguishes the various quarks from each other is called its *flavour*. Thus in addition to the standard notation,  $I$  isospin,  $Q$  electric charge, B baryon number, we introduce the strangeness quantum number  $S$ , the charm quantum number  $C$ , the bottom quantum number  $B$  and the top quantum number  $T$ . In accordance with the convention of *The Review of Particle Properties* (Particle Data Group, 1992) the sign of the flavour of a quark is taken to be the same as the sign of its electric charge, so that  $S(s) = -1$ ,  $C(c) = +1$ ,  $B(b) = -1$  and  $T(t) = +1$ . The quantum number assignment of the quarks is shown in Table 9.1.

Note that the Gell-Mann–Nishijima formula generalizes to

$$Q = I_3 + \frac{1}{2}(B + S + C + B + T). \quad (9.1.7)$$

## 9.2 Quark mixing

Returning now to the weak interactions, it would be bizarre if in the quark sector the Cabibbo mixing only took place between  $d$  and  $s$ . So we generalize the Cabibbo scheme by assuming that the coupling in the weak interactions is to *three* linearly independent combinations of  $d$ ,  $s$  and  $b$ :

$$\begin{aligned} d' &= V_{udd} + V_{us}s + V_{ub}b \\ s' &= V_{cdd} + V_{cs}s + V_{cb}b \\ b' &= V_{tdd} + V_{ts}s + V_{tb}b \end{aligned} \quad (9.2.1)$$

The matrix  $\mathbf{V}$  with elements  $V_{ij}$  where  $i = u, c, t$  and  $j = d, s, b$  must be unitary as discussed in Section 1.1.

	$Y_W$	$I_W$		$I_{3W}$	$I_{3W} + Y_W/2$
$q_{1L}$	1/3	1/2	$\left\{ \begin{array}{l} u_L \\ d'_L \end{array} \right.$	1/2 -1/2	2/3 -1/3
$d'_R$	-2/3	0		0	-1/3
$u_R$	4/3	0		0	2/3

Table 9.2. Weak interaction quantum numbers of the quarks of the first generation. The same quantum numbers apply to members of each generation. Note that  $Q = I_{3W} + Y_W/2$  holds. Compare with the lepton properties given in Table 4.1.

It is then assumed that the weak interactions couple to the left-handed weak isospin doublets

$$q_{1L} = \begin{pmatrix} u \\ d' \end{pmatrix}_L \quad q_{2L} = \begin{pmatrix} c \\ s' \end{pmatrix}_L \quad q_{3L} = \begin{pmatrix} t \\ b' \end{pmatrix}_L \quad (9.2.2)$$

and that each of these doublets transforms under the gauge transformations in the same way as do the left-handed lepton doublets (see Section 4.2).

$$\begin{pmatrix} \nu_e \\ e^- \end{pmatrix}_L \quad \begin{pmatrix} \nu_\mu \\ \mu^- \end{pmatrix}_L \quad \begin{pmatrix} \nu_\tau \\ \tau^- \end{pmatrix}_L \quad (9.2.3)$$

In this way we have a complete parallelism between the three lepton doublets and the three quark doublets. The transformations under  $SU(2)$  are identical, but because of the fractional charges one needs

$$q_{jL} \rightarrow e^{-i\theta(x)/6} q_{jL} \quad j = 1, 2, 3 \quad (9.2.4)$$

under  $U(1)$ .

Just as for the leptons, we require right-handed parts for  $u, d', c, s', t$  and  $b'$  in order to have the correct electromagnetic current, and these are taken to be invariant under the  $SU(2)$  gauge transformations. To achieve a gauge invariant theory they must transform under the  $U(1)$  transformations as follows:

$$\left. \begin{array}{l} u_R \rightarrow e^{-2i\theta/3} u_R, \\ d'_R \rightarrow e^{i\theta/3} d'_R, \end{array} \right\} \quad (9.2.5)$$

and similarly for  $c, s'$  and  $t, b'$ .

Analogously to Table 4.1 we show in Table 9.2 the weak interaction quantum numbers of the various quarks.

The above extension of the Cabibbo scheme is due to Kobayashi and Maskawa (1973). Because of the success of the Cabibbo theory it must be true that the new pieces in the mixtures which played a rôle earlier, must

be a small perturbation of the Cabibbo mixture. So, for example, we would expect  $V_{ud} \sim \cos \theta_C$ ,  $V_{us} \sim \sin \theta_C \ll V_{ud}$ ,  $|V_{ub}| \ll |V_{us}|$ . The precise determination of the values of the elements of the Kobayashi–Maskawa (KM) matrix is of great interest at present, and will be discussed in detail in Chapter 18.

We note here the important fact that the *order of magnitude* of the KM matrix elements will turn out to be

$$\begin{pmatrix} V_{ud} & V_{us} & V_{ub} \\ V_{cd} & V_{cs} & V_{cb} \\ V_{td} & V_{ts} & V_{tb} \end{pmatrix} \approx \begin{pmatrix} 1 - \lambda^2/2 & \lambda & \lambda^3 \\ -\lambda & 1 - \lambda^2/2 & \lambda^2 \\ \lambda^3 & -\lambda^2 & 1 \end{pmatrix} \quad (9.2.6)$$

where  $\lambda \approx \sin \theta_C \approx 0.22$ . Thus the diagonal elements are very close to unity in magnitude and off-diagonal elements vary from small to exceedingly small. This will be helpful in our study of deep inelastic scattering in assessing the relative importance of various contributions.

Although the extension from Cabibbo mixing, which involves a  $2 \times 2$  matrix, to KM mixing with its  $3 \times 3$  matrix may seem inconsequential, there is, in fact, a fundamental difference connected with CP violation, as was stressed by Kobayashi and Maskawa in their original paper.

Suppose that we had  $n$  quark doublets, i.e.  $n$  quark generations. The most general mixing would involve an  $n \times n$  unitary matrix which is specified by  $n^2$  real parameters. Each quark wave function or field being defined only up to a relative phase, there are  $(2n - 1)$  real parameters that can be absorbed as phases in the definition of the quark fields so that we are left with  $(n - 1)^2$  measurable real parameters. On the other hand, an orthogonal  $n \times n$  matrix depends on  $\frac{1}{2}n(n - 1)$  real angles. Therefore, our  $(n - 1)^2$  parameters can be broken up into  $\frac{1}{2}n(n - 1)$  real angles and  $(n - 1)^2 - \frac{1}{2}n(n - 1) = \frac{1}{2}(n - 1)(n - 2)$  phases. The presence of phases means that some of the elements of the matrix must be complex and this leads to CP violating transitions, and because CPT is assumed valid, also to time reversal violation.

In a four-quark model,  $n = 2$ , there is just one real rotation (the Cabibbo angle) and no phase; CP must be conserved (at least so long as no other interaction, outside the weak interaction gauge scheme, is introduced, or larger gauge groups used). But, as is well known, CP violation effects *have* been observed in the weak decays  $K_L \rightarrow 2\pi$ ,  $K_S \rightarrow 2\pi$  where  $K_{L,S}$  are the long lived and short lived neutral K mesons. In a six-quark scheme,  $n = 3$ , we have three ‘Cabibbo’ angles and one phase so that CP can be violated naturally (i.e. without altering the interaction). It is a topic of major interest at present to decide whether the observed effects are consistent with this natural CP violation. This is discussed extensively in Chapter 19.

There are many conventions for the choice of variables to parametrize the KM matrix. We follow the parametrization of *The Review of Particle Properties* (Particle Data Group, 1992):

$$\mathbf{V} = \begin{pmatrix} c_{12}c_{13} & s_{12}c_{13} & s_{13}e^{-i\delta} \\ -s_{12}c_{23} - c_{12}s_{23}s_{13}e^{i\delta} & c_{12}c_{23} - s_{12}s_{23}s_{13}e^{i\delta} & s_{23}c_{13} \\ s_{12}s_{23} - c_{12}c_{23}s_{13}e^{i\delta} & -c_{12}s_{23} - s_{12}c_{23}s_{13}e^{i\delta} & c_{23}c_{13} \end{pmatrix} \quad (9.2.7)$$

where  $c_{ij} \equiv \cos \theta_{ij}$  and  $s_{ij} \equiv \sin \theta_{ij}$ . It can be shown that one may take all the angles  $\theta_{12}, \theta_{23}, \theta_{13}$  to lie in the range  $0 \leq \theta_{ij} \leq \pi/2$  so that  $c_{ij} \geq 0$  and  $s_{ij} \geq 0$ , and the phase  $\delta$  to lie in  $0 \leq \delta \leq 2\pi$ .

A detailed discussion of the evaluation from experiment of the KM matrix elements is given in Chapter 18. The rôle of the KM matrix in CP violation is studied in Chapter 19.

### 9.3 Electroweak interaction of the quarks

In complete analogy with the leptonic case, the coupling in  $\mathcal{L}$  of the quarks to the neutral boson  $Z^0$  is given by [see (4.2.44)]

$$\frac{e}{2 \sin \theta_W \cos \theta_W} [h_3^\mu - 2 \sin^2 \theta_W h_{\text{em}}^\mu] Z_\mu \quad (9.3.1)$$

where  $h_{\text{em}}^\mu$  is the hadronic (i.e. quark) em current, which can be written

$$h_{\text{em}}^\mu = \sum_{j=1}^3 \bar{q}_j \gamma^\mu \frac{1}{2} (\tau_3 + \frac{1}{3} I) q_j \quad (9.3.2)$$

and

$$\begin{aligned} h_3^\mu &= \sum_{j=1}^3 \bar{q}_j \gamma^\mu (1 - \gamma_5) \frac{1}{2} \tau_3 q_j \\ &= \sum_j \bar{q}_{jL} \gamma^\mu \tau_3 q_{jL}. \end{aligned} \quad (9.3.3)$$

When colour is introduced it is postulated that the electroweak interactions are ‘colour blind’, i.e. that  $W$  and  $Z$  interact identically with a given type of quark irrespective of its colour. A sum over colour, though not shown, is *always* implied in *all* the quark currents.

As expected, when we substitute for  $q_j$  in terms of  $u, d; c, s; t, b$  all cross-terms disappear and there is no changing of strangeness, as desired. There is in fact no changing of *any* flavour. Thus, one finds, leaving out the matrices  $\gamma^\mu$

$$h_{\text{em}}^\mu = \frac{2}{3} (\bar{u}u + \bar{c}c + \bar{t}t) - \frac{1}{3} (\bar{d}d + \bar{s}s + \bar{b}b) \quad (9.3.4)$$

and leaving out the matrices  $\frac{1}{2}\gamma^\mu(1 - \gamma_5)$

$$h_3^\mu = (\bar{u}u + \bar{c}c + \bar{t}t) - (\bar{d}d + \bar{s}s + \bar{b}b). \quad (9.3.5)$$

Thus the weak neutral current conserves  $S, C, B$  and  $T$ .

Note that we can write (9.3.1) in the form

$$\left(\frac{2G}{\sqrt{2}}\right)^{\frac{1}{2}} M_Z h_Z^\mu Z_\mu \quad (9.3.6)$$

with

$$h_Z^\mu \equiv h_3^\mu - 2 \sin^2 \theta_W h_{\text{em}}^\mu. \quad (9.3.7)$$

The coupling of the quarks in  $\mathcal{L}$  to the charged bosons is of the form [see (4.2.27)]

$$- \frac{e}{2\sqrt{2} \sin \theta_W} [h_-^\mu W_\mu^- + h_+^\mu W_\mu^+] \quad (9.3.8)$$

where  $h_\pm^\mu$  is the charged weak current of the quarks, e.g.

$$h_+^\mu = 2 \sum_{j=1}^3 \bar{q}_{jL} \gamma^\mu \tau_+ q_{jL} \quad (9.3.9)$$

$$= \bar{u} \gamma^\mu (1 - \gamma_5) d' + \bar{c} \gamma^\mu (1 - \gamma_5) s' + \bar{t} \gamma^\mu (1 - \gamma_5) b'. \quad (9.3.10)$$

The Feynman diagram vertices corresponding to the interactions (9.3.1) and (9.3.8) are given in Section 9.6.

Recall that in the Cabibbo theory

$$d' = \cos \theta_C d + \sin \theta_C s \quad s' = \cos \theta_C s - \sin \theta_C d \quad (9.3.11)$$

with  $\cos \theta_C \gg \sin \theta_C$ , so that in (9.3.10) the strongest transitions are  $d \leftrightarrow u$  and  $s \leftrightarrow c$ . The latter will be important later in the identification of reactions arising from charm quarks. Note also that even in  $\theta_C = 0$ , the isospin properties of  $h_+^\mu$  are no longer simple. Only the first term  $\bar{u}d$  is a combination of genuine isospin currents,  $J_1 + iJ_2$ .

## 9.4 The GIM mechanism

Because of its historical importance we shall briefly discuss one of the original motivations for introducing a charm quark.

Consider the calculations of the  $K_L - K_S$  mass difference, to second order, via the *charged* weak currents.

The virtual transitions between  $K^0 = \bar{s}d$  and  $\bar{K}^0 = \bar{s}\bar{d}$  that are responsible for the mass difference are given by the diagrams in Fig. 9.1. (The precise relation between the mass difference and the Feynman amplitude is derived in Sections 19.2 and 19.3.) The Feynman amplitudes

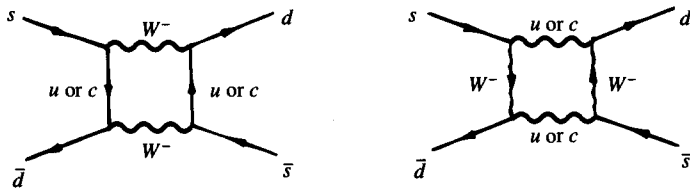


Fig. 9.1. Feynman diagrams contributing to  $K_L, K_S$  mass difference.

(not including the external spinors) are clearly proportional to  $g^4$ . Dimensionally, they must be like  $[M]^{-2}$ . Given that  $M_W \gg$  quark mass (indeed the quark masses could be zero), we are bound to find that

$$A(K^0 \rightarrow \bar{K}^0) \sim g^4/M_W^2 \sim \alpha G. \quad (9.4.1)$$

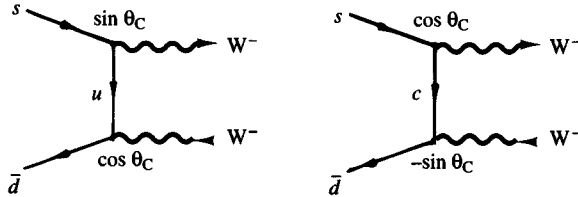
Now it can be shown that to be consistent with the experimental result

$$m_{K_L} - m_{K_S} = (3.522 \pm 0.016) \times 10^{-6} \text{ eV} \quad (9.4.2)$$

one requires

$$A(K_0 \rightarrow \bar{K}_0) \sim m_p^2 G^2 \sim 10^{-5} G. \quad (9.4.3)$$

So the result (9.4.1) is apparently much too large. However, if we look in more detail at the couplings implied by (9.3.10), we see that for the pieces making up the first diagram in Fig. 9.1 we have the factors shown below:



To the extent that  $m_u = m_c$  the propagators in the figure are the same, and the combined contribution will be proportional to

$$\sin \theta_C \cos \theta_C - \cos \theta_C \sin \theta_C,$$

i.e. it will vanish. A similar result holds for the second diagram of Fig. 9.1. Thus  $A(K^0 \rightarrow \bar{K}^0)$  must be proportional to  $m_u - m_c$ . Indeed one finds

$$\begin{aligned} A(K^0 \rightarrow \bar{K}^0) &\sim \frac{\alpha G (m_u - m_c)^2}{M_W^2} (\sin \theta_C \cos \theta_C)^2 \\ &\sim [G \sin \theta_C \cos \theta_C (m_u - m_c)]^2. \end{aligned} \quad (9.4.4)$$

Hence if the quark masses, or mass differences, are small, i.e. comparable with  $m_p$ , (9.4.4) will be compatible with (9.4.3).

A similar argument holds for the decay  $K^0 \rightarrow \mu^+ \mu^-$  which can also proceed via the chain  $K^0 \rightarrow W^+ W^- \rightarrow \mu^+ \mu^-$  and which would give much too large a rate if there were no cancellation between the terms involving  $u$  and  $c$  quarks.

We see, therefore, that the theory is only compatible with experiment because of the vital rôle played by the charm quark.

Later, when we come to study CP violation in Chapter 19 we shall re-examine the above calculation in the light of the existence of  $b$  and  $t$  quarks.

## 9.5 Colour

Up to the present we have utilized six different quarks  $u, d, c, s, t, b$ , which are referred to as different *flavour states* of the quarks: quarks come in six flavours.

There are several indications that the quarks possess a further internal degree of freedom, labelled by a new quantum number, which (rather arbitrarily) has been called *colour*. (Needless to say ‘colour’ should not be interpreted at all literally.) Each quark is supposed to exist in three colours, say yellow, blue, red, and the strong interactions are supposed to be ‘colour blind’, i.e. invariant under an  $SU(3)$  group of transformations that mixes up the colours. This  $SU(3)$  has nothing to do with the usual  $SU(3)$  which mixes up flavours, so it will be best to distinguish it by writing  $SU(3)_C$  and  $SU(3)_F$  for the two kinds of transformations. Since none of the known *hadrons* has any unforeseen degeneracy, as would surely occur if they were available in different colour states, it is presumed that  $SU(3)_C$  is a perfect symmetry of the strong interactions and the known hadrons are all *colour singlets*. It is believed to be true, but is far from proved, that it will emerge from the dynamical model of the strong interactions, QCD, based on the idea of the colour, that the only stable eigenstates are colour singlets.

### 9.5.1 The quark statistics

The lowest lying states, in the naive quark model (Gell-Mann, 1964; Zweig, 1964) of the most common baryons, consist of triplets ( $qqq$ ) of  $u, d$  and  $s$  quarks in relative s-wave configurations, since if the kinetic energy is to be a minimum the space wave function cannot have nodes and must be symmetric. Phenomenologically, in order to agree with the spectra of known particles, one finds that the spin and isospin parts must also be symmetric. Thus we have totally symmetric wave functions in violation of the Pauli principle if quarks are fermions as they have to be.

The classic example is the  $N^*$  resonance  $\Delta(1238)$  with spin  $\frac{3}{2}$  and isospin  $\frac{3}{2}$ . It thus requires all quark spins and isospins pointing in the same direction, and is completely symmetric, e.g.  $\Delta^{++}(s_Z = \frac{3}{2}) = u^\dagger u^\dagger u^\dagger$  where  $u^\dagger = u(s_z = \frac{1}{2})$ .

At a more sophisticated level, if one tries to incorporate ordinary spin with the usual  $SU(3)$  one is led to the celebrated  $SU(6)$  symmetry group (Gursey and Radicati, 1964; Sakita, 1964) (in analogy to what is done in nuclear physics where one combines  $SU(2)$  for spin with the  $SU(2)$  for isospin to get  $SU(4)$ ), where the quarks form a representation, the 6, with components

$$q = (u^\dagger, u^\dagger, d^\dagger, d^\dagger, s^\dagger, s^\dagger). \quad (9.5.1)$$

The  $SU(6)$  content of baryons is then given by

$$\begin{aligned} B &\sim qqq \sim \underline{\mathbf{6}} \otimes \underline{\mathbf{6}} \otimes \underline{\mathbf{6}} \\ &= \underline{\mathbf{56}} \oplus \underline{\mathbf{70}} \oplus \underline{\mathbf{70}} \oplus \underline{\mathbf{20}}. \end{aligned}$$

Of these the 56 is totally symmetric whereas the 20 is totally antisymmetric.

According to the generalized Pauli principle, one expects the complete wave function of the baryon to be antisymmetric, and since the ground state baryon  $SU(6)$  supermultiplet is a symmetric s-state, the favoured  $SU(6)$  representation ought to be the 20, whose content in terms of flavour and ordinary spin is

$$\begin{aligned} \underline{\mathbf{20}} \text{ of } SU(6) &\rightarrow [SU(3) \text{ octet with spin } \frac{1}{2}] \\ &+ [SU(3) \text{ singlet with spin } \frac{3}{2}] \end{aligned}$$

or

$$\underline{\mathbf{20}} \rightarrow (8, 2) + (1, 4),$$

and which has even parity. However, not only is there no known even parity, unitary singlet, spin  $\frac{3}{2}$  low mass resonance, but the predicted magnetic moments for the spin  $\frac{1}{2}$  octet disagree in sign and magnitude with the observed baryon magnetic moments.

Although one could simply conclude that  $SU(6)$  is a bad symmetry, the surprising fact is that the *symmetric* 56 representation for baryons leads to the decomposition

$$\underline{\mathbf{56}} \rightarrow (8, 2) \oplus (10, 4),$$

which beautifully fits the observed positive parity spin  $\frac{1}{2}$  octet ( $N, \Lambda, \Sigma, \Xi$ ) and the spin  $\frac{3}{2}$  decuplet ( $\Delta, \Sigma^*, \Xi^*, \Omega$ ). Furthermore, both  $SU(6)$  and the non-relativistic quark model predict  $\mu(p)/\mu(n) = -\frac{3}{2}$  in good agreement

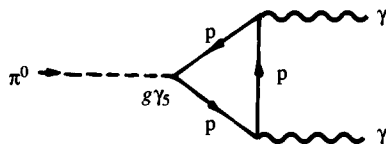


Fig. 9.2. Feynman diagram for  $\pi^0 \rightarrow 2\gamma$  decay amplitude used by Steinberger in 1949.

with the experimental values of the magnetic moments, and give reasonable values for the other baryon magnetic moments.

One can reverse this argument to estimate quark masses as follows. The quarks require a magnetic moment  $\mu_j = 2.79Q_j \times (e\hbar/2m_{pc})$ , where  $eQ_j$  is the quark charge. If they are *point-like* Dirac particles, i.e. have no anomalous moment, they must have an effective mass  $m_q \approx m_p/2.79 \approx 335 \text{ MeV}/c^2$ . This effective mass is referred to as the ‘constituent mass’.

There is clearly a conflict with the generalized Pauli principle unless there exists a further, new quantum number (colour) whose wave function is antisymmetric.

With minor variations, all the proposals for colour (Greenberg, 1964; Han and Nambu, 1965; Struminsky, 1965) were originally motivated by the statistics argument. Recently, colour has become a very handy tool to perhaps explain why quarks cannot get free. It is believed that all stable states are colour singlets and that colour is an exact symmetry. This will prevent any colour carrying object (quark, gluon, ...) from materializing in the laboratory. Most confining models are based on this idea.

In summary, if  $q^a$  is a quark of colour  $a$  ( $a = 1, 2, 3$ ), then colour confinement demands that observed hadrons be in either of the following colour singlet states:

$$\begin{aligned} \epsilon_{abc} q^a q^b q^c &\quad \text{for baryons.} \\ \delta_{ab} q^a \bar{q}^b &\quad \text{for mesons.} \end{aligned}$$

### 9.5.2 $\pi^0 \rightarrow 2\gamma$

Steinberger (1949) calculated the rate for the decay  $\pi^0 \rightarrow 2\gamma$  in the proton-antiproton or one-loop approximation as shown in Fig. 9.2.

Using a pseudo-scalar  $\pi N\bar{N}$  coupling, with coupling constant  $g^2/4\pi = 14.6$ , and a point Dirac coupling without anomalous magnetic moment for the  $\gamma N\bar{N}$  vertices, the result was

$$\begin{aligned}\Gamma(\pi^0 \rightarrow 2\gamma) &= \frac{\alpha^2}{16\pi^2} \frac{g^2}{4\pi^2} \frac{m_\pi^3}{m_p^2} \\ &\simeq 13.8 \text{ eV},\end{aligned}\quad (9.5.2)$$

as compared with the experimental value of  $7.8 \pm 1.0$  eV —good agreement granted that this is a strong interaction calculation.

If we now believe that the fundamental hadrons are the quarks, we should redo the calculation using quarks rather than protons for the internal lines of the diagram. The  $\pi^0$  contains only  $u$  and  $d$  quarks, so the triangle will consist of  $u$  or  $d$  quarks and we require the coupling of the  $\pi^0$  to these.

We take  $u$  and  $d$  to form an isodoublet  $q = \begin{pmatrix} u \\ d \end{pmatrix}$  just like  $N = \begin{pmatrix} p \\ n \end{pmatrix}$  so that the isospin invariant coupling to the quarks will be identical in form to that between pions and nucleons, namely,

$$g_q \bar{q} \gamma_5 \tau \cdot \pi q \quad \text{and} \quad g \bar{N} \gamma_5 \tau \cdot \pi N \quad (9.5.3)$$

so that the coupling to the  $\pi^0$  is

$$g_q \bar{q} \gamma_5 \tau_3 \pi^0 q = g_q [\bar{u} \gamma_5 u - \bar{d} \gamma_5 d] \pi^0. \quad (9.5.4)$$

But because we are dealing with the strong interactions it is a non-trivial matter to relate  $g_q$  to  $g$ . As pointed out to us by M. Scadron, one can attack the problem using the so-called Goldberger–Treiman relation (see Bailin, 1982, for a clear explanation) which suggests that

$$\frac{g_q}{m_q} \approx \frac{g}{m_p}. \quad (9.5.5)$$

Bearing in mind (9.5.4) and the charges of the quarks, the quark result can be obtained from the nucleon result for Fig. 9.2 by the substitutions:

$$\begin{aligned}\alpha &\rightarrow \alpha \left[ \left( \frac{2}{3} \right)^2 - \left( \frac{1}{3} \right)^2 \right] = \frac{\alpha}{3} \\ \frac{g}{m_p} &\rightarrow \frac{g_q}{m_q} = \frac{g}{m_p}.\end{aligned}\quad (9.5.6)$$

The net result is that (9.5.2) must be multiplied by a factor  $1/9$  and the calculation using quarks is too small by a factor of 5.

If, however, quarks come in three colours, the  $\pi^0$ , being a colour singlet, couples equally strongly to each colour. Thus summing over the colour of the quarks in the triangle will give a factor of 3 in the amplitude which will then cancel the factor of  $1/9$  in the rate, and leave us with the original Steinberger result (9.5.2).

A more sophisticated calculation using current algebra (Adler, 1969) gives a rate

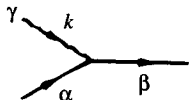
$$\Gamma(\pi^0 \rightarrow 2\gamma) = 7.29 \text{ eV} \quad (9.5.7)$$

when colour is included—this is in remarkably good agreement with experiment but wrong by a factor of 9 without colour.

### 9.5.3 Triangle anomalies

We mentioned earlier that there are some technical restrictions in constructing models of gauge theories if renormalizability is to be ensured. We will not attempt to analyse the details but indicate heuristically the origin of these restrictions and the conditions required to satisfy them.

To begin with, consider the simplest and best known gauge theory—QED. As a result of the gauge invariance there are equations of constraint (the Ward-Takahashi identities mentioned in Section 1.1) that must be satisfied by certain matrix elements. For example, because the photon is coupled to the electromagnetic current in the form  $A_\mu J_{\text{em}}^\mu$ , the amplitude for a photon to cause a transition from some state  $|\alpha\rangle$  to  $|\beta\rangle$  as shown,



is of the form

$$\epsilon_\mu(k) M^\mu(\beta, \alpha), \quad (9.5.8)$$

where  $\epsilon_\mu(k)$  is the polarization vector of the photon and

$$M^\mu(\beta, \alpha) \sim \int d^4x e^{ik \cdot x} \langle \beta | J_{\text{em}}^\mu(x) | \alpha \rangle. \quad (9.5.9)$$

The consequence of the gauge invariance, (1.1.4), implies here that

$$k^\mu M^\mu(\beta, \alpha) = 0. \quad (9.5.10)$$

This is a formal property. It was derived in a very general fashion. It sometimes happens, however, that when we calculate a particular  $M^\mu(\beta, \alpha)$  in perturbation theory it diverges, and in removing the divergence there may be difficulties in satisfying (9.5.10) or analogous relations, as we shall presently see.

Although irrelevant for most electrodynamic processes, but, in fact, important in deep inelastic reactions (see Section 16.8), we can consider, within the realm of QED, the following axial-vector current

$$A_\mu = \bar{\psi} \gamma_\mu \gamma_5 \psi \quad (9.5.11)$$

and pseudo-scalar current

$$P = \bar{\psi} \gamma_5 \psi. \quad (9.5.12)$$

Using just the equations of motion one can show that

$$\partial_\mu A^\mu = 2im_0 P \quad (9.5.13)$$

where  $m_0$  is the bare mass of the electron.



Fig. 9.3. General amplitudes for coupling of two photons to axial-vector and pseudo-scalar currents.

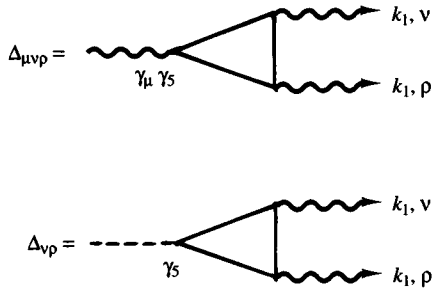


Fig. 9.4. ‘Triangle diagram’ contributions to the amplitudes of Fig. 9.3.

This relationship, like  $\partial_\mu J_{\text{em}}^\mu = 0$ , gives rise to constraints amongst certain matrix elements. We shall refer to these as the axial Ward identities. For example, if we consider the diagrams in Fig. 9.3 in which two photons couple to the axial current and the pseudo-scalar current respectively then we ought to find, because of (9.5.13), that the scalar product of  $(k_1 + k_2)_\mu$  with the first amplitude should equal the second amplitude.

Unfortunately in perturbation theory we run into trouble at an early stage. Consider the ‘triangle diagram’ contributions to the amplitudes of Fig. 9.3 shown in Fig. 9.4. Gauge invariance requires

$$k_{1\nu} \Delta_{\mu\nu\rho} = k_{2\rho} \Delta_{\mu\nu\rho} = 0. \quad (9.5.14)$$

The axial Ward identity requires

$$(k_1 + k_2)_\mu \Delta_{\mu\nu\rho} = 2m_0 \Delta_{\nu\rho}. \quad (9.5.15)$$

The actual Feynman integral for  $\Delta_{\mu\nu\rho}$  is divergent. Nevertheless when we compute the LHS of (9.5.15) an algebraic cancellation occurs, the integral becomes finite, and we get the expected answer, namely the RHS of (9.5.15).

However, when we try to compute the LHS of (9.5.14) we get the difference of two divergent integrals. The diagram for  $\Delta_{\mu\nu\rho}$  has, of course, to be subjected to renormalization to make it finite; and when this is done it can be arranged that (9.5.14) comes out correctly, but now (9.5.15) fails to hold! It can be shown that there is *no* consistent method of regularization such that *both* (9.5.14) and (9.5.15) hold. One of the bizarre features is that the result depends upon the choice of integration variables, i.e.

upon what momentum labels are attached to the lines in the Feynman diagram!

This unwelcome discovery is potentially catastrophic for our unified weak and electromagnetic gauge theory. There we have lots of gauge invariance, many conserved currents, both vector and axial-vector, and hence many Ward identities. Moreover the Ward identities play a vital rôle in proving that the theory is renormalizable. It is the subtle inter-relation of matrix elements that allows certain infinities to cancel out and render the theory finite. Thus we cannot tolerate a breakdown of the Ward identities, and we have to ensure that in our theory these triangle anomalies do not appear.

It turns out, similar to the above, that regularization of the triangle diagrams leads to correct results for the vector current Ward identities. The analogue of (9.5.13) is that the divergence of the axial-vector current vanishes, so the RHS of (9.5.15) should be zero, and this fails to hold. We must therefore construct our theory so that the coefficient of  $\gamma_5$  in the expression for  $(k_1 + k_2)_\mu \Delta_{\mu\nu\rho}$  is zero for *algebraic reasons*.

In general we have gauge vector bosons  $W_\mu$  coupled gauge-invariantly to the left-handed parts of a set of fermions

$$f_L = \begin{bmatrix} f_1 \\ f_2 \\ \vdots \\ f_j \\ \vdots \end{bmatrix}$$

in the form  $\bar{f}_L \gamma^\mu M^a f_L W_\mu^a$  and to the right-handed parts of the same or some other set of fermions

$$F_R = \begin{bmatrix} F_1 \\ F_2 \\ \vdots \\ F_i \\ \vdots \end{bmatrix}$$

via  $\bar{F}_R \gamma^\mu N^b F_R W_\mu^b$  where  $M^a$  and  $N^b$  are sets of matrices representing the generators of the gauge transformations [analogous to the  $L_j$  of (2.3.28)].

We consider the general triangle diagram shown in Fig. 9.5, bearing in mind that we must include both the left-handed and right-handed fermion contributions, and also that each fermion labelled  $i, j, k$  can either flow towards or away from a particular vertex. (In Fig. 9.5 we show only the left-handed fermions. Similar diagrams occur for the right-handed ones.)

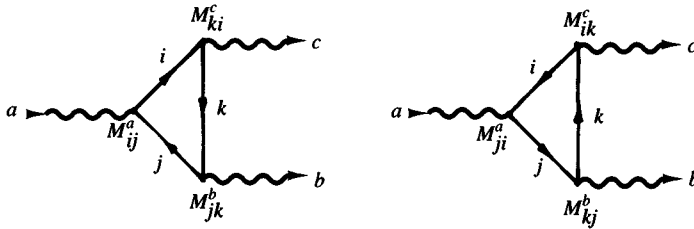


Fig. 9.5. Detailed structure of triangle diagram contributions to  $W^a \rightarrow W^b + W^c$  in a general gauge theory.

The amplitudes will contain various Feynman propagators (which are irrelevant to our discussion) and, as is easy to see, there will be overall factors of

$$(1 - \gamma_5) M_{ij}^a M_{jk}^b M_{ki}^c \quad \text{and} \quad (1 - \gamma_5) M_{ji}^a M_{ik}^c M_{kj}^b$$

in the diagrams shown. When added, the result is

$$(1 - \gamma_5) \text{Tr}\{M^a [M^b, M^c]_+\} \quad (9.5.16)$$

where  $[ ]_+$  stands for the anti-commutator of the matrices.

In similar fashion the right-handed fermions give

$$(1 + \gamma_5) \text{Tr}\{N^a [N^b, N^c]_+\}. \quad (9.5.17)$$

In order therefore to eliminate the  $\gamma_5$  term, which is the source of all the trouble, we must require our couplings to the fermions to satisfy

$$\text{Tr}\{M^a [M^b, M^c]_+\} - \text{Tr}\{N^a [N^b, N^c]_+\} = 0 \quad (9.5.18)$$

This is quite general and we now turn to its implications in the standard model.

Charge conservation limits the number of cases we have to examine. For  $Z \rightarrow W^+ W^-$  from (9.3.1) and (9.3.8), the coupling is only to the left-handed fermions and (9.5.18) becomes

$$\text{Tr}\{(2 \sin^2 \theta_W Q - \tau_3)[\tau_-, \tau_+]_+\} = 0, \quad (9.5.19)$$

where  $Q$  is a diagonal matrix whose elements are the charges of the fermions in units of  $e$ . Now  $[\tau_+, \tau_-]_+ = I$ ,  $\text{Tr} \tau_3 = 0$  and so we are left with the requirement

$$\text{Tr} Q = 0. \quad (9.5.20)$$

But  $\text{Tr} Q = \sum_j Q_j$ . Thus we have the remarkable condition that the algebraic sum of the charges of *all* the left-handed fermions in the theory must be zero:

$$\sum_{j \in f_L} Q_j = 0. \quad (9.5.21)$$

The other triangle diagrams turn out to add no further requirement than this.

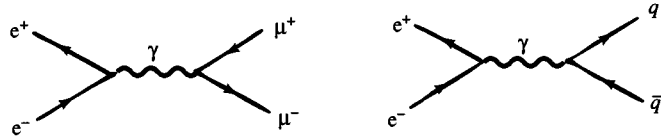
Let us examine (9.5.21). The charges of the leptons ( $e^-$ ,  $\nu_e$ ,  $\mu^-$ ,  $\nu_\mu$ ,  $\tau^-$ ,  $\nu_\tau$ ) add up to  $(-3)$ . If there are six quarks ( $u, d, c, s, t, b$ ) their charges add up to  $1$ . But if each quark comes in three colours the charge sum becomes  $(+3)$ . In this case

$$\sum_{j \in f_L} Q_j = 0$$

and the anomaly is removed!

#### 9.5.4 The cross-section for $e^+e^- \rightarrow \text{hadrons}$

For energies well below  $M_Z$ ,  $Z^0$  exchange should be a small correction to  $\gamma$  exchange. As a result, in the quark model, the *basic* amplitudes involved in  $e^+e^- \rightarrow \mu^+\mu^-$  and in  $e^+e^- \rightarrow \text{hadrons}$  are almost identical:



and differ only by the ratio of the charges  $eQ_q/(-e)$ .

Since quarks, by decree, cannot appear in the laboratory, their branching ratio into ordinary particles must be 100% and almost all of this, say  $> 99\%$ , will be into hadrons.

Thus for a given quark-antiquark pair  $q_j\bar{q}_j$  one has

$$\left| \frac{A(e^+e^- \rightarrow \text{hadrons via } q_j\bar{q}_j)}{A(e^+e^- \rightarrow \mu^+\mu^-)} \right|^2 = Q_j^2. \quad (9.5.22)$$

Experimentally, one measures the famous ratio  $R$  defined as

$$R \equiv \frac{\sigma(e^+e^- \rightarrow \text{anything}) - \sigma(e^+e^- \rightarrow e^+e^-) - \sigma(e^+e^- \rightarrow \mu^+\mu^-)}{\sigma(e^+e^- \rightarrow \mu^+\mu^-)_{\text{QED}}} \quad (9.5.23)$$

$$= \frac{\sigma(e^+e^- \rightarrow \text{'hadrons'}}{\sigma(e^+e^- \rightarrow \mu^+\mu^-)_{\text{QED}}}. \quad (9.5.24)$$

where  $\sigma(e^+e^- \rightarrow \mu^+\mu^-)_{\text{QED}}$  is given in (8.3.5). We have written ‘hadrons’ in inverted commas because as mentioned earlier there is evidence for the existence of a new heavy lepton  $\tau$ , and what is measured in (9.5.23) includes the production of this or any other so far unrecognized leptons that couple directly to a photon.

Now spectroscopic evidence suggests that the quark constituent masses are very roughly  $m_u \approx m_d \approx 300 \text{ MeV}/c^2$ ,  $m_s \approx 500 \text{ MeV}/c^2$ ,  $m_c \approx$

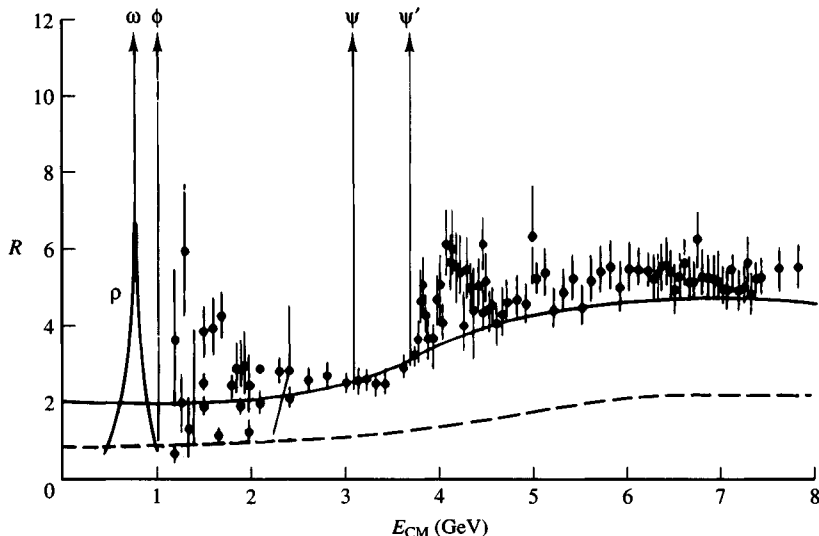


Fig. 9.6. Comparison between experiment and theory for the ratio  $R$  as function of CM energy. Solid line corresponds to quarks in three colours; dashed line to no colour.

$1.5 \text{ GeV}/c^2$ ,  $m_b \approx 5 \text{ GeV}/c^2$  and it is believed that  $m_t \approx 130 \text{ GeV}/c^2$  [eqns (8.6.20) and (7.8.2)].

Consider then the contribution to  $R$  of a particular quark-antiquark pair. At a given CM energy, the cross-section ratio (9.5.24) will differ from the ratio (9.5.22) because of the different phase space for  $\mu^+\mu^-$  and  $q_j\bar{q}_j$ . Indeed for  $E_{\text{CM}} < 2m_j$  there should be no contribution from  $q_j\bar{q}_j$ . As  $E_{\text{CM}}$  passes through the threshold energy  $2m_j$  we expect a gradual rise of the contribution to  $R$ , and for  $E_{\text{CM}} \gg 2m_j$  phase space effects will be negligible and we expect

$$(\text{Contribution to } R \text{ from } q_j\bar{q}_j) \xrightarrow{E_{\text{CM}} \gg 2m_j} Q_j^2. \quad (9.5.25)$$

Thus, as a function of energy,  $R$  should rise in a series of ‘rounded’ steps at  $E_{\text{CM}} \simeq 2m_j$ , each step being of height  $N_j Q_j^2$ , where  $N_j$  is the number of quarks of charge  $Q_j$  and mass  $m_j$ . There will be additional steps of height  $Q_j^2$  for each new lepton of mass  $m_j$  and charge  $Q_j$  at  $E_{\text{CM}} \sim 2m_j$ .

In Fig. 9.6 we show  $R$  vs  $E_{\text{CM}}$  at moderate energies, compared with our theoretical picture. The dashed line corresponds to no colour. The full line corresponds to quarks coming in three colours, so that  $N_j$  in the previous paragraph has value 3 for each quark flavour.

Note that below the charm production threshold the height of  $R \sim 2.5$

is in reasonable agreement with the value

$$\sum_{j=u,d,s} Q_j^2 = 3 \times \left( \frac{4}{9} + \frac{1}{9} + \frac{1}{9} \right) = 2 \quad (9.5.26)$$

whereas there would be serious disagreement with the value  $\frac{2}{3}$  in the absence of colour.

Above the charm and heavy lepton thresholds we expect

$$\sum_{j=u,d,s,c,\tau} Q_j^2 = 3 \times \left( \frac{4}{9} + \frac{1}{9} + \frac{1}{9} + \frac{4}{9} \right) + 1 = 4.33, \quad (9.5.27)$$

as compared with the experimental value  $R \sim 5$  in Fig. 9.6.

Given the uncertainties in the experimental calibration one sees that the measured values of  $R$  are in reasonable agreement with a scheme based on coloured quarks with the usual fractional charges, and with the existence of a heavy lepton. Note too that the data is compatible with the charge assignment  $Q_c = \frac{2}{3}$  for the charm quark.

As mentioned in Chapter 1, colour is a basic ingredient of QCD, and we shall see in Section 22.1 that there are strong interaction corrections to (9.5.22) coming from gluon exchange between the outgoing  $q\bar{q}$  pair. This slightly alters the energy dependence of  $R$  and can be used to estimate the strong interaction gluon-quark coupling strength.

Note that the behaviour of  $R$  changes at energies approaching  $M_Z$  (see Figs. 8.2 and 8.3). At LEP energies  $Z^0$  exchange dominates and the couplings to the  $q_j\bar{q}_j$  pairs is no longer just  $Q_j^2$ . In Chapter 8 we discussed the reaction  $e^+e^- \rightarrow f\bar{f}$  in the LEP energy region. The treatment of  $e^+e^- \rightarrow q\bar{q}$  is the same in so far as electroweak interactions are concerned, but clearly will be significantly altered by strong interactions, e.g. gluon exchange.

## 9.6 Summary of the quark sector of the standard model

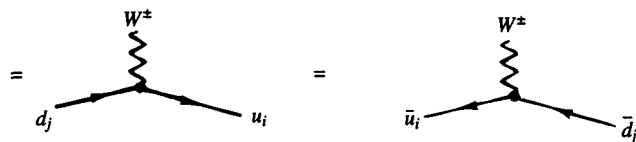
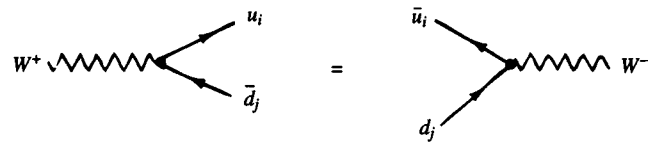
For ease of reference we here summarize the physical content of that part of the full standard model Lagrangian involving the interaction of the gauge bosons, the quarks and the Higgs. The full Feynman rules are given in Appendix 2.3. Here we give just the vertices. All results are independent of the quark colour.

By convention all topologically similar vertices are given the same sign in a Feynman diagram. The overall sign of the diagram has to be determined by comparing the order of the fermion operators in the diagram with their normal order in the S operator. An example is worked out in Section 5.1.1.

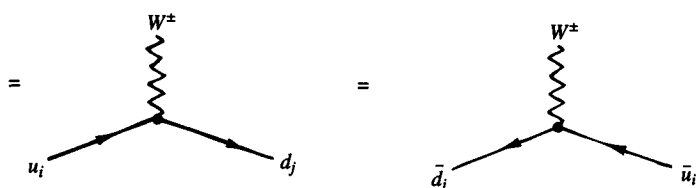
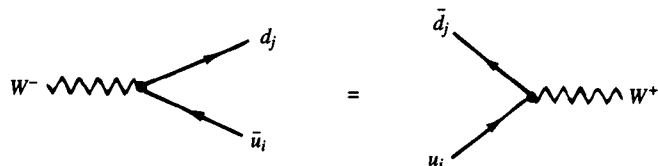
1. *Charged weak hadronic interaction.* Let us introduce generation labels  $i, j = 1, 2, 3$  such that

$$(u_1, u_2, u_3) \equiv (u, c, t) \quad \text{and} \quad (d_1, d_2, d_3) \equiv (d, s, b) \quad (9.6.1)$$

Then from (9.3.8), (9.3.10) and (9.2.1) one deduces

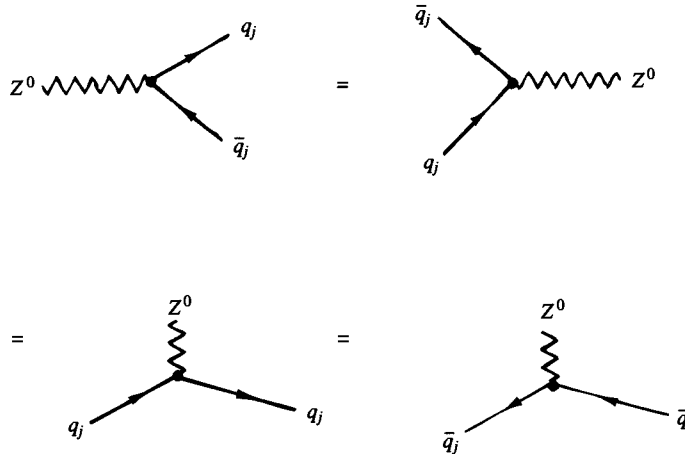


$$= -\frac{ie}{2\sqrt{2}\sin\theta_W} V_{ij} \gamma^\mu (1 - \gamma_5) \quad (9.6.2)$$



$$= -\frac{ie}{2\sqrt{2}\sin\theta_W} V_{ij}^* \gamma^\mu (1 - \gamma_5) \quad (9.6.3)$$

2. *Neutral weak hadronic interaction.* From (9.3.1), (9.3.2) and (9.3.3) we get, with  $q_j = u_j$  or  $d_j$



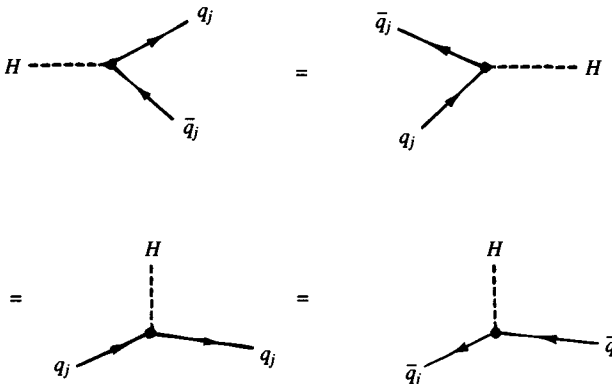
$$= ie\gamma^\mu(v_j - a_j\gamma_5) \quad (9.6.4)$$

where

$$\left. \begin{aligned} v_j &= \frac{I_3^{jL} - 2Q_j \sin^2 \theta_W}{2 \sin \theta_W \cos \theta_W} & a_j &= \frac{I_3^{jL}}{2 \sin \theta_W \cos \theta_W} \\ &\equiv \frac{g_V^j}{2 \sin \theta_W \cos \theta_W} & &\equiv \frac{g_A^j}{2 \sin \theta_W \cos \theta_W} \end{aligned} \right\} \quad (9.6.5)$$

where \$I\_3^{jL}\$ is the third component of weak isospin of the left-handed part of the quark \$j\$, i.e. \$I\_3^{jL} = \frac{1}{2}\$ for \$u, c, t\$; \$= -\frac{1}{2}\$ for \$d, s, b\$.

### 3. Higgs coupling to quarks.



$$= i \frac{\sqrt{\pi\alpha}}{\sin \theta_W} \left( \frac{m_j}{M_W} \right) I \quad (9.6.6)$$

where \$m\_j\$ is the mass of quark \$j\$ and \$I\$ is the unit \$4 \times 4\$ matrix.

### 9.7 Quark masses and the KM matrix

In Section 4.2 we showed how the leptons could be coupled to the Higgs (scalar) field in such a way that the non-zero value of  $\phi$  in the vacuum generated mass terms for the leptons  $e, \mu, \tau$  while leaving their neutrinos massless. The interaction was of the form (4.2.48)

$$\mathcal{L}_{S-Lept} = -G_\ell(\bar{L}\phi)\mathbf{R} + \text{h.c.} \quad (9.7.1)$$

where L and R refer to the lepton left-handed doublet and right-handed singlet of a given generation. There is one such term for each generation  $\ell = e, \mu, \tau$ .

A similar mechanism can be invoked to give mass to the quarks [though there may be other sources of mass for the quarks (see Section 20.3)], but this would leave the up-type quarks, the analogues of the neutrinos, massless. In order to construct an interaction invariant under weak  $SU(2)$  and weak  $U(1)$  which will give mass to the quarks with  $I_{3W} = 1/2$ , it turns out, on the basis of Table 9.2, that we need a Higgs doublet with  $Y_W = -1$ . Recall that  $\phi \equiv \begin{pmatrix} \phi^+ \\ \phi^0 \end{pmatrix}$  has  $Y_W = 1$ , and is a weak isospin doublet. Recall also, that for ordinary isospin, the nucleon doublet  $N \equiv \begin{pmatrix} p \\ n \end{pmatrix}$  and the anti-nucleon doublet  $\bar{N} \equiv \begin{pmatrix} \bar{n} \\ -\bar{p} \end{pmatrix}$  (note the minus sign!) transform identically under isospin rotations. By analogy

$$\tilde{\phi} \equiv \begin{pmatrix} \bar{\phi}^0 \\ -\bar{\phi}^- \end{pmatrix} \quad (9.7.2)$$

will transform just like  $\phi$  under weak  $SU(2)$ , and it has  $Y_W = -1$ .

Invariant couplings of the form

$$-G_j^d(\bar{q}_{jL}\phi)d'_{jR} - G_j^u(\bar{q}_{jL}\tilde{\phi})u_{jR} + \text{h.c.} \quad (9.7.3)$$

with one such term for each generation  $j$ , would then generate masses for all the quarks. However, instead of proceeding in this fashion we think it worthwhile to discuss the mass question from a slightly different point of view which, interestingly, links it to the question of the existence of the KM matrix. Suppose that the original Lagrangian involves ‘bare’ quarks

$$q_{1L}^0 = \begin{pmatrix} u^0 \\ d^0 \end{pmatrix} \quad q_{2L}^0 = \begin{pmatrix} c^0 \\ s^0 \end{pmatrix} \quad q_{3L}^0 = \begin{pmatrix} t^0 \\ b^0 \end{pmatrix} \quad (9.7.4)$$

$$\left. \begin{array}{lll} u_{1R}^0 = u_R^0 & u_{2R}^0 = c_R^0 & u_{3R}^0 = t_R^0 \\ d_{1R}^0 = d_R^0 & d_{2R}^0 = s_R^0 & d_{3R}^0 = b_R^0 \end{array} \right\} \quad (9.7.5)$$

which couple to the electroweak bosons exactly as do the lepton doublets and singlets (see Section 4.2). There is then perfect universality between

leptons and bare quarks and there is no KM mixing to start with.

But now postulate that these bare quarks are not eigenstates of mass, i.e. that their mass-like couplings are *non-diagonal*. The mass-generating interaction can then be of the form

$$\mathcal{L}_{S-Quarks} = -D_{ij}(\bar{q}_{iL}^0 \phi) d_{jR}^0 - U_{ij}(\bar{q}_{iL}^0 \tilde{\phi}) u_{jR}^0 + \text{h.c.} \quad (9.7.6)$$

where  $\mathbf{D}$  and  $\mathbf{U}$  are arbitrary  $3 \times 3$  matrices, i.e. not necessarily hermitian.

The non-zero value of  $\phi$  in the vacuum state

$$\phi_{\text{VAC}} = \begin{pmatrix} 0 \\ v/\sqrt{2} \end{pmatrix} \quad \tilde{\phi}_{\text{VAC}} = \begin{pmatrix} v/\sqrt{2} \\ 0 \end{pmatrix} \quad (9.7.7)$$

then yields non-diagonal mass-like terms

$$\begin{aligned} & \frac{v}{\sqrt{2}} \left\{ D_{ij} \bar{d}_{iL}^0 d_{jR}^0 + U_{ij} \bar{u}_{iL}^0 u_{jR}^0 \right\} + \text{h.c.} \\ &= \frac{v}{\sqrt{2}} \left\{ \bar{d}_L^0 \mathbf{D} d_R^0 + \bar{u}_L^0 \mathbf{U} u_R^0 \right\} + \text{h.c.} \end{aligned} \quad (9.7.8)$$

where we have introduced

$$\mathbf{d}_R^0 = \begin{pmatrix} d_1^0 \\ d_2^0 \\ d_3^0 \end{pmatrix}_R = \begin{pmatrix} d_R^0 \\ s_R^0 \\ b_R^0 \end{pmatrix} \quad (9.7.9)$$

and

$$\mathbf{u}_R^0 = \begin{pmatrix} u_1^0 \\ u_2^0 \\ u_3^0 \end{pmatrix}_R = \begin{pmatrix} u_R^0 \\ c_R^0 \\ t_R^0 \end{pmatrix} \quad (9.7.10)$$

and similarly for the left-handed parts.

We now wish to diagonalize  $\mathbf{D}$  and  $\mathbf{U}$  in order to find linear combinations of the bare quarks which have definite mass. Since  $\mathbf{D}$  (and  $\mathbf{U}$ ) is an arbitrary matrix it cannot be diagonalized by one single unitary matrix as would be the case for a hermitian matrix. But it is possible to find pairs of unitary matrices  $\mathbf{U}_L^D, \mathbf{U}_R^D$  and  $\mathbf{U}_L^U, \mathbf{U}_R^U$  such that

$$\mathbf{U}_L^D \mathbf{D} \mathbf{U}_R^D = \hat{\mathbf{D}} \quad (9.7.11)$$

$$\mathbf{U}_L^U \mathbf{U} \mathbf{U}_R^U = \hat{\mathbf{U}} \quad (9.7.12)$$

where  $\hat{\mathbf{D}}$  and  $\hat{\mathbf{U}}$  are diagonal matrices with real positive elements.

We now write

$$\frac{v}{\sqrt{2}} \mathbf{U}_L^D \mathbf{D} \mathbf{U}_R^D = \begin{pmatrix} m_d & & \\ & m_s & \\ & & m_b \end{pmatrix} \quad (9.7.13)$$

$$\frac{v}{\sqrt{2}} \mathbf{U}_L^U \mathbf{U} \mathbf{V}_R^U = \begin{pmatrix} m_u & & \\ & m_c & \\ & & m_t \end{pmatrix} \quad (9.7.14)$$

and define new quark fields

$$\begin{aligned} u_L &\equiv \mathbf{U}_L^U u_L^0 & u_R &\equiv \mathbf{U}_R^U u_R^0 \\ d_L &\equiv \mathbf{U}_L^D d_L^0 & d_R &\equiv \mathbf{U}_R^D d_R^0 \end{aligned} \quad (9.7.15)$$

In terms of these fields  $\mathcal{L}_{S-Quarks}$  in (9.7.6) becomes a sum of standard, diagonal, mass-like terms of the form  $m\bar{\psi}\psi$ , one for each quark.

In accord with the assumption of exact universality between leptons and *bare* quarks, the interaction of the bare quarks with the  $W$  boson will be given by terms analogous to (4.2.26), which are, of course, diagonal in flavour. But these terms, when re-expressed in terms of the fields in (9.7.15) become non-diagonal in flavour.

For example the coupling to  $W^+$  involves

$$\begin{aligned} \sum_j \bar{q}_{jL}^0 \tau_+ q_{jL}^0 &= \sum_j \bar{u}_{jL}^0 d_{jL}^0 = \bar{u}_L^0 d_L^0 \\ &= \bar{u}_L \mathbf{U}_L^U \mathbf{U}_L^{D^\dagger} d_L. \end{aligned} \quad (9.7.16)$$

This is precisely of the form (9.3.10) provided we identify  $\mathbf{U}_L^U \mathbf{U}_L^{D^\dagger}$  as the Kobayashi–Maskawa matrix  $\mathbf{V}$  of (9.2.1).

In this approach  $\mathbf{V}$  has appeared as a consequence of transforming to quark fields which have definite mass.

It is easy to check that the diagonal neutral current  $h_3^\mu$  and the electromagnetic current  $h_{em}^\mu$  remain diagonal under (9.7.15).

# 10

## Phenomenology of semi-leptonic reactions

In the leptonic sector, once we are given the values of  $\alpha$ ,  $G$  and  $M_Z$ , there are no free parameters left (at least at Born approximation level) so that the entire phenomenology of leptonic reactions is calculable.

In the hadronic sector, matters are not so clear cut. The coupling strengths  $V_{ij}$  which involve four parameters are introduced at the quark level. Thus we have to find a convincing way to relate information at the quark level to the calculation of hadronic reactions. This step, in principle, involves the strong interactions and is therefore highly non-trivial. From this point of view the least difficult reactions are the semi-leptonic ones and we shall concentrate upon them in this chapter.

Clearly none of the results of the old Cabibbo theory pertaining to the classic low energy weak interactions discussed in Chapter 1 will be altered, so the most interesting information will come from reactions involving the ‘new’ particles and from high energy weak interactions. For this reason we shall not attempt an analysis of  $V_{ij}$  in this chapter. Rather, we shall gather information on the  $V_{ij}$  when discussing the discovery and properties of the new particles in the following chapters, in Chapter 18 and in the study of CP violation in Chapter 19.

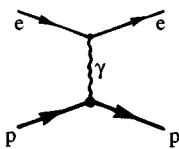
As always with hadrons the strong interactions play a dominant rôle, which is largely not understood. Our weak interaction theory is very precise as far as quarks are concerned, but to translate this into precise statements about hadrons requires a model of the quark content of hadrons and the rôle of the quarks in scattering processes.

One of the most remarkable discoveries of the past few years is the existence of a large cross-section for the ‘inclusive’ reactions

$$\ell_1 + p \rightarrow \ell_2 + X,$$

where  $\ell_{1,2}$  are leptons and  $X$  implies a summation over everything else that emerges from the reaction. The cross-section remains big even when

the momentum transfer  $q$  and the energy transfer  $\nu$  from  $p$  to  $X$  are large. Indeed the inclusive cross-sections are found to be essentially independent of  $q^2$  (aside from some naturally occurring kinematic factors) and this is in marked contrast, for example, to the ‘exclusive’ reaction  $e + p \rightarrow e + p$ , where the number of events with large momentum transfer drops rapidly as  $q^2$  increases; much faster than one would expect from the  $1/q^2$  behaviour of the photon exchange in the amplitude shown.



The leptons bouncing back so often with large momentum transfer in the inclusive reaction are reminiscent of Rutherford’s  $\alpha$ -particles scattering through large angles in inelastic  $\alpha$ -atom collisions, and suggest a similar interpretation. Just as the atom is showing the existence of a hard, tiny core—the nucleus—here the proton is perhaps showing the existence of some tiny granular inner structure—‘partons’—with which the photon is interacting in a point-like manner.

There is an elaborate and beautiful picture built upon this idea, the quark-parton model, which we shall investigate in detail in Chapters 15–17. In the framework of this model very precise and detailed tests of the standard model can be made, and we shall be content, at this point, to note that all aspects of the SM theory are consistent with experiments of the inclusive type up to the present.

Here we should like to see what tests can be made that are relatively independent of a specific hadron model.

We discuss the evidence for the existence of neutral current reactions and show that rates for neutral current, charged current and electromagnetic reactions are related to each other in a way that is perfectly compatible with the theory. We also examine the remarkable and beautiful new parity-violating effects that arise from the interference between  $\gamma$  and  $Z^0$  exchange, namely the asymmetry in the scattering of longitudinally polarized electrons on unpolarized nuclear targets, and the rotation of the plane of polarization of linearly polarized light passing through the vapour of a substance with large atomic number.

We shall return to the question of the Kobayashi–Maskawa matrix in Chapter 18. We shall also discuss the intriguing question as to whether the SM can provide an explanation of CP violating phenomena in Chapter 19.

### 10.1 Model independent tests

We shall examine the following questions:

1. What is the evidence for the existence of neutral current events involving hadrons?
2. Is this evidence consistent with the structure implied by (9.3.1), in particular its relationship to charged current events?

Let us examine these questions in more detail.

1. In the first place the very existence of neutral current (NC) events involving hadrons is highly significant. All of the reactions  $\nu_\mu p \rightarrow \nu_\mu p$ ,  $\bar{\nu}_\mu p \rightarrow \bar{\nu}_\mu p$ ,  $\nu_\mu p \rightarrow \nu_\mu X$ ,  $\bar{\nu}_\mu p \rightarrow \bar{\nu}_\mu X$  have been seen to occur with rates comparable with the analogous charged current (CC) reactions  $\nu_\mu n \rightarrow \mu^- p$ ,  $\bar{\nu}_\mu p \rightarrow \mu^+ n$ ,  $\nu_\mu p \rightarrow \mu^- X$ ,  $\bar{\nu}_\mu p \rightarrow \mu^+ X$ . The reason why muon rather than electron neutrinos are used was explained in Section 5.1.2.

A recent measurement (Ahrens *et al.*, 1987) gives for the ‘elastic’ events,

$$\left. \begin{aligned} \frac{\sigma(\nu_\mu + p \rightarrow \nu_\mu + p)}{\sigma(\nu_\mu + n \rightarrow \mu^- + p)} &= 0.153 \pm 0.018 \\ \frac{\sigma(\bar{\nu}_\mu + p \rightarrow \bar{\nu}_\mu + p)}{\sigma(\bar{\nu}_\mu + p \rightarrow \mu^+ + n)} &= 0.218 \pm 0.025. \end{aligned} \right\} \quad (10.1.1)$$

For the inclusive reactions, the targets have mostly been heavy nuclei with roughly equal numbers of protons and neutrons, and they are usually interpreted as being ‘isoscalar’ targets which we shall label collectively as  $N_0$ . The ratios

$$R_\nu \equiv \frac{\sigma(\nu_\mu + N_0 \rightarrow \nu_\mu + X)}{\sigma(\nu_\mu + N_0 \rightarrow \mu^- + X)} \quad (10.1.2)$$

and

$$R_{\bar{\nu}} \equiv \frac{\sigma(\bar{\nu}_\mu + N_0 \rightarrow \bar{\nu}_\mu + X)}{\sigma(\bar{\nu}_\mu + N_0 \rightarrow \mu^+ + X)} \quad (10.1.3)$$

have been measured by several groups over a wide range of neutrino energies, from a few GeV up to a few hundred GeV. The results are consistent with each other and with  $R_\nu$ ,  $R_{\bar{\nu}}$  being essentially independent of energy. The most recent determinations (Allaby *et al.*, 1987; Blondel *et al.*, 1989) yield (we have taken a simple average)

$$\left. \begin{aligned} R_\nu &= 0.307 \pm 0.003 \\ R_{\bar{\nu}} &= 0.390 \pm 0.016. \end{aligned} \right\} \quad (10.1.4)$$

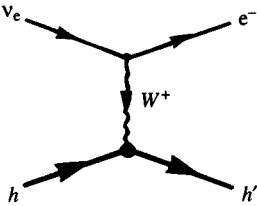
NC events are thus unquestionably comparable with CC ones.

2. Let us consider first the general structure in a gauge vector boson theory for a reaction of the type

$$\nu_e h \rightarrow e^- h',$$

where  $h$  is any hadron and  $h'$  any hadron or group of hadrons.

The amplitudes will be given by diagrams of the type



and will have the form

$$\frac{e}{2\sqrt{2} \sin \theta_W} \bar{u}(e) \gamma_\mu (1 - \gamma_5) u(\nu) \frac{1}{M_W^2 - q^2} \langle h' | h_+^\mu | h \rangle, \quad (10.1.5)$$

where  $q = p(\nu) - p(e^-)$  is the four-momentum transfer and  $h_+^\mu$  is the weak charged current of the hadrons.

The differential cross-section will depend on various factors that can be exactly calculated, and a hadronic term  $W^{\mu\nu}$  of the form

$$\begin{aligned} W_+^{\mu\nu} &\sim \langle h' | h_+^\mu | h \rangle^* \langle h' | h_+^\nu | h \rangle \\ &= \langle h | h_-^\mu | h' \rangle \langle h' | h_+^\nu | h \rangle. \end{aligned} \quad (10.1.6)$$

In (10.1.6) the spin or spins of  $h'$  are summed over and the spin of  $h$  is averaged. For an exclusive reaction  $h'$  will be one or a definite set of hadrons. For inclusive reactions we would sum over all possible hadrons making up  $h'$ .

Certain limited tests can be made without any model of the strong interactions (Paschos and Wolfenstein, 1973). What is tested is the relationship between cross-sections that depend on the electromagnetic current  $h_{\text{em}}^\mu$ , the charged current  $h_+^\mu$ , and neutral current  $h_Z^\mu$  which is coupled to the  $Z^0$ :

$$h_Z^\mu = h_3^\mu - 2 \sin^2 \theta_W h_{\text{em}}^\mu. \quad (10.1.7)$$

If we work at energies low enough so that there is effectively no production of charm particles, and if we take  $\cos \theta_C \approx 1$ , then we have  $h_+^\mu \approx h_1^\mu + i h_2^\mu$ , where the  $h_j^\mu (j = 1, 2, 3)$  are the components of an isotriplet of currents. Using (1.3.12) we deduce that

$$[h_3^\mu, T_+] = h_+^\mu, \quad [T_+, h_-^\nu] = 2h_3^\nu, \quad (10.1.8)$$

where  $T_+$  is the isospin raising operator.

To simplify the argument let us suppress the  $\mu, \nu$  indices. Let us average over the cross-sections for a given lepton projectile colliding with all

possible isospin states of the target  $h$ , i.e. if  $h$  has isospin  $I$  one uses as targets  $|h; I_3 = I\rangle, |h; I_3 = I - 1\rangle, \dots, |h; I_3 = -I\rangle$ . This is equivalent to replacing  $h$  by an isospin zero target. Let us further sum the cross-section over all possible values of  $I_3$  in the set of final hadrons  $h'$  (this is automatic for an inclusive reaction). This is equivalent to having an isospin zero final state.

Let us denote by  $\langle W_+ \rangle$  the result of this summation and averaging. For example for the inclusive reaction  $\nu p \rightarrow e^- X$  we have

$$\langle W_+ \rangle \sim \frac{1}{2} \sum_X \{ \langle p | h_- | X \rangle \langle X | h_+ | p \rangle + \langle n | h_- | X \rangle \langle X | h_+ | n \rangle \} \quad (10.1.9)$$

or, in general,

$$\langle W_+ \rangle \sim \frac{1}{2I+1} \sum_{I_3 I'_3} \langle h; I_3 | h_- | h'; I'_3 \rangle \langle h'; I'_3 | h_+ | h; I_3 \rangle. \quad (10.1.10)$$

The sums

$$\sum_{I_3} |h; I_3\rangle \langle h; I_3|, \quad \sum_{I'_3} |h'; I'_3\rangle \langle h'; I'_3|$$

are isoscalars and therefore commute with the generators of isotopic rotations.

Using (10.1.8) one then deduces that

$$\langle W_+ \rangle = 2\langle W_3 \rangle, \quad (10.1.11)$$

where

$$W_3 \sim \langle h' | h_3 | h \rangle^* \langle h' | h_3 | h \rangle. \quad (10.1.12)$$

Using (10.1.7) and (10.1.11) we have

$$\begin{aligned} \langle W_Z \rangle &= 4 \sin^2 \theta_W \langle W_{em} \rangle + \frac{1}{2} \langle W_+ \rangle - \\ &\quad - 2 \sin^2 \theta_W \left\{ \sum \langle h' | h_{em} | h \rangle^* \langle h' | h_3 | h \rangle + \right. \\ &\quad \left. + \sum \langle h' | h_3 | h \rangle^* \langle h' | h_{em} | h \rangle \right\}. \end{aligned} \quad (10.1.13)$$

The last term,  $\{\}$ , can be bounded by the Schwartz inequality, and using (10.1.11) we get

$$|\{\}|^2 \leq \langle W_{em} \rangle \langle W_+ \rangle. \quad (10.1.14)$$

We denote by  $\langle d\sigma \rangle$  the differential cross-section for CC, NC or em reactions into some specified kinematic range of final states, suitably averaged and summed over isospin as described above. Then putting in all the

factors, (10.1.5), (10.1.13) and (10.1.14) lead to

$$\begin{aligned} \frac{1}{2} \left\{ 1 - \sin^2 \theta_W \frac{GQ^2}{\pi\alpha} \sqrt{\frac{\langle d\sigma_{em} \rangle}{\langle d\sigma_{CC} \rangle}} \right\}^2 &\leq \frac{\langle d\sigma_{NC} \rangle}{\langle d\sigma_{CC} \rangle} \\ &\leq \frac{1}{2} \left\{ 1 + \sin^2 \theta_W \frac{GQ^2}{\pi\alpha} \sqrt{\frac{\langle d\sigma_{em} \rangle}{\langle d\sigma_{CC} \rangle}} \right\}^2, \end{aligned} \quad (10.1.15)$$

where all cross-sections have to be taken over the same kinematic range and  $Q^2 = -q^2$ .

If (10.1.15) is used for the *total* cross-sections then, experimentally, the coefficient of  $\sin^2 \theta_W$  is largely independent of energy, and its value is  $\sim 1.2$ . Thus we have

$$\frac{1}{2}(1 - 1.2 \sin^2 \theta_W)^2 \leq \frac{\langle \sigma_{NC} \rangle}{\langle \sigma_{CC} \rangle} \leq \frac{1}{2}(1 + 1.2 \sin^2 \theta_W)^2. \quad (10.1.16)$$

The value  $R_\nu = 0.307$  thus implies

$$\sin^2 \theta_W \geq 0.2, \quad (10.1.17)$$

which is perfectly compatible with the value deduced from the leptonic sector (see Fig. 5.6).

A more striking result can be achieved, if, for the type of isospin averaged data just discussed, one has also data for the antineutrino cross-sections. At the *leptonic* vertex, going from a  $\nu$  reaction to a  $\bar{\nu}$  one has the effect of changing  $\gamma_5$  to  $-\gamma_5$  as explained in Section 1.3. At the hadronic vertex  $h_+ \rightarrow h_-$  and vice versa. But with our isotopically neutral initial and final states we can make a rotation of  $\pi/2$  about the ‘1’ axis in isospace without affecting the states, and thereby change  $h_-$  back to  $h_+$ , provided we are in a situation where it is a good approximation to take  $h_\pm \sim h_1 \pm i h_2$ . So the *hadronic* expression in the  $\bar{\nu}$  cross-section is the same as it was in the  $\nu$  reaction.

We must now consider the vector ( $V$ ) and axial-vector ( $A$ ) aspects of the currents. If we write for the leptonic current

$$l = V_l + A_l \quad (10.1.18)$$

then, schematically, in the cross-section there will be terms like  $V_l^2 + A_l^2 + (V_l A_l + A_l V_l)$  for  $\nu$  reactions and, by the above,  $V_l^2 + A_l^2 - (V_l A_l + A_l V_l)$  for  $\bar{\nu}$  reactions.

For the hadron current we write

$$h = V + A \quad (10.1.19)$$

and the hadron vertex in both  $\nu$  and  $\bar{\nu}$  reactions will contribute terms like

$$V^2 + A^2 + (VA + AV).$$

Since we are considering spin-averaged cross-sections, the answer must be scalar, so the leptonic term  $\pm(V_l^\mu A_l^\nu + A_l^\mu V_l^\nu)$ , an axial tensor, can only be coupled to the analogous hadronic term  $(V^\mu A^\nu + A^\mu V^\nu)$ .

Therefore, when we form the difference  $\langle d\sigma^\nu \rangle - \langle d\sigma^{\bar{\nu}} \rangle$ , it can only depend on the form  $(VA + AV)$  from the hadronic vertex.

Consider now the structure of this cross-section difference for NC reactions. Putting  $h_Z = V_Z + A_Z$ , (10.1.7) yields

$$\left. \begin{aligned} V_Z &= (1 - 2 \sin^2 \theta_W) V_3 - 2 \sin^2 \theta_W V_{SC}, \\ A_Z &= A_3, \end{aligned} \right\} \quad (10.1.20)$$

where  $V_{SC}$  is the isoscalar part of  $h_{em}$ . When we look at the terms  $(V_Z A_Z + A_Z V_Z)$  using (10.1.20) there will be cross-terms  $V_{SC} A_3$  and  $A_3 V_{SC}$  which must vanish since there is no way to construct an answer that is an isovector with our isotopically neutral initial and final states.

Schematically, we are left with

$$\begin{aligned} V_Z A_Z + A_Z V_Z &= (1 - 2 \sin^2 \theta_W)(V_3 A_3 + A_3 V_3) \\ &= \frac{1}{2}(1 - 2 \sin^2 \theta_W)(V_+ A_+ + A_+ V_+) \end{aligned} \quad (10.1.21)$$

by (10.1.11). We have achieved a relation between the NC and CC reactions. When all details are taken care of one finds the remarkable result (Paschos and Wolfenstein, 1973), independent of any model of the hadrons,

$$\frac{\langle d\sigma_{NC}^\nu \rangle - \langle d\sigma_{NC}^{\bar{\nu}} \rangle}{\langle d\sigma_{CC}^\nu \rangle - \langle d\sigma_{CC}^{\bar{\nu}} \rangle} = \frac{1}{2}(1 - 2 \sin^2 \theta_W). \quad (10.1.22)$$

Let us utilize (10.1.22) for total cross-sections. Defining

$$r \equiv \frac{\langle \sigma_{CC}^{\bar{\nu}} \rangle}{\langle \sigma_{CC}^\nu \rangle} \quad (10.1.23)$$

and using the notation (10.1.2), (10.1.3) gives

$$\frac{R_\nu - r R_{\bar{\nu}}}{1 - r} = \frac{1}{2}(1 - 2 \sin^2 \theta_W). \quad (10.1.24)$$

In utilizing (10.1.24) care must be taken to remember that its derivation assumed no charm particle production, an assumption only reasonable at moderately low energies. We thus use the weighted values of  $R_\nu$  and  $R_{\bar{\nu}}$  and the weighted mean of several measurements of  $r$  given by Winter (1978)

$$R_\nu = 0.29 \pm 0.01 \quad r = 0.48 \pm 0.01 \quad R_{\bar{\nu}} = 0.35 \pm 0.025 \quad (10.1.25)$$

rather than the later high energy values, and find

$$\sin^2 \theta_W = 0.231 \pm 0.035 \quad \left( \begin{array}{l} \text{NC and CC} \\ \nu \text{ and } \bar{\nu} \text{ total} \\ \text{cross-sections} \end{array} \right) \quad (10.1.26)$$

There is a great deal of new data at higher energies which requires a more detailed theoretical analysis. We shall deal with this in Section 17.2.

Thus the model independent results on semi-leptonic reactions seem to be consistent with the SM expectations. It will be interesting to see in later sections how the model stands up to more detailed experimental studies.

We end this section with some comments about the energy and momentum transfer dependence expected for the cross-sections.

In a picture in which the weak interactions are mediated by the exchange of vector bosons we expect to see a characteristic  $q^2$  dependence coming from the boson propagator. [For leptonic reactions we have already seen an explicit example of this, viz. (5.1.15).] Such behaviour ought soon to be seen as available  $q^2$  values increase.

In the parton model, where the interaction is with *point-like* objects inside the hadron one finds an energy dependence analogous to that of purely leptonic scattering [see, for example, (5.1.27)].

In particular one finds the total cross-sections

$$\sigma_{\text{CC}}^\nu(E), \sigma_{\text{CC}}^{\bar{\nu}}(E), \sigma_{\text{NC}}^\nu(E) \text{ and } \sigma_{\text{NC}}^{\bar{\nu}}(E)$$

all proportional to  $E$  ( $E = \text{lab. energy of lepton}$ ) for  $m_p \ll E \ll M_W$  or  $M_Z$ . Thus the ratios  $R_\nu, R_{\bar{\nu}}$  and  $r$  should be essentially independent of energy.

Neutrino and antineutrino CC total cross-sections divided by  $E$  are shown in Fig. 10.1 taken from the Particle Data Group (1992). The proportionality to  $E$  is convincingly demonstrated.

## 10.2 Parity violation in electron–nucleus scattering

Just as  $Z$  exchange interfered with photon exchange in  $e^+e^- \rightarrow \mu^+\mu^-$ , so in the scattering of electrons from nuclei both  $Z$  and photon exchange will contribute, and will interfere with each other. For momentum transfers  $q^2 \ll M_Z^2$  the  $Z^0$  exchange is much weaker than the usual em term so the best possibility is to look for effects which would be totally absent if there were no  $Z^0$ . The most dramatic possibility is to look for parity-violating effects. Just as a non-zero longitudinal polarization of the muon in  $e^+e^- \rightarrow \mu^+\mu^-$  signals parity violation, so too does any difference between the cross-sections  $d\sigma_L$  and  $d\sigma_R$  for  $e^-A \rightarrow e^-A'$  starting

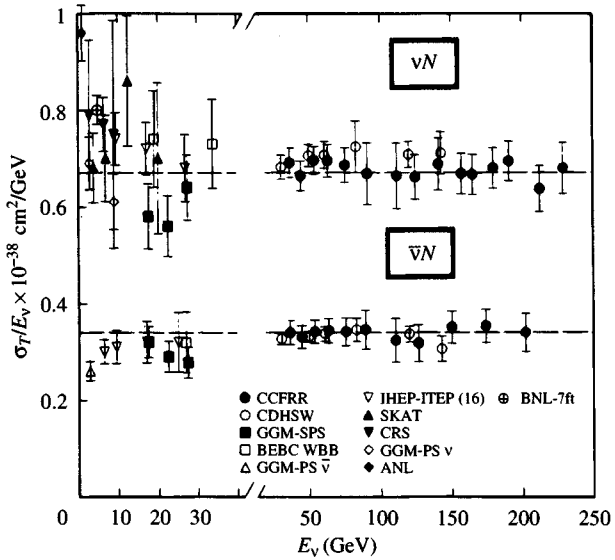


Fig. 10.1.  $\sigma_T/E_\nu$  for the muon neutrino and antineutrino charged-current total cross-section as a function of neutrino energy.

with left-handed or right-handed electrons, i.e. electrons longitudinally polarized opposite to or along their motion. The target  $A$  is unpolarized and no final spins are detected.

Let us try to estimate the sort of effects expected. We consider

$$e^- N_0 \rightarrow e^- X,$$

where  $N_0$  is an isoscalar target, at fairly high energies ( $E \gg m_p$ ) and moderately large momentum transfers ( $|q^2| > 1 \text{ GeV}^2/c$ ). In this regime of ‘deep inelastic scattering’ one assumes elastic scattering between the electron and partons in the target and one sums *incoherently* over the various type of partons and their possible momenta. The exact result depends upon details of the parton model (Cahn and Gilman, 1978). Here we make the simplifying assumptions that only  $u$  and  $d$  quark-partons exist in the target, and because it is isoscalar, the probabilities for finding  $u$  or  $d$  will be the same.

The scattering on a quark of type  $j$

$$e^- + q_j \rightarrow e^- + q_j$$

is analogous to  $\nu e \rightarrow \nu e$  discussed in Section 5.1.

The photon and  $Z_0$  exchange amplitudes are of the form [see (5.1.13)]

and (5.1.14)]

$$-iQ_j e^2 (\bar{u}_e \gamma^\mu u_e) \frac{1}{q^2} (\bar{u}_j \gamma_\mu u_j) \quad (10.2.1)$$

and

$$ie^2 [\bar{u}_e \gamma^\mu (v_e - a_e \gamma_5) u_e] \frac{1}{q^2 - M_Z^2} [\bar{u}_j \gamma_\mu (v_j - a_j \gamma_5) u_j] \quad (10.2.2)$$

where  $Q_j$  is the quark charge in units of  $e$ .

Breaking these up into transitions involving left-handed or right-handed particles, using the  $\theta$  dependence discussed in Section 8.5, and keeping only the dominant terms for  $q^2 \ll M_Z^2$ , one gets [with  $C \equiv (2 \sin \theta_W \cos \theta_W M_Z^2)^{-1}$ ]

$$\left. \begin{aligned} d\sigma_{LL \leftarrow LL}^j &\propto \left[ -\frac{Q_j}{q^2} + C(v_e + a_e)(2 \sin^2 \theta_W Q_j - 2I_3^{jL}) \right]^2, \\ d\sigma_{RL \leftarrow RL}^j &\propto \left[ -\frac{Q_j}{q^2} + C(v_e + a_e)2 \sin^2 \theta_W Q_j \right]^2 (1-y)^2, \\ d\sigma_{RR \leftarrow RR}^j &\propto \left[ -\frac{Q_j}{q^2} + C(v_e - a_e)2 \sin^2 \theta_W Q_j \right]^2, \\ d\sigma_{LR \leftarrow LR}^j &\propto \left[ -\frac{Q_j}{q^2} + C(v_e - a_e)(2 \sin^2 \theta_W Q_j - 2I_3^{jL}) \right]^2 (1-y)^2, \end{aligned} \right\} \quad (10.2.3)$$

where, analogously to (5.1.23)

$$y = \left( \frac{E_e - E'_e}{E_e} \right)_{LAB} \simeq \frac{1}{2}(1 - \cos \theta)_{CM}. \quad (10.2.4)$$

With

$$\left. \begin{aligned} d\sigma_L^j &\equiv d\sigma_{LL \leftarrow LL}^j + d\sigma_{RL \leftarrow RL}^j, \\ d\sigma_R^j &\equiv d\sigma_{RR \leftarrow RR}^j + d\sigma_{LR \leftarrow LR}^j, \end{aligned} \right\} \quad (10.2.5)$$

the experimental asymmetry is

$$A_0 \equiv \frac{d\sigma_R - d\sigma_L}{d\sigma_R + d\sigma_L} = \frac{\sum_j (d\sigma_R^j - d\sigma_L^j)}{\sum_j (d\sigma_R^j + d\sigma_L^j)}. \quad (10.2.6)$$

In the last step the probability functions for finding quark  $j$ , being independent of  $j$  for an isoscalar target, have cancelled out.

In the denominator we can ignore the  $Z^0$  contribution completely. In the numerator we keep just the dominant  $\gamma - Z^0$  interference terms and

find

$$A_0 = -\frac{1}{2 \sin \theta_W \cos \theta_W} \left( \frac{q^2}{M_Z^2} \right) \times \frac{\sum_j Q_j \left\{ v_e I_3^{jL} [1 - (1-y)^2] - a_e (4 \sin^2 \theta_W Q_j - I_3^{jL}) [1 + (1-y)^2] \right\}}{[1 + (1-y)^2] \sum_j Q_j^2} \quad (10.2.7)$$

Taking

$$j = u, d; \quad Q_u = \frac{2}{3}, Q_d = -\frac{1}{3}, I_3^{uL} = \frac{1}{2}; \quad I_3^{dL} = -\frac{1}{2};$$

$$v_e = \frac{2 \sin^2 \theta_W - 1/2}{2 \sin \theta_W \cos \theta_W}; \quad a_e = -\frac{1/2}{2 \sin \theta_W \cos \theta_W}$$

yields

$$\begin{aligned} A_0 &= -\left(\frac{1}{2 \sin \theta_W \cos \theta_W}\right)^2 \left(\frac{Q^2}{M_Z^2}\right) \frac{9}{10} \left[ \left(1 - \frac{20}{9} \sin^2 \theta_W\right) \right. \\ &\quad \left. + (1 - 4 \sin^2 \theta_W) \frac{1 - (1-y)^2}{1 + (1-y)^2} \right], \end{aligned} \quad (10.2.8)$$

where  $Q^2 = -q^2 > 0$ . Note that  $A_0$  does not depend explicitly on beam energy.

For  $Q^2 \approx 1(\text{GeV}/c)^2$  we see that the asymmetry is tiny!

$$|A_0| \sim 9 \times 10^{-5}. \quad (10.2.9)$$

An experiment of extraordinary delicacy has been carried out at SLAC (Prescott *et al.*, 1978). The polarized electrons are produced by optical pumping of a gallium arsenide crystal using circularly polarized photons, and a mean electron polarization of 0.37 is obtained. The measured asymmetry is

$$A_{\text{expt}} = P_e A_0 \quad (10.2.10)$$

where  $P_e$  is the beam polarization, taken as positive for right-handed electrons. Many checks were carried out to avoid systematic errors, including the following:

1. The variation of  $A_{\text{expt}}$  as the beam polarization is varied from positive through zero to negative values.
2. The variation of  $A_{\text{expt}}$  as the beam energy is altered.  $A_0$  itself does not vary with energy, but since the beam is bent magnetically in the apparatus the spin precesses between source and target as a result of the anomalous magnetic moment of the electron [for a discussion of

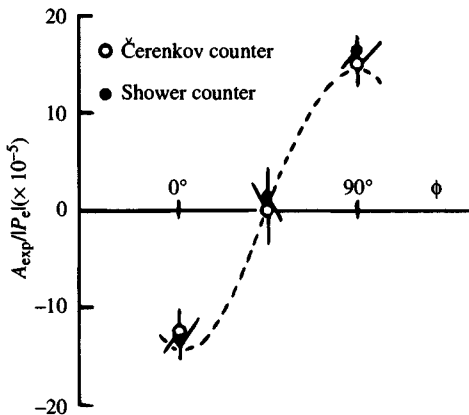
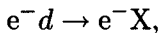


Fig. 10.2. The experimental asymmetry shows the expected variation (dashed line) as the beam polarization changes. The polarization is written as  $P_e = |P_e| \cos 2\phi$ , where  $\phi$  is an angle giving the orientation of the prism that polarizes the light. (From Prescott *et al.*, 1978.)

spin precession see, for example, Berestetskii, Lifshitz and Pitaevskii (1971)], and the precession angle varies with energy. So, varying  $E$  has the effect of varying the beam polarization at the target without altering it at the source, and causes  $A_{\text{exp}}$  to change.

The results of these studies (shown in Figs. 10.2 and 10.3) suggest that the experiment is capable of detecting an asymmetry of order  $10^{-5}$ .

The reaction is



with  $E \sim 20$  GeV,  $Q^2 \sim 1.6$   $(\text{GeV}/c)^2$ ,  $y \sim 0.2$ , and the result is

$$\frac{A_0}{Q^2} = (-9.5 \pm 1.6) \times 10^{-5} (\text{GeV}/c)^{-2}. \quad (10.2.11)$$

Thus the existence of a parity-violating component interfering with the em interaction is confirmed! The  $y$ -dependence in (10.2.8) for the range  $0.15 \leq y \leq 0.38$  has been studied and is compatible with the SM result with  $\sin^2 \theta_W = 0.224 \pm 0.020$ —a further success for the theory.

### 10.3 Optical rotation

Another remarkable result of the interference between weak and em interactions is that the refractive index of a substance can be different for right and left circularly polarized light, even when the material is in a non-crystalline form. We shall consider the passage of a plane polarized

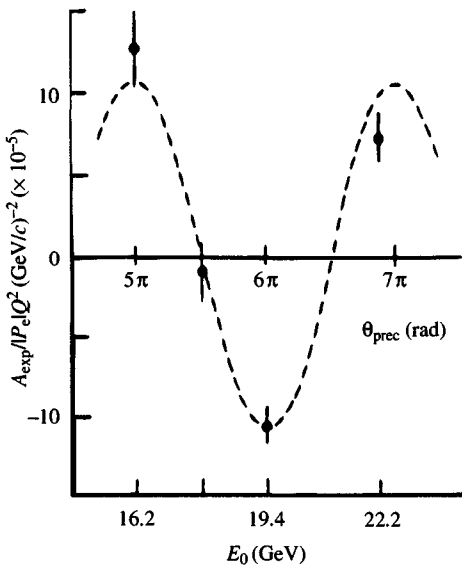


Fig. 10.3. The experimental asymmetry shows the expected variation (dashed line) as the beam polarization changes as a function of beam energy owing to the  $g - 2$  precession in the beam transport system. (From Prescott *et al.*, 1978.)

beam of light moving in the positive  $Z$  direction through the vapour of a substance with large atomic number. The electric field of the incoming beam, say polarized along  $OX$ , can be written as a superposition of right and left circularly polarized electric fields

$$\mathbf{E}_x = \frac{1}{\sqrt{2}}(\mathbf{E}_R - \mathbf{E}_L). \quad (10.3.1)$$

If  $n_R, n_L$  are the refractive indices (complex if there is absorption) for right and left circularly polarized light of angular frequency  $\omega$  then at a point  $z$  inside the vapour

$$\left. \begin{aligned} \mathbf{E}_R &= E_0 \epsilon_R e^{i\omega[t-(n_R/c)z]}, \\ \mathbf{E}_L &= E_0 \epsilon_L e^{i\omega[t-(n_L/c)z]}, \end{aligned} \right\} \quad (10.3.2)$$

where  $E_0$  is a constant and  $\epsilon_{R,L}$  are the vectors

$$\epsilon_R = \frac{1}{\sqrt{2}}(\hat{i} - i\hat{j}), \quad \epsilon_L = -\frac{1}{\sqrt{2}}(\hat{i} + i\hat{j}), \quad (10.3.3)$$

$\hat{i}$  and  $\hat{j}$  being unit vectors along  $OX$  and  $OY$ .

It is easy then to see that the resultant electric field at  $z$  is plane

polarized along a direction making angle  $\phi(z)$  with the  $X$ -axis, with

$$\phi(z) = \frac{\omega}{2c} \operatorname{Re}(n_L - n_R)z.$$

Clearly then, if any plane polarized light beam traverses a length  $l$  of the vapour its plane of polarization will be rotated by

$$\phi(l) = \frac{\omega}{2c} \operatorname{Re}(n_L - n_R)l. \quad (10.3.4)$$

Note that since under a space reflection  $R \leftrightarrow L$  the fact that  $n_R \neq n_L$  can only arise from the parity-violating parts of the Hamiltonian. Our task is to relate  $n_R, n_L$  to the weak interaction Hamiltonian.

Firstly we recall the famous relation [see, for example, Goldberger and Watson (1964)] between index of refraction and forward scattering amplitude  $f$  for a dilute material:

$$n = 1 + \frac{2\pi\rho f}{k^2}, \quad (10.3.5)$$

where  $\rho$  is the number density of scatterers and  $k$  is the momentum.

We will have two scattering amplitudes,  $f_R$  and  $f_L$  for the scattering of right and left circularly polarized light from the atoms of the vapour.

Let us suppose that the frequency of the light used is close to the frequency of a transition from some state  $|\alpha\rangle$  of the atom to a higher state  $|\beta\rangle$  whose width is  $\Gamma$ . The scattering of the light can then be thought of as a process of absorption and re-emission of a photon, so that for light with polarization vector  $\epsilon$ , and momentum  $\mathbf{k}$ , the effective scattering amplitude is

$$f(\epsilon) \propto \frac{1}{2J_\alpha + 1} \sum_{m_\alpha, m_\beta} \frac{\langle \mathbf{k}, \epsilon; \alpha m_\alpha | H'_{\text{em}} | \beta m_\beta \rangle \langle \beta m_\beta | H'_{\text{em}} | \mathbf{k}, \epsilon; \alpha m_\alpha \rangle}{k + E_\alpha - E_\beta + \frac{1}{2}i\Gamma} \quad (10.3.6)$$

the sums being over magnetic substates. Here

$$H'_{\text{em}} = -e \int d^3x J_{\text{em}}^\mu A_\mu \quad (10.3.7)$$

is the em interaction responsible for the photon absorption and emission.

It can be shown (Sakurai, 1967) that in the non-relativistic regime

$$\langle \beta | H'_{\text{em}} | \mathbf{k}, \epsilon; \alpha \rangle \propto -\frac{e}{m} \sum_j \langle \psi_\beta | e^{i\mathbf{k} \cdot \mathbf{x}} \{ \epsilon \cdot \hat{\mathbf{p}}_j + \frac{1}{2}i(\mathbf{k} \times \epsilon) \cdot \boldsymbol{\sigma}_j \} | \psi_\alpha \rangle, \quad (10.3.8)$$

where the summation is over the electrons in the atom and  $\hat{\mathbf{p}}_j$  is the momentum operator for the  $j$ th electron and  $\frac{1}{2}\boldsymbol{\sigma}_j$  its spin operator.  $|\psi_{\alpha,\beta}\rangle$  are the ordinary non-relativistic quantum mechanical state vectors for the atom.

If the wavelength  $\lambda$  of the light is very much greater than the size  $r_A$  of the atom then, since  $k = 1/\lambda$ , the exponential in (10.3.8) can be expanded

and by far the largest contribution comes from the electric dipole (E1) amplitude\*

$$\epsilon \cdot \langle \beta | \hat{\mathbf{p}}_j | \alpha \rangle \quad (10.3.9)$$

provided it does not vanish because of the symmetry of the states  $\alpha, \beta$ .

Normally the states  $a, \beta$  are eigenstates of parity and the E1 transition is allowed provided

$$\left. \begin{aligned} |J_\beta - J_\alpha| &= 0 \text{ or } 1 \text{ (not } 0 \rightarrow 0), \\ P_\beta &= -P_\alpha. \end{aligned} \right\} \quad (10.3.10)$$

The second term in (10.3.8), when  $e^{i\mathbf{k}\cdot\mathbf{x}}$  is replaced by unity, is an example of a magnetic dipole (M1) amplitude. It is allowed provided

$$\left. \begin{aligned} |J_\beta - J_\alpha| &\leq 1 \text{ (not } 0 \rightarrow 0), \\ P_\beta &= P_\alpha. \end{aligned} \right\} \quad (10.3.11)$$

If however  $Z^0$  exchange as well as  $\gamma$  exchange (in this case mainly the Coulomb force) provides the interaction we must expect the eigenstates to be not entirely of one parity. Since  $Z^0$  is so heavy it provides an interaction between electrons and nucleus that is of extremely short range, essentially a  $\delta$ -function potential. The parity-violating (PV) part is, from (5.1.3), (5.1.4) and (9.3.1)

$$\begin{aligned} H_{\text{PV}} = -\frac{G}{\sqrt{2}} &\left[ (4 \sin^2 \theta_W - 1)(\bar{e} \gamma^\mu e)(\bar{N} \gamma_\mu \gamma_5 \frac{1}{2} \tau_3 N) + (\bar{e} \gamma^\mu \gamma_5 e) \right. \\ &\times \left. \left( \bar{N} \gamma_\mu \frac{2 \sin^2 \theta_W + (2 \sin^2 \theta_W - 1) \tau_3}{2} N \right) \right]. \end{aligned} \quad (10.3.12)$$

Note that we have introduced nucleon field operators  $N$  instead of quark operators to express simply the nucleon contribution to  $h_Z^\mu$ . The first term in (10.3.12) is negligible since the nuclear matrix element will be proportional to the nuclear spin and therefore small, whereas the second term, which non-relativistically is dominated by the  $\gamma_0$  component, gives rise to a coherent nuclear contribution, with matrix element proportional to

$$\begin{aligned} Q_W &\equiv -[2 \sin^2 \theta_W (N + Z) + (2 \sin^2 \theta_W - 1)(Z - N)] \\ &= -[(4 \sin^2 \theta_W - 1)Z + N], \end{aligned} \quad (10.3.13)$$

where  $N$  and  $Z$  are the number of neutrons and protons in the nucleus.

\* By the uncertainty relation we expect  $|\mathbf{p}_j| \sim h/r_A$  and thus the spin term should be of order  $r_A/\lambda$  relative to it.

<sup>†</sup> If the  $N$  are considered as free field operators then we should include a factor  $G_A = 1.24$  in the axial-vector nucleon term.

If we assume a point nucleus, the main extra, parity-violating potential with which each electron interacts is then

$$V_{\text{PV}} = \frac{G}{\sqrt{2}} \frac{Q_W}{4m_e} [\boldsymbol{\sigma} \cdot \hat{\mathbf{p}} \delta^3(\mathbf{r}) + \delta^3(\mathbf{r}) \boldsymbol{\sigma} \cdot \hat{\mathbf{p}}], \quad (10.3.14)$$

where a symmetrized form of the non-relativistic limit of  $\gamma^\mu \gamma_5$  has been used and  $\delta^3(\mathbf{r}) = (1/4\pi r^2)\delta(r)$ .

Because this potential is so weak we may use perturbation theory to calculate the new atomic states

$$|\alpha'\rangle = |\alpha\rangle + \sum_{n_\alpha} \frac{\langle n_\alpha | V_{\text{PV}} | \alpha \rangle | n_\alpha \rangle}{E_\alpha - E_{n_\alpha}}, \quad (10.3.15)$$

where the  $|n_\alpha\rangle$  that occur in (10.3.15) have opposite parity to  $|\alpha\rangle$  but the same  $J$  value since  $V_{\text{PV}}$  is a pseudo-scalar. Usually the sum is dominated by one level. Let us call it  $|\bar{\alpha}\rangle$ . We write (10.3.15) as

$$|\alpha'\rangle = |\alpha\rangle + \eta_\alpha |\bar{\alpha}\rangle, \quad (10.3.16)$$

where  $|\bar{\alpha}\rangle$  has opposite parity to  $|\alpha\rangle$  and  $|\eta_\alpha| \ll 1$ , and similarly for  $|\beta'\rangle$ .

If now an E1 transition between  $|\alpha\rangle$  and  $|\beta\rangle$  is allowed, it will totally dominate the transition  $|\alpha'\rangle \rightarrow |\beta'\rangle$  since transitions like  $|\alpha\rangle \rightarrow |\bar{\beta}\rangle$  or  $|\bar{\alpha}\rangle \rightarrow |\beta\rangle$  will be magnetic dipole and thus down by a factor of order

$$\left( \frac{r_A}{\lambda} \right) \left( \frac{V_{\text{PV}}}{\Delta E} \right),$$

where  $\Delta E$  is a typical level spacing in the unperturbed atom. So there would be no hope of detecting the effects of the parity-violating term.

We must therefore look for a pair of levels  $\alpha, \beta$  for which the E1 transition is forbidden, but M1 allowed<sup>†</sup>. The main term in the transition  $|\alpha'\rangle \rightarrow |\beta'\rangle$  will then be an M1  $|\alpha\rangle \rightarrow |\beta\rangle$  transition and there will be in addition E1 transitions  $|\alpha\rangle \rightarrow |\bar{\beta}\rangle$  or  $|\bar{\alpha}\rangle \rightarrow |\beta\rangle$ . The fact that  $|E1| \gg |M1|$  will somewhat compensate for the minuteness of the admixture of  $|\bar{\alpha}\rangle$  in  $|\alpha'\rangle$  or  $|\bar{\beta}\rangle$  in  $|\beta'\rangle$ .

We return to consider the resonance scattering amplitude (10.3.6) now between the mixed parity levels  $|\alpha'\rangle, |\beta'\rangle$ . The electromagnetic interaction conserves parity and is rotationally invariant. It is thus invariant under a reflection  $Y = e^{-i\pi J_y} P$  in the  $XZ$  plane, which turns  $\epsilon_R$  into  $\epsilon_L$  and vice versa, and which has the following effect on the states:

$$Y|\mathbf{k}, \epsilon_R; \alpha, m_\alpha\rangle = P_\gamma P_\alpha (-1)^{J_\alpha - m_\alpha} |\mathbf{k}, \epsilon_L; \alpha, -m_\alpha\rangle. \quad (10.3.17)$$

---

<sup>†</sup> Electric quadrupole (E2) transitions have the same selection rules as M1. It is assumed that we are choosing levels for which E2 is negligible.

Putting  $Y^\dagger H'_{\text{em}} Y = H'_{\text{em}}$  in the matrix elements in (10.3.6) in which we assume a transition with  $P_\alpha = P_\beta$  and using (10.3.17) one finds

$$\left. \begin{aligned} f_R &\cong f(M1) + f', \\ f_L &\cong f(M1) - f', \end{aligned} \right\} \quad (10.3.18)$$

where, schematically, and suppressing the  $\mathbf{k}, \epsilon_R$  labels,

$$f(M1) \propto \frac{\langle \alpha | M1 | \beta \rangle \langle \beta | M1 | \alpha \rangle}{\omega - \omega_0 + \frac{1}{2}i\Gamma}, \quad (10.3.19)$$

wherein we have put  $k = \omega c = \omega, E_\beta - E_\alpha = \omega_0$ , the resonant angular frequency, and

$$f' \propto \frac{\langle \alpha | M1 | \beta \rangle \langle \beta' | E1 | \alpha' \rangle + \langle \alpha' | E1 | \beta' \rangle \langle \beta | M1 | \alpha \rangle}{\omega - \omega_0 + \frac{1}{2}i\Gamma}. \quad (10.3.20)$$

For the E1 matrix elements we have, for example,

$$\langle \beta' | E1 | \alpha' \rangle \simeq \eta_\alpha \langle \beta | E1 | \bar{\alpha} \rangle + \eta_\beta^* \langle \bar{\beta} | E1 | \alpha \rangle. \quad (10.3.21)$$

Note that with standard conventions  $\langle \alpha | M1 | \beta \rangle$  is real whereas  $\langle \alpha' | E1 | \beta' \rangle$  is pure imaginary.

Let us now consider the size of the expected rotation of the plane of polarization. A good measure is the angle of rotation per mean free path in the vapour.

From (10.3.2) the absorption coefficient is

$$a = -\frac{2\omega \operatorname{Im} n}{c} \quad (10.3.22)$$

so that the angle of rotation per mean free path is, using (10.3.5),

$$\hat{\phi} = \frac{\phi(l)}{la} = \frac{\operatorname{Re}(n_L - n_R)}{-4 \operatorname{Im} n}. \quad (10.3.23)$$

The magnitude of  $\hat{\phi}$  is then

$$\begin{aligned} &\simeq \frac{2 \operatorname{Re} f'}{-r \operatorname{Im} f(M1)} \\ &\simeq \frac{\operatorname{Im} \langle \beta' | E1 | \alpha' \rangle}{\langle \beta | M1 | \alpha \rangle} \frac{\omega - \omega_0}{\frac{1}{2}\Gamma} \equiv R \frac{\omega - \omega_0}{\Gamma/2} \end{aligned} \quad (10.3.24)$$

The accurate calculation of the matrix elements is difficult because we clearly wish to make the parity mixing as large as possible and to do this we need to use heavy atoms. This ensures: (a) that  $Q_W$  is large in (10.3.14) and (b) that  $\langle V_{PV} \rangle$  is relatively large on account of its being proportional to  $Z^3$ . (This is because the  $\delta$  function makes  $|V_{PV}| \propto |\text{wave function at origin}|^2$ , and the latter is inversely proportional to the volume of the atom.)

Experiment	Transition used (Å)	Optical rotation parameter $R \times 10^8$	
		Experiment	Theory
Oxford	8757	$-10.12 \pm 0.20$	$-10 \pm 1$
Seattle	8757	$-10.4 \pm 1.7$	
Oxford	6480	$-9.3 \pm 1.4$	$-12 \pm 3$
Moscow	6480	$-7.8 \pm 1.8$	
Novosibirsk	6480	$-20.6 \pm 3.2$	

Table 10.1. Optical rotation parameters.

Unfortunately for heavy atoms the use of single particle ‘hydrogenic’ wave functions is inadequate, and relativistic effects may not be completely negligible. The computations are subtle and difficult and may not be very reliable.

The results for  $\hat{\phi}$ , not surprisingly, are exceedingly small. Calculations for atomic bismuth 209 ( $Z = 83$ ) yield values for  $\hat{\phi} \sim 10^{-7}$  radians, depending on the frequency of the transition used (Henley and Wilets, 1976). Experiments of great delicacy using tunable lasers to provide a sufficiently intense light source have been carried out at Oxford (Taylor *et al.*, 1987; Macpherson *et al.*, 1987), Seattle (Hollister *et al.*, 1981), Moscow (Birich *et al.*, 1984) and Novosibirsk (Barkov and Zolotorev, 1980). After an initial stage of disagreement, most groups are now compatible with each other, the only exception being the early experiment at Novosibirsk. The results are summarized in Table 10.1.

The extraordinary quality of the experiment at Oxford can be seen in Fig. 10.4 which shows the optical rotation spectrum for the 8757 Å line in atomic bismuth. The dispersion shaped profiles are centred on the positions of the hyperfine components (indicated by arrows). The curve shows the theoretical expectations in the SM and is in amazing agreement with the data. Note that the spectrum would be flat and featureless without the parity violation. (For the latest data see Macpherson *et al.*, 1991.)

The theoretical result for 6480 Å is not very precise but it seems clear that there is general agreement with the predictions of the SM for this most beautiful phenomenon.

There are many other approaches to the detection of the electroweak-induced parity violating transitions. One of the most accurate involves looking for the highly forbidden M1 transitions  $6S_{1/2} \rightarrow 7S_{1/2}$  in cesium induced by a circularly polarized laser beam in the presence of crossed electric and magnetic fields. The results are expressed in terms of a

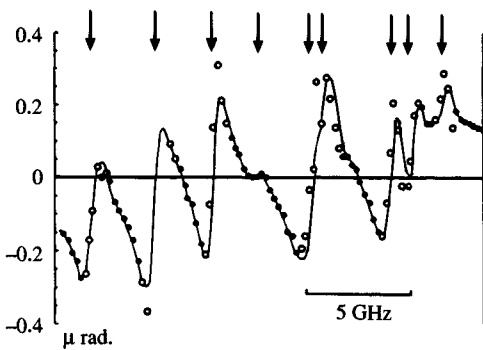


Fig. 10.4. Optical rotation spectrum for the 8757 Å line in atomic bismuth, in the current Oxford experiment of Macpherson, Zetie, Hoare, Stacey and Warrington (courtesy of Dr D. N. Stacey). See text for explanation.

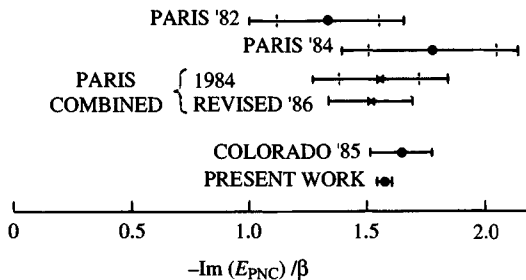


Fig. 10.5. Evolution of experimental measurement of parity violation in cesium.

quantity  $\text{Im}(E_{\text{PNC}})/\beta$  where  $E_{\text{PNC}}$  and  $\beta$  are measures of the parity non-conserving E1 transition and the stark, electric field induced, transition respectively.

The theoretical value expected (Bouchiat *et al.*, 1984, 1986) is

$$-\frac{\text{Im}(E_{\text{PNC}})}{\beta} = 1.56 \pm 0.17 \pm 0.12 \text{ mV/cm} \quad (10.3.25)$$

Figure 10.5 taken from the work of Noecker, Masterton and Witman (1988) shows the evolution of the experimental measurements over the past few years. The improvement in accuracy is impressive, as is the agreement with (10.3.25).

For an up to date summary of this highly specialized subject the reader is referred to the review by Sandars (1989), to whom we are indebted for advice on this subject.

**10.4 Summary**

The standard model developed by Weinberg, Salam and Glashow provides a beautiful unification of the weak and electromagnetic interactions of the leptons and hadrons. At the level of lowest order perturbation theory it provides expressions for a large number of physical observables in many different reactions in terms of one single parameter  $\theta_W$ . That the values of  $\theta_W$  obtained from many different sources are compatible, as shown in Fig 5.6, testifies to the remarkable success of the theory.

# 11

## The discovery of the narrow vector resonances

Perhaps the most remarkable development in particle physics in the 1970s was the discovery of several families of extremely narrow (i.e. long lived) vector mesons. We give here a brief survey of these particles, of their interpretation in terms of quark constituents and of the consequent implications for the parallelism between quarks and leptons. Some features of QCD needed in this analysis are explained.

Next, we discuss in detail the properties of the members of the  $J/\Psi$  family (bound states of a charm–anticharm pair), their quantum numbers, decay patterns and the dynamical and kinematical reasons for their narrow widths. We then turn to the most recently discovered family ( $\Upsilon$ ) whose members are remarkably heavy ( $\gtrsim 10 \text{ GeV}/c^2$ ) and which are supposed to be bound states of the heaviest quark–antiquark pair so far identified ('bottom' or 'beauty').

The study of the quarkonium picture ('charmonium' and 'bottomonium', respectively) in which the narrow resonances are visualized as loosely bound states of heavy  $Q\bar{Q}$  pairs, interacting almost non-relativistically through a static potential, is deferred to the next chapter but some general considerations are made here.

### 11.1 Introduction

The spectroscopy of atomic and molecular levels has long been in a state of perfection. During and after the Second World War much effort went into the study of nuclear levels, and we are at present witnessing a massive effort to come to terms with what can reasonably be called the 'spectroscopy of elementary particles', i.e. their levels, decay schemes and constitution. The last three decades have witnessed the discovery of a tremendous number of particles and resonances.

From the point of view of their quantum numbers, the few hundred hadronic resonances classified in the tables of particles up to the end of

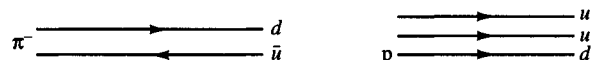
1974 could all be understood qualitatively as bound (resonant) states of just three ‘elementary’ (but, alas, elusive) constituents, the light  $u$ ,  $d$  and  $s$  quarks which we have already mentioned in Chapter 9.

Starting from the pioneering efforts of the early days (Fermi and Yang, 1949), various ways of classifying these particles have been explored, either in terms of unitary symmetries, the celebrated  $SU(3)$  eight-fold way of Gell-Mann and Neéman, or by combining internal quantum number with spin [ $SU(6)$ ] or in terms of dynamical models (recurrences on Regge trajectories, harmonic oscillator-like model etc.).

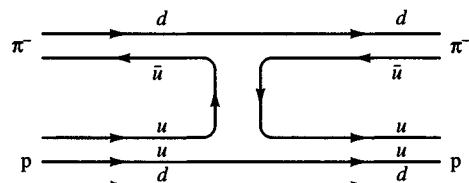
We shall not review the detailed development of the particle spectroscopy of the ‘older’ particles and we refer the interested reader to specialized books on the subject. However, while reasonable success was achieved in classification schemes, in attributing quantum numbers to the various levels, the dynamical models proposed to explain the spectrum of particles built from the  $u$ ,  $d$ ,  $s$  quarks (and from the corresponding antiquarks) had little predictive power. By this we mean that mass splitting had to be invoked and attributed to more or less *ad hoc* symmetry breakings to make realistic the rather degenerate levels predicted by the theory.

However a simple, mnemonic rule emerges: each mesonic (baryonic) state has the quantum number content of an appropriate quark–antiquark (three quark) system. The structure of mesons and baryons in terms of quarks and antiquarks is outlined below and the reader is referred for details to Lichtenberg (1978).

It has therefore become customary to visualize mesons diagrammatically as systems of quark–antiquark lines and baryons as systems of three-quark lines where ‘quarks’ and ‘antiquarks’ are simply represented by lines with arrows in opposite direction. We have already given an example of this in Section 1.2 for the weak interactions. As an example for the strong interactions, we have the following pictorial representations of a  $\pi^-$  and a proton:



leading to the pictorial representation of, for example,  $\pi^-$ p elastic scattering:



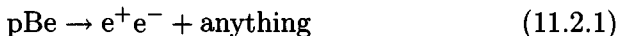
As already mentioned, these diagrams are for purely mnemonic help in keeping track of internal quantum numbers and have no dynamical

content. They are *not* Feynman diagrams.

The same convenient representation of hadronic states in terms of quark and antiquark lines will be carried over to the new sector of heavy quarks (charm  $c$ , bottom or beauty  $b$ , top  $t, \dots$ ).

## 11.2 The ‘new’ particles

In November 1974 the world of physics was shaken by the discovery of a very odd new particle, the  $J/\Psi(3097)$ . The discovery was made simultaneously by two independent groups. The first (Aubert *et al.*, 1974) saw it as an enhancement in the  $e^+e^-$  mass spectrum in the reaction



at Brookhaven (naming it  $J$ ) while the second (Augustin *et al.*, 1974) saw it in the reaction

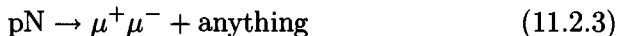


using the SPEAR machine at SLAC and named it  $\Psi$ .

Further, independent confirmation of the existence of the new particle (Bacci *et al.*, 1974) came from the ADONE accelerator at Frascati by looking at reaction (11.2.2).

Aside from its large mass ( $3097 \text{ MeV}/c^2$ ), the most remarkable property of the  $J/\Psi$  is its extreme narrowness (long lifetime) as compared with ordinary strong interaction resonances. In fact, while the latter typically have widths of the order of few hundred MeV, and the widths seem to grow (linearly?) with mass, the  $J/\Psi(3097)$  while having a large mass, has a *total* width of only  $86 \pm 6 \text{ keV}$ ! The leptonic width, on the other hand, into the  $e^+e^-$  channel is about  $5.36 \pm 0.29 \text{ keV}$  which is typical of vector mesons.

The discovery of the  $J/\Psi$  was soon followed by the unveiling of a whole family of ‘new’ particles which gave a totally unexpected course to particle physics. A few days after the discovery of the  $J/\Psi$  a second, heavier particle, a recurrence of the  $J/\Psi$ , was found at SPEAR. Optimistically labelled  $\Psi'$  it has a mass of  $3686 \text{ MeV}/c^2$  and full width of  $278 \pm 32 \text{ keV}$ . Needless to say, several other members of the  $J/\Psi$  family have since been found. In 1977, the first member of a new generation of narrow resonances was found, the upsilon  $\Upsilon$ , with a mass of  $9.46 \text{ GeV}/c^2$  and a full width of  $52.1 \pm 2.1 \text{ keV}$ . It was discovered at Fermilab (Herb *et al.*, 1977) by looking at  $\mu$  pairs in the reaction



Possible recurrences of the  $\Upsilon$  were soon found and their properties have since been studied in great detail mostly at DESY, Cornell and SLAC.

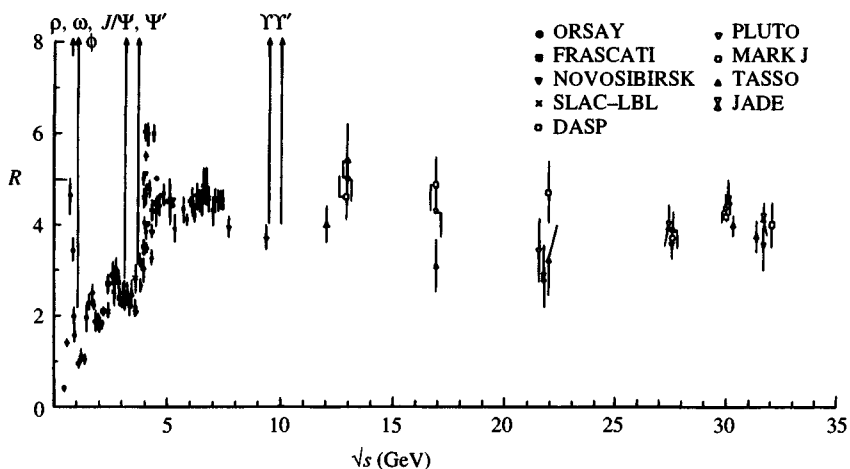


Fig. 11.1. The ratio  $R$  as a function of energy up to the CM energy  $\sqrt{s} \approx 30$  GeV. (From Brandelik *et al.*, 1979.)

The properties of these families and their experimental and theoretical implications will be the subject of the next chapters.

Fig. 11.1 shows the ratio  $R = \sigma(e^+e^- \rightarrow \text{'hadrons'})/\sigma(e^+e^- \rightarrow \mu^+\mu^-)$  (discussed in Section 6.2.5) up to about 30 GeV (i.e. where electroweak effects can be neglected). As shown in Fig. 11.1, the ‘new’ particles appear as very narrow spikes in the  $e^+e^-$  cross-section. Much effort on the theoretical side has been expended in understanding these particles. The dust has long settled and it seems convincingly demonstrated that the  $J/\Psi$  is the first manifestation of particles built out of the heavy quark (mass  $\simeq 1.5$   $GeV/c^2$ ), i.e. the charm quark introduced in Chapter 9, and whose existence was demanded for the gauge theory of weak interactions to make sense (Glashow, Iliopoulos and Maiani, 1970). The  $J/\Psi$  is visualized as a loosely bound state of  $c\bar{c}$ . Similarly, the  $\Upsilon(9.46)$  particle is interpreted as the first manifestation of a  $b\bar{b}$  bound state.

In Chapter 12 we will discuss the ‘spectroscopy’ of hidden charm and bottom or ‘charmonium’ and ‘bottomonium’ in which the actual hadrons have charm and bottom quantum number equal zero. However, when one combines a charm or bottom quark with the old light  $u$ ,  $d$ ,  $s$  quarks, new families of ‘charm’ or ‘bottom’ hadrons are predicted to exist. This will be taken up in Chapter 13.

As already mentioned in Chapter 9 (and Section 9.5.3 in particular), some theoretical arguments support the need for more than four quarks (i.e. to go beyond charm) as a consequence of the discovery in 1977 of the new heavy lepton  $\tau$  (Perl *et al.*, 1977). Its properties will be discussed in Chapter 14.

### 11.3 Some qualitative features of QCD

One of the most interesting and distinctive features of the narrow resonance spectroscopy as compared with the spectroscopy of the older particles, where only light  $u$ ,  $d$ ,  $s$  quarks come into play, i.e. up to masses below  $3 \text{ GeV}/c^2$ , is the highly satisfactory predictive power of the phenomenological models used to describe the particle spectrum in this new sector. This is mainly due to the fact that the large mass of the quarks involved allows one to make use of non-relativistic dynamics (i.e. Schrödinger equation) which would not have been a sensible approximation in the old sector with light quarks.

The conventional ‘constituent’ masses of the old quarks are  $m_u \simeq m_d \simeq 336 \text{ MeV}/c^2$  and  $m_s \simeq 500 \text{ MeV}/c^2$ . Notice (Lichtenberg, 1978) that  $m_u$  is of the order of  $\frac{1}{3}m_{\text{Nucleon}}$  and very close to  $m_p/\mu_p = 938/2.793 \text{ MeV}/c^2$ . The mass difference  $m_d - m_u$  is supposed to be very close to  $m_N - m_p$  and not much different from  $m_e - m_\nu$ ; in other words, this mass difference should be accounted for by electromagnetic effects in the ‘old’ spectroscopy, their origin being the breaking of  $SU(2)$  symmetry. The fact that  $m_s - m_u \simeq 100 - 200 \text{ MeV}/c^2$  is much larger than  $m_d - m_u$  accounts for the fact that  $SU(3)$  is more severely broken. By the same argument, given that the best estimate for the charm quark mass ( $m_c \simeq 1.5 \text{ GeV}/c^2$ ) leads to mass differences of the order of  $\sim 1000 \text{ MeV}/c^2$ , we expect the larger symmetry  $SU(4)$  which includes charm to be even more badly broken. This is why we do not consider larger symmetries.

To describe the second ingredient that makes the non-relativistic approach a practical tool for numerical computation in the heavy quark sector, we have to briefly review here some of the basic characteristics of QCD, the candidate theory of strong interactions which will be used to describe the interaction potential between quarks. QCD will be discussed in detail in Chapters 20–23.

It is believed that confinement, i.e. the absence of free quarks, is due to the quarks being endowed with the new quantum number *colour* and that ordinary hadrons that appear as free particles have to be colour singlets. QCD is a non-Abelian gauge analogue of QED where six flavoured quarks, each coming in three colours, are the analogue of the electron, and the exactly conserved colour quantum number or colour charge is the analogue of electric charge. In this way one is naturally led to assume a gauge theory of the strong interactions in which the symmetry group is  $SU(3)_C$  acting on the colour indices.

In such a theory, one requires eight massless coloured vector bosons (called gluons) to mediate the strong interaction. With colour as an exact symmetry one cannot expect to see free gluons, but their existence has

several consequences, which will be discussed in Chapters 20–25.

Thus, we have the following formal analogy

QED	$\Rightarrow$	QCD,
electron	$\Rightarrow$	colour triplets of six flavoured quarks,
photon	$\Rightarrow$	colour octet of massless vector bosons called gluons,
charge	$\Rightarrow$	colour.

Colour, like charge, cannot be destroyed but, contrary to charge, physical states (hadrons) must be colourless (i.e. colour singlets). Although no one has so far been able to prove that confinement is a property of QCD, this is usually assumed to be the case.

It will be shown in Chapters 20 and 21 that in the case of non-Abelian gauge theories, such as QCD, certain vertex corrections can be summed to all orders, with the result that what would normally be regarded as the strong interaction *coupling constant* is here replaced by a function of the virtual mass  $k^2$  of the gluon attached to the vertex, and this function is, somewhat infelicitously, referred to as the ‘running coupling constant’. We shall refer to it as the running or effective coupling. Specifically, one can show that the running coupling, which plays the rôle of an effective coupling constant, in perturbation theory is given by

$$\alpha_s \left( \frac{k^2}{\mu^2} \right) = \frac{g^2/4\pi}{1 + b(g^2/4\pi) \ln(k^2/\mu^2)} + O(\alpha_s^2), \quad (11.3.1)$$

where  $g^2/4\pi$  is the physical coupling constant ( $\alpha_s(1) \equiv g^2/4\pi \equiv \alpha_s$ ),  $\mu$  is some fixed mass scale, and  $b$  depends on the group structure. For  $SU(3)_C$

$$b = \frac{1}{12\pi}(33 - 2N_F), \quad (11.3.2)$$

where  $N_F$  is the number of flavours taken to be 6. If this perturbative result is *assumed* to give the dominant contribution (see Chapter 20 for details), then one sees that  $b$  is positive so long as we do not have more than 16 flavours! In this case the effective coupling  $\alpha_s$  tends logarithmically to zero as  $k^2/\mu^2 \rightarrow \infty$  and the theory is called asymptotically free (or ultraviolet free). The opposite happens for QED as well as for any Abelian gauge theory, where  $b$  is always negative.

As an example of a practical consequence of the above *assumptions*, the formula (9.5.25) for  $R$  (Fig. 11.1) is altered, and to second order in  $\alpha_s$  becomes (below the region of electroweak interference)

$$\begin{aligned} R &= \frac{\sigma(e^+e^- \rightarrow \text{hadrons})}{\sigma(e^+e^- \rightarrow \mu^+\mu^-)_{\text{QED}}} \\ &= \sum_j Q_j^2 \left[ 1 + \frac{\alpha_s}{\pi} + \left( \frac{\alpha_s}{\pi} \right)^2 (1.98 - 0.116N_F) \right]. \end{aligned} \quad (11.3.3)$$

Returning now to the key problem of what potential to use to describe the heavy quark (charm, bottom, ...) interactions, from our previous considerations we see that at large distances we should require the potential to grow in such a way as to confine the constituents within its boundaries. In the small  $r$  domain, which corresponds to large momenta, we may hope that the effective coupling constant is small so that we can apply perturbation theory and invoke an analogy between one-gluon and one-photon exchange. So we shall have a potential which looks like the Coulomb potential at small distances but which grows at large  $r$ . This, in essence, is the approach that we shall use in Chapter 12 when discussing ‘charmonium’ and ‘bottomonium’. Unfortunately, rather serious complications arise when trying to include spin effects in the problem.

#### 11.4 Quark-lepton parallelism

There is, presently, evidence for a sequence of three ‘generations’ of leptons, whose left-handed parts behave as doublets in the weak interactions

$$\left( \begin{array}{c} \nu_e \\ e^- \end{array} \right)_L, \left( \begin{array}{c} \nu_\mu \\ \mu^- \end{array} \right)_L, \left( \begin{array}{c} \nu_\tau \\ \tau^- \end{array} \right)_L \quad (11.4.1)$$

and whose right-handed parts as singlets  $e_R^-, \mu_R^-, \tau_R^-$  (of these only the  $\tau$  neutrino  $\nu_\tau$  has not yet been conclusively detected experimentally). That just three families of leptons exist is strongly supported by LEP data.

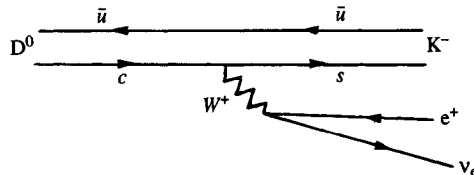
To these, there seem to correspond a sequence of quark doublets

$$\left( \begin{array}{c} u \\ d' \end{array} \right), \left( \begin{array}{c} c \\ s' \end{array} \right), \left( \begin{array}{c} t \\ b' \end{array} \right) \quad (11.4.2)$$

(each of which in fact comes in three colours) which also interact in a left-handed fashion in the weak interactions. For instance, the direct semi-leptonic decay involving the  $c$  quark

$$D^0 \rightarrow K^- + \nu_e + e^+, \quad (11.4.3)$$

is visualized in the simplest picture as



The above picture is actually oversimplified and other diagrams are needed to account for the data (see Chapter 13).

Although the data (mostly from neutrino experiments) on the  $c - s$  coupling are not conclusive, the evidence suggests that it is also left-handed. The apparent connection between quarks and leptons is fascinating. Both sets of doublets are point-like  $s = \frac{1}{2}$  fermions; their electric charges are quantized in a related way ( $Q, Q - 1$ ; with  $Q = 0$  for leptons and  $Q = \frac{2}{3}$  for quarks); furthermore, the sum of the electric charges of all fermions (in a colour scheme) vanishes as required to cancel triangle anomalies (see Section 9.5.3). It should be noted, however, that serious questions arise if one tries to put the above quark-lepton connection on a quantitative basis. For instance, it is very reasonable that the quark doublet  $\begin{pmatrix} u \\ d \end{pmatrix}_L$  should be heavier than the corresponding lepton doublet  $\begin{pmatrix} \nu_e \\ e^- \end{pmatrix}$  since the former responds also to strong interactions. In this sense it is nice that  $m_d - m_u \approx m_e - m_{\nu_e}$  since one can attribute this mass difference to electromagnetic effects ( $\nu_e$  and  $e$  differ only in their em interaction). On the other hand, going to the second pair of doublets, their electroweak and strong interaction response appears to be exactly the same as for the first pair of doublets and yet the mass pattern is totally different. Not only are the  $\mu - \nu_\mu$  and the  $c - s$  mass differences much larger than those of  $e - \nu_e$  and  $d - u$  (so that it is hard to attribute them to electroweak effects), but the quark mass difference is reversed:  $c$  is heavier than  $s$  while  $d$  is heavier than  $u$ . To complicate matters further the  $t - b$  mass difference has the same sign as  $c - s$ , but the mass spectrum is entirely different from the first set of doublets. On the other hand, there is no doubt that the quark responsible for the  $\Upsilon(9.46)$  is indeed  $b$  and not  $t$ . This will be discussed in Chapter 12, but the simplest argument is in terms of  $R$ , shown in Fig. 11.1. The expected value of  $R$  above the new quark threshold is obtained from (9.5.27) by adding an extra  $3Q_b^2 = 3 \times \frac{1}{9} = \frac{1}{3}$  for  $b$  or  $3Q_t^2 = 3 \times \frac{4}{9} = \frac{4}{3}$  for  $t$ . The experimental value of  $R$  is far too low to agree with the latter. To summarize, the theory is based on pairs of quarks of charges  $\frac{2}{3}$  and  $-\frac{1}{3}$ , each of which comes in three colours, and there is a parallelism between these pairs of quarks and the leptons. Some questions remain unanswered. Are all the neutrinos massless? Is the coupling always of the  $V - A$  type? Are the quarks really confined and, if so, do we understand the mechanism?

## 11.5 Flavour classification of hadrons

As already mentioned, the flavour symmetry  $SU(3)_F$  of Gell-Mann and Néeman was very successful in providing a classification of the old (i.e. pre-charm) spectroscopy. The quantum numbers of each hadron were

obtained from combinations of  $q\bar{q}$  (where  $q = u, d$  or  $s$ ) and  $qqq$  for mesons and baryons respectively. Multiplets of particles are thus obtained, e.g. singlets and octets of pseudo-scalar and vector mesons by coupling quarks and antiquarks in their fundamental representations ( $3$  and  $\bar{3}$ ) according to

$$3 \otimes \bar{3} = 1 \oplus 8. \quad (11.5.1)$$

Examples of the quark–antiquark content are given in Fig. 11.2. The quark content of the particles at the centre of the diagrams, assuming  $SU(3)_F$  symmetry, are

$$\left. \begin{aligned} \pi^0 &= \frac{1}{\sqrt{2}}(u\bar{u} - d\bar{d}) \\ \eta &= \frac{1}{\sqrt{6}}(u\bar{u} + d\bar{d} - 2s\bar{s}) \\ \eta' &= \frac{1}{\sqrt{3}}(u\bar{u} + d\bar{d} + s\bar{s}). \end{aligned} \right\} \quad (11.5.2)$$

Similarly, for the vectors

$$\left. \begin{aligned} \varrho^0 &= \frac{1}{\sqrt{2}}(u\bar{u} - d\bar{d}) \\ \omega &= \frac{1}{\sqrt{2}}(u\bar{u} + d\bar{d}) \\ \phi &= s\bar{s}. \end{aligned} \right\} \quad (11.5.3)$$

Similarly, singlets, octets and decuplets of baryons are obtained by combining quarks according to

$$3 \otimes 3 \otimes 3 = 1 \oplus 8 \oplus 8 \oplus 10. \quad (11.5.4)$$

For examples, see Fig. 11.3. For the baryon octet,  $SU(3)_F$  does not uniquely specify the flavour wave function.

Concerning the decuplet, it is worth recalling how the existence of the  $\Omega^- (sss)$  was actually predicted theoretically and later found at about the right mass — a triumph for  $SU(3)_F$ .

The correctness of the above quantum number assignments can be checked from Table 7.1.

Now that we believe that quarks come in six flavours,  $SU(3)_F$  cannot be an exact symmetry. It is somewhat ironic that a new  $SU(3)$  symmetry [ $SU(3)_C$ ] has now emerged as an exact symmetry of nature.

Even in the absence of flavour symmetry, the quark model of hadrons correctly predicts the quantum numbers of the hadrons, the charm pseudo-scalars  $D^+ = (c\bar{d})$ ,  $D^0 = (c\bar{u})$ ,  $D_s^+ = (c\bar{s})$ , their vector counterparts  $D^{+*} = (c\bar{d})$  etc. and the bottom pseudo-scalars  $B^- = (b\bar{u})$ ,  $\bar{B}^0 = (b\bar{d})$ ,  $\bar{B}_s^0 = (b\bar{s})$  etc. Detailed tables of heavy flavoured hadrons are given in Chapter 13.

There are two possible sets of octet wave function shown in Table 11.1. The first is symmetric, the second antisymmetric under the interchange of the flavour indices of the first two quarks.

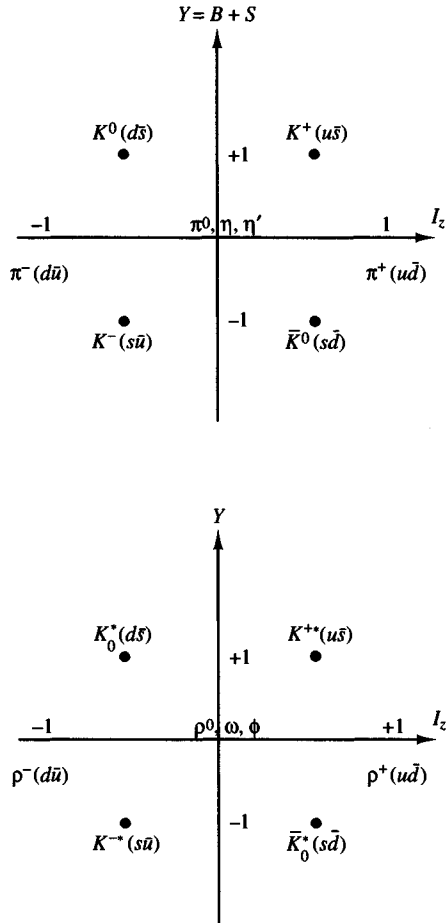


Fig. 11.2. The pseudoscalar and vector  $q\bar{q}$  octets according to  $SU(3)_F$ .

For the spin  $\frac{3}{2}$  decouplet, the  $SU(3)_F$  wave function is shown in Table 11.2.

In the pure quark model only negative intrinsic parity mesons can exist as the lowest lying bound states of a  $q\bar{q}$  pair. Scalar or axial-vector mesons would therefore signal new mechanisms such as glueballs, i.e. bound states of gluons expected in QCD. Charm and bottom baryons should analogously exist and some have been discovered, e.g.  $\Lambda_c = (cds)$ . The baryons are considered bound states of three quarks, and, according to the discussion of Section 9.5.1, the wave function is completely anti-symmetric under exchange of colour, isospin, spin and space coordinates. If we denote eigenstates of colour of the quarks by  $y$  (yellow),  $b$  (blue) and  $r$  (red)

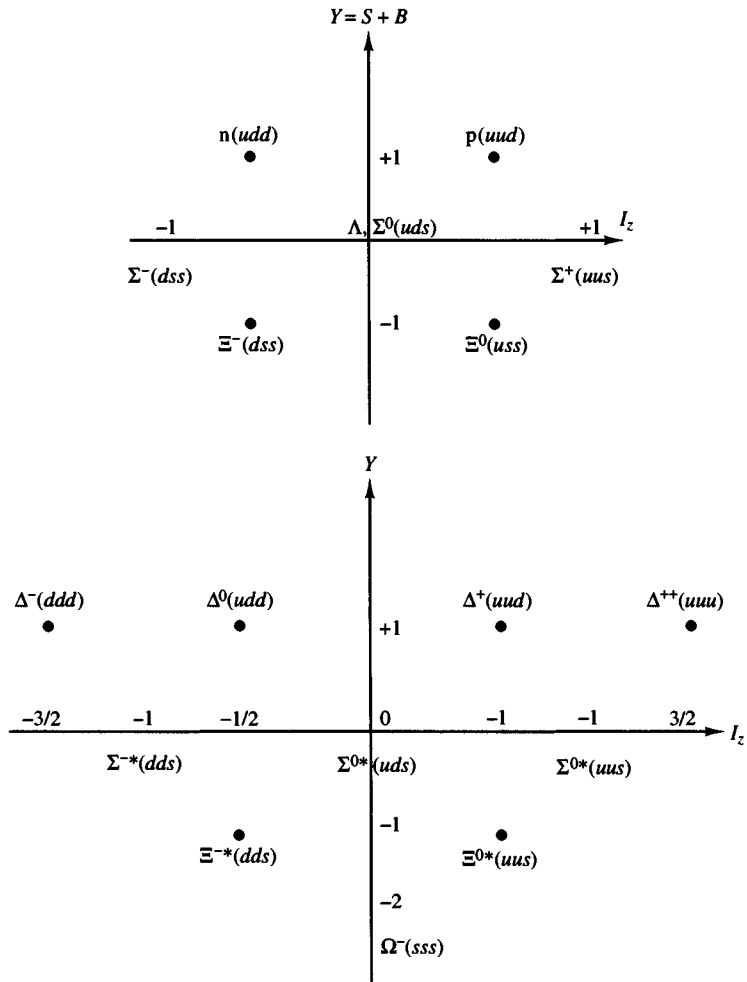


Fig. 11.3. The octet and decuplet of  $qqq$  states according to  $SU(3)_F$ .

the colour part of the baryon wave function will be

$$B_{\text{colour}} = \frac{1}{\sqrt{6}}(ybr + ryb + bry - yrb - rby - byr). \quad (11.5.5)$$

Similarly, we will have for mesons

$$M_{\text{colour}} = \frac{1}{\sqrt{3}}(y\bar{y} + b\bar{b} + r\bar{r}). \quad (11.5.6)$$

Whereas the spatial part of the wave function requires detailed information about the interaction, the spin and flavour parts of the wave function can be worked out in a straightforward way if exact flavour symmetry is

Baryon	Octet 1(S)	Octet 2(A)
p	$(2uud - udu - duu)/\sqrt{6}$	$(udu - duu)\sqrt{2}$
n	$(udd + dud - 2ddu)/\sqrt{6}$	$(udd - dud)/\sqrt{2}$
$\Lambda^0$	$\frac{1}{2}(usd + sud - dsu - sdu)$	$(2uds - 2dus + sdu - dsu + usd - sud)/\sqrt{12}$
$\Sigma^+$	$(2uus - usu - suu)/\sqrt{6}$	$(usu - suu)/\sqrt{2}$
$\Sigma^0$	$(2uds + 2dus - usd - dsu - sud - sdu)/\sqrt{12}$	$\frac{1}{2}(usd + dsu - sud - sdu)$
$\Sigma^-$	$(2dds - dsd - sdd)/\sqrt{6}$	$(dsd - sdd)/\sqrt{2}$
$\Xi^0$	$(uss + sus - 2ssu)/\sqrt{6}$	$(uss - sus)/\sqrt{2}$
$\Xi^-$	$(dss + sds - 2ssd)/\sqrt{6}$	$(dss - sds)/\sqrt{2}$

Table 11.1. Baryon octets (flavour wave function).

Baryon	Flavour wave function
$\Delta^{++}$	$uuu$
$\Delta^+$	$(uud + udu + duu)/\sqrt{3}$
$\Delta^0$	$(udd + dud + ddu)/\sqrt{3}$
$\Delta^-$	$ddd$
$\Sigma^{*+}$	$(uus + usu + suu)/\sqrt{3}$
$\Sigma^{*0}$	$(uds + usd + dus + dsu + sud + sdu)/\sqrt{6}$
$\Sigma^{*-}$	$(dds + dsd + sdd)/\sqrt{3}$
$\Xi^{*0}$	$(uss + sus + ssu)/\sqrt{3}$
$\Xi^{*-}$	$(dss + sds + ssd)/\sqrt{3}$
$\Omega^-$	$sss$

Table 11.2. Baryon decouplet.

assumed.

In dynamical calculations, e.g. the quarkonium model, one does not impose exact flavour symmetry. However, attempts have been made to extend  $SU(3)_F$  to more flavours. Details can be found in Lichtenberg (1978).

## 11.6 The $J/\Psi$ and the OZI rule

As already mentioned (Section 11.2), the first and most surprising very narrow vector meson resonance, the  $J/\Psi$  (3097), was discovered in 1974

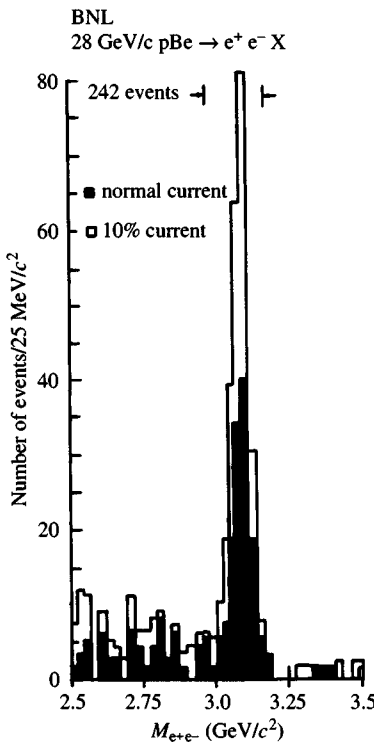


Fig. 11.4. The  $e^+e^-$  effective mass spectrum from the reaction  $pBe \rightarrow e^+e^-X$ . (From Aubert *et al.*, 1974.)

simultaneously at BNL and at SLAC (Figs. 11.4 and 11.5). In the  $e^+e^-$  channel, the enhancement factor at the  $J/\Psi$  mass is about 1000.

The very small width of this resonance,  $\Gamma \simeq 70$  keV (about a factor 1000 smaller than a typical hadronic width), indicates that its decay mode into ordinary hadrons is highly suppressed. This discovery triggered a vast experimental search and stimulated much theoretical work. The present interpretation of the  $J/\Psi$  is that it is the first manifestation of a  $c\bar{c}$  bound state ('hidden charm') occurring below the threshold for charm particle production.

The fact that the  $J/\Psi$  is produced with such a large cross-section in the  $e^+e^-$  channel makes it very plausible that its  $J^{PC}$  quantum numbers should be  $1^{--}$ , i.e. the same as the photon's. The decay properties and quantum numbers of  $J/\Psi$  have been thoroughly explored and it can now be used for calibration purposes.

The qualitative explanation of the narrowness of the  $J/\Psi$  can most simply be understood in terms of the so-called OZI rule which was invented independently by Okubo (1963), Zweig (1964) and Iizuka (1966).

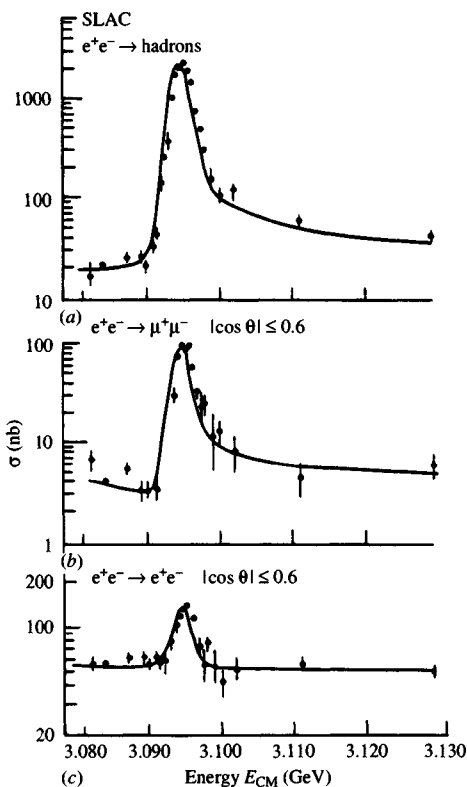
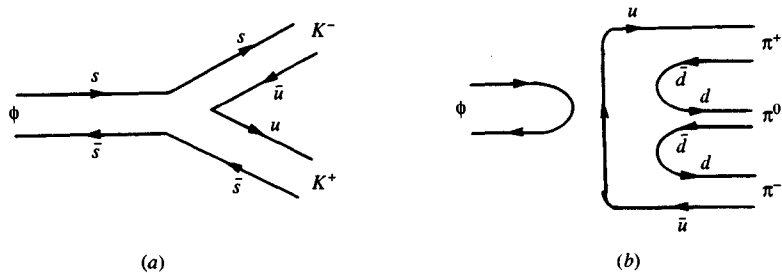


Fig. 11.5. Energy dependence of  $e^+e^-$  cross-sections in the vicinity of the  $J/\Psi$ . (From Augustin *et al.*, 1974.)

It postulates that ‘disconnected quark diagrams are suppressed relative to connected ones’. In practice, this implies that hadronic reactions are suppressed (‘OZI forbidden’) when their quark diagrams are such that one cannot trace a continuous quark line from the initial hadrons to the final ones.

The best and most celebrated example is  $\phi$  decay for which the OZI rule was invented. Given that the quark content of  $\phi$  is  $s\bar{s}$  [see (11.5.3)], OZI allowed (a) and forbidden (b) decay diagrams are



implying that the decay  $\phi \rightarrow 3\pi$  is suppressed compared with  $\phi \rightarrow K^+K^-$ , as is experimentally verified.

That the  $\phi$  width ( $\Gamma \sim 4$  MeV) is a factor 20–50 smaller than a typical hadronic decay width is, in turn, due to the fact that the OZI allowed decay  $\phi \rightarrow K\bar{K}$  has very little phase-space available since the  $\phi$  mass (1020 MeV/c<sup>2</sup>) is barely above  $K\bar{K}$  threshold.

There is ample phenomenological verification of the OZI rule in pre-charm physics and we quote a few examples of rates:

$$\begin{aligned}\Gamma(\phi \rightarrow 3\pi) &\ll \Gamma(\omega \rightarrow 3\pi), \\ \sigma(\pi N \rightarrow \phi N) &\ll \sigma(\pi N \rightarrow \omega N), \\ \sigma(pp \rightarrow pp\phi) &\ll \sigma(pp \rightarrow pp\omega)\end{aligned}$$

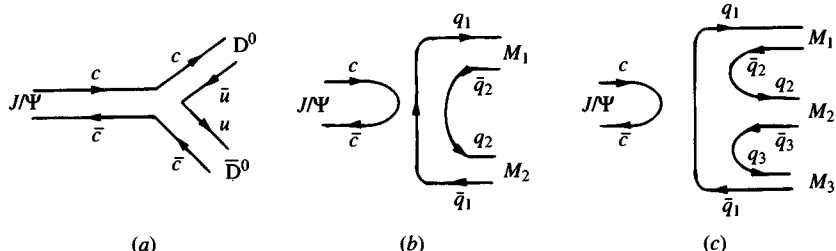
and the coupling constant relation

$$g_{NN\phi}^2 \ll g_{NN\omega}^2.$$

Similarly, one has, among OZI allowed processes

$$\begin{aligned}\sigma(K^- p \rightarrow \phi \Lambda) &\sim \sigma(K^- p \rightarrow \omega \Lambda), \\ g_{KK\phi}^2 &\simeq g_{KK\omega}^2, \text{ etc.}\end{aligned}$$

With the interpretation that  $J/\Psi$  (3097) is a  $c\bar{c}$  bound state, the same mechanism would be responsible for the very narrow width of  $J/\Psi$  (as well as of  $\Psi'$ (3684)). The corresponding OZI allowed (a) and forbidden (b), (c) decays would be, typically,



where  $q_1, q_2, q_3$  denote any light ( $u, d, s$ ) quarks and  $M_1, M_2, M_3$  are mesons with zero charm. Thus, in analogy with the  $\phi$  case, we would expect the  $J/\Psi$  to decay predominantly into pairs of charm–anticharm mesons.

It turns out, however, that the lightest charm meson  $D^0$  has a mass of 1863 MeV/c<sup>2</sup> so that  $J/\Psi(3097)$  [as well as  $\Psi'(3684)$ ] is *below* the threshold for decay into  $D^0\bar{D}^0$  in contradistinction to  $\phi$  which was just able to decay into  $K\bar{K}$ . As a result, the  $J/\Psi$  *must* decay via OZI forbidden modes and its suppression factor  $\sim 1000$  is much larger than the  $\phi$ s. To summarize, the  $J/\Psi(3097)$  is so narrow because by energy-momentum conservation it can only decay through OZI suppressed channels.

Let us now try to see how the OZI mechanism can be rephrased in the language of QCD. An OZI forbidden decay, by definition, has final state quark lines disconnected from initial state ones. Thus the only way the initial quark–antiquark ( $s\bar{s}$  or  $c\bar{c}$ ) pair can interact with the final quarks is by exchange of gluons. Single-gluon exchange is not possible because gluons carry colour (i.e. belong to a colour octet) while the initial and final states are colour singlets. A colour singlet can be made with two gluons but a  $J^{PC} = 1^{--}$  state cannot couple to a two-gluon state since, as we shall show, the latter must be even under charge conjugation, just as, in the electromagnetic case, the  $1^{--}$  state, known as orthopositronium, does not decay into two photons.

To see why two gluons coming from the decay of charmonium are in a  $C$ -even state, instead of the original gluon fields  $A_\mu^a$  ( $a = 1, \dots, 8$ ) let us use the combinations  $G_{\mu,j}^i = \sum_a (\frac{1}{2}\lambda^a)_{ij} A_\mu^a$ , where  $i, j = 1, 2, 3$  are colour labels and  $G_i^i = 0$ .

The Lagrangian for the quark–gluon interaction is then proportional to

$$\bar{q}_i \gamma^\mu \left( \frac{\lambda^a}{2} \right)_{ij} q_j A_\mu^a = \bar{q}_i \gamma^\mu q_j G_{\mu,j}^i. \quad (11.6.1)$$

As a generalization of the fact that the photon field is odd under charge conjugation, the gluon field transforms like

$$G_j^i \xrightarrow{C} -G_i^j, \quad (11.6.2)$$

which makes the Lagrangian (11.6.1) invariant (remember that a quark field transforms like a spinor under charge conjugation; see Appendix 1).

If we now consider a two-gluon colour singlet state which we denote by  $\mathbf{G}_1 \mathbf{G}_2 = G_{1j}^i G_{2i}^j$  (where  $\mathbf{G}_1$  and  $\mathbf{G}_2$  stand for the first and second gluon fields), the product  $\mathbf{G}_1 \mathbf{G}_2$  remains unchanged under charge conjugation and the corresponding two-gluon state is therefore  $C$ -even.

For the three-coloured gluons, on the other hand, there are two independent ways of forming a colour singlet state. The totally symmetric colour combination

$$D \sim \text{Tr}(\mathbf{G}_1 \mathbf{G}_2 \mathbf{G}_3) + \text{Tr}(\mathbf{G}_1 \mathbf{G}_3 \mathbf{G}_2) \quad (11.6.3)$$

is odd under  $C$ -parity and is traditionally referred as a  $D$ -type state while the antisymmetric combination

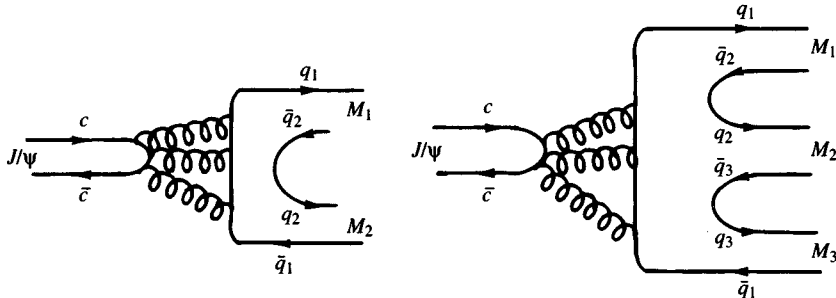
$$F \sim \text{Tr}(\mathbf{G}_1 \mathbf{G}_2 \mathbf{G}_3) - \text{Tr}(\mathbf{G}_1 \mathbf{G}_3 \mathbf{G}_2) \quad (11.6.4)$$

is referred to as an  $F$ -type state and is even under charge conjugation.

Recalling finally, that a  $q\bar{q}$  state is an eigenstate of  $C$  with eigenvalue  $(-1)^{L+S}$ , where  $L$  and  $S$  are the orbital angular momentum and spin of the pair, one finally obtains (Navikov *et al.*, 1978) the selection rules for hadronic and photon decay of charmonium in Table 11.3.

Charmonium state	$^1S_0$	$^3S_1$	$^1P_1$	$^3P_0$	$^3P_1$	$^3P_2$
$J^{CP}$	$0^{-+}$	$1^{--}$	$1^{+-}$	$0^{++}$	$1^{++}$	$2^{++}$
Hadron decay	$2G$	$(3G)_D$	$(3G)_D$	$2G$	$\left\{ \begin{array}{l} (3G)_F \\ q\bar{q}G \end{array} \right.$	$2G$
Photon decay	$2\gamma$	$3\gamma$	$3\gamma$	$2\gamma$	$\left\{ \begin{array}{l} q\bar{q}\gamma \\ 4\gamma \end{array} \right.$	$2\gamma$

Table 11.3. Charmonium selection rules.

Fig. 11.6. QCD diagrams for the decays  $J/\Psi \rightarrow$ two mesons and  $J/\Psi \rightarrow$ three mesons.

Thus, the lowest gluonic intermediate state which has the right quantum numbers to couple to a  $1^{--}$  particle has three gluons, just as orthopositronium decays into at least three real photons. The  $J/\Psi$  decay is now visualized as proceeding via the quark-gluon diagrams of Fig. 11.6, where quarks are denoted by continuous lines and gluons by helices.

The diagrams of Fig. 11.6 as yet have no dynamical content and are meant to provide only an heuristic description of the interaction responsible for the underlying processes. The dynamical model will be treated in Chapters 21 and 22.

We can, however, already appreciate why it is usually stated that charm-anticharm quark states can be better dealt with in perturbation theory than the bound states of light quarks can. To see this, we make use of the QCD idea that the quark-quark-gluon coupling



is given by an effective coupling whose numerical value decreases with increasing masses [see (11.3.1)].

At the three-gluon vertex of Fig. 11.6, i.e.



a (heavy) charm quark is exchanged so that the annihilation occurs over a relatively short distance ( $\sim 1/m_c$ ) and the momentum transferred to the gluonic system is large (the mass of the bound state). The gluons are relatively ‘hard’, so the effective coupling constant is expected to be small and in this case the diagram can be treated in perturbation theory. In perturbation theory the rate for the emission of  $n$  hard gluons (each carrying and average mass squared  $s$ ) will be proportional to  $[\alpha_s(s)]^n$ . Thus, the amplitudes for a narrow vector meson to decay into three gluons which then materialize into hadrons are expected to be proportional to  $[\alpha_s(s)]^3$  and should thus be rather small when  $\alpha_s$  itself is small.

The fact that the  $\phi \rightarrow 3\pi$  decay amplitude is fairly small leads one to hope that a perturbative approach will be adequate for  $J/\Psi$  decay since the effective coupling constant  $\alpha_s$  decreases when going from the  $\phi$  to the  $J/\Psi$  mass. An approximate calculation, to which we shall return when discussing charmonium, yields a value  $\alpha_s \simeq 0.5$  for  $\phi$  decay while a value  $\alpha_s \simeq 0.16$  is found at the  $J/\Psi$  mass—a rather rapid drop. However, it will turn out, when discussing ‘bottomonium’ that the variation of  $\alpha_s$  from the  $J/\Psi(3.097)$  to the  $\Upsilon(9.46)$  mass is rather weak.

In conclusion, the OZI rule is a useful phenomenological selection rule. Small violations may be attributed to admixtures of light  $q\bar{q}$  pairs in the  $\phi, J/\Psi, \dots$  wave functions.

## 11.7 Experimental status of the $J/\Psi$ spectroscopy

The present experimental status of the  $J/\Psi$  spectroscopy is shown in Fig. 11.7 and the details are given in Table 11.4.

All the states shown in Fig. 11.7 are excitations of the  $c\bar{c}$  bound state. Their spectroscopic classification  $n^{2S+1}L_J$  is given together with their conventional symbol. The  $J^{PC}$  assignment is shown at the bottom of the figure. The even charge conjugation pseudo-scalar states  $\eta_c(2980)$  and  $\eta'_c(3592)$  are indicated with a dashed line. They are placed close to their spin 1 (triplet) partners [ $\Psi'(3685)$  and  $J/\Psi(3097)$ ] from which they are reached via an M1 transition. Branching fractions are given in Table 11.4 (Particle Data Group, 1992.)

In Fig. 11.7 a label on an arrow indicates the type of transition.

Notice that there is a whole set of spectroscopic recurrences of the  $1^{--}$  ground state. This, in a strict sense, is the  $J/\Psi$  family and is the analogue of orthopositronium in the case of  $e^+e^-$  bound states (just as the pseudo-

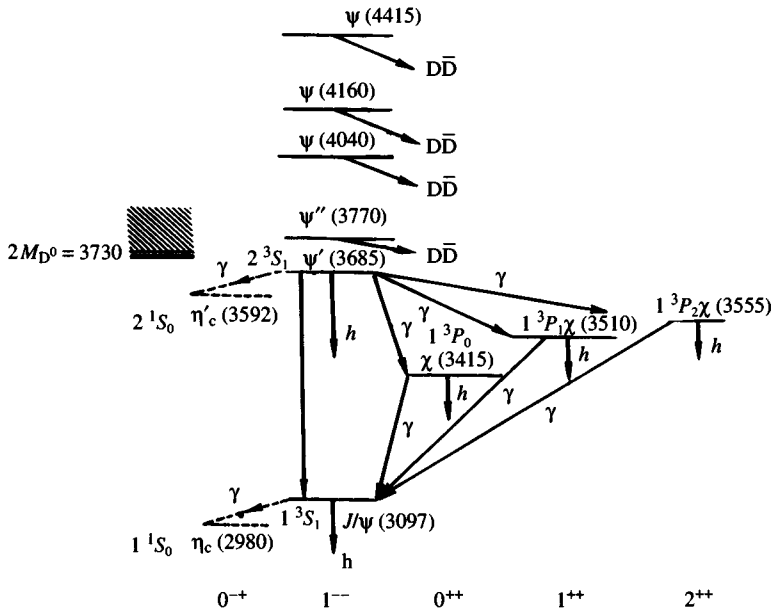


Fig. 11.7. Level diagram for  $J/\Psi$  family (see text).

scalar and its recurrences would be the analogue of parapositronium). This analogy has led to the name ‘charmonium’ for the  $c\bar{c}$  states.

A (small) mass splitting between the triplet (or vector)  ${}^3S_1$  and the singlet (or pseudo-scalar)  ${}^1S_0$  states is expected from spin dependent effects which are also responsible for the mass splitting between the  $P$  levels.

Table 11.4 summarizes the properties and main decays of the various levels. Note that the total width is in MeV, whereas the leptonic decay width  $\Gamma_e$  is in keV.

The degree to which lepton universality is satisfied in the  $J/\Psi$  family, can be seen from

$$\begin{aligned}
 B_{ee}(J/\Psi) &= 6.27 \pm 0.20 \\
 B_{\mu\mu}(J/\Psi) &= 5.97 \pm 0.25 \\
 B_{ee}(\Psi'(3685)) &= 0.88 \pm 0.13 \\
 B_{\mu\mu}(\Psi'(3685)) &= 0.77 \pm 0.17
 \end{aligned}$$

In Fig. 11.7 the threshold for  $D\bar{D}$  production is shown and by comparison with Table 11.4 one can check that those vector states that lie above this threshold are fairly broad resonances, whereas those lying below [the  $J/\Psi(3097)$  and  $\Psi'(3685)$ ] are very narrow. As explained in Section 11.6, this is expected on the basis of the OZI rule. This is further illustrated in Fig. 11.8, where the ratio  $R$  (Fig. 11.1) is shown in this energy region in more detail.

Particle	$I^G(J^{PC})$	Mass(MeV/ $c^2$ )	$\Gamma$ (MeV)	$\Gamma_e$ (keV)	Main decay modes	Branching ratio %
$\eta_c(2980)$	$0^+(0^{-+})$	$2978.8 \pm 1.9$	$10.3 \begin{array}{l} +3.8 \\ -3.4 \end{array}$		Mostly hadrons	
$\Psi(1S) \equiv J/\Psi(3097)$	$0^-(1^{--})$	$3096.93 \pm 0.09$	$0.086 \pm 0.006$	$5.36 \pm 0.29$	$\gamma\gamma$ $e^+e^-$ $\mu^+\mu^-$ direct hadrons	$\left(\begin{array}{l} +6 \\ -5 \end{array}\right) 10^{-4}$ $6.27 \pm 0.20$ $5.97 \pm 0.25$ $86 \pm 2$
$\chi(3415)$	$0^+(0^{++})$	$3415.1 \pm 1.0$	$13.5 \pm 1.0$		$\gamma J/\Psi(3097)$ hadrons	$0.66 \pm 0.18$
$\chi(3510)$	$0^+(1^{++})$	$3510.6 \pm 0.5$	$0.88 \pm 0.14$		$\gamma J/\Psi(3097)$ hadrons	$27.3 \pm 1.6$
$\chi(3555)$	$0^+(2^{++})$	$3556.17 \pm 0.13$	$2.00 \pm 0.18$		$\gamma J/\Psi(3097)$ hadrons	$13.5 \pm 1.1$
$\Psi(2S) \equiv \Psi'(3685)$	$0^-(1^{--})$	$3686.00 \pm 0.10$	$0.278 \pm 0.032$	$2.14 \pm 0.21$	$e^+e^-$ $\mu^+\mu^-$ $J/\Psi + X$ $J/\Psi + \text{neutrals}$ $J/\Psi\pi^+\pi^-$ $J/\Psi\pi^0\pi^0$ $J/\Psi\eta$ $\gamma\chi(3415)$ $\gamma\chi(3510)$ $\gamma\chi(3550)$	$0.88 \pm 0.13$ $0.77 \pm 0.17$ $57 \pm 4$ $23.2 \pm 2.6$ $32.4 \pm 2.6$ $18.4 \pm 2.7$ $2.7 \pm 0.4$ $9.3 \pm 0.8$ $8.7 \pm 0.8$ $7.8 \pm 0.8$
$\Psi''(3770)$	$0^-(1^{--})$	$3769.9 \pm 2.5$	$23.6 \pm 2.7$	$0.26 \pm 0.04$	$e^+e^-$ $D\bar{D}$	$(1.12 \pm 0.17) 10^{-5}$ dominant
$\Psi(4040)$	? $(1^{--})$	$4040.0 \pm 10.0$	$52.0 \pm 10.0$	$0.75 \pm 0.15$	$e^+e^-$	$(1.4 \pm 0.4) 10^{-5}$
$\Psi(4160)$	? $(1^{--})$	$4159.0 \pm 20.0$	$78.0 \pm 20.0$	$0.77 \pm 0.23$	charm mesons	$(10 \pm 4) 10^{-6}$
$\Psi(4415)$	? $(1^{--})$	$4415 \pm 6$	$43 \pm 15$	$0.47 \begin{array}{l} +0.10 \\ -0.09 \end{array}$	$e^+e^-$ charm mesons	$(1.1 \pm 0.4) 10^{-5}$

Table 11.4. The  $J/\Psi$  spectroscopy.

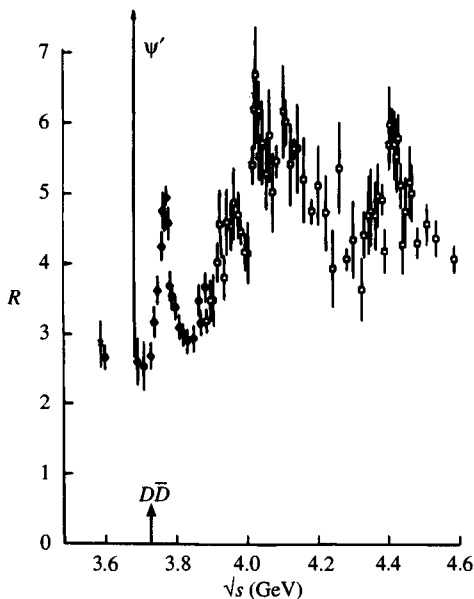


Fig. 11.8.  $R$  in the charm threshold region as measured by the SLAC-LBL collaboration at SLAC. (From Feldman, 1977.)

Needless to say, only vector states are directly accessible to the  $e^+e^-$  channel (at least through the dominant one-photon exchange), and therefore all the even charge conjugation states can be studied only by looking at radiative decays of  $\Psi'(3685)$ . It is this exceptional situation of having both  $J/\Psi$  and  $\Psi'$  below the  $D\bar{D}$  threshold that makes it possible to study the rich spectroscopy of radiative excitations (the  $\chi$  states of Table 11.4).

Experimentally, in  $e^+e^-$  physics, the mass of a new particle can be determined from two kinds of measurement:

(i) from peaks in the  $e^+e^- \rightarrow \text{hadrons}$  cross-section (see e.g. Fig. 11.5). This method is very efficacious but only for  $1^{--}$  particles. Special care is required when a resonance is narrower than the experimental energy resolution, as in the case for  $J/\Psi$  (see Section 12.3.1).

(ii) by studying the invariant masses calculated from the momenta of the (charged) decay products. If the resonance decays into two particles whose momenta are at an angle  $\theta$  the invariant mass is given by

$$M_{\text{inv}}^2 = m_1^2 + m_2^2 + 2(E_1 E_2 - |\mathbf{p}_1||\mathbf{p}_2| \cos \theta). \quad (11.7.1)$$

All combinations of particles must be tried since one cannot tell which particle in the final state originated from the resonance. Phase space decays (i.e. decays governed purely by phase space, assuming a constant matrix element) and wrong combinations produce a slowly varying back-

ground in the distribution of  $M_{\text{inv}}$ , whereas the right combination will produce a sharp peak on top of this background. The method requires the determination of all decay particles and is therefore not very useful if neutral particles are produced or if the identification of particles in the final state is not good (e.g.  $\pi - K$  separation is difficult) or if some particles fall outside the spectrometer's acceptance.

Some cases are of special interest. If the decaying system is at rest ( $\mathbf{p}_1 = -\mathbf{p}_2 = \mathbf{p}$ ) and  $M'$  is its mass, then the  $Q$ -value, i.e. the energy release of the decay, is

$$\begin{aligned} Q &= M' - m_1 - m_2 = \sqrt{\mathbf{p}^2 + m_1^2} - m_1 + \sqrt{\mathbf{p}^2 + m_2^2} - m_2 = \\ &= \mathbf{p}^2[(m_1 + \sqrt{\mathbf{p}^2 + m_1^2})^{-1} + (m_2 + \sqrt{\mathbf{p}^2 + m_2^2})^{-1}]. \end{aligned} \quad (11.7.2)$$

If, furthermore,  $p \ll (m_1, m_2)$  then  $Q$  is proportional to  $p^2$  and even a somewhat crude measurement of  $p$  gives a reasonable estimate of  $M'$ . This procedure is useful when resonances are produced just above threshold (as in the case of  $e^+e^- \rightarrow \Psi'(3770) \rightarrow D\bar{D}$ ).

If a particle of mass  $M$  and momentum  $\mathbf{p}$  decays into two  $\gamma$ s, the minimum opening angle between the photons will occur when both have the same energy  $k$  and their momenta are symmetrical about  $\mathbf{p}$ . In this case if  $\frac{1}{2}\theta$  is the angle between  $\mathbf{p}$  and the photon's momentum  $\mathbf{k}$ ,

$$\cos \frac{1}{2}\theta = \frac{p}{2k} = \frac{p}{\sqrt{p^2 + M^2}}. \quad (11.7.3)$$

If, in particular, the particle  $M$  is, in turn, the decay product of a one-photon transition, i.e. if the original resonance  $M'$  goes into three photons via a two-step process as in the case

$$\begin{array}{c} J/\Psi \rightarrow \gamma \eta_c \\ \searrow \\ \gamma \gamma \end{array} \quad (11.7.4)$$

then one can try to combine (11.7.2) and (11.7.3), with  $m_1 = M, m_2 = M_\gamma = 0$  and one gets for the invariant mass of the  $\eta_c$

$$M = M' \sin \frac{1}{2}\theta / (1 + \cos \frac{1}{2}\theta). \quad (11.7.5)$$

In this case the mass of the intermediate resonance can in principle be determined by a measurement of the photon direction alone.

How complicated things can be in practice is shown in the saga of the search for reaction (11.7.4) by looking for three final  $\gamma$ s. Originally, a clear signal was claimed for a pseudo-scalar  $1^1S_0$  state at 2820 MeV/ $c^2$  by two different groups while finally this was found at 2980 MeV/ $c^2$ .

If not all of the decay products of the resonance in question ( $R$ ) can be detected (either because they are neutral or do not fall in the acceptance

of the spectrometers), it is still possible to determine its mass if  $R$  is produced together with one other resonance  $R'$  or particle. From the masses  $m_i$  and momenta  $\mathbf{p}_i$  of the decay products of  $R'$ , the mass recoiling off  $R$  can be calculated

$$M_{\text{recoil}}^2 = \left( E - \sum_i \sqrt{\mathbf{p}_i + m_i^2} \right)^2 - \left( \sum_i \mathbf{p}_i \right)^2. \quad (11.7.6)$$

If the recoiling mass is associated with a resonance  $R'$ , one finds a peak in the recoil mass distribution at  $M_{\text{recoil}} = M_{R'}$ . From this, the mass  $M_R$  is calculable using energy momentum conservation.

To the extent that strong interactions are expected to conserve charm, the decays that  $c\bar{c}$  bound states will undergo are:

(a) decay into charm particles. This OZI allowed mode, by energy conservation, is open only to the higher  $\Psi$  states and will not be considered further, since it is just like ordinary hadronic decay.

(b) decay into light  $q\bar{q}$  pairs with emission of photons (if the electromagnetic channel is considered) or gluons (in the case of strong decay). In the latter case, the gluons are expected to materialize by converting into hadrons.

(c) by cascading from higher to lower  $c\bar{c}$  states radiating either photons or gluons. These are studied in Chapter 12.

### 11.7.1 Mass determination of the $J/\Psi$

The  $J/\Psi$  mass has been measured with good precision in the Novosibirsk  $e^+e^-$  storage ring (Zholentz *et al.*, 1980) and in collisions of a stochastically cooled antiproton beam (Van der Meer, 1981) with an internal jet target at the ISR (Baglin *et al.*, 1987). The limit to the precision of the  $J/\Psi$  mass determination in  $e^+e^-$  rings comes from the calibration uncertainty in the absolute energy scale ( $\sim 1$  MeV/ $c^2$ ).

This limitation has been overcome by using the resonance depolarization method pioneered by the Novosibirsk group (Derbenev *et al.*, 1978) which requires the measurement of the spin precession frequency  $\Omega$  of the polarized electron beam. The latter is related to the beam energy by the relation

$$E_e = m_e \kappa^{-1} \left( \frac{\Omega}{\omega} - 1 \right), \quad (11.7.7)$$

where  $\kappa$  is the ratio of the anomalous to the normal part of the electron's magnetic moment and  $\omega$  is the cyclotron frequency of the particles in the storage ring, known to an accuracy of better than one part in  $10^6$ . The spin precession frequency  $\Omega$  is obtained by slowly varying the frequency ( $\omega_d$ ) of a depolarizing field. This leads to significant depolarization when

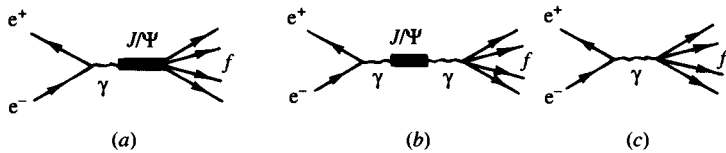


Fig. 11.9. Possible mechanisms for the annihilation reaction  $e^+e^- \rightarrow f$  important in the vicinity of the  $J/\Psi$ .

$\omega_d = \Omega$ . The relative accuracy of the determination of the beam energy obtained this way ( $\sim 3 \times 10^{-5}$ ) is ten times better than with previous methods and the final result for the  $J/\Psi$  mass is given in Table 11.4 (radiative corrections have been taken into account).

## 11.8 Properties of the $J/\Psi(3097)$ and $\Psi'(3685)$

Since the  $J/\Psi$  family is directly and copiously produced in the  $e^+e^-$  annihilation channel, the simplest conjecture is that it has the quantum numbers of the photon.  $e^+e^-$  cannot decay into one real photon because of momentum conservation but it can couple to one *virtual* photon, or to two (or more) real or virtual photons.

The dominant lowest order coupling is to one virtual photon, so the simplest assumption is that  $J/\Psi$  is a  $J^{PC} = 1^{--}$  state reached through one virtual photon exchange via mechanisms familiar from the theory of ‘vector meson dominance’ used in discussing the  $\varrho, \omega, \phi$  mesons. Fig. 11.9 shows various possibilities for the process  $e^+e^- \rightarrow f$  in the region of the  $J/\Psi$  mass.

Diagram (a) involves the direct decay  $J/\Psi \rightarrow f$ . Diagrams (b) and (c) are not really independent. The  $J/\Psi$  in (b) provides a correction to the bare photon propagator in (c), and the two contributions interfere with each other. In Fig. 11.9  $f$  is any final state, but if it consists of just  $e^+e^-$  or  $\mu^+\mu^-$  then only (b) and (c) occur since we always assume that  $e$  and  $\mu$  couple directly only to photons (aside, of course, from their weak interaction which is irrelevant here). The latter assumption is indeed corroborated by the data. Table 11.4 shows that the direct  $J/\Psi$  decay into leptons is actually quite small.

### 11.8.1 $J/\Psi$ and $\Psi'$ widths

Given that the  $J/\Psi$  width is much smaller than the experimental resolution of both  $e^+e^-$  machines ( $\sim 2$  MeV) as well as of  $p\bar{p}$  machines ( $\sim 0.7$  MeV), the width cannot be read off directly from the shape of the

$J^{PC}$	Differential cross-section $\frac{d\sigma}{d\Omega}$	Interference in $\sigma_{\mu\mu}(s)$	$F/B$ asymmetry
$0^\pm$	$\frac{2\alpha^2}{3s} \left\{ \frac{3}{8}(1 + \cos^2 \theta) + \frac{g^4}{e^4} \frac{s^2}{(M^2 - s)^2 + M^2 \Gamma^2} \right\}$ $\begin{array}{ccc} \uparrow & & \uparrow \\  QED ^2 & &  R ^2 \end{array}$	no	no
$1^-$	$\frac{\alpha^2}{4s} (1 + \cos^2 \theta) \left\{ 1 - 2 \frac{g^2}{e^2} \frac{(M^2 - s)s}{(M^2 - s)^2 + M^2 \Gamma^2} + \frac{g^4}{e^4} \frac{s^2}{(M^2 - s)^2 + M^2 \Gamma^2} \right\}$ $\begin{array}{ccc} \uparrow & & \uparrow \\  QED ^2 & &  R ^2 \\ \uparrow & & \uparrow \\ 2QEDR^* & &  R ^2 \end{array}$	yes	no
$1^+$	$\frac{\alpha^2}{4s} \left\{ (1 + \cos^2 \theta) \left( 1 + \frac{g^4}{e^4} \frac{s^2}{(M^2 - s)^2 + M^2 \Gamma^2} \right) - 2 \cos \theta \frac{g^2}{e^2} \frac{(M^2 - s)s}{(M^2 - s)^2 + M^2 \Gamma^2} \right\}$	no	yes

Table 11.5.  $\mu$  pair production in the neighbourhood of a resonance  $R$  of mass  $M$ ;  $g$  is the coupling of the resonance  $R$  to  $\mu^+ \mu^-$ .

resonance curve and must be obtained from data which are independent of the resolution, such as the cross-section integrated over the resonance.

Assuming that Fig. 11.9 (a) dominates near the resonance mass and parametrizing the resonant amplitude à la Breit-Wigner (see, for example, Blatt and Weisskopf, 1979), for the reaction

$$e^+e^- \rightarrow J/\Psi \rightarrow f \quad (11.8.1)$$

at energy  $\sqrt{s}$  we have

$$\sigma_f = \pi \frac{2J+1}{s} \frac{\Gamma_e \Gamma_f}{(M - \sqrt{s})^2 + \frac{1}{4}\Gamma^2}, \quad (11.8.2)$$

where  $\Gamma_e, \Gamma_f$  are the widths for decay into  $e^+e^-$  and  $f$  respectively and  $J$  is the spin of the resonance.

Integrating (11.8.2) over the resonance region and defining

$$\sum_f \equiv \int_{\text{resonance}} \sigma_f d\sqrt{s} \quad (11.8.3)$$

and setting  $J = 1$ , we find for the reactions  $f = e^+e^-$ ,  $f = \mu^+\mu^-$ ,  $f = \text{hadrons}$ :

$$\left. \begin{array}{l} \sum_e = \frac{6\pi^2}{M^2} \frac{\Gamma_e^2}{\Gamma}, \\ \sum_\mu = \frac{6\pi^2}{M^2} \frac{\Gamma_e \Gamma_\mu}{\Gamma}, \\ \sum_h = \frac{6\pi^2}{M^2} \frac{\Gamma_e \Gamma_h}{\Gamma}. \end{array} \right\} \quad (11.8.4)$$

In practice, the integral of (11.8.2) is carried out by first replacing  $1/s$  by  $1/M^2$  and then integrating between  $-\infty$  to  $+\infty$  in the variable  $x = \sqrt{s} - M$ . The total width  $\Gamma$  is given by

$$\Gamma = \Gamma_h + \Gamma_e + \Gamma_\mu \quad (11.8.5)$$

in terms of the leptonic ( $\Gamma_e, \Gamma_\mu$ ) and hadronic ( $\Gamma_h$ ) widths.

In principle, (11.8.4) and (11.8.5) allow us to solve completely for  $\Gamma_e \Gamma_\mu$  and  $\Gamma_h$  if the three corresponding cross-sections are separately measured. In practice, given that  $\Gamma_e$  and  $\Gamma_\mu \ll \Gamma_h$  and  $\Gamma_h \simeq \Gamma$  we see, from the last of (11.8.4) that the total integrated cross-section essentially determines  $\Gamma_e$  and this, together with the integrated measured  $\sum_e$ , gives the full width:

$$\Gamma \simeq \Gamma_e \frac{\sum_{\text{tot}}}{\sum_e}. \quad (11.8.6)$$

From the values of  $\Gamma_e \simeq 5.36 \pm 0.29$  keV and from  $\int \sigma_h d\sqrt{s} \simeq (10.4 \pm 1.5) \mu\text{b MeV}$  and  $\int \sigma_{e\text{ed}} d\sqrt{s} \simeq 790 \text{ nb MeV}$ , one gets the value already quoted:  $\Gamma \simeq (86 \pm 6)$  keV for  $J/\Psi(3097)$ . Similarly, one gets  $\Gamma^{\Psi'} \simeq (278 \pm 32)$  keV.

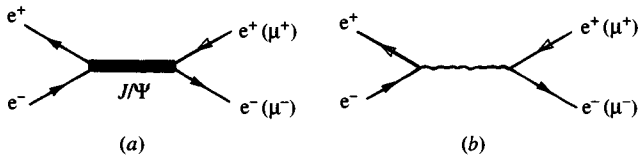


Fig. 11.10. Annihilation diagrams for  $e^+e^- \rightarrow e^+e^-$  or  $\mu^+\mu^-$  involving  $J/\Psi$  or  $\gamma$  intermediate states.

Needless to say, complementary information can be found from other reactions such as

$$pp \rightarrow e^+e^- + X. \quad (11.8.7)$$

### 11.8.2 $J^{PC}$ assignments

Suppose  $J/\Psi$  has arbitrary spin. Then, the processes  $e^+e^- \rightarrow e^+e^-$  or  $\mu^+\mu^-$  will receive contributions from the diagrams shown in Fig. 11.10.

The spin and parity of  $J/\Psi$  can be deduced from a study of the interference between  $\mu^+\mu^-$  pair production via  $J/\Psi$  and via pure QED. In Table 11.5 the differential cross-sections expected for various spin parity assignments of  $J/\Psi$  are given. The coupling of  $J/\Psi$  to  $\mu^+\mu^-$  is denoted by  $g$ .

In Table 11.5,  $\sigma_{\mu\mu}$  is the total cross-section for  $e^+e^- \rightarrow \mu^+\mu^-$  and the column  $F/B$  refers to the forward-backward asymmetry in the angular distribution of the final  $\mu$ . Notice that in the case of  $J^P = 0^+$  or  $1^+$  there is no interference term in the cross-section, whereas for  $J^P = 1^-$  the cross-section  $\sigma_{\mu\mu}(s)$  has an interference effect which is destructive below and constructive above the resonance. On the other hand, a  $1^-$  assignment gives a symmetric forward-backward differential cross-section, whereas an axial vector  $1^+$  would lead to a forward-backward asymmetry.

The data are shown in Figs. 11.11, 11.12 and 11.13.

In Fig. 11.11 the ratio  $\sigma_{\mu^+\mu^-}/\sigma_{e^+e^-}$  is shown rather than  $\sigma_{\mu^+\mu^-}$  since one is seeking very small effects and this helps to eliminate systematic errors due to normalization. In calculating  $\sigma_{e^+e^-}$  it is assumed that  $\mu^-e$  universality holds, i.e. the same coupling of  $J/\Psi$  to  $e^+e^-$  and  $\mu^+\mu^-$  is used. The coupling  $g$  of Table 11.5 is related to  $\Gamma_e$  by  $g^2 = 12\pi\Gamma_e/M$ . The interference based on the  $1^{--}$  assignment fits the data very well. In support of this assignment, Fig. 11.12 shows no forward-backward asymmetry. Finally, Fig. 11.13 shows the angular distribution of one of the leptons in the pair. The non-QED contribution for electrons is consistent with the  $1 + \cos^2\theta$  form expected for a  $1^{--}$  resonance (see discussion of  $Z^0$  exchange in Section 8.5). This excludes higher spin assignments. (The

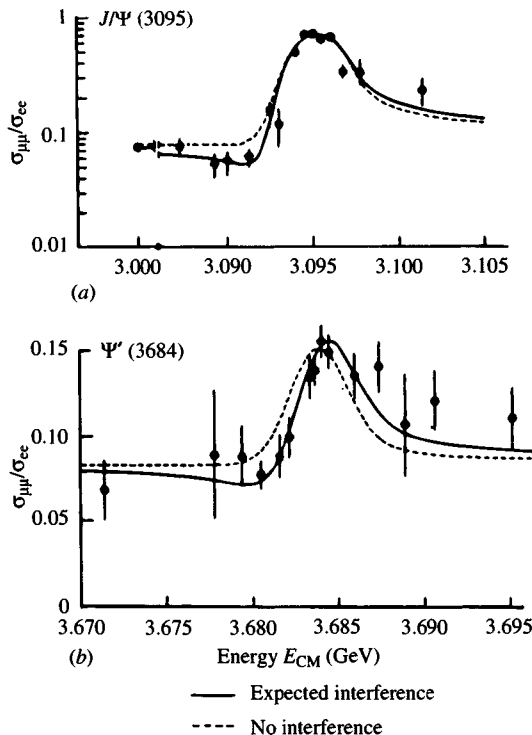


Fig. 11.11. Ratio of lepton pair cross-sections  $\sigma_{\mu\mu}/\sigma_{ee}$  in the vicinity of the  $J/\Psi$  and the  $\Psi'$ . (From Boyarski *et al.*, 1975.)

fact that there is difference between the angular distribution of the  $\mu$  and the  $e$ , within QED, has been discussed in Section 8.3.)

Now notice that the combined operation of  $CP$  does not alter a state containing just  $\mu^+\mu^-$ . Such states must therefore have  $C = P$ . The negative parity implied by the  $1^{--}$  assignment then implies also  $C = -1$ . Thus, the original guesses of  $J^{PC} = 1^{--}$  for the  $J/\Psi(3097)$  and for the  $\Psi'(3685)$  are well corroborated by the experimental evidence.

### 11.8.3 $I^G$ assignment

On analysing the  $J/\Psi$  multipion decay modes (Trippe *et al.*, 1977), it turns out that the  $J/\Psi$  decays approximately ten times more frequently into an odd than into an even number of pions. *Both* types of decay, however, do occur. Since pions have  $G$  parity ( $-1$ ) and as a consequence the  $G$  parity of a non-strange neutral meson should be even or odd according to whether it decays into an even or odd numbers of pions, we might conclude that  $G$  is not a good quantum number for  $J/\Psi$  decay.

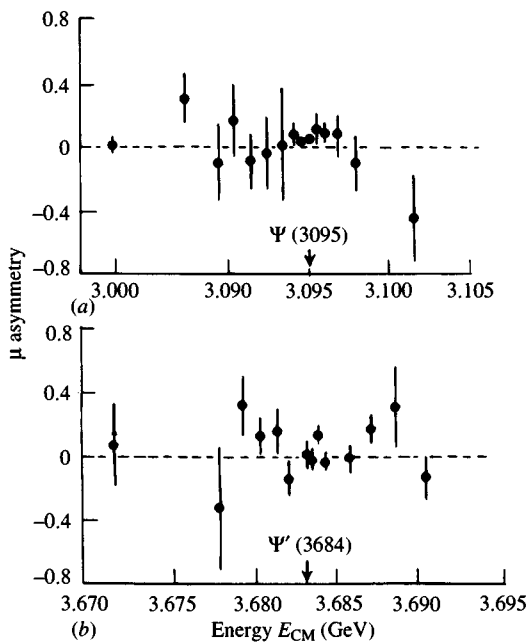


Fig. 11.12. Forward-backward asymmetry for  $e^+e^- \rightarrow \mu^+\mu^-$  in the vicinity of the  $J/\Psi$  and the  $\Psi'$ . (From Boyarski *et al.*, 1975.)

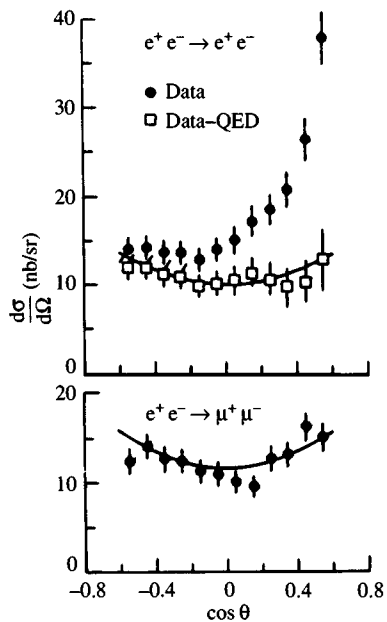


Fig. 11.13. Differential cross-sections for  $J/\Psi$  production followed by decay into  $e^+e^-$  or  $\mu^+\mu^-$ . (From Boyarski *et al.*, 1975.)

However, electromagnetic interactions violate  $G$  conservation so the decay diagrams [(Fig. 11.9(b) and (c)] can lead to states  $f$  with either even or odd numbers of pions.

It is thus not unreasonable to assume that  $J/\Psi$  has a definite (negative)  $G$  parity and that while the direct decay [Fig. 11.9(a)] is  $G$  parity conserving the one-photon contribution [Fig. 11.9(b)] gives the observed violation of  $G$  parity. To check this, we notice that, off resonance, the ratio of the one-photon contribution to multipion final states and to  $\mu^+\mu^-$  pairs must be insensitive as to whether the multipion final states have an even or an odd number of pions. Thus, a plot of

$$\alpha_n = \frac{\sigma_{n\pi}(\text{on resonance})/\sigma_{\mu\mu}(\text{on resonance})}{\sigma_{n\pi}(\text{off resonance})/\sigma_{\mu\mu}(\text{off resonance})} \quad (11.8.8)$$

should change dramatically as  $n$  varies through odd and even values, if indeed  $J/\Psi$  has a well-defined  $G$  parity. As shown in Fig. 11.14, this is in fact the case, and the conclusion is that the  $G$  parity of  $J/\Psi(3097)$  is negative.

As for isospin, we certainly have  $I \leq 3$  since decay into three pions is observed. Then, from the relation valid for charge zero mesons,

$$G = C(-1)^I; \quad (11.8.9)$$

given that  $C$  and  $G$  are negative, it follows that  $I = 0$  or  $2$ . To see that  $I = 0$  it is sufficient to notice that the decay into  $3\pi$  goes mainly via  $\varrho\pi$  and that  $\Gamma_{\varrho^0\pi^0} \simeq \Gamma_{\varrho^+\pi^-} \simeq \Gamma_{\varrho^-\pi^+}$ . Indeed

$$\frac{\Gamma(J/\Psi \rightarrow \varrho^0\pi^0)}{\Gamma(J/\Psi \rightarrow \varrho^0\pi^0) + \Gamma(J/\Psi \rightarrow \varrho^+\pi^-) + \Gamma(J/\Psi \rightarrow \varrho^-\pi^+)} \simeq 0.328 \pm 0.005 \pm 0.027. \quad (11.8.10)$$

For  $I = 0$  one expects equal amounts of neutral and charged  $\varrho\pi$  production, whereas  $I = 2$  would require  $\Gamma_{\varrho^0\pi^0} = 4\Gamma_{\varrho^+\pi^-}$  which is excluded by the data.

Similar assignments  $I^G = 0^-$  have been made for  $\Psi'(3685)$  on the basis of its cascade decay

$$\Psi'(3685) \rightarrow J/\Psi(3097) + X, \quad (11.8.11)$$

which accounts for almost 60% of its entire decay

$$\frac{\Gamma[\Psi'(3685) \rightarrow J/\Psi(3097) + X]}{\Gamma[\Psi'(3685) \rightarrow X]} \simeq 0.57 \pm 0.05. \quad (11.8.12)$$

The typical and most common decay of type (11.8.11) is  $X = \pi^+\pi^-$ , an example of which is shown in Fig. 11.15 and

$$\frac{\Gamma[\Psi'(3685) \rightarrow J/\Psi(3097) + \pi^+\pi^-]}{\Gamma_{\text{tot}}[\Psi'(3685)]} \simeq 0.332 \pm 0.033. \quad (11.8.13)$$

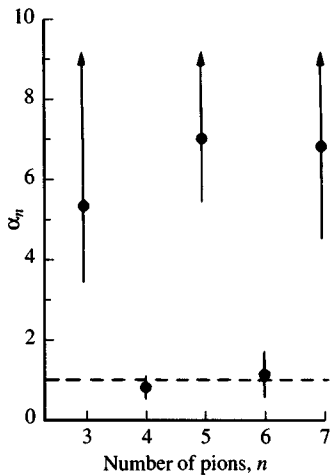


Fig. 11.14. Ratio of multipion cross-section to muon pair cross-section at the  $J/\Psi$  (ON) and at 3.0 GeV (OFF), as a function of the number of produced pions. (From Jean-Marie *et al.*, 1976.)

If we assume isospin conservation in the decay, the ratio for  $J/\Psi 2\pi^0$  to  $J/\Psi \pi^+\pi^-$  production would be 0.5 if  $\Psi'$  had  $I = 0$ , 0 for  $I = 1$  and 2 for  $I = 2$ . The experimental value  $0.57 \pm 0.08$  is a convincing argument in favour of  $I = 0$ .

### 11.9 Baryonic decay of $J/\Psi$

Special interest attaches to the decay of  $J/\Psi$  into baryons. The majority of these decays produce two-body final states. In general, the angular distribution must then be of the form (Section 25.2.1)

$$\frac{dN}{d \cos \theta_B} \propto 1 + \alpha \cos^2 \theta_B, \quad (11.9.1)$$

where  $\theta_B$  is the angle between the baryon and the  $e^+$  beam direction. The results for  $p\bar{p}$ ,  $\Lambda\bar{\Lambda}$  and  $\Sigma\bar{\Sigma}$  are shown in Fig. 11.16, where the curves correspond to fits using (11.9.1) (see Köpke and Wermes, 1989, for details).

Unfortunately the values of  $\alpha$  vary somewhat inconsistently from experiment to experiment. Nonetheless taking averages one finds

$$\left. \begin{aligned} \alpha_{p\bar{p}} &= 0.63 \pm 0.08, \\ \alpha_{\Lambda\bar{\Lambda}} &= 0.65 \pm 0.19, \\ \alpha_{\Sigma\bar{\Sigma}} &= 0.26 \pm 0.30. \end{aligned} \right\} \quad (11.9.2)$$

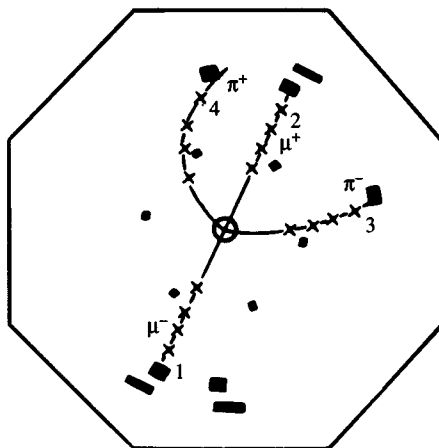


Fig. 11.15. Example of tracks in the decay  $\Psi' \rightarrow J/\Psi + \pi^+\pi^-$  followed by  $J/\Psi \rightarrow \mu^+\mu^-$ . (From Abrams *et al.*, 1975.)

The angular distribution provides a severe challenge to our understanding of non-perturbative QCD. A possible mechanism for the decay is shown in Fig. 11.17.

Since the quarks are almost at rest, the process of hadronization, a non-perturbative effect, will significantly influence the angular distribution. (This is very different from say  $c\bar{c}$  production in  $e^+e^-$  collisions at *high* energy, where one expects the energetic  $c$  and  $\bar{c}$  to materialize into jets moving basically along their directions of motion.) Despite the danger, perturbative calculations based on diagrams like Fig. 11.17 yield sensible values for  $\alpha$ . For example,  $\alpha_{p\bar{p}} = 0.69$ ,  $\alpha_{\Lambda\bar{\Lambda}} = 0.51$  and  $\alpha_{\Sigma\bar{\Sigma}} = 0.43$  (Carimalo, 1987).

A fascinating suggestion (Törnquist, 1981) is to use the decay

$$\begin{array}{c} J/\Psi \rightarrow \Lambda\bar{\Lambda} \\ \downarrow \\ \pi^+\bar{p} \\ \downarrow \\ \pi^-\bar{p} \end{array} \quad (11.9.3)$$

as a sort of Einstein–Podolski–Rosen (1935) experiment. The weak decays of the hyperons function as analyzers of the spin state of the  $\Lambda$ ,  $\bar{\Lambda}$ , so that quantum mechanical correlations at macroscopic distances can be measured and compared with the Bell inequality. Preliminary results (Tixier, 1988) are consistent with quantum mechanical expectations.

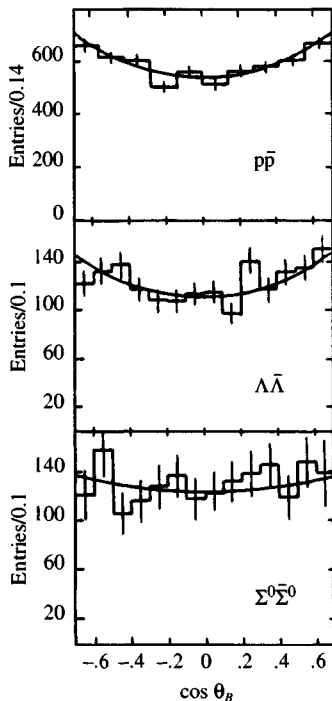


Fig. 11.16. Angular distribution in two baryon production. Polar angle distribution of (a) proton, (b)  $\Lambda$ , and (c)  $\Sigma^0$  with respect to the positron direction. (Köpke and Wermes, 1989).

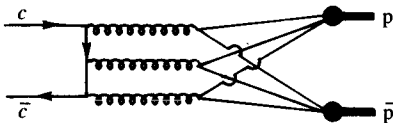


Fig. 11.17. Possible decay mechanism for  $J/\Psi \rightarrow p\bar{p}$ .

### 11.10 The $\Upsilon$ family and its experimental status

No further narrow vector resonances were discovered in the mass range  $4.5 \text{ GeV}/c^2 < \sqrt{s} \lesssim 9.5 \text{ GeV}/c^2$ , but a few years after the discovery of the  $J/\Psi$ , a narrow resonance was found as an enhancement in the dimuon mass spectrum in proton–nucleus collisions at  $400 \text{ GeV}/c$  at Fermilab in the reactions

$$p + (\text{Cu} + \text{Pb}) \rightarrow \mu^+ \mu^- + X. \quad (11.10.1)$$

The new resonance (Herb *et al.*, 1977; Ledermann, 1978) at a mass of  $9.46 \text{ GeV}/c^2$  was named  $\Upsilon(9.46)$ . Its rich spectroscopy had actually been anticipated (Eichten and Gottfried, 1976) on the basis of the theoretical scheme discussed in the next Chapter.

The results are shown in Fig. 11.18. In Fig. 11.19 the data are shown after subtraction of a smooth background and are compared with the data obtained later at DORIS in  $e^+e^-$  collisions. Two indisputable peaks  $\Upsilon(9.46)$  and  $\Upsilon'(10.02)$  are seen. However, attempts to fit the Fermilab data using a form based on two Breit-Wigner resonances led to a separation  $M_{\Upsilon'} - M_\Upsilon$  significantly larger than that of the actual peaks. This is because there is an excess of events around  $E \simeq 10.5 \text{ GeV}/c^2$  and the  $\Upsilon'$  Breit-Wigner is somehow trying to accommodate for them. Although there was no visible peak at  $10.5 \text{ GeV}/c^2$  it turned out that an excellent fit was obtained with *three* Breit-Wigner resonances,  $M_\Upsilon$  being constrained in the fit by the DORIS data, with the third peak  $M_{\Upsilon''}$  located at  $10.41 \pm 0.05 \text{ GeV}/c^2$  by the fit. A two resonance Breit-Wigner fit, with  $M_{\Upsilon'}$  forced to lie at  $10.02 \text{ GeV}/c^2$ , was 11 standard deviations worse than the three resonance fit.

Remarkably, the  $\Upsilon''$  was then confirmed by the  $e^+e^-$  machine CESR at Cornell University. The remarkably clear resolution of the peaks is shown in Fig. 11.20.

The very rich spectroscopy unveiled mainly at Cornell and SLAC is summarized in Table 11.6. Much the same kind of analysis as for the  $J/\Psi$  family applies here *mutatis mutandis*.

The ratio  $R$  shown in Fig. 11.21 indicates the complicated structure in the  $\Upsilon$  family above the  $B\bar{B}$  threshold.

Table 11.6 gives a summary of the main properties of the members of the  $\Upsilon$  family. Notice that three  $1^{--}$  states are now very narrow [ $\Upsilon(1S)$ ,  $\Upsilon(2S)$  and  $\Upsilon(3S)$ ] with widths, typically, between 50 and 20 keV, whereas the other recurrences lying above the  $B\bar{B}$  threshold have widths  $\sim 10^3$  times larger. Note also, the high degree to which  $e - \mu - \tau$  universality is satisfied.

The  $\Upsilon$  family members are interpreted as  $b\bar{b}$  bound states. All members are  $J^{PC} = 1^{--}$  states.

There are several arguments in favour of the assignment, charge  $-\frac{1}{3}$ , to the quark involved, rather than charge  $\frac{2}{3}$ , which could be the charge of the quark  $t$  on the assumption that there exists a new type of quark doublet of the standard type  $\begin{pmatrix} t \\ b \end{pmatrix}$ . The calculated leptonic widths are proportional to  $Q_b^2$  but are of course model dependent. Nevertheless, in a large class of potential models the leptonic widths given in Table 11.6 favour  $Q_b^2 = \frac{1}{9}$ . This assignment is supported by the behaviour of  $R$  in

Particle	$I^G(J^{PC})$	Mass (GeV/ $c^2$ )	$\Gamma$ (keV)	$\Gamma_e$ (keV)	Decay mode	Fraction (%)
$\Upsilon(1S, 9460)$	$(1^{--})$	$9460.32 \pm 0.22$	$52.1 \pm 2.1$	$1.34 \pm 0.04$	$e^+e^-$	$2.52 \pm 0.17$
					$\mu^+\mu^-$	$2.48 \pm 0.06$
					$\tau^+\tau^-$	$2.97 \pm 0.35$
					$J/\Psi + X$	$\sim 0.11 \pm 0.04$
					$\gamma + X$	$< 0.2$
$\chi_{b0}(1P)$	$?(0^{++})$	$9859.8 \pm 1.3$			$\gamma\Upsilon(1S)$	$< 6$
$\chi_{b1}(1P)$	$?(1^{++})$	$9891.9 \pm 0.7$			$\gamma\Upsilon(1S)$	$35 \pm 8$
$\chi_{b2}(1P)$	$?(2^{++})$	$9913.2 \pm 0.6$			$\gamma\Upsilon(1S)$	$22 \pm 4$
$\Upsilon(2S)$	$?(1^{--})$	$10023.30 \pm 0.31$	$43 \pm 8$	$0.586 \pm 0.029$	$e^+e^-$	$1.36 \pm 0.26$
					$\mu^+\mu^-$	$1.31 \pm 0.21$
					$\tau^+\tau^-$	$1.7 \pm 1.6$
					$\sum_i \gamma\chi_{bi}$	$\sim 18$
					$\Upsilon(1S)\pi\pi$	27
$\chi'_{b0}(2P)$	$?(0^{++?})$	$10232.0 \pm 0.7$	$416 \pm 135 \pm 76$		$\gamma\Upsilon(1S)$	$1.4 \pm 1.0$
					$\gamma\Upsilon(2S)$	$7 \pm 4$
$\chi'_{b1}(2P)$	$?(1^{++?})$	$10255.2 \pm 0.4$	$89 \pm 7 \pm 16$		$\gamma\Upsilon(1S)$	$7.9 \pm 1.1$
					$\gamma\Upsilon(2S)$	$22 \pm 4$
$\chi'_{b2}(2P)$	$?(2^{++?})$	$10268.4 \pm 0.6$	$128 \pm 12 \pm 15$		$\gamma\Upsilon(1S)$	$7.0 \pm 1.1$
					$\gamma\Upsilon(2S)$	$19 \pm 4$
$\Upsilon(3S)$	$?(1^{--})$	$10355.3 \pm 0.5$	$24.3 \pm 2.9$	$0.44 \pm 0.03$	$e^+e^-$	$1.81 \pm 0.25$
					$\mu^+\mu^-$	$1.81 \pm 0.17$
					$\Upsilon(2S) + X$	$10.1 \pm 1.7$
					$\sum_i \gamma\chi_{bi}$	$\sim 30$
$\Upsilon(4S)$	$?(1^{--})$	$10580.0 \pm 3.5$	$23.8 \pm 2.2$ MeV	$0.24 \pm 0.05$		
$\Upsilon(5S)$	$?(1^{--})$	$10865 \pm 8$	$110 \pm 13$ MeV	$0.31 \pm 0.07$		
$\Upsilon(6S)$	$?(1^{--})$	$11019 \pm 8$	$79 \pm 16$ MeV	$0.130 \pm 0.030$		

Table 11.6. The  $\Upsilon$  spectroscopy.

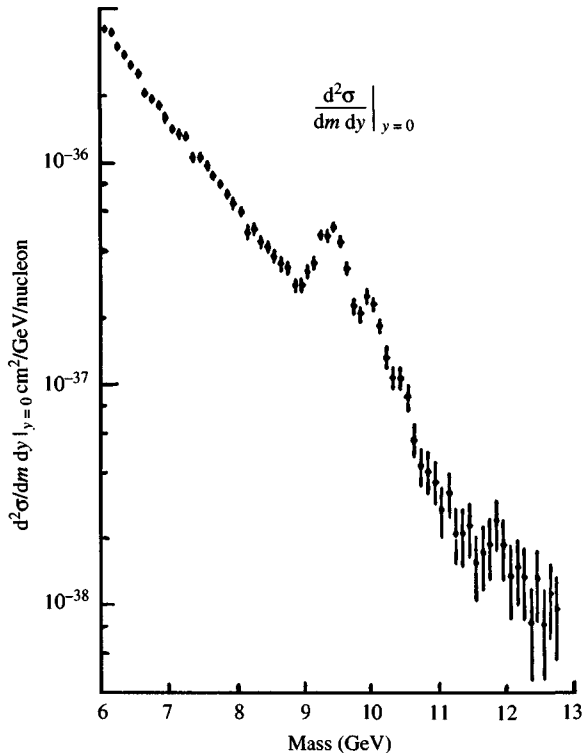


Fig. 11.18. Enhancement in the production cross-sections for  $\mu^+ \mu^-$  masses near 9.46  $\text{GeV}/c^2$ . (From Herb *et al.*, 1977.)

the region above the  $\Upsilon$  mass. The increase of  $R$  across the  $b\bar{b}$  threshold is compatible with the addition of a new flavour with  $Q_b^2 = \frac{1}{9}$ , but is too small to be compatible with a  $\frac{2}{3}$  charge assignment (see Fig. 11.1).

From Tables 11.4 and 11.6 we notice that the mass differences between the low lying members of the  $J/\Psi$  and  $\Upsilon$  families are very similar.

$$\left. \begin{aligned} m[\Upsilon_{2S}(10.02)] - m[\Upsilon_{1S}(9.46)] &= 0.560 \pm 0.003 \text{ GeV}/c^2 \simeq \\ &\simeq m[\Psi_{2S}(3685)] - m[J/\Psi_{1S}(3097)] = 0.585 \pm 0.003 \text{ GeV}/c^2, \\ m[\Upsilon_{3S}(10.36)] - m[\Upsilon_{1S}(9.46)] &= 0.90 \text{ GeV}/c^2 \simeq \\ &\simeq m[\Psi_{3S}(4040)] - m[J/\Psi_{1S}(3097)] = 0.95 \pm 0.02 \text{ GeV}/c^2. \end{aligned} \right\} \quad (11.10.2)$$

The application of non-relativistic dynamics to the description of the bottomonium system is quite successful and is discussed in Chapter 12.

The fact that there are three  $\Upsilon$  states below the  $B\bar{B}$  threshold, compared with the two  $J/\Psi$  states below  $D\bar{D}$ , is predicted in this model.

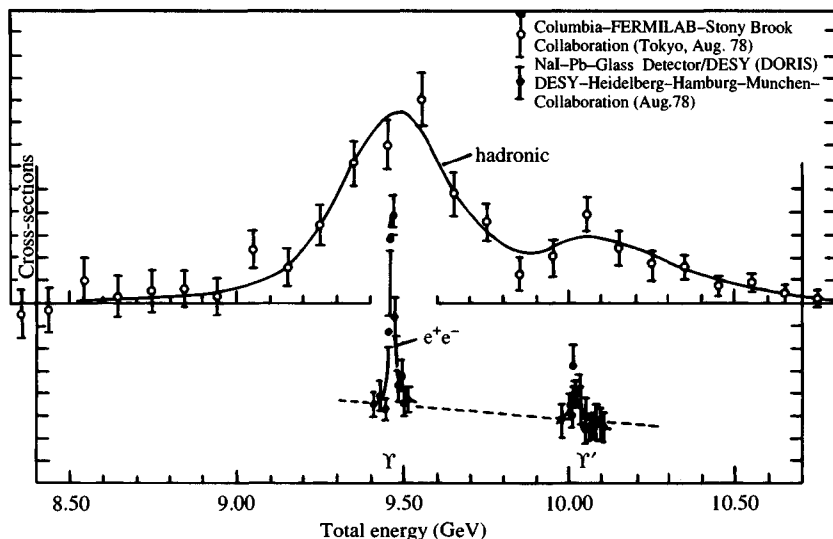


Fig. 11.19. Comparison of data on  $\Upsilon$  and  $\Upsilon'$  production in hadronic and in  $e^+e^-$  reactions. (From Flügge, 1978.)

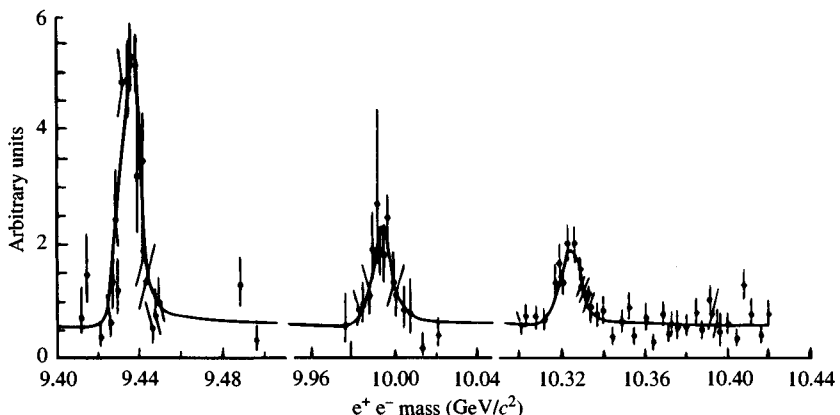


Fig. 11.20. The 'upsilon' family as seen at CESR.

Much information has been collected at CESR on the  $\chi_b$  and  $\chi'_b$  states, from the radial excitations of  $\Upsilon(1S)$  and  $\Upsilon(2S)$ , by studying the radiative transitions from the  $\Upsilon(3S)$ . The  $\chi'_b(2P)$  states were observed for the first time by CUSB (Han *et al.*, 1982; Eigen *et al.*, 1982).

Unlike the charmonium case, the hadronic widths of the  $\chi'_b$  states (see Table 11.6) are very narrow. An estimate of their hadronic widths has been given by using the  $E1$  rates calculated in potential models (Kwong and Rosner, 1988; Gupta *et al.*, 1984). Typical results are (Particle

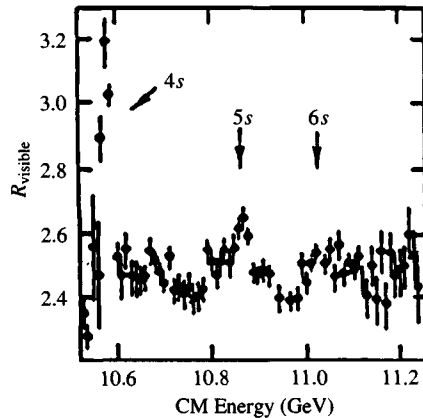


Fig. 11.21. The ratio  $R$  above bottom threshold from Lovelock *et al.* (1985).

Data Group, 1992)

$$\begin{aligned}\Gamma_{\text{had}}(\chi'_{b_2}) &= 100 \pm 12 \pm 16 \text{ keV}, \\ \Gamma_{\text{had}}(\chi'_{b_1}) &= 63 \pm 7 \pm 16 \text{ keV}, \\ \Gamma_{\text{had}}(\chi'_{b_0}) &= 396 \pm 135 \pm 76 \text{ keV},\end{aligned}\quad (11.10.3)$$

not inconsistent with QCD estimates.

Finally, there is great interest in the fact that the  $\Upsilon$ , even more so than the  $J/\Psi$  system, may be a natural source of ‘gluon jets’. This point will be mentioned in Chapter 25 but the idea is that the  $q\bar{q}$  system forming the  $\Upsilon$  family is sufficiently massive so that each of the three gluons into which the primary decay is supposed to occur will have sufficient momentum to materialize independently into hadrons which will then ‘remember’ the direction of their parent gluon. One should thus see events with three coplanar jets of hadrons.

# 12

## Hidden flavour bound states

The term *quarkonium* is used to denote any  $q\bar{q}$  bound state system in analogy to positronium in the  $e^+e^-$  system. But it is only for heavy quarks that a non-relativistic approach can be justified. In this chapter we deal with the charmonium and bottomonium states whose data was analysed in Chapter 11. We also briefly consider glueballs. There exist several good reviews on the subject (Berkelman, 1986; Kwong *et al.*, 1987; Lichtenberg, 1987; Schindler, 1986).

While the non-relativistic potential remains the most successful and simplest approach for calculating and predicting energy levels and decay rates, other, more sophisticated, methods have been devised including bag models, QCD sum rules (Shifman *et al.*, 1978; Reinders *et al.*, 1985) and lattice calculations (Rebbi, 1983; Creutz, 1983; Creutz *et al.*, 1983). The properties of quarkonia test some aspects of both perturbative and non-perturbative QCD; the heavier the quarkonium system, the less important are both relativistic effects and higher order perturbative QCD corrections. For a more recent approach to the problem of heavy flavours, see Isgur and Wise (1989, 1990) and for a comprehensive review, Neubert (1992).

### 12.1 Quarkonium

In this section we consider  $c\bar{c}$  and  $b\bar{b}$  bound states treated within the non-relativistic potential picture. Light quarks are excluded from our present considerations.

The picture incorporates ‘ideas’ of QCD and translates them into the familiar language of potential scattering by making the following assumptions:

- (i)  $c$  and  $b$  quarks are heavy, and so non-relativistic dynamics can be used to lowest order and relativistic corrections should be small;

- (ii) one-gluon exchange should dominate at small distances and the corresponding potential should behave like the Coulomb one, *i.e.* like  $1/r$  for small  $r$ ;
- (iii) at large distances the potential should be confining to comply with the assumption that quarks cannot appear as free particles;
- (vi) coupled channels may play an important role above  $D\bar{D}$  threshold where the decay becomes OZI allowed (Section 11.6);
- (v) annihilation into light particles is OZI suppressed.

If a potential is chosen, it is used in a wave equation and the solutions are obtained numerically in some approximation scheme. For most of the wave equations, the errors made in the numerical approximation are negligible. The sources of uncertainty are the lack of knowledge of the exact form of the potential and the lack of knowledge about what wave equation to use. Indeed, the very concept of a local potential is an approximation, and it is surprising that it works so well for quarkonium. The most commonly used wave equation is the non-relativistic Schrödinger equation.

However, relativistic effects are large in bound states containing at least one light quark, despite the superficial successes of some authors in correlating data with non-relativistic models. When relativistic effects are important, we do not really know what is the best wave equation to describe quarkonium states. The relativistic two-body problem with strong coupling remains an unsolved problem, and it may be that any attempt to deal with it without including virtual pair production can achieve only qualitative success. Relativistic effects are less important in heavy quarkonia, being about 20 to 30% in charmonium, and about 5 to 10% in bottomonium. Since we want to use quarkonium to learn something about the potential and to test QCD, we want to be as free as possible from uncertainties arising from relativistic effects. Clearly, of the known quarkonia, bottomonium is the best system to explore in detail.

### 12.1.1 The positronium analogy

Suppose we want to treat quarkonium using QCD. How do we go about it? Bound state problems cannot be treated by conventional perturbation theory. And so far, field theories can only be evaluated in perturbation theory. It seems as if there is a mismatch between field theory and the bound state problem.

Let us first recall how bound state problems like positronium are treated in the simpler theory of QED. First, we use perturbation theory to calculate a scattering amplitude between electron and positron. Then we identify a potential which will give the amplitude in Born approximation. Last, we substitute the potential in the wave equation, for example, the

Schrödinger equation and solve for the bound-state energy levels. To obtain decay rates, we again use perturbation theory to calculate transition matrix elements between the bound-state levels.

In lowest-order perturbation theory, the QED potential arises from one-photon exchange. This potential contains a static part (i.e. a velocity independent part), which is the Coulomb potential, and non-static corrections. These non-static terms are most commonly treated in the Fermi–Breit approximation, which gives the corrections to order  $v^2/c^2$ . The Fermi–Breit terms include a spin–spin interaction, a spin–orbit interaction, and a tensor interaction. They also include a spin-independent part which depends on the particle momenta.

### 12.1.2 The QCD potential

The procedure for obtaining the QED potential cannot be directly taken over into QCD to calculate the properties of quarkonium. The reason is that in contrast to QED, QCD is a non-Abelian field theory. Because of this, the running coupling of QCD is weak at very small distances between quarks (asymptotic freedom), but becomes strong at large interquark separations. Therefore, we can use lowest-order QCD perturbation theory to describe the quark–antiquark potential only at very small distances.

The value of  $r$  beyond which perturbative QCD cannot be used is determined by the confinement scale  $\Lambda$ , which is roughly 200 MeV, corresponding to about 1 fm. Unfortunately, however, the potential appears to deviate substantially from the lowest-order perturbative result (arising from one-gluon exchange) at considerably smaller distances, and is probably good at only  $r < 0.1$  fm. At somewhat larger distances we can use higher-order perturbative theory to calculate the potential, but at some distance perturbation theory breaks down. It is not easy to obtain the value of  $r$  for which the perturbation theory is no longer valid, but we roughly estimate it to be somewhat less than 0.3 fm. The size of a typical meson is greater than this, and therefore some knowledge of the interaction in the non-perturbative region is essential for understanding the basic properties of mesons.

Because the running coupling  $\alpha_s$  increases with increasing distance, it is believed that quarks are confined, and that if QCD could be evaluated non-perturbatively, it would predict confinement. So, unlike the case of QED, in QCD the *potential itself* must be calculated non-perturbatively at distances exceeding some critical value. We know how to make non-perturbative calculations only in various approximation schemes, perhaps the best justified of which is to put QCD on a lattice. It is important to stress that none of the approximation schemes used so far is mathe-

matically controlled because so far there is no way of making a reliable estimate of the errors.

The procedure for obtaining the potential in QCD is as follows: One divides the potential into two intervals of  $r$ . In the short-distance interval one uses QCD perturbation theory to calculate the potential. This may be done either analogously to the case of QED or by other suitable procedures. The resulting potential, which in lowest-order perturbation theory arises from one-gluon exchange, is a Coulomb potential plus Fermi–Breit corrections to order  $v^2/c^2$ .

In long-distance interval one calculates the potential in a model which is assumed to be a good approximation to QCD, usually in lattice QCD, but also in string and flux-tube models. One can use a smooth interpolating function for the transition region, smoothly join the non-perturbative potential to the perturbative one or simply add the perturbative and nonperturbative contributions.

If lattice QCD (see Section 27.2) is used to calculate QCD in the so-called ‘quenched’ or ‘valence’ approximation, one obtains a linear potential at large distances between quark and antiquark.

The potential between two static colour charges as derived by Stack (1984) in lattice calculations is shown in Fig. 12.1.

At smaller distances some lattice calculations give a  $1/r$  correction to the linear term. However, it is not clear that this represents the contribution from one-gluon exchange. In a string model, for example, transverse vibrations of the string give a  $1/r$  correction to a linear potential (Lüscher *et al.*, 1980).

The quenched approximation is one that neglects creation and annihilation of quark–antiquark pairs. Use of this approximation cannot be right, since at large distances it becomes energetically favourable to produce such pairs. Therefore, the potential concept breaks down. If quark–antiquark pairs are included, the time required to do a lattice calculation is very long with present techniques, and so far the calculation has been done only on lattices which are too small to give a reliable result.

It has been estimated that the present quarkonium data approximately determine the potential only within an interval

$$0.1 < r < 1 \text{ fm}.$$

Therefore, it is not clear that lowest-order QCD perturbation theory is at all relevant to the bound-state problem.

More precise data on both energy levels and decay rates, plus additional theoretical work, will be needed to get more information about the short-distance behaviour of the static potential. Experimental studies of the  $b\bar{b}$  system, being the heaviest observed so far, and therefore the most non-relativistic, can play an important role in giving us this information.

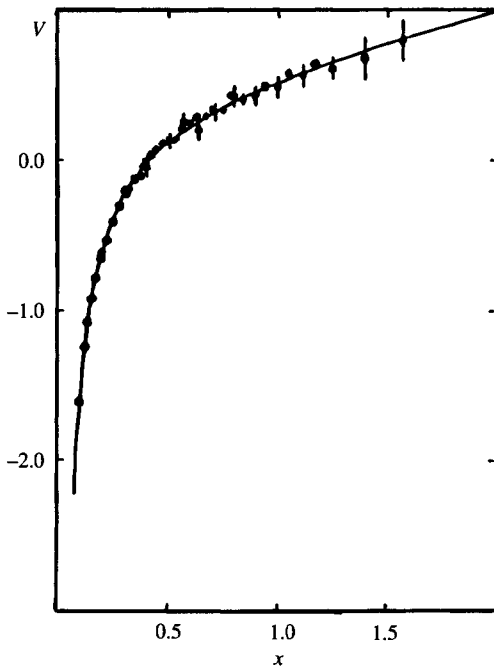


Fig. 12.1. The potential between static colour charges versus distance, in dimensionless lattice units. The points represent the Monte Carlo data of Stack (1984). The bold line corresponds to the linear plus Coulomb fit to the data.

The spin-dependent splitting of energy levels in bottomonium appears to be especially sensitive to the potential at short distances, and good measurements may enable us to obtain information at  $r < 0.1$  fm and to test perturbative QCD.

Many authors have computed corrections to the static QCD perturbative potential (Coulomb potential). The simplest correction is to let the coupling run in accordance with asymptotic freedom. Also, one-loop terms have been computed, for example, by Pantaleone *et al.* (1986). But, so far, even the Coulomb nature of the short-distance potential has not been established from quarkonium data, much less the nature of the higher-order corrections.

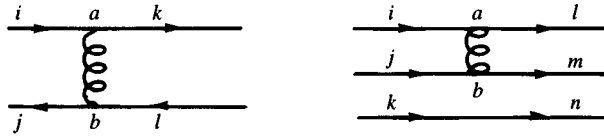
Phenomenologically, it appears as if the static potential is flavour independent to a good approximation. The static potential determined from QCD in lowest-order perturbation theory is also independent of quark flavour. The situation is more complicated for the non-perturbative part of the potential. In the quenched approximation the strength of the linear potential also appears to be independent of flavour, at least for sufficiently heavy quarks. A flavour-independent potential means that the same static

potential should be used to calculate the properties of all quarkonia, from lightest to heaviest. The most popular potential motivated by QCD is the Cornell potential (Eichten *et al.*, 1975, 1978 and 1980), which is a Coulomb plus linear potential. Another popular potential motivated from QCD is that of Richardson (1979) and many more potentials have been proposed. If a phenomenological potential is used, usually its parameters are fixed and applied to all quarkonia.

### 12.1.3 The strength of the potential

To see what coupling constant to use for the  $1/r$  potential, aside from replacing the fine structure constant  $\alpha$  by the effective coupling constant  $\alpha_s$ , we must work out how the colour  $SU(3)_C$  coupling is modified by the fact that quarks and gluons are coloured while hadrons are colour singlets.

The colour singlet  $q\bar{q}$  wave function  $\delta_{ij}/\sqrt{3}$  (where  $i, j$  label colours) corresponds to  $|q\bar{q}\rangle = (1/\sqrt{3}) \sum_i |q_i\bar{q}_i\rangle$  [see (11.5.4)] while colour singlet baryons are in a singlet totally antisymmetric state  $\varepsilon_{ijk}/\sqrt{6}$  corresponding to the wave function (11.5.3). The relevant gluon exchange diagrams, whose amplitudes yield the potential, are



so that the effective  $q\bar{q}$  coupling is

$$\begin{aligned} \alpha_s^{(\text{eff})}(q\bar{q}) &= \sum_{a,b} \sum_{ijkl} \frac{1}{\sqrt{3}} \delta_{ij} \left( \frac{\sqrt{\alpha_s}}{2} \lambda_{lj}^a \right) \left( -\frac{\sqrt{\alpha_s}}{2} \lambda_{ik}^b \right) \frac{1}{\sqrt{3}} \delta_{kl} \\ &= -\frac{\alpha_s}{12} \sum_{ab} \sum_{lj} \lambda_{jl}^a \lambda_{lj}^b = -\frac{\alpha_s}{12} \sum_{ab} \text{Tr} \lambda^a \lambda^b \\ &= -\frac{\alpha_s}{6} \sum_{ab} \delta_{ab} = -\frac{8}{6} \alpha_s = -\frac{4}{3} \alpha_s, \end{aligned} \quad (12.1.1)$$

where  $\lambda_{il}^a$  are the usual Gell-Mann  $SU(3)$  matrices (see Appendix 2.6 for the evaluation of traces).

In the  $qqq$  state we have

$$\begin{aligned} \alpha_s^{(\text{eff})}(qqq) &= \sum_{ab} \sum_{ijk} \sum_{lmn} \frac{\varepsilon_{ijk}}{\sqrt{6}} \left( \frac{\sqrt{\alpha_s}}{2} \lambda_{il}^a \right) \left( \frac{\sqrt{\alpha_s}}{2} \lambda_{jm}^b \right) \frac{\varepsilon_{lmn}}{\sqrt{6}} \delta_{kn} \\ &= \frac{\alpha_s}{24} \sum_{ab} \sum_{ijlm} \lambda_{il}^a \lambda_{jm}^b \sum_k \varepsilon_{ijk} \varepsilon_{lmk} \end{aligned}$$

and using

$$\sum_k \varepsilon_{ijk} \varepsilon_{lmk} = \delta_{il} \delta_{jm} - \delta_{im} \delta_{jl}$$

we get

$$\alpha_s^{(\text{eff})}(qqq) = \frac{\alpha_s}{24} \sum_{ab} \{ (\text{Tr } \lambda^a)(\text{Tr } \lambda^b) - (\text{Tr } \lambda^a \lambda^b) \} = -\frac{2}{3} \alpha_s. \quad (12.1.2)$$

Thus, in the case of interest, the one-gluon exchange potential at small distances will be

$$V_G(r)_{r \rightarrow 0} \simeq -\frac{4\alpha_s}{3r}. \quad (12.1.3)$$

The question of how the large distance confining potential should behave is a central one though it is not clear how meaningful it is. Recall that this corresponds to the large distance interaction between static sources: surely not the most accurate description of nature. Various suggestions have been made:

- (i) a linearly growing potential;
- (ii) a harmonic oscillator potential;
- (iii) a potential growing like  $r^\delta$  with the  $\delta$  between 0 and 2;
- (iv) a logarithmically growing potential.

The excited state levels for (a) purely Coulomb, (b) harmonic oscillator, and (c) Coulomb plus linearly rising potentials are shown in Fig. 12.2. Notice how the spectrum of the latter qualitatively resembles the experimental spectra, for instance, in the charmonium case.

General conditions (Martin, 1977; Grosse, 1977) on the confining part of the potential  $V_c(r)$  which ensure that the level spectrum has the experimentally found ordering of energy levels

$$E(1S) < E(1P) < E(2S) < E(1D) < \dots \quad (12.1.4)$$

have been worked out.

These conditions are

$$\left. \begin{aligned} \frac{d^3}{dr^3}(r^2 V_c) &> 0 \\ \frac{d}{dr} \left[ \frac{1}{r} \frac{d}{dr} \left( 2V_c + r \frac{dV_c}{dr} \right) \right] &< 0 \\ \lim_{r \rightarrow 0} \left[ 2rV_c + r^2 \frac{dV_c}{dr} \right] &= 0 \end{aligned} \right\} \text{for all } r. \quad (12.1.5)$$

Conditions (12.1.5) are satisfied by any long range potential of the form

$$V_c(r) \propto r^\delta \quad 0 < \delta < 2, \quad (12.1.6)$$

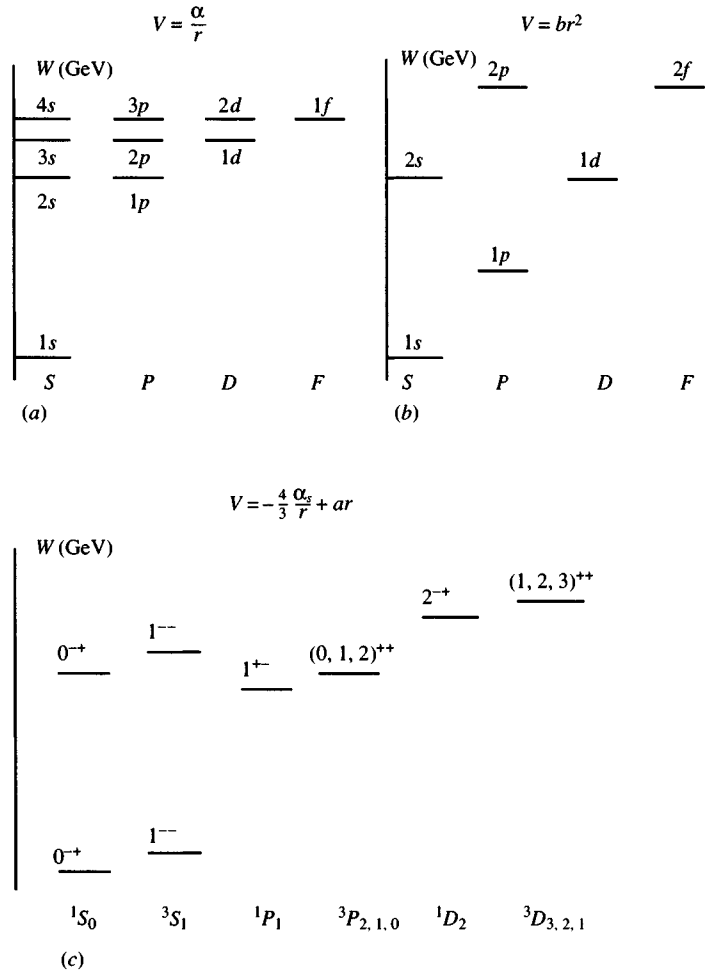


Fig. 12.2. Energy level scheme computed using (a) pure Coulomb potential  $V = \alpha/r$ , (b) harmonic oscillator potential  $V = br^2$ , (c)  $V = -\frac{4}{3}\alpha_s(m^2)/r + ar$ . (From Wiik and Wolf, 1978.)

as well as by logarithmic potentials

$$V_c(r) \propto \ln r. \quad (12.1.7)$$

It can be shown that the relative magnitude of the radial part of the  $1S$  and  $2S$  wave functions at the origin ( $r=0$ ) is controlled by the sign of  $V''(r)$ . Indeed,

$$V'' \geq 0 \text{ for all } r \Rightarrow \left| \frac{R_{2S}(0)}{R_{1S}(0)} \right| \geq 1. \quad (12.1.8)$$

From what we shall see later, it follows that

$$\left| \frac{R_{2S}(0)}{R_{1S}(0)} \right| < 1 \quad (12.1.9)$$

is demanded by the data on the leptonic decay widths, i.e. by  $\Gamma_e(\Psi'(3684)) < \Gamma_e(J/\Psi(3097))$ , so we shall demand  $V''(r) < 0$  for all  $r$ . Such a condition is always satisfied by a superposition of Coulomb plus linear potentials or Coulomb plus logarithmic potentials, but not by Coulomb plus  $r^\delta$  ( $1 < \delta < 2$ ) potentials.

Thus, either

$$V = -\frac{4}{3} \frac{\alpha_s}{r} + \frac{r}{a^2} \quad (12.1.10)$$

(where  $a \simeq 2 \text{ GeV}^{-1}$ ), or

$$V = -\frac{4}{3} \frac{\alpha_s}{r} + br^c \quad (0 < c < 1) \quad (12.1.11)$$

(where  $c \sim 0.1$ ), or

$$V = -\frac{4}{3} \frac{\alpha_s}{r} + k \ln r \quad (12.1.12)$$

(where  $k \simeq 0.7 \text{ GeV}$ ;  $r$  in units of  $\hbar c (\text{GeV})^{-1}$ ) seem to have the right qualities to comply with the experimental requirements.

#### 12.1.4 Spin dependence of the potential

Although the static quarkonium potential is flavour independent to a good approximation, nevertheless, the potential does contain flavour dependence in its non-static parts. These include both spin-dependent and spin-independent terms. We shall focus mainly on the spin-dependent corrections, as these are directly testable by measurements of the fine and hyperfine splittings in quarkonium.

To order  $v^2/c^2$ , the one-gluon-exchange contributions to the non-static potential are known as the Fermi–Breit terms. These Fermi–Breit terms include a spin–spin interaction, a spin–orbit interaction, and a tensor interaction. They go inversely as the square of one or the other of the quark masses or inversely as their product.

The existence of spin–spin, spin–orbit, and tensor interactions is well established by the quarkonium data. The heavier the quarks, the smaller the corrections arising from these non-static terms, but the splitting of energy levels arising from these terms is significant even in bottomonium.

The spin-dependent Fermi–Breit terms can give information about the Lorentz transformation properties of the potential. Most attention has

been focused on potentials, denoted by  $V$ , which transform as a component of a Lorentz four-vector (like the energy), and on potentials, denoted by  $S$ , which transform like a Lorentz scalar (like a mass). If  $V$  and  $S$  are inserted into a Bethe-Salpeter equation and a non-relativistic reduction is made to order  $v^2/c^2$ , one obtains generalized Fermi-Breit corrections to the static potential. These calculations have been made by a number of authors, for example, by Gromes (1977). See Lichtenberg (1987) for additional references.

In terms of  $V$  and  $S$ , the generalized Fermi-Breit spin-spin, spin-orbit, and tensor potentials are given by (for the equal-mass case)

$$\begin{aligned} V_S &= 2 \nabla^2 V \mathbf{S}_1 \cdot \mathbf{S}_2 / (3m^2), \\ V_{LS} &= \frac{1}{2m^2 r} \left( 3 \frac{dV}{dr} - \frac{dS}{dr} \right) \mathbf{L} \cdot \mathbf{S}, \\ V_T &= \frac{1}{12m^2} \left( \frac{1}{r} \frac{dV}{dr} - \frac{d^2 V}{dr^2} \right) S_{12}. \end{aligned} \quad (12.1.13)$$

The tensor operator is given by

$$S_{12} = 2 \left( \frac{\mathbf{S}_1 \cdot \mathbf{r} \mathbf{S}_2 \cdot \mathbf{r}}{r^2} - \mathbf{S}_1 \cdot \mathbf{S}_2 \right), \quad (12.1.14)$$

and has diagonal matrix elements only for  $L \neq 0$ . The expectation values of  $S_{12}$  in the  ${}^3P_2$ ,  ${}^3P_1$  and  ${}^3P_0$  states are  $-2/5$ ,  $2$ , and  $-4$  respectively. The matrix elements of  $\mathbf{L} \cdot \mathbf{S}$  in these same states are  $1$ ,  $-1$ , and  $-2$  respectively. A slightly more complicated form emerges for the case of unequal mass quarks (Pantaleone *et al.*, 1986).

One expects from lowest-order QCD that the short range part of the potential (which arises mainly from one-gluon exchange) is vector in character. On the other hand, lattice QCD calculations and some flux-tube models indicate that the confining potential is a scalar. The experimental evidence is not conclusive, but is consistent with this picture. If these ideas are correct, then there should not be any appreciable spin-spin splitting in quarkonium states with  $L > 0$  because in such states the wave function is small at short distances because of the centrifugal barrier. Measurements of the spin-spin splitting in  $L > 0$  states therefore provide important tests of QCD-motivated potentials.

### 12.1.5 Comparison with the data

Only a very brief account of the comparison of quarkonia predictions with the data will be possible and we shall confine ourselves to discussing the situation below threshold, i.e. to bound states.

A preliminary question is to what extent the non-relativistic scheme is adequate for  $q\bar{q}$  systems. As shown in Table 12.1, this seems quite

	Charm	Bottom
Mass	$1.5 \text{ GeV}/c^2$	$4.5 \text{ GeV}/c^2$
$\langle \beta^2 \rangle$	$\sim 0.20$	$< 0.1$
$\langle r^2 \rangle^{1/2}$	0.4 fm	0.2 fm
Number of bound states	8	$\sim 30$

Table 12.1.

safe for  $\bar{b}b$  states whereas the case may not be so clear cut for the  $c\bar{c}$  system. Table 12.1 gives the average  $\beta^2 = v^2/c^2$  and the mean square radii of the ground states. The number of bound states (i.e. states below the meson–antimeson production threshold) is also shown for both charm and bottom.

It is amusing that a similar computation for a toponium ( $\bar{t}t$ ) system taking  $m_t \sim 130 \text{ GeV}/c^2$  yields over 300 bound states!

Details of the various  $c\bar{c}$  and  $b\bar{b}$  states expected in quarkonia schemes are given in Figs. 12.3 and 12.4 respectively. The thresholds are shown by the shaded lines. Continuous lines denote states that have been experimentally observed whereas broken lines are theoretical predictions. Numbers above the states denote the principal quantum numbers.

It must be stressed that only the fine details depend on the specific choice of the potential. The qualitative picture is largely independent of which of the potentials discussed previously one actually uses.

The observed and expected transitions and decays for the charmonium states are shown in Fig. 12.5 whereas Fig. 12.6 exhibits separately the expected radiative and hadronic transitions in the  $b\bar{b}$  system.

Concerning the comparison of the spectra of Figs. 12.3 and 12.4 with the data (Tables 11.4 and 11.6) the agreement is generally good. It is excellent for the lower  $n^3S_1$  levels and for the mean values of the various  $P$  levels. In these cases, the predictions are, typically, within few  $\text{MeV}/c^2$  of the data. However, things become slightly worse when we go to higher and higher  $n$  quantum numbers (where coupled channel complications arise) or when spin splitting is considered. This is exemplified in Table 12.2 where the result of a best fit to energy level *differences* is given for bottomonium. Various different potentials are compared with the data. No potential had more than three parameters (two for the potential denoted ‘Indiana’) plus the bottom quark mass. Details can be found in Lichtenberg *et al.* (1989).

As a general strategy, one fits the parameters of the potential and the quark masses to the lowest states and then predicts the higher lying states;

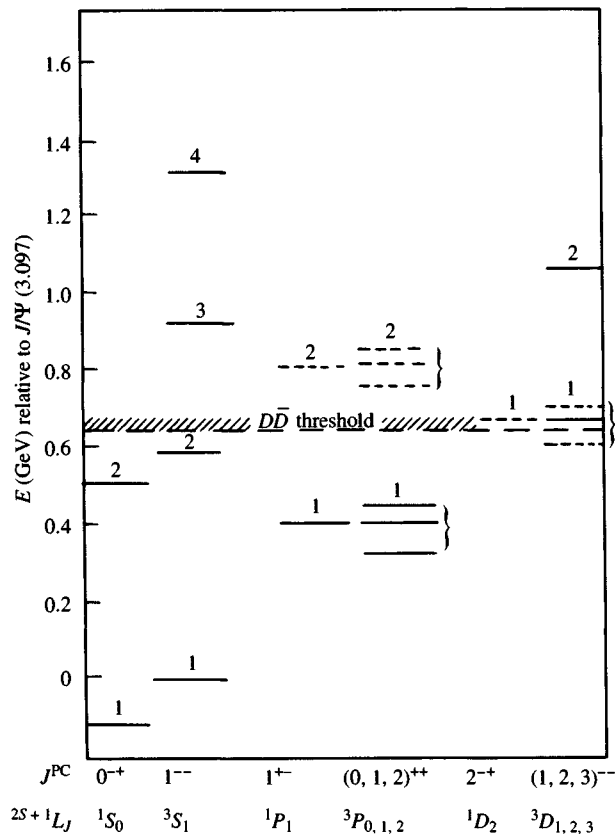


Fig. 12.3. Theoretical charmonium levels.

State	Experiment	Cornell	Indiana	Turin
$2S - 1S$	566 $\pm 4$	553	569	567
$3S - 1S$	900 $\pm 4$	891	902	901
$4S - 1S$	1124 $\pm 8$	1166	1157	1157
$5S - 1S$	1413 $\pm 12$	1407	1371	1373
$6S - 1S$	1568 $\pm 13$	1627	1558	1563
$1P - 1S$	450 $\pm 3$	454	445	447
$2P - 1P$	362 $\pm 3$	348	360	358

Table 12.2. Best fit to bottomonium energy level differences with various potentials. All figures in  $\text{MeV}/c^2$ .

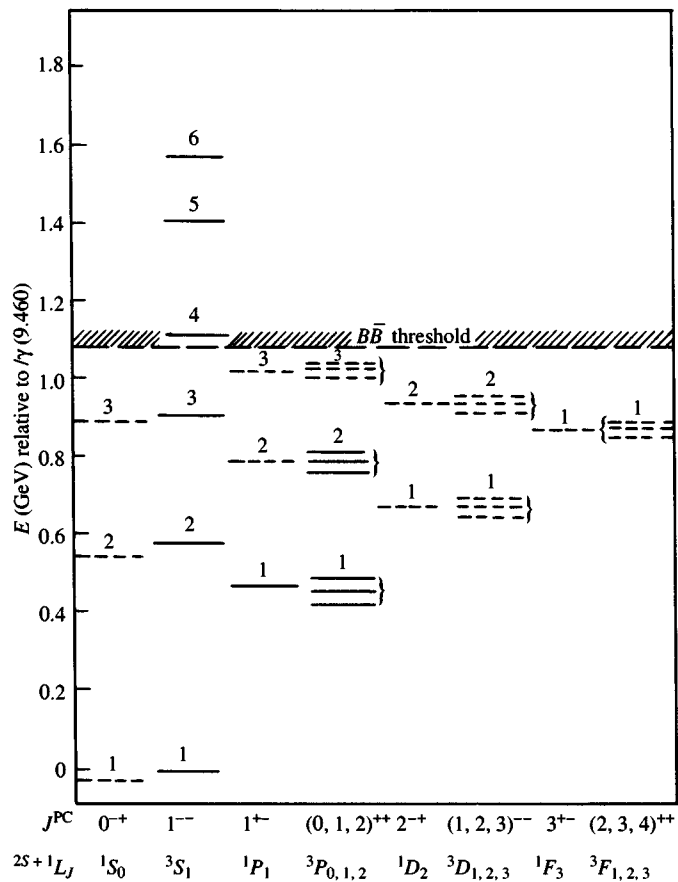


Fig. 12.4. Theoretical bottomonium levels.

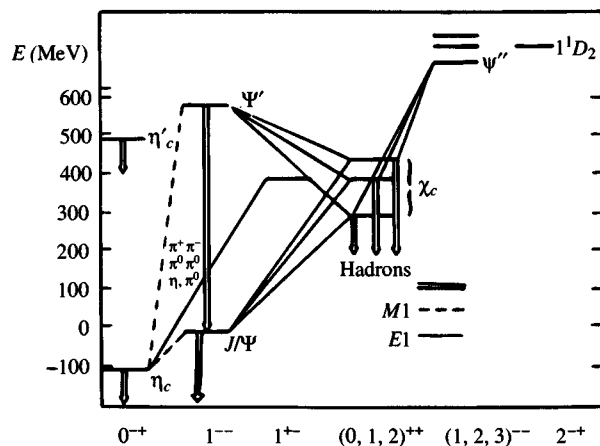


Fig. 12.5. Observed (double lines) and expected transitions and decays of charmonium states (from Schindler, 1986).

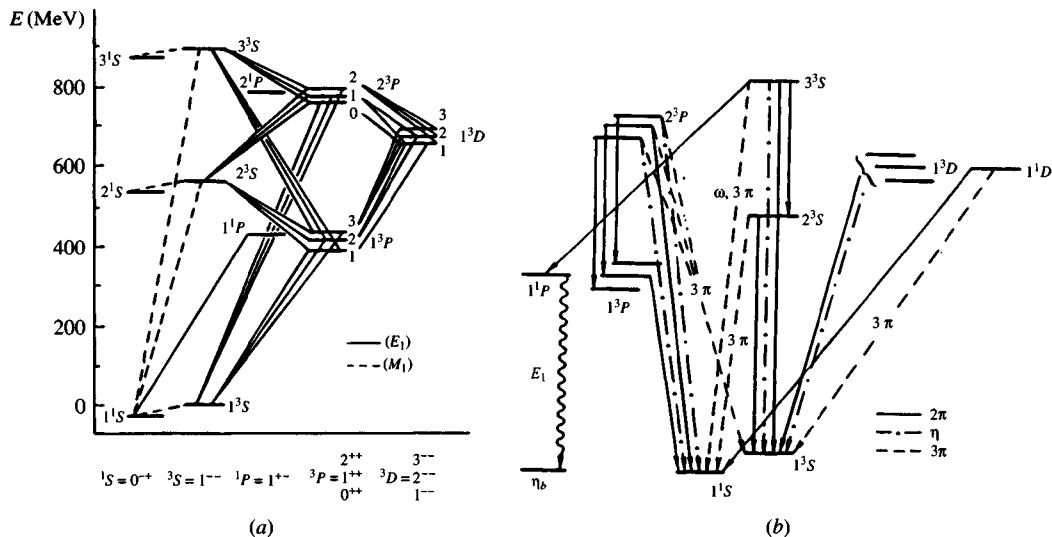


Fig. 12.6. (a) Expected radiative transitions in the  $b\bar{b}$  system; (b) same for hadronic transitions (from Schindler, 1986).

alternatively, a global fit to the data is performed (this was the procedure leading to Table 12.2). Often, the scheme is then extended to predict the spectrum of mesons having at least one heavy flavour; occasionally, it is even stretched to light quarks. Here, however, relativistic effects become important.

The same kind of approach has been applied with some success to baryon bound states (Godfrey and Isgur, 1985). The three-body calculations involved, however, demand further dynamical assumptions.

A few remarks concerning the spectrum of  $\chi$  states (Table 11.4) are necessary. The spectrum agrees very well with the hypothesis that the  $\chi$  states are the radial excitations of bound  $c\bar{c}$  or  $b\bar{b}$  pairs. Thus, the  $\chi$  states in  $e^+e^-$  collisions can only be reached from  ${}^3S_1$  states via  $E1$  electromagnetic transitions (e.g. the  $\chi_c$  states from the  $\Psi'(3685)$ , Fig. 12.5).  $M1$  transitions, on the other hand, are necessary to go from the  ${}^3S_1$  states to the pseudo-scalar  ${}^1S_0$  states (e.g. the  $\eta_c$ ).

Concerning the  $\eta_c$  it is worth recalling that it was originally located at 2830 MeV/ $c^2$ , an uncomfortably low value compared with the theoretical predictions. The present value, 2980 MeV/ $c^2$ , is very close to what is expected in the scheme discussed above.

The decay  $J/\Psi \rightarrow \gamma + \text{pseudo-scalar}$  gives a clear signal for the  $\eta_c(2980)$ . This is seen in Fig. 12.7 where the inclusive  $\gamma$  spectrum is shown (Bloom and Peck, 1983). The peak at 200 MeV arises from charged particles not tagged by the tracking system. The peaks at the endpoint are from

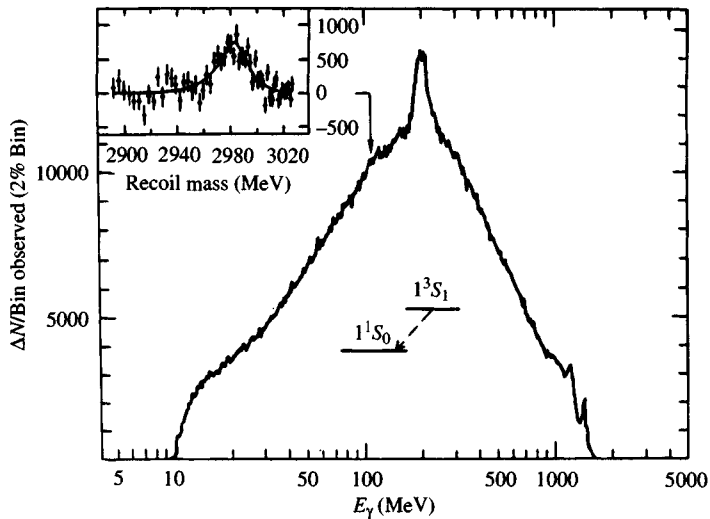


Fig. 12.7. Evidence for the  $\eta_c$  ( $1^1S_0$ ) in the inclusive  $\gamma$  spectrum at the  $J/\Psi$  ( $1^3S_1$ ).

$J/\Psi \rightarrow \gamma\eta'$  and  $J/\Psi \rightarrow \gamma\eta(1440)$  whereas the signals  $J/\Psi \rightarrow \gamma\eta$  and  $J/\Psi \rightarrow \gamma\pi^0$  have been removed by cuts. The region of the  $\eta_c$ , background subtracted, is displayed in the insert.

Note that radiative  $J/\Psi$  decays may be an ideal laboratory for glueball searches. This point will be briefly discussed in Section 12.4.

Thus far we have focused on the comparison with data below threshold, i.e. on bound states.

Above threshold, the situation is much more complex (see the data in Figs. 11.8 and 11.19). In this region a coupled channel approach is necessary and Fig. 12.8 shows a typical example of how each channel contributes to  $R$ .

For a detailed discussion of the merits and limitations of a potential approach and of its aspects (wave equations, relativistic effects, flavour dependence and ambiguities connected with spin dependence), see Lichtenberg *et al.* (1988 and 1989).

## 12.2 $J/\Psi$ decays. Calculation of the widths

By now several tens of millions of  $J/\Psi$ s have been analysed. The information on decay rates and angular distributions provides an ideal testing ground for models of  $q\bar{q}$  bound states.

In a non-relativistic fermion–antifermion bound state picture, the hadronic and leptonic decays can be mediated by both photons and gluons as shown in Fig. 12.9.

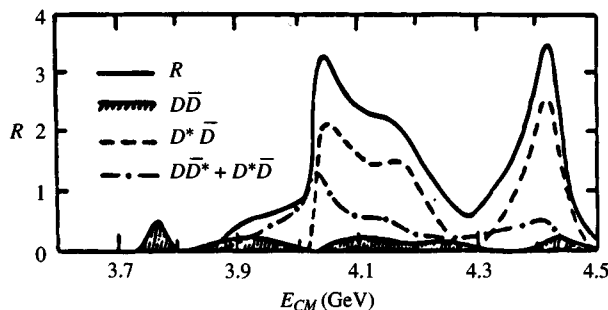


Fig. 12.8. The coupled channel calculation above charm threshold of Eichten *et al.* (1978).

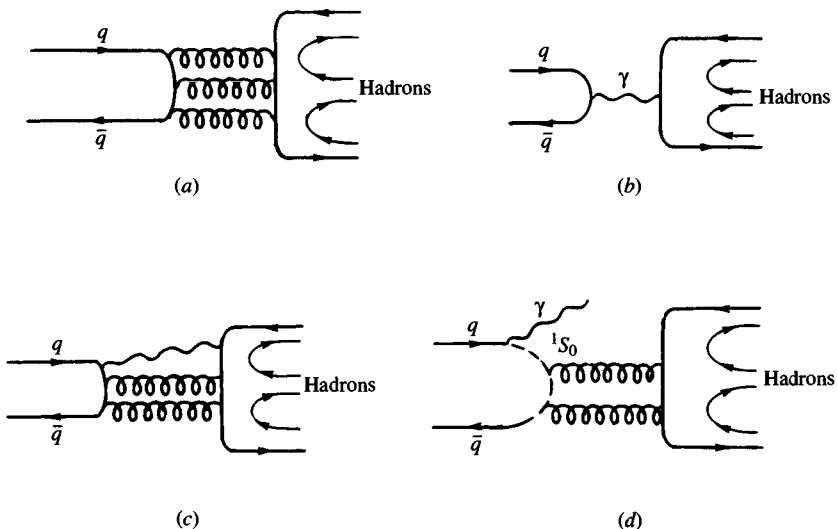


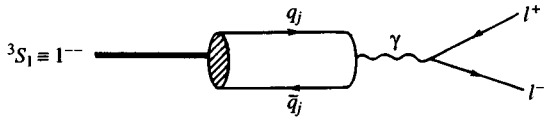
Fig. 12.9.

In particular, Fig. 12.9(a) represents the hadronic decay via  $q\bar{q}$  annihilation into three gluons, (b) the electromagnetic decay via  $q\bar{q}$  annihilation into a virtual photon, (c) the vector meson radiative decay via  $q\bar{q}$  annihilation into a photon and two gluons and (d) the magnetic dipole transition to the  $q\bar{q}^1S_0$  state [the  $\eta_c(2980)$  in the  $c\bar{c}$  case] followed by annihilation into two gluons.

We shall return to this point later (Section 12.5.1) but it is worth pointing out here the particular importance of Fig. 12.9(d). Should a resonance peak be observed in the energy distribution of the inclusive photon or in the mass of the hadronic final state, this would be an unequivocal signal for a glueball, i.e. for a flavourless bound state made of two gluons.

For decay into a leptonic  $l^+l^-$  pair, only diagram (b) occurs. According to the Van Royen–Weisskopff approach (1967a, b), in the above scheme the decay width can be computed once the magnitudes of the bound state wave functions at the origin are known. For the hadronic widths one also needs the conversion rate for gluons into hadrons. We shall continue to assume that gluons materialize into hadrons with unit probability without paying any attention to the questions that this assumption raises.

The leptonic width for a non-relativistic  $q\bar{q}$  system in a vector  $1^{--}$  state of mass  $M_v$  to decay into  $l^+l^-$  via one (virtual) photon,



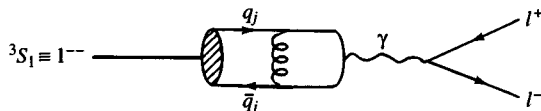
as will be explained below, is given by (Appelquist *et al.*, 1978; Krammer and Kraseman, 1979).

$$\Gamma(n^3S_1 \rightarrow l^+l^-) = 16\pi\alpha^2 Q_j^2 \frac{|\psi_n(0)|^2}{M_v^2} \left(1 + \frac{2m_l^2}{M_v^2}\right) \left(1 - \frac{4m_l^2}{M_v^2}\right)^{\frac{1}{2}}.$$

Ignoring terms like  $m_l^2/M_v^2$  one has

$$\Gamma(n^3S_1 \rightarrow l^+l^-) = 16\pi\alpha^2 Q_j^2 \frac{|\psi_n(0)|^2}{M_v^2}, \quad (12.2.1)$$

where  $M_v$  is the mass of the vector particle in the  $n^3S_1$  state, and  $Q_j$  is the charge of the relevant quark (in units of  $e$ ).  $\psi_n(0)$  is the non-relativistic wave function of the bound  $q\bar{q}$  system at the origin. If, in (12.2.1),  $\psi_n$  is the *exact* wave function, then (12.2.1) is the whole story. Sometimes, however,  $\psi_n$  is calculated approximately by using just the long range, confining part of the potential. In that case one should add corrections, involving gluon exchange, that correspond to the *short* range part of the interaction, as shown:



If ' $\psi_n$ ' is the approximate wave function, then in (12.2.1) the factor  $|\psi_n(0)|^2$  can be corrected into  $|\psi'_n(0)|^2(1 - \frac{16}{3}\alpha_s/\pi)$ . The correction factor, in this approach, is uncomfortably large. The relativistic kinematic terms, which are ignored in (12.2.1), are likely to be relevant only for decay into  $\tau^+\tau^-$  pairs.

Note that compared with the analogous case of QED [for a detailed derivation of (12.2.1) in the QED case see Jauch and Rohrlich (1955)] a colour factor of 3 has been taken into account in writing (12.2.1).

Let us sketch how one can derive (12.2.1). The quantity we are interested in is the decay rate from the state  $\Psi$  to a final state  $f$ , i.e. the modulus squared  $\Gamma_\Psi = |A_\Psi|^2$  of the corresponding transition amplitude

$$A_\Psi = \langle f | T | \Psi \rangle. \quad (12.2.2)$$

Normally, when computing the cross-section  $\sigma(p)$  for a process like  $q\bar{q} \rightarrow f$  one utilizes plane wave states for the initial particles. In that case, the relevant transition amplitude is

$$A(p) = \langle f | T | p \rangle. \quad (12.2.3)$$

But, by completeness, the transition amplitude of interest is

$$A_\Psi = \sum_p \langle f | T | p \rangle \langle p | \Psi \rangle = \int d^3p A(\mathbf{p}) \hat{\psi}(\mathbf{p}), \quad (12.2.4)$$

where  $\hat{\psi}(\mathbf{p})$  is the momentum space wave function corresponding to the state  $|\Psi\rangle$ .

We shall see in a moment that for our case

$$A(p) \simeq A = \text{constant} \quad (12.2.5)$$

for the range of  $p$  involved, in which case

$$\begin{aligned} A_\Psi &= A \int d^3p \hat{\psi}(\mathbf{p}) \\ &= A \int d^3p \int \frac{e^{i\mathbf{p}\mathbf{r}}}{(2\pi)^{3/2}} \psi(\mathbf{r}) d^3r \\ &= (2\pi)^{3/2} A \psi(0), \end{aligned} \quad (12.2.6)$$

so that the transition rate we are interested in is given by

$$\Gamma_\Psi = |A_\Psi|^2 \simeq (2\pi)^3 |A|^2 |\psi(0)|^2. \quad (12.2.7)$$

We now compute  $|A|^2$ . With incoming plane waves we have

$$\Gamma(p) \equiv |A(p)|^2 = \frac{v}{(2\pi)^3} \sigma_{q\bar{q} \rightarrow l^+l^-} \quad (12.2.8)$$

where  $\sigma_{q\bar{q} \rightarrow l^+l^-}$  is the spin averaged cross-section and  $v$  is the relative quark velocity (expected to be small) and  $v/(2\pi)^3$  is the flux factor.

If we neglect the lepton mass, the  $q\bar{q} \rightarrow l^+l^-$  cross-section as given by the following diagram:



is given by (see Appendix 1)

$$\sigma_{q_j\bar{q}_j \rightarrow l^+l^-} = \frac{\pi\alpha^2 Q_j^2 k}{sp} \left( 1 + \frac{v^2}{3} + \frac{4m^2}{s} \right). \quad (12.2.9)$$

where  $p$  and  $k$  are the CM momenta of the quarks and the leptons respectively,  $s$  is the usual squared CM energy and  $m$  is the mass of the constituent quark.

For fairly small momentum (12.2.9) yields

$$|A|^2 \equiv \Gamma(p) = \frac{v}{(2\pi)^3} \sigma_{q\bar{q} \rightarrow l^+l^-}(p) \simeq \frac{\pi\alpha^2 Q_j^2}{(2\pi)^3 m^2}, \quad (12.2.10)$$

which is indeed independent of momentum.

The actual transition rate, with  $\Gamma_\Psi$  given by (12.2.7) and (12.2.10), is then

$$\Gamma_\Psi = \frac{4\pi\alpha^2 Q_j^2}{M_v^2} |\psi(0)|^2, \quad (12.2.11)$$

where use has been made of  $M_v \simeq 2m$ .

We now recall that the result (12.2.9) for  $q\bar{q} \rightarrow l^+l^-$  involves an average over four initial spin states. These may be considered as consisting of three spin-triplet states and one singlet, of which only the former contributes on account of the  $J = 1$  photon exchange. For the spin 1 ( $J/\Psi$  or  $\Upsilon$ ) only the triplet initial state occurs and so we must multiply (12.2.11) by  $\frac{4}{3}$ . In addition there is a factor 3 needed to account for the colour. With these factors (12.2.11) reduces to (12.2.1).

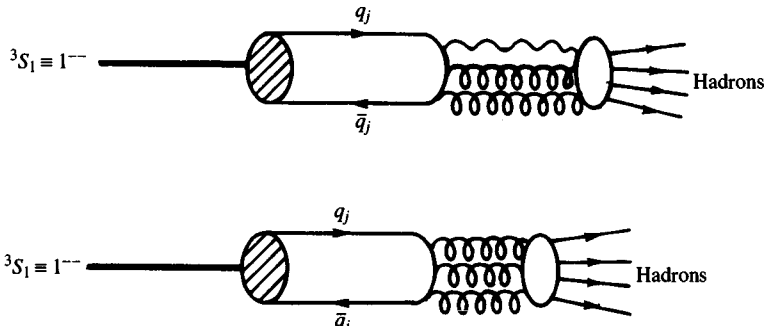
Concerning eqn (12.2.1), an inherent ambiguity is the mass to be used in the denominator on the RHS. Should it be  $M_v^2$  or  $(2m_q)^2$ ? Therefore, predictions of *ratios* of rates should be more reliable than absolute rates (Kwong *et al.*, 1987).

Going back to the general problem of decay via gluons and/or photons, we first recall that one-gluon exchange is not allowed by colour conservation. Neither two-photon nor two-gluon transitions are allowed, as already explained (Section 11.6) so the next lowest order annihilation into processes of a  $1^{--}$  state can occur via  $1\gamma 2G$ ,  $3G$ , and  $3\gamma$ .

The annihilation into  $3\gamma$  is negligibly small, but its calculation for orthopositronium (Jauch and Rohrlich, 1955) allows us to write down the width for the  $1\gamma 2G$  and  $3G$  cases by simply taking care of colour factors. Thus for an  $n^3S_1$ ,  $q_j\bar{q}_j$  decay one finds

$$\Gamma(n^3S_1 \rightarrow 3\gamma) = \frac{64}{3}(\pi^2 - 9)\alpha^3 Q_j^6 \frac{|\psi_n(0)|^2}{M_v^2}. \quad (12.2.12)$$

For the  $1\gamma 2G$  and  $3G$  diagrams



one finds

$$\Gamma(n^3S_1 \rightarrow 1\gamma 2G) = \frac{128}{9}(\pi^2 - 9)\alpha Q_j^2 \alpha_s^2 \frac{|\psi_n(0)|^2}{M_v^2}. \quad (12.2.13)$$

$$\Gamma(n^3S_1 \rightarrow 3G) = \frac{160}{81}(\pi^2 - 9)\alpha_s^3 \frac{|\psi_n(0)|^2}{M_v^2}. \quad (12.2.14)$$

where  $\psi_n$  is the wave function for the particular  $n^3S_1$  state under consideration.

As discussed above, perturbative QCD effects can be incorporated by replacing  $|\psi_n(0)|^2$  by  $|'\psi_n(0)'|^2$  and multiplying by

$$(1 - 12.6\alpha_s/\pi), (1 - 0.9\alpha_s/\pi) \text{ and } (1 + 4.9\alpha_s/\pi), \quad (12.2.15)$$

in eqns. (12.2.12), (12.2.13) and (12.2.14) respectively.

The lowest order annihilation processes for the pseudo-scalar states  $n^1S_0$  (or  $0^{-+}$ ) are into  $2\gamma$  or  $2G$  and the results are

$$\Gamma(n^1S_0 \rightarrow 2\gamma) = 48\pi\alpha^2 Q_j^4 |\psi_n(0)|^2 / M_v^2 \quad (12.2.16)$$

and

$$\Gamma(n^1S_0 \rightarrow 2G) = \frac{32}{3}\pi\alpha_s^2 Q_j^4 |\psi_n(0)|^2 / M_v^2. \quad (12.2.17)$$

The results (12.2.13), (12.2.14), (12.2.16) and (12.2.17) are less accurate than (12.2.1). In the present case of decay into several particles the  $q\bar{q}$  interaction is not strictly point-like. Its range is likely to be of order  $1/m_c$ , where  $m_c$  is the charmed quark mass. On the other hand, the size of charmonium is about 1 fm. Since 1 fm  $\gg 1/m_c$  it is not too bad an approximation to use the value  $\psi_n(0)$  of the wave function at the origin.

The relative factor between the  $2G$  and the  $2\gamma$  rates coming from colour is given to lowest order by

$$\frac{\Gamma_{2G}}{\Gamma_{2\gamma}} = \frac{\alpha_s^2}{\alpha^2 Q_j^4} \frac{1}{9} \sum_{ab} \left| \text{Tr} \left( \frac{\lambda_a}{2} \frac{\lambda_b}{2} \right) \right|^2 = \frac{\alpha_s^2}{\alpha^2 Q_j^4} \times \frac{2}{9}.$$

Similarly, the conversion factor between the  $3G$  and  $3\gamma$  decay involves a sum over colour indices of the trace of the symmetric combination of  $\lambda_a \lambda_b \lambda_c$  which is the only one to have negative  $C$ -parity as was pointed out in Section 11.6. One has then

$$\frac{\Gamma_{3G}}{\Gamma_{3\gamma}} = \frac{\alpha_s^3}{\alpha^3 Q_j^6} \frac{1}{9} \sum_{a,b,c} \left| \text{Tr} \left( \frac{\lambda_a}{2} \left\{ \frac{\lambda_b}{2}, \frac{\lambda_c}{2} \right\} \right) \right|^2 = \frac{5}{54} \frac{\alpha_s^3}{\alpha^3 Q_j^6}.$$

The assumption that gluons convert into hadrons with unit probability of course implies that, whenever in the previous formulae ‘gluons’ are produced, they really must be interpreted as the production of ‘hadrons’.

Radiative gluon corrections are expected in the previous formulae.

Many other decay rates are similarly obtained. Sum rules and bounds have also been worked out and we refer to the literature (Köpke and Weremes, 1989) for a detailed account of the subject as well as for a comparison with the measured transition rates.

Particularly interesting are the following ratios which will be used to estimate the value of  $\alpha_s$  in the next section.

From (12.2.1), (12.2.14) and (12.2.15) we get

$$\begin{aligned} \frac{\Gamma(^3S_1 \rightarrow 3G)}{\Gamma(^3S_1 \rightarrow e^+e^-)} &\simeq \frac{10}{81} \frac{\pi^2 - 9}{\pi} \frac{\alpha_s^3}{\alpha^2 Q_j^2} \left( 1 + 10.2 \frac{\alpha_s}{\pi} \right) \\ &\simeq \frac{4}{9} \times 1440 \times \frac{\alpha_s^3}{Q_j^2} \left( 1 + 10.2 \frac{\alpha_s}{\pi} \right). \end{aligned} \quad (12.2.18)$$

Similarly,

$$\frac{\Gamma(^3S_1 \rightarrow 1\gamma 2G)}{\Gamma(^3S_1 \rightarrow e^+e^-)} \simeq \frac{8}{9} \frac{\alpha_s^2}{\alpha \pi} (\pi^2 - 9) \left( 1 + 4.4 \frac{\alpha_s}{\pi} \right). \quad (12.2.19)$$

### 12.3 Determination of $\alpha_s$

The results of the previous section can be used to estimate the value of the strong coupling  $\alpha_s$ . From the diagrams of Fig. 12.9 the total hadronic width of any  ${}^3S_1$  states can be written

$$\Gamma_h = \Gamma_h(3G) + \Gamma_h(1\gamma) + \Gamma_h(1\gamma 2G) + \Gamma_h({}^1S_0 2G). \quad (12.3.1)$$

Now the width into  $l^+l^-$  is given by the analogue of Fig. 12.9(b) for the production of a  $q_j \bar{q}_j$  pair. Thus allowing for the quark charges and colour and summing over quark flavour we expect

$$\Gamma_h(1\gamma) = \sum_j \Gamma({}^3S_1 \rightarrow q_j \bar{q}_j).$$

For the  $J/\Psi$  we have

$$\Gamma_h^{J/\Psi}(1\gamma) = 3\Gamma(^3S_1 \rightarrow l^+l^-) \sum_j Q_j^2 \quad (12.3.2)$$

$$= 2\Gamma(J/\Psi \rightarrow l^+l^-) \quad (12.3.3)$$

$$= (10.72 \pm 0.58) \text{ keV from Table 11.4} \quad (12.3.4)$$

Now according to Partridge *et al.* (1980), measurements of the  $J/\Psi$  inclusive  $\gamma$  spectrum indicate that  $\Gamma(J/\Psi \rightarrow \eta_c\gamma) = (0.94 \pm 0.29)$  keV, which suggests that the diagram Fig. 12.9(d) is negligible. Hence we get for the  $J/\Psi$

$$\Gamma_h(3G) + \Gamma_h(1\gamma 2G) \simeq \Gamma_h - 2\Gamma(J/\Psi \rightarrow l^+l^-), \quad (12.3.5)$$

i.e.

$$\frac{\Gamma(J/\Psi \rightarrow 3G)}{\Gamma(J/\Psi \rightarrow l^+l^-)} + \frac{\Gamma(J/\Psi \rightarrow 1\gamma 2G)}{\Gamma(J/\Psi \rightarrow l^+l^-)} \simeq \frac{\Gamma_h}{\Gamma(J/\Psi \rightarrow l^+l^-)} - 2 \quad (12.3.6)$$

where

$$\Gamma_h = \Gamma_{\text{total}} - \Gamma(J/\Psi \rightarrow e^+e^-) - \Gamma(J/\Psi \rightarrow \mu^+\mu^-). \quad (12.3.7)$$

Using eqns (12.2.18) and (12.2.19) with  $Q_j^2 = 4/9$  and Table 11.4 yields an equation for  $\alpha_s(M_{J/\Psi}^2)$ , from which one obtains

$$\alpha_s(M_{J/\Psi}^2) \simeq 0.16. \quad (12.3.8)$$

With this value of  $\alpha_s$  from (12.2.13) and (12.2.14) one finds

$$\left. \frac{\Gamma(1\gamma 2G)}{\Gamma(3G)} \right|_{J/\Psi} \simeq 10\% \quad (12.3.9)$$

implying that, as expected, the largest contribution to the decay into hadrons comes from Fig. 12.9(a).

Making similar assumptions at the  $\Upsilon(9640)$  eqn (12.3.2) now gives

$$\Gamma_h^\Upsilon(1\gamma) = 3\Gamma(\Upsilon \rightarrow l^+l^-) \sum_{j=u,d,s,c} Q_j^2 \quad (12.3.10)$$

$$= (4.5 \pm 0.1) \text{ keV from Table 11.6.} \quad (12.3.11)$$

Repeating the above analysis, but taking  $Q_j^2 = 1/9$  in eqns (12.2.18) and (12.2.19) eventually leads to

$$\alpha_s(M_\Upsilon^2) = 0.15. \quad (12.3.12)$$

This implies, via (12.2.13) and (12.2.14),

$$\left. \frac{\Gamma(1\gamma 2G)}{\Gamma(3G)} \right|_\Upsilon \simeq 3\%. \quad (12.3.13)$$

Similar arguments using LEP data at the  $Z^0$  peak suggest  $\alpha_s(M_Z^2) = 0.12$ .

The above value of  $\alpha_s$  is compatible with a slow running of  $\alpha_s(k^2)$  with  $k^2$ . However, if we use the standard QCD formula

$$\alpha_s(k^2) = \frac{12\pi}{(33 - 2N_f) \ln(k^2/\Lambda^2)} \quad (12.3.14)$$

the above variation corresponds to  $\Lambda \approx 50$  MeV, a value somewhat lower than suggested by deep inelastic scattering data.

A possible cause for this discrepancy could be the neglect of relativistic corrections (Consoli, private communication). A crude estimate of these can be found in Kwong *et al.* (1987). Actually, in the absence of a reliable calculation of these effects, we can only make a qualitative assessment. From Table 12.1, we see that relativistic corrections could change branching ratios by some 20% at the  $J/\Psi$ . In this case, from (12.2.18), which goes as  $\alpha_s^3$ , we see that the determination of  $\alpha_s$  at the  $J/\Psi$  may be modified by about 7%. We can then ascribe a theoretical uncertainty due to relativistic corrections alone of the order of

$$\Delta\alpha_s|_{\text{rel}} \simeq 0.01 \quad (J/\Psi)$$

$$\Delta\alpha_s|_{\text{rel}} \simeq 0.003 \quad (\Upsilon)$$

This, however, is not enough to account for the above mentioned discrepancy.

Note that the above estimates are very much to be taken with a pinch of salt given the large uncertainties in the analysis.

If we blindly repeat the same calculation for the  $\phi$  decay (which is *a priori* dangerous) we get a very rough estimate of  $\alpha_s(M_\phi^2) = 0.4 - 0.6$ .

These results suggest that perturbation theory is probably safe at the  $\Upsilon$  and perhaps at the  $J/\Psi$  but certainly not at the  $\phi$ .

## 12.4 Leptonic widths

An interesting empirical feature concerning the leptonic widths of all the vector mesons (ground states of each family), old and new, was noticed by Sakurai (1978). For the decay of a vector meson made of  $q_j\bar{q}_j$

$$\Gamma(^3S_1 \rightarrow e^+e^-)/\langle Q_j^2 \rangle = \text{const.} \simeq 12 \text{ keV} \quad (12.4.1)$$

where  $\langle Q_j^2 \rangle$  is the mean squared charge. Table 12.3 shows the evidence for this.

This rule can be interpreted as support for the assignments  $Q_c = \frac{2}{3}$ ,  $Q_b = -\frac{1}{3}$ .

	$\Gamma_e$ (keV)	Quark content	$\langle Q_j^2 \rangle$	$\Gamma_e/Q_j^2$ (keV)
$\rho$	$6.77 \pm 0.32$	$\frac{1}{\sqrt{2}}(u\bar{u} - d\bar{d})$	$\left  \frac{1}{\sqrt{2}} \left( \frac{2}{3} + \frac{1}{3} \right) \right ^2 = \frac{1}{2}$	$13.54 \pm 0.64$
$\omega$	$0.60 \pm 0.02$	$\frac{1}{\sqrt{2}}(u\bar{u} + d\bar{d})$	$\left  \frac{1}{\sqrt{2}} \left( \frac{2}{3} - \frac{1}{3} \right) \right ^2 = \frac{1}{18}$	$12.00 \pm 0.04$
$\phi$	$1.37 \pm 0.05$	$s\bar{s}$	$\left  \frac{1}{3} \right ^2 = \frac{1}{9}$	$12.33 \pm 0.45$
$J/\Psi$	$4.72 \pm 0.35$	$c\bar{c}$	$\left  \frac{2}{3} \right ^2 = \frac{4}{9}$	$10.6 \pm 0.7$
$\Upsilon$	$1.34 \pm 0.04$	$b\bar{b}$	$\left  -\frac{1}{3} \right ^2 = \frac{1}{9}$	$12.1 \pm 0.4$

Table 12.3.

Equation (12.4.1) used in (12.2.1) would imply that

$$|\psi_n(0)|^2 \propto M_v^2 \quad (12.4.2)$$

and the question arises as to what kind of potential would produce it. As argued below, a potential of the form  $V(r) = A(m)r^\delta$ , where  $m$  is the mass of the particle in the potential, will give

$$|\psi_n(0)|^2 \simeq [mA(m)]^{3/(\delta+2)}. \quad (12.4.3)$$

We use the Heisenberg uncertainty relation,  $\Delta r \Delta p \simeq 1$ , to estimate the ground state energy  $\langle E \rangle = \langle p^2/2m \rangle + \langle V(r) \rangle$ . To do this we put  $\langle V(r) \rangle = A\langle r^\delta \rangle \simeq A(\Delta r)^\delta$  and  $\langle p^2/2m \rangle \simeq (\Delta p)^2/2m$  and then minimize  $\langle E \rangle$  with respect to  $\Delta r$ . The result is

$$\langle E \rangle_{\min} \propto A(m)m^{-\delta(\delta+2)} \quad (12.4.4)$$

with

$$\Delta r_{\min} \propto [m\delta A(m)]^{-1/(\delta+2)}. \quad (12.4.5)$$

For an  $S$ -state,  $|\psi(0)|^2 \neq 0$  and  $|\psi(r)|^2$  decreases with  $r$  so, for a normalized wave function, we have approximately

$$|\psi(0)|^2 \propto \Delta r^{-3} \simeq [mA(m)]^{3/(\delta+2)}. \quad (12.4.6)$$

Although very crude, this method gives the correct dependence on the particle mass for essentially any non-pathological potential at least for the ground state. To the extent that we can further assume that the mass of the bound state is roughly twice the mass of the constituent quark and that the form of the potential does not change in ranging from the  $\varrho$  to the  $\Upsilon$ , we can compare the result (12.4.3) with the empirical form (12.4.1).

We see that no mass independent ( $A(m) = \text{constant}$ ) confining ( $\delta > 0$ ) potential can give the  $M_v^2$  growth suggested by (12.4.1). A logarithmic potential yields a result comparable with  $\delta = 0$ , i.e. an  $M_v^{3/2}$  growth and could simulate the data (Quigg and Rosner, 1977a, b).

## 12.5 Exotics: glueballs, hybrids, etc.

Among flavourless states, a special role is played by glueballs ( $G\bar{G}$  bound states) and hybrid states ( $q\bar{q}G$ ), i.e. states which can exist only because gluons attract each other because of their non-Abelian colour charge. These states are predicted in QCD as a consequence of its non-Abelian character and their unambiguous identification would be an important step towards proving that QCD is *the* theory of strong interactions. Glueballs, as singlet states of both  $SU(3)_C$  and  $SU(3)_F$  are not only colourless and flavourless, but also they are charge neutral and have no isospin. The combinations of  $J^{PC}$  allowed for each state are listed in Table 12.4 from Köpke and Wermes (1989). Notice that if gluons are massless, the states marked by an asterisk are forbidden by Yang's theorem (Landau, 1948; Yang, 1950) and a  $0^{+-}$  hybrid is allowed only with one unit of angular momentum between the  $q\bar{q}$  and the  $G$ . States with quantum numbers inaccessible to  $q\bar{q}$  are particularly interesting, providing an unequivocal signature for an exotic bound state.

Predictions for glueball masses have been made in all approaches: lattice calculations, QCD sum rules, bag models, effective Lagrangians and potential models. There is an extensive literature on the subject; see Köpke and Wermes (1989).

Theoretical predictions for the masses of those glueballs, which have been most intensively searched for, are shown in Fig. 12.10.

One can make a naive estimate of the production rate for the various species of particles, mesons ( $M$ ), hybrids ( $H$ ) and glueballs ( $\mathcal{G}$ ) by simply counting powers of  $\alpha m$  and strong coupling constants (Chanowitz, 1987).

$$\left\{ \begin{array}{l} \Gamma(^3S_1 \rightarrow \gamma\mathcal{G}) \sim O(\alpha\alpha_s^2); \quad \Gamma(^3S_1 \rightarrow \gamma H) \sim O(\alpha\alpha_s^3) \\ \Gamma(^3S_1 \rightarrow \gamma M) \sim O(\alpha\alpha_s^4); \quad \Gamma(^3S_1 \rightarrow MH) \sim O(\alpha_s^5) \\ \Gamma(^3S_1 \rightarrow MM') \sim O(\alpha_s^6); \quad \Gamma(^3S_1 \rightarrow MG) \sim O(\alpha_s^6) \end{array} \right. \quad (12.5.1)$$

The experimental situation is still extremely controversial. We mention

$J^{PC}$	$q\bar{q}$	$qq\bar{q}\bar{q}$	$q\bar{q}G$	$GG$	$GGG$
$0^{++}$	x	x	x	x	x
$0^{+-}$		x	x		x
$0^{-+}$	x	x	x	x	x
$0^{--}$		x	x		x
$1^{++}$	x	x	x	x*	x
$1^{+-}$	x	x	x		x
$1^{-+}$		x	x	x*	x
$1^{--}$	x	x	x		x
$2^{++}$	x	x	x	x	x
$2^{+-}$		x	x		x
$2^{-+}$	x	x	x	x	x
$2^{--}$	x	x	x		x

Table 12.4.

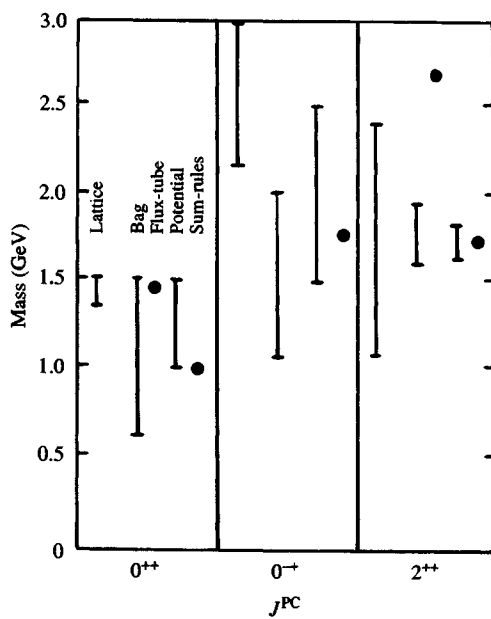


Fig. 12.10. Some predicted glueball masses.

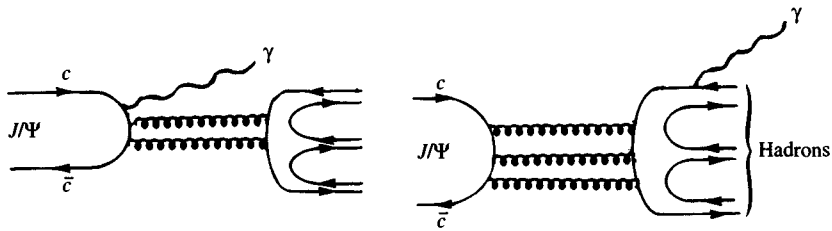


Fig. 12.11.

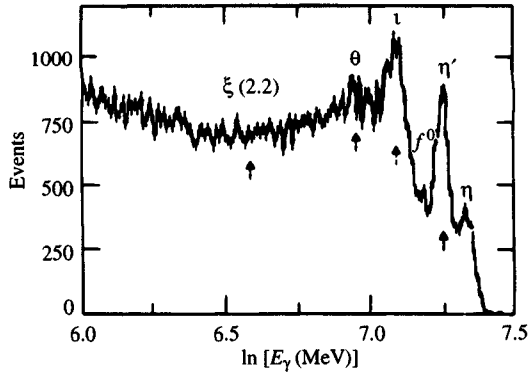


Fig. 12.12. Inclusive measurement of  $J/\Psi \rightarrow \gamma + X$ . The distribution is not normalized. The particle names label the regions where resonances should appear.

only those aspects of the quest for glueballs which are directly connected with the narrow resonances, namely the radiative  $J/\Psi$  decays.

As already mentioned, radiative  $J/\Psi$  decay is the type of reaction where evidence for glueballs might be particularly clean. The  $\gamma$  energy spectrum in

$$J/\Psi \rightarrow \gamma + X \quad (12.5.2)$$

would then show a peak corresponding to glueballs dominating the diagrams of Fig. 12.11.

In Fig. 12.12 we show Crystal Ball results for the reaction (12.5.2) (Bloom, 1982, 1985).

As can be seen, not all the resonances for which there is evidence are glueball candidates. But some are, noticeably the most famous glueball candidates, the pseudo-scalar  $\iota(1440)$ , now renamed  $\eta(1440)$  by the Particle Data Group, with  $I^G(J^{PC}) = 0^+(0^-)$ , and the tensor  $\theta(1690)$ , now renamed  $f_2(1720)$ , with  $I^G(J^{PC}) = 0^+(2^{++})$ .

The evidence for glueball states is clearly not conclusive from Fig. 12.12, but shows the potential power of the radiative decay approach and this is the reason why the new experiment E852 with its great capability for detecting neutral (gammas) as well as charged particles should soon change the perspective about glueballs. For an updating on glueballs, see Burchell (1992).

## 12.6 $\Psi' \rightarrow \varrho\pi$ : a puzzle

In the quarkonium picture the width for the hadronic decays  $J/\Psi \rightarrow \varrho\pi$  and  $\Psi' \rightarrow \varrho\pi$  are dominated by the diagram Fig. 12.9(a) on account of (12.3.9). There are two unknown factors involved in calculating these widths:  $|\psi_n(0)|^2$  and the probability  $\mathcal{P}_{\varrho\pi}^{3G}$  for  $3G$  to materialize as a  $\varrho\pi$  state. In forming branching ratios the factor  $|\psi_n(0)|^2$  cancels out. Moreover it seems very reasonable to assume

$$\mathcal{P}_{\varrho\pi}^{3G}|_{M_{J/\Psi}} \approx \mathcal{P}_{\varrho\pi}^{3G}|_{M_{\Psi'}}. \quad (12.6.1)$$

Then we would expect

$$\begin{aligned} \frac{B(\Psi' \rightarrow \varrho\pi)}{B(J/\Psi \rightarrow \varrho\pi)} &= \frac{B(\Psi' \rightarrow 3G)}{B(J/\Psi \rightarrow 3G)} \\ &= \frac{\Gamma(\Psi' \rightarrow e^+e^-)}{\Gamma_{\text{tot}}(\Psi')} \frac{\Gamma_{\text{tot}}(J/\Psi)}{\Gamma(J/\Psi \rightarrow e^+e^-)} \end{aligned} \quad (12.6.2)$$

where we have used the fact that

$$\Gamma(n^3S_1 \rightarrow 3G) = \text{constant} \times \Gamma(n^3S_1 \rightarrow e^+e^-), \quad (12.6.3)$$

the constant being independent of  $n$ .

Using Table 11.4 we then find from (12.6.2)

$$\left. \frac{B(\Psi' \rightarrow \varrho\pi)}{B(J/\Psi \rightarrow \varrho\pi)} \right|_{\text{theory}} = (12.8 \pm 2.4)\% \quad (12.6.4)$$

to be compared with the measured ratio of branching fractions

$$\left. \frac{B(\Psi' \rightarrow \varrho\pi)}{B(J/\Psi \rightarrow \varrho\pi)} \right|_{\text{expt.}} < 0.006 \text{ at } 90\% CL. \quad (12.6.5)$$

Such an enormous discrepancy between theory and experiment is disastrous; but, interestingly, a nice escape route exists (Brodsky et al., 1987). The trouble may be a signal for the existence of a glueball state of mass  $M_G$  close to the  $J/\Psi$  (Freund and Nambu, 1975). Looked at this way it is the  $J/\Psi \rightarrow \varrho\pi$  width that is enhanced by the nearby resonance. The calculated ratio of branching fractions (12.6.4) should now be multiplied

by Breit–Wigner type factors

$$\frac{(M_{J/\Psi} - M_G)^2 + \Gamma_G^2/4}{(M_{\Psi'} - M_G)^2 + \Gamma_G^2/4}. \quad (12.6.6)$$

For example, the reasonable choice

$$M_G = 3.0 \text{ GeV}/c^2, \quad \Gamma_G = 140 \text{ MeV} \quad (12.6.7)$$

turns the result (12.6.4) into the acceptable value 0.004. A similar problem exists for the decays into  $K^*\bar{K}$ . These are, perhaps, indirect evidence for a glueball state.

## 12.7 Conclusions

The quarkonium approach seems to provide a reasonable description of the levels and decays of the  $J/\Psi$  and  $\Upsilon$  families. There is even some hope that perturbative QCD effects can be detected.

On the experimental side it may come as a surprise to learn that despite  $\approx 20$  million  $J/\Psi$  decays it is believed that only some 25% of all hadronic decay channels have been identified. Similarly, for the radiative decays, some 50% of the modes may still be unidentified. The situation should improve dramatically with the high luminosity ( $5 \times 10^{30} \text{ cm}^{-2}\text{s}^{-1}$ ) and small energy spread ( $\Delta E \approx 0.6 \text{ MeV}$ )  $e^+e^-$  collider BEPC in Beijing. A similar situation is envisaged for the  $\Upsilon$  when the  $B$ -meson factories now under discussion are built.

# 13

## Open heavy flavours

The subject of heavy flavours has expanded tremendously in recent years stretching from the ‘static’ properties (mainly spectroscopy, i.e. energy levels, lifetimes, branching ratios, decays, mixing etc.) of hadrons with one or more heavy quarks, e.g. bottom or charm, to more dynamical properties (like fragmentation, structure functions, jets etc.) and on to more exotic topics, e.g. production and decay of as yet undiscovered flavours like top, or speculations on a fourth generation or implications on Higgs or on non-standard effects and so on.

Some of these topics are covered in other chapters (for energy levels, see Chapters 11 and 12; for Kobayashi–Maskawa matrix elements and CP violation, see Chapters 18 and 19; for structure functions, see Chapters 16 and 17). Here we discuss the discovery of particles with heavy flavours, their lifetimes, decays, mixing and other properties. For more detailed discussions, we refer to the specialized literature (see e.g. Ellis and Kernan, 1990, Kühn *et al.*, 1989 and references therein).

We note that if the electromagnetic and strong interactions conserve flavour, then we should expect ‘associated production’ of heavy flavours, i.e. that production always occurs with pairs of particles of opposite charm or bottom (this is, of course, *not* the case for production in neutrino interactions via *weak forces*). Further, the decay of a heavy particle should be generated by the weak interactions, implying very narrow widths and effects of parity non conservation.

The absence of  $D^0 - \bar{D}^0$  mixing will be mentioned in Section 13.2.3 and Chapter 19 and is in agreement with the non-existence of charm-changing *neutral* currents (as expected from the GIM mechanism, see Chapter 9). The decays, therefore, are due to the charged weak current. Nonetheless  $B^0 - \bar{B}^0$  mixing is not negligible, as we will see, and this has important consequences for CP violation (see Chapter 19).

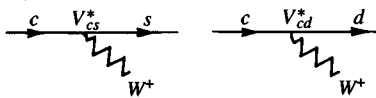


Fig. 13.1. Charm quark transitions in the standard model.

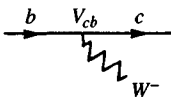


Fig. 13.2. Bottom quark transition in the standard model.

### 13.1 Discovery and basic properties of charm and bottom particles

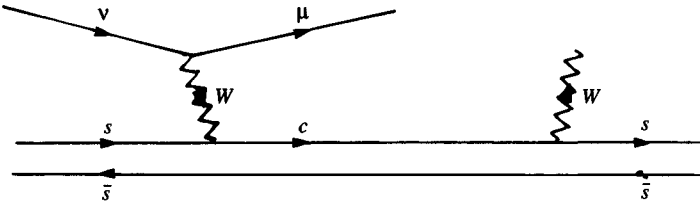
In terms of quark diagrams (Fig. 13.1), a charm particle will decay into ordinary hadrons, according to the standard model, via the dominant quark transitions (see Section 9.2)

$$c \rightarrow V_{cs}^* s + V_{cd}^* d \simeq s \cos \theta_C - d \sin \theta_C. \quad (13.1.1)$$

The transition  $c \rightarrow s + W^+$  occurs with a strength proportional to  $\cos \theta_C$  and is therefore a Cabibbo allowed transition (Chapter 1) whereas  $c \rightarrow d + W^+$  is Cabibbo suppressed being proportional to  $\sin \theta_C$ .

Thus, in general terms, we expect charm particle decays to be signalled by the detection of one strange particle in the decay debris. By analogy, bottom decays predominantly via  $b \rightarrow c + W^-$  (Fig. 13.2). (Its ‘allowed’ mode as discussed in Chapters 9 and 19 would be  $b \rightarrow t + W$  but this is not permitted energetically.) In this case also, production of strange particles is expected.

Of course production of two strange particles can occur through the interaction with one strange quark from the sea via the process



This process proceeds via a Cabibbo allowed transition and, although it is depressed by comparison with an interaction with a valence quark,

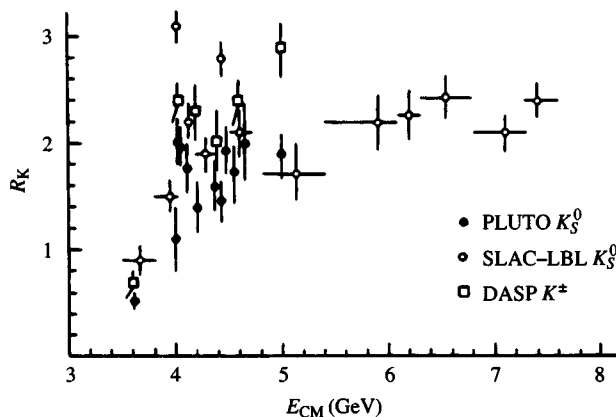
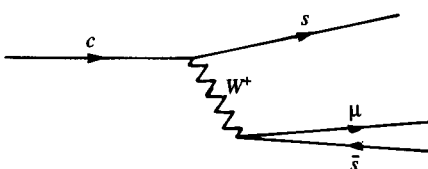


Fig. 13.3. Ratio of cross-sections for  $e^+e^- \rightarrow K^0X$  and the sum of cross-sections for  $e^+e^- \rightarrow K^\pm X$  to the cross-section for  $e^+e^- \rightarrow \mu^+\mu^-$ . (From Wiik and Wolf, 1978.)

its overall rate is comparable with that of a Cabibbo forbidden reaction such as coming from



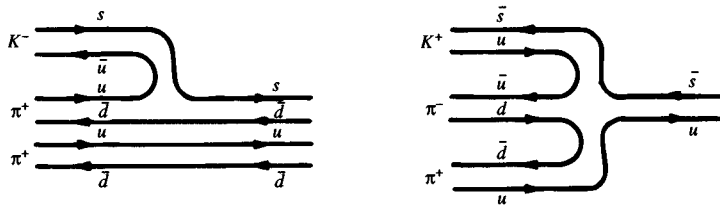
These decays have been seen.

The predicted increase of strange particle yield above the charm threshold is indeed borne out by the data on inclusive  $K^0$  and  $K^\pm$  production in  $e^+e^-$  interactions. In Fig. 13.3 the ratios

$$\begin{aligned} R_{K^0} &= 2\sigma(e^+e^- \rightarrow K^0X)/\sigma(e^+e^- \rightarrow \mu^+\mu^-) \text{ and} \\ R_{K^\pm} &= \sigma(e^+e^- \rightarrow K^\pm X)/\sigma(e^+e^- \rightarrow \mu^+\mu^-) \end{aligned}$$

are plotted as functions of the CM energy [ $\sigma(e^+e^- \rightarrow K^\pm X)$  being the sum of the inclusive  $K^+$  and  $K^-$  cross-sections].

On the basis of the previous mechanism, one expects  $D^+ (= c\bar{d})$  decay into  $K^-\pi^+\pi^+$ , but not into  $K^+\pi^+\pi^-$  since  $s$  has strangeness  $-1$ . The former is what used to be called an ‘exotic’ meson state (meaning that it is not reducible to a combination of ordinary  $q\bar{q}$ , i.e. light quarks) whereas the latter is ‘non-exotic’.



According to ‘pre-charm’ prejudices, the non-exotic channel should have been much more favoured, whereas experimentally the opposite occurs, in agreement with the prediction from mechanism (13.1.1).

These exotic channels have provided the first direct evidence (Goldhaber *et al.*, 1976) for ‘naked’ charm, i.e. for particles with charm quantum number different from zero, in  $e^+e^-$  collisions at SPEAR.

Fig. 13.4 shows early evidence for the ‘exotic’ decay  $D^+ \rightarrow K^-\pi^+\pi^+$  and the absence of any signal in the ‘non-exotic’ channel  $K^+\pi^+\pi^-$ .

In May 1976 a narrow neutral state called  $D^0$  was observed at 1863 MeV/ $c^2$  through its decay into  $K^-\pi^+$  and  $K^-\pi^-\pi^+\pi^+$ . In terms of the previous diagrams this corresponds to a hadronic decay of charm according to the scheme of Fig. 13.5 where the  $W^+$  converts into a  $q\bar{q}$  pair ( $u\bar{d}$ ).

After some claim of baryon charm decay seen at Fermilab the first actual complete reconstruction of a charm baryon event has come from leptonic (neutrino induced) reactions (Angelini *et al.*, 1979) at CERN where all the momenta have been measured and the particles identified, allowing the determination of both the proper decay time and mass. The event corresponds to the decay of the charm baryon  $\Lambda_c^+(ucd)$

$$\Lambda_c^+ \rightarrow p K^- \pi^+. \quad (13.1.2)$$

The decay time measured was

$$t_{\Lambda_c} \simeq (7.3 \pm 0.1) \times 10^{-13} \text{ seconds} \quad (13.1.3)$$

and the mass was determined to be

$$m_{\Lambda_c} = 2290 \pm 15 \text{ MeV}/c^2. \quad (13.1.4)$$

which is consistent with the presently accepted value (Particle Data Group, 1992)

$$m_{\Lambda_c} \simeq 2284.9 \pm 0.6 \text{ MeV}/c^2. \quad (13.1.5)$$

If we use the elementary process  $c \rightarrow s + \ell^+ + \nu_e$  as an approximate way to estimate the lifetime of  $\Lambda_c$ , we can apply the same formulae as for  $\mu$ -decay (4.2.33) and we get

$$\tau_c \simeq (\text{BR})_\ell \left( \frac{m_\mu}{m_c} \right)^5 \tau_\mu. \quad (13.1.6)$$

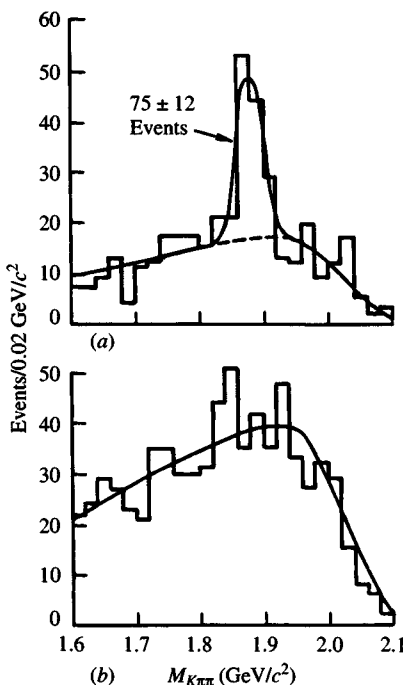


Fig. 13.4. (a) Evidence for the decay  $D^+ \rightarrow K^-\pi^+\pi^+$  and (b) absence of a signal for  $D^+ \rightarrow K^+\pi^+\pi^-$ . (From Goldhaber *et al.*, 1976.)

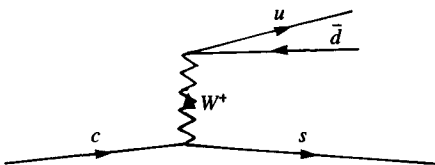


Fig. 13.5. Leading contribution to  $c \rightarrow u\bar{d}s$  decay.

If we take  $m_c \simeq 1600 \text{ MeV}/c^2$  for the charm quark mass, the presently established  $\Lambda_c$  lifetime ( $\simeq 1.9 \times 10^{-13} \text{ s}$ , see Table 13.1) is obtained with  $(\text{BR})_\ell = \Gamma_\ell/\Gamma_{\text{tot}} \simeq 0.07$ , not an unreasonable value.

The first indirect evidence for bottom production was seen in 1980 at CESR (CLEO, 1980; Franzini, 1981).

Fig. 13.6 shows how the value of  $R$ , in crossing the  $\Upsilon(4s)$  peak at  $\sqrt{s} \approx 10.55 \text{ GeV}$ , rises by about 0.33 signalling the production of a new flavour with charge  $\frac{1}{3}$ . The detailed reconstruction of  $B$  meson decays is extremely difficult and was first achieved by the Argus and the CESR groups in 1987 (ARGUS, 1987b; CLEO, 1987).

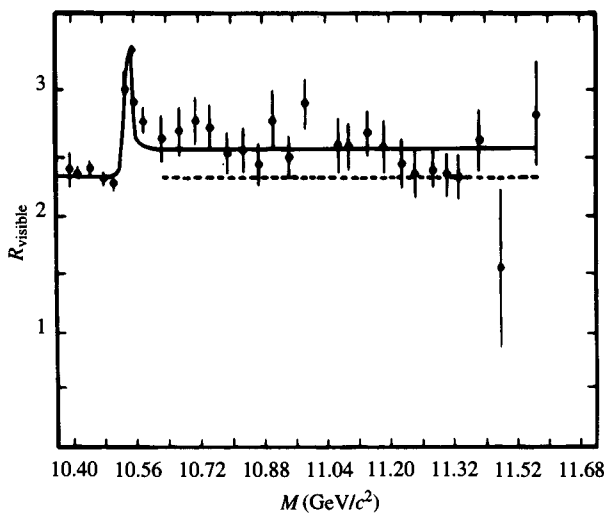


Fig. 13.6.  $R_{\text{visible}}$  just below and above the flavour threshold. CUSB data.

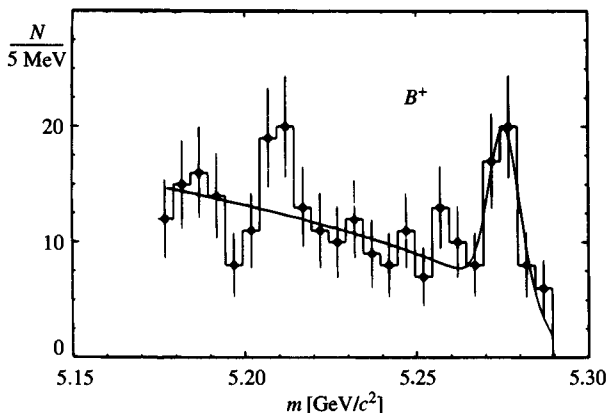


Fig. 13.7. Mass distribution of  $B^\pm$  candidates.

Amongst others the following channels were studied:

$$\begin{aligned}\bar{B}^0 &\rightarrow D^{*+}\pi^-, \quad D^{*+}\pi^-\pi^0, \quad D^{*+}\pi^-\pi^-\pi^+ \\ B^- &\rightarrow D^{*+}\pi^-\pi^-, \quad D^{*+}\pi^-\pi^-\pi^0.\end{aligned}$$

As an example Fig. 13.7 shows the mass distribution in channels occurring in charged  $B$  decays. The clear  $B$ -peak at  $5275.8 \pm 1.3 \pm 3.0$  MeV/ $c^2$  is evident. It is found that  $B_s$  decay predominantly into charm mesons, in agreement with the decay mechanism illustrated in Fig. 13.2.

Since the first observations, data on charm and bottom particles have accumulated rapidly. A summary of data is given in Table 13.1 (for

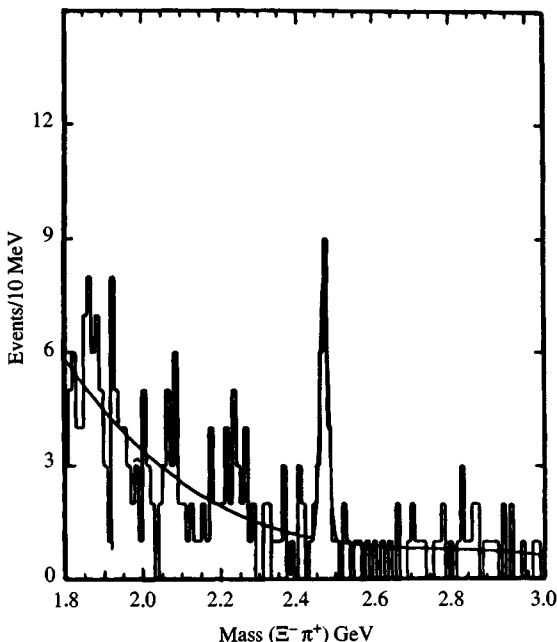


Fig. 13.8. CLEO data showing the  $\Xi_c^0$  in  $\Xi^- \pi^+$  mass combinations (from Morrison, 1990).

charm) and Table 13.2 (for bottom). Another example of evidence of a charm particle is given in Fig. 13.8 with the CLEO data showing the  $\Xi_c^0(dsc)$  in the  $\Xi^- \pi^+$  mass combination (Morrison, 1990).

As far as the masses are concerned, the techniques discussed in Chapter 12 give quite accurate results. Much less satisfactory is the situation concerning the theoretical prediction of the lifetimes, as we will discuss later.

Although we shall not give details of the wave functions of the various multiplets,  $SU(4)_F$  for charm and  $SU(5)_F$  for bottom mesons and baryons (for  $SU(4)$  see Lichtenberg, 1978), the quark content of each baryon is specified in Tables 13.1 and 13.2. All the charm mesons expected (both pseudo-scalar and vector) have been found, but the list is far from complete for both charm baryons and bottom hadrons. For the masses of the as yet undiscovered hadrons, rather precise predictions are available in some cases (see e.g. Godfrey and Isgur, 1985) or inequalities have been derived (see e.g. Anselmino *et al.*, 1990a). There is also a rather interesting approach which tries to connect ground state energy levels of baryons to those (much better known) of mesons (Basdevant *et al.*, 1990).

We draw attention in Tables 13.1 and 13.2 to the large difference between the lifetimes of non-strange charged and neutral charm mesons. We shall return to this point in Section 13.2.1.

### 13.1.1 Detection of heavy flavours

Several techniques have been devised to identify charm and bottom hadrons, such as: (a) invariant mass peaks, (b) direct analysis of the decay vertex, (c) detection of leptons from semi-leptonic decays of heavy quarks. The key ingredients in these analyses are: (i) the relatively long lifetime and (ii) the lepton signature of heavy hadron decays.

(a) *Invariant mass peak analysis* is very useful in  $e^+e^-$  colliders (as already mentioned in Chapters 8 and 11) where  $\sigma_{Q\bar{Q}}/\sigma_{\text{tot}}$  is large, the combinatorial background relatively low, particle identification enhances the signal and the  $Q\bar{Q}$  CM energy is well determined and provides a useful constraint.

As we have already seen, the first evidence for charm ( $D$  meson production) came from analysing the  $K\pi\pi$  invariant mass produced in  $e^+e^-$  collisions above 4 GeV. The sharp narrow enhancement visible in the  $K^-\pi^+\pi^+$  exotic channel is absent in the non-exotic  $K^+\pi^+\pi^-$  channel (Fig. 13.9) and is convincing evidence that what is seen is indeed the decay of a  $D$  meson.

By far the best way to study the  $D$  meson properties, however, is to analyse the decay of the  $1^3D_1$  state of charmonium, the so-called  $\Psi''(3772)$  (see Chapter 11) whose mass lies less than 50 MeV/ $c^2$  above the  $D\bar{D}$  threshold (so that the  $D$ s move slowly) and is below the threshold for  $D^*$  production. This situation allows a very precise measurement of the mass from  $m = (E^2 - p^2)^{\frac{1}{2}}$  where  $E \simeq M_{\Psi''}/2$  is the energy of the beam which is known with only 1 MeV/ $c^2$  uncertainty. The momentum is very small, being so close to threshold ( $p^2 \simeq 0.08(\text{GeV}/c)^2$ ) that any uncertainty in its value is irrelevant in the mass determination, whose resolution is then  $\sim 3$  MeV/ $c^2$ . The invariant mass spectra for various  $K\pi$  combinations are shown in Fig. 13.10.

The angular distributions for the  $K^\pm\pi^\mp$  and  $K^\mp\pi^\pm\pi^\pm$  decays of  $D^0$ ,  $\bar{D}^0$  and  $D^\pm$  respectively, are shown in Fig. 13.11. Parametrizing angular distributions as  $d\sigma/d\Omega \propto 1 + \alpha \cos^2 \theta$  it is found that  $\alpha_{D^+} \simeq -1.04 \pm 0.10$ ,  $\alpha_{D^0} \simeq -1.00 \pm 0.09$ . According to eqn (25.2.19) this is clear evidence that the  $D$  spin is 0.

An important point that has already been mentioned is that charm conservation in strong and electromagnetic reactions requires charm particles to be produced in associated production only. The present situation is particularly favourable since we can look at the recoil mass to verify that a  $\bar{D}^0$  has been produced in association with the  $D^0$ . The result shown

Particle	$I(J^P)$	Mass (MeV/ $c^2$ )	Main decay modes	Branching fraction (%)	Mean life or full width
$D^0$ $(c\bar{u})$	$\frac{1}{2}(0^-)$	$1869.3 \pm 0.4$	$e^+X$	$7.7 \pm 1.2$	$(4.20 \pm 0.08)10^{-13}s$
			$K^-X$	$46 \pm 4$	
			$K^+X$	$3.5^{+0.6}_{-0.5}$	
			$K^-\bar{e}^+\nu_e$	$42 \pm 5$	
			$\pi^-\bar{e}^+\nu_e$	$3.31 \pm 0.29$ $(3.9^{+2.3}_{-1.2})10^{-3}$	
$D^+$ $(c\bar{d})$	$\frac{1}{2}(0^-)$	$1869.3 \pm 0.4$	$e^+X$	$17.2 \pm 1.9$	$(10.66 \pm 0.23)10^{-13}s$
			$K^-X$	$20.8 \pm 2.8$	
			$K^+X$	$5.8 \pm 1.4$	
			$K^0(\bar{K}^0)X$	$59 \pm 7$	
$D_s^+$ $(c\bar{s})$	$0(0^-)$	$1968.8 \pm 0.7$	$K^0(\bar{K}^0)X$	$39 \pm 28$	$(4.50^{+0.30}_{-0.26})10^{-13}s$
			(non $K\bar{K}$ ) $X$	$64 \pm 17$	
$D^{0*}$	$\frac{1}{2}(1^-)$	$2007.1 \pm 1.4$	$D^0\pi^0$ $D^0\gamma$	$55 \pm 6$ $45 \pm 6$	$\Gamma < 2.1 MeV$
$D^{+*}$	$\frac{1}{2}(1^-)$	$2010.1 \pm 0.6$	$D^0\pi^+$ $D^+\pi^0$ $D^+\gamma$	$55 \pm 4$ $27.2 \pm 2.5$ $18 \pm 4$	$\Gamma < 1.1 MeV$
$D_s^*$	?(?)	$2110.3 \pm 2$	$D_s\gamma$	dominant	$\Gamma < 4.5 MeV$
$\Lambda_c^+$ $(udc)$	$0(\frac{1}{2}^+)$	$2284.9 \pm 0.6$	$p\bar{K}^0$ $e^+X$	$1.6 \pm 0.6$ $4.5 \pm 1.7$	$(1.19^{+0.15}_{-0.12})10^{-13}s$
$\Sigma_c$	$1(\frac{1}{2}^+)$	2455	$\Lambda_c^+\pi$	100	
$\Xi_c^+$ $(usc)$	$(\frac{1}{2}^+)$	$2466 \pm 2.1$			$(3.0^{+1.0}_{-0.6})10^{-13}s$
$\Xi_c^0$ $(dsc)$	$(\frac{1}{2}^+)$	$2472 \pm 2.1$			$(0.82^{+0.59}_{-0.30})10^{-13}s$
$\Omega_c^0$ $(ssc)$					$(7.9 \pm 3.4)10^{-13}s$

Table 13.1. Experimental properties of charm particles (from the Particle Data Group, 1992).

Particle	$I(J^P)$	Mass (MeV/ $c^2$ )	Main decay modes	Branching fraction (%)	Mean life or full width
$B^+$ $(u\bar{b})$	$\frac{1}{2}(0^-)$	$5278.6 \pm 2.0$	$e\nu X$ $D^\pm X$ $D^0(\bar{D}^0)X$ $D^{*\pm} X$ $D_s^+ X$	$23.1 \pm 1.1$ $22.7 \pm 3.3$ $46 \pm 5$ $26.9 \pm 3.5$ $11.5 \pm 2.8$	$(12.9 \pm 0.5)10^{-13}\text{s}$
$B^0$ $(d\bar{b})$	$\frac{1}{2}(0^-)$	$5278.7 \pm 2.1$	$D^-\ell^+\nu$ $D^{*-}\ell'\nu$	$1.8 \pm 0.5$ $4.9 \pm 0.8$	$\frac{\pi_{B^+}}{\pi_{B^0}} = 0.93 \pm 0.16$

Table 13.2. Experimental properties of bottom particles (from the Particle Data Group, 1992)

in Fig. 13.12 yields dramatic confirmation of associated production and therefore of charm conservation in the production process.

The branching ratios given in Table 13.1 follow from the analysis of the  $\Psi''(3772)$  decay under the assumptions that the latter has a definite isospin (0 or 1) and that its only decay mode is  $D\bar{D}$ . The missing fraction of  $D$  decay is attributed to neutral channels, small unidentified channels and, mostly, inadequate detection efficiency.

If it were possible to produce a  $D$  without a  $\bar{D}$  then one should see  $D$  production at energies below  $2m_D$ . As a test of associated production, in Fig. 13.10 samples of events in the reaction  $e^+e^- \rightarrow$  anything are plotted for different energies. The energies chosen are  $\sqrt{s} \simeq m_{J/\Psi}, m_{\Psi'}, 4.028$  GeV and  $3.9 \leq \sqrt{s} \leq 4.6$  GeV.

The  $K^*(890)$  is seen at all energies but no sign of  $D^0, \bar{D}^0(1863)$  is seen at the  $J/\Psi$  and  $\Psi'$  masses, while it becomes quite evident at the two higher energies.

(b) *Vertex detection*, i.e. the reconstruction of the vertex where the interaction has occurred, has been particularly successful in fixed target experiments (as an example, E691 at FNAL has accumulated more than  $10^4$  charm hadrons with negligible background and the total  $c\bar{c}$  production cross-section measured on Be has been found to be  $4.70 \pm 0.07 \pm 0.80 \mu\text{b}$  [Raab *et al.*, 1988]). In  $e^+e^-$  collisions, the difficulty of reconstructing the production vertex say of a  $B$  meson due to the problem that a large fraction of the tracks originate from secondary vertices is partly overcome by using the centroid of the beam spot (the area over which the  $e^+$  and  $e^-$  beams interact) as an estimate of the production vertex.

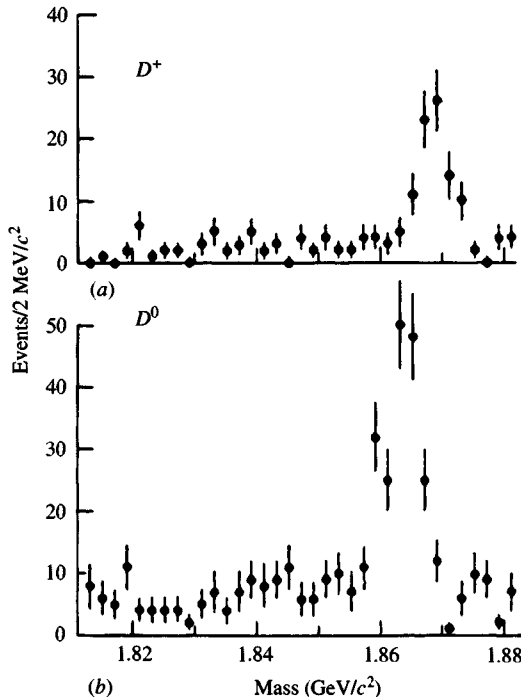


Fig. 13.9. Invariant mass spectra (a)  $K^-\pi^+\pi^+$ , and (b)  $K^-\pi^+$  showing peaks at  $D^+$  and  $D^0$  respectively. (From Rapidis *et al.*, 1977.)

(c) *Detection of semileptonic decays.* Charged leptons have proved efficient tags both in  $e^+e^-$  and in hadron colliders where the current generation of detectors has been specifically designed to detect high  $p_T$  leptons and jets. These detectors have a lepton  $p_T$  threshold; for instance, UA1 detects muons with  $p_T \gtrsim 3$  GeV/ $c$  and electrons with  $p_T \gtrsim 10$  GeV/ $c$ .

### 13.1.2 Charge of the charm and bottom quarks

We have repeatedly remarked that the assumption that the charm quark has electric charge 2/3 makes it the natural candidate to be the missing partner in the SM doublet  $\begin{pmatrix} c \\ s_c \end{pmatrix}$  and we have noted that this charge assignment is in accord with several pieces of data. The ultimate proof that  $Q_c = +2/3$  comes from noticing that the observed  $D^+(c\bar{d})$  and  $D_s^+(c\bar{s})$  do indeed have charge +1 and  $D^0 (= c\bar{u})$  has charge zero, as expected from their quark content. Similarly  $Q[\Lambda_c(ucd)] = 1$  is experimentally verified and so is the fact, for instance, that the  $\Sigma_c$  come in three charge states  $\Sigma_c^{++}(cuu)$ ,  $\Sigma_c^+(cud)$  and  $\Sigma_c^0(cdd)$ .

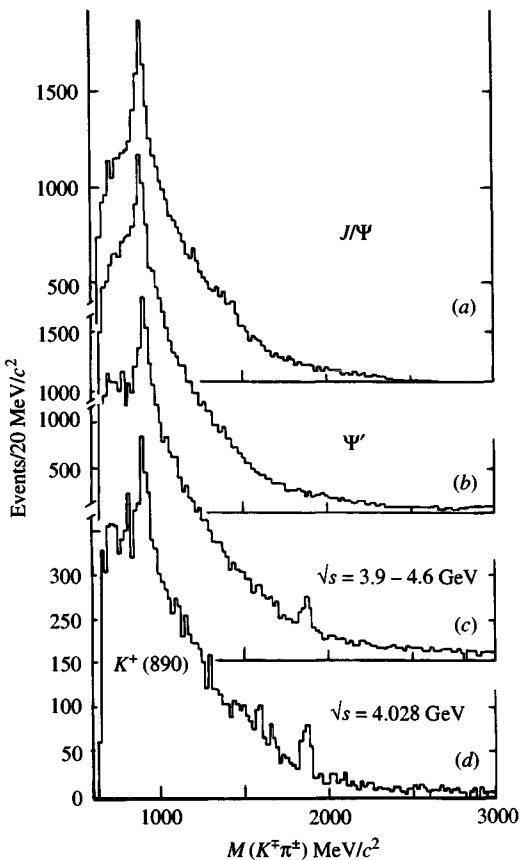


Fig. 13.10.  $K^\mp\pi^\pm$  invariant mass spectra at different CM energies showing emergence of  $D^0$  or  $\bar{D}^0$  at higher energies only (see text). (From Goldhaber, 1976.)

That the charm quark charge is  $2/3$  is also borne out by the size of the increase in the ratio  $R$  (see Fig. 14.1) on crossing the charm threshold (i.e. much bigger than would be the case for a  $|Q| = 1/3$  quark).

Because the  $b$  quark is part of an entirely new doublet, no ‘natural’ assumption is possible in the sense that its partner (the top) is still missing.

In contrast to the charm case, the bottom quark charge assignment  $Q_b = -1/3$  comes from the moderate increase of  $R$  above the  $b$  threshold. This assignment is confirmed by the charge of the  $B^+(u\bar{b})$ .

### 13.1.3 Heavy flavour masses

As compared with the case of ‘hidden’ charm, discussed in the previous chapters, the spectroscopy of heavy flavoured particles, especially charm

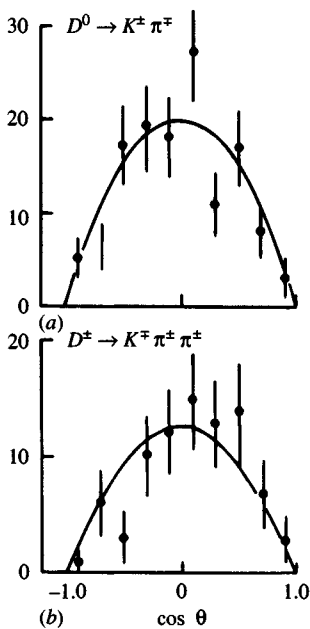


Fig. 13.11. Decay angular distributions for neutral and charged  $D$  mesons.  
(From Schopper, 1977.)

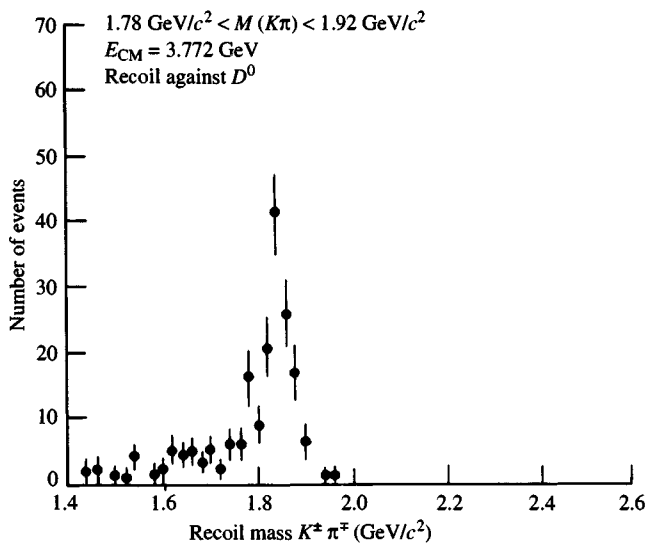


Fig. 13.12. ‘Recoil mass’ spectrum in  $D^0$  production. (From Schopper, 1977.)

$M_{D^0} \simeq 1830 \text{ MeV}/c^2$
$M_{D^+} - M_{D^0} \simeq M_{D^{*+}} - M_{D^{*0}} \simeq 15 \text{ MeV}/c^2$
$M_{D^*} - M_D \simeq 130 \text{ MeV}/c^2$
$M_{D_s^*} - M_{D_s} \simeq 80 \text{ MeV}/c^2$
$M_{\Sigma_c^*} - M_{\Sigma_c} \simeq 60 \text{ MeV}/c^2$
$M_{\Sigma_c} - M_{\Lambda_c} \simeq 160 \text{ MeV}/c^2$

Table 13.3. Predictions for charm hadron masses (de Rujula *et al.*, 1975).

ones, is *a priori* more difficult because at least one light quark is now present so that the non-relativistic approach is probably inadequate.

Despite this, the masses of charm mesons were predicted (by, for example, de Rujula, Georgi and Glashow, 1975) before their actual discovery. That these predictions (Table 13.3) are quite reasonable can be seen by comparing with the experimental data reported in Table 13.1.

The accuracy of present calculations is much higher (see Godfrey and Isgur, 1985) but the theoretical basis and limitations are much the same as discussed in Chapter 12.

Some calculations use very general arguments to derive bounds for as yet undiscovered heavy flavoured particles. For example, Anselmino *et al.*, (1990a) isolate the effects of colour-hyperfine terms and use experimental information to make predictions about the masses of baryons containing at least one heavy quark. Typical results are the predictions  $64 < \Omega_c^* - \Omega_c < 107 \text{ MeV}/c^2$ , and  $23 < \Omega_b^* - \Omega_b < 39 \text{ MeV}/c^2$ . These imply that  $\Omega_c^*$  and  $\Omega_b^*$  cannot decay strongly. By the same technique one finds also  $23 < \Sigma_b^* - \Sigma_b < 39 \text{ MeV}/c^2$  so  $\Sigma_b^*$  cannot decay strongly into  $\Sigma_b$  but both decay strongly into  $\Lambda_b$ .

### 13.2 Charm decay

To a large degree the considerations that follow can be extended to bottom with only minor changes. We will continue to refer to charm for simplicity.

If we assume charm to be a good quantum number under strong and electromagnetic interaction (see Section 13.3), the pseudo-scalar charm mesons  $D^0, D^+$  and  $D_s^+$  can only decay weakly into ‘old’ mesons. By contrast,  $D^*$ s can decay both strongly and electromagnetically whereas only the latter mode is available to  $D_s^*$  due to its mass threshold, as can be seen from Table 13.1. The naive expectation that heavy flavoured hadron decays are entirely determined by the so-called spectator diagram (Fig. 13.13) leads to immediate predictions for the lifetimes of these

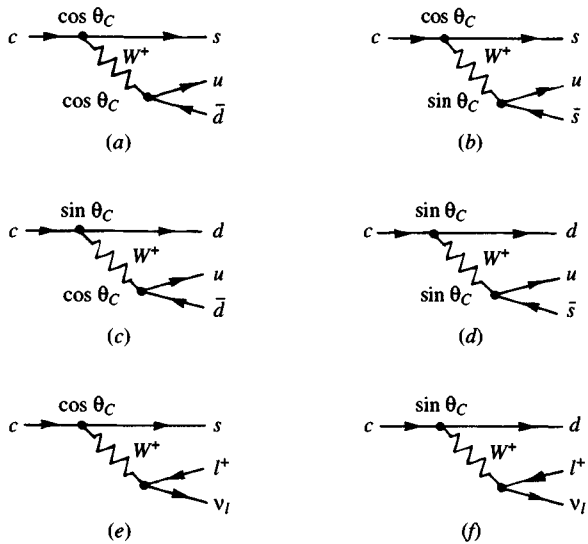


Fig. 13.13. Quark transitions in the standard model. The Kobayashi–Maskawa matrix elements are approximated by Cabibbo angle factors.

hadrons. These predictions, as will be seen, do not comply with experiment.

The relative strengths of the various possible hadronic and semi-leptonic charm decays can be estimated from the couplings to the Cabibbo allowed and forbidden channels and can be read off from Fig. 13.13.

Ignoring phase space and dynamical considerations, we expect the following relative rates (the factors of 3 are explained below):

$$\left. \begin{array}{ll} (a) c \rightarrow su\bar{d} \propto 3 \cos^4 \theta_C; & (b) c \rightarrow su\bar{s} \propto 3 \cos^2 \theta_C \sin^2 \theta_C \\ (c) c \rightarrow d\bar{d}u \propto 3 \sin^2 \theta_C \cos^2 \theta_C; & (d) c \rightarrow du\bar{s} \propto 3 \sin^4 \theta_C \\ (e) c \rightarrow sl^+\nu_l \propto \cos^2 \theta_C; & (f) c \rightarrow dl^+\nu_l \propto \sin^2 \theta_C. \end{array} \right\} (13.2.1)$$

To see the origin of the colour factor 3 in the hadronic rates, recall that  $W$  couples to quarks of each colour with the strength  $g \cos \theta_C$  or  $g \sin \theta_C$ .

The vertex  $W \rightarrow$  hadrons  $h$  involves  $\sum_{(\text{colour})i} A(W \rightarrow u_i\bar{d}_i) \times \langle u_i\bar{d}_i | h \rangle = g \cos \theta_C \sum_i \langle u_i\bar{d}_i | h \rangle$ . The hadrons are colour singlets, and so we assume unit amplitude for the normalized singlet state  $|\text{colour singlet}\rangle = (1/\sqrt{3})(|ud\rangle_{\text{yellow}} + |u\bar{d}\rangle_{\text{blue}} + |d\bar{d}\rangle_{\text{red}})$  to convert into hadrons. Then  $\sum_i \langle u_i\bar{d}_i | h \rangle = \sqrt{3} \langle \text{colour singlet} | h \rangle = \sqrt{3}$ .

By just counting diagrams, from (13.2.1) one would conservatively expect semi-leptonic decays to be  $\sim 1/3$  of the hadronic ones but not orders of magnitude smaller.

As we shall see the naive decay model has to be revised on the basis

of dynamical considerations, leading to the estimate that semi-leptonic decays are only a few per cent of the hadronic ones. In this case, hadronic decays should be the most important channels for charm decay.

All Cabibbo allowed decays of non-strange charm particles involve a single strange particle which therefore provides a prominent signal for charm. As already mentioned, the same signal is expected for bottom particles given that  $b \rightarrow c + W^-$  is the main decay mode of  $b$  quarks.

### 13.2.1 Heavy flavour lifetimes

The typical momentum transfer in weak decays of hadrons containing a heavy quark  $Q$  and light quarks is of the order of the mass  $m_Q$ . For sufficiently large values of  $m_Q$ , inclusive decay properties such as total lifetimes and semi-leptonic branching ratios should be dominated by the dynamics at short distances, where according to QCD, interparticle forces become weak. In this ideal situation, the light quarks should play the purely passive role of spectators and, as already mentioned, all lifetimes should be determined by the spectator diagram Fig. 13.13. Under such an approximation, all lifetimes of hadrons with one particular heavy quark  $Q$  should be equal and all should reflect the intrinsic lifetime of  $Q$  itself. The latter, as already stated, can be calculated in exactly the same way as the  $\mu$ -lifetime was calculated, *to the extent that a quark can be considered as a free particle*. Thus, infinitely heavy quarks could presumably be treated as free objects but this may (and does) lead to complications for finite masses. Hence, while it may make sense to use the free quark picture for bottom, we must expect sizeable subasymptotic corrections to the spectator model for charm particles. Indeed, instead of the naive expectation

$$\tau(D^+) \simeq \tau(D^0) \simeq \tau(D_s^+) \simeq \tau(\Lambda_c^+)$$

we find, from the data (Table 13.1),

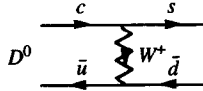
$$\tau(D^+) > \tau(D^0) \simeq \tau(D_s^+) > \tau(\Lambda_c^+),$$

i.e. the various charm particles have considerable variations in their lifetimes.

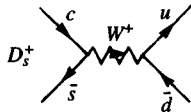
Aside from the spectator contribution to all charm particle decays (this is sometimes called ‘ $W$ -radiation’), several approaches have been suggested in order to estimate possible corrections. Among these, we have:

- (i)  $W$ -exchange which could, for instance, contribute to  $c\bar{u} \rightarrow s\bar{d}$ , i.e. to

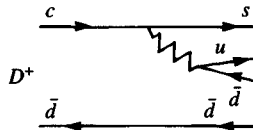
$D^0$  decay via



(ii)  $W$ -annihilation which could contribute to  $c\bar{s} \rightarrow u\bar{d}$ , i.e. to  $D_s^+$  decay as in



(iii) Final state interactions of various types, e.g. Pauli effect interference, such as can be found when identical quarks are present in the final state. An example is



(iv) Diquark contribution. This may just be a curiosity but the  $\Lambda_c^+$  lifetime calculated from the knowledge of  $D^+$  decay assuming a quark-diquark structure of baryons coincides exactly with the experimental value (Bediaga *et al.*, 1985).

All these mechanisms improve the agreement with the data to some extent. For detailed calculations, we refer the reader to the specialized literature (Gittelman, 1991; Kühn *et al.*, 1989; Basdevant *et al.*, 1987 and references therein).

Before proceeding further however, let us show that naive arguments at least lead to the *correct order of magnitude* for both charm and bottom lifetimes.

Using eqn (13.1.5) with  $m_c \simeq 1.6 \text{ GeV}/c^2$ , recalling that  $|V_{cs}| \simeq 1$ , noting from (13.2.1) or Fig. 13.13 which decays are Cabibbo allowed and taking colour into account (a factor of 3 for  $c \rightarrow s u \bar{d}$  as compared with  $c \rightarrow s \ell^+ \nu_\ell$ ), we find

$$\tau_c \simeq \frac{1}{5} \left( \frac{m_\mu}{m_c} \right)^5 \tau_\mu \simeq 6 \times 10^{-13} \text{s.} \quad (13.2.2)$$

In the case of bottom decay, taking  $m_b \simeq 4.5 \text{ GeV}/c^2$ ,  $|V_{cb}| \simeq \sin^2 \theta_C \simeq 0.05$  [see (9.2.6)] and recalling that a further channel (due to the  $\tau$ -lepton) contributes, we find

$$\tau_b \simeq \frac{1}{6} \frac{1}{|V_{cb}|^2} \left( \frac{m_\mu}{m_b} \right)^5 \tau_\mu \simeq 1 \times 10^{-13} \text{s.} \quad (13.2.3)$$

The above values are in qualitative agreement with the experimental

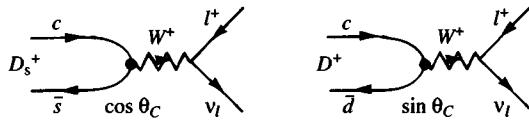


Fig. 13.14.

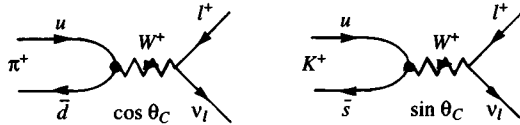


Fig. 13.15.

data of Tables 13.1 and 13.2.

### 13.2.2 Purely leptonic charm decays

Let us assume that leptonic charm decays proceed via (13.1.1), i.e. neglecting the other contributions listed in Section 13.2.1. We show in Fig. 13.14 examples of Cabibbo allowed and suppressed decays.

To get an estimate for the leptonic decay rates, note that vector boson effects are unimportant, so that from Section 1.2 the Feynman amplitude for the pseudo-scalar \$P \rightarrow \ell^+ \nu\_\ell\$ decay will be given by (0 means vacuum)

$$\mathcal{M} = \frac{G}{\sqrt{2}} \langle 0 | h^\alpha | P \rangle [\bar{\ell} \gamma_\alpha (1 - \gamma_5) \nu_\ell]. \quad (13.2.4)$$

We define the meson decay constants

$$\left. \begin{aligned} \langle 0 | h^\alpha | \pi^-(q) \rangle &= i f_\pi \cos \theta_C q^\alpha, \\ \langle 0 | h^\alpha | K^-(q) \rangle &= i f_K \sin \theta_C q^\alpha, \\ \langle 0 | h^\alpha | D^-(q) \rangle &= -i f_D \sin \theta_C q^\alpha, \\ \langle 0 | h^\alpha | D_s^-(q) \rangle &= i f_{D_s} \cos \theta_C q^\alpha, \end{aligned} \right\} \quad (13.2.5)$$

where the origin of the \$\theta\_C\$ dependence of the first two decays is indicated in Fig. 13.15.

To the extent that \$SU(4)\_F\$ is not too badly broken a rough estimate of leptonic charm decay can be obtained by assuming \$f\_\pi \simeq f\_K \simeq f\_D \simeq f\_{D\_s}\$.

Taking \$|\mathcal{M}|^2\$ in (13.2.4), summing over the spins of the leptons and using the definitions (13.2.5) one gets for the process \$P \rightarrow \ell^+ \nu\_\ell\$ (\$P \equiv \pi, K, D, F\$)

$$\Gamma(P \rightarrow \ell^+ \nu_\ell) = \frac{G^2}{8\pi} f_P^2 \left\{ \frac{\cos^2 \theta_C}{\sin^2 \theta_C} \right\} m_\ell^2 \left( 1 - \frac{m_\ell^2}{m_P^2} \right)^2 m_P \quad (13.2.6)$$

according to whether the transition is Cabibbo allowed or forbidden.

The pion decay can be used to set the scale; using the experimental value  $\Gamma_\pi \simeq 3.84 \times 10^7 \text{ s}^{-1}$  one gets  $f_\pi \simeq 0.131 \text{ GeV}$ . The phase space factor  $[1 - (m_\ell^2/m_P^2)]^2$  is already  $\simeq 0.91$  for  $K^+ \rightarrow \mu^+ \nu_\mu$  decay and becomes totally irrelevant in the decay of heavier pseudo-scalars.

Thus, we get approximately

$$\frac{\Gamma(D^+ \rightarrow \mu^+ \nu_\mu)}{\Gamma(K^+ \rightarrow \mu^+ \nu_\mu)} \simeq \frac{m_D}{m_K}, \quad \frac{\Gamma(D_s^+ \rightarrow \mu^+ \nu_\mu)}{\Gamma(K^+ \rightarrow \mu^+ \nu_\mu)} \simeq \frac{m_{D_s^+}}{m_K} \cot^2 \theta_C, \quad (13.2.7)$$

from which we estimate the  $D_s \rightarrow \ell^+ \nu_\ell$  decay rate to be of the order of  $\Gamma \sim 10^9 \text{ s}^{-1}$  whereas  $D \rightarrow \ell^+ \nu_\ell$  is suppressed relative to this by a factor of  $\tan^2 \theta_C \simeq 0.05$ .

As can be seen from (13.2.6), decays into  $\mu^+ \nu_\mu$  will totally dominate over decays into  $e^+ \nu_e$  because of the very large mass ratio  $(m_\mu/m_e)^2$ . The decay rate  $D_s^+ \rightarrow \tau^+ \nu_\tau$  (heavy lepton) is expected to be about 16 times larger than  $D_s^+ \rightarrow \mu^+ \nu_\mu$  but is unfortunately very difficult to observe.

As we shall soon see, the total decay rate of  $D$  and  $D_s^+$  (into hadrons) can be estimated to be of the order of  $10^{12} - 10^{13} \text{ s}^{-1}$  so that the purely leptonic decay rate of charm mesons leads to branching ratios which are, at most, of order  $10^{-3} - 10^{-4}$  and can, therefore, be neglected. Indeed up to the present, none of the leptonic decays has been observed (on this question, the Particle Data Group (1992) reports  $\text{BR}(D_s^+ \rightarrow \mu^+ \nu_\mu) < 3 \times 10^{-2}$  and  $\text{BR}(D^+ \rightarrow \mu^+ \nu_\mu) < 7.2 \times 10^{-4}$ ).

### 13.2.3 Semi-leptonic and hadronic decays of charm mesons

Semi-leptonic decays should, in principle, provide the best way to test our ideas about charm currents since the hadronic current appears only once and is multiplied by the well-known leptonic part.

Semi-leptonic decays of charm mesons with an electron in the final state were first observed at DESY by the DASP collaboration shortly after the first evidence for charm had been reported in hadronic decays.

Let us consider first semi-leptonic three-body decays. It follows from Fig. 13.13 that possible transitions obey the following selection rules:

Cabibbo allowed (i.e. proportional to  $\cos \theta_C$ )

$$\Delta S = \Delta C = \Delta Q \quad \text{with} \quad \Delta I = 0. \quad (13.2.8a)$$

Cabibbo forbidden (i.e. proportional to  $\sin \theta_C$ )

$$\Delta Q = \Delta C, \quad \Delta S = 0, \quad \Delta I = \frac{1}{2}. \quad (13.2.8b)$$

Thus, a  $D$  meson should predominantly go to  $\ell^+ \nu_\ell \bar{K}^0$  or  $\ell^+ \nu_\ell \bar{K}^{0*}$ , whereas events like  $D^+ \rightarrow \ell^+ \nu_\ell \pi^0$  should be depressed by  $\tan^2 \theta_C$ .

Taking into account the different Cabibbo structure ( $K \rightarrow \pi\ell^+\nu_\ell$  has a  $\sin\theta_C$  one gets, using  $m_\pi \ll m_K$  and  $m_K \ll m_D$ ,

$$\Gamma(D^+ \rightarrow \bar{K}^0\ell^+\nu_\ell) \simeq \left(\frac{m_D}{m_K}\right)^5 \cot^2\theta_C \Gamma(K^0 \rightarrow \pi^-\ell^+\nu_\ell) \frac{f(m_K/m_D)}{f(m_\pi/m_K)} \quad (13.2.9)$$

where (Jackson, 1963)  $f(x) = 1 - 8x^2 + 8x^6 - x^8 - 24x^4 \ln x$  comes from phase space.

The ratio of the above functions is of order unity and can be ignored. Whence, on using

$$\Gamma(K^0 \rightarrow \pi^-\ell^+\nu_\ell) \simeq 7.5 \times 10^6 \text{s}^{-1}$$

one gets the estimate for  $D_{\ell 3}$  decay

$$\Gamma(D^+ \rightarrow \bar{K}^0\ell^+\nu_\ell) \simeq \Gamma(D^0 \rightarrow K^-\ell^+\nu_\ell) \sim 1.4 \times 10^{11} \text{s}^{-1}. \quad (13.2.10)$$

Similarly

$$\Gamma(D^+ \rightarrow \bar{K}^{*0}\ell^+\nu_\ell) \simeq \Gamma(D^0 \rightarrow K^{*-}\ell^+\nu_\ell) \sim 0.7 \times 10^{11} \text{s}^{-1}. \quad (13.2.11)$$

As a comparison, from the Particle Data Group we get  $\Gamma_{\text{exp}}(D^0 \rightarrow K^-e^+\nu_e) \simeq 0.8 \times 10^{11} \text{s}^{-1}$  and  $\Gamma_{\text{exp}}(D^+ \rightarrow \bar{K}^{*0}e^+\nu_e) \simeq 0.4 \times 10^{11} \text{s}^{-1}$  whose agreement with (13.2.11) is fair but not spectacular.

The problem lies in the same theoretical mechanisms that were discussed in Section 13.2.1, i.e. the contribution from non-spectator diagrams.

As for the strange charm meson  $D_s(c\bar{s})$  it transforms into  $s\bar{s}$  with a  $\cos\theta_C$  amplitude and into  $\bar{s}d$  with a  $\sin\theta_C$  one. Thus, we expect  $\Gamma(D_s^+ \rightarrow K^0\ell^+\nu_\ell)$  to be suppressed by  $\tan^2\theta_C$  compared with  $\Gamma(D_s^+ \rightarrow \ell^+\nu_\ell)$ .

If hadronic rates are governed principally by quark rates, one would roughly expect for  $D_s^+ \rightarrow \eta\ell^+\nu_\ell$  a rate of the same order of magnitude as  $D^+ \rightarrow \bar{K}^0\ell^+\nu_\ell$ , but the former is not yet measured.

If we now go to inclusive semi-leptonic and hadronic decays, our understanding of these reactions is severely limited by our poor knowledge of the hadronic effects involved.

Estimates can be made, however, if we use the free quark-parton model and assume that partons convert into hadrons with unit probability. A very rough estimate for the inclusive semi-leptonic  $D$  decay can be obtained along the lines given previously [eqn (13.2.2)] if we forget all complications coming from non-spectator diagrams and assume that the light quark behaves purely like a spectator while the charm quark decay proceeds as if it were a free particle. In this case one has

$$\Gamma(D \rightarrow \ell + \nu_\ell + h) \simeq \left(\frac{m_c}{m_\mu}\right)^5 \Gamma(\mu \rightarrow e + \nu_\mu + \bar{\nu}_e) < 10^{12} \text{s}^{-1}, \quad (13.2.12)$$

where  $m_c$  is the mass of the charm quark.

A naive argument based purely on counting diagrams in (13.2.1) led us to conclude that the hadronic decay contribution should be about 3 times larger than the semi-leptonic one. However, it is believed that an enhancement factor comes into play here.

If one considers the dominant term ( $\propto \cos^2 \theta_C$ ) in the charged-current-charged-current interaction

$$\left. \begin{aligned} h_\alpha h^{\alpha+} &\propto \cos^2 \theta_C [(\bar{u}d)(\bar{d}u) + (\bar{c}s)(\bar{s}c) + (\bar{u}d)(\bar{s}c) + (\bar{d}u)(\bar{c}s)] \\ &+ \sin \theta_C \cos \theta_C [(\bar{u}d)(\bar{s}u) - (\bar{u}d)(\bar{d}c) + (\bar{c}s)(\bar{s}u) - (\bar{c}s)(\bar{d}c)] \\ &+ \sin^2 \theta_C [(\bar{u}s)(\bar{s}u) + (\bar{c}d)(\bar{d}c) - (\bar{u}s)(\bar{d}c) - (\bar{s}u)(\bar{c}d)] + \text{h.c.} \end{aligned} \right\} \quad (13.2.13)$$

one sees that the only  $\Delta S = 1$  decay involving ordinary (light) quarks solely is  $(\bar{u}d)(\bar{s}u)$ , the isospin content of which is like

$$(\bar{u}d)(\bar{s}u) \sim \pi^- K^+ = \sqrt{\frac{2}{3}} \left( I = \frac{1}{2} \right) - \sqrt{\frac{1}{3}} \left( I = \frac{3}{2} \right). \quad (13.2.14)$$

Thus the current interaction possesses a roughly comparable mixture of  $\Delta I = \frac{1}{2}$  and  $\Delta I = \frac{3}{2}$  terms, whereas experimentally the  $\Delta I = \frac{3}{2}$  term is only about 5% of the total. In the  $SU(3)_F$  pre-charm days, this was explained by the postulate of ‘octet enhancement’ (over the 27-plet). If one extrapolates from the  $\Delta C = 0$  to the charm case, one might postulate an enhancement of the  $SU(4)_F$  20-plet which could increase the hadronic rate by an order of magnitude as compared with the naive estimate based on (13.2.1).

The present evidence for semi-leptonic decays comes from a study of inclusive electron production. Some care is necessary in separating the products of  $D$  decay from those of the heavy lepton  $\tau$ , since  $D$  and  $\tau$  are very close in mass.

The present estimates for inclusive semi-leptonic modes (Table 13.1)

$$\text{BR}(D^0 \rightarrow \ell X) \simeq (7.7 \pm 1.2)\%, \quad \text{BR}(D^+ \rightarrow \ell X) \simeq (17.2 \pm 1.9)\%$$

indicate that there may be some enhancement of the hadronic mode, but not as high as originally guessed.

Summarizing, as an order of magnitude we have

$$\left. \begin{aligned} \Gamma(D \rightarrow h) &\sim 10^{13} \text{s}^{-1} \\ \Gamma(D \rightarrow \ell \nu h) &\sim 10^{12} \text{s}^{-1} \\ \Gamma(D \rightarrow K \ell \nu) &\sim 10^{11} \text{s}^{-1} \\ \Gamma(D \rightarrow \ell \nu) &\sim 10^9 \text{s}^{-1} \end{aligned} \right\} \quad (13.2.15)$$

(where we have disregarded the indication that charged charm particles seem to be longer lived than neutral ones), which explains why the first direct observation of  $D^+$  decay occurred in the exotic channel  $K^- \pi^+ \pi^+$  (Fig. 13.3), while the absence of any decay into the non-exotic channel  $K^+ \pi^+ \pi^-$  via the neutral weak current is in line with the absence of  $D^0 -$

$\bar{D}^0$  mixing which, in turn, is evidence of the fact that charm-changing neutral currents are suppressed experimentally.  $D^0 - \bar{D}^0$  mixing would, in fact, go via

$$D^0 = c\bar{u} \leftrightarrow \bar{c}u = \bar{D}^0$$

(just as  $K^0 - \bar{K}^0$  mixing occurs via  $K^0 = d\bar{s} \leftrightarrow \bar{d}s = \bar{K}^0$ ). The discussion on  $D^0 - \bar{D}^0$  mixing parallels very much that on  $K^0 - \bar{K}^0$  of Section 9.4. Mixing in general is dealt with in Chapter 19. We simply recall that in the standard model the mixing is the result of the exchange of two  $W$ s as a second order process via charged currents (Fig. 9.1).

If one looks at the associated production of charm particles in  $e^+e^-$ , one expects copious contribution from  $e^+e^- \rightarrow D^0\bar{D}^0X$ . In the absence of significant  $D^0 - \bar{D}^0$  mixing, events with two charged kaons in the final state should consist only of pairs of oppositely charged kaons (more properly, the final state should have strangeness zero) since  $D^0$  and  $\bar{D}^0$  go only into final states containing  $K^-$  and  $K^+$  respectively, e.g.  $\bar{D}^0 \rightarrow K^+\pi^-$ ,  $D^0 \rightarrow K^-\pi^+$ .

The present experimental evidence is

$$\frac{\Gamma(D^0 \rightarrow \bar{D}^0 \rightarrow K^+\pi^-)}{\Gamma(D^0 \rightarrow K^-\pi^+)} < 0.0037$$

compatible with the expectation from the standard model decay modes.

As a final comment, we notice that (13.2.1) leads to a series of predictions concerning Cabibbo suppressed decays, of which we list a few:

$$\begin{aligned} \frac{\Gamma(D^0 \rightarrow \pi^+\pi^-)}{\Gamma(D^0 \rightarrow K^-\pi^+)} &\simeq 2 \frac{\Gamma(D^+ \rightarrow \pi^+\pi^0)}{\Gamma(D^+ \rightarrow K^0\pi^+)} \\ &\simeq \frac{\Gamma(D^0 \rightarrow K^-K^+)}{\Gamma(D^0 \rightarrow K^-\pi^+)} \simeq \frac{1}{2} \frac{\Gamma(D_s^+ \rightarrow K^0\pi^+)}{\Gamma(D_s^+ \rightarrow \eta\pi^+)} \\ &\simeq \tan^2 \theta_C \simeq 0.05. \end{aligned} \quad (13.2.16)$$

The present indication from the Particle Data Group (1992) is that

$$\frac{\Gamma(D^0 \rightarrow \pi^+\pi^-)}{\Gamma(D^0 \rightarrow K^-\pi^+)} \simeq 0.045 \pm 0.005, \quad (13.2.17)$$

but that

$$\frac{\Gamma(D^0 \rightarrow K^-K^+)}{\Gamma(D^0 \rightarrow K^-\pi^+)} \simeq 0.131 \pm 0.007. \quad (13.2.18)$$

### 13.3 $B$ physics

Turning now to the  $b$  sector, much less data exist here (compare Table 13.1 and 13.2) and the situation is to some extent simpler since the naive

expectations based on the spectator diagram dominance are believed to be closer to the data. The present estimate by the Particle Data Group (1992) is

$$\frac{\tau_{B^+}}{\tau_{B^0}} = 0.93 \pm 0.16.$$

Before the above value was established, at the 25th International Conference on High Energy Physics, Gittelman, (1991) presented the results

$$\begin{aligned} \frac{\tau_{B^-}}{\tau_{B^0}} &\simeq (0.89 \pm 0.19 \pm 0.13) \frac{f_{00}}{f_{+-}} (\text{CLEO}) \\ &= (1.00 \pm 0.23 \pm 0.14) \frac{f_{00}}{f_{+-}} (\text{ARGUS}) \end{aligned} \quad (13.3.1)$$

where  $f_{+-}$  and  $f_{00}$  are the fractions of  $\Upsilon(4s)$  decays to  $B^+B^-$  and to  $B^0\bar{B}^0$  respectively. Unfortunately, these fractions are not known though it is believed that  $f_{+-} \simeq f_{00} \simeq 0.5$ , yielding roughly equal lifetimes for  $B^0$  and  $B^-$  in agreement with the spectator diagram predictions. Theoretical expectations for the difference of  $B^+$  and  $B^0$  lifetimes range from some 30% (Kühn *et al.*, 1989) to  $\lesssim 10\%$  (Bediaga *et al.*, 1988). Most of our knowledge of  $B$  physics comes from CESR (CUSB and CLEO collaborations) and from DORIS (ARGUS collaboration) i.e. from  $\Upsilon$  spectroscopy but some important issues in  $B$  physics, such as  $B^0 - \bar{B}^0$  mixing (see Chapter 19), have originated from  $\bar{p}p$  physics (UA1 collaboration).

Semi-leptonic and exclusive  $B$  decay channels have been observed [BR( $B \rightarrow e + \nu + \text{hadrons}$ )  $\simeq 10.7 \pm 0.5\%$  and BR( $B \rightarrow \mu + \nu + \text{hadrons}$ )  $\simeq 10.3 \pm 0.5\%$ ] but it is fair to say that  $B$  physics has barely begun and offers great potential for an extremely rich experimental programme both at electron and hadron machines. The most crucial question that we expect to be answered from  $B$  physics concerns CP violating asymmetries. This subject will be discussed in Chapter 19.

$B_s$  mesons have not yet been sufficiently firmly established to be given an entry in the main listing of the Particle Data Group. Recently, however, CUSB II (1990) has reported evidence from the study of the photon signal in  $B^* \rightarrow B + \gamma$  and  $B_s^* \rightarrow B_s + \gamma$  that a significant number of  $B_s$  mesons are produced in  $\Upsilon(5S)$  decays and that the hyperfine splitting  $M(B_s^*) - M(B_s) \simeq 47 \text{ MeV}/c^2$  is compatible with  $M(B^*) - M(B) \simeq 45 \text{ MeV}/c^2$ . Both, in turn are not incompatible with the empirical rule on the universality of  $M_{\text{vector}}^2 - M_{\text{pseudo-scalar}}^2 \simeq 0.54 - 0.58(\text{GeV}/c)^2$ .

### 13.3.1 The decay $\bar{B}^0 \rightarrow D^{*+}\ell^-\bar{\nu}$

It is, perhaps, worth illustrating some details of  $B$  physics using the decay  $\bar{B}^0 \rightarrow D^{*+}\ell^-\bar{\nu}$  as an example. This reaction can be monitored if the

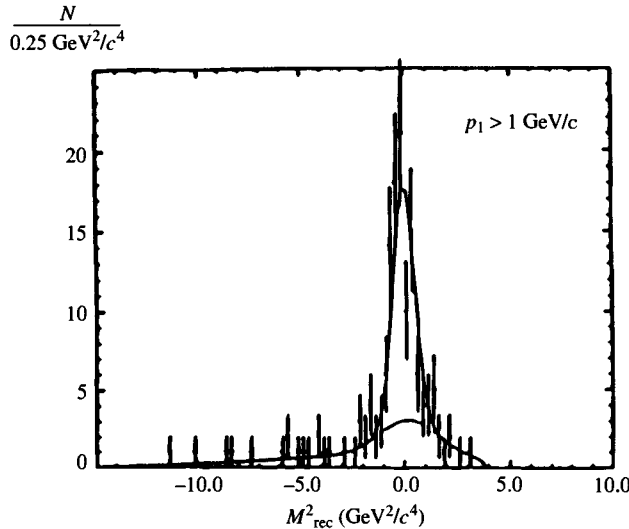


Fig. 13.16.  $M_{\text{rec}}^2$  distribution in the decay  $\bar{B}^0 \rightarrow D^{*+} \ell^- \nu$ .

apparatus has a high efficiency for detecting electrons and muons as well as for reconstructing  $D^*$ s as is the case at the CESR detectors. The neutrino is inferred from

$$M_\nu^2 = [E_B - (E_{D^*} + E_{\ell^-})]^2 - [\mathbf{p}_B - \mathbf{p}_{D^*} - \mathbf{p}_{\ell^-}]^2 = 0. \quad (13.3.2)$$

The  $B^0$  mesons are the decay products of a  $\Upsilon(4S)$  at rest so that  $E_B = E_{\text{beam}} \simeq \frac{1}{2}m(\Upsilon)$  and  $\mathbf{p}_B \simeq 0$ . The decay  $\bar{B}^0 \rightarrow D^{*+} \ell^- \nu$  is thus seen as a peak in the recoil mass squared spectrum  $M_{\text{rec}}^2$  at  $M_{\text{rec}}^2 = 0$  (see Fig. 13.16).

$$M_{\text{rec}}^2 = [E_{\text{beam}} - (E_{D^*} + E_{\ell^-})]^2 - (\mathbf{p}_{D^*} + \mathbf{p}_\ell)^2. \quad (13.3.3)$$

The prominent peak at  $M_{\text{rec}}^2 = 0$  has  $75 \pm 11$  events on a background of  $23 \pm 5$  events. The branching ratio is found to be

$$\text{BR}(\bar{B}^0 \rightarrow D^{*+} \ell^- \bar{\nu}) \simeq (7.0 \pm 1.2 \pm 1.9)\% \quad (13.3.4)$$

and represents about 60–70% of the total semi-leptonic branching ratio *i.e.* it dominates the inclusive lepton spectrum in  $B$  decays.

Combining this with  $\tau_{B^0} = (1.15 \pm 0.14)10^{-12}\text{s}$  yields information on  $V_{cb}$  as is explained in Section 19.1. One finds from the above reaction (Schröder, 1989)

$$|V_{cb}| = 0.051 \pm 0.010. \quad (13.3.5)$$

Collider	Beams	$\sqrt{s}$ TeV	$\sigma_{\bar{b}b}(\mu\text{b})$	$\sigma_{\text{tot}}/\sigma_{\bar{b}b}$
<i>SppS</i>	$\bar{p}p$	0.63	10	5000
TeV 1	$\bar{p}p$	1.8	50	1000
SSC	$p\bar{p}$	40	500	200
CESR	$e^+e^-$	$1.1 \times 10^{-2}$	$5 \times 10^{-3}$	4
LEP	$e^+e^-$	$9 \times 10^{-2}$	$5 \times 10^{-3}$	7

Table 13.4. Comparison of  $b\bar{b}$  production at  $e^+e^-$  and  $\bar{p}p$  colliders.

### 13.4 Production of heavy flavours

Charm and bottom are produced in large abundance at hadron colliders but their detection is made difficult by the high total inelastic cross-section and by the very high multiplicity of particles produced in the TeV region. An interesting comparison (from Ellis and Kernan, 1990) of  $b\bar{b}$  production at CESR ( $e^+e^-$ ) and at the CERN *SppS* colliders is shown in Table 13.4. The production rate is much larger at hadron machines but the ratio  $\sigma_{b\bar{b}}/\sigma_{\text{tot}}$  is only about 0.01% at the CERN *SppS* whereas it is  $\sim 23\%$  at CESR. Expectations for the Tevatron, for SSC and LEP are also given.

#### 13.4.1 Theoretical estimates of heavy flavour production

The production of heavy flavours is a classical process in QCD and is linked with jet physics (Chapters 24, 25). Here, we limit ourselves to a few qualitative considerations.

The  $b$  quark production cross-sections calculated to order  $\alpha_s^2$  and to order  $\alpha_s^3$  in QCD are shown in Fig. 13.17 as function of  $\sqrt{s}$  (from Ellis and Kernan, 1990) whereas the cross-section for charm production is given in Fig. 13.18 (Altarelli *et al.*, 1988). In both cases, one feels quite uneasy about the large changes brought about by higher order contributions (Fig. 13.17) or by changing the various parameters (Fig. 13.18). Examples of calculated heavy quark differential cross-sections as functions of the transverse momenta for various rapidities are given in Fig. 13.19 (Dawson *et al.*, 1988, 1989, 1990; see also Beenaker *et al.*, 1989).

Note the peculiar feature that 2.3 times the lowest order result (LO) is remarkably close to the higher order one (LO+NLO). This so-called ‘ $K$ -factor’ also shows up in the Drell–Yan process (see Section 17.4).

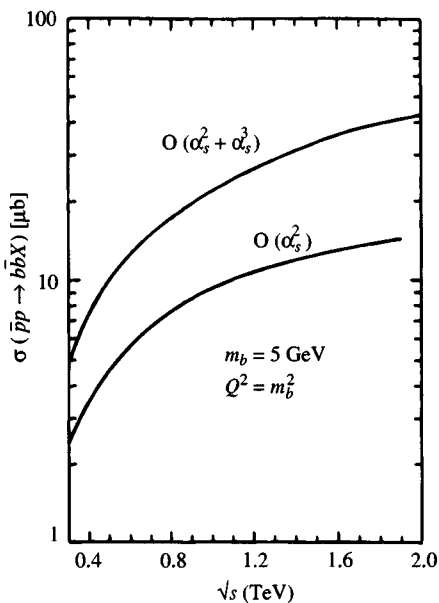


Fig. 13.17. Cross-section for bottom production versus  $\sqrt{s}$  (from Ellis and Kernan, 1990).

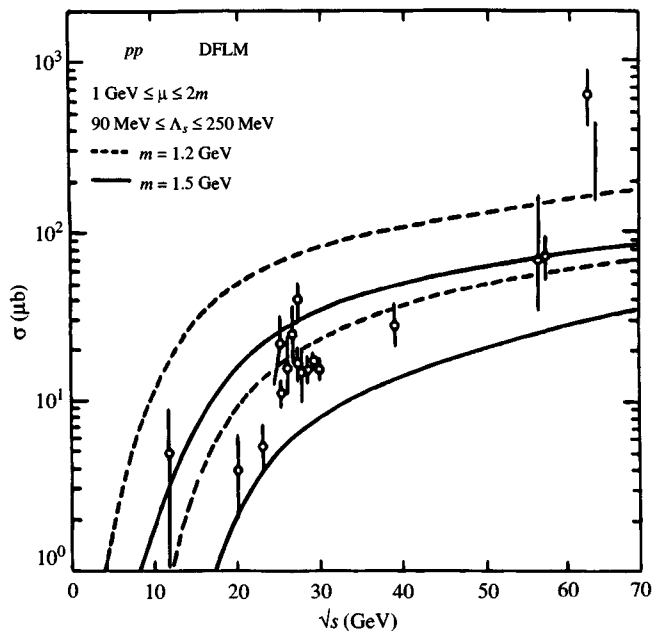


Fig. 13.18. Cross-section for charm production versus  $\sqrt{s}$  (from Altarelli *et al.*, 1988).

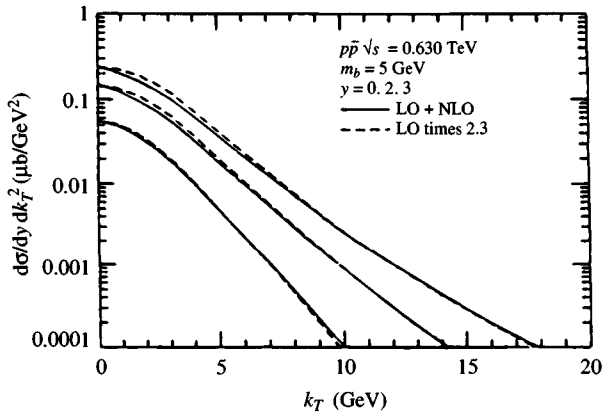


Fig. 13.19. Cross-section for bottom production (from Ellis and Kernan, 1990).

### 13.5 Heavy flavours at LEP

A new chapter on heavy flavour physics has been initiated at LEP in its studies of  $Z^0$  decays. The main motivation for heavy flavour searches, i.e. the quest for top (and Higgs), has been frustrating so far and we have repeatedly commented about the top mass limits set by LEP [eqn (8.6.20)]:

$$m_t \approx 130 \pm 40 \text{ GeV}/c^2.$$

If the above estimate is correct, the direct detection of top in  $e^+e^-$  colliders is not just around the corner. Nonetheless LEP 1 has already given much information on heavy flavours (for a detailed review, see Tenchini, 1990).

#### 13.5.1 Production of $c$ and $b$ quarks at the $Z^0$ pole

In the standard model the coupling of the  $Z^0$  to each flavour depends only on the weak isospin of the  $q\bar{q}$  pair. The widths in the Born approximation are from (8.6.9)

$$\left. \begin{aligned} \Gamma^{\text{Born}}(Z \rightarrow c\bar{c}) &\simeq 280 \text{ MeV}, \\ \Gamma^{\text{Born}}(Z \rightarrow b\bar{b}) &\simeq 360 \text{ MeV}. \end{aligned} \right\} \quad (13.5.1)$$

Taking into account QCD corrections [see (8.6.13)], we find

$$\left. \begin{aligned} \Gamma(Z \rightarrow c\bar{c})/\Gamma_{\text{had}} &\simeq 0.171, \\ \Gamma(Z \rightarrow b\bar{b})/\Gamma_{\text{had}} &\simeq 0.217. \end{aligned} \right\} \quad (13.5.2)$$

These theoretical results are in quite nice agreement with the data. For instance, from the detection of the lepton produced in semi-leptonic

$\sigma$	Born		$O(\alpha)$		$O(\alpha^2)$ + exponentiation	
	$\sqrt{s}(\text{GeV})$	$\sigma(\text{nb})$	$\sqrt{s}(\text{GeV})$	$\sigma(\text{nb})$	$\sqrt{s}(\text{GeV})$	$\sigma(\text{nb})$
$\sigma(\mu\bar{\mu})$	90.984	2.0090	91.166	1.4219	91.090	1.4834
$\sigma(b\bar{b})$		8.6882		6.1211		6.3880
$\frac{\sigma(b\bar{b})}{\sigma(\mu\bar{\mu})}$		4.346		4.3049		4.3063

Table 13.5.  $\mu^+\mu^-$  and  $b\bar{b}$  cross-sections at the  $Z^0$ : comparison of Born and radiatively corrected approximations.

decays, ALEPH and L3 find

$$\left. \begin{aligned} \Gamma(Z \rightarrow c\bar{c})/\Gamma_{\text{had}}|_{\text{ALEPH}} &= 0.148 \pm 0.044(\text{stat})^{+0.045}_{-0.038}(\text{syst}) \\ \Gamma(Z \rightarrow b\bar{b})/\Gamma_{\text{had}}|_{\text{ALEPH}} &= 0.220 \pm 0.016(\text{stat}) \pm 0.024(\text{syst}) \end{aligned} \right\} \quad (13.5.3)$$

and

$$\Gamma(Z \rightarrow b\bar{b})/\Gamma_{\text{had}}|_{\text{L3}} = 0.218 \pm 0.010(\text{stat}) \pm 0.021(\text{syst}). \quad (13.5.4)$$

Semi-leptonic branching ratios have also been measured yielding

$$\text{BR}(b \rightarrow \ell X \nu)|_{\text{ALEPH}} = 0.102 \pm 0.010 \quad (13.5.5)$$

$$\text{BR}(b \rightarrow \ell X \nu)|_{\text{L3}} = 0.118 \pm 0.011 \quad (13.5.6)$$

which are compatible with the values quoted in Section 13.3.

### 13.5.2 Production cross-section

In Section 8.5 we gave results for the differential cross-section for  $e^+e^- \rightarrow f\bar{f}$  including  $Z^0 - \gamma$  interference and higher order corrections.

Upon integrating (8.5.21) or (8.5.27) over  $d\Omega$  we get results for the total cross-section for  $e^+e^- \rightarrow f\bar{f}$  in the SM.

The QED corrections are very important (see Kühn and Zerwas, 1990) and give substantial contributions to cross-sections around the  $Z^0$  peak. Their effects, however, largely cancel when ratios are taken. This can be seen from Table 13.5 where the Born cross-sections for  $\mu\bar{\mu}$  and  $b\bar{b}$  at the peak are compared with initial state radiative corrections calculated to order  $O(\alpha)$  and to order  $O(\alpha^2)$  [in the latter, an attempt is made to estimate higher orders by exponentiation (Berends *et al.*, 1987, 1988b)].

The  $s$  dependence around the  $Z^0$  mass of the various cross-sections ( $\mu^+\mu^-$ ,  $b\bar{b}$ ,  $c\bar{c}$  and their ratios) is shown in Fig. 13.20.

The detailed results from box amplitudes and interference between initial and final state emissions calculated at the parton level can be found in Kühn and Zerwas (1990) together with the original references.

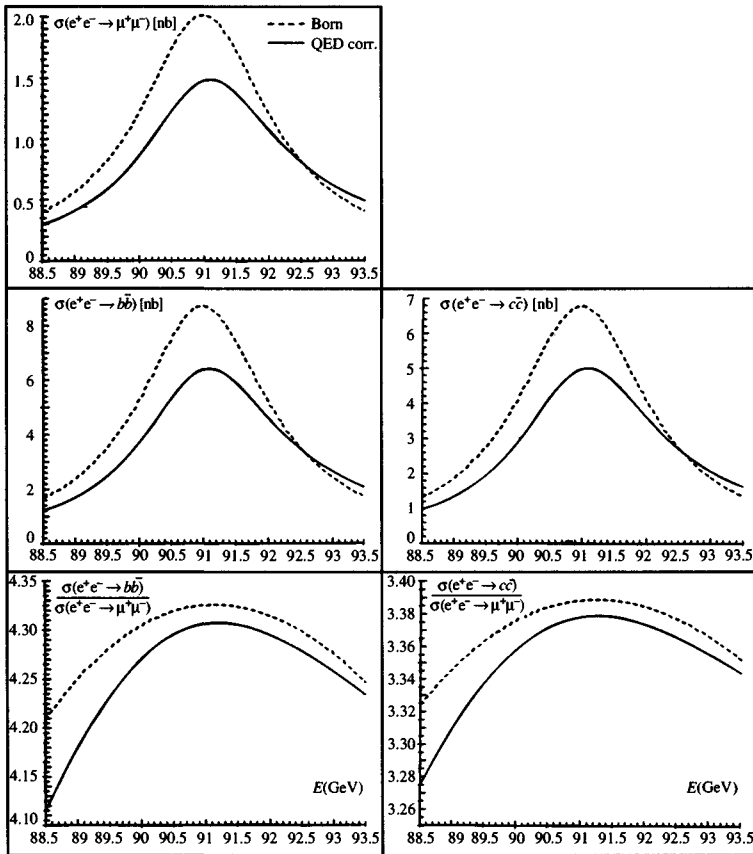


Fig. 13.20. Impact of QED corrections on the  $\mu^+\mu^-$ ,  $b\bar{b}$  and  $c\bar{c}$  cross-sections and on their ratio with parameters as described in the text.

### 13.5.3 Miscellaneous

A number of other studies are presently under way. For instance, asymmetries due to  $\gamma - Z^0$  interference can be studied in much the same way as in the case of lepton pair production which was considered in detail in Section 8.5.

Fig. 13.21 shows the forward-backward asymmetry as function of  $\cos\theta$  as measured by ALEPH (Dydak, 1991). This figure should be compared e.g. with Fig. 8.20.

Another matter under intense investigation is  $B^0 - \bar{B}^0$  mixing which is treated in detail in Chapter 19. Briefly, in semi-leptonic decays of  $b$  hadrons the charge of the lepton is correlated in sign with that of the initial quark. Therefore,  $B^0 - \bar{B}^0$  mixing can be measured from hadronic  $Z^0$  decays by monitoring pairs of high  $p_T$  leptons moving in roughly op-

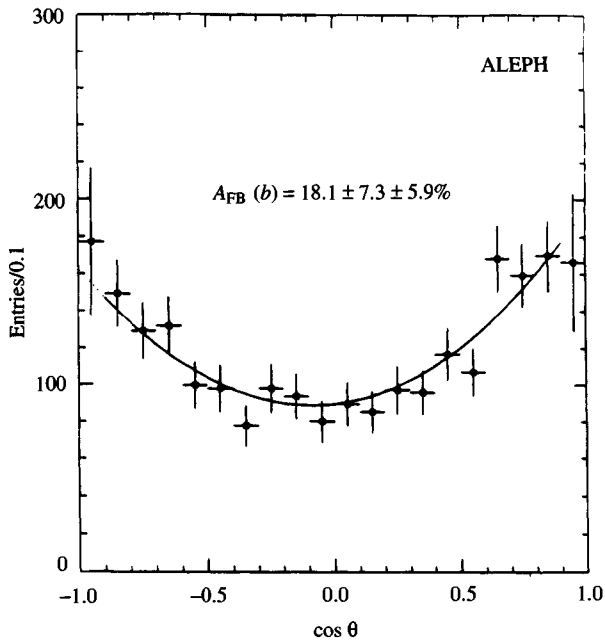


Fig. 13.21. Forward-backward asymmetry. (From Dydak, 1991).

posite directions. At LEP energies both  $B_d^0$  and  $B_s^0$  are produced so that what is measured is the average mixing parameter (see Section 19.1)

$$\chi_{\text{meas}} = \chi_d f_d + \chi_s f_s \quad (13.5.7)$$

where  $f_d(f_s)$  is the fraction of  $B_d^0(B_s^0)$  produced and

$$\chi_{d,s} = \frac{\text{Prob } (B_{d,s}^0 \rightarrow \bar{B}_{d,s}^0)}{\text{Prob } (B_{d,s}^0 \rightarrow B_{d,s}^0) + \text{Prob } (B_{d,s}^0 \rightarrow \bar{B}_{d,s}^0)}. \quad (13.5.8)$$

Ideally,  $\chi_{\text{meas}}$  is obtained by comparing the number of like-sign dileptons with the total number of dileptons. The preliminary results by ALEPH (1991)

$$\chi_{\text{meas}} = 0.132^{+0.027}_{-0.026}$$

and L3 (1991)

$$\chi_{\text{meas}} = 0.178^{+0.049}_{-0.040}$$

show significant  $b$  mixing.

In closing, we mention the measurement of the  $B$  lifetime  $\tau_b$  at LEP by

ALEPH (Tenchini, 1990)

$$\tau_b = [1.29 \pm 0.11(\text{stat}) \pm 0.12(\text{syst})] 10^{-12} \text{s} \quad (13.5.9)$$

quite close to, and well compatible with, the value quoted in Table 13.2.

### 13.6 Final comments

Heavy flavour physics has really just begun. We expect it to become one of the major subjects of the next few years with an impact on all aspects of the standard model on QCD and on CP violation.

Before closing this chapter, we should mention a new approach which has received considerable attention in recent years. The idea (Isgur and Wise, 1989, 1990) is that a great simplification occurs in the description of hadronic processes involving (at least) one heavy flavour  $Q$  if one takes the limit  $m_Q \rightarrow \infty$ . In this limit, the dynamical complications of strong interactions are considerably reduced. As an example, the large number of hadronic form factors describing the semi-leptonic transitions between two heavy pseudo-scalar or vector mesons reduce to just one (unknown) universal function (called the Isgur–Wise form factor) which depends on the change of velocity between the two heavy mesons. Not unexpectedly, the complications arise at the next order (i.e. the order  $1/m_Q$ ) where one is forced to reintroduce new different (non-perturbative) form factors to characterize the properties of the light quarks beyond the picture in which they move in the fixed static colour field of the infinitely heavy quark.

For a summary of both results and applications and a rather complete list of references on the subject, see Neubert (1992).

# 14

## The heavy lepton $\tau$

### 14.1 Introduction

The ratio  $R = \sigma(e^+e^- \rightarrow \text{anything})/\sigma(e^+e^- \rightarrow \mu^+\mu^-)|_{\text{QED}}$  around the charm threshold is shown in Fig. 14.1 which indicates how complicated this energy region is.

In the low energy region (i.e. below charm threshold  $\sqrt{s} \leq 3.5$  GeV) the quark model result  $R \simeq \sum_j Q_j^2$  gives the correct value within 20% once the various narrow peaks have been subtracted out.

In the 3.5–4 GeV region, a *very* complex structure emerges which was partly explained within the charmonium picture. However, the experimental jump  $\Delta R \simeq 2.5$  in going from 3.5 to 4.5 GeV fails to be explained by the jump expected theoretically on crossing the charm threshold

$$(\Delta R)_{\text{th}} = \sum_{\text{colour}} Q_c^2 = 3 \left( \frac{2}{3} \right)^2 = 1.33.$$

The possibility of new quarks in this mass range is made unlikely by the overall qualitative success of the charmonium model (Chapter 11), which assumes that only the charm quarks have come into play in the strong interaction sector, and the next known quark (the  $b$ ) lies too high up in mass to be of any relevance here.

The only possibility left to explain the jump in  $\Delta R$  within this framework is that new leptons (heavy ones\*) are produced and are mixed with the hadrons as a result of their large mass. Any such charged lepton

---

\* The term ‘heavy lepton’ is of course self-contradictory (an oxymoron) since ‘lepton’ is borrowed from the Greek for ‘weak’ or ‘light’ as compared with ‘hadron’ for ‘strong’ or ‘heavy’. The  $\tau$  is heavier than most known hadrons, which means that mass alone does not allow one to characterize the ‘elementarity’ of a particle. In the following, the ‘elementarity’ of leptons will be taken to imply their nearly point-like behaviour at least down to distances  $\approx 10^{-16}$  cm.

would (asymptotically) contribute one unit to the  $\Delta R$  jump and, therefore, in the energy range  $3.5 \text{ GeV} \lesssim \sqrt{s} < 4.5 \text{ GeV}$ , the contribution of just one heavy lepton would restore the validity of the charge counting rule to within 20%. Furthermore, as seen from Fig. 8.1, no further contribution from heavy leptons would seem to be needed up to the highest energies presently attainable, i.e. up to LEP energies. This, of course, has to be expected if the quark-lepton parallelism works and if only three generations of neutrinos exist.

From the previous discussion, we would expect the heavy lepton mass to be around 1.8–2.0 GeV, i.e. extremely close to the mass of the charm meson. That there are no heavy leptons with mass  $\leq 1.5 \text{ GeV}$  has been established (Bernardini *et al.*, 1973; Zichichi, 1977) by earlier experimental searches. The cross-section for lepton pair production, within QED, i.e.  $e^+e^- \rightarrow \gamma \rightarrow \tau^+\tau^-$ , assuming point-like spin  $\frac{1}{2}$  particles, is given by

$$\sigma_{\tau\tau} = \sigma_{\mu\mu}\beta(3 - \beta^2)/2 \quad (14.1.1)$$

where  $\sigma_{\mu\mu}$  is the usual lowest order QED  $\mu^+\mu^-$  cross-section (with  $m_\mu/\sqrt{s}$  neglected)

$$\sigma_{\mu\mu} = 4\pi\alpha^2/3s \quad (14.1.2)$$

and  $\beta$  is the  $\tau$  velocity. Therefore,  $\sigma_{\tau\tau}$  rises rapidly from threshold (at  $\sqrt{s} = 2m_\tau$ ) towards its asymptotic value  $\sigma_{\mu\mu}$  (14.1.2).

## 14.2 Discovery of the $\tau$ lepton

The final evidence for a new lepton was seen by the SLAC-LBL group at SLAC in 1975 and soon after by the PLUTO group at DESY in 1976 in  $e^+e^-$  collisions producing ‘anomalous’  $e\mu$  events (Perl *et al.*, 1975, 1976, 1977; Feldman *et al.*, 1976; PLUTO, 1977; DASP, 1977).

Given that lepton conservation forbids the reaction  $e^+e^- \rightarrow \mu^\mp e^\pm$  the appearance of  $e\mu$  events could be interpreted as the signal for a two-step process of the kind

$$\begin{array}{c} e^+e^- \rightarrow \tau^+\tau^- \\ \downarrow \\ e^-\bar{\nu}_e\nu_\tau \\ \downarrow \\ \mu^+\nu_\mu\bar{\nu}_\tau \end{array} \quad (14.2.1)$$

where  $\tau$  is a new heavy lepton.

In this picture the simplest option is that the heavy lepton is a ‘sequential’ lepton (i.e. endowed with lepton quantum number of its own, distinct from those of both the electron and the muon). This case can

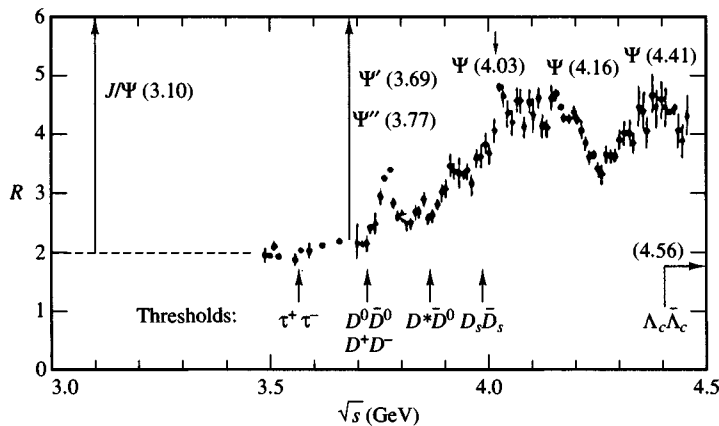


Fig. 14.1.  $R$  value versus the centre of mass energy in the  $\tau$ -charm energy range.

easily be accommodated within the standard model by simply adding a new doublet  $\begin{pmatrix} \nu_\tau \\ \tau^- \end{pmatrix}$ . This has already been mentioned several times.

Other possibilities that have been considered in the literature are that  $\tau^-$  could be a new lepton with: (i) the quantum numbers of either the electron or the muon (this has occasionally been referred to as the ‘ortholepton’ hypothesis)—in this case the  $\tau$  neutrino,  $\nu_\tau$  would be identical with either  $\nu_e$  or  $\nu_\mu$ ; (ii) with the quantum numbers of one of the light antileptons (the ‘paralepton’ hypothesis)—in this case  $\nu_\tau$  would be identical with either  $\bar{\nu}_e$  or  $\bar{\nu}_\mu$ . All these hypotheses have by now been dismissed on experimental grounds.

For paraleptons (with  $V \pm A$  coupling and massless neutrino) it turns out that there is a factor of 2 in the ratio of electron and muon decay modes. For example, in the electron-type case  $\tau^- \equiv E^-$  one would have

$$BR(E^- \rightarrow \bar{\nu}_e e^- \bar{\nu}_e) / BR(E^- \rightarrow \bar{\nu}_e \mu^- \bar{\nu}_\mu) = 2, \quad (14.2.2)$$

whereas for the muon type the ratio would be 0.5. The data in Table 14.1 rule out this possibility.

The simplest case of an ortholepton, where the  $\tau$  would be an excited state of either  $e$  or  $\mu$  that decays *electromagnetically*, is again excluded by the data. This, on the other hand, does not rule out ortholepton with weak decays only. We shall not discuss this point in detail but we simply mention that, in this case, a neutral current coupling could occur and produce semi-hadronic or three-charged-lepton decays. Ortholeptons with conventional coupling are, again, excluded by the data (see Table 14.2). Moreover, the overwhelming evidence in favour of the standard model

Parameter	Units	Prediction <sup>†</sup>	Exp. value
Mass	$\text{MeV}/c^2$		$1784.1^{+2.7}_{-3.6}$
Neutrino mass	$\text{MeV}/c^2$		$< 35$
Spin		1/2	1/2
Lifetime	$10^{-13}\text{s}$	2.8	$3.05 \pm 0.06$
Michel parameter		0.75	$0.734 \pm 0.055 \pm 0.026$
One-prong BR%			
$X^- \nu \nu$		$\sim 50$	$50.3 \pm 0.6$
$e^- \nu \nu$		18.9	$17.93 \pm 0.26$
$\mu^- \nu \nu$		18.4	$17.58 \pm 0.27$
$\varrho^- \nu$		22.7	$22.7 \pm 0.8$
$\pi^- \nu$		10.8	$11.6 \pm 0.4$
Topological $n$ -prong branching ratios			world averages
$B_1$			$86 \pm 0.3$
$B_3$			$13.9 \pm 0.3$
$B_5$			$0.15 \pm 0.03$
$B_{>5}$			$< 0.019 \quad 90\% \text{CL}$

Table 14.1. Summary of  $\tau$  parameters (the one-prong predictions are normalized assuming  $BR_\mu = 0.973 \ BR_e$ ).

<sup>†</sup> The origin of the predicted values is explained in the text.

makes it very unlikely that the  $\tau$  could be a singlet, in contradistinction to the  $(e, \nu_e)$  and  $(\mu, \nu_\mu)$  doublets.

To make sure that the  $e\mu$  events seen are really produced in reaction (14.2.1) several conditions must be met: for example, (i) there must be  $\mu^+ e^-$  (or a  $\mu^- e^+$ ) pair; and so, (ii) care must be taken to avoid misidentification between hadron and leptons—in the case of the SLAC-LBL detector this required the lepton momenta to be rather large (typically larger than  $650 \text{ MeV}/c$ , whereas no such cut was necessary at PLUTO); (iii) there must be no photons. One could have events with no associated photons from two virtual photon processes  $e^+ e^- \rightarrow e^+ e^- \mu^+ \mu^-$ . This contribution can be calculated and is negligibly small but can anyway be eliminated by further demanding that: (iv) there are no other charged particles; (v) the process should not be a two-body process, which implies

that there should be some missing energy and that the two charged prongs should be reasonably acoplanar with the incident beam (typically, by at least 20'); (vi) criteria must be given to discriminate against charm production and decay. This is not difficult because, as seen in Chapter 13, the latter goes mostly via production of hadrons and, in general, of more than two charged tracks. Furthermore, as repeatedly emphasized,  $D$  mesons tend to decay mostly into kaons, whereas the heavy lepton, being slightly below the charm mass, has a very low branching ratio into kaons.

An example of one of the consistency checks is given in Fig. 14.2 where the data from SLAC are shown. The expected momentum spectrum of the  $e$  or  $\mu$  produced in the reaction (14.2.1) through the three-body decays  $\tau \rightarrow \nu_\tau e \bar{\nu}_e$  or  $\tau \rightarrow \nu_\tau \mu \bar{\nu}_\mu$  is shown in Fig. 14.2(a) and compared with that expected from a two-body decay  $\tau \rightarrow e\nu$  or  $\tau \rightarrow \mu\nu$  (dashed curve). Fig. 14.2(b) shows the SLAC-LBL data; at low momenta the acceptance did not allow the identification of the particle, but at large momentum the data agree with the three-body decay, and two-body decays of the  $\tau$  are excluded. Fig. 14.2(c) shows a reconstruction of the momentum spectrum at PLUTO, leading to the same conclusions.

The final evidence that no hadrons are present in the  $e\mu$  events has come from PLUTO. (This does not mean that  $\tau$  cannot decay into hadrons. We shall see later that it decays weakly into several hadrons; see Table 14.2, which is a combination of data from the Particle Data Group (1992) and data presented at the 1990 Singapore High Energy Conference.)

To make the above analysis convincing is very tricky, and a large number of extensive articles exist. For a review, see the Proceedings of the Tau-charm Factory Workshop (SLAC-343, 1989).

### 14.3 Properties of the $\tau$ lepton

#### 14.3.1 The $\tau$ mass

The  $\tau$  mass was first determined from the threshold behaviour of the cross-section (14.1.1). From (14.1.1) the quantity

$$R_{eh} \equiv \frac{\sigma(e^+e^- \rightarrow \tau^+\tau^- \rightarrow eh)}{\sigma(e^+e^- \rightarrow \mu^+\mu^-)}$$

is given by

$$R_{eh} = P_{eh}\beta(3 - \beta^2)/2, \quad (14.3.1)$$

where  $P_{eh}$  (which should not vary rapidly for small  $\beta$ ) is the probability that a  $\tau^+\tau^-$  pair decays into an electron plus a charged hadron.

$R_{eh}$  is shown in Fig. 14.3(a). Notice that the shape of the energy dependence agrees with that in (14.3.1) and is strictly a consequence of

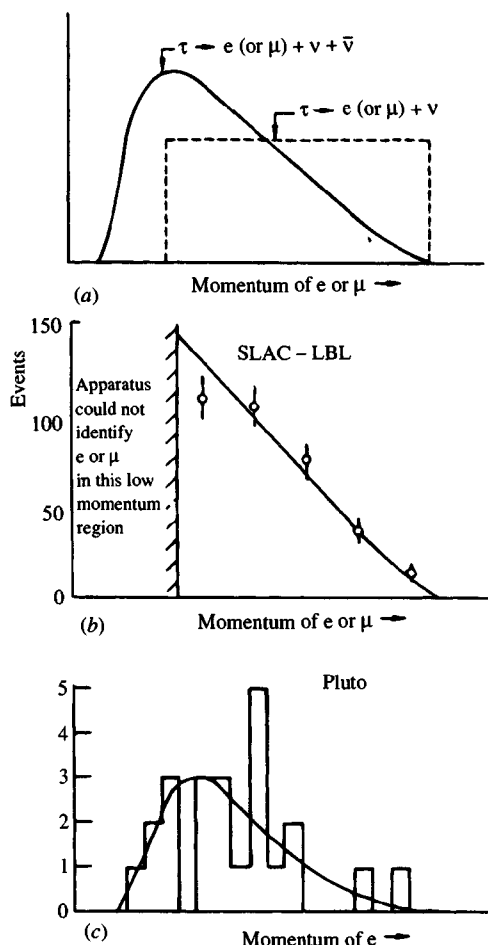


Fig. 14.2. Momentum spectra of  $e$  or  $\mu$  from  $\tau$  decay: (a) expected spectra of two-body and three-body decays, (b) and (c) SLAC-LBL and PLUTO data, respectively, compared with three-body spectrum. (From Perl, 1978.) More recent data are shown in Fig. 14.7.

the assumption that  $\tau$  is a lepton. Below threshold,  $R_{eh}$  is zero and it starts rising at  $\sqrt{s} = 2m_\tau$ . As the energy increases,  $\beta \rightarrow 1$  and  $R_{eh} \rightarrow P_{eh}$ . Fig. 14.3(b) shows the behaviour of

$$R_{e\mu} \equiv \frac{\sigma(e^+e^- \rightarrow \tau^+\tau^- \rightarrow \mu e)}{\sigma(e^+e^- \rightarrow \mu^+\mu^-)}, \quad (14.3.2)$$

where the numerator is the cross-section to produce  $e\mu$  pairs. The consistency of the data in Fig. 14.3(b) with (14.3.1) supports the claim that  $\tau$  is indeed a lepton.

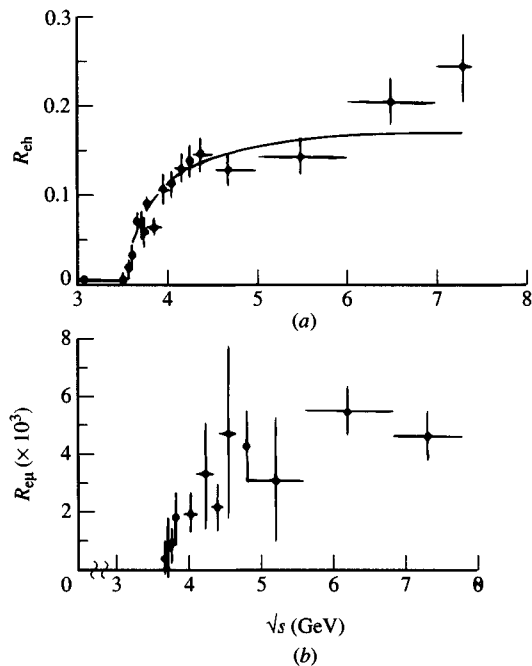


Fig. 14.3. Ratio of the cross-sections  $e^+e^- \rightarrow \tau^+\tau^- \rightarrow eh$  and  $e^+e^- \rightarrow \tau^+\tau^- \rightarrow e\mu$  to the cross-section for  $e^+e^- \rightarrow \mu^+\mu^-$ , denoted by  $R_{eh}$  and  $R_{e\mu}$  respectively. (From Perl, 1978.)

The best value for  $m_\tau$  is presently (Particle Data Group, 1992)

$$m_\tau = 1784.1^{+2.7}_{-3.6} \text{ MeV}/c^2 \quad (14.3.3)$$

i.e. slightly below the charm  $D$  meson mass.

### 14.3.2 The $\tau$ lifetime

In the SM one has for the  $\tau$  lifetime (using  $BR_e = 17.7 \pm 0.4$ )

$$\tau_\tau = \left( \frac{m_\mu}{m_\tau} \right)^5 BR_e \tau_\mu \simeq (2.81 \pm 0.06) 10^{-13} \text{ s}, \quad (14.3.4)$$

very close to the present world average (Particle Data Group, 1992)

$$\tau_\tau(\text{expt}) = (3.05 \pm 0.06) 10^{-13} \text{ s}. \quad (14.3.5)$$

Fig. 14.4 shows a compilation of results where the average is denoted by a vertical line to show the quick convergence of the measurements toward the present value of  $\tau_\tau$ .

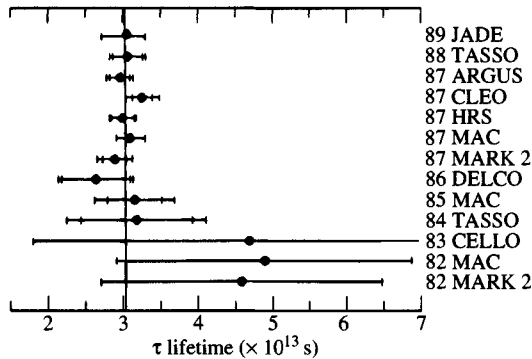


Fig. 14.4. A compilation of old results showing the quick convergence of  $\tau_\tau$  toward its present value (14.3.5).

#### 14.3.3 The spin of the $\tau$

Some of the data are compared in Fig. 14.5 with the behaviour expected from various spin assignments for the  $\tau$ , assuming that the particles produced are point-like.

The spin 0 result would tend, asymptotically, to

$$\sigma_{\tau\tau}(\text{spin } 0) = \frac{1}{4}\sigma_{\mu\mu}\beta^3|F_\tau|^2 BR_e BR_{ns}, \quad (14.3.6)$$

where  $\sigma_{\mu\mu} = 4\pi\alpha^2/3s$ ,  $F_\tau$  is the  $\tau$  form factor,  $BR_e$  is the branching ratio and  $BR_{ns}$  is the branching ratio for one non-showering track.

Assuming  $F_\tau = 1$  (see Section 14.3.4), and taking  $BR_e = 0.175$ , we see the curve to be lower by almost an order of magnitude as compared with the data. Spin 0 is therefore ruled out. So is the spin  $\frac{3}{2}$  result, which increases too fast.

For spin  $\frac{1}{2}$  we have

$$\sigma_{\tau\tau}(\text{spin } \frac{1}{2}) = \sigma_{\mu\mu}\beta\frac{1}{2}(3 - \beta^2)|F_\tau|^2 BR_e BR_{ns}, \quad (14.3.7)$$

whereas for spin 1

$$\sigma_{\tau\tau}(\text{spin } 1) = \sigma_{\mu\mu}\beta^3 \left[ \left( \frac{s}{4m_\tau^2} \right)^2 + 5 \left( \frac{s}{4m_\tau^2} \right) + \frac{3}{4} \right] BR_e BR_{ns} |F_\tau|^2. \quad (14.3.8)$$

The fit was made treating the  $\tau$  mass and the product  $BR_e BR_{ns}$  as free parameters and taking  $F_\tau = 1$ . Although spin 1 does not describe well the data, it could not be ruled out by the data shown in Fig. 14.5. The curve for spin 1, however, continues to grow with energy, while higher energy data flatten out to a constant in agreement with the assignment for spin  $\frac{1}{2}$  (14.3.7). The fit to the  $\frac{1}{2}$  curve, with the proper mass assignment, yields  $BR_{ns} \simeq 0.5 \pm 0.1$ .

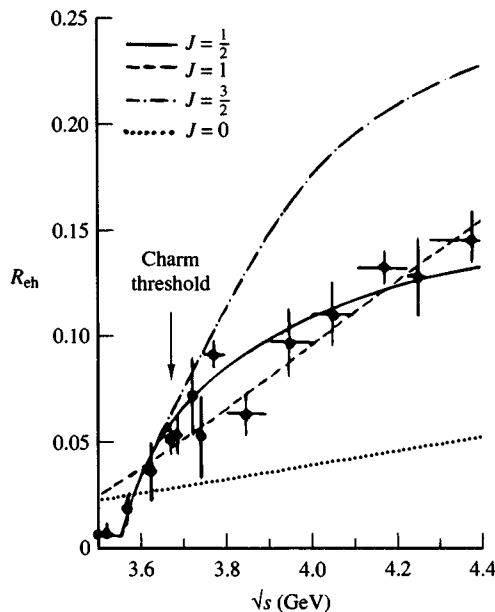


Fig. 14.5. Expectations for  $R_{eh}$  for various spins of the  $\tau$  lepton (from Bacino *et al.*, 1978).

#### 14.3.4 Point-like structure

The data are compatible with the curves calculated assuming point-like particles. Just as in the usual tests of QED, one can quantify this statement by introducing a form factor, which was denoted by  $F_\tau(s)$  in (14.3.7). If  $F_\tau(s)$  is parametrized as

$$F_\tau(s) = 1 \pm s/\Lambda_\pm^2, \quad (14.3.9)$$

the best fit to the cut-off parameter gives  $\Lambda_\pm > 50$  GeV showing essentially no deviation from point-like behaviour.

All in all, one has

$$\sigma_{\tau\tau}(9.4 \text{ GeV}) = (0.94 \pm 0.25)\sigma_{\tau\tau}(\text{QED}).$$

It seems safe, therefore, to conclude that the  $\tau$  is indeed a new spin  $\frac{1}{2}$  lepton, i.e. a point-like elementary particle whose behaviour is controlled by QED. In summary, the new lepton appears to have its own lepton quantum number, i.e. to be a ‘sequential’ lepton, with its own neutrino (as is discussed later), and its spin coupling structure is consistent with the traditional  $V - A$  coupling of its lighter companions  $e$  and  $\mu$ . It therefore seems to be a genuine recurrence in the  $\begin{pmatrix} \nu_e \\ e \end{pmatrix}, \begin{pmatrix} \nu_\mu \\ \mu \end{pmatrix}$  sequence.

We shall return later on the evidence in favour of a  $V - A$  coupling (Section 14.5).

#### 14.3.5 $\tau - e - \mu$ universality

This important concept has already been commented upon many times in previous chapters. It is worth recalling that from the  $\tau \rightarrow \mu$  and  $\tau \rightarrow e$  data one gets the following relation between the weak coupling constants  $G_{\tau\mu}$  and  $G_{\tau e}$  (Gerber, 1987)

$$G_{\tau\mu}/G_{\tau e} = 1.00 \pm 0.02. \quad (14.3.10)$$

Also *assuming* lepton universality, the  $\tau$  lifetime can be obtained by scaling the  $\mu$  lifetime and is related to the leptonic decay branching ratio  $BR_e = BR(\tau \rightarrow e\nu\bar{\nu})$  through eqn (14.3.4)

$$BR_e = \frac{\tau_\tau}{\tau_\mu} \left( \frac{m_\tau}{m_\mu} \right)^5 \quad (14.3.11)$$

(note that electroweak radiative corrections are only at the level of  $\sim 3 \times 10^{-4}$ ).

Putting into eqn (14.3.11) the lifetime measurements one gets  $BR_e = 18.9 \pm 0.49$ .

The data shown in Table 14.1 for the one-prong events make use of  $\mu - e$  universality. Taking account of the phase-space difference one has  $BR_\mu = 0.973BR_e$ .

## 14.4 $\tau$ decay

Granted the sequential lepton hypothesis, the origin of the ‘anomalous’  $e\mu$  events described in Section 14.2 is most naturally attributed to the decay (14.2.1). In this case, the various decay modes expected for the  $\tau$  lepton can be read off from the diagrams in Fig. 14.6.

It may seem odd that a spin 1 particle like the  $W$  can transform directly into a spin 0  $\pi$  in Fig. 14.6(c). The reason for this is rather subtle (Leader, 1968). In a Feynman diagram the propagator of a vector meson *off mass shell* is really a mixture of spin 1 and spin 0 pieces. Only *on mass shell* does it reduce to pure spin 1. However, if the vector meson couples to a conserved current (as does the photon) the spin 0 part gives no contribution. The axial part of the current to which the  $W$  couples is, of course, not conserved, which explains its ability to transform into the pseudo-scalar  $\pi$ . On the other hand, according to CVC (see Section 1.2), the  $W$  couples to a conserved vector current and thus it cannot transmute into a spin 0 *scalar* particle.

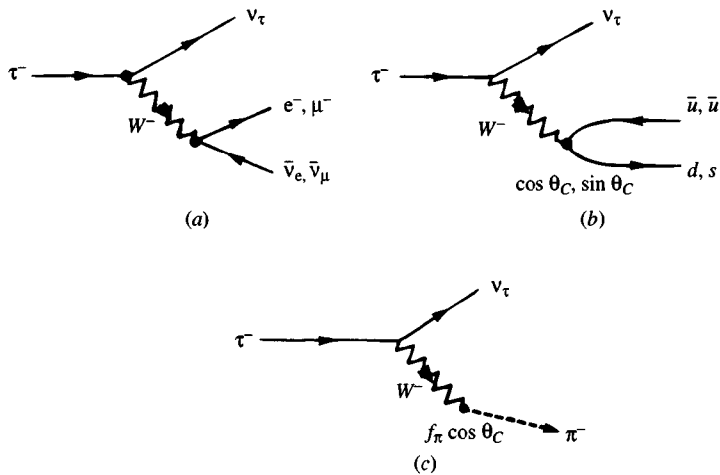


Fig. 14.6. Diagrams contributing to  $\tau$  decay (see text).

To the extent that lepton–quark universality holds, the mere counting of decay modes (the lepton modes, Fig. 14.6(a), contributing twice and the hadronic Cabibbo favoured mode, Fig. 14.6(b), contributing three times because of colour) yields the very naive prediction

$$\left. \begin{aligned} BR_e &\sim BR_\mu \simeq 0.2 \\ BR_h &\sim 3BR_e \simeq 0.6 \end{aligned} \right\}. \quad (14.4.1)$$

This is close to the prediction from  $\mu\tau$  universality (14.3.11) and is nicely confirmed by the data for which the world average is (Table 14.1).

$$BR_e \sim BR_\mu / 0.973 \simeq 17.7 \pm 0.4\%. \quad (14.4.2)$$

As was mentioned earlier, this rules out the paralepton hypothesis and makes it unlikely that the  $\tau$  is not a sequential lepton.

#### 14.4.1 Semi-leptonic $\tau$ decays

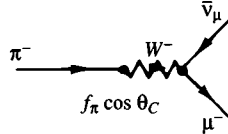
Owing to its large mass, the  $\tau$  lepton can decay into hadrons according to the graph shown in Fig. 14.6(b). However, because the  $\tau$  lies below charm threshold, its decays into strange particles will be Cabibbo suppressed.

Semi-leptonic decays are ideal for checking that the  $\tau$  really has the weak interaction properties expected within the standard model, since it should couple to hadrons of both vector  $J^P = 1^-$  and axial  $J^P = 0^-, 1^+$  types. Notice that no scalar  $J^P = 0^+$  final states can occur because of CVC as explained above.

As an example of a reaction controlled by the vector current, the theoretical prediction for  $\tau \rightarrow \nu_\tau \rho$ , on assuming the standard model

and using  $BR_e \simeq 17\%$ ,  $m_\varrho = 0.77 \text{ GeV}/c^2$  and  $m_\tau \simeq 1.8 \text{ GeV}/c^2$ , is  $BR(\tau \rightarrow \nu_\tau \varrho) \sim 25\%$  which is in reasonable agreement with the data.

As for the axial-vector current, of particular interest is the decay  $\tau \rightarrow \nu_\tau \pi$  (Fig. 14.6(c)) which is just the inverse of the usual  $\pi$  decay



and can therefore be unambiguously predicted from the pion decay constant (see (13.2.5))  $f_\pi \approx 0.132 \text{ GeV}$  to be  $BR(\tau \rightarrow \nu\pi) \simeq 11\%$ . The data (Table 14.1) are in good agreement with this prediction.

#### 14.4.2 QCD tests from $\tau$ decay

The inclusive semi-leptonic decay rate of the  $\tau$  lepton could provide an important testing ground for QCD if and when a  $\tau$  factory is constructed. The simplest quantity to look at is the ratio

$$r = \frac{\Gamma(\tau^- \rightarrow \nu_\tau + \text{hadrons})}{\Gamma(\tau^- \rightarrow \nu_\tau + e^- \bar{\nu}_e)} \quad (14.4.3)$$

which according to the naive argument of Section 14.4 is, to lowest order, essentially due to colour, i.e.

$$r = N_c(|V_{ud}|^2 + |V_{us}|^2) \simeq 3. \quad (14.4.4)$$

On the other hand, from the data on the branching fraction  $BR_e$  for a  $\tau$  to decay into an electron (or into a muon,  $BR_\mu = 0.973 BR_e$ ) we have (see Table 14.1)

$$r = \frac{1 - 1.973 BR_e}{BR_e} \simeq 3.68 \pm 0.08 \quad (14.4.5)$$

which is not so far from the naive expectation one would get by directly using the  $\tau$  lifetime value (14.3.5) in

$$\frac{1}{\tau_\tau} = \Gamma(\tau^-) = \Gamma(\tau^- \rightarrow \nu_\tau e^- \bar{\nu}_e)[1.973 + r] \quad (14.4.6)$$

using the theoretical value for the semi-leptonic width obtained in an obvious way from (4.2.33).

Since the accuracy of both measurements should increase considerably in the near future, let us briefly discuss the corrections expected to the naive prediction (4.3.4). These come from contributions such as (i) electroweak, (ii) perturbative QCD and (iii) non-perturbative QCD.

The electroweak corrections are small but are not negligible as they are proportional to  $\ln(M_Z/m_\tau)$ . The estimate (Marciano and Sirlin, 1988)

is that electroweak corrections add about  $\sim 2.4\%$  to the naive estimate (14.4.4).

QCD perturbative corrections are in principle calculable by treating the reactions as the decay into  $\bar{u}d$  (or  $\bar{u}s$ ) plus gluons and additional  $q\bar{q}$  pairs, as if the latter were free particles. This gives (Narison and Pich, 1988; Braaten, 1989a)

$$r_{\text{pert}} = 3 \left\{ 1 + \frac{1}{\pi} \alpha_s(m_\tau^2) + \frac{5.20}{\pi^2} \alpha_s^2(m_\tau^2) \right\} \quad (14.4.7)$$

which leads to  $r \approx 3.49$  if  $\alpha_s(m_\tau^2) \simeq 0.33$  is used. Higher order calculations are in progress. These could be important because of the rather large value of  $\alpha_s$  at the  $\tau$  mass.

Attempts have been made (Braaten, 1989b; Pich, 1989) to estimate the non-perturbative QCD contribution to  $r$  based upon QCD sum rules and the operator product expansion.

## 14.5 The $\tau$ neutrino

While the heavy lepton neutrino  $\nu_\tau$  has not yet been identified with absolute certainty, there are good reasons to believe that it exists. If not, it would be meaningless to assign a new lepton number to the  $\tau$ , and the  $\tau$  would be able to decay into  $\mu$  or  $e$ . In that case, a non-negligible contribution to  $\tau$  decay would for instance come from the reaction

$$\tau^- \rightarrow e^- + \bar{\nu}_e + \nu_e, \quad (14.5.1)$$

while, experimentally,

$$\frac{\Gamma(\tau^- \rightarrow e^- + \bar{\nu}_e + \nu_e)}{\Gamma(\tau^- \rightarrow \text{anything})} < 0.6\%, \quad (14.5.2)$$

so that we conclude that  $\nu_\tau$  must exist and  $\nu_\tau \neq \nu_\mu \neq \nu_e$ .

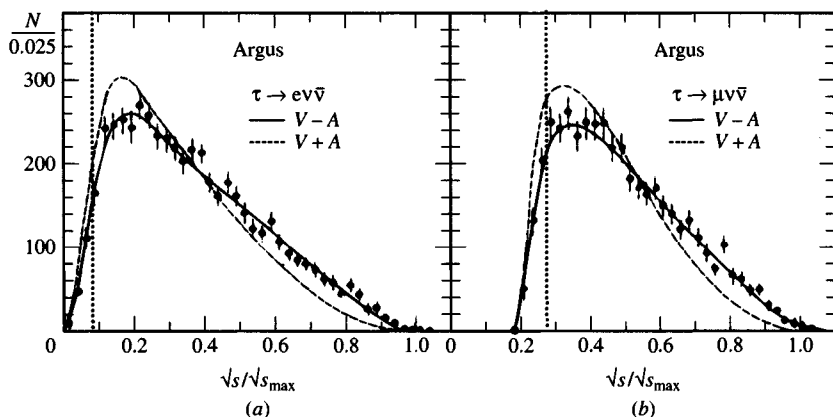
For many more limits testing lepton number conservation in  $\tau$  decays, see the 1992 edition of the Review of Particle Properties (Particle Data Group, 1992); see also Table 14.2.

Fig. 14.7 shows the ARGUS data on decay electron and muon energy distributions (ARGUS, 1990) with the form expected in the SM with  $V - A$ ,  $\tau - \nu_\tau$  coupling (continuous curves) and  $V + A$  coupling (dashed curves). These data are based on a total integrated luminosity of  $455 \text{ pb}^{-1}$ .

If a  $V - A$  coupling is assumed, the structure of the  $\tau$   $\beta$ -decay spectrum is given in terms of the usual Michel parameter  $\varrho^M$  (Section 1.4), i.e. the energy spectrum of the emitted lepton in the  $\tau$  rest frame is

$$\frac{1}{x^2} \frac{d\Gamma}{dx} = 12(1-x) - \frac{8}{3}(3-4x)\varrho^M + r(x) \quad (14.5.3)$$

Decay mode	$Q[\text{GeV}/c]$	Limit	Remarks
$\tau \rightarrow e\gamma$	0.9	$\sim 4 \times 10^{-5}$	Permitted
$\tau \rightarrow \mu\gamma$	0.9	$6 \times 10^{-4}$	if massive $\nu$ ,
$\tau \rightarrow e^+e^-e$	0.9	$3 \times 10^{-5}$	but doubly
$\tau \rightarrow e^+e^-\mu$	0.9	$3 \times 10^{-5}$	weak
$\tau \rightarrow e\mu^+\mu^-$	0.8	$3 \times 10^{-5}$	
$\tau \rightarrow \mu^+\mu^-\mu$	0.8	$3 \times 10^{-5}$	
$\tau \rightarrow \varrho^0 e$	0.5	$4 \times 10^{-5}$	
$\tau \rightarrow \varrho^0 \mu$	0.5	$4 \times 10^{-5}$	
$\tau \rightarrow \pi^0 e$	0.8	$2 \times 10^{-3}$	Most likely
$\tau \rightarrow \pi^0 \mu$	0.8	$8 \times 10^{-4}$	leptoquark
$\tau \rightarrow K^0 e$	0.6	$1.3 \times 10^{-3}$	mediated
$\tau \rightarrow K^0 \mu$	0.6	$1 \times 10^{-3}$	

Table 14.2. Searches for rare  $\tau$  decays (Particle Data Group, 1992).Fig. 14.7. Electron momentum distribution in  $\tau$  decay (ARGUS data) compared with  $V - A$  (continuous curve) and  $V + A$  (dashed curve) coupling.

where  $x$  is the momentum of the outgoing lepton divided by half the  $\tau$  mass and  $r(x)$  contains all radiative corrections.  $\varrho^M$  is given by

$$\varrho^M = \frac{3}{8} \frac{(g_V + g_A)^2}{g_V^2 + g_A^2} \quad (14.5.4)$$

so that one expects  $\varrho^M = \frac{3}{4}$  for  $V - A$  ( $g_V = g_A$ ), 0 for  $V + A$  ( $g_V = -g_A$ ) and  $3/8$  for pure  $A$  or  $V$  ( $g_V = 0$  or  $g_A = 0$ ).

The first results from various experiments gave hints of possible problems with

$$\varrho_e^M = 0.64 \pm 0.06 < 3/4$$

$$\varrho_\mu^M = 0.84 \pm 0.11 > 3/4$$

However, the latest high statistics ARGUS data (see e.g. Kühn, 1991) yield

$$\varrho^M = 0.734 \pm 0.055 \pm 0.026 \quad (14.5.5)$$

which favours the  $V - A$  coupling over either pure  $V$  or pure  $A$  and essentially excludes the  $V + A$  possibility.

From the  $V - A$  assumption one is led to the limit on the  $\tau$  neutrino mass given in Table 14.1, namely  $m_{\nu_\tau} < 35 \text{ MeV}/c^2$ .

The new generation of experiments under consideration presently should lower the above limit considerably, perhaps to some  $10 \text{ MeV}/c^2$ .

## 14.6 Rare $\tau$ decays

Rare decays are important in providing information about interactions not dominant under ordinary conditions. Rare lepton decays involving flavour changes are thus sensitive to interactions that go beyond the SM.

A compilation of experimental limits on some rare  $\tau$  decays is shown in Table 14.2 (from Heusch, 1989). Such decays could best be pursued at a  $\tau$  factory. Such facilities have already been advocated.

One suggestion is to have colliding high luminosity  $e^+e^-$  beams with energy in the range 3.0–4.2 GeV with the aim of producing up to  $10^8 \tau$  leptons per year. This would involve production of about  $10^{10} J/\Psi$  and  $10^8$  charm mesons per year. The design luminosity is  $10^{33} \text{ cm}^2/\text{s}$ .

It should be noted that the heavy mass of the  $\tau$  (and, therefore, its ability to decay weakly into ordinary hadrons) makes it a unique probe of the coupling to the standard quarks and leptons of any new weak boson. Also, the  $\tau$  may represent one of the dominant and more tractable decay modes of charged Higgs bosons.

It should, finally, be mentioned that excited  $\tau$  leptons which would manifest themselves through  $e^+e^- \rightarrow \tau^{*+}\tau^{*-} \rightarrow \tau^+\tau^-\gamma\gamma$  or  $e^+e^- \rightarrow \tau^*\tau \rightarrow \tau^+\tau^-\gamma$  have been excluded by LEP searches up to masses as high as  $45 \text{ GeV}/c^2$  (see, for instance, L3, 1990c).

## 14.7 Miscellaneous and conclusions

Recently, various results have been reported which seem to settle any controversy about the sequential lepton hypothesis for the  $\tau$ . In particular,

the correct amount of parity violation expected on the basis of the SM has been reported by the ARGUS collaboration in the analysis of  $\tau \rightarrow \nu 3\pi$  (see e.g. Kühn, 1991). As already shown (Fig. 14.7), the ARGUS collaboration has also given very strong indication that the  $\tau$  coupling is  $V - A$  to both electrons and muons and that the Michel parameter is very close to what is expected from the  $V - A$  theory. Strictly speaking, however, the value  $\varrho_\mu = \varrho_e = 0.75$  does not by itself guarantee the  $V - A$  coupling. Although unlikely, a  $V + A$  coupling with a new right-handed gauge boson  $W_R^-$  would also give  $\varrho^M = 0.75$ . To settle the issue one must measure the helicity of the  $\nu_\tau$  and this has been inferred from the  $\nu 3\pi$  decay as suggested long ago (Kühn and Wagner, 1984).

One measures the dependence of the decay rate upon the correlation between the normal to the triangle formed by the momenta of the three pions and the direction of the  $3\pi$  system in the LAB. Such a dependence signals parity violation in  $\tau$  decay. (The fact that parity is violated in  $\tau$  decay allows one to deduce its state of polarisation from the angular distribution of its decay products (see, e.g. Bourrely *et al.*, 1980). The importance of the polarisation of the  $\tau s$  produced in  $e^+e^- \rightarrow \tau^+\tau^-$  is discussed in Section 8.8.) The measured asymmetry leads to the conclusion that the  $\nu_\tau$  is indeed left-handed.

This, in turn, combined with the LEP demonstration of three neutrino species, gives strong support to the hypothesis of three left-handed lepton doublets  $\begin{pmatrix} \nu_e \\ e^- \end{pmatrix}_L, \begin{pmatrix} \nu_\mu \\ \mu^- \end{pmatrix}_L, \begin{pmatrix} \nu_\tau \\ \tau^- \end{pmatrix}_L$  and reinforces the conclusion that the discovery of the top quark should be forthcoming and should, at least provisionally, stop the hunt for more ‘elementary particles’ (but would still leave open the Higgs problem).

Ultimately, of course, this remains one of the crucial questions, i.e. how many more elementary objects, either leptons or quarks, we are going to find. And, if there are many, should one really think of them as elementary? In a sense, our experience with molecules, atoms, nuclei, nucleons and quarks suggests that it would be surprising if there ever are any *final* elementary constituents, a depressing thought which we may perhaps have to face. But a step beyond quarks is even more disturbing since it is the first time we will be postulating constituents of objects which themselves have never been seen (and can never be seen if the confinement hypothesis holds). In this case, any ‘proof’ of either elementarity or compositeness of quarks would be highly indirect: not a trivial problem when distances smaller than  $10^{-16}$  cm are involved!

# 15

## Towards the parton model—deep inelastic scattering

We have seen in earlier chapters that there seems to be a close parallelism between the sets of leptons and the sets of quarks, at least in so far as the unified weak and electromagnetic interaction is concerned. The leptons are essentially ‘point-like’ in their behaviour, and it is not inconceivable that the quarks too enjoy this property. In that case we might expect the hadrons to behave, in certain situations, in a less complicated fashion than usual. If we think of the hadrons as complicated ‘atoms’ or ‘molecules’ of quarks, then at high energies and momentum transfers, where we are probing the inner structure, we may discover a relatively simple situation, with the behaviour controlled by almost free, point-like constituents. The idea that hadrons possess a ‘granular’ structure and that the ‘granules’ behave as hard point-like, almost free (but nevertheless confined) objects, is the basis of Feynman’s (1969) *parton* model.

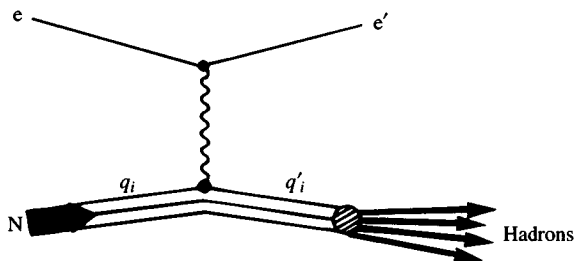
We shall discuss the model in some detail in the following chapters, in particular the question as to whether the partons can be identified with the quarks. The introductory material of the chapter is largely based upon lecture notes of F. Close (1973) (see also Close, 1979). We shall also study more sophisticated versions of the picture, wherein the quark-partons are not treated as free, but are allowed to interact with each other via the exchange of gluons, in the framework of QCD.

The essence of the parton model is the assumption that, when a sufficiently high momentum transfer reaction takes place, the projectile, be it a lepton or a parton inside a hadron, sees the target as made up of almost free constituents, and is scattered by a single, free, effectively massless constituent. Moreover the scattering from individual constituents is incoherent. The picture thus looks much like the impulse approximation of nuclear physics.

A typical process, ‘deep inelastic electron scattering’ on a nucleon, i.e.

$$e + N \rightarrow e' + X,$$

with large momentum transfer from electron to nucleon, would be viewed schematically as shown:



The fundamental interaction is the electromagnetic scattering of the electron on a parton  $q_i$ . The details of how the struck parton recombines with those partons that did not interact, so as to form physical hadrons, is not well understood. Since partons or quarks are assumed not to exist as real physical particles there must be unit probability for them to transmute into physical hadrons.

In order to understand the parton model properly one clearly requires a good understanding of the basic lepton-quark process

$$e + q \rightarrow e' + q',$$

i.e. the electromagnetic scattering of two spin-half point-like particles.

We thus begin with a pedagogical example. We study the very simple reaction:

$$e + \mu \rightarrow e' + \mu'$$

and at first consider only unpolarized cross-sections. The very interesting new discoveries using polarized targets (Ashman *et al.*, 1988) are dealt with in Section 15.6.

## 15.1 Electron-muon scattering

In lowest order perturbation theory of QED the reaction is described by the one-photon exchange diagram shown in Fig. 15.1.

Using the rules given in Appendix 2 the Feynman amplitude can be written down and has the form

$$M \sim [\bar{u}_e(k')\gamma_\beta u_e(k)] \frac{1}{q^2} [\bar{u}_\mu(p')\gamma^\beta u_\mu(k)]. \quad (15.1.1)$$

Taking the modulus squared of the amplitude, multiplying by the appropriate phase space and flux factors [see formula (A2.1.6) of Appendix 2], one finds that the differential cross-section for the electron to be scattered into solid angle  $d\Omega$  and final energy range  $E' \rightarrow E' + dE'$  in the

LAB frame is of the form

$$\frac{d^2\sigma}{d\Omega dE'} = \frac{1}{2} \frac{\alpha^2}{m_\mu q^4} \frac{E'}{E} L_{\alpha\beta}(e, e) W^{\alpha\beta}(\mu, \mu), \quad (15.1.2)$$

where  $\alpha$  is the fine structure constant, and in the LAB

$$p = (m_\mu, 0), \quad k = (E, \mathbf{k}), \quad k' = (E', \mathbf{k}'). \quad (15.1.3)$$

As usual the momentum transfer is

$$q = k - k'. \quad (15.1.4)$$

For our elastic reaction  $E'$  is of course fixed by energy-momentum conservation, but to facilitate comparison with later formulae we have hidden the energy  $\delta$ -function inside  $W^{\alpha\beta}(\mu, \mu)$ .

The tensors  $L_{\alpha\beta}(e, e)$ ,  $W^{\alpha\beta}(\mu, \mu)$  come from averaging over initial spins and summing over final spins in the factors arising from the electron and muon vertices when (15.1.1) is squared. Thus

$$\begin{aligned} L_{\alpha\beta}(e, e) &= \frac{1}{2} \sum_{\substack{\text{initial} \\ \text{spins}}} \sum_{\substack{\text{final} \\ \text{spins}}} [\bar{u}_e \gamma_\alpha u_e]^* [\bar{u}_e \gamma_\beta u_e] \\ &= \frac{1}{2} \text{Tr}\{(\not{k}' + m_e) \gamma_\alpha (\not{k} + m_e) \gamma_\beta\} \\ &= 2\{k_\alpha k'_\beta + k'_\alpha k_\beta - g_{\alpha\beta}(k \cdot k' - m_e^2)\}. \end{aligned} \quad (15.1.5)$$

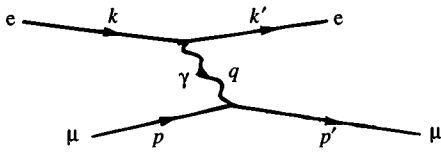
Note that with our normalization for the spinors, which holds for both massive leptons and neutrinos, the usual energy projection operators are  $\Lambda_\pm(p) = \pm \not{p} + m$  and there is no factor of  $2m$  in the denominator.

For  $W_{\alpha\beta}(\mu, \mu)$  we have a similar expression, except that we include in it the energy conserving  $\delta$ -function present in  $d^2\sigma/d\Omega dE'$ . Thus we have

$$W_{\alpha\beta}(\mu, \mu) = \frac{1}{2} \sum_{\substack{\text{initial} \\ \text{spins}}} \sum_{\substack{\text{final} \\ \text{spins}}} [\bar{u}_\mu \gamma_\alpha u_\mu]^* [\bar{u}_\mu \gamma_\beta u_\mu] \frac{\delta(p'_0 - p_0 - q_0)}{2p'_0} \quad (15.1.6)$$

$$\begin{aligned} &= 2\{p_\alpha p'_\beta + p'_\alpha p_\beta - g_{\alpha\beta}(p \cdot p' - m_\mu^2)\} \frac{\delta(p'_0 - p_0 - q_0)}{2p'_0} \\ &= 2\{2p_\alpha p_\beta + p_\alpha q_\beta + q_\alpha p_\beta - (p \cdot q)g_{\alpha\beta}\} \frac{\delta(p'_0 - p_0 - q_0)}{2p'_0}. \end{aligned} \quad (15.1.7)$$

[A more general version of this, valid for a transition between two different elementary fermions is given in (16.9.24).]

Fig. 15.1. Feynman diagram for  $e\mu \rightarrow e\mu$ .

We can rewrite the energy conserving  $\delta$ -function as follows. Since  $p'_0$  is positive,

$$\begin{aligned} \frac{1}{2p'_0} \delta(p'_0 - p_0 - q_0) &= \delta\{(p'_0 - p_0 - q_0)(p'_0 + p_0 + q_0)\} \\ &= \delta\{(p'_0)^2 - (p_0 + q_0)^2\}, \end{aligned} \quad (15.1.8)$$

and since  $\mathbf{p}' = \mathbf{p} + \mathbf{q}$  the RHS of (15.1.8) is just

$$\begin{aligned} \delta\{(p')^2 - (p + q)^2\} &= \delta\{m_\mu^2 - (m_\mu^2 + q^2 + 2p \cdot q)\} \\ &= \delta(q^2 + 2p \cdot q), \end{aligned} \quad (15.1.9)$$

which clearly shows its invariant character.

Carrying out the scalar product gives

$$\begin{aligned} L_{\alpha\beta}(e, e) W^{\alpha\beta}(\mu, \mu) &= 8[(p' \cdot k')(p \cdot k) + (p' \cdot k)(p \cdot k')] \\ &\quad - m_e^2(p \cdot p') - m_\mu^2(k \cdot k') + 2m_e^2m_\mu^2] \\ &\quad \times \delta(q^2 + 2p \cdot q). \end{aligned} \quad (15.1.10)$$

We shall always be in a region of high energies and momentum transfers where we can neglect the electron mass. In that case

$$q^2 \simeq -2k \cdot k', \quad (15.1.11)$$

and our formula (15.1.10) simplifies to

$$\begin{aligned} L_{\alpha\beta}(e, e) W^{\alpha\beta}(\mu, \mu) &= 8 \left\{ \left[ 2(p \cdot k)(p \cdot k') + \frac{p^2 q^2}{2} \right] - \left[ (p \cdot q) \frac{q^2}{2} \right] \right\} \\ &\quad \times \delta(q^2 + 2p \cdot q), \end{aligned} \quad (15.1.12)$$

where we have grouped terms that will later simplify.

*In the LAB frame*, we define

$$\nu = E - E' \quad (15.1.13)$$

as the energy transfer from the electrons to the target. The target muon being at rest we have also

$$\nu = \frac{q \cdot p}{m_\mu}. \quad (15.1.14)$$

Further, if  $\theta$  is the LAB scattering angle of the electron, from (15.1.11),

$$\begin{aligned} q^2 &\simeq -2EE' + 2\mathbf{k} \cdot \mathbf{k}' \\ &\simeq -2EE'(1 - \cos\theta) \\ &\simeq -4EE'\sin^2\frac{1}{2}\theta. \end{aligned} \quad (15.1.15)$$

Since  $q^2$  is negative in the scattering region it is common practice to introduce  $Q^2 = -q^2 > 0$  so that

$$Q^2 \equiv -q^2 \simeq 4EE'\sin^2\frac{1}{2}\theta. \quad (15.1.16)$$

Then (15.1.12) can be written

$$L_{\alpha\beta}(e, e)W^{\alpha\beta}(\mu, \mu) = 16m_\mu^2EE' \left[ \cos^2\frac{1}{2}\theta + \frac{\nu}{m_\mu} \sin^2\frac{1}{2}\theta \right] \delta(2q \cdot p - Q^2) \quad (15.1.17)$$

If we substitute in (15.1.2), and use (15.1.14), the cross-section in the LAB becomes

$$\frac{d^2\sigma}{d\Omega dE'} = \frac{\alpha^2}{4E^2 \sin^4\frac{1}{2}\theta} \left( \cos^2\frac{1}{2}\theta + \frac{Q^2}{2m_\mu^2} \sin^2\frac{1}{2}\theta \right) \delta\left(\nu - \frac{Q^2}{2m_\mu}\right), \quad (15.1.18)$$

where we have used the fact that  $\delta(az) = (1/a)\delta(z)$ .

It must be stressed that (15.1.18) holds in the LAB frame where the target muon is at rest.

If we are interested in the differential cross-section into angle  $d\Omega$  we can integrate (15.1.18) over  $E'$ , being careful to remember that  $Q^2$  depends on  $E'$  when  $\theta$  is held fixed [see (15.1.16)], to obtain

$$\frac{d\sigma}{d\Omega} = \left( \frac{d\sigma}{d\Omega} \right)_M \left( 1 + \frac{Q^2}{2m_\mu^2} \tan^2\frac{1}{2}\theta \right) \left( 1 + \frac{2E}{m_\mu} \sin^2\frac{1}{2}\theta \right)^{-1}, \quad (15.1.19)$$

where the ‘Mott’ cross-section is, at high energies,

$$\left( \frac{d\sigma}{d\Omega} \right)_M = \frac{\alpha^2 \cos^2\frac{1}{2}\theta}{4E^2 \sin^4\frac{1}{2}\theta}. \quad (15.1.20)$$

The Mott cross-section is just the cross-section for the scattering of a spin  $\frac{1}{2}$  particle in the Coulomb field of a massive (spinless) target. The extra factors in (15.1.19) arise (i) because the target has spin  $\frac{1}{2}$  and there is a contribution due to the *magnetic* interaction between electron and muon, and (ii) because the target has finite mass and recoils.

In the above, the electron and muon are treated as point-like spin  $\frac{1}{2}$  Dirac particles and thus possess only the intrinsic magnetic moments of magnitude  $e\hbar/2m_e c$  and  $e\hbar/2m_\mu c$  respectively. We now generalize to electron–proton scattering where the proton will be allowed an additional, i.e. anomalous, magnetic moment and will not be considered point-like.

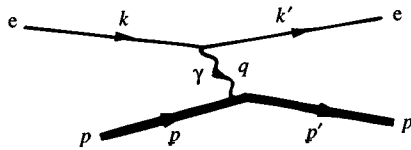


Fig. 15.2. Feynman diagram for elastic ep scattering.

The study of elastic ep scattering will set the stage for the remarkable and unexpected results that we shall find when we investigate *inelastic* ep scattering.

## 15.2 Elastic electron–proton scattering

Much effort has been expended over many years to study the charge distribution or form factors of the nucleon by probing it with beams of electrons (Hofstadter, 1957). The ‘classical period’ dealt principally with elastic scattering, which in lowest order perturbation theory of QED looks very similar to  $e\mu$  scattering; the only difference being that the vertex linking the  $\gamma$  to the proton is no longer point-like and should be given the most general form possible (see Fig. 15.2). Essentially we require an expression for  $\langle \text{proton } p' | J_{\text{em}}^\alpha | \text{proton } p \rangle$ .

Whereas for the muon or electron we had

$$\langle \text{electron } p' | J_{\text{em}}^\alpha | \text{electron } p \rangle = \bar{u}_e(p') \gamma^\alpha u_e(p),$$

we shall now have

$$\langle \text{proton } p' | J_{\text{em}}^\alpha | \text{proton } p \rangle = \bar{u}_p(p') \Gamma^\alpha u_p(p), \quad (15.2.1)$$

where the most general form of  $\Gamma^\alpha$  allowed by parity conservation and time reversal invariance is

$$\Gamma_\alpha = F_1(q^2) \gamma_\alpha + \frac{\kappa}{2m_p} F_2(q^2) i \sigma_{\alpha\beta} q^\beta + F_3(q^2) q_\alpha, \quad (15.2.2)$$

and

$$\sigma_{\alpha\beta} = \frac{i}{2} [\gamma_\alpha, \gamma_\beta]. \quad (15.2.3)$$

The  $F_j(q^2)$  are the electromagnetic ‘elastic structure functions’ or ‘elastic form factors’ of the proton, which can only depend on the momentum transfer  $q$ . In (15.2.2)  $\kappa$  is the anomalous magnetic moment of the proton measured in Bohr magnetons,  $\kappa = 1.79$ , and the term  $\kappa/2m_p$  is factored out for convenience.

For the electromagnetic case we are now dealing with,  $J_{\text{em}}^\alpha$  is a conserved current. Use of (1.1.4) then shows that  $F_3(q^2) \equiv 0$  so, in fact,

$$\Gamma_\alpha^{\text{em}} = F_1(q^2)\gamma_\alpha + \frac{\kappa}{2m_p}F_2(q^2)i\sigma_{\alpha\beta}q^\beta. \quad (15.2.4)$$

When we come to deal with neutrino scattering we shall have a current that is not conserved and the  $F_3$  type form factor will appear. The form factors  $F_1, F_2$  are defined in such a way that for  $q^2 = 0$ , which physically corresponds to the proton interacting with a static electro-magnetic field, one has

$$\left. \begin{aligned} F_1(0) &= 1 \\ F_2(0) &= 1 \end{aligned} \right\} \quad (15.2.5)$$

to ensure the correct electrostatic and magnetostatic interaction. (Note that if there is no anomalous magnetic moment one has  $F_2(0) = 0$ . If the particle is electrically neutral, e.g. the neutron, one has  $F_1(0) = 0$ .) The form factors  $F_{1,2}$  are usually referred to as the Dirac form factors. Often, however, one utilizes linear combinations of them. Thus one can use the Dirac equation to replace  $\bar{u}(p')i\sigma_{\alpha\beta}q^\beta u(p)$  by  $\bar{u}(p')[2m_p\gamma_\alpha - (p+p')_\alpha]u(p)$  and then

$$\Gamma_\alpha^{\text{em}} = G_M(q^2)\gamma_\alpha + \frac{G_E(q^2) - G_M(q^2)}{1 - q^2/4m_p^2} \times \frac{(p+p')_\alpha}{2m_p}, \quad (15.2.6)$$

where

$$\left. \begin{aligned} G_E(q^2) &= F_1 + \frac{\kappa q^2}{4m_p^2}F_2, \\ G_M(q^2) &= F_1 + \kappa F_2 \end{aligned} \right\} \quad (15.2.7)$$

are the Sachs electric and magnetic form factors. Note that  $G_E(0) = 1$ ,  $G_M(0) = 1 + \kappa$ .

The cross-section for  $e p \rightarrow e p$  is structurally the same as for  $e \mu \rightarrow e \mu$  except that  $\gamma_\alpha$  at the muon vertex is replaced by  $\Gamma_\alpha$  in the proton vertex. Thus (15.1.2) becomes

$$\frac{d^2\sigma}{d\Omega dE'} = \frac{1}{2} \frac{\alpha^2}{m_p q^4} \frac{E'}{E} L_{\alpha\beta}(e, e) W^{\alpha\beta}(p, p), \quad (15.2.8)$$

where

$$W_{\alpha\beta}(p, p) = \frac{1}{2} \text{Tr} \left\{ (\not{p}' + m_p) \Gamma_\alpha^{\text{em}} (\not{p} + m_p) \Gamma_\beta^{\text{em}} \right\} \frac{\delta(p'_0 - p_0 - q_0)}{2p'_0}. \quad (15.2.9)$$

After some algebra one arrives at the analogues of (15.1.18) and (15.1.19):

$$\frac{d^2\sigma}{d\Omega dE'} = \frac{\alpha^2}{4E^2 \sin^4 \frac{1}{2}\theta} \left[ \left( F_1^2 + \frac{\kappa^2 Q^2}{4m_p^2} F_2^2 \right) \cos^2 \frac{1}{2}\theta + \right.$$

$$+ \frac{Q^2}{2m_p^2} (F_1 + \kappa F_2)^2 \sin^2 \frac{1}{2}\theta \Big] \delta \left( \nu - \frac{Q^2}{2m_p} \right), \quad (15.2.10)$$

wherein  $F_{1,2}$  is short for  $F_{1,2}(q^2)$  and

$$\frac{d\sigma}{d\Omega} = \left( \frac{d\sigma}{d\Omega} \right)'_M \left[ \left( F_1^2 + \frac{\kappa^2 Q^2}{4m_p^2} F_2^2 \right) + \frac{Q^2}{2m_p^2} (F_1 + \kappa F_2)^2 \tan^2 \frac{1}{2}\theta \right] \quad (15.2.11)$$

where

$$\left( \frac{d\sigma}{d\Omega} \right)'_M \equiv \left( 1 + \frac{2E}{m_p} \sin^2 \frac{1}{2}\theta \right)^{-1} \left( \frac{d\sigma}{d\Omega} \right)_M.$$

Note that we recover the  $e\mu$  result by putting  $F_1 = 1$ ,  $F_2 = 0$  and  $m_p = m_\mu$ . We can thus say that the elastic form factor of a *point-like* particle such as the  $\mu$  is a constant, independent of  $Q^2$ . This fact is of vital importance for the parton idea.

Eqn (15.2.10), known as the Rosenbluth formula, is the basis of all experimental studies of the electromagnetic structure of nucleons.

Notice that both for nucleon and muon targets one has

$$\frac{d\sigma}{d\Omega} / \left( \frac{d\sigma}{d\Omega} \right)'_M = A + B \tan^2 \frac{1}{2}\theta, \quad (15.2.12)$$

where for a muon target

$$A = 1, \quad B = Q^2/2m_\mu^2 \quad (15.2.13)$$

and for a nucleon target

$$A = F_1^2 + \frac{\kappa^2 Q^2}{4m_p^2} F_2^2, \quad B = \frac{Q^2}{2m_p^2} (F_1 + \kappa F_2)^2. \quad (15.2.14)$$

The relation (15.2.12) is characteristic of single-photon exchange. By varying  $\theta$  at fixed  $Q^2$  one can check whether (15.2.12) holds, i.e. whether a one-photon exchange description is adequate. Experimentally, as shown in Fig. 15.3, (15.2.12) seems to hold remarkably well. By varying  $Q^2$  one can unravel the values of  $F_1$  and  $F_2$  as functions of  $q^2$ .

Experimentally  $F_1$  and  $F_2$  (or equivalently  $G_E$  and  $G_M$ ) have been studied from  $Q^2 = 0$  out to  $Q^2 \simeq 30$  (GeV/c)<sup>2</sup>. They are found to drop rapidly as  $Q^2$  increases. Roughly the behaviour is

$$G_E(q^2) \propto G_M(q^2) \propto \frac{1}{(1 + Q^2/0.71)^2}, \quad (15.2.15)$$

the so-called ‘dipole’ form.

Since in any case  $(d\sigma/d\Omega)_M$  is dropping rapidly, like  $1/Q^4$  as  $Q$  increases, we see that the *elastic* cross-section dies out very quickly as one

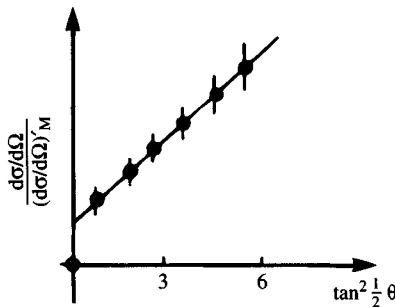


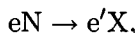
Fig. 15.3. Typical test of angular dependence in (15.2.12).

moves to large  $Q^2$  and it becomes increasingly difficult to carry out accurate measurements.

The remarkable discovery (Panofsky, 1968) that for *inelastic* reactions the analogous form factors do *not* decrease at large  $Q^2$  is the basis for the idea that the nucleon has a granular structure. The granules, or partons, give rise to far more events with large momentum transfer than would be expected with a continuous distribution of matter, just as, in Rutherford's famous experiment, the nucleus had caused many more alpha particles to bounce back through large angles than would have been expected from an atom with a smooth continuous distribution of matter.

### 15.3 Inelastic electron–nucleon scattering

We turn at last to the reaction of central interest to us,



where  $X$  stands for a sum over all the hadronic debris created in the inelastic collision. The reaction, which for large momentum transfer is usually referred to as 'deep inelastic electron scattering', is simply the inclusive scattering of the electron on the nucleon with measurement of the final energy and scattering angle of the scattered electron only.

It is assumed that the process is dominated by one-photon exchange, shown in Fig. 15.4 but direct tests of this are not as complete as in the elastic case.

One can test for the importance of two-photon exchange by comparing cross-sections using positrons and electrons as projectiles. It is intuitively easy to see why two-photon exchange will lead to a difference between the positron and electron cross-sections. Symbolically, one has

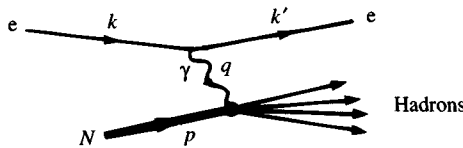


Fig. 15.4. Feynman diagram for deep inelastic lepton-nucleon scattering  $eN \rightarrow eX$ .

$$\begin{aligned} \sigma(e^+) &= | \text{diagram } 1 + \text{diagram } 2 |^2 \\ &\propto \{ae^2 + be^4 + ce^3\} \\ \sigma(e^-) &= | \text{diagram } 1 + \text{diagram } 2 |^2 \\ &\propto \{ae^2 + be^4 - ce^3\} \end{aligned}$$

The interference term changes sign under  $e^+ \rightarrow e^-$ . The same argument holds for  $\mu^\pm p \rightarrow \mu^\pm X$ . In Fig. 15.5 the ratio  $\sigma(\mu^+)/\sigma(\mu^-)$  is plotted vs  $Q^2$ . Within errors the ratio is certainly compatible with the value 1.

For large values of  $Q^2$  one in any case expects weak interaction effects to alter the one-photon behaviour, but for the present we shall proceed on the assumption that one-photon exchange is adequate.

The differential cross-section (we label it ‘em’ for later comparison with neutrino induced reactions) in the LAB can again be written in the form ( $N = \text{proton or neutron}$ )

$$\frac{d^2\sigma_{\text{em}}}{d\Omega dE'} = \frac{1}{2} \frac{\alpha^2}{m_N q^4} \frac{E'}{E} L_{\alpha\beta}(e, e) W_{\text{em}}^{\alpha\beta}(N) \quad (15.3.1)$$

where  $L_{\alpha\beta}(e, e)$  is the same as earlier [see (15.1.5)], but  $W_{\text{em}}^{\alpha\beta}(N)$  is now more complicated. It corresponds to electromagnetic transitions of the target nucleon to all possible final states. It is thus given by

$$\begin{aligned} W_{\alpha\beta}^{\text{em}}(N) &= \frac{1}{2} \sum_{\substack{\text{initial} \\ \text{spins}}} \sum_{\substack{\text{all} \\ \text{states } X}} \langle X | J_\alpha^{\text{em}}(0) | N \rangle^* \\ &\times \langle X | J_\beta^{\text{em}}(0) | N \rangle (2\pi)^3 \delta^4(p_X - p - q), \quad (15.3.2) \end{aligned}$$

where  $p_X$  is the total four-momentum of the state  $|X\rangle$ .

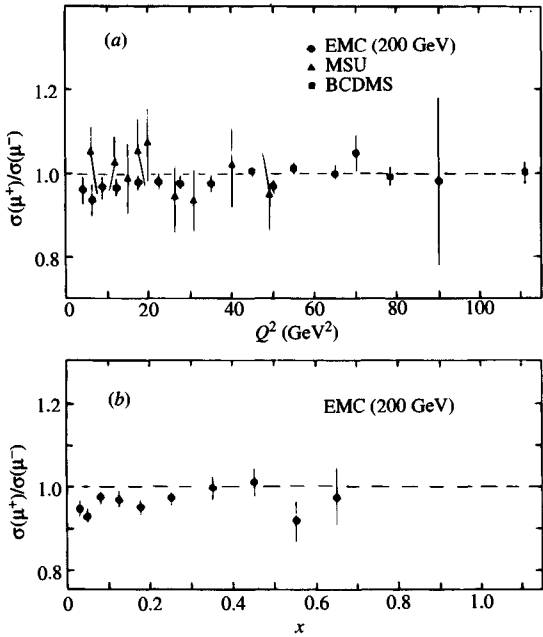


Fig. 15.5. Ratio of cross-section  $\sigma(\mu^+)/\sigma(\mu^-)$  for  $\mu^\pm p \rightarrow \mu^\pm X$  as function of square of momentum transfer. From EMC (1986). Note different scales.

Note that:

- (15.3.2) holds with states normalized so that

$$\langle \mathbf{p} | \mathbf{p}' \rangle = (2\pi)^3 2p_0 \delta^3(\mathbf{p} - \mathbf{p}'), \quad (15.3.3)$$

- the sum over all states X includes an integration

$$\int \frac{d^3 \mathbf{p}_j}{(2\pi)^3 2E_j}$$

for each particle  $j$  making up the system X as well as a sum over all spins involved.

Let us check that (15.3.2) reduces to our earlier result (15.2.9) when N is a proton and we restrict X also to be a proton. Then

$$\begin{aligned}
 W_{\alpha\beta}^{\text{elastic}}(N) &= \frac{1}{2} \sum_{\substack{\text{initial} \\ \text{spins}}} \sum_{\substack{\text{final} \\ \text{spins}}} \int \frac{d^3 \mathbf{p}'}{(2\pi)^3 2p'_0} (2\pi)^3 \delta^4(p' - p - q) \\
 &\quad \times [\bar{u}(p') \Gamma_\alpha u(p)]^* [\bar{u}(p') \Gamma_\beta u(p)] \\
 &= \frac{\delta(p'_0 - p_0 - q_0)}{2p'_0} \frac{1}{2} \sum_{\text{spins}} [\bar{u}(p') \Gamma_\alpha u(p)]^* [\bar{u}(p') \Gamma_\beta u(p)] \\
 &= W_{\alpha\beta}(p, p) \text{ as expected.}
 \end{aligned} \quad (15.3.4)$$

Despite the fact that each possible final state may give a very complicated contribution to  $W_{\alpha\beta}(N)$ , the resultant sum over spins has a relatively simple structure. Since  $J_\alpha^{\text{em}}$  is Hermitian we can write (15.3.2) as

$$W_{\alpha\beta}^{\text{em}}(N) = \frac{1}{2} \sum (2\pi)^3 \delta^4(p_X - p - q) \langle N | J_\alpha^{\text{em}} | X \rangle \langle X | J_\beta^{\text{em}} | N \rangle. \quad (15.3.5)$$

It is easily seen from (15.3.2) that

$$W_{\alpha\beta}^{\text{em}*}(N) = W_{\beta\alpha}^{\text{em}}(N). \quad (15.3.6)$$

We can then break up  $W_{\alpha\beta}^{\text{em}}$  into a symmetric and an anti-symmetric piece under  $\alpha \leftrightarrow \beta$ :

$$W_{\alpha\beta}^{\text{em}}(N) = W_{\alpha\beta}^{(S)}(N) + iW_{\alpha\beta}^{(A)}(N), \quad (15.3.7)$$

with both  $W^{(S)}$  and  $W^{(A)}$  real. [The split in (15.3.7) corresponds also to breaking  $W_{\alpha\beta}$  into its real and imaginary parts.] Because  $L_{\alpha\beta}(e, e)$  is explicitly symmetric under  $\alpha \leftrightarrow \beta$  [see (15.1.5)], when contracted with  $W_{\alpha\beta}$  in (15.3.1) only the symmetric part of  $W_{\alpha\beta}$  will contribute, i.e.

$$L^{\alpha\beta}(e, e)W_{\alpha\beta}^{\text{em}}(N) = L^{\alpha\beta}(e, e)W_{\alpha\beta}^{(S)}(N). \quad (15.3.8)$$

Moreover:

- the electromagnetic interaction conserves parity, so  $W_{\alpha\beta}$  has to be a genuine second rank tensor,
- all momenta are integrated over except  $p, q$  and  $p_X$ , and  $p_X = p + q$  because of the  $\delta$ -function,
- all spins are summed over.

Thus the final result can only depend on  $p$  and  $q$  and, of course, the metric tensor  $g_{\alpha\beta}$ .

The most general form possible for  $W_{\alpha\beta}^{(S)}$  is then

$$W_{\alpha\beta}^{(S)}(N) = A g_{\alpha\beta} + B q_\alpha q_\beta + C (q_\alpha p_\beta + q_\beta p_\alpha) + D p_\alpha p_\beta, \quad (15.3.9)$$

where the coefficients can depend only on the independent *scalars* formed from  $p$  and  $q$  which we can choose as  $\nu$  and  $q^2$ .

However, current conservation implies [see (1.1.4)] that

$$q^\alpha W_{\alpha\beta}^{\text{em}} = W_{\alpha\beta}^{\text{em}} q^\beta = 0, \quad (15.3.10)$$

and this must hold for both real and imaginary parts of  $W_{\alpha\beta}$ . Thus we require

$$(A + Bq^2 + Cp \cdot q)q_\beta + (Cq^2 + Dp \cdot q)p_\beta = 0. \quad (15.3.11)$$

Since  $q$  and  $p$  are independent vectors, the scalar coefficients in (15.3.11) must separately vanish. This is easily seen by going to the LAB frame where  $p = (m, 000)$  and first choosing  $\beta = x$  component, whereupon the first term must vanish, and then  $\beta =$  time component, whereupon the second must also vanish. Thus eliminating  $B$  and  $C$ , and introducing the conventional notation

$$W_1^{\text{eN}} = -\frac{A}{2m_N}, \quad \frac{W_2^{\text{eN}}}{m_N^2} = \frac{D}{2m_N}$$

one arrives at

$$\begin{aligned} \frac{1}{2m_N} W_{\alpha\beta}^{(\text{S})}(N) &= \left[ \frac{q_\alpha q_\beta}{q^2} - g_{\alpha\beta} \right] W_1^{\text{eN}}(\nu, q^2) \\ &\quad + \frac{1}{m_N^2} \left[ \left( p_\alpha - \frac{p \cdot q}{q^2} q_\alpha \right) \left( p_\beta - \frac{p \cdot q}{q^2} q_\beta \right) \right] W_2^{\text{eN}}(\nu, q^2). \end{aligned} \quad (15.3.12)$$

$W_{1,2}(\nu, Q^2)$  are known as the *structure functions* of the nucleon. They are the generalization to the inelastic case of the elastic form factors.

If we substitute (15.3.12) and (15.1.5) into (15.3.8) and neglect the lepton mass,

$$\begin{aligned} \frac{1}{2m_N} L^{\alpha\beta}(\text{e}, \text{e}) W_{\alpha\beta}^{\text{em}}(N) &= 4k \cdot k' W_1^{\text{eN}} + 2[2(p \cdot k)(p \cdot k') \\ &\quad - (k \cdot k') m_N^2] \frac{W_2^{\text{eN}}}{m_N^2}. \end{aligned} \quad (15.3.13)$$

Evaluating (15.3.13) in the LAB frame where  $p \cdot k = m_N E$ ,  $p \cdot k' = m_N E'$  and using (15.1.11) and (15.1.15), we get the simple result

$$\frac{1}{2m_N} L^{\alpha\beta}(\text{e}, \text{e}) W_{\alpha\beta}^{\text{em}}(N) = 4EE' (2W_1^{\text{eN}} \sin^2 \frac{1}{2}\theta + W_2^{\text{eN}} \cos^2 \frac{1}{2}\theta). \quad (15.3.14)$$

Note that we shall not append the subscript ‘em’ to the  $W_j$ . It ought not to be forgotten however.

Substituting in (15.3.1) we get finally for the LAB cross-section

$$\frac{d^2\sigma_{\text{em}}}{d\Omega dE'} = \frac{4\alpha^2(E')^2}{q^4} (2W_1^{\text{eN}} \sin^2 \frac{1}{2}\theta + W_2^{\text{eN}} \cos^2 \frac{1}{2}\theta), \quad (15.3.15)$$

where  $W_{1,2}$  are short for  $W_{1,2}(\nu, Q^2)$ , or

$$\frac{d^2\sigma_{\text{em}}}{d\Omega dE'} = \frac{\alpha^2}{4E^2 \sin^4 \frac{1}{2}\theta} (2W_1^{\text{eN}} \sin^2 \frac{1}{2}\theta + W_2^{\text{eN}} \cos^2 \frac{1}{2}\theta). \quad (15.3.16)$$

Our definitions of  $W_{1,2}$  agree with those usually used in the literature, and (15.3.15) and (15.3.16) are the standard forms for the differential cross-sections.

We note that the expression for  $d^2\sigma/d\Omega dE'$  has once again the characteristic angular dependence that we found for  $e\mu \rightarrow e\mu$  and for  $ep \rightarrow ep$ .

Comparing (15.3.16) with (15.2.10), we see, for example, that the *elastic* contribution to  $W_{1,2}^{ep}$  is

$$\left. \begin{aligned} W_2^{ep}(\nu, Q^2)_{\text{el}} &= \left( F_1^2 + \frac{\kappa^2 Q^2}{4m_p^2} F_2^2 \right) \delta \left( \nu - \frac{Q^2}{2m_p} \right), \\ W_1^{ep}(\nu, Q^2)_{\text{el}} &= \frac{Q^2}{4m_p^2} (F_1 + \kappa F_2)^2 \delta \left( \nu - \frac{Q^2}{2m_p} \right), \end{aligned} \right\} \quad (15.3.17)$$

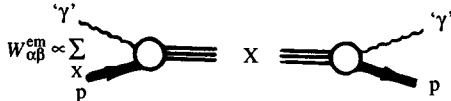
where  $F_{1,2}$  are the proton form factors.

Were we to be studying the reaction  $e\mu \rightarrow e'X$  we would conclude from the discussion after (15.2.11) that the elastic contribution to  $W_{1,2}^{e\mu}$  is

$$\left. \begin{aligned} W_2^{e\mu}(\nu, Q^2)_{\text{el}} &= \delta \left( \nu - \frac{Q^2}{2m_\mu} \right), \\ W_1^{e\mu}(\nu, Q^2)_{\text{el}} &= \frac{Q^2}{4m_\mu^2} \delta \left( \nu - \frac{Q^2}{2m_\mu} \right). \end{aligned} \right\} \quad (15.3.18)$$

The structure of these equations will be very important later on.

It is also important to interpret the  $W_{1,2}$  from a somewhat different point of view. Diagrammatically we have



where ‘ $\gamma$ ’ is an off-shell, i.e. virtual-photon, and the states  $|X\rangle$  consist of all possible physical particles. So  $W_{\alpha\beta}$  must be related, via the optical theorem [see, for example, Landau and Lifshitz (1977)], to the imaginary part (more correctly ‘absorptive part’) of the Feynman amplitude for forward scattering of virtual photons on nucleons, i.e. to the forward virtual Compton amplitude. Indeed (as will be shown in Section 15.6), if one introduces polarization vectors  $\epsilon^\alpha(\lambda)$  for *virtual* photons of mass  $q^2$  and helicity  $\lambda$ , where  $\lambda = \pm 1, 0$ , corresponding to the three possible states of polarization of a *massive* photon, and if  $K$  denotes the flux of incoming virtual photons, then the total cross-sections for photo-absorption of virtual photons on an unpolarized nucleon  $N$  are

$$\sigma_\lambda^{\gamma N} = \frac{4\pi^2 \alpha}{K 2m_N} \epsilon^{\alpha*}(\lambda) W_{\alpha\beta}^S(N) \epsilon^\beta(\lambda). \quad (15.3.19)$$

There are two problems to be solved.

- What are the polarization vectors for a virtual photon?

- What is the flux for a ‘beam’ of virtual photons?

The first is straightforward. One simply uses the polarization vectors for a massive spin-one particle. If the photon of mass  $q^2$  is moving along the  $Z$ -axis with energy  $\nu$  then

$$\epsilon^\alpha(\pm 1) = \mp \frac{1}{\sqrt{2}}(0, 1, \pm i, 0), \quad (15.3.20)$$

and, for the longitudinal mode [c.f. (2.1.13)]

$$\epsilon^\alpha(0) = \frac{1}{\sqrt{q^2}} \left( \sqrt{\nu^2 - q^2}, 0, 0, \nu \right). \quad (15.3.21)$$

Parity invariance implies  $\sigma_{+1} = \sigma_{-1}$  for an unpolarized target, so there are two independent cross-sections, usually taken as the transverse (T) and longitudinal (L) cross-sections

$$\sigma_T^{\gamma N} \equiv \frac{1}{2}(\sigma_{+1}^{\gamma N} + \sigma_{-1}^{\gamma N}), \quad \sigma_L^{\gamma N} \equiv \sigma_0^{\gamma N}. \quad (15.3.22)$$

Whereas for a real photon the flux factor is  $K = \nu$ , for virtual photons there is no unambiguous definition. It is simply a matter of convention.

Gilman (1967) uses

$$K^{\text{Gil}} = \sqrt{\nu^2 - q^2} \xrightarrow{\nu \rightarrow \infty} \nu + \frac{Q^2}{2\nu}, \quad (15.3.23)$$

whereas Hand (1963) takes  $K$  to be the energy that a real photon would need in order to create the final state involved. The final state has mass  $M^*$  given by

$$M^{*2} = (p + q)^2 = m_N^2 + 2m_N\nu - Q^2$$

so we must have

$$2m_N K^{\text{Han}} = 2m_N\nu - Q^2,$$

i.e.

$$K^{\text{Han}} = \nu - \frac{Q^2}{2m_N}. \quad (15.3.24)$$

Naturally both  $K^{\text{Gil}}$  and  $K^{\text{Han}}$  reduce to  $\nu$  at  $Q^2 = 0$ . In what follows, the convention is not relevant. In either convention, using (15.3.19), (15.3.22) and (15.3.12) one finds

$$\left. \begin{aligned} W_1^{\text{eN}} &= \frac{K}{4\pi^2\alpha} \sigma_T^{\gamma N}, \\ W_2^{\text{eN}} &= \frac{K}{4\pi^2\alpha} \frac{Q^2}{Q^2 + \nu^2} (\sigma_T^{\gamma N} + \sigma_L^{\gamma N}). \end{aligned} \right\} \quad (15.3.25)$$

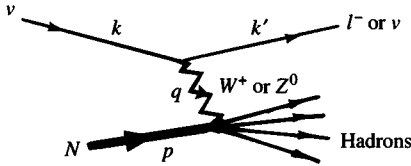


Fig. 15.6. Feynman diagram for deep inelastic neutrino-nucleon scattering:  $\nu N \rightarrow \ell^- (\text{or } \nu) X$ .

A fundamental quantity is the ratio

$$R = \frac{\sigma_L^{\gamma N}}{\sigma_T^{\gamma N}} = \frac{W_2^{eN}(\nu, Q^2)}{W_1^{eN}(\nu, Q^2)} \left( 1 + \frac{\nu^2}{Q^2} \right) - 1, \quad (15.3.26)$$

whose value, as will be seen later, is an indicator of the spin of the hadron's constituents.

Finally, we note that in the literature the inclusive cross-section (15.3.16) for  $eN \rightarrow e'X$  is sometimes written in terms of  $\sigma_T^{\gamma N}$  and  $\sigma_L^{\gamma N}$ :

$$\frac{d^2\sigma_{em}}{d\Omega dE'} = \Gamma(\sigma_T^{\gamma N} + \epsilon\sigma_L^{\gamma N}), \quad (15.3.27)$$

$$\left. \begin{aligned} \text{where } \epsilon &= \left( 1 + 2 \frac{Q^2 + \nu^2}{Q^2} \tan^2 \frac{1}{2}\theta \right)^{-1} \\ \text{and } \Gamma &= \frac{K\alpha}{2\pi^2 Q^2} \times \frac{E'}{E} \times \frac{1}{1 - \epsilon}. \end{aligned} \right\} \quad (15.3.28)$$

## 15.4 Inelastic neutrino-nucleon scattering

We consider now reactions of the type

$$\nu N \rightarrow \ell^- X \quad \text{and} \quad \nu N \rightarrow \nu X$$

where  $\ell^-$  is any lepton. These reactions are clearly very similar to inelastic electron-nucleon scattering, the main differences being that the nucleon is here probed by one of the gauge vector bosons rather than by the photon, and that the coupling at the leptonic vertex now contains both vector and axial-vector pieces. The process is visualized as in Fig. 15.6, which structurally is quite similar to Fig. 15.4. For later convenience we shall always think of this as the *emission* of a gauge boson by the leptons and the *absorption* of the gauge boson by the hadron. Because of the similarity to the electromagnetic case we shall be brief in our treatment.

The inclusive cross-section will be given by a formula closely analogous to (15.3.1) in which the following replacements must be made:

1. If  $\ell = e^-$  or  $\mu^-$ , i.e. we have a charged current reaction (CC),

$$\left. \begin{array}{l} q^2 \rightarrow q^2 - M_W^2, \\ e^2 \rightarrow \frac{G}{\sqrt{2}} M_W^2 \end{array} \right\} \quad (15.4.1)$$

[where we have used (5.1.1) and (5.1.2)], and  $L_{\alpha\beta}(ee) \rightarrow 8L_{\alpha\beta}(\nu)$  (the factor 8 is for later convenience), where the  $\nu$  tensor is obtained from (15.1.5) by changing  $\gamma_\alpha$  to  $\gamma_\alpha(1 - \gamma_5)$  and omitting the factor of  $\frac{1}{2}$  that corresponded to averaging over the two spin states of the initial electron. One then finds

$$L_{\alpha\beta}(\nu) = k_\alpha k'_\beta + k'_\alpha k_\beta - g_{\alpha\beta} k \cdot k' + i\epsilon_{\alpha\beta\gamma\delta} k^\gamma k'^\delta, \quad (15.4.2)$$

the new term, antisymmetric under  $\alpha \leftrightarrow \beta$ , and a pseudo-tensor under space inversion, having arisen from the vector–axial-vector interference at the vertex.

2. If  $\ell = \nu_e$  or  $\nu_\mu$ , i.e. we have a neutral current reaction (NC),

$$\left. \begin{array}{l} q^2 \rightarrow q^2 - M_Z^2, \\ e^2 \rightarrow \frac{GM_Z^2}{2\sqrt{2}} \end{array} \right\} \quad (15.4.3)$$

[where we have used (5.1.10) and (5.1.2) and the SM relation  $M_W = M_Z \cos \theta_W$ ], and  $L_{\alpha\beta}(ee) \rightarrow 8L_{\alpha\beta}(\nu)$  as in (1) above.

Later, when we consider higher order corrections,  $G$  as used in this chapter should be thought of as shorthand for  $e^2/(4\sqrt{2}\sin^2 \theta_W M_W^2)$ .

Thus we have, for  $\nu N \rightarrow \ell^- X$

$$\frac{d^2\sigma_{CC}^\nu}{d\Omega dE'} = \frac{1}{2m_N} \left( \frac{G}{2\pi} \right)^2 \left( \frac{M_W^2}{Q^2 + M_W^2} \right)^2 \frac{E'}{E} L_{\alpha\beta}(\nu) W_{CC}^{\alpha\beta}(\nu N), \quad (15.4.4)$$

where, by analogy with (15.3.2), and using (8.3.6)

$$\begin{aligned} W_{CC}^{\alpha\beta}(\nu N) &= \frac{1}{2} \sum_{\substack{\text{initial} \\ \text{spins}}} \sum_{\text{all} \atop \text{states } X} (2\pi)^3 \delta^4(p_X - p - q) \langle X | h_+^\alpha | N \rangle^* \langle X | h_+^\beta | N \rangle \\ &= \frac{1}{2} \sum (2\pi)^3 \delta^4(p_X - p - q) \langle N | h_-^\alpha | X \rangle \langle X | h_+^\beta | N \rangle, \end{aligned} \quad (15.4.5)$$

where we have used the fact that

$$h_+^{\alpha\dagger} = h_-^\alpha. \quad (15.4.6)$$

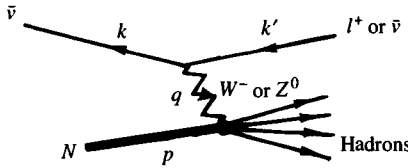


Fig. 15.7. Feynman diagram for deep inelastic antineutrino-nucleon scattering:  $\bar{\nu}N \rightarrow \ell^+(\text{or } \bar{\nu})X$ .

For  $\nu N \rightarrow \nu X$  we have

$$\frac{d^2\sigma_{NC}^\nu}{d\Omega dE'} = \frac{1}{2m_N} \left( \frac{G}{2\pi} \right)^2 \left( \frac{M_Z^2}{Q^2 + M_Z^2} \right)^2 \frac{E'}{E} L_{\alpha\beta}(\nu) W_{NC}^{\alpha\beta}(\nu N), \quad (15.4.7)$$

where via (7.5.2) and (8.3.6)

$$W_{NC}^{\alpha\beta}(\nu N) = \frac{1}{2} \sum (2\pi)^3 \delta^4(p_X - p - q) \langle N | h_Z^\alpha | X \rangle \langle X | h_Z^\beta | N \rangle. \quad (15.4.8)$$

Finally, to complete our armoury, we need expressions for the cross-sections induced by *antineutrinos* as visualized in Fig. 15.7. The change required at the leptonic vertex was explained in Section 1.3.2. The propagator is unchanged, and at the hadronic vertex, for CC reactions,  $h_+ \rightarrow h_-$ . For NC reactions the hadronic vertex is unchanged.

We end up therefore with expressions completely analogous to (15.4.4) and (15.4.7), in which the label  $\nu \rightarrow \bar{\nu}$  and wherein

$$L_{\alpha\beta}(\bar{\nu}) = k_\alpha k'_\beta + k'_\alpha k_\beta - g_{\alpha\beta} k \cdot k' - i\epsilon_{\alpha\beta\gamma\delta} k^\gamma k'^\delta. \quad (15.4.9)$$

For  $\bar{\nu}N \rightarrow \ell^+X$  there will occur in (15.4.4)

$$W_{CC}^{\alpha\beta}(\bar{\nu}N) = \frac{1}{2} \sum (2\pi)^3 \delta^4(p_X - p - q) \langle N | h_+^\alpha | X \rangle \langle X | h_-^\beta | N \rangle, \quad (15.4.10)$$

while for  $\bar{\nu}N \rightarrow \bar{\nu}X$  there will appear in (15.4.7)

$$W_{NC}^{\alpha\beta}(\bar{\nu}N) = W_{NC}^{\alpha\beta}(\nu N). \quad (15.4.11)$$

Note from (15.4.5) and (15.4.10) that in general

$$W_{CC}^{\alpha\beta}(\nu N) \neq W_{CC}^{\alpha\beta}(\bar{\nu}N). \quad (15.4.12)$$

The precise relation between the  $\nu N$  and  $\bar{\nu}N$  tensors depends very much on the structure of the currents used. Since charm particles are rather heavy there is an energy regime in which it is reasonable to assume that charm particle production is negligible. In this regime we may take for the charged weak current

$$h_+^\alpha = \bar{u} \gamma^\alpha (1 - \gamma_5) (\cos \theta_C d + \sin \theta_C s). \quad (15.4.13)$$

The region *below charm threshold* will occasionally be referred to as BCT. If further we neglect  $\sin^2 \theta_C$  compared with  $\cos^2 \theta_C$ , which, bearing in

mind the difficulty of neutrino experiments and the inherently large experimental errors, is quite justified, we may take as the effective current

$$h_+^\alpha \simeq \bar{u}\gamma^\alpha(1 - \gamma_5)d. \quad (15.4.14)$$

We shall refer to this approximation as the ' $\theta_C = 0$ ' approximation. In this case  $h_+^\alpha$  has simple properties under isotopic spin rotations and we may obtain some general relations between the  $\nu N$  and  $\bar{\nu}N$  cases.

Thus, as discussed in Section 9.1, if our target has isospin zero, or if we average our measurements over all possible  $I_3$  values of the target so that in effect we have an isotopically neutral target (which we indicate by  $N_0$ ), then

$$W_{CC}^{\alpha\beta}(\nu N_0) = W_{CC}^{\alpha\beta}(\bar{\nu}N_0) \quad (\text{BCT}; \theta_C = 0). \quad (15.4.15)$$

In the case that  $N$  is a neutron or proton we can make a rotation of  $\pi$  around the '1' axis in isospace, using the fact that  $\sum_X |X\rangle\langle X|$  is isotopically neutral, to obtain, analogously to the manipulations leading to (1.3.20),

$$W_{CC}^{\alpha\beta}(\nu n) = W_{CC}^{\alpha\beta}(\bar{\nu}p) \quad (\text{BCT}; \theta_C = 0). \quad (15.4.16)$$

The case of the more general structure for the weak charged current will be discussed in Chapter 16.

For any of the  $\nu$  or  $\bar{\nu}$  induced reactions discussed above, the most general form of  $W_{\alpha\beta}$  is considerably more complicated than in the electromagnetic case. This is because there is no current conservation equation like (15.3.10) and because the non-symmetric form of  $L_{\alpha\beta}(\nu)$  implies the need to utilize that part of  $W_{\alpha\beta}$  which is antisymmetric under  $\alpha \leftrightarrow \beta$ . The latter has an antisymmetric part, even for the unpolarized case, because it can be a mixture of a pure tensor and a pseudo-tensor, since parity is violated.

One has for CC, NC,  $\nu$  or  $\bar{\nu}$  and unpolarized target,

$$\begin{aligned} \frac{1}{2m_N} W_{\alpha\beta} &= -g_{\alpha\beta}W_1 + \frac{p_\alpha p_\beta}{m_N^2}W_2 - \frac{i\epsilon_{\alpha\beta\gamma\delta}p^\gamma q^\delta}{2m_N^2}W_3 + \frac{q_\alpha q_\beta}{m_N^2}W_4 \\ &\quad + \frac{p_\alpha q_\beta + p_\beta q_\alpha}{2m_N^2}W_5 + i\frac{p_\alpha q_\beta - p_\beta q_\alpha}{2m_N^2}W_6. \end{aligned} \quad (15.4.17)$$

But this complexity is only temporary. When contracted with the leptonic tensor  $L^{\alpha\beta}(\nu)$  in (15.4.2), and upon neglecting lepton masses, the terms involving  $W_{4,5,6}$  disappear. The only new term in the result is then  $W_3$  which arises from the contraction of the vector–axial-vector interference term at the leptonic vertex with the analogous interference term at the hadronic vertex.

Although the kinematic coefficients of  $W_{1,2}$  in (15.4.17) look different from those in (15.3.12), the neglect of the lepton mass when using the

latter has the effect that only those parts of the coefficients in (15.3.12) that also appear in (15.4.17) actually contribute to the final answer. The final result for the cross-section in terms of structure functions then looks very similar to the electromagnetic case.

Remembering the relationship between  $L_{\alpha\beta}(\nu)$  and  $L_{\alpha\beta}(\bar{\nu})$  [see (15.4.2) and (15.4.9)] one has for CC, NC,  $\nu$  and  $\bar{\nu}$  reactions

$$\begin{aligned}\frac{d^2\sigma^{\nu,\bar{\nu}}}{d\Omega dE'} = & \frac{G^2}{2\pi^2} \left( \frac{M^2}{M^2 + Q^2} \right)^2 (E')^2 [2W_1^{\nu,\bar{\nu}} \sin^2 \frac{1}{2}\theta \right. \\ & \left. + W_2^{\nu,\bar{\nu}} \cos^2 \frac{1}{2}\theta \mp W_3^{\nu,\bar{\nu}} \frac{E + E'}{m_N} \sin^2 \frac{1}{2}\theta],\end{aligned}\quad (15.4.18)$$

where the upper (lower) sign holds for neutrino (antineutrino) induced reactions, and where for CC reactions  $M = M_W$  and for NC reactions  $M = M_Z$ .

Finally we remark that like the electromagnetic case one can relate the structure functions to total cross-sections for the absorption of virtual  $W$  (or  $Z^0$ ) of various helicities on unpolarized nucleons. The analogue of (15.3.25) is

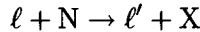
$$\left. \begin{aligned}W_1 &= \frac{K}{\pi GM^2\sqrt{2}}(\sigma_1 + \sigma_{-1}), \\ W_2 &= \frac{K}{\pi GM^2\sqrt{2}} \frac{Q^2}{Q^2 + \nu^2} (\sigma_1 + \sigma_{-1} + 2\sigma_0), \\ W_3 &= \frac{K}{\pi GM^2\sqrt{2}} \frac{2m_N}{\sqrt{Q^2 + \nu^2}} (\sigma_1 - \sigma_{-1}).\end{aligned}\right\} \quad (15.4.19)$$

Previously we had  $\sigma_1 = \sigma_{-1} \Rightarrow W_3^{\text{em}} = 0$ . Now because of the parity-violating  $V - A$  structure,  $\sigma_1 \neq \sigma_{-1}$ .

The above relations will be important in understanding the parton model for the structure functions  $W_j$ .

## 15.5 Deep inelastic scattering and scaling behaviour

The term ‘deep inelastic’ for the reaction



refers to the kinematical domain where both  $Q^2$  and the mass  $M_X$  of the produced hadrons are large compared with typical hadron masses. Since

$$M_X^2 = (p + q)^2 = m_N^2 + 2m_N\nu - Q^2 \quad (15.5.1)$$

we see that also  $\nu$  must be large.

For  $\nu$  and  $Q^2$  such that  $M_X$  is small, a plot of  $d\sigma/dM_X$  vs  $M_X$  shows typical resonance bumps as  $M_X$  crosses values corresponding to the pro-

duction of hadron resonances like  $N^*$ . As  $M_X$  increases one reaches a region where smooth behaviour sets in. This is the deep inelastic region.

Note that for elastic scattering  $Q^2 = 2m_N\nu$ . Also that for fixed  $Q^2$  one approaches the deep inelastic domain by increasing  $\nu$ .

Aside from the energy of the initial lepton, the cross-sections etc. can be taken to depend on any *two* of the variables  $Q^2, \nu, M_X^2$ . In practice other variables are often used. The most important are

$$x \equiv \frac{1}{\omega} \equiv \frac{Q^2}{2m_N\nu} = \frac{Q^2}{2p \cdot q}, \quad y \equiv \frac{\nu}{E} = \frac{p \cdot q}{p \cdot k} \quad (15.5.2)$$

with  $0 \leq x \leq 1$  and  $1 \leq \omega \leq \infty; 0 \leq y \leq 1$ .

It is easiest to measure cross-sections at a fixed LAB angle  $\theta$ , picking up the scattered leptons with various energies  $E'$ . This will correspond to a range of values for  $\nu$  and  $Q^2$ . However, from (15.3.16) or (15.4.18), we will not be able to get exact values of the individual structure functions  $W_j$  unless we can vary  $\theta$  adequately. If we assume that the  $W_j$  are of roughly the same magnitude, then for very small  $\theta$  the  $\sin^2 \frac{1}{2}\theta$  terms can be neglected and a measurement of the cross-section should yield a sensible estimate of the value of  $W_2$ .

Measurements at several angles for the electromagnetic cases yielded values of the ratio  $W_2/W_1$  or, as usually presented, of the ratio  $R$  defined in (15.3.26), but accurate answers seem notoriously difficult to achieve and new generations of experiments have several times resulted in changes in the accepted values of  $R$ . The dependence of  $R$  upon  $(\nu, Q^2)$  or  $(x, Q^2)$  is of great theoretical interest, as will be discussed in Section 23.8 but is not very well determined. Some data, for two values of  $x$ , as functions of  $Q^2$ , are shown in Fig. 15.8 (the curves will be discussed later). It is seen that there is a wide spread in the experimental values, but some hint of a decrease at the largest value of  $Q^2$  shown. The reader is warned that sometimes in experimental analyses it is *assumed* that  $R$  is a constant or zero for simplicity.

We remarked earlier in Section 15.2 that the nucleon *elastic* form factors drop rapidly with  $Q^2$ , roughly as  $Q^{-4}$ . On the other hand the elastic form factors of the *point-like* muon were constants independent of  $Q^2$ .

One of the most remarkable discoveries of the recent past is shown in Fig. 15.9. When values of the inelastic electromagnetic structure function  $W_2$  measured at SLAC are displayed in the form  $\nu W_2$  vs  $Q^2$  at fixed values of  $\omega$  or  $x$  [see (15.5.2)] it seems to be largely independent of  $Q^2$  for  $Q^2 \geq 1(\text{GeV}/c)^2$  in complete contrast to the behaviour of the elastic form factors. [This would not be true for  $Q^2 \rightarrow 0$  since because of (15.3.25)  $W_2 = 0$  at  $Q^2 = 0$ ].

*A priori*,  $\nu W_2$  is a function of two variables  $(\nu, Q^2)$  or, equivalently,  $(x, Q^2)$ . The notion that  $\nu W_2$ , considered as a function of  $(x, Q^2)$ , depends

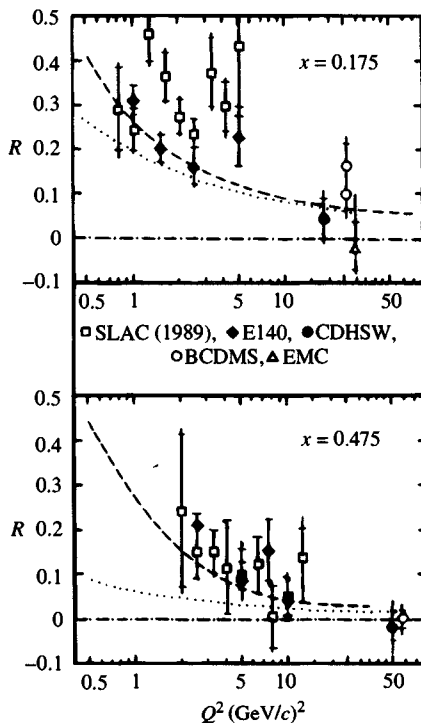


Fig. 15.8.  $R(x, Q^2)$  at fixed  $x$  as function of  $Q^2$  for two values of  $x$ ; from Feltesse (1989). Experimental data are SLAC (1989), SLAC E140 (1988), CDHSW (1991), BCDMS (1987) and EMC (1986).

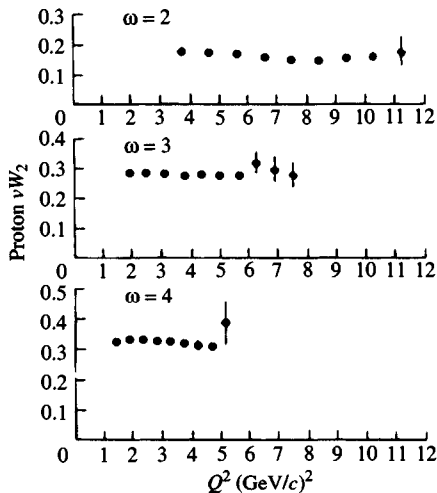


Fig. 15.9. Scaling behaviour of electromagnetic structure function  $\nu W_2$  at various  $\omega$  values. There is virtually no variation with  $Q^2$ . (From Panofsky, 1968.)

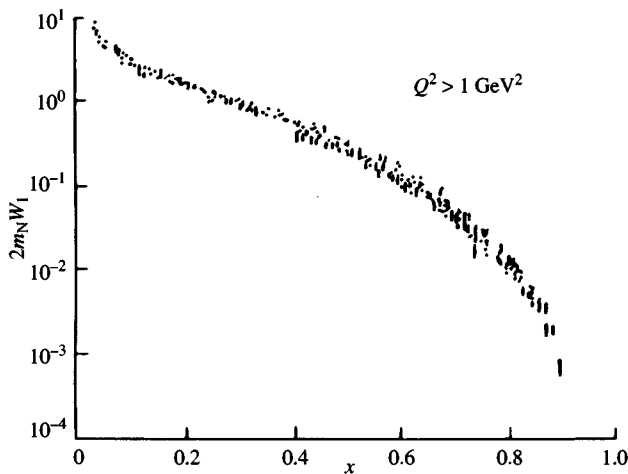


Fig. 15.10. Scaling behaviour of electromagnetic structure function  $2m_N W_1$ . Almost no  $Q^2$  dependence is visible. (From Panofsky, 1968.)

only on  $x$  is known as *scaling*, and the fact that it does not decrease as  $Q^2$  increases suggests that some sort of collision with *point-like* objects is the underlying dynamical mechanism at work.

Fig. 15.10 is a diagram of historic importance. It shows  $2m_N W_1$  plotted against  $x$  for a wide range of values of  $Q^2$ . It is seen that at each  $x$  there is hardly any dependence on  $Q^2$ .

The surprising lack of dependence of  $\nu W_2$  and  $W_1$  on  $Q^2$  was in a sense predicted by Bjorken (1969). He studied  $W_{\alpha\beta}(\nu, Q^2)$  in the following mathematical limit (now referred to as the ‘Bjorken limit’)

$$Q^2 \rightarrow \infty, \quad \nu \rightarrow \infty, \quad x = \frac{Q^2}{2m_N \nu} \quad \text{fixed} \quad (15.5.3)$$

and argued that

$$\left. \begin{aligned} \lim_{B_j} m_N W_1(\nu, Q^2) &= F_1(x), \\ \lim_{B_j} \nu W_2(\nu, Q^2) &= F_2(x), \\ \lim_{B_j} \nu W_3(\nu, Q^2) &= -F_3(x). \end{aligned} \right\} \quad (15.5.4)$$

Our sign convention for  $F_3$  differs from that used in the earlier literature. It agrees, however, with present conventions and has the minor merit of making the quark contribution to  $F_3(x)$  positive, as will emerge later.

It is important to be clear as to what is and is not remarkable about (15.5.4). With  $Q^2 \rightarrow \infty$  it is *not* surprising that the value in the limit

depends on only one variable. But that the limiting value is not zero is amazing.

The fact that the quantities on the LHS of (15.5.4) show so little  $Q^2$  dependence in the presently explored kinematic domain is also surprising. After all  $Q^2 \geq 1(\text{GeV}/c)^2$  is not quite  $Q^2 = \infty$ !

Later we shall learn that the scaling is *not* perfect and that small deviations from scaling (a logarithmic dependence on  $Q^2$ ) are predicted by QCD. Because of the importance of these effects it has become customary to re-express all the DIS cross-section formulae in terms of the ‘scaling functions’  $F_j(x; Q^2)$  which, to first approximation, do not vary with  $Q^2$ . It is also, by now, conventional to use as kinematic variables  $x, y$  [see eqn (15.5.2)] and  $Q^2$ . Since there is no  $\phi$  dependence for unpolarized collisions we may take  $d\Omega = 2\pi d\cos\theta$ . The Jacobian then leads to

$$\frac{d^2\sigma}{dxdy} = \frac{2\pi m_N y E}{E'} \frac{d^2\sigma}{d\Omega dE'}. \quad (15.5.5)$$

We also eliminate  $m_N E$  using  $s = (p + k)^2 \approx 2m_N E$  for  $E \gg m_N$ . Finally, in anticipation of inclusion of higher order electroweak effects and of the testing of the minimal Higgs mechanism we replace  $G$  by the expression (5.1.2) involving  $e$  and  $\sin\theta_W$ , for which it was just a shorthand notation in the above.

Then we obtain the following standard formulae, in Lorentz invariant form, from (15.3.16) and (15.4.18):

- For purely electromagnetic reactions:

$$\frac{d^2\sigma_{\text{em}}}{dxdy} = \frac{4\pi\alpha^2 s}{Q^4} \left\{ xy^2 F_1^\gamma(x; Q^2) + \left(1 - y - \frac{xy m_N^2}{s}\right) F_2^\gamma(x; Q^2) \right\} \quad (15.5.6)$$

where the label  $\gamma$  on the  $F_{1,2}$  reminds us that it is a virtual  $\gamma$  absorbed by the hadronic target.

For  $E \gg m_N$  one ignores the last term in the coefficient of  $F_2$ .

- For CC reactions initiated by a  $\nu$  or  $\bar{\nu}$ , i.e.  $\nu p \rightarrow \ell^- X$  or  $\bar{\nu} p \rightarrow \ell^+ X$

$$\begin{aligned} \frac{d^2\sigma_{\text{CC}}^{\nu,\bar{\nu}}}{dxdy} &= \pi s \left( \frac{\alpha}{2\sin^2\theta_W M_W^2} \right)^2 \left( \frac{M_W^2}{M_W^2 + Q^2} \right)^2 \left\{ xy^2 F_1^{W^\pm}(x; Q^2) \right. \\ &\quad + \left( 1 - y - \frac{xy m_N^2}{s} \right) F_2^{W^\pm}(x; Q^2) \\ &\quad \left. \pm \left( y - \frac{y^2}{2} \right) x F_3^{W^\pm}(x; Q^2) \right\} \end{aligned} \quad (15.5.7)$$

where the label  $W^\pm$  indicates that the hadron target absorbs a virtual  $W^+$  or  $W^-$  for  $\nu, \bar{\nu}$  interactions respectively.

- For CC reactions initiated by a charged lepton, i.e.  $\ell^+ p \rightarrow \bar{\nu} X$  or  $\ell^- p \rightarrow \nu X$  one has

$$\begin{aligned} \frac{d^2\sigma_{CC}^{\ell^+, \ell^-}}{dxdy} = & \frac{\pi s}{2} \left( \frac{\alpha}{2 \sin^2 \theta_W M_W^2} \right)^2 \left( \frac{M_W^2}{M_W^2 + Q^2} \right)^2 \left\{ xy^2 F_1^{W^\pm}(x; Q^2) \right. \\ & + \left( 1 - y - \frac{xym_N^2}{s} \right) F_2^{W^\pm}(x; Q^2) \\ & \left. \mp \left( y - \frac{y^2}{2} \right) x F_3^{W^\pm}(x; Q^2) \right\} \end{aligned} \quad (15.5.8)$$

- For NC reactions initiated by a  $\nu$  or  $\bar{\nu}$ :

$$\begin{aligned} \frac{d^2\sigma^{\nu, \bar{\nu}}}{dxdy} = & \pi s \left( \frac{\alpha}{2 \sin^2 \theta_W \cos^2 \theta_W M_Z^2} \right)^2 \left( \frac{M_Z^2}{M_Z^2 + Q^2} \right)^2 \\ & \times \left\{ xy^2 F_1^Z(x; Q^2) + \left( 1 - y - \frac{xym_N^2}{s} \right) F_2^Z(x; Q^2) \right. \\ & \left. \pm \left( y - \frac{y^2}{2} \right) x F_3^Z(x; Q^2) \right\} \end{aligned} \quad (15.5.9)$$

where the superscript  $Z$  indicates that a virtual  $Z^0$  is absorbed by the hadron target.

For the NC scattering of *charged* leptons we should of course also include  $Z^0$  exchange—there is no longer any such thing as a *purely* electromagnetic reaction. So, strictly speaking, eqn (15.5.6) is an idealization. However for all fixed target experiments up to the present,  $Q^2 \leq 200$  ( $\text{GeV}/c$ ) $^2$ , so that  $M_Z^2 \gg Q^2$ . Upon using the fact that  $G^2 M_Z^4 = \pi^2 \alpha^2 / (2 \sin^4 \theta_W \cos^4 \theta_W)$  we see that the  $Z^0$  contribution to  $d\sigma_{\text{em}}$  is totally negligible in the present experimental context.

However, the great new electron–proton collider HERA at DESY will produce collisions between 820 GeV protons and 30 GeV electrons corresponding to a CM energy of about 314 GeV. This is equivalent, for a fixed target experiment with an electron beam, to  $E \simeq 50$  TeV.

The range  $x$  and  $Q^2$  for which it is estimated that systematic errors in the measurement can be kept to less than 10% is shown in Fig. 15.11.

We see that at HERA it will be possible to explore out to  $Q^2 = 10^4$  ( $\text{GeV}/c$ ) $^2$  at which point  $Q^2 \approx M_Z^2$ . Also that incredibly small values of  $x$  ( $\approx 10^{-4}$ ) will be attainable. Hence:

- For HERA physics we *must* replace  $d\sigma_{\text{em}}$  by a charged lepton NC cross-section which includes both  $\gamma$  and  $Z^0$  exchange. In this case there is an important new feature. Because of the parity-violating

weak coupling, the cross-section will be different for left- or right-handed leptons, *even when the target is unpolarized*. Moreover it is likely that HERA will eventually have a polarized electron beam. We thus calculate the cross-sections for left- and right-handed leptons separately. Using the  $Z^0$  couplings given in (5.1.3) we eventually find for the scattering of an L- or R-handed charge lepton  $\ell = \ell^-$  in NC reactions:

$$\begin{aligned} \frac{d^2\sigma_{NC}^{L,R}}{dxdy}(\ell) = & \frac{4\pi\alpha^2 s}{Q^4} \left\{ \left[ xy^2 F_1^\gamma(x; Q^2) + (1-y) F_2^\gamma(x; Q^2) \right] \right. \\ & - \left( \frac{Q^2}{Q^2 + M_Z^2} \right)^2 \frac{(v_\ell \pm a_\ell)}{2 \sin \theta_W \cos \theta_W} \left[ xy^2 F_1^Z(x; Q^2) \right. \\ & \left. \left. + (1-y) F_2^{\gamma Z}(x; Q^2) \pm \left( y - \frac{y^2}{2} \right) x F_3^{\gamma Z}(x; Q^2) \right] \right. \\ & + \left( \frac{Q^2}{Q^2 + M_Z^2} \right)^2 \left( \frac{v_\ell \pm a_\ell}{2 \sin \theta_W \cos \theta_W} \right)^2 \left[ xy^2 F_1^Z(x; Q^2) \right. \\ & \left. \left. + (1-y) F_2^Z(x; Q^2) \pm \left( y - \frac{y^2}{2} \right) x F_3^Z(x; Q^2) \right] \right\} \end{aligned} \quad (15.5.10)$$

where the lepton couplings  $v_\ell, a_\ell$  are given in (5.1.3) and (5.1.6).

The new scaling functions  $F_j^{\gamma Z}$  coming from  $\gamma$ - $Z$  interference, are defined in terms of functions  $W_j^{\gamma Z}$  via (15.5.4), the  $W_j^{\gamma Z}$  being the functions appearing in the expansion (15.4.17) of  $W_{\alpha\beta}^{\text{INT}}$  where

$$\begin{aligned} W_{\alpha\beta}^{\text{INT}} = & \frac{1}{2} \sum_{\substack{\text{initial} \\ \text{spins}}} \sum_X (2\pi)^3 \delta^4(p_X - p - q) \left\{ \langle X | h_Z^\alpha | N \rangle^* \langle X | h_{\text{em}}^\beta | N \rangle \right. \\ & \left. + \langle X | h_{\text{em}}^\alpha | N \rangle^* \langle X | h_Z^\beta | N \rangle \right\} \end{aligned} \quad (15.5.11)$$

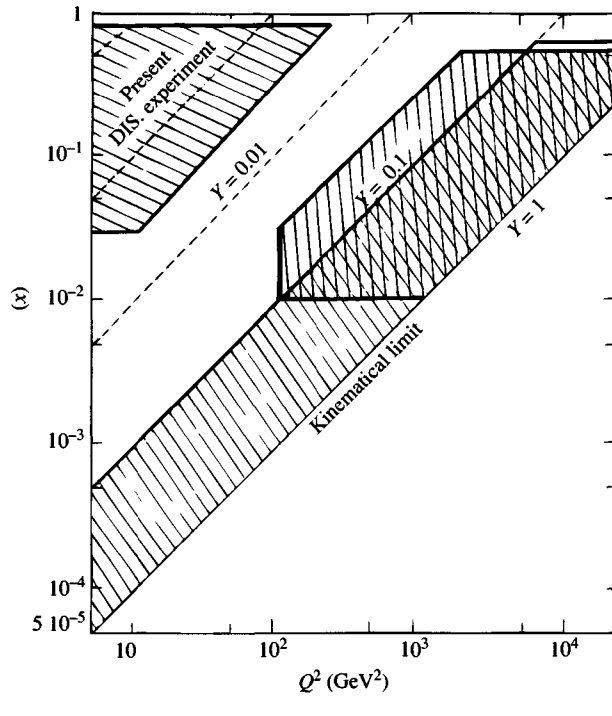
From Section 1.3.2 we can obtain the scattering of an antilepton,  $\bar{\ell} = \ell^+$ , in an NC reaction, from (15.5.10) by changing the sign of the vector coupling to the  $\gamma$  and the  $Z^0$  at the leptonic vertex. In the end this is equivalent to the replacement

$$a_\ell \rightarrow -a_\ell \quad (15.5.12)$$

in (15.5.10).

For an unpolarized lepton beam or a partially polarized beam the cross-section is an obvious linear combination of  $d\sigma^L$  and  $d\sigma^R$ .

For a purely electromagnetic interaction a polarization asymmetry can only arise if *both* a polarized lepton beam *and* a polarized target are used.



Domains where systematic errors are below 10% for:

: electron measurement

: hadron flow measurement

Fig. 15.11. Kinematic ranges of  $(x, Q^2)$  at HERA where systematic errors can be kept below 10%. Also shown is the range of pre-HERA deep inelastic experiments. From Feltesse (1987).

In that case, as we shall see in the next section, we are probing a different aspect of the hadron and a different, independent set of scaling functions is involved.

### 15.6 Polarization effects in deep inelastic scattering

In all of the previous treatment it has been assumed that the target spin is averaged over. Thus  $W_{\alpha\beta}^{\text{em}}$  in (15.3.2) and  $W_{CC}^{\alpha\beta}$  or  $W_{NC}^{\alpha\beta}$  in (15.4.5) and (15.4.8) are defined with an average over the spin of the nucleon  $|N\rangle$ .

Experiments using polarized electrons on polarized targets had already been carried out at SLAC as early as 1978 (Algard *et al.*, 1978). Further information has come from the SLAC-Yale group (Baum *et al.*, 1983) with

fascinating implications about the internal structure of the proton, which we shall discuss in Sections 16.8 and 17.1.2. And then, more recently, very startling results were obtained by the European Muon Collaboration (EMC) who scattered a polarized muon beam of energy 100–200 GeV on a polarized hydrogen target at CERN (Ashman *et al.*, 1988). The unexpectedly low asymmetry found by EMC led to what was termed a ‘spin crisis’ (Leader and Anselmino, 1988) and raised serious questions as to how the spin of a proton is made up from the spin of its constituents. It also seemed, for a while, to imply the first failure of the parton model.

The EMC result, as will be discussed, catalysed a great deal of theoretical research and the ‘crisis’ is now believed to be resolved as a consequence of the discovery of a deep and beautiful connection between the observable measured by the EMC and the axial anomaly (which was briefly referred to in Section 9.5.3). We shall only treat the pure electromagnetic case, since it does not seem feasible to contemplate neutrino scattering on a polarized target; nor can one foresee deep inelastic scattering of polarized electrons on polarized protons at the  $Q^2$  values where it would be important to take account of  $Z^0$  exchange. We should mention, however, that the general formalism for  $W$  and  $Z^0$  exchange is much more complicated than for the purely electromagnetic case (Gambino, 1990). For a general introduction to polarization phenomena the reader is referred to Bourrely, Leader and Soffer (1980).

We consider the collision of longitudinally polarized electrons or muons (helicity  $\lambda = \pm \frac{1}{2}$ ) with a polarized nucleon described by a covariant spin vector  $S_\mu$ .

The essential property of  $S_\mu$  is that if  $p = (E, \mathbf{p})$  is the four-momentum of the nucleon then

$$S \cdot p = 0 \quad \text{and} \quad S^2 = -1. \quad (15.6.1)$$

For a nucleon with helicity  $\lambda = \pm \frac{1}{2}$  one has

$$S^\mu(\lambda) = \frac{2\lambda}{m_N}(|\mathbf{p}|, E\hat{\mathbf{p}}). \quad (15.6.2)$$

For the theory behind this see Bjorken and Drell (1965).

At high energies we neglect the lepton mass, and in that case the lepton emits the virtual photon without changing its helicity, as explained in Section 1.3. Also, helicity is then the same as chirality.

The lepton tensor (15.1.5) now generalizes to

$$L_{\alpha\beta}^{(\pm)} = L_{\alpha\beta}^{(S)} + iL_{\alpha\beta}^{(A)}(\pm), \quad (15.6.3)$$

where

$$L_{\alpha\beta}^{(S)} \equiv L_{\alpha\beta}(ee) \quad (15.6.4)$$

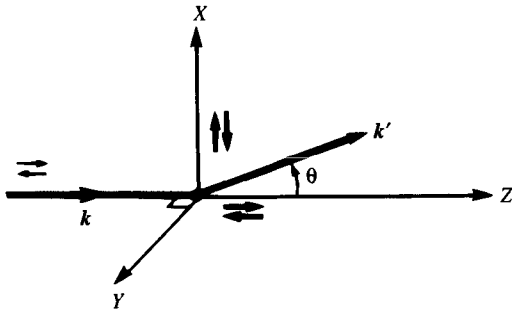


Fig. 15.12. Specification of spin directions used in defining polarized deep inelastic cross-sections.

of (15.1.5). The additional, antisymmetric, term is

$$L_{\alpha\beta}^{(A)}(\lambda = \pm \frac{1}{2}) = \mp 2\epsilon_{\alpha\beta\gamma\delta}k^\gamma k'^\delta. \quad (15.6.5)$$

In a similar fashion the antisymmetric part of  $W_{\alpha\beta}^{\text{em}}$  now plays a rôle. We have

$$W_{\alpha\beta}^{\text{em}}(S) = W_{\alpha\beta}^{(S)} + iW_{\alpha\beta}^{(A)}(S), \quad (15.6.6)$$

where  $W_{\alpha\beta}^{(S)}$  is, as before, given by (15.3.12) and the antisymmetric term can be shown to be expressible in the form (Bjorken, 1966, 1971)

$$\begin{aligned} \frac{1}{2m_N}W_{\alpha\beta}^{(A)}(S) &= \epsilon_{\alpha\beta\delta\gamma}q^\gamma \left\{ S^\delta \left[ m_N G_1(\nu, q^2) + \frac{p \cdot q}{m_N} G_2(\nu, q^2) \right] \right. \\ &\quad \left. - p^\delta \frac{S \cdot q}{m_N} G_2(\nu, q^2) \right\}. \end{aligned} \quad (15.6.7)$$

Clearly  $W^{(A)}$  changes sign under reversal of the nucleon's polarization.

It will be shown in Chapter 16 that the new structure functions  $G_{1,2}$  depend upon the spin wave function of the constituents of the hadron.

It should be noted that  $G_{1,2}$  cannot be obtained from an experiment with just a polarized beam or just a polarized target. Both must be polarized, otherwise the term  $L_{\alpha\beta}^{(A)}W^{(A)\alpha\beta}$  drops out.

To specify the various spin directions unambiguously let the lepton move in the positive  $OZ$  direction in the LAB as shown in Fig. 15.12. Let the initial and final lepton moment be  $\mathbf{k}$  and  $\mathbf{k}'$  respectively. The axis  $OY$  is taken along  $\mathbf{k} \times \mathbf{k}'$ , which then fixes the direction of  $OX$  as shown. The longitudinal spin of the incoming lepton, along or opposite to its momentum, is denoted by  $\rightarrow$  or  $\leftarrow$ . The longitudinal ( $\rightarrow$  or  $\leftarrow$ ) and transverse ( $\uparrow$  or  $\downarrow$ ) spin of the target is as shown ( $\rightarrow$  is along  $OZ$ ;  $\uparrow$  is along  $OX$ ).

Then for the differential cross-sections with initial state of definite polarization, one finds (Hey and Mandula, 1972)

$$\frac{d^2\sigma_{\leftarrow}^{\rightarrow}}{d\Omega dE'} + \frac{d^2\sigma_{\rightarrow}^{\rightarrow}}{d\Omega dE'} = \frac{8\alpha^2(E')^2}{Q^4} (2W_1 \sin^2 \frac{1}{2}\theta + W_2 \cos^2 \frac{1}{2}\theta), \quad (15.6.8)$$

which is just twice the unpolarized cross-section [see (15.3.15)], and

$$\frac{d^2\sigma_{\leftarrow}^{\rightarrow}}{d\Omega dE'} - \frac{d^2\sigma_{\rightarrow}^{\rightarrow}}{d\Omega dE'} = \frac{4\alpha^2 E'}{Q^2 E} [(E + E' \cos \theta) m_N G_1 - Q^2 G_2]. \quad (15.6.9)$$

For transverse target polarization one gets

$$\frac{d^2\sigma^{\rightarrow\downarrow}}{d\Omega dE'} - \frac{d^2\sigma^{\rightarrow\uparrow}}{d\Omega dE'} = \frac{4\alpha^2(E')^2}{Q^2 E} \sin \theta (m_N G_1 + 2EG_2). \quad (15.6.10)$$

We see that by performing experiments with both longitudinally and transversely polarized targets one can measure  $G_1$  and  $G_2$  individually.

Note that in principle one could separate  $G_1$  from  $G_2$  say in (15.6.9) from a study of the energy dependence. In practice the limited statistics have not allowed this.

In analogy to (15.3.25) and (15.3.26) the functions  $G_{1,2}$  can be related to the off-shell photo-absorption cross-sections with polarized photons and nucleons. There are four independent amplitudes, specified by the helicities of the virtual photon and nucleon; the rest are related to these by parity and time-reversal invariance. Conventionally the four transitions are labelled by the total  $J_Z$  involved and a label L or T to indicate a ‘longitudinal’ photon ( $\lambda_\gamma = 0$ ) or a ‘transverse’ photon ( $\lambda_\gamma = \pm 1$ ). The following is the pattern of transitions:

Initial		Final		Z-axis
$\lambda_\gamma$	$\lambda_N$	$\lambda_\gamma$	$\lambda_N$	$J_Z$
1	$-\frac{1}{2}$	1	$-\frac{1}{2}$	$\frac{3}{2}, T$
1	$\frac{1}{2}$	1	$\frac{1}{2}$	$\frac{1}{2}, T$
1	$\frac{1}{2}$	0	$-\frac{1}{2}$	$\frac{1}{2}, TL$
0	$-\frac{1}{2}$	0	$-\frac{1}{2}$	$\frac{1}{2}, L$

The relations between the structure functions, imaginary parts of the forward virtual Compton amplitudes  $A_{\lambda_\gamma\lambda'_N;\lambda_\gamma\lambda_N}$  and the photo-

absorption cross-sections are

$$\left. \begin{aligned} W_1 &= \frac{1}{2}(A_{1\frac{1}{2};1\frac{1}{2}} + A_{1-\frac{1}{2};1-\frac{1}{2}}) \propto \frac{1}{2}(\sigma_{1/2}^T + \sigma_{3/2}^T), \\ \left(1 + \frac{\nu^2}{Q^2}\right) W_2 - W_1 &\equiv W_L = A_{0\frac{1}{2};0\frac{1}{2}} \propto \sigma_{1/2}^L, \\ \nu m_N G_1 - Q^2 G_2 &= \frac{1}{2}(A_{1\frac{1}{2};1\frac{1}{2}} - A_{1-\frac{1}{2};1-\frac{1}{2}}) \propto \frac{1}{2}(\sigma_{1/2}^T - \sigma_{3/2}^T), \\ \sqrt{2Q^2}(m_N G_1 + \nu G_2) &= A_{1\frac{1}{2};0-\frac{1}{2}} \propto \sigma_{1/2}^{TL}. \end{aligned} \right\} \quad (15.6.11)$$

[We have written  $\propto$  because, as discussed in connection with eqn (15.3.25), the cross-section for a virtual photon is somewhat ambiguous.]

Note that the above cross-sections are related to the unpolarized ones used in Section 15.3 by

$$\sigma_T = \frac{1}{2}(\sigma_{1/2}^T + \sigma_{3/2}^T) \quad \text{and} \quad \sigma_L = \sigma_{1/2}^L.$$

One sometimes introduces an asymmetry parameter for virtual photon–nucleon scattering

$$A_1 = \frac{\sigma_{1/2}^T - \sigma_{3/2}^T}{\sigma_{1/2}^T + \sigma_{3/2}^T} \quad (15.6.12)$$

which must lie between  $-1$  and  $+1$ . On substituting (15.6.11) one finds

$$W_1 \geq |\nu m_N G_1 - Q^2 G_2|. \quad (15.6.13)$$

It can also be shown, using the Schwartz inequality, that

$$A_{1\frac{1}{2};1\frac{1}{2}} A_{0\frac{1}{2};0\frac{1}{2}} \geq (A_{1-\frac{1}{2};0\frac{1}{2}})^2, \quad (15.6.14)$$

which leads to

$$Q^2(m_N G_1 + \nu G_2)^2 \leq R W_1^2, \quad (15.6.15)$$

where

$$R \equiv \frac{\sigma_L}{\sigma_T} = \frac{\sigma_{1/2}^L}{\frac{1}{2}(\sigma_{3/2}^T + \sigma_{1/2}^T)}$$

was introduced in (15.3.26). It will be recalled that experimentally  $R$  is rather small (Fig. 15.8), so that (15.6.15) suggests that  $m_N G_1 + \nu G_2$  will be very small compared with  $W_1$  at large  $Q^2$ .

There are two sum rules that shed some light on the expected value of the asymmetry parameter  $A_1$  (15.6.12). Using an unsubtracted dispersion relation for the forward spin-flip amplitude  $f_2(\nu)$  for genuine Compton

scattering on nucleons, and the low energy theorem

$$\lim_{\nu \rightarrow 0} \frac{f_2(\nu)}{\nu} = -\frac{\alpha \kappa^2}{2m_N^2}, \quad (15.6.16)$$

where  $\kappa$  is the anomalous magnetic moment of the nucleon, Drell and Hearn (1966) and Gerasimov (1966) obtained the result

$$\frac{2\pi^2 \alpha \kappa^2}{m_N^2} = \int_{v_0}^{\infty} \frac{d\nu}{\nu} [\sigma_{3/2}(\nu) - \sigma_{1/2}(\nu)]. \quad (15.6.17)$$

Since we here have real photons, the  $\sigma(\nu)$  are of the transverse type.

For on-shell photons the forward Compton scattering amplitude is written in the CM as

$$f(\nu) = \chi_f^\dagger [\epsilon_f^* \cdot \epsilon_i f_1(\nu) + i\sigma \cdot (\epsilon_f^* \times \epsilon_i) f_2(\nu)] \chi_i, \quad (15.6.18)$$

where  $\chi_{i,f}$  are two-component spinors for the nucleon and  $\epsilon_{i,f}$  the polarization vectors for the photons. One has

$$\begin{aligned} \text{Im}f_1(\nu) &= \frac{\nu}{8\pi} [\sigma_{1/2}(\nu) + \sigma_{3/2}(\nu)] = \frac{\nu}{4\pi} \sigma_{\text{total}} \\ \text{Im}f_2(\nu) &= \frac{\nu}{8\pi} [\sigma_{1/2}(\nu) - \sigma_{3/2}(\nu)]. \end{aligned} \quad (15.6.19)$$

Studies of the DHG sum rule at fairly low energy (the resonance region) suggest that at these energies for protons  $\sigma_{3/2} > \sigma_{1/2}$ . This would imply that at  $Q^2 = 0$ , for protons,

$$A_1(\nu, 0) < 0 \quad (15.6.20)$$

for some range of  $\nu$ .

The second sum rule due to Bjorken (1966, 1971) states that

$$\lim_{Q^2 \rightarrow \infty} \int_0^{\infty} \frac{d\nu}{\nu} [\nu W_2(\nu, Q^2)] \frac{A_1(\nu, Q^2)}{1+R} = Z \neq 0 \quad (15.6.21)$$

but  $Z$  is in general not calculable. However if one subtracts neutron data from proton data, and invokes isotopic spin invariance one gets

$$Z_p - Z_n = \frac{1}{3} \frac{G_A}{G_V}, \quad (15.6.22)$$

$G_{A,V}$  being the usual vector and axial-vector nucleon  $\beta$ -decay constants defined in (1.2.6).

If we were to assume  $SU(6)$  symmetry we would have  $Z_p = \frac{5}{9}, Z_n = 0$  which would imply  $A_1 > 0$  for protons at large  $Q^2$ , in contrast to (15.6.20). We shall see later that  $A_1 > 0$  also emerges from the parton model.

What has actually been measured in polarized deep inelastic experiments is the asymmetry

$$A_{||} \equiv \frac{\frac{d^2\sigma_{\leftarrow}}{d\Omega dE'} - \frac{d^2\sigma_{\rightarrow}}{d\Omega dE'}}{\frac{d^2\sigma_{\leftarrow}}{d\Omega dE'} + \frac{d^2\sigma_{\rightarrow}}{d\Omega dE'}}, \quad (15.6.23)$$

which can be related to the structure functions via (15.6.8) and (15.6.9). For historical reasons one sometimes writes

$$A_{||} = D(A_1 + \eta A_2) \quad (15.6.24)$$

where  $A_1$  is defined in (15.6.12) and

$$A_2 = \frac{\sigma^{\text{TL}}}{\sigma_T}, \quad (15.6.25)$$

$$D = \frac{y(2-y)}{y^2 + 2(1-y)(1+R)}, \quad (15.6.26)$$

and

$$\eta = \frac{2(1-y)\sqrt{Q^2}}{y(2-y)E}. \quad (15.6.27)$$

The bound (15.6.15) leads to

$$|A_2| \leq \sqrt{R}. \quad (15.6.28)$$

Since also  $\eta \ll 1$  in the usual kinematic range of the experiments, (15.6.24) is often approximated as

$$A_{||} \approx DA_1. \quad (15.6.29)$$

The behaviour of  $A_1$  vs  $x$  for protons, as measured by the SLAC-Yale and EMC groups, is shown in Fig. 15.13. Note that  $A_1$  seems to tend to 1 as  $x \rightarrow 1$ . This feature will be seen to have important implications for the spin dependence of the proton's wave function.

In analogy to the spin independent case [see eqn (15.5.4)] the functions  $G_{1,2}(\nu, Q^2)$  multiplied by kinematic factors are expected to obey Bjorken scaling. One thus writes

$$\begin{aligned} m_N^2 \nu G_1(\nu, Q^2) &\equiv g_1(x, Q^2) \\ m_N \nu^2 G_2(\nu, Q^2) &\equiv g_2(x, Q^2) \end{aligned} \quad (15.6.30)$$

and expects  $g_{1,2}$  to depend only weakly (logarithmically) on  $Q^2$  in the Bjorken limit of large  $Q^2$  at fixed  $x$ .

Since our real interest is in the functions  $g_{1,2}(x, Q^2)$  it is best to relate the experimentally measured asymmetry  $A_{||}$  directly to them. One

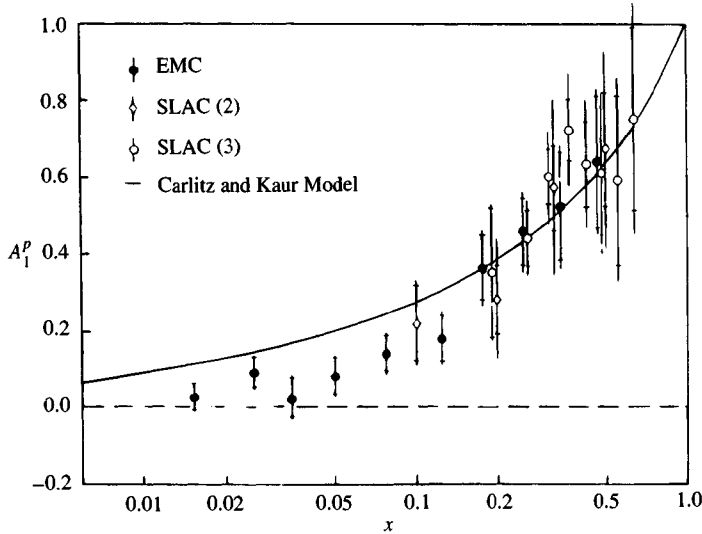


Fig. 15.13. The asymmetry  $A_1^P(x)$  as measured at SLAC and CERN. The curve is from a theoretical model which had been adjusted to agree with the SLAC data.

constructs the experimental quantity

$$\mathcal{G}_{||}(x, Q^2, E) \equiv \frac{m_N \nu Q^2 E}{2\alpha^2 E'(E + E' \cos \theta)} \cdot \frac{d^2\sigma}{d\Omega dE'} \cdot A_{||} \quad (15.6.31)$$

and one then finds from (15.6.8), (15.6.9) and (15.6.30)

$$\begin{aligned} \mathcal{G}_{||}(x, Q^2, E) &= g_1(x, Q^2) - \frac{2xm_N}{E + E' \cos \theta} g_2(x, Q^2) \\ &\simeq g_1(x, Q^2) - \frac{xm_N}{E - Q^2/4m_N x} g_2(x, Q^2). \end{aligned} \quad (15.6.32)$$

Because of the  $E$  in its denominator the second term can generally be neglected, though this could be dangerous at ultra-small  $x$  where, as will be discussed,  $g_2(x, Q^2)$  might diverge like  $1/x^2$ . In any event it seems important to try to test the usual approximation

$$\mathcal{G}_{||}(x, Q^2, E) \approx g_1(x, Q^2) \quad (15.6.33)$$

by studying the energy dependence of the LHS of (15.6.32).

In terms of the spin dependent scaling functions, one has from (15.6.12)

$$A_1 = \frac{1}{F_1(x, Q^2)} \left[ g_1(x, Q^2) - \frac{4m_N^2 x^2}{Q^2} g_2(x, Q^2) \right]. \quad (15.6.34)$$

Using this and (15.3.26) in the Bjorken sum rule (15.6.21) and (15.6.22)

one obtains

$$\lim_{Q^2 \rightarrow \infty} \int_0^1 [g_1^p(x, Q^2) - g_1^n(x, Q^2)] dx = \frac{1}{6} \frac{G_A}{G_V}. \quad (15.6.35)$$

This is, in fact, a very fundamental sum rule, and any violation of it would signal a major failure in our understanding of weak and electromagnetic interactions. A propos of this rule, Feynman (1972) has written

... (it) tests simultaneously the quark view, and the interpretation of the weak current  $\gamma_\mu(1 - \gamma_5)$  not only for  $e, \nu, \mu \dots$  but also for quarks. ... Its verification, or failure, would have a most decisive effect on the direction of future high energy theoretical physics.

It has never been tested experimentally! Experiments to do so are under construction at CERN and SLAC. There are also plans at HERA using a polarized gas jet target, since the main proton beam will remain unpolarized for the foreseeable future.

There is some controversy about the behaviour expected for  $G_2(\nu, Q^2)$ . Hey and Mandula (1972) give the sum rule

$$\lim_{Q^2 \rightarrow \infty} \int_0^\infty G_2(\nu, Q^2) d\nu = 0$$

which is equivalent to

$$\lim_{Q^2 \rightarrow \infty} \int_0^1 g_2(x, Q^2) dx = 0 \quad (15.6.36)$$

but it may well be that the integral does not converge (Heimann, 1973).

It is thus of great interest to measure  $g_2$  directly using the asymmetry (15.6.10) with the proton polarized transversely. The problem is that the event rate is reduced by the tiny factor  $\sin \theta$  in (15.6.10). An attempt to measure  $g_2$  will be made soon at SLAC.

Let us define the transverse asymmetry as

$$A_\perp \equiv \frac{\frac{d^2\sigma^{\downarrow}}{d\Omega dE'} - \frac{d^2\sigma^{\uparrow}}{d\Omega dE'}}{\frac{d^2\sigma^{\downarrow}}{d\Omega dE'} + \frac{d^2\sigma^{\uparrow}}{d\Omega dE'}}, \quad (15.6.37)$$

(where the denominator is twice the unpolarized cross-section) and construct the experimental quantity

$$\mathcal{G}_\perp(x, Q^2, E) \equiv \frac{m_N \nu Q^2}{4\alpha^2 (E')^2 \sin \theta} \cdot \frac{d^2\sigma}{d\Omega dE'} \cdot A_\perp. \quad (15.6.38)$$

Then from (15.6.10) and (15.6.30)

$$\mathcal{G}_\perp(x, Q^2, E) = g_2(x, Q^2) + \frac{\nu}{2E} g_1(x, Q^2). \quad (15.6.39)$$

For some range of  $\nu$  it will be safe to take

$$\mathcal{G}_\perp(x, Q^2, E) \approx g_2(x, Q^2) \quad (15.6.40)$$

but once both  $\mathcal{G}_{||}$  and  $\mathcal{G}_\perp$  are measured we can avoid approximations and simply solve (15.6.39) and (15.6.32) for  $g_1$  and  $g_2$ .

A comprehensive and intelligible discussion of what can be measured in various types of polarized deep inelastic experiments can be found in Anselmino (1979).

In the following chapter we shall see how the quark–parton model explains the occurrence of Bjorken scaling and we shall obtain expressions for all the scaling functions in terms of number densities for the quark–partons in a hadron.

# 16

## The quark–parton model

As with all theories of strong interactions things look simple to begin with, but as experimental accuracy improves models are forced to become increasingly complicated, with the continuous addition of new features much, it must be admitted, like the Ptolemaic cycles and epi-cycles of old. Thus the behaviour of the structure functions in deep inelastic lepton scattering will lead us initially to a simple picture of a hadron composed of granular constituents, partons. Soon thereafter we shall discover the need for antipartons and the beautiful association between partons and quarks. But the gross failure of the ‘momentum sum rules’ will indicate that some constituents are still missing; presumably the ‘gluons’. Although the gluons do not interact directly with the virtual photon used in our picture of deep inelastic scattering they are supposed to mediate the strong interactions and to give rise to the QCD corrections to the quark–parton model. These will be discussed in Chapters 20 and 21.

Finally we warn the reader that to meet the phenomenal accuracy of recent experiments it is necessary to give careful attention to kinematic details which to some extent detract from the elegant simplicity of the original picture. These effects are treated in the appendix to this chapter (Section 16.9) in which the parton model is reformulated as an impulse approximation which allows better control of the kinematic factors. The chapter can be perfectly well understood without reading the appendix.

### 16.1 The introduction of partons

We begin with a qualitative discussion of the quark–parton model. A more careful and quantitative description is gradually developed thereafter.

The data on  $W_{1,2}$  in deep inelastic electron scattering discussed in the last chapter have shown two remarkable features. The structure functions do not decrease as  $Q^2$  increases and  $\nu W_2, W_1$  depend on the variables  $Q^2, \nu$

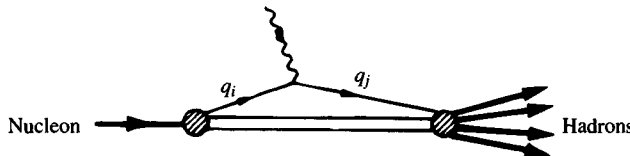


Fig. 16.1. Parton model interpretation of ' $\gamma$ N → hadrons'.

largely in the combination

$$x \equiv \frac{1}{\omega} = \frac{Q^2}{2m_N\nu} \quad \text{only.}$$

But these are exactly the properties of the *elastic* contribution to the structure functions for  $e\mu \rightarrow e'\chi$ . Using  $\delta(az) = (1/a)\delta(z)$  we can rewrite (15.3.18) as

$$\left. \begin{aligned} W_{1\text{el}}^{e\mu} &= \frac{Q^2}{4m_\mu^2\nu} \delta\left(1 - \frac{Q^2}{2m_\mu\nu}\right), \\ \nu W_{2\text{el}}^{e\mu} &= \delta\left(1 - \frac{Q^2}{2m_\mu\nu}\right), \end{aligned} \right\} \quad (16.1.1)$$

which shows that the dependence on the variables is solely in the combination  $Q^2/\nu$ . Clearly a similar result holds for electrons scattering on any *point-like* spin-half particle. For a particle of mass  $m_j$  and charge  $Q_j$  (in units of  $e$ ),

$$\left. \begin{aligned} W_{1\text{el}}^{ej} &= Q_j^2 \frac{Q^2}{4m_j^2\nu} \delta\left(1 - \frac{Q^2}{2m_j\nu}\right), \\ \nu W_{2\text{el}}^{ej} &= Q_j^2 \delta\left(1 - \frac{Q^2}{2m_j\nu}\right), \end{aligned} \right\} \quad (16.1.2)$$

If then the nucleon is composed of point-like spin-half constituents (partons) and if the structure functions for deep inelastic reactions can be viewed as built up from an *incoherent* sum of *elastic* scatterings of the virtual photon on these constituents, as shown in Fig. 16.1, then we shall find a dependence upon only the variable  $Q^2/\nu$  as desired.

Note that we are guilty of deception in (16.1.2). We are using  $\nu$  to mean the time component of  $q$  in the rest frame of the target nucleon. Strictly, what should appear in (16.1.2) is the time component of  $q$  in the rest frame of the constituent. To the extent that this difference is important the model breaks down. We shall ignore it in the following and return to consider it in the appendix to this chapter (Section 16.9).

However, although the idea of constituents is a very familiar one, new subtleties are demanded in the parton picture, as can be seen as follows. Suppose the constituents had a definite mass  $m_j$ . Then  $W_1$  and  $\nu W_2$  would have a  $\delta$ -function shape with the peak at the point  $Q^2/2m_j\nu = 1$  or  $Q^2/2m_N\nu = m_j/m_N$ . The data shown in Fig. 15.10 indicate on the contrary a smooth, wide dependence on the variable  $Q^2/2m_N\nu$ . It could be argued that if we took into account the Fermi motion of the constituents inside the hadron then the  $\delta$ -function would get smeared out into a smooth bump. In low energy nuclear physics, where the constituents are the nucleons, this is exactly what does happen.

In our case it can be shown that the smearing is of order Fermi momentum/ $\sqrt{m_N\nu}$ , which tends to zero as  $\nu \rightarrow \infty$ , so very sharp peaks would remain. Moreover, where the binding energies are enormous we cannot expect to find a few constituents with fixed masses. Indeed we cannot even expect a fixed *number* of constituents, since the huge potential energy can surely create ‘pairs’.

What is needed to build a smooth flat curve out of  $\delta$ -functions is clearly a continuous distribution of masses. We thus introduce  $f_j(x')dx'$  as the *parton densities*, i.e. as the number of partons of type  $j$  with mass  $x'm_N$  with  $0 \leq x' \leq 1$ . The effective mass of the constituents thus varies between 0 and  $m_N$  and is not a fixed number.

Later, in the appendix Section 16.9, we shall show that, in the presence of non-zero Fermi momentum, it is more fundamental to define  $x'$  as the fraction of the nucleon’s  $Z$ -component of momentum carried by the parton, when measured in the CM of the high energy lepton–nucleon collision. By making a Lorentz transformation to the CM it is easy to see that the two definitions coincide when there is no Fermi momentum.

With these assumptions we can proceed to calculate the structure functions  $W_{1,2,3}$ . However, some care must be exercised as to what is *additive*. From (15.3.25) we see that  $W_{1,2}$  are essentially total cross-sections. It is natural in a constituent model that cross-sections should be additive and it is thus not unreasonable to assume that

$$W_{1,2} = \sum_j W_{1,2\text{el}}^{(j)}. \quad (16.1.3)$$

We thus have

$$\begin{aligned} W_1^{\text{eN}}(\nu, Q^2) &= \sum_j W_{1\text{el}}^{ej} \\ &= \sum_j \int_0^1 dx' f_j(x') Q_j^2 \frac{Q^2}{4x'^2 m_N^2 \nu} \delta\left(1 - \frac{Q^2}{2m_N x' \nu}\right) \end{aligned}$$

$$\begin{aligned}
&= \sum_j Q_j^2 \int_0^1 dx' f_j(x') \frac{x' x}{2m_N x'^2} \delta(x' - x) \\
&= \frac{1}{2m_N} \sum_j Q_j^2 f_j(x).
\end{aligned} \tag{16.1.4}$$

Similarly one finds

$$\nu W_2^{eN}(\nu, Q^2) = \sum_j Q_j^2 x f_j(x) = x \sum_j Q_j^2 f_j(x). \tag{16.1.5}$$

We see that for given  $\nu, Q^2$  only one value of  $x'$ , namely  $x' = x \equiv Q^2/2m_N \nu$ , plays a rôle. We have thus obtained the remarkable features of the deep inelastic structure functions mentioned earlier, and satisfied the Bjorken result (15.5.4). Indeed, in the above ‘naive’ parton model we have

$$m_N W_1^{eN}(\nu, Q^2) = F_1^\gamma(x) = \frac{1}{2} \sum_j Q_j^2 f_j(x), \tag{16.1.6}$$

$$\nu W_2^{eN}(\nu, Q^2) = F_2^\gamma(x) = x \sum_j Q_j^2 f_j(x), \tag{16.1.7}$$

for all  $\nu, Q^2$ , but the result is only to be taken seriously when  $\nu, Q$  and  $M_X$  are all  $\gg$  typical hadron masses. The superscript  $\gamma$  is to remind us that the hadron absorbs a virtual photon. The behaviour of  $\nu W_2$  per nucleon, obtained from  $eD \rightarrow e'X$  at SLAC for smaller  $Q^2$ , and from  $\mu Fe \rightarrow \mu'X$  by the European Muon Collaboration (EMC) at CERN for larger  $Q^2$ , is shown in Fig. 16.2.

Any dependence on  $Q^2$  is very weak. The scale in Fig. 16.2 should be carefully noted. Over such a  $Q^2$  range the *elastic* form factors drop by many orders of magnitude! So the scaling behaviour holds remarkably well over a huge range of  $Q^2$ .

But the model has further implications. From (16.1.6) and (16.1.7) we see that

$$F_2^\gamma(x) = 2x F_1^\gamma(x), \tag{16.1.8}$$

a result known as the Callan–Gross relation.

From (15.3.26) we see that (16.1.8) is equivalent to

$$R = \frac{4m_N^2 x^2}{Q^2}. \tag{16.1.9}$$

Some data on  $R$  were shown in Fig. 15.8, where there was an indication of a decrease with  $Q^2$  as suggested by (16.1.9). But the data decrease with  $x$  at fixed  $Q^2$  which contradicts (16.1.9). This disagreement is irrelevant—the whole picture is only valid when  $Q^2 \gg m_N^2$  so (16.1.9) cannot be expected to be accurate. It should simply be interpreted as indicating

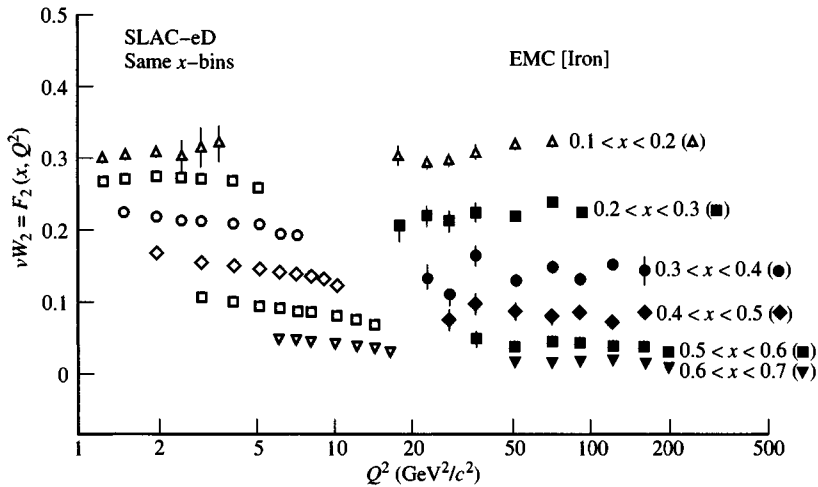


Fig. 16.2. Comparison of SLAC data on  $eD \rightarrow eX$  and EMC data on  $\mu Fe \rightarrow \mu X$  showing the remarkable absence of dependence on  $Q^2$ . (From Gabathuler, 1979.) Newer data are discussed in Chapter 20.

$R \approx 0$ . In fact, as will be seen later,  $R$  is particularly sensitive to QCD corrections and the form (16.1.9) is severely modified. Indeed at large  $Q^2$   $R$  is expected to decrease only very slowly, but to have a very small value.

However, if partons had spin 0, then the scattering  $e + \text{parton} \rightarrow e + \text{parton}$  would be given by the Mott cross-section (15.1.20), which, as can be seen by looking at (15.1.18) and (15.3.16) corresponds to having  $W_1^{\text{parton}} = 0$  or by (15.3.25)  $\sigma_T^{\gamma\text{parton}} = 0$ . This would imply  $R = \infty$ . So at least the small value  $R \approx 0$  in Fig. 15.8 lends some support to the idea that the partons are spin-half objects. But the experimental correctness of (16.1.8) does not *prove* that partons have spin-half. Indeed a strongly correlated parton–parton pair with spin 1 (a ‘vector diquark’) which, while not fundamental, could be important at medium values of  $Q^2$ , would also yield a contribution to  $F_{1,2}$  which satisfies (16.1.8) (Anselmino *et al.*, 1990b).

The parton picture can be extended to cover the deep inelastic neutrino induced reactions in an obvious way. If we allow the gauge bosons to couple to a parton of type  $j$  through a current which is generically of the form  $\gamma_\mu(\lambda_V^j - \lambda_A^j \gamma_5)$ , then the analogue of (16.1.2) is

$$\left. \begin{aligned} W_1^{(j)} &= \left[ (\lambda_V^j)^2 + (\lambda_A^j)^2 \right] \frac{Q^2}{4m_j^2 \nu} \delta \left( 1 - \frac{Q^2}{2m_j \nu} \right), \\ \nu W_2^{(j)} &= \left[ (\lambda_V^j)^2 + (\lambda_A^j)^2 \right] \delta \left( 1 - \frac{Q^2}{2m_j \nu} \right), \\ \nu W_3^{(j)} &= -2 \left[ \lambda_V^j \lambda_A^j \right] \delta \left( 1 - \frac{Q^2}{2m_j \nu} \right), \end{aligned} \right\} \quad (16.1.10)$$

where we have suppressed the labels indicating what the reaction is and which gauge boson is involved.

As before, in a constituent model, it is natural to take  $W_{1,2} = \sum_j W_{1,2}^{(j)}$ . But  $W_3$  is more subtle and it would be incorrect to take  $W_3$  as given by  $\sum_j W_3^{(j)}$ . This can be seen in (15.4.19) from which it is clear the  $W_3/m$  and not  $W_3$  behaves like a cross-section. Thus we must take

$$\frac{W_3}{m_N} = \sum_j \frac{W_3^{(j)}}{m_j}. \quad (16.1.11)$$

With  $F_{1,2}$  defined as in (16.1.7) and with

$$\nu W_3 = -F_3(x) \quad (16.1.12)$$

we shall find, analogously to (16.1.6) and (16.1.7)

$$\left. \begin{aligned} F_1 &= \frac{1}{2} \sum_j \left[ (\lambda_V^j)^2 + (\lambda_A^j)^2 \right] f_j(x), \\ F_2 &= x \sum_j \left[ (\lambda_V^j)^2 + (\lambda_A^j)^2 \right] f_j(x), \\ F_3 &= 2 \sum_j [\lambda_V^j \lambda_A^j] f_j(x). \end{aligned} \right\} \quad (16.1.13)$$

The scaling functions  $F_i(x)$  ( $i = 1, 2, 3$ ) should be labelled analogously to (16.1.6) and (16.1.7) by a symbol to indicate which gauge boson is *absorbed* by the hadron. We will thus have the following possibilities:

$$\left. \begin{aligned} \nu CC : \quad \nu_e N \rightarrow e^- X &\text{ or } \nu_\mu N \rightarrow \mu^- X : & F_i^{W^+}(x), \\ \bar{\nu} CC : \quad \bar{\nu}_e N \rightarrow e^+ X &\text{ or } \bar{\nu}_\mu N \rightarrow \mu^+ X : & F_i^{W^-}(x), \\ \nu NC : \quad \nu_e N \rightarrow \nu_e X &\text{ or } \nu_\mu N \rightarrow \nu_\mu X : & F_i^Z(x), \\ \bar{\nu} NC : \quad \bar{\nu}_e N \rightarrow \bar{\nu}_e X &\text{ or } \bar{\nu}_\mu N \rightarrow \bar{\nu}_\mu X : & F_i^Z(x). \end{aligned} \right\} \quad (16.1.14)$$

In the interest of legibility we shall usually leave out the superscripts when writing formulae which apply to all of the above reactions. Strictly speaking the  $F$ 's should also have a label to indicate the hadron involved. By convention no label means a proton. Occasionally, when essential, we shall add a further label for the hadron and/or the absorbed vector boson.

The case of NC reactions induced by charged leptons at very large values of  $Q^2$ , where  $\gamma$ - $Z^0$  interference needs to be taken into account, will be dealt with later in Section 16.5.

As an example of how the  $F_i(x)$  can depend on the reaction, let us take the partons to be quarks. Then for example in  $\nu_e N \rightarrow e^- X$  the nucleon absorbs a  $W^+$  via the reaction  $W^+ + d \rightarrow u$  so that  $f_j(x)$  will here refer to the number density of  $d$  quarks in the nucleon.

For  $\bar{\nu}_e N \rightarrow e^+ X$  the hadron absorbs a  $W^-$  via  $W^- + u \rightarrow d$  so in this case  $f_j(x)$  would refer to  $u$  quarks.

Note that, as for the electromagnetic case, we have from (16.1.13)

$$F_2(x) = 2x F_1(x). \quad (16.1.15)$$

Let us now consider some of the physical consequences of the scaling form of the cross-section formulae (15.5.7) and (15.5.8). For this qualitative discussion we shall revert to the use of  $G$ , via (5.1.2), to simplify the notation.

Ideally, if there is enough data, we can isolate the scaling functions  $F_{1,2,3}$  experimentally and study their properties in detail. For the moment let us be content to check some general aspects that are implied by the forms (15.5.7) and (15.5.8).

Let us concentrate on the region  $E \gg m_N, M_W^2 \gg Q^2 \gg m_N^2$ . Then integrating over  $y$  yields a result of the form

$$\frac{d\sigma^{\nu,\bar{\nu}}}{dx} \approx \frac{G^2 m_N E}{\pi} \left[ \frac{1}{3} x F_1(x) + \frac{1}{2} F_2(x) \pm \frac{1}{3} x F_3(x) \right]. \quad (16.1.16)$$

The total cross-sections are obtained by integrating over  $x$  and it is clear that we will have  $\sigma_{CC}^\nu, \sigma_{CC}^{\bar{\nu}}, \sigma_{NC}^\nu, \sigma_{NC}^{\bar{\nu}}$  all proportional to  $E$ , which is in agreement with experiment as discussed in Section 10.1. (See Fig. 10.1.) The above will hold only if  $E$  is small enough so that the  $Q^2$  dependence of the propagator term in (15.5.7) and (15.5.8) is negligible. If we define generically

$$A(x) = \left( \frac{2x F_1(x)}{F_2(x)} \right), \quad (16.1.17)$$

$$B(x) = \left( \frac{x F_3(x)}{F_2(x)} \right), \quad (16.1.18)$$

then (15.5.7), (15.5.8) and (16.1.16) in the above kinematic region have the form

$$\frac{d^2\sigma^{\nu,\bar{\nu}}}{dxdy} = \frac{G^2 m_N E}{\pi} F_2(x) \left[ (1-y) + \frac{1}{2} y^2 A(x) \pm (y - \frac{1}{2} y^2) B(x) \right] \quad (16.1.19)$$

$$\frac{d\sigma^{\nu,\bar{\nu}}}{dx} = \frac{G^2 m_N E}{\pi} F_2(x) \left[ \frac{1}{2} + \frac{1}{6} A(x) \pm \frac{1}{3} B(x) \right]. \quad (16.1.20)$$

Let us now restrict our attention to CC reactions.

In the simple parton model we have from (16.1.15), for both  $\nu$  and  $\bar{\nu}$ ,

$$A(x) = 1 \quad (16.1.21)$$

and if we assume that the partons couple to the charged gauge bosons as quarks are supposed to, then in (16.1.10) and (16.1.13) we shall have

$$\lambda_V^j = \lambda_A^j = 1, \quad (16.1.22)$$

i.e. for  $V - A$  coupling and then for both  $\nu$  and  $\bar{\nu}$

$$B(x) = 1. \quad (16.1.23)$$

Then, restoring the detailed labelling,

$$\frac{d\sigma_{CC}^{\nu,\bar{\nu}}}{dx} = \frac{G^2 m_N E}{\pi} F_2^{W^\pm}(x) (\frac{2}{3} \pm \frac{1}{3}). \quad (16.1.24)$$

There are very good reasons to believe that for an isoscalar target  $N_0$ ,  $F_2^{W^+ N_0} = F_2^{W^- N_0}$ . Below charm production threshold this follows from (15.4.15). Above charm production threshold it will be justified in Section 16.4. Then, for the total cross-section ratio introduced in Section 10.1, we find

$$r \equiv \frac{\sigma_{CC}^{\bar{\nu}}}{\sigma_{CC}^{\nu}} = \frac{1}{3}, \quad (16.1.25)$$

which disagrees with the low energy experimental value  $0.48 \pm 0.01$  given there.

## 16.2 Antipartons

It would be possible to argue from the above that the coupling to partons is not pure  $V - A$ . But a more natural approach, when we identify partons with quarks, is to insist on pure  $V - A$  coupling for quarks, but to allow the presence of quark-antiquark pairs in the hadrons. The antiquarks or antipartons, like antineutrinos, will couple through  $V + A$  and the deviation of  $r_{\text{exp}}$  from  $\frac{1}{3}$  will measure the proportion of antiquarks present in the hadron.

A more demanding test of the coupling can be made by looking at the  $y$  distributions. From (16.1.19), using (16.1.21)

$$\frac{d^2\sigma^{\nu,\bar{\nu}}}{dxdy} = \frac{G^2 m_N E}{\pi} F_2(x) [(1 - y + \frac{1}{2}y^2) \pm (y - \frac{1}{2}y^2)B(x)]. \quad (16.2.1)$$

If (16.1.23) held for all  $x$ , we would have

$$\begin{aligned} \frac{d^2\sigma^\nu}{dxdy} &= \frac{G^2 m_N E}{\pi} F_2^{W^+}(x) \\ \frac{d^2\sigma^{\bar{\nu}}}{dxdy} &= \frac{G^2 m_N E}{\pi} F_2^{W^-}(x)(1-y)^2, \end{aligned} \quad (16.2.2)$$

which, not surprisingly, are just like angular distributions found for  $\nu e \rightarrow \nu e$  and  $\bar{\nu} e \rightarrow \bar{\nu} e$  in Section 5.1 [see (5.1.26) and (5.1.29)].

The data shown in Fig. 16.3 for an iron target indicate that the  $y$  distribution for  $\nu$  reactions is indeed much flatter than for  $\bar{\nu}$  reactions, but is not quite in accord with (16.2.2).

If we integrate (16.2.1) over  $x$  to get the distribution in  $y$ , we obtain

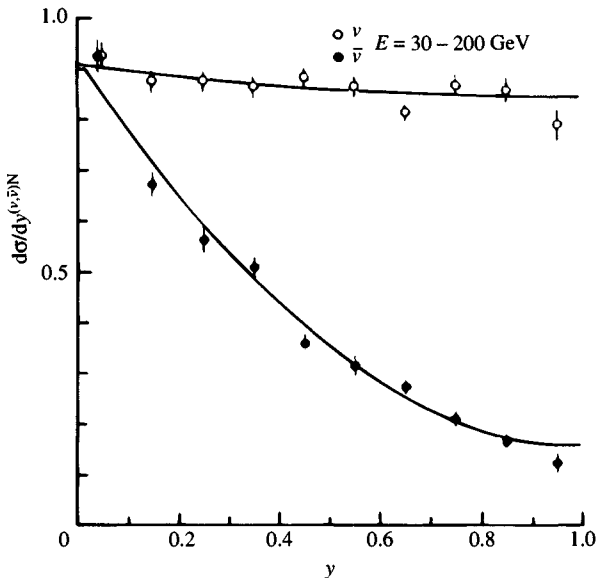


Fig. 16.3. Comparison of  $y$  distribution for neutrino and antineutrino reactions.  
(From de Groot *et al.*, 1979.)

for isoscalar targets  $N_0$  (using  $F_k^{W+N_0} = F_k^{W-N_0}$ )

$$\frac{d\sigma^{(\nu, \bar{\nu})N_0}}{dy} = \frac{G^2 m_N E}{\pi} [(1 - y + \frac{1}{2}y^2) \pm (y - \frac{1}{2}y^2)B] \int_0^1 F_2(x) dx, \quad (16.2.3)$$

where the constant  $B$  is defined by

$$B \equiv \frac{\int_0^1 x F_3(x) dx}{\int_0^1 F_2(x) dx}. \quad (16.2.4)$$

The curves in Fig. 16.3 are a fit to the data using (16.2.3), and yield  $B \simeq 0.7$  as against the value 1 expected from pure  $V - A$  partons alone.

We therefore generalize our approach to allow for both ‘partons’ and ‘antipartons’ as constituents, where partons by definition couple strictly through  $V - A$ , ( $\lambda_V^j = \lambda_A^j = 1$ ) and antipartons through  $V + A$ , ( $\lambda_V^j = -\lambda_A^j = 1$ ). We must introduce in place of  $f_j(x')$  in (16.1.13) two separate sets of functions,  $q_j(x')$  and  $\bar{q}_j(x')$ , as the number densities of partons and antipartons respectively with momentum in the CM of the lepton–nucleon collision  $p_z^{\text{constituent}} = x' p_z^{\text{nucleon}}$ .

Then (16.1.3) becomes for CC reactions

$$\left. \begin{aligned} F_1(x) &= \sum_j [q_j(x) + \bar{q}_j(x)], \\ F_2(x) &= 2x \sum_j [q_j(x) + \bar{q}_j(x)], \\ F_3(x) &= 2 \sum_j [q_j(x) - \bar{q}_j(x)]. \end{aligned} \right\} \quad (16.2.5)$$

Note that we still have (16.1.21)

$$A(x) = \left( \frac{F_2(x)}{2xF_1(x)} \right) = 1, \quad (16.2.6)$$

but now, from (16.1.18) and (16.2.5), instead of (16.1.23),

$$B(x) = \frac{\sum_j [q_j(x) - \bar{q}_j(x)]}{\sum_j [q_j(x) + \bar{q}_j(x)]} \quad (16.2.7)$$

depends on  $x$  and is a measure of the relative probabilities for finding partons or antipartons with a given  $x$ .

The data are consistent with (16.2.6). As for  $B(x)$  we show in Fig. 16.4 some data on  $xF_3$  and  $F_2$  for neutrinos with energies between 30 and 200 GeV scattering on iron. It is clear that  $B(x) \sim 1$  for larger  $x$  but  $B(x) \ll 1$  at small  $x$ . We conclude from (16.2.7) that there are few antipartons at large  $x$  but many at small  $x$ .

Returning to Fig. 16.3, we see that the data are consistent with

$$\lim_{y \rightarrow 0} \frac{d^2\sigma^{\nu N_0}}{dxdy} = \lim_{y \rightarrow 0} \frac{d^2\sigma^{\bar{\nu} N_0}}{dxdy}, \quad (16.2.8)$$

which follows from (16.1.19) provided  $F_2^{W^+N_0} = F_2^{W^-N_0}$ .

### 16.3 Partons as quarks

Since the Cabibbo theory of weak interactions and its successor the SM gauge theory of weak and electromagnetic interactions are most simply formulated in terms of leptons and quarks, and since the low energy data are nicely consistent with this and a picture of the hadrons as built up from quarks, it would be most natural to expect that the point-like granules, the partons, discovered inside the hadrons, are in fact the quarks. From the point of view of hadron model building one tends to think of quarks as particles with a well-defined mass, whereas our partons have a continuous range of mass  $m_j = xm_N$  ( $0 < x < 1$ ). But, as mentioned earlier, the

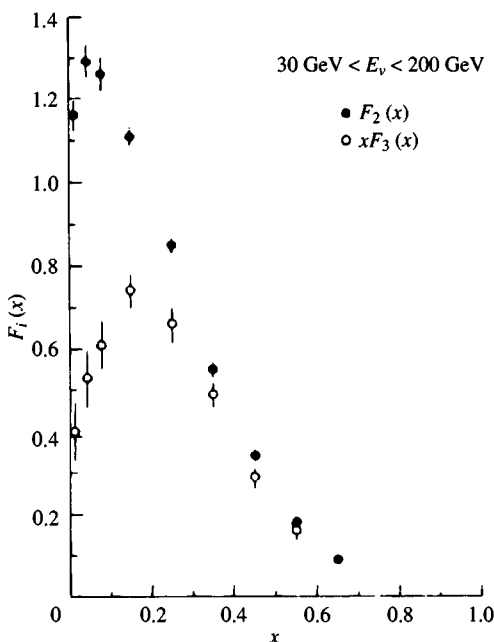


Fig. 16.4. Some data on neutrino deep inelastic structure functions (see text). (From de Groot *et al.*, 1979.)

parton model is a rather subtle form of impulse approximation and the mass  $xm_N$  is an effective mass. We should thus not take the varying mass  $xm_N$  of our partons as an argument against them being quarks.

We have already seen, however, that there must be antipartons present in the hadrons. Thus the *naive* quark model in which a proton say is just made up of *uud* quarks is not adequate and we must allow for the existence of quark-antiquark pairs inside the hadrons.

From the point of view of strong interactions this is a perfectly natural situation. We have long been used to visualizing hadrons as a core surrounded by a cloud of virtual particles, mainly pions but including some  $K\bar{K}$  pairs or even  $p\bar{p}$  pairs. So there is no conceptual difficulty in generalizing our quark picture. Henceforth the hadron will consist principally of those quarks attributed to it in the naive model [these will be termed its ‘valence’ (V) quarks], and which will give it its required  $SU(3)$  properties, and a ‘sea’ of quark-antiquark pairs, behaving neutrally or almost so, i.e. as a singlet, under  $SU(3)$ . On the basis of the experimental results on  $B(x)$  (Fig. 16.4) we expect valence quarks to predominate at large  $x$  and the sea to become increasingly important at small  $x$ . Later we shall see that gluons, too, are important at small  $x$ .

Further evidence for the  $q\bar{q}$  sea can be obtained by considering the

experimental value of  $\int W_2^{\text{ep}} d\nu$  at fixed  $Q^2$ . One has

$$\begin{aligned}\int W_2^{\text{ep}} d\nu &= \int (\nu W_2^{\text{ep}}) \frac{d\nu}{\nu} = \int (\nu W_2^{\text{ep}}) \frac{d\omega}{\omega} \\ &= \int_0^1 F_2^{\gamma}(x) \frac{dx}{x} = \sum_j Q_j^2 \int_0^1 f_j(x) dx\end{aligned}\quad (16.3.1)$$

where we have used (16.1.6). Now if there were only valence quarks in the proton so that  $f_j(x) = q_j(x)$  then the integral, which is counting the number of partons, would give 2 for  $u$  quarks and 1 for  $d$  quarks. Thus the result of (16.3.1) would be

$$\int (\nu W_2^{\text{ep}}) \frac{d\omega}{\omega} = \left(\frac{2}{3}\right)^2 \times 2 + \left(-\frac{1}{3}\right)^2 \times 1 = 1. \quad (16.3.2)$$

Experimentally, however,  $\nu W_2^{\text{ep}}$  does not seem to decrease as  $\omega$  increases at fixed  $Q^2$  (see Fig. 16.5) suggesting that the LHS of (16.3.1) might diverge. This would imply that the sum over  $j$  on the RHS would have to include more and more terms as  $\nu$  increases, i.e. the sea becomes more and more activated as  $\nu$  increases at fixed  $Q^2$ .

It is amusing to note that the regime  $\nu \rightarrow \infty$ ,  $Q^2$  fixed, corresponds to high energy Compton scattering of virtual photon of mass  $q^2 = -Q^2$ , and thus is the region of diffractive or Regge scattering. A link is therefore suggested between diffractive scattering and the quark-antiquark sea.

If this interpretation is correct, then the sea, assuming it is isotopically neutral, will give the same contribution to protons and neutrons. In that case if we consider

$$\int_1^\infty \frac{d\omega}{\omega} (\nu W_2^{\text{ep}} - \nu W_2^{\text{en}}) = \int_0^1 \frac{dx}{x} (\nu W_2^{\text{ep}} - \nu W_2^{\text{en}}) \quad (16.3.3)$$

the sea effects should cancel out, and from (16.1.6) we expect, since a neutron contains one  $u$  and two  $d$  quarks,

$$\int_0^1 \frac{dx}{x} (\nu W_2^{\text{ep}} - \nu W_2^{\text{en}}) = \left(2 \times \frac{4}{9} + \frac{1}{9}\right) - \left(2 \times \frac{1}{9} + \frac{4}{9}\right) = \frac{1}{3}, \quad (16.3.4)$$

a sum rule due to Gottfried.

Some early experimental data are shown in Fig. 16.6. It is seen that  $\nu W_2^{\text{ep}} - \nu W_2^{\text{en}}$  decreases as  $x \rightarrow 0$ , i.e.  $\omega \rightarrow \infty$  and the result of the integration is  $0.28 \pm 0.06$ , in reasonable agreement with (16.3.4). Our identification of partons with quarks has thus passed its most elementary test.

We should warn the reader that newer data, comparing  $\mu p$  and  $\mu n$  deep inelastic scattering suggest values uncomfortably different from the Gottfried value (16.3.4). This will be discussed in Section 17.1.

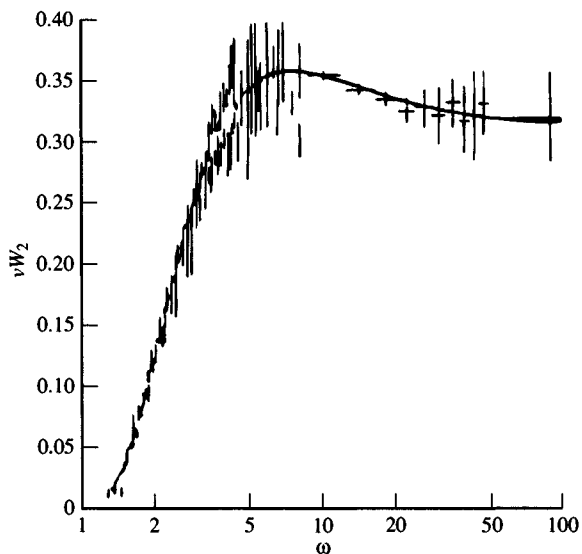


Fig. 16.5. Dependence of electromagnetic structure function  $\nu W_2$  upon  $\omega$ . (From Atwood *et al.*, 1975.)

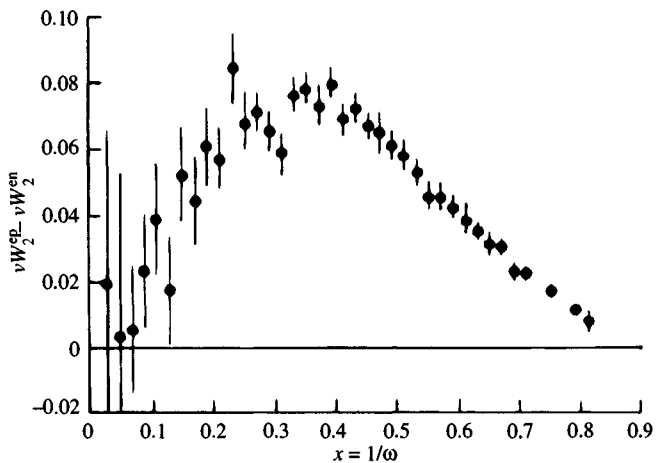


Fig. 16.6. Data on difference of  $\nu W_2$  for ep and en reactions as function of  $x = 1/\omega$ . (From Nachtmann, 1976.)

Taken seriously the quark–parton model is exciting because it offers a host of testable relations to which we now turn.

#### 16.4 The detailed quark–parton model

For each type (flavour) of quark–parton or antiquark–antiparton we now allow a separate distribution function  $u(x)$ ,  $d(x)$ ,  $s(x)$  and  $\bar{u}(x)$ ,  $\bar{d}(x)$ ,  $\bar{s}(x)$  giving the number densities of such objects with momentum fraction be-

tween  $x$  and  $x + dx$  in the proton.

Note that we do not consider any fundamental component of  $c$ ,  $b$  or  $t$  quarks in the nucleon. Their presence, in the form of  $q\bar{q}$  pairs, is better thought of as a dynamic effect arising from pair production from gluons (see Fig. 16.10), i.e. a QCD effect, and will be treated in Section 23.8. This means that the formulae for the scaling functions to be presented in this section *require additional contributions to be added to them* when the kinematics is such as to allow charm or bottom production. Given present estimates of the top mass the production of top is not a relevant consideration.

All the above will be normalized so that

$$\int_0^1 q_j(x) dx = \text{number of quarks of type } j \text{ in the proton.} \quad (16.4.1)$$

Because of the existence of the sea, whose excitation seems to depend upon  $\nu$ , we should not expect the RHS of (16.4.1) to be a constant, nor indeed to be particularly meaningful. On the other hand, if we ask for the *net* number of say  $u$  quarks in the proton we must find 2. Thus

$$\int_0^1 dx[u(x) - \bar{u}(x)] = 2. \quad (16.4.2)$$

Similarly we require, in a proton,

$$\int_0^1 dx[d(x) - \bar{d}(x)] = 1, \quad (16.4.3)$$

$$\int_0^1 dx[s(x) - \bar{s}(x)] = 0. \quad (16.4.4)$$

A more rigorous derivation of these results is given in Section 16.9.3 in the appendix to this chapter. The above equations, which simply express the overall quark content of a proton, will be the basis for various sum rules that can be tested experimentally. Notice that they do not imply  $s(x) = \bar{s}(x)$ , though this seems very reasonable and is often assumed in the following.

Because, by definition, the valence quarks give the proton its correct  $SU(2)$  or  $SU(3)$  properties, we expect the sea to be basically neutral, i.e. singlet under these transformations. But the above symmetries are not perfect, and while  $SU(2)$  is well respected, in nature  $SU(3)$  is broken somewhat. It thus seems reasonable, for the proton, to insist in the simple picture that

$$\left. \begin{aligned} u_{\text{sea}}(x) &= d_{\text{sea}}(x), \\ \bar{u}_{\text{sea}}(x) &= \bar{d}_{\text{sea}}(x), \end{aligned} \right\} \quad (16.4.5)$$

but not to insist that these are identical with  $s(x)$ . (It should be noted that in a proton  $s(x)$  can only arise from the sea.) Note that for an

antiquark in a proton,  $\bar{q}(x)$  is  $\bar{q}_{\text{sea}}(x)$  by definition. For  $u$  and  $d$  quarks in a proton, on the other hand, we separate  $q(x)$  into a valence and sea contribution by *defining*

$$q_{\text{sea}}(x) \equiv \bar{q}_{\text{sea}}(x) \quad (16.4.6)$$

so that

$$q(x) = q_V(x) + q_{\text{sea}}(x) = q_V(x) + \bar{q}_{\text{sea}}(x). \quad (16.4.7)$$

Then, for example, in a proton,

$$u(x) - \bar{u}(x) = u_V(x) + u_{\text{sea}}(x) - \bar{u}_{\text{sea}}(x) = u_V(x) \quad (16.4.8)$$

consistent with the counting rules (16.4.2) to (16.4.4).

#### 16.4.1 The scaling functions for purely electromagnetic interactions

For a proton target, and for  $Q^2 \ll M_Z^2$ , from (16.1.7) and (16.1.8), the scaling functions to be used in (15.5.6) are, assuming  $\bar{s}(x) = s(x)$ ,

$$F_2^{\gamma p} = x \left\{ \frac{4}{9}[u(x) + \bar{u}(x)] + \frac{1}{9}[d(x) + \bar{d}(x) + 2s(x)] \right\} \quad (16.4.9)$$

and

$$F_1^{\gamma p}(x) = \frac{1}{2x} F_2^{\gamma p}(x). \quad (16.4.10)$$

If we now compare scattering on proton and neutron targets, and if we temporarily attach a label to the distributions to signify the hadron involved, then on the grounds of isospin invariance we expect

$$u_p(x) = d_n(x), d_p(x) = u_n(x), \quad (16.4.11)$$

and similarly for the antiquarks. This relation is always assumed.

Thus, reverting to the convention that no label refers to distributions in the proton, we have

$$F_2^{\gamma n} = x \left\{ \frac{4}{9}[d(x) + \bar{d}(x)] + \frac{1}{9}[u(x) + \bar{u}(x) + 2s(x)] \right\} \quad (16.4.12)$$

and

$$F_1^{\gamma n}(x) = \frac{1}{2x} F_2^{\gamma n}(x). \quad (16.4.13)$$

We would naturally expect the structure of a hadron to be dominated by its valence quarks— $u$  and  $d$  for a nucleon. So we might expect the contribution from the sea to be small. But this cannot be true for all  $x$  as we saw from the discussion of  $B(x)$  in Section 16.2. And QCD arguments indicate that the sea should become increasingly important for small  $x$ .

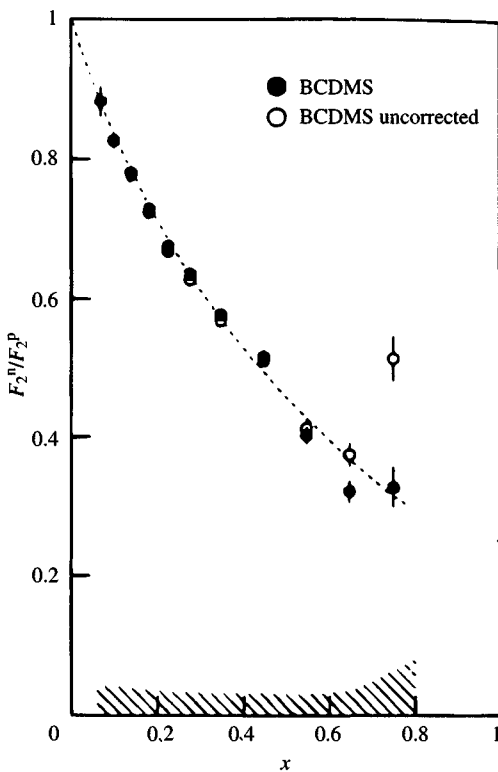


Fig. 16.7. Ratio of  $F_2$  for neutron and proton targets.

With this in mind consider the ratio of scaling functions obtained from ep and en reactions:

$$\frac{F_2^{\gamma n}(x)}{F_2^{\gamma p}(x)} = \frac{u + \bar{u} + 4(d + \bar{d}) + 2s}{4(u + \bar{u}) + d + \bar{d} + 2s}. \quad (16.4.14)$$

Since the distribution functions are positive one obtains the Nachtmann inequality:

$$\frac{1}{4} \leq \frac{F_{1,2}^{en}(x)}{F_{1,2}^{ep}(x)} \leq 4. \quad (16.4.15)$$

The data shown in Fig. 16.7 are most interesting. For large  $x$  one is close to the lower limit of  $\frac{1}{4}$  which can only be reached if  $d = \bar{d} = s = 0$ . This suggests a picture in which the *high momentum* partons in a proton are mainly  $u$  quarks.

For small  $x$  the ratio is close to 1 suggesting little influence of valence quarks at small  $x$  and dominance of a symmetric sea contribution in which  $u + \bar{u} \approx d + \bar{d}$ . All this is nicely consistent with the conclusions following from the behaviour of  $B(x)$  discussed in Section 16.2.

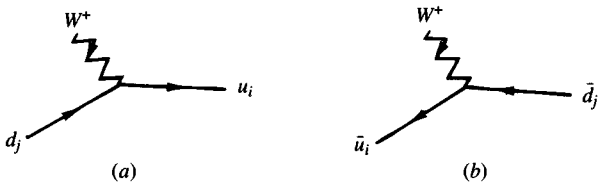


Fig. 16.8. Quark (a) and antiquark (b) transitions for neutrino induced charged current reactions.

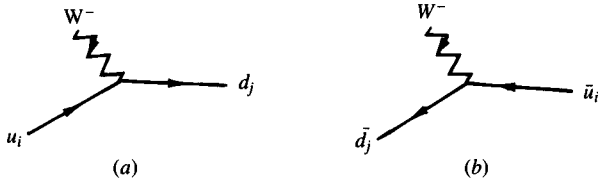


Fig. 16.9. Quark (a) and antiquark (b) transitions involved in antineutrino induced charged current reactions.

#### 16.4.2 Charged current scaling functions

For CC reactions the relevant term in the Lagrangian for the hadron to absorb a  $W^+$  is  $h_+^\mu W_\mu^+$  which according to (9.3.10) and (9.2.1) describes the quark transitions at the hadronic vertex, shown in Fig. 16.8 (a) ( $d_j = d, s, b; u_i = u, c, t$ ).

Similarly the above term in the Lagrangian generates the antiquark transitions shown in Fig. 16.8 (b).

The transitions do not all have the same strength and are controlled by the elements of the KM matrix introduced in Section 9.2 and whose determination is studied in Chapter 18. From the form of  $h_+^\mu$  one has the following couplings for the quark and antiquark transitions:

$$\begin{aligned} d_j \rightarrow u_i &: V_{ij}\gamma^\mu(1 - \gamma_5) \\ \bar{u}_i \rightarrow \bar{d}_j &: -V_{ij}^*\gamma^\mu(1 - \gamma_5) \end{aligned} \quad (16.4.16)$$

For CC reactions in which the hadron absorbs a  $W^-$  the relevant term in the Lagrangian is  $h_-^\mu W_\mu^-$ , leading to transitions shown in Fig. 16.9 (a), (b).

The couplings in  $h_-^\mu$  are:

$$\begin{aligned} u_i \rightarrow d_j &: V_{ij}^*\gamma^\mu(1 - \gamma_5) \\ \bar{d}_j \rightarrow \bar{u}_i &: -V_{ij}\gamma^\mu(1 - \gamma_5) \end{aligned} \quad (16.4.17)$$

In writing down the contributions to the scaling functions we have to compute matrix elements of these couplings. Then in comparing an antiquark matrix element with that of the analogous quark matrix element

we need, according to Section 1.3, simply reverse the relative sign of the vector-axial-vector couplings. This means that in the general result (16.1.13), which was derived for quarks, we must change the sign of  $F_3$  when dealing with antiquarks.

(a) *Threshold corrections for charm and bottom production.* Below the charm production threshold the part of the currents  $h_{\pm}^{\mu}$  which change the charm quantum number will be inoperative. As we go up through the charm production threshold we should not expect scaling to hold since with respect to the charm particles we are not yet in the ‘deep inelastic’ region. Only when we are well above the charm threshold should scaling again hold. In practice, however, much data lies in the threshold region and we should therefore try to take into account the most important corrections.

In the appendix to this chapter we shall develop a picture of the parton model as an impulse approximation in which better control of kinematic effects is possible. It turns out from eqn (16.9.36) that for CC reactions involving a transition from a light quark  $j$  to a heavy quark  $k$  the principal kinematic corrections are the following:

$$\left. \begin{aligned} \text{In } F_{1,3} : q_j(x) &\rightarrow q_j(\xi_k)\theta(1 - \xi_k), \\ \text{In } F_2 : 2xq_j(x) &\rightarrow 2\xi_k q_j(\xi_k)\theta(1 - \xi_k), \end{aligned} \right\} \quad (16.4.18)$$

where

$$\xi_k \equiv x \left( 1 + \frac{m_k^2}{Q^2} \right) \quad (16.4.19)$$

and  $\theta$  is the *step function* defined by

$$\left. \begin{aligned} \theta(z) &= 1 && \text{for } z \geq 0, \\ &= 0 && \text{for } z < 0. \end{aligned} \right\} \quad (16.4.20)$$

Note that the replacement of  $x$  by  $\xi_k$  implies that the scaling functions  $F_i$  will have some  $Q^2$ -dependence and will only scale for  $Q^2 \gg m_k^2$ . (Of course, as mentioned earlier, QCD corrections also induce a dynamical breaking of scaling.)

In the case that we have a transition from a light quark to a  $c$  or  $b$  quark, the final state will contain charm or bottom particles which are considerably heavier than the nucleon. But from (15.5.1) the mass of the final state is given by

$$M_X^2 = m_N^2 + Q^2 \left( \frac{1}{x} - 1 \right) \quad (16.4.21)$$

so that for a given  $x$ , only sufficiently large  $Q^2$  will allow such a process to take place. What the minimum mass of the final state is, will depend upon

Transition	Minimum $M_X$
$d \rightarrow c$	$M_X^{cd} \equiv m_N + m_D \approx 2.8 \text{ GeV}/c^2$
$s \rightarrow c$	$M_X^{cs} \equiv m_\Lambda + m_D \approx 3 \text{ GeV}/c^2$
$u \rightarrow b$	$M_X^{bu} \equiv m_N + m_B \approx 6.2 \text{ GeV}/c^2$

Table 16.1. Minimum mass of the final state X corresponding to a given CC quark transition.

the quark transition involved. Bearing in mind baryon conservation, and that  $s$  quarks only exist in a nucleon in the sea in pairs  $s\bar{s}$ , the minimum masses  $M_X$  for various quark transitions are given in Table 16.1.

For a given  $x$  a particular transition can thus only occur for

$$Q^2 \geq \left( \frac{x}{1-x} \right) \left[ (M_X^{\min})^2 - m_N^2 \right]. \quad (16.4.22)$$

On the other hand when we are considering fixed  $Q^2$  the condition that  $\xi_k \leq 1$  implies

$$x \leq \frac{Q^2}{Q^2 + m_k^2} \quad (16.4.23)$$

whereas (16.4.22) implies

$$x \leq \frac{Q^2}{Q^2 + \Delta_k^2} \quad (16.4.24)$$

where, for  $k = c$ ,

$$\Delta_c^2 = (M_X^{cd})^2 - m_N^2 \simeq (M_X^{cs})^2 - m_N^2 \simeq 7.5 (\text{GeV}/c^2)^2$$

and for  $k = b$ ,

$$\Delta_b^2 = (M_X^{bu})^2 - m_N^2 \simeq 37.5 (\text{GeV}/c^2)^2. \quad (16.4.25)$$

Given that  $m_c^2 \approx 2.3 (\text{GeV}/c^2)^2$  and  $m_b^2 \approx 25 (\text{GeV}/c^2)^2$ , it is seen that (16.4.24) is more restrictive than (16.4.23).

Thus the condition  $\xi_k \leq 1$  and the condition on the final state mass (16.4.22) can both be taken into account by replacing  $\theta(1-\xi_k)$  in (16.4.18) by  $\theta(x_k - x)$  where

$$x_k(Q^2) = \frac{Q^2}{Q^2 + \Delta_k^2}. \quad (16.4.26)$$

(b) *Expressions for the CC scaling functions.* As discussed in Section 15.5, CC reactions can be initiated either by neutrinos or by charged leptons.

Up to the present the field has been dominated by neutrino physics, but  $e^-$  induced CC reactions will become important at HERA.

With the above kinematic effects taken into account we present expressions for the CC scaling functions which should be reliable even close to the charm and bottom thresholds. Using (16.1.13) with the coupling  $\lambda_V, \lambda_A$  chosen to correspond to (16.4.16) and (16.4.17), we find for the CC scaling functions for the reactions  $\nu p \rightarrow \ell^- X$  or  $\ell^+ p \rightarrow \bar{\nu} X$ , to be used in (15.5.7) or (15.5.8),

$$\begin{aligned} F_1^{W^+p}(x, Q^2) = & d(x)|V_{ud}|^2 + d(\xi_c)|V_{cd}|^2\theta(x_c - x) \\ & + \bar{u}(x)(|V_{ud}|^2 + |V_{us}|^2) + \bar{u}(\xi_b)|V_{ub}|^2\theta(x_b - x) \\ & + s(x)|V_{us}|^2 + s(\xi_c)|V_{cs}|^2\theta(x_c - x). \end{aligned} \quad (16.4.27)$$

$F_2^{W^+p}(x, Q^2)$  is obtained from (16.4.27) by the replacements, for quarks and antiquarks,

$$q(x) \rightarrow 2xq(x), \quad q(\xi_k) \rightarrow 2\xi_k q(\xi_k). \quad (16.4.28)$$

$\frac{1}{2}F_3^{W^+p}(x, Q^2)$  is obtained from (16.4.27) by the replacement, for the anti-quarks,

$$\bar{q} \rightarrow -\bar{q}. \quad (16.4.29)$$

Note that to the extent that  $\xi_k$  differs from  $x$ , we have

$$F_2^{W^+p} \neq 2xF_1^{W^+p}. \quad (16.4.30)$$

For a neutron target replace  $u \leftrightarrow d$  and  $\bar{u} \leftrightarrow \bar{d}$ .

In similar fashion one finds for  $\bar{\nu} p \rightarrow \ell^+ X$  or  $\ell^- p \rightarrow \nu X$

$$\begin{aligned} F_1^{W^-p}(x, Q^2) = & u(x)(|V_{ud}|^2 + |V_{us}|^2) + u(\xi_b)|V_{ub}|^2\theta(x_b - x) \\ & + \bar{d}(x)|V_{ud}|^2 + \bar{d}(\xi_c)|V_{cd}|^2\theta(x_c - x) \\ & + \bar{s}(x)|V_{us}|^2 + \bar{s}(\xi_c)|V_{cs}|^2\theta(x_c - x) \end{aligned} \quad (16.4.31)$$

and  $F_{2,3}^{W^-p}$  are obtained from (16.4.31) by the substitutions (16.4.28) and (16.4.29) respectively. For a neutron target one substitutes  $u \leftrightarrow d$  and  $\bar{u} \leftrightarrow \bar{d}$ .

It is useful to have approximate simpler expressions for the CC scaling functions which take into account just the dominant contributions.

As discussed in Section 9.2 the success of the Cabibbo theory implies that

$$\begin{aligned} |V_{ud}|^2 &\approx \cos^2 \theta_C \approx 0.95 \\ |V_{us}|^2 &\approx \sin^2 \theta_C \approx 0.05 \end{aligned} \quad (16.4.32)$$

and further, from (9.2.6) we see that

$$|V_{cd}|^2 \approx |V_{us}|^2, \quad |V_{ub}|^2 \ll |V_{us}|^2. \quad (16.4.33)$$

Also we shall see later that the strange sea is less important than  $\bar{u}$  or  $\bar{d}$ . If therefore we ignore effects of a few per cent we may keep only the largest terms and neglect the  $m^2/Q^2$  corrections. Then we have

$$\left. \begin{aligned} F_1^{W^+p}(x) &\approx d(x) + \bar{u}(x), \\ F_2^{W^+p}(x) &\approx 2xF_1^{W^+p}(x), \\ F_3^{W^+p}(x) &\approx 2[d(x) - \bar{u}(x)], \end{aligned} \right\} \quad (16.4.34)$$

and

$$\left. \begin{aligned} F_1^{W^-p}(x) &\approx u(x) + \bar{d}(x), \\ F_2^{W^-p}(x) &\approx 2xF_1^{W^-p}(x), \\ F_3^{W^-p}(x) &\approx 2[u(x) - \bar{d}(x)]. \end{aligned} \right\} \quad (16.4.35)$$

The above simplified expressions should yield the dominant contributions to the scaling functions.

Returning to the accurate formulae we see that certain combinations of scaling functions simplify as a consequence of  $s = \bar{s}$  and the fact that  $s(x)$  is the same in protons and neutrons.

Thus

$$\begin{aligned} F_1^{W^+p} - F_1^{W^-p} &= d_V(x)|V_{ud}|^2 + d_V(\xi_c)|V_{cd}|^2\theta(x_c - x) \\ &\quad - u_V(x)(|V_{ud}|^2 + |V_{us}|^2) - u_V(\xi_b)|V_{ub}|^2\theta(x_b - x) \end{aligned} \quad (16.4.36)$$

and thus depends only on the valence quark distribution, as does

$$\begin{aligned} \frac{1}{2}(F_3^{W^+p} + F_3^{W^-p}) &= d_V(x)|V_{ud}|^2 + d_V(\xi_c)|V_{cd}|^2\theta(x_c - x) \\ &\quad + u_V(x)(|V_{ud}|^2 + |V_{us}|^2) + u_V(\xi_b)|V_{ub}|^2\theta(x_b - x) \end{aligned} \quad (16.4.37)$$

Utilizing the analogous result for neutrons we obtain

$$\begin{aligned} F_1^{W^+p} - F_1^{W^-p} + F_1^{W^+n} - F_1^{W^-n} &= -[d_V(x) + u_V(x)]|V_{us}|^2 \\ &\quad + [d_V(\xi_c) + u_V(\xi_c)]|V_{cd}|^2\theta(x_c - x) \\ &\quad - [d_V(\xi_b) + u_V(\xi_b)]|V_{ub}|^2\theta(x_b - x). \end{aligned} \quad (16.4.38)$$

The RHS of (16.4.38) involves only small non-diagonal elements of the KM matrix. Thus to a good approximation we can ignore the  $Q^2$  dependence and conclude that for an isoscalar target  $N_0$

$$F_1^{W^+N_0} - F_1^{W^-N_0} \approx [u_V(x) + d_V(x)] \{ |V_{cd}|^2 - |V_{us}|^2 - |V_{ub}|^2 \}$$

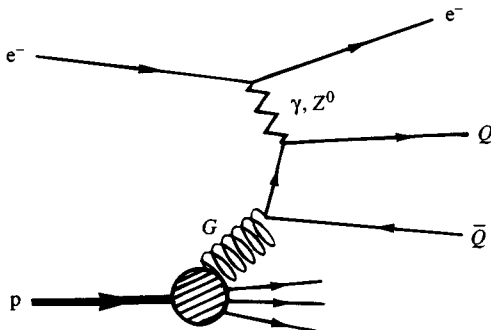


Fig. 16.10. Mechanism for producing a heavy quark-antiquark pair  $Q\bar{Q}$ . There is also a crossed diagram.

Using the unitarity of the KM matrix  $|V_{us}|^2 + |V_{ub}|^2 = 1 - |V_{ud}|^2$  and the above can be written

$$F_1^{W^+N_0} - F_1^{W^-N_0} \approx -[u_V(x) + d_V(x)]|V_{td}|^2. \quad (16.4.39)$$

The  $td$  matrix element is exceedingly tiny,  $|V_{td}|^2 \approx 10^{-4}$  as will be discussed in Chapter 18.

Thus to a very high degree of accuracy one has

$$F_1^{W^+N_0} = F_1^{W^-N_0}. \quad (16.4.40)$$

Moreover, the larger  $Q^2$  is, the more exact the equality becomes.

### 16.4.3 Neutrino and antineutrino neutral current scaling functions

Comparing (15.4.8) with (15.4.10) and using the expression for  $h_Z^\mu$  in the SM given in (9.3.7), or directly from (9.6.5), we see that  $\lambda_V$  and  $\lambda_A$  in (16.1.13) must be chosen as follows:

$$\begin{aligned} \text{For } u : \lambda_V &= \frac{1}{2} - \frac{4}{3} \sin^2 \theta_W \equiv g_V^u, & \lambda_A &= \frac{1}{2} \equiv g_A^u, \\ \text{For } d, s : \lambda_V &= \frac{2}{3} \sin^2 \theta_W - \frac{1}{2} \equiv g_V^d, & \lambda_A &= -\frac{1}{2} \equiv g_A^d. \end{aligned} \quad (16.4.41)$$

Because NC interactions do not change the quark flavour, the only way to produce heavy quarks in the final state is for the vector boson to interact with the heavy quark itself. As mentioned earlier it is sensible to assume that there is no primitive  $c$  or  $b$  content to a nucleon so that the process relies on  $Q\bar{Q}$  production by gluons, as illustrated in Fig. 16.10.

Since this is an essentially QCD mechanism we shall postpone its discussion until Section 23.8. Note that the analogue of the diagram of Fig. 16.10 for CC reactions involves subprocesses of the type  $WG \rightarrow c\bar{s}$  or  $s\bar{c}$ . This implies that the effective  $s$  and  $c$  content of the proton will be different when probed in NC and CC reactions! (Barone *et al.*, 1991.)

$Q\bar{Q}$ pair	Minimum $M_X$
$c\bar{c}$	$m_N + m_{J/\Psi} \approx 4 \text{ GeV}/c^2$
$b\bar{b}$	$m_N + m_Y \approx 10.5 \text{ GeV}/c^2$

Table 16.2. Minimum mass of the final state  $X$  corresponding to a given NC transition.

The minimum final state masses for NC reactions are given in Table 16.2.

The expressions to follow do not include charm or bottom production. But it is important to emphasize that the  $Q\bar{Q}$  contribution will turn out to be exceedingly small except for very small  $x$ . Thus the formulae below are strictly accurate only below charm threshold, but are still highly accurate even above charm threshold provided  $x \geq 0.01$ .

Thus the parton model expressions for the scaling functions to be used in (15.5.9) are:

$$\begin{aligned} F_1^{Zp}(x) &= \frac{1}{2} \left\{ \left[ (g_V^u)^2 + (g_A^u)^2 \right] (u(x) + \bar{u}(x)) \right. \\ &\quad \left. + \left[ (g_V^d)^2 + (g_A^d)^2 \right] (d(x) + \bar{d}(x) + 2s(x)) \right\}, \end{aligned} \quad (16.4.42)$$

$$F_2^{Zp}(x) = 2xF_1^{Zp}(x), \quad (16.4.43)$$

$$F_3^{Zp}(x) = 2 \left[ g_V^u g_A^u u_V(x) + g_V^d g_A^d d_V(x) \right]. \quad (16.4.44)$$

As usual for a neutron target make the replacements  $u \leftrightarrow d, \bar{u} \leftrightarrow \bar{d}$ .

This completes the specification of the quark-parton model formulae for the scaling functions relevant to scattering on an unpolarized nucleon target in the region  $Q^2 \ll M_Z^2$ .

## 16.5 Charged lepton induced reactions for $Q^2$ of order $M_Z^2$

In NC reactions initiated by a charged lepton, as discussed in Section 15.5, it becomes necessary to take into account interference between  $\gamma$  and  $Z^0$  exchange when  $Q^2$  cannot be neglected compared with  $M_Z^2$ . The cross-section formula (15.5.10) requires the scaling functions  $F_i^\gamma, F_i^Z$  discussed already and the ‘interference’ scaling functions  $F_i^{\gamma Z}$  defined in terms of the currents in (15.5.11).

Bearing in mind the structure of the electromagnetic current  $h_{\text{em}}^\alpha$  and  $h_Z^\beta$  it is straightforward to read off from (16.1.10) the formula for the  $F_i^{\gamma Z}$ . One finds

$$F_1^{\gamma Z}(x) = \frac{2}{3}g_V^u[u(x) + \bar{u}(x)] - \frac{1}{3}g_V^d[d(x) + \bar{d}(x) + 2s(x)], \quad (16.5.1)$$

$$F_2^{\gamma Z}(x) = 2xF_1^{\gamma Z}(x), \quad (16.5.2)$$

$$F_3^{\gamma Z}(x) = \frac{4}{3}g_A^u u_V(x) - \frac{2}{3}g_A^d d_V(x), \quad (16.5.3)$$

where the couplings  $g_V^{u,d}, g_A^{u,d}$  were given in (16.4.41).

In CC reactions we are now in a region where  $Q^2 \gg m_b^2$  so the formulae (16.4.27) etc. greatly simplify. One has, to a very high degree of accuracy:

$$\left. \begin{aligned} F_1^{W^+ p}(x) &= d(x) + s(x) + \bar{u}(x), \\ F_2^{W^+ p}(x) &= 2xF_1^{W^+ p}(x), \\ F_3^{W^+ p}(x) &= 2[d(x) + s(x) - \bar{u}(x)], \end{aligned} \right\} \quad (16.5.4)$$

and

$$\left. \begin{aligned} F_1^{W^- p}(x) &= u(x) + \bar{d}(x) + \bar{s}(x), \\ F_2^{W^- p}(x) &= 2xF_1^{W^- p}(x), \\ F_3^{W^- p}(x) &= 2[u(x) - \bar{d}(x) - \bar{s}(x)]. \end{aligned} \right\} \quad (16.5.5)$$

The only error in the above comes from neglecting the KM matrix elements  $|V_{td}|^2$  and  $|V_{ts}|^2$ , which are of order  $10^{-4}$ , compared with unity. We are assuming that there is no top production even at these values of  $Q^2$ . When in fact top is produced then obvious modifications must be made to (16.4.27) etc. near the threshold for top production, and (16.5.4) and (16.5.5) become exact well beyond the threshold.

## 16.6 Behaviour of the quark number densities as $x \rightarrow 0$

Because of their connection with ‘virtual photon’ nucleon scattering, the behaviour of the structure functions  $W_{1,2}$  in the high energy limit of that process, i.e.  $\nu \rightarrow \infty$ , with  $Q^2$  fixed, should be given by Regge theory (Abarbanel, Goldberger and Treiman, 1969) as

$$\left. \begin{aligned} W_1(\nu, Q^2) &\rightarrow \nu^\alpha f_\alpha^{(1)}(Q^2), \\ W_2(\nu, Q^2) &\rightarrow \nu^{\alpha-2} f_\alpha^{(2)}(Q^2), \end{aligned} \right\} \quad (16.6.1)$$

where  $\alpha$  is the intercept of the appropriate Regge trajectory ( $\alpha = 1$  for ‘Pomeron’;  $\alpha \simeq \frac{1}{2}$  for  $\rho, \omega, f, A_2$  exchange).

If the form (16.6.1) continues to hold as  $Q^2 \rightarrow \infty$ , i.e. in the scaling region, then to get scaling we need, for large  $Q^2$ ,

$$\left. \begin{aligned} f_\alpha^{(1)}(Q^2) &\approx (Q^2)^{-\alpha}, \\ f_\alpha^{(2)}(Q^2) &\approx (Q^2)^{1-\alpha}. \end{aligned} \right\} \quad (16.6.2)$$

Combining (16.6.2) and (16.6.1) suggests that the  $x \rightarrow 0$  behaviour of the scaling functions is

$$\left. \begin{aligned} F_1(x) &\sim x^{-\alpha}, \\ F_2(x) &\sim x^{1-\alpha}. \end{aligned} \right\} \quad (16.6.3)$$

In particular, the leading (Pomeron) contribution would suggest

$$\left. \begin{aligned} F_1(x) &\xrightarrow{x \rightarrow 0} \frac{1}{x}, \\ F_2(x) &\xrightarrow{x \rightarrow 0} \text{constant.} \end{aligned} \right\} \quad (16.6.4)$$

We have already remarked in Section 16.3 that  $\nu W_2$  does not decrease as  $\omega \rightarrow \infty$ . Since  $\omega \rightarrow \infty$  corresponds to  $x \rightarrow 0$  we see that the electromagnetic data are not incompatible with  $F_2(x) \rightarrow \text{constant}$  as  $x \rightarrow 0$ . The distributions shown in Figs. 16.4 and 17.5 support this. Taken literally this implies that the parton or antiparton distribution functions diverge as  $x \rightarrow 0$ , i.e.

$$q_j(x), \bar{q}_j(x) \propto \frac{1}{x} \quad (16.6.5)$$

so that the total number of any type of parton is infinite:

$$\int_0^1 dx q_j(x) \rightarrow \infty. \quad (16.6.6)$$

The combination of Regge plus scaling behaviour has a further consequence. Since the Pomeron is even under charge conjugation and since it has isospin zero, it will contribute equally to ' $\gamma' p$ ', ' $\gamma' n$ ', ' $\gamma' \bar{p}$ ', ' $\gamma' \bar{n}$ ' scattering. We thus expect

$$F_{1,2}^{\text{ep}}(x) = F_{1,2}^{\text{en}}(x) = F_{1,2}^{\text{e}\bar{p}}(x) = F_{1,2}^{\text{e}\bar{n}}(x) \quad \text{as } x \rightarrow 0,$$

which implies

$$\left. \begin{aligned} u(x) &= \bar{u}(x) = d(x) = \bar{d}(x), \\ s(x) &= \bar{s}(x), \end{aligned} \right\} \text{as } x \rightarrow 0. \quad (16.6.7)$$

That this is indeed so seems to be borne out by the data in Fig. 16.7.

Note that if we took the Pomeron to be an  $SU(3)$  singlet we would have, in addition,  $s(x) = u(x)$  as  $x \rightarrow 0$  etc. The fact that the  $\pi p$  and  $K p$  total cross-sections remain unequal at very high energies indicates that the Pomeron is probably not an  $SU(3)$  singlet.

The above arguments are suggestive but not rigorous. How precisely, the number densities behave at small  $x$  is a theoretical topic of great

interest at present and is related to deep questions about the dynamical structure of the Pomeron in QCD. We shall comment briefly on this in Section 23.6.

### 16.7 The missing constituents—gluons

We defined  $q_j(x') dx'$  as the number of partons of type  $j$  whose mass lies between  $x'm_N$  and  $(x' + dx')m_N$ . As already mentioned, it is more fundamental to define  $q_j(x') dx'$  as the number of partons of type  $j$  whose  $Z$  component of momentum, *as measured in the CM reference frame in which the nucleon is travelling very fast* (we call this an ‘infinite momentum frame’), lies between  $x'p_{zN}$  and  $(x' + dx')p_{zN}$ . Generally, a parton with  $Z$  component of momentum  $x'p_{zN}$  in an infinite momentum frame will *not* have mass  $x'm_N$ . The two statements are equivalent only if the parton is at rest in the rest frame of the nucleon. (This is explained in the appendix to this chapter.) But the latter property was effectively assumed when in Section 16.1 we identified the time component of  $q$  in the partons rest frame as  $\nu$ . Thus the two interpretations of the physical meaning of  $q_j(x')$  are equivalent, and this equivalence is essential for the derivation of many of the detailed formulae of the model.

Granted this, it is clear that the total  $Z$  component of momentum carried by a given type of parton is  $\int_0^1 dx [p_{zN} x q_j(x)]$ . Thus the *fraction* of the proton’s CM momentum carried by a given constituent is  $\int_0^1 x q_j(x) dx$ .

The total fraction of the proton’s CM momentum carried by the quarks and antiquarks is thus

$$F = \int_0^1 x(u + \bar{u} + d + \bar{d} + s + \bar{s}) dx \quad (16.7.1)$$

and should equal 1 if these quarks and antiquarks are the *only constituents*.

Now from (16.4.9), (16.4.12) and (16.4.27) we see that to a very good approximation, below charm threshold,

$$F \approx \int_0^1 dx \left\{ \frac{9}{2}[F_2^{ep}(x) + F_2^{en}(x)] - \frac{3}{4}[F_2^{\nu p}(x) + F_2^{\nu n}(x)] \right\}. \quad (16.7.2)$$

Experimentally, the RHS is measured over a wide range of  $Q^2$  to be  $0.45 \pm 0.03$ . We are forced to conclude that the quarks and antiquarks carry only about 50% of the momentum of the proton!

It is usually concluded from this that there must be other constituents. But since the model using just quarks and antiquarks has worked so successfully in describing both weak and electromagnetic interactions it is reasonable to guess that the new constituents do not interact either electromagnetically or via the weak interactions. It is suggested that the

new constituents are the electrically neutral ‘gluons’, the quanta of the colour field that mediates the strong interaction between quarks in the framework of QCD. The QCD gluons have acceptable properties for this rôle. Moreover, in analogy to electromagnetic pair production, they will provide a mechanism for the generation of the quark–antiquark sea that we have been utilizing as shown in Fig. 16.10.

We shall see later that diagrams of this type play a crucial rôle in the breaking of Bjorken scaling and in providing a slow  $Q^2$  dependence for the scaling functions. This behaviour will turn out to be one of the pieces of evidence in favour of QCD.

### 16.8 The parton model in polarized deep inelastic scattering

In Section 15.6 we introduced the formalism necessary for studying deep inelastic scattering using polarized electron or muon beams on polarized nucleon targets. Here we briefly present the parton model predictions for the structure functions  $G_{1,2}$  and consider what may be learnt from the experiments with polarized beams and targets.

The original Bjorken analysis when applied to  $G_{1,2}$  would suggest

$$\left. \begin{aligned} \lim_{B_j} m_N^2 \nu G_1(\nu, Q^2) &= g_1(x), \\ \lim_{B_j} m_N \nu^2 G_2(\nu, Q^2) &= g_2(x). \end{aligned} \right\} \quad (16.8.1)$$

In the parton model we have a virtual photon undergoing a high energy collision with a parton. Since the parton mass is then irrelevant we expect that the parton helicity is unchanged in the collision (see Section 1.3) and as a consequence there is no mechanism to alter the helicity of the nucleon in the collision. From (15.6.11) we see that the combination  $m_N G_1 + \nu G_2$  is proportional to an amplitude in which the nucleon helicity is flipped. Thus, in the parton model we expect

$$m_N G_1 + \nu G_2 \approx 0, \quad (16.8.2)$$

which implies that  $G_2$  is negligible compared with  $G_1$  in the Bjorken limit. It is sometimes argued that (16.8.2) implies that  $g_1(x) + g_2(x) \approx 0$ , but this is incorrect (Anselmino and Leader, 1992). The RHS of (16.8.2) should be interpreted as  $O(m_N/Q)$  and one then finds

$$g_1(x) + g_2(x) = O(1). \quad (16.8.3)$$

Consider now a proton with helicity  $+\frac{1}{2}(\rightarrow)$ . We can introduce number densities

$$f_j^P(x) = f_j^{\rightarrow}(x) \quad \text{and} \quad f_j^A(x) = f_j^{\leftarrow}(x) \quad (16.8.4)$$

for partons of type  $j$  whose helicity is parallel or antiparallel to the proton's helicity respectively. By parity invariance

$$f_j^{\leftarrow} = f_j^{\rightarrow} \quad \text{and} \quad f_j^{\leftarrow} = f_j^{\rightarrow}. \quad (16.8.5)$$

$f_j^{\mathcal{P},\mathcal{A}}(x)$  are the two independent number densities. The usual unpolarized number density is then, clearly,

$$f_j(x) = f_j^{\mathcal{P}}(x) + f_j^{\mathcal{A}}(x) \quad (16.8.6)$$

A simple way to obtain the parton model formula for  $g_1(x)$  is to note that from (15.6.11) and (16.1.4)

$$\begin{aligned} F_1(x) &= \frac{m_N}{2} \left( A_{1\frac{1}{2};1\frac{1}{2}} + A_{1-\frac{1}{2};1-\frac{1}{2}} \right) \\ &= \frac{1}{2} \sum_j Q_j^2 f_j(x) \\ &= \frac{1}{2} \sum_j Q_j^2 [f_j^{\mathcal{P}}(x) + f_j^{\mathcal{A}}(x)] \end{aligned} \quad (16.8.7)$$

whereas from (15.6.11) and (16.8.2)

$$g_1(x) = \frac{m_N}{2} \left( A_{1\frac{1}{2};1\frac{1}{2}} - A_{1-\frac{1}{2};1-\frac{1}{2}} \right) + O\left(\frac{m^2}{Q^2}\right). \quad (16.8.8)$$

Bearing in mind (16.8.5) we deduce that

$$g_1(x) = \frac{1}{2} \sum_j Q_j^2 [f_j^{\mathcal{P}}(x) - f_j^{\mathcal{A}}(x)]. \quad (16.8.9)$$

It has become conventional to define

$$\Delta f_j(x) \equiv f_j^{\mathcal{P}}(x) - f_j^{\mathcal{A}}(x) \quad (16.8.10)$$

as the 'polarized parton number densities', so that

$$g_1(x) = \frac{1}{2} \sum_j Q_j^2 \Delta f_j(x) = \frac{1}{2} \sum_j Q_j^2 [\Delta q_j(x) + \Delta \bar{q}_j(x)]. \quad (16.8.11)$$

We see that  $G_1$  or  $g_1$  measures the extent to which a parton's helicity is influenced by the helicity of its parent hadron. Presumably this is a measure of the spin dependent forces at work.

To end this brief survey we show how to derive the scaling version of the Bjorken sum rule (15.6.35) from the parton model (Hey, 1974).

First we note that in the quark–parton model we have, as can be seen from Table 9.1,

$$Q_j^2 = \frac{2}{3} B_j + \frac{1}{6} Y_j + \frac{1}{3} I_{3j} + \frac{1}{3} C_j, \quad (16.8.12)$$

where  $B, Y, I_3$  and  $C$  refer to baryon number, hypercharge, third component of isospin and charm respectively. Secondly we introduce integrated distribution functions,

$$\Delta f_j \equiv \int_0^1 \Delta f_j(x) dx \quad (16.8.13)$$

so that, for the first moment of  $g_1(x)$ ,

$$\Gamma \equiv \int_0^1 g_1(x) dx = \frac{1}{2} \sum_j Q_j^2 \Delta f_j = \frac{1}{2} \sum_j Q_j^2 [\Delta q_j + \Delta \bar{q}_j]. \quad (16.8.14)$$

Consider now the axial-vector quark current defined by

$$\mathcal{A}_\mu \equiv \sum_j Q_j^2 \bar{\psi}_j \gamma_\mu \gamma_5 \psi_j. \quad (16.8.15)$$

Writing

$$\gamma_5 = \frac{1}{2}(1 + \gamma_5) + \frac{1}{2}(1 - \gamma_5)$$

and remembering (1.3.2) that  $\frac{1}{2}(1 \mp \gamma_5)$  projects out left-handed and right-handed fast particles, respectively, one finds, as explained in the appendix to this chapter

$$\langle p, \frac{1}{2} | \mathcal{A}_\mu | p, \frac{1}{2} \rangle = 2m_N S_\mu \sum_j Q_j^2 (\Delta q_j + \Delta \bar{q}_j) \quad (16.8.16)$$

for the matrix element between a nucleon state of four-momentum  $p_\mu$  and helicity  $+\frac{1}{2}$ . Here  $S_\mu$  is the covariant spin vector for a nucleon of helicity  $+\frac{1}{2}$  as given in (15.6.2).

Now, using (16.8.12), we can express  $\mathcal{A}_\mu$  as a sum of various currents. Amongst them the axial-vector isotopic spin current

$$A_3^\mu = \sum_j I_{3j} \bar{\psi}_j \gamma^\mu \gamma_5 \psi_j \quad (16.8.17)$$

is exactly the isotopic partner of the axial current that appears in the weak interactions [see Section 1.2; especially (1.2.21)] and therefore its hadronic matrix element is known from  $\beta$ -decay measurements. One has from (1.3.17)

$$\langle p | A_3^\mu | n \rangle = \langle p | A_3^\mu | p \rangle - \langle n | A_3^\mu | n \rangle$$

where  $|p\rangle, |n\rangle$  refer to proton and neutron states. The LHS is known from  $\beta$ -decay [see Appendix 3 and eqn (1.2.6)]

$$\langle p, \frac{1}{2} | A_3^\mu | n, \frac{1}{2} \rangle = 2m_N S^\mu \frac{G_A}{G_V}. \quad (16.8.18)$$

The factor  $G_V$  in the denominator arises from the Cabibbo  $\cos \theta_C$  factor (or in the Kobayashi–Maskawa scheme  $V_{ud}$ ) [see (1.2.23) or (9.2.21)].

The hadronic matrix element of  $A_3^\mu$  is thus known *provided* one subtracts neutron and proton matrix elements. When this is done for the current  $\mathcal{A}_\mu$  all the other terms on the RHS of (16.8.12) cancel out so one obtains

$$\begin{aligned} \langle p, \frac{1}{2} | \mathcal{A}^\mu | p, \frac{1}{2} \rangle - \langle n, \frac{1}{2} | \mathcal{A}^\mu | n, \frac{1}{2} \rangle &= \frac{1}{3} \left\{ \langle p, \frac{1}{2} | A_3^\mu | p, \frac{1}{2} \rangle - \langle n, \frac{1}{2} | A_3^\mu | n, \frac{1}{2} \rangle \right\} \\ &= 2m_N S^\mu \frac{1}{3} \frac{G_A}{G_V}. \end{aligned} \quad (16.8.19)$$

Finally using (16.8.16) and (16.8.14) and analogous expressions for neutron matrix elements, in (16.8.19) one finds

$$\int_0^1 [g_1^p(x) - g_1^n(x)] dx = \frac{1}{6} \frac{G_A}{G_V} \quad (16.8.20)$$

which agrees with (15.6.35).

Let us now consider what can be learnt about the parton structure from polarized deep inelastic experiments. In the quark-parton model (16.8.11) becomes

$$g_1^p(x) = \frac{1}{2} \left\{ \frac{4}{9} [\Delta u(x) + \Delta \bar{u}(x)] + \frac{1}{9} [\Delta d(x) + \Delta \bar{d}(x) + \Delta s(x) + \Delta \bar{s}(x)] \right\}. \quad (16.8.21)$$

From (15.6.11) and (15.6.12) the asymmetry  $A_1$  discussed in Section 15.6 is then given by

$$A_1(x) = \frac{\frac{4}{9} [\Delta u(x) + \Delta \bar{u}(x)] + \frac{1}{9} [\Delta d(x) + \Delta \bar{d}(x) + \Delta s(x) + \Delta \bar{s}(x)]}{\frac{4}{9} [u(x) + \bar{u}(x)] + \frac{1}{9} [d(x) + \bar{d}(x) + s(x) + \bar{s}(x)]} \quad (16.8.22)$$

Now we noted that  $A_1(x)$  appears to approach the value 1 as  $x \rightarrow 1$  (Fig. 15.13). We already know that the sea is negligible at large  $x$  and also that in a proton  $d(x) \ll u(x)$  as  $x \rightarrow 1$  (Section 16.4.1). Thus for  $x \rightarrow 1$  we have

$$A_1(x) \approx \frac{\Delta u(x)}{u(x)} \quad (16.8.23)$$

from which we conclude that

$$\Delta u(x) \approx u(x) \quad \text{for } x \rightarrow 1. \quad (16.8.24)$$

In other words the fastest moving up quark in a proton seems to be 100% polarized in the direction of the spin of the proton.

In Section 17.1.2 we shall return to discuss the startling EMC experiment described in Section 15.6. The interpretation of the EMC results is the first to contradict the naive parton model in the sense that QCD effects are operative which do not vanish as  $Q^2 \rightarrow \infty$ .

### 16.9 Appendix to Chapter 16: The parton model as an impulse approximation

In the previous chapters we saw that in so far as deep inelastic *lepton–nucleon* scattering was concerned the nucleon could be visualized as a bound system of constituent quark–partons, with which the lepton interacted as if they were free particles. Our aim now is to try to give some sort of justification for such a picture, and to derive more reliable results for deep inelastic scattering in which allowance is made for the internal longitudinal and transverse (Fermi) motion of the quark–partons. The approach also allows us to evaluate the *forward* hadronic matrix elements of currents which appear in the sum rules discussed in Chapters 16 and 17 in terms of parton number densities.

#### 16.9.1 The parton model as an impulse approximation

Let us consider the nucleon as a bound state of several constituents. In what way does it differ significantly from other bound state systems such as atoms or nuclei? The most important difference lies in the ratio of binding energy to total energy or mass of the constituents:

$$\text{Atoms} \quad \frac{\text{few eV}}{0.5 \text{ MeV}} \approx 10^{-5},$$

$$\text{Nuclei} \quad \frac{8 \text{ MeV}}{940 \text{ MeV}} \approx 10^{-2},$$

$$\text{Nucleons} \quad \frac{1 \text{ GeV}}{\leq 1 \text{ GeV}} \geq 1.$$

The higher the ratio, the more important is the potential energy of the constituent, and this has two consequences:

- It is less reasonable to pretend that the constituent is quasi-free. We shall see that this statement is reference-frame dependent and that, although the above comment is valid in the rest frame of the system, it may not be so in a frame in which the system is moving sufficiently fast;
- It is not sensible to think of the system as composed of a fixed number of constituents. The enormous potential energy can cause pair production with consequent fluctuations in the number of constituents.

If in a given reference frame we imagine taking a snapshot of the target as seen by the projectile we may see a set of constituents of mass  $m_j$  and

momenta  $\mathbf{k}_j$  and we may ask for how long this fluctuation or virtual state will exist. Its lifetime,  $\tau_V$ , by the uncertainty principle, is likely to be of the order of

$$\tau_V \simeq \frac{1}{\Delta E} = \frac{1}{E_V - E_N}, \quad (16.9.1)$$

where  $E_V$  is the energy of the virtual state and  $E_N$  the energy of the nucleon, in the given reference frame.

The impulse approximation treats the collision of the projectile with the constituent as if the latter were a free particle. It will be a valid approximation when:

1. the time of interaction  $\tau_{int}$  between the projectile and the constituent is much smaller than  $\tau_V$ , so that the constituent is basically free during the period of its interaction with the projectile, and
2. the impulse given to the constituent is so large that after the interaction its energy is much larger than the binding energy, and so it continues to behave as a free particle.

The second condition is automatically satisfied in the deep inelastic regime since one imparts a very large momentum to the struck constituent.

To analyse the first condition let us look at the high energy lepton-nucleon collision in a frame in which the proton is moving very fast, i.e. one in which  $E_N \gg m_N$ , loosely referred to as an ‘infinite momentum frame’. The simplest choice of frame is first to rotate the LAB frame so as to make the momentum transfer vector  $\mathbf{q}$  lie along  $OZ$ , and then to transform to a frame moving very fast along this  $OZ$  axis. We shall label this frame  $S^\infty$ .

The components of the nucleon’s four-momentum in  $S^\infty$  will be

$$\begin{aligned} p &= (E_N = \sqrt{P^2 + m_N^2}, 0, 0, -P) \\ &\simeq \left( P + \frac{m_N^2}{2P}, 0, 0, -P \right), \end{aligned} \quad (16.9.2)$$

where the speed of the reference frame as seen in the LAB is

$$\beta = \frac{P}{E_N} \simeq 1.$$

The four-momentum transfer  $\mathbf{q}$  has components

$$\begin{aligned} q &= (\nu, 0, 0, \sqrt{\nu^2 + Q^2}) \\ &= (\nu, 0, 0, \sqrt{\nu^2 + 2m_N\nu x}) \end{aligned} \quad (16.9.3)$$

in the rotated LAB frame, where  $x$ , as defined earlier, is equal to  $Q^2/2m_N\nu$ .

Transforming to the reference frame  $S^\infty$ , for  $\nu \gg m_N$  it will have components given by

$$\begin{aligned} q &= (q_0^*, q_x^*, q_y^*, q_z^*) \\ &= \left[ -xP \left( 1 - \frac{x^2 m_N^2}{Q^2} \right) + \frac{m_N \nu}{2P}, 0, 0, xP \left( 1 - \frac{x^2 m_N^2}{Q^2} \right) \right. \\ &\quad \left. + \frac{m_N \nu}{2P} \left( 1 + \frac{2x^2 m_N^2}{Q^2} \right) \right] \end{aligned} \quad (16.9.4)$$

Note the odd feature, that although  $\mathbf{q}$  pointed along  $OZ$ ,  $q_z^*$  increases as  $S^\infty$  moves faster along  $OZ$ . The reason is that  $q$  is *not* the four-momentum of a particle. Indeed it is a space-like four-vector.

It is a typical feature of quantum mechanics that, in attempting to cause a momentum change  $q^*$  in a quantum mechanical system, the times  $t$  and distances  $z$  of importance are always those that keep the phase factor  $e^{iq^* \cdot z}$  close to one in value.

We can write

$$q^* \cdot z = \frac{1}{2}(q_0^* - q_z^*)(t + z) + \frac{1}{2}(q_0^* + q_z^*)(t - z)$$

and substituting from (16.9.4)

$$q^* \cdot z \simeq \frac{1}{2} \left[ -2xP(t + z) + \frac{m_N \nu}{P}(t - z) \right]. \quad (16.9.5)$$

Thus as  $P \rightarrow \infty$  the important times and distances must satisfy

$$t + z < \frac{\text{constant}}{P},$$

or

$$z \simeq -t.$$

The second term in (16.9.5) will then be small provided that

$$\frac{m_N \nu}{P} t < 1.$$

We can thus say the relevant interaction time  $\tau_{\text{int}}$  will satisfy

$$\tau_{\text{int}} \leq \frac{P}{2m_N \nu}. \quad (16.9.6)$$

To estimate the lifetime of a virtual state, let the  $j$ th constituent have mass  $m_j$ , momentum perpendicular to  $OZ$ ,  $\kappa_{jT}$ , and let the momentum along  $OZ$  be specified in terms of the nucleon's momentum by

$$\kappa_{jz} = x'_j p_{Nz} = -x'_j P. \quad (16.9.7)$$

To conserve momentum we require

$$\sum_j \kappa_{jT} = 0, \quad \sum_j x'_j = 1. \quad (16.9.8)$$

Then the quantity needed in (16.9.1) is

$$\begin{aligned} E_V - E_N &= \sum_j (x_j'^2 P^2 + \kappa_{jT}^2 + m_j^2)^{1/2} - (P^2 + m_N^2)^{1/2} \\ &\simeq \sum_j x'_j P + \sum_j \frac{\kappa_{jT}^2 + m_j^2}{2x'_j P} - P - \frac{m_N^2}{2P} \end{aligned}$$

*provided*  $x'_j P$  is not small.

Using (16.9.8) we get

$$E_V - E_N \simeq \frac{1}{2P} \left[ \sum_j \left( \frac{\kappa_{jT}^2 + m_j^2}{x'_j} \right) - m_N^2 \right]. \quad (16.9.9)$$

We assume that the internal motion of the constituents is limited and that the quantity in parentheses is some finite quantity; let us call it  $\mathcal{M}^2$ , perhaps of order  $m_N^2$ .

Then, from (16.9.9)

$$\frac{\tau_{\text{int}}}{\tau_V} = \frac{\mathcal{M}^2}{4m_N \nu}, \quad (16.9.10)$$

and this will be  $\ll 1$  provided

$$m_N \nu \gg \frac{1}{4} \mathcal{M}^2. \quad (16.9.11)$$

From the form of  $\mathcal{M}^2$  and (16.9.11), it is clear that condition (1) for the validity of the impulse approximation will also be satisfied when  $\nu \rightarrow \infty$  provided  $x'_j \neq 0$ .

Since, as we learn in Chapter 16, a scattering with a given value of  $x$  involves only constituents with  $x'_j \approx x$ , we can say that the parton-like picture is justified in the deep inelastic limit in the  $S^\infty$  frame except at  $x = 0$ . Of course the region  $x \approx 1$  is also excluded, since it corresponds to elastic scattering, where it is surely nonsense to claim unit probability for the struck parton to reunite to form a nucleon.

We can try to specify the dangerous regions a little more precisely.

For the region  $x \approx 1$ , the requirement that many hadrons can be produced in the final state implies that the produced hadronic mass  $M_X^*$  be much greater than the mass  $M_X^{\min}$  of the lightest hadron allowed by the internal quantum number conservation laws. Thus we require, by (16.4.21) or (16.4.22)

$$2m_N \nu (1 - x) + m_N^2 \gg (M_X^{\min})^2$$

or

$$(1 - x) \gg \frac{(M_X^{\min})^2 - m_N^2}{2m_N\nu}. \quad (16.9.12)$$

For the region  $x \approx 0$  we require

$$xP \gg (m_j^2 + \langle \kappa_T^2 \rangle)^{1/2}.$$

Since  $P$  can be made arbitrarily large it might seem that only the *point*  $x = 0$  is excluded. It should not be forgotten though that we have assumed  $\nu, Q^2 \gg m_N^2$ ; and later we shall require  $Q^2 \gg \langle \kappa_T^2 \rangle$  in order to use the approximation of incoherence. So, in a given experiment, a safe value for  $x$  near zero is simply one for which these conditions are satisfied.

Given that the impulse approximation is valid in the frame  $S^\infty$ , we now attempt a more careful calculation of the deep inelastic cross-section allowing for non-zero internal transverse motion of the constituents.

### 16.9.2 The parton model including transverse motion

We now go to the reference frame  $S^\infty$  in which the impulse approximation is supposed to hold. In this frame we shall calculate the *inelastic* nucleon tensor  $W^{\alpha\beta}(N)$  in terms of the partonic tensors  $W^{\alpha\beta}(k, j)$  for a lepton scattering on a quark  $j$  and turning it into a quark of type  $k$ . Although the impulse approximation is a simple idea, there are subtleties in the derivation so we shall go through the analysis in some detail.

Let us use the labels  $P$  and  $q^*$  to denote the components of the four-momentum of the nucleon and of  $q$  in the frame  $S^\infty$ . The inelastic nucleon tensors for the various kinds of reactions are defined in (15.3.2), (15.4.5) and (15.4.8). We shall write

$$W_{\alpha\beta}(N) = \frac{1}{2} \sum_X \langle P | J_\alpha^\dagger(0) | X \rangle \langle X | J_\beta(0) | P \rangle (2\pi)^3 \delta^4(P_X - P - q^*) \quad (16.9.13)$$

where a sum over initial spin is implied and where  $J^\alpha$  could be any of the currents discussed in Chapter 15.

We now make the following assumptions:

1. When  $P_X^2 = (P + q^*)^2 \gg m_N^2$ , so that the states  $|X\rangle$  contain many hadrons, it is permissible to replace the sum over  $|X\rangle$  by a sum over all possible parton states  $|\kappa_1\rangle, |\kappa_1\kappa_2\rangle, |\kappa_1\kappa_2\kappa_3\rangle, \dots$  with the same total four-momentum as  $|X\rangle$ . This is equivalent to stating that there is unit probability for the partons to transmute into hadrons.
2. The interaction of the photon with the nucleon is viewed as a sum

of interactions with the various constituents. Thus

$$J^\alpha = \sum_j J_j^\alpha, \quad (16.9.14)$$

where we sum over all the distinct types of constituent.

3. The  $J_j^\alpha$  are ‘one-body’ operators, i.e. they act only on partons of type  $j$  and the partons scatter under the action of  $J_j^\alpha$  in a point-like fashion.
4. The nucleon can be viewed as a superposition of states of different numbers of partons which are essentially free during the time of the interaction.

When we substitute for  $|P\rangle$  a superposition over states with  $n$  partons, it is clear that since the  $J_j^\alpha$  do not change the number of partons present we shall end up with a sum for (16.9.13) of the form

$$\begin{aligned} W_{\alpha\beta}(N) &= \sum_n \mathcal{P}_n \sum_{\kappa_1 \dots \kappa_n} \langle P; n | J_\alpha^\dagger(0) | \kappa_1 \dots \kappa_n \rangle \langle \kappa_1 \dots \kappa_n | J_\beta(0) | P; n \rangle \\ &\quad \times (2\pi)^3 \delta^4(\kappa_1 + \dots + \kappa_n - P - q^*), \end{aligned} \quad (16.9.15)$$

where  $\mathcal{P}_n$  is the probability of finding an  $n$ -parton state in the proton and  $|P; n\rangle$  means the  $n$ -parton component of the nucleon state.

Because of the relativistic normalization of the states [see (15.3.3)] which is essential in order to have covariant matrix elements, the sum over  $\kappa_i$  in (16.9.15) must be of the form

$$\sum_{\kappa_i} \rightarrow \int \frac{d^3 \kappa_i}{(2\pi)^3 2\epsilon_i}, \quad (16.9.16)$$

where  $\epsilon_i$  is the energy corresponding to  $\kappa_i$ .

We now write

$$\begin{aligned} |P, n\rangle &= [(2\pi)^3 2P_0]^{1/2} \int \frac{d^3 \kappa_1}{\sqrt{(2\pi)^3 2\epsilon_1}} \dots \int \frac{d^3 \kappa_n}{\sqrt{(2\pi)^3 2\epsilon_n}} \psi(\kappa_1 \dots \kappa_n) \\ &\quad \times \delta(P - \kappa_1 - \dots - \kappa_n) |\kappa_1 \dots \kappa_n\rangle \end{aligned} \quad (16.9.17)$$

in order to ensure that  $\psi(\kappa_i)$  is a true probability amplitude for finding the momenta  $\kappa_1 \dots \kappa_n$  in  $|P; n\rangle$ , so that we have

$$\int d^3 \kappa_1 \dots d^3 \kappa_n |\psi(\kappa_1 \dots \kappa_n)|^2 \delta(P - \kappa_1 - \dots - \kappa_n) = 1. \quad (16.9.18)$$

(Note that we are insisting that the sum of the parton three-momenta equals that of the nucleon.)

To avoid a jungle of algebra we study the structure of the terms in (16.9.15) using a highly symbolic notation and limiting ourselves to the case  $n = 2$ , though the general case is quite straightforward.

Suppose that the two partons involved are of different types, say ‘*a*’ and ‘*b*’. Then one will have the terms of the form

$$\sum_{\substack{a,b,a' \\ b',a'',b''}} \delta(P - a - b) \psi^*(a, b) \langle a, b | J_a^\dagger + J_b^\dagger | a', b' \rangle \langle a', b' | J_a + J_b | a'', b'' \rangle \\ \times \psi(a'', b'') \delta(P - a'' - b'') \delta(a' + b' - P - q^*).$$

Using the assumption that the partons are free, so that

$$\langle a, b | J_a | a', b' \rangle = \delta(b - b') \langle a | J_a | a' \rangle$$

etc., one will end up with ‘diagonal’ terms of the form

$$\sum_{\kappa_a} |\psi(a, P - a)|^2 \langle a | J_a^\dagger | a + q^* \rangle \langle a + q^* | J_a | a \rangle \\ + \sum_{\kappa_b} |\psi(P - b, b)|^2 \langle b | J_b^\dagger | b + q^* \rangle \langle b + q^* | J_b | b \rangle,$$

where, for example,  $|\psi(a, P - a)|^2$  measures the probability of finding the type *a* parton with momentum  $\kappa_a$ .

The cross-terms lead eventually to expressions of the type

$$\sum_{\kappa_a} \psi^*(a, P - a) \psi(a + q^*, P - a - q^*) \langle a | J_a^\dagger | a + q^* \rangle \\ \times \langle P - a | J_b | P - a - q^* \rangle,$$

which involve a product or overlap of wave functions evaluated at momenta  $\kappa_a$  and  $\kappa_a + q^*$ . In the deep inelastic region of large  $q^*$  this should become totally negligible. Thus all cross-terms disappear and one is left with an incoherent sum involving probabilities and not probability amplitudes.

When all the details are put in, one obtains the result

$$W^{\alpha\beta}(N) = \sum_n \mathcal{P}_n \sum_j N_j(n) \int d^3 \kappa_j \left( \frac{P_0}{\epsilon_j} \right) \mathcal{P}(\kappa_j) W^{\alpha\beta}(k, j), \quad (16.9.19)$$

where  $\mathcal{P}_n$  is the probability of finding *n* partons in the nucleon,  $N_j(n)$  is the number of partons of type *j* in the *n*-parton state, and  $\mathcal{P}(\kappa_j)$  is the probability of finding a type *j* parton with momentum  $\kappa_j$ . The sum *j* goes over distinct types of parton.

As written (16.9.19) refers to the production of a particular quark type *k*. To get the fully inclusive result we must sum over the different *k* that may originate from a given type *j* quark. For electromagnetic or NC reactions we always have *k* = *j*. But for CC reactions we can have, for example, transitions like  $d \rightarrow u$  and  $d \rightarrow c$ .

One sees that the result (16.9.19) is just what one would have written down intuitively in an impulse approximation with incoherence assumed,

were it not for the factor  $P_0/\epsilon_j$  which has arisen from the necessary relativistic normalization of states.

There is one important point that is hidden in the above derivation.  $W^{\alpha\beta}(k, j)$  is defined with conservation of both energy and momentum between initial and final states. Our nucleon, on the other hand, was decomposed into virtual states with the same three-momentum as the nucleon, but not with the same energy, so it might appear that the initial and final partons will not have the same energy. However, precisely because we are in the frame  $S^\infty$ , this failure of energy conservation is of the order of  $m_N/P$  and vanishes as  $P \rightarrow \infty$ , as can be seen from (16.9.9).

Finally we rewrite (16.9.19) in simpler form. Let  $n_j(\boldsymbol{\kappa})d^3\boldsymbol{\kappa}$  be the mean number of partons of *distinct type*  $j$  with momentum in the range  $\boldsymbol{\kappa} \rightarrow \boldsymbol{\kappa} + d\boldsymbol{\kappa}$  in the nucleon as seen in frame  $S^\infty$ . Then (16.9.19) becomes

$$W^{\alpha\beta}(N) = \sum_j \int d^3\boldsymbol{\kappa} \left( \frac{P_0}{\epsilon} \right) n_j(\boldsymbol{\kappa}) W^{\alpha\beta}(k, j), \quad (16.9.20)$$

where the sum runs over the various distinct kinds of partons, or constituents in general.

Although the formal derivation has made no use of it, it must be remembered that the whole picture utilized is only valid in a frame where the proton is moving very fast, as was emphasized in Section 16.9.1.

*The scaling functions allowing for partonic transverse motion.* The last stage of the analysis compares the forms of  $W^{\alpha\beta}(N)$  and  $W^{\alpha\beta}(k, j)$  in  $S^\infty$  and leads to formulae for the scaling functions  $F_i(x)$  which take account of the transverse motion of the constituents.

The most general form for  $W^{\alpha\beta}(N)$  in terms of  $W_i$ , or equivalently the scaling function  $F_i$ , was given in (15.3.12) for the electromagnetic case and in (15.4.17) for the NC and CC cases. Using the notation  $P_\alpha$  and  $q_\alpha^*$  for the nucleon and vector boson four-momenta in the  $S^\infty$  frame the scaling functions  $F_j(j = 1, 2, 3)$  can be projected out from  $W^{\alpha\beta}(N)$  in the following fashion.

Define

$$\left. \begin{aligned} \mathcal{P}_{\alpha\beta} &\equiv \frac{1}{4} \left( \frac{Q^2}{4x^2} + m_N^2 \right)^{-1} \left( P_\alpha + \frac{q_\alpha^*}{2x} \right) \left( P_\beta + \frac{q_\beta^*}{2x} \right), \\ Q_{\alpha\beta} &\equiv \frac{1}{4} \left( \frac{q_\alpha^* q_\beta^*}{q^2} - g_{\alpha\beta} \right). \end{aligned} \right\} \quad (16.9.21)$$

Then, after a considerable amount of algebra, one finds

$$\left. \begin{aligned} F_1 &= (\mathcal{P}_{\alpha\beta} + Q_{\alpha\beta}) W^{\alpha\beta}(N), \\ F_2 &= 2x \left[ 1 + \frac{4x^2 m_N^2}{Q^2} \right]^{-1} (\mathcal{P}_{\alpha\beta} + 3Q_{\alpha\beta}) W^{\alpha\beta}(N), \\ F_3 &= \mathcal{R}_{\alpha\beta} W^{\alpha\beta}(N), \end{aligned} \right\} \quad (16.9.22)$$

where

$$\mathcal{R}_{\alpha\beta} = \frac{i}{8x} \left[ \frac{Q^2}{4x^2} + m_N^2 \right]^{-1} \left( q^{*\gamma} P^\delta - P^\gamma q^{*\delta} \right) \epsilon_{\gamma\delta\alpha\beta}. \quad (16.9.23)$$

The partonic tensor  $W^{\alpha\beta}(k, j)$  for the transition  $j \rightarrow k$  with a current  $\gamma_\alpha(\lambda_V - \lambda_A \gamma_5)$  is obtained in a manner analogous to (15.1.7). One finds, recalling that the initial quark momentum is  $\kappa_\mu$ ,

$$\begin{aligned} W_{\alpha\beta}(k, j) = & \left\{ 2(\lambda_V^2 + \lambda_A^2) \left[ 2\kappa_\alpha \kappa_\beta + \kappa_\alpha q_\beta^* + q_\alpha^* \kappa_\beta - g_{\alpha\beta} (\kappa \cdot q^* + m_j^2) \right] + \right. \\ & + 2(\lambda_V^2 - \lambda_A^2) m_j m_k g_{\alpha\beta} + 4i \lambda_V \lambda_A \kappa^\gamma q^{*\delta} \epsilon_{\gamma\delta\alpha\beta} \Big\} \\ & \times \delta(2\kappa \cdot q^* - Q^2 + m_j^2 - m_k^2). \end{aligned} \quad (16.9.24)$$

In the above we have kept all quark mass terms so that we can deal with the case of heavy quark production when  $Q^2$  is not much greater than  $m_k^2$ . As previously we specify  $\kappa_z$  by

$$\kappa_z \equiv x' P_z = -x' P, \quad (16.9.25)$$

where it is assumed that  $x' P \gg m_j^2$ , and we assume, as always, that  $\kappa_T$  is bounded. Then in  $S^\infty$  the components of  $\kappa$  will be

$$\kappa \simeq \left( x' P + \frac{m_j^2 + \kappa_T^2}{2x' P}, \kappa_T, -x' P \right). \quad (16.9.26)$$

If we use (16.9.4), the argument in the  $\delta$ -function in (16.9.24) then involves

$$2\kappa \cdot q^* = 2m_N \nu x' \left( 1 + \frac{x^2 m_N^2}{Q^2} \right) - \frac{x}{x'} \left( m_j^2 + \kappa_T^2 \right). \quad (16.9.27)$$

The  $\delta$ -function then becomes, to leading order,

$$\begin{aligned} \delta \left( 2\kappa \cdot q^* - Q^2 + m_j^2 - m_k^2 \right) = & \frac{(1 - x^2 m_N^2 / Q^2)}{2m_N \nu} \\ & \times \delta \left[ x' - x \left( 1 + \frac{m_j^2 + \kappa_T^2}{2m_N \nu x'} \right) + \frac{m_j^2 - m_k^2 + x^2 m_N^2}{2m_N \nu} \right]. \end{aligned} \quad (16.9.28)$$

We see that, with the exception of the point  $x' = 0$ , as  $\nu \rightarrow \infty$ , the  $\delta$ -function forces

$$x = x'. \quad (16.9.29)$$

Thus the spread expected from the internal motion is negligible as  $\nu \rightarrow \infty$ .

In practice of course  $\nu$  is large but finite, so it is probably worth while to solve for  $x'$  more accurately in (16.9.28), especially for use near  $x = 0$ .

In that case keeping terms to order  $m^2/Q^2$  we have

$$\begin{aligned} \delta(2\kappa \cdot q^* - Q^2 + m_j^2 - m_k^2) &= \frac{x'}{2m_N\nu x} \left[ 1 - \frac{m_j^2 + m_k^2 + 2\kappa_T^2}{Q^2} \right] \\ &\quad \times \delta \left[ x' - x \left( 1 + \frac{m_k^2 + \kappa_T^2 - x^2 m_N^2}{Q^2} \right) \right] \end{aligned} \quad (16.9.30)$$

where we have deliberately left the factor  $x'$  in the numerator since it will cancel the term  $P_0/\epsilon = 1/x'$  in (16.9.20).

We now use (16.9.22) to project out the  $F_j$  from the expression (16.9.20) using (16.9.24) for the partonic tensor. After some algebra one finds

$$\begin{aligned} F_1(x, Q^2) &= \sum_{j,k} \int d^3\kappa n_j(\kappa) \left[ \frac{1}{2}(\lambda_V^2 + \lambda_A^2)_{kj} - \frac{m_j m_k (\lambda_V^2 - \lambda_A^2)_{kj}}{Q^2} \right] \\ &\quad \times \delta(x' - \xi'_k), \\ F_2(x, Q^2) &= 2x \sum_{j,k} \int d^3\kappa n_j(\kappa) \frac{1}{2}(\lambda_V^2 + \lambda_A^2)_{kj} \\ &\quad \times \left[ 1 + \frac{m_j^2 + m_k^2 + 4\kappa_T^2 - 4x^2 m_N^2}{Q^2} \right] \delta(x' - \xi'_k), \\ F_3(x, Q^2) &= \sum_{j,k} \int d^3\kappa n_j(\kappa) (2\lambda_V \lambda_A)_{kj} \left[ 1 - \frac{3x^2 m_N^2}{Q^2} \right] \delta(x' - \xi'_k), \end{aligned} \quad (16.9.31)$$

where

$$\xi'_k \equiv x \left( 1 + \frac{m_k^2 + \kappa_T^2 - x^2 m_N^2}{Q^2} \right) \quad (16.9.32)$$

In (16.9.31) we have indicated that the currents involved in the transitions  $j \rightarrow k$  depend upon  $j$  and  $k$ .

Finally, we define  $q_j(x')dx'$  as the number density, i.e. the mean number of partons of type  $j$  with  $Z$  component of momentum between  $x'P_z$  and  $(x' + dx')P_z$  in  $S^\infty$ , do the  $x'$  integration, and carry out the integration over  $d^2\kappa_T$  by simply replacing  $\kappa_T^2$  by its mean value  $\langle \kappa_T^2 \rangle$  everywhere. The latter step is justified if  $q_j(x')$  is a smooth function over a range in  $x'$  around the point  $x$  of order  $m_N^2/Q^2$ . Then

$$\begin{aligned} F_1(x, Q^2) &= \sum_{j,k} q_j(\xi'_k) \left[ \frac{1}{2}(\lambda_V^2 + \lambda_A^2)_{kj} - \frac{m_j m_k (\lambda_V^2 - \lambda_A^2)_{kj}}{Q^2} \right] \\ &\quad \times \theta(1 - \xi'_k), \end{aligned}$$

$$\begin{aligned}
F_2(x, Q^2) &= 2x \sum_{j,k} q_j(\xi'_k) \frac{1}{2} (\lambda_V^2 + \lambda_A^2)_{kj} \\
&\quad \times \left[ 1 + \frac{m_j^2 + m_k^2 + 4\langle \kappa_T^2 \rangle_j - 4x^2 m_N^2}{Q^2} \right] \theta(1 - \xi'_k), \\
F_3(x, Q^2) &= 2 \sum_{j,k} q_j(\xi'_k) (\lambda_V \lambda_A)_{kj} \left[ 1 - \frac{3x^2 m_N^2}{Q^2} \right] \theta(1 - \xi'_k), \quad (16.9.33)
\end{aligned}$$

where the step function [ $\theta(z) = 1$  if  $z \geq 0$ ,  $= 0$  if  $z < 0$ ] reflects the fact that the upper limit of the  $x'$  integration was 1.

As  $Q^2 \rightarrow \infty$  we recover exactly our earlier results (16.1.4) and (16.1.5).

It is interesting to note that these results now emerge without the need to assume a continuous spread of parton masses between 0 and  $m_N$ . Indeed we can, if we wish, fix the masses or put them to zero, at will. The presence of the internal motion allows  $x'$  to vary between 0 and 1 without forcing the mass of the parton to vary.

As will be discussed later, the mean intrinsic transverse momentum of the quarks is small  $\langle \kappa_T^2 \rangle < m_N^2$ . In the following we always assume that

$$Q^2 \gg m_N^2. \quad (16.9.34)$$

In that case it is not meaningful to retain the correction terms involving  $\langle \kappa_T^2 \rangle$  or  $x^2 m_N^2$ , nor indeed light quark mass terms.

Finally, then, we define

$$\left. \begin{aligned} \xi_k &\equiv x \left( 1 + \frac{m_k^2}{Q^2} \right) & (k = c, b), \\ &\equiv x & (k = u, d, s), \end{aligned} \right\} \quad (16.9.35)$$

and have

$$\begin{aligned}
F_1(x, Q^2) &= \sum_{j,k} q_j(\xi_k) \left[ \frac{1}{2} (\lambda_V^2 + \lambda_A^2)_{kj} - \frac{m_j m_k (\lambda_V^2 - \lambda_A^2)_{kj}}{Q^2} \right] \\
&\quad \times \theta(1 - \xi_k), \\
F_2(x, Q^2) &= 2 \sum_{j,k} \left( \frac{\xi_k \xi_j}{x} \right) q_j(\xi_k) \frac{1}{2} (\lambda_V^2 + \lambda_A^2)_{kj} \theta(1 - \xi_k), \\
F_3(x, Q^2) &= 2 \sum_{j,k} q_j(\xi_k) (\lambda_V \lambda_A)_{kj} \theta(1 - \xi_k). \quad (16.9.36)
\end{aligned}$$

Note that the correction term in  $F_1$  does not contribute in CC reactions since  $\lambda_V = \lambda_A$ .

Compared with our previous results we note the following:

1. The scaling functions now depend weakly on  $Q^2$ , so that perfect scaling will not hold. What we measure at a given  $x$  is not  $q_j(x' = x)$

but  $q_j(x' = \xi_k)$ . (It should not be forgotten that scaling is also violated as a consequence of dynamical QCD effects.)

2. The Callan–Gross relation (16.1.8) is no longer exactly valid. Of course it becomes exact for  $Q^2 \gg (\text{heavy quark mass})^2$ .

Finally we note that the internal Fermi motion in a *nucleus* can be treated by the above approach. This will be discussed in relation to the so-called ‘EMC effect’ in Section 17.1.3.

### 16.9.3 Current matrix elements in the quark–parton model

In the SM all hadronic currents are expressed in terms of quark fields  $\psi_f(x)$  where  $f$  labels the flavour. As in Sections 1.2, 16.8 and 18.1, we often require the forward matrix elements of these currents taken between nucleon states. We shall use the quark–parton model to evaluate these in the frame  $S^\infty$ .

Consider the generic current

$$J_f = \bar{\psi}_f \Gamma \psi_f \quad (16.9.37)$$

where  $\Gamma = \gamma^\alpha$  or  $\gamma^\alpha \gamma_5$ , evaluated at the space-time origin  $x_\mu = 0$ . We shall evaluate the forward matrix elements of  $J_f$  in a proton state with covariant spin vector  $S_\mu$ .

Analogously to (16.9.15) we insert complete sets of quark states, corresponding to partons of momentum  $\kappa$  and helicity  $\lambda$ .

Because the proton is polarized we need to slightly generalize the number densities  $n_j(\kappa)$  used previously. Thus we introduce  $n_f(\kappa, \lambda; \mathbf{S}) d^3\kappa$  as the number of flavour  $f$  quarks with momentum in the range  $\kappa \rightarrow \kappa + d\kappa$  and with helicity  $\lambda$  inside a proton of momentum  $\mathbf{P}$  and covariant spin vector  $S_\mu$  [see eqn (15.6.2)]. After some algebra one finds for the *forward* hadronic matrix elements,

$$\langle \mathbf{P}, \mathbf{S} | J_f | \mathbf{P}, \mathbf{S} \rangle = \sum_{\lambda} \int \frac{P_0}{\epsilon} n_f(\kappa, \lambda; \mathbf{S}) \langle \kappa, \lambda | J_f | \kappa, \lambda \rangle d^3\kappa \quad (16.9.38)$$

where we have utilized the fact [see (1.3.6)] that for fast quarks  $\gamma^\alpha$  and  $\gamma^\alpha \gamma^5$  conserve helicity.

Let us now define more specifically

$$J_f^\alpha = \bar{\psi}_f \gamma^\alpha \psi_f, \quad J_f^{5\alpha} = \bar{\psi}_f \gamma^\alpha \gamma_5 \psi_f. \quad (16.9.39)$$

Then treating the quark–partons as ‘free’ particles in  $S^\infty$  one has [see eqn (A1.1.23) of Appendix 1]

$$\langle \kappa, \lambda | J_f^\alpha | \kappa, \lambda \rangle = \bar{u}_\lambda \gamma^\alpha u_\lambda = 2\kappa^\alpha \quad (16.9.40)$$

and

$$\langle \kappa, \lambda | J_f^{5\alpha} | \kappa, \lambda \rangle = \bar{u}_\lambda \gamma^\alpha \gamma^5 u_\lambda = 2m_f s^\alpha(\lambda) \quad (16.9.41)$$

where  $s^\alpha(\lambda)$  is the parton's covariant spin vector corresponding to a helicity state  $\lambda = \pm \frac{1}{2}$

$$s^\alpha(\lambda) = \frac{2\lambda}{m_f}(|\kappa|, \epsilon \hat{\kappa}). \quad (16.9.42)$$

On grounds of Lorentz covariance the forward nucleonic matrix elements have a similar structure:

$$\langle \mathbf{P}, \mathbf{S} | J_f^\alpha | \mathbf{P}, \mathbf{S} \rangle = 2v_f P^\alpha \quad (16.9.43)$$

and

$$\langle \mathbf{P}, \mathbf{S} | J_f^{5\alpha} | \mathbf{P}, \mathbf{S} \rangle = 2m_N a_f S^\alpha \quad (16.9.44)$$

where  $v_f, a_f$  are numbers (Lorentz scalars) that measure the strength of the vector and axial-vector matrix elements. As explained in Appendix 3, the numbers  $v_f$  are exactly known when the currents  $J_f^\alpha$  are conserved currents.

Substituting (16.9.40) and (16.9.41) into (16.9.38), and using (16.9.43) and (16.9.44), one finds

$$P^\alpha v_f = \sum_{\lambda} \int \frac{P_0}{\epsilon} n_f(\kappa, \lambda; \mathbf{S}) \kappa^\alpha d^3\kappa \quad (16.9.45)$$

and

$$m_N S^\alpha a_f = \sum_{\lambda} \int \frac{P_0}{\epsilon} n_f(\kappa, \lambda; \mathbf{S}) m_f s^\alpha(\lambda) d^3\kappa. \quad (16.9.46)$$

Now using (16.9.26) in (16.9.42), and taking

$$S^\alpha(\Lambda) = \frac{2\Lambda}{m_N} \left( P, 0, 0, -P - \frac{m_N^2}{2P} \right)$$

for a proton of helicity  $\Lambda = \pm \frac{1}{2}$  as follows from (15.6.2) and (16.9.2), we find eventually

$$v_f = \int_0^1 dx' [q_f^P(x') + q_f^A(x')] = \int_0^1 q_f(x) dx$$

and

$$a_f = \int_0^1 dx' [q_f^P(x') - q_f^A(x')] = \int_0^1 \Delta q_f(x) dx.$$

In the above we considered only quarks. A similar argument holds for antiquark constituents, where the partonic matrix elements are

$$\left. \begin{aligned} \langle \bar{\kappa}, \lambda | J_f^\alpha | \bar{\kappa}, \lambda \rangle &= -\bar{v}_\lambda \gamma^\alpha v_\lambda = -2\kappa^\alpha, \\ \langle \bar{\kappa}, \lambda | J_f^{5\alpha} | \bar{\kappa}, \lambda \rangle &= -\bar{v}_\lambda \gamma^\alpha \gamma^5 v_\lambda = 2m_f s^\alpha(\lambda), \end{aligned} \right\} \quad (16.9.47)$$

where we have used (1.3.11) in the last step.

Finally then one finds

$$v_f = \int_0^1 [q_f(x) - \bar{q}_f(x)] dx \quad (16.9.48)$$

$$a_f = \int_0^1 [\Delta q_f(x) + \Delta \bar{q}_f(x)] dx. \quad (16.9.49)$$

It is these relations together with the exact results for the hadronic matrix elements of conserved currents discussed in Appendix 3 that provide the real basis for the sum rules quoted in eqns (16.4.2) to (16.4.4).

Because charge, baryon number, isospin, strangeness, etc. are all conserved by the strong interactions, combinations of  $v_f$ s corresponding to these currents are exactly known.

Thus taking

$$\left. \begin{aligned} J_{\text{em}}^\alpha &= \sum_f Q_f \bar{\psi}_f \gamma^\alpha \psi_f, \\ J_{I_3}^\alpha &= \frac{1}{2} (\bar{\psi}_u \gamma^\alpha \psi_u - \bar{\psi}_d \gamma^\alpha \psi_d), \\ J_s^\alpha &= -\bar{\psi}_s \gamma^\alpha \psi_s, \end{aligned} \right\} \quad (16.9.50)$$

we have, for proton matrix elements,

$$\left. \begin{aligned} \sum_f Q_f v_f &= 1, \\ \frac{1}{2}(v_u - v_d) &= \frac{1}{2}, \\ v_s &= 0, \end{aligned} \right\} \quad (16.9.51)$$

and using (16.9.39) and (16.9.48) one finds respectively:

$$\left. \begin{aligned} 1 &= \int_0^1 dx [\frac{2}{3}(u - \bar{u}) - \frac{1}{3}(d - \bar{d} + s - \bar{s})], \\ \frac{1}{2} &= \frac{1}{2} \int_0^1 dx [u - \bar{u} - (d - \bar{d})], \\ 0 &= - \int_0^1 dx [s - \bar{s}], \end{aligned} \right\} \quad (16.9.52)$$

which lead directly to (16.4.2) to (16.4.4).

Also from (16.9.49), (16.9.44) and (16.8.15) we immediately obtain the result

$$\langle p, \frac{1}{2} | \mathcal{A}_\mu | p, \frac{1}{2} \rangle = 2m_N S_\mu \sum_j Q_j^2 [\Delta q_j + \Delta \bar{q}_j] \quad (16.9.53)$$

quoted in (16.8.16).

# 17

## Experimental tests of the quark–parton model

The quark–parton model was developed in great detail in the previous chapter. Here we discuss the experimental situation and confront the theory with the vast amount of data on deep inelastic scattering and related reactions. It must be borne in mind that we have not yet discussed the QCD corrections to the model. These are not small, but their *dominant* effect can be taken into account by allowing the parton number densities to depend upon  $Q^2$  in a way calculable in QCD, so that, fortuitously, the entire formalism is basically unchanged, except that each  $q_j(x) \rightarrow q_j(x, Q^2)$ . As mentioned earlier this implies a dynamical breaking of perfect Bjorken scaling. It also implies that if one is seeking accurate information about the  $q_j(x)$  from experiment then care must be taken to specify the  $Q^2$  involved.

*In this chapter we shall continue to write just  $q_j(x)$  but the above considerations should not be forgotten.*

We shall also look at some other reactions where the model provides a direct and successful description of the physics:  $e^+e^- \rightarrow$  hadrons, the Drell–Yan process  $h_A + h_B \rightarrow \ell^+\ell^-X$  and the hadronic production of heavy vector bosons.

### 17.1 Deep inelastic scaling functions for $Q^2 \ll M_Z^2$

In the previous chapter we expressed all the measurable scaling functions in terms of the quark distributions or number densities. Notice that there are many more experimental scaling functions than quark number densities  $u, d, s, \bar{u}, \bar{d}, \bar{s} = s$ , so that the predictive power is in principle very great.

It would be naive to imagine that all the relations can be tested experimentally. Electromagnetic deep inelastic scattering experiments are difficult enough, but that analogous experiments can be performed at all

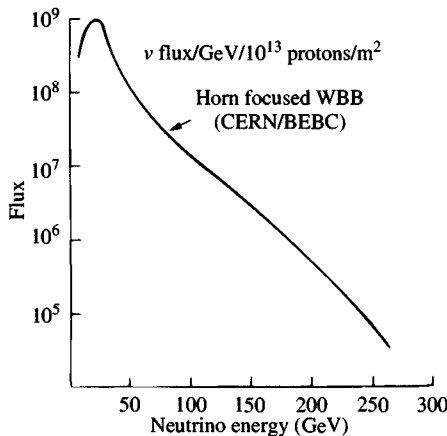


Fig. 17.1. Spectrum of a wide band neutrino beam. (From Dydak, 1978.)

with neutrinos is a technical miracle and it will be a long time before a rigorous check of *all* relationships is completed.

In an electromagnetic experiment the electron or muon beam is almost monochromatic and the energy  $E$  of the beam particles well known. The laboratory angle  $\theta$  and the energy  $E'$  of the scattered electron or muon can also be accurately determined, so that for each event  $(E, Q^2, \nu)$  or  $(E, x, y)$  are known, and detailed differential studies are possible, though the practical possibility of varying  $\theta$  significantly in a given experiment by altering the position of a huge spectrometer, is limited. This makes it particularly difficult to measure  $R$  (15.3.26) and therefore to separate  $F_1$  and  $F_2$  from the data.

High energy neutrino beams are never monochromatic. They are constructed as follows. A high intensity beam of protons strikes a heavy atom target and the resulting pions and kaons are focused and sent down a high vacuum ‘decay tunnel’. The neutrinos are produced by the decay in flight of fast  $\pi$ s and  $K$ s (via  $\pi \rightarrow \mu\nu$  and  $K \rightarrow \mu\nu$ ) in the decay tunnel. The muons and hadrons that do not decay have to be absorbed in a huge shield. There are two main types of beam. If the principal aim is intensity rather than energy resolution, one focuses as many  $\pi$ s and  $K$ s as possible, irrespective of their momenta, into the decay tunnel and there results a ‘wide band beam’ (WBB). An example of such a spectrum is shown in Fig. 17.1.

If good energy resolution is required the  $\pi$ s and  $K$ s are first momentum selected so that the neutrinos are being emitted by particles whose momentum is essentially known. This gives rise to a ‘narrow band beam’ (NBB). There is clearly a loss of intensity in this selection, but it now

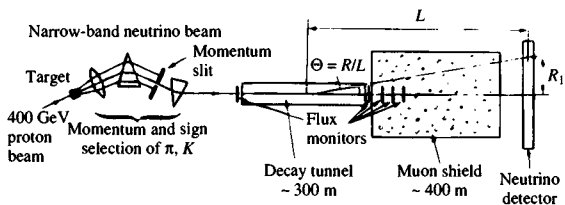


Fig. 17.2. Schematic layout of narrow band neutrino beam of the CDHS group at CERN. (From Dydak, 1978.)

proves possible to estimate the energy of the neutrino from a knowledge of its interaction point in the target (itself a huge ‘neutrino detector’), as we shall show. In the rest frame of its parent hadron the neutrino is emitted with a well-defined energy  $E_0$  and at a variable angle  $\Theta_0$  relative to the beam axis. The decay rate is isotropic, i.e. independent of  $\cos \Theta_0$ . Applying a Lorentz transformation, the laboratory energy  $E$  and laboratory angle  $\Theta$  of the neutrino are related by

$$E = \frac{E_0}{\gamma(1 - \beta \cos \Theta)}$$

where  $\gamma = E_{\text{parent}}/m_{\text{parent}}$  and  $\gamma\beta = \sqrt{\gamma^2 - 1}$ .

Thus from a knowledge of  $\Theta$  we can deduce  $E$ , but only up to a two-fold ambiguity since we don’t know whether its parent was a  $\pi$  or a  $K$ . The beam is thus ‘diachromatic’. Unfortunately, as shown in Fig. 17.2, there is an inherent uncertainty in deducing  $\Theta$  from the measurement of the interaction position  $R_I$ —one does not know where in the decay tunnel the neutrino was produced. The neutrino energy spectrum of the CERN-Dortmund-Heidelberg-Saclay (CDHS) narrow band beam at CERN is shown in Fig. 17.3.

The uncertainty in the neutrino energy makes it imperative in CC reactions to monitor not only the energy and angle of the outgoing muon or electron but also the total energy  $E_H$  carried away by the hadronic shower  $X$ , or, better still, its total momentum  $p_H$  as well. This can be done in a bubble chamber, but large corrections are necessary to allow for the undetected neutral particles; or using electronic detectors, which have the advantage that the target mass can be gargantuan, up to about 1000 tons, of great help in studying the very small cross-sections involved.

For NC reactions one cannot detect the final neutrino at all, so one has to rely entirely on the reconstruction of the hadron shower energy and direction, and of course on the point of interaction. In principle if  $E, E_H$  and  $p_H$  are known then  $(E, x, y)$  are fixed. Since

$$E_H = m_N + \nu = m_N + E y$$

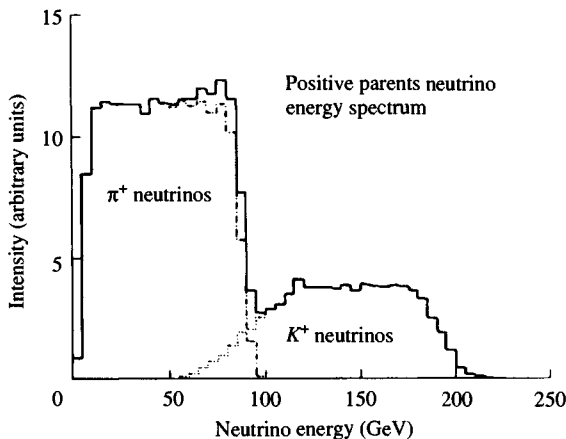


Fig. 17.3. Neutrino energy spectrum of the CDHS group's narrow band beam. (From de Groot *et al.*, 1979.)

a study of the distribution in  $E_H$  allows one to deduce the  $y$  dependence once the beam energy spectrum is known.

The avoidance of systematic errors in the study of  $y$  distributions is clearly very difficult for NC reactions. A very promising approach is to study directly the ratio of NC to CC events occurring in a given  $E_H$  bin and in the same radial distance ( $R_I$ ) bin. This has the effect of greatly reducing systematic errors and has been used successfully to determine the NC  $y$  distribution.

In the past few years there has been a significant improvement experimentally due to a better understanding of background events arising from neutrinos from unfocused parent particles and to a more accurate determination of the transverse position of the interaction.

As regards  $x$  distributions, even in electromagnetic and CC reactions, it is particularly hard to get reliable estimates of  $F_1(x)$  and  $F_3(x)$  for very small  $x$  because what is actually measured [see (15.5.6) and (15.5.7)] is  $xF_1(x)$  and  $xF_3(x)$ , and dividing a measured quantity by  $x$ , for  $x \approx 0$ , leads to large uncertainties.

For this reason some papers prefer to deal only with the quantities  $xq_j(x)$  rather than the distributions  $q_j(x)$ . This is of course perfectly reasonable, but the reader is warned that some of these papers thoughtlessly use the notation  $q_j(x)$  to stand for  $xq_j(x)$ !

In order to compare the parton model predictions with experiment we must be aware that data presented for  $F_1$  or  $F_2$  have often involved an

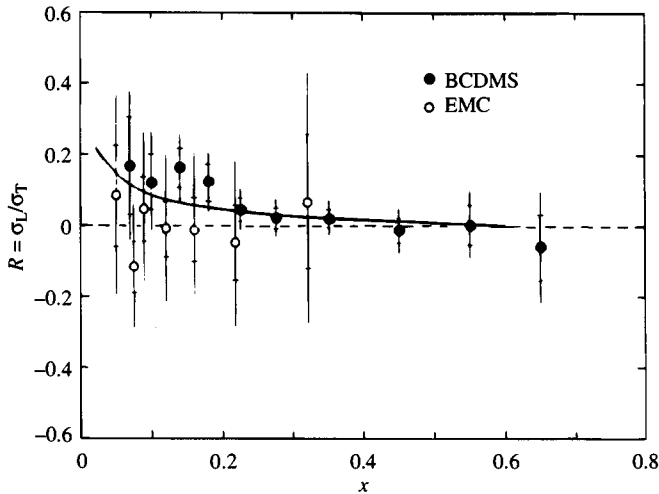


Fig. 17.4. Data on  $R$  from BCDMS and EMC groups. Curve is QCD prediction (see Section 23.8).

assumption as to the value of  $R$  (15.3.26) in analysing the data. Thus many papers dealing with large  $Q^2$  data take  $R = 0$ , which corresponds to assuming the validity of  $F_2(x) = 2xF_1(x)$ . Others use a value of  $R$  calculated from a QCD formula. The latter is preferable since a high statistics measurement of  $R$  in muon-proton scattering (BCDMS, 1989) seems to be in reasonable agreement with a QCD calculation [see eqn. (23.8.13)], as regards its  $x$  dependence [in contrast to the naive result (16.1.9)!]. This is shown in Fig. 17.4 where the EMC data (EMC, 1985) are also indicated. But it should be noted that even here it was assumed that  $R$  did not vary with  $Q^2$  for the range of the experiment, i.e.  $7 \leq Q^2 \leq 260$  (GeV) $^2$ . Nonetheless it seems clear that  $R$  is generally *very* small except for  $x \leq 0.2$  where it is non-zero but still not large, at least down to  $x \approx 0.1$ .

Some effort has been made to test the relation  $F_2(x) = 2xF_1(x)$  in  $\nu$  and  $\bar{\nu}$  CC reactions by looking at the  $y$  distributions using (16.1.19). The data are compatible with  $A(x) = 1$ , i.e. with the validity of  $F_2(x) = 2xF_1(x)$ , but the experimental constraints on the value of  $A(x)$  are rather poor. From the  $y$  distributions alone, i.e. (16.1.19) integrated over  $x$ , one has the result

$$A \equiv \frac{\int_0^1 2xF_1(x)dx}{\int_0^1 F_2(x)dx} = 1.02 \pm 0.12. \quad (17.1.1)$$

### 17.1.1 Sum rules and their experimental tests

Let us now look at some of the relations amongst the scaling functions in the quark–parton model. We shall see that where these have been tested the results are, with one exception at present, generally in agreement with the predictions.

There is a set of sum rules, based upon the relations (16.4.2–4), which involve integrating the scaling functions over the region  $0 \leq x \leq 1$ . The presence of production thresholds in the formulae for the  $F_i(x, Q^2)$  complicates the results at finite  $Q^2$ ; in addition there are sometimes QCD corrections. It is only in the limit  $Q^2 \rightarrow \infty$  that truly simple results emerge. And since we now believe the top quark to be very massive,  $Q^2 \rightarrow \infty$  means  $Q^2 \gg m_t^2$ !

Firstly, because (16.4.36) involves only valence contributions, we obtain via (16.4.28)

$$\lim_{Q^2 \rightarrow \infty} \int_0^1 \frac{dx}{x} [F_2^{W^-p}(x, Q^2) - F_2^{W^+p}(x, Q^2)] = 2 \quad (17.1.2)$$

where we have allowed for a transition  $d \rightarrow t$  not included in (16.4.36) and have used the unitarity of the KM matrix.

Analogously

$$\lim_{Q^2 \rightarrow \infty} \int_0^1 \frac{dx}{x} [F_2^{W^-n}(x, Q^2) - F_2^{W^+n}(x, Q^2)] = -2. \quad (17.1.3)$$

These results were originally derived by Adler, prior to the invention of the parton model.

At finite  $Q^2$  the result is not simple. But because of the dominance of  $|V_{ud}|^2$  the full expression in (16.4.36) will lead to a result differing from (17.1.2) and (17.1.3) by at most a few per cent. There are no QCD corrections. The Adler sum rule has been tested by the WA25 Group (WA25, 1985) and is in agreement with the data for  $1 < Q^2 < 40$  (GeV/c)<sup>2</sup>.

Similar arguments apply to (16.4.37) from which we obtain

$$\lim_{Q^2 \rightarrow \infty} \frac{1}{2} \int_0^1 dx [F_3^{W^+p}(x, Q^2) + F_3^{W^-p}(x, Q^2)] = 3 \quad (17.1.4)$$

and

$$\lim_{Q^2 \rightarrow \infty} \frac{1}{2} \int_0^1 dx [F_3^{W^+n}(x, Q^2) + F_3^{W^-n}(x, Q^2)] = 3. \quad (17.1.5)$$

Again at finite  $Q^2$  the results should differ from (17.1.4,5) by at most a few per cent. The sum rules (17.1.4,5) were due to Gross and Llewellyn-Smith. An average of early experiments (Sciulli, 1986) using iron targets, i.e. essentially equal numbers of n and p, yielded a value of  $2.81 \pm 0.16$ . In

this case there is a significant QCD correction, and the RHS of (17.1.4,5) should be altered to

$$3[1 - \alpha_s(Q^2)/\pi]. \quad (17.1.6)$$

The mean  $Q^2$  is about  $3(\text{GeV}/c)^2$  so that  $\alpha_s(Q^2) \approx 0.2$  and the QCD correction is about 6% in the right direction, yielding good agreement with the experimental value.

Recently, however, a much more accurate determination has come from the CCFR Collaboration (CCFR, 1990a) also using an iron target. They obtain  $2.66 \pm 0.03 \pm 0.08$ . The discrepancy (10%) is too large to attribute to the QCD correction. Moreover use of the more accurate expression (16.4.37) with allowance for finite  $Q^2$  effects will only reduce the RHS of (17.1.4,5) by about 1%. Thus theory and experiment are barely compatible and further data will be of great interest.

The Gottfried sum rule already mentioned in (16.3.4) is not immediately evident from our scaling function formulae (16.4.9,12). We have

$$\frac{1}{x} [F_2^{\gamma p}(x) - F_2^{\gamma n}(x)] = \frac{1}{3} [u(x) + \bar{u}(x) - d(x) - \bar{d}(x)], \quad (17.1.7)$$

but we can rewrite this as

$$\frac{1}{x} [F_2^{\gamma p}(x) - F_2^{\gamma n}(x)] = \frac{1}{3} [u(x) - \bar{u}(x) - d(x) + \bar{d}(x) + 2\bar{u}(x) - 2\bar{d}(x)],$$

so that, using (16.4.2,3)

$$\int_0^1 \frac{dx}{x} [F_2^{\gamma p}(x) - F_2^{\gamma n}(x)] = \frac{1}{3} + \frac{2}{3} \int_0^1 dx [\bar{u}(x) - \bar{d}(x)]. \quad (17.1.8)$$

If the sea is isotopically neutral,  $\bar{u}(x) = \bar{d}(x)$  and we recover (16.3.4).

Early tests of this sum rule were compatible with the value  $\frac{1}{3}$ , but recent data seem to be giving results on the low side. However there is some ambiguity coming from the form of the extrapolation to  $x = 0$ . When this is included one has the values

$$\left. \begin{array}{l} 0.235^{+0.110}_{-0.099} \text{ from EMC (1987),} \\ 0.197 \pm 0.036 + (0.07 \text{ to } 0.22) \text{ from BCDMS (1990).} \end{array} \right\} \quad (17.1.9)$$

The most recent study of this question (NMC, 1990) reaches the smallest values of  $x$  thus far:  $x = 0.004$ . The results, at two values of  $Q^2$ , are:

$$\begin{aligned} Q^2 = 4 (\text{GeV}/c)^2 : & 0.230 \pm 0.013 \pm 0.027 + (0.012 \text{ to } 0.040), \\ Q^2 = 15 (\text{GeV}/c)^2 : & 0.219 \pm 0.008 \pm 0.021 + (0.010 \text{ to } 0.020). \end{aligned} \quad (17.1.10)$$

These remarkably precise values are significantly different from  $\frac{1}{3}$  and have led to the suggestion that the sum rule is not satisfied. There are

no large QCD corrections to (16.3.4) or (17.1.8). An obvious explanation is that the sea is not isotopically neutral, so that  $\bar{u}(x) \neq \bar{d}(x)$ . There is nothing unreasonable about this. Any mechanism for the production of  $q\bar{q}$  pairs will lead to different densities of  $\bar{u}$  and  $\bar{d}$  since the pairs are produced in an environment which is not symmetric with respect to  $u$  and  $d$ , e.g. in the proton production of  $(u\bar{u})$  will be different from  $(d\bar{d})$  in the  $(uud)$  environment; at the very least due to Pauli exclusion principle effects.

In Section 16.6 we argued that as  $x \rightarrow 0$  we must have  $\bar{u}(x) = \bar{d}(x)$ ; and this is sufficient to explain the en vs ep data discussed in Section 16.4 which indicated that  $u(x) + \bar{u}(x) \approx d(x) + \bar{d}(x)$  at small  $x$ , so away from this region they could differ. But what is perhaps puzzling is the large size of the effect in the Gottfried sum rule.

Finally, one might be left a little uneasy by the knowledge that the neutron data are extracted from scattering on deuterium. But the deuteron is a loosely bound system, so that one might have expected very little effect from the binding at large  $Q^2$ . Nonetheless it turns out that there are several nuclear effects, for example the enhanced probability of the ' $\gamma$ ' interacting with a virtual pion, shadowing, parton recombination etc., which, although their effect is small in  $F_2^D$ , are important when studying the small difference  $2F_2^P - 2F_2^D$ , the latter being the observable that is interpreted as  $F_2^P - F_2^n$ . (See Epele *et al.*, 1994. Note that  $F_2^D$  is usually defined *per nucleon*.) In any event we shall refrain from putting  $\bar{u}(x) = \bar{d}(x)$  in the following.

An interesting relation due to Llewellyn-Smith connects electromagnetic and CC reactions. In the approximation (16.4.33,34)

$$F_3^{W^-p} - F_3^{W^+p} \approx 2[u(x) + \bar{u}(x) - d(x) - \bar{d}(x)] \quad (17.1.11)$$

so that via (16.4.9,12)

$$F_3^{W^-p}(x) - F_3^{W^+p}(x) \approx \frac{6}{x} \left\{ F_2^{\gamma p}(x) - F_2^{\gamma n}(x) \right\}. \quad (17.1.12)$$

As far as we are aware this relation has not been tested yet.

Finally we consider a relation between the electromagnetic and approximate CC scaling functions which yields further information about the sea. We have from (16.4.33)

$$F_2^{W^+p} + F_2^{W^+n} \approx 2x[u(x) + d(x) + \bar{u}(x) + \bar{d}(x)] \quad (17.1.13)$$

and from (16.4.9, 12), neglecting  $s(x)$ ,

$$F_2^{\gamma p} + F_2^{\gamma n} = 2x \frac{5}{18} [u(x) + d(x) + \bar{u}(x) + \bar{d}(x)] \quad (17.1.14)$$

$$\approx \frac{5}{18} \left\{ F_2^{W^+p}(x) + F_2^{W^+n}(x) \right\}. \quad (17.1.15)$$

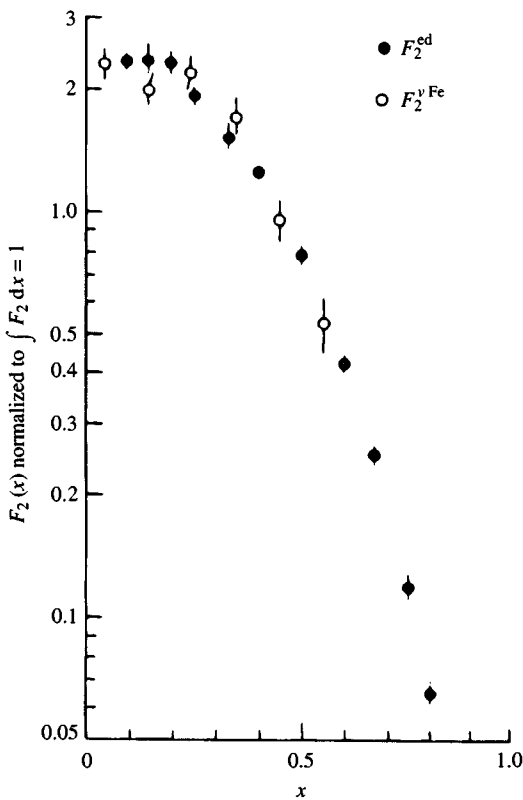


Fig. 17.5. Comparison of electromagnetic and neutrino structure functions for various  $x$  values. (From de Groot *et al.*, 1979.)

For an isoscalar target  $N_0$  we thus have

$$F_2^{\gamma N_0}(x) \approx \frac{5}{18} F_2^{W^+ N_0}(x). \quad (17.1.16)$$

In Fig. 17.5 we compare  $F_2(x)$  obtained from SLAC electron-deuteron data and from CERN neutrino-iron data. The neutrino energy range is  $20 \text{ GeV} < E_\nu < 30 \text{ GeV}$  and the range of  $Q^2$  is similar for both reactions. The data have been scaled so as to make  $\int F_2(x) dx = 1$  in both. Clearly the dependence on  $x$  is very similar for the two reactions.

Note that despite the fact that  $F_2(x)$  depends on parton distribution functions in the form  $xq(x)$  there is no doubt that  $F_2(x) \not\rightarrow 0$  as  $x \rightarrow 0$ . The implication that, as  $x \rightarrow 0$ ,

$$q(x) \propto \frac{1}{x} \quad (17.1.17)$$

was discussed in Section 16.6.

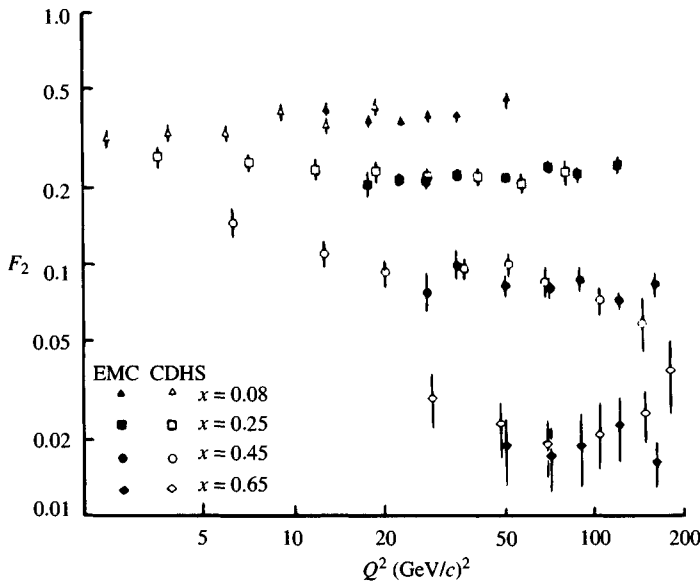


Fig. 17.6. Comparison of high energy data for  $\mu\text{Fe} \rightarrow \mu\text{X}$  and  $\nu_\mu\text{Fe} \rightarrow \mu^-\text{X}$ . The neutrino data has been multiplied by  $\frac{5}{18}$  (see text). (From Gabathuler, 1979.)

Fig. 17.6 compares early data on  $F_2(x)$  from the EMC and CDHS groups at CERN as obtained from  $\mu\text{Fe} \rightarrow \mu'\text{X}$  and  $\nu_\mu\text{Fe} \rightarrow \mu^-\text{X}$  respectively. The neutrino data has been multiplied by  $\frac{5}{18}$ . The agreement is remarkable! The good agreement with the data confirms that  $s(x)$  is relatively small, even at low values of  $x$ . A quantitative estimate of the strange sea is given in the next section.

### 17.1.2 Polarized scattering sum rule and the ‘spin crisis’

The EMC measurement of the asymmetry in polarized deep inelastic  $\mu\text{p}$  scattering was discussed in Section 15.6 and the measured  $A_1(x)$  shown in Fig. 15.12. We shall show now that this result has some rather unexpected implications which caused much excitement and led to interesting theoretical developments.

If in (15.6.34) we neglect the term involving  $g_2(x)$ , since it is multiplied by a small coefficient, and if we feed in the very accurately measured  $F_1(x)$  we can extract the scaling function  $g_1(x)$ . The result is shown in Fig. 17.7 where also earlier SLAC data are included.

From this one finds, from the EMC data, for the first moment,

$$\Gamma_p \equiv \int_0^1 g_1^p(x) dx = 0.126 \pm 0.010 \pm 0.015. \quad (17.1.18)$$

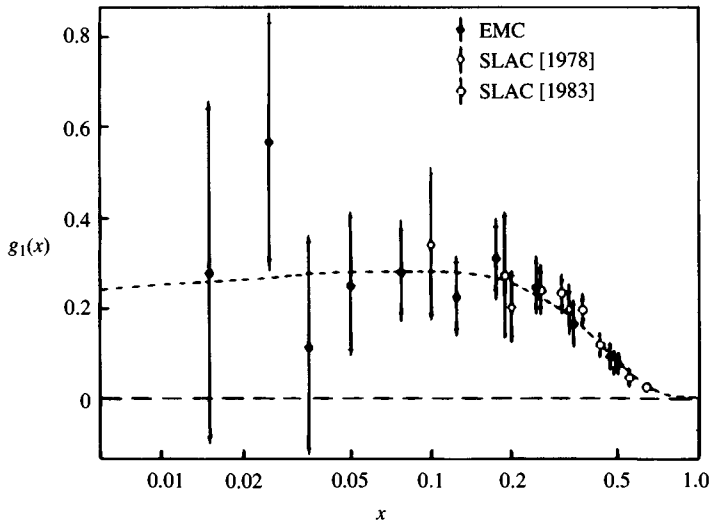


Fig. 17.7. EMC and SLAC data on the scaling function  $g_1(x)$ . Note the logarithmic  $x$  scale.

For flavours  $f = u, d, s$  let us define

$$\Delta_f = \int_0^1 [\Delta q_f(x) + \Delta \bar{q}_f(x)] dx \quad (17.1.19)$$

Then using the quark-parton model expression (16.8.21) for  $g_1^p(x)$ , (17.1.18) implies

$$\frac{2}{9}\Delta_u + \frac{1}{18}(\Delta_d + \Delta_s) = 0.126 \pm 0.010 \pm 0.015. \quad (17.1.20)$$

The Bjorken sum rule (16.8.20) yields

$$\Delta_u - \Delta_d = G_A/G_V = 1.254 \pm 0.006. \quad (17.1.21)$$

In order to solve for the individual  $\Delta_f$  we need one more relation. This can be obtained from a study of hyperon  $\beta$ -decays, the data for which seem to be in good agreement with  $SU(3)_F$  invariance. If  $SU(3)_F$  invariance holds, all decay amplitudes are expressed in the form [see (18.1.2) and (18.1.16)]

$$(KM \text{ matrix element } V_{fi}) \times (\text{hadronic matrix element of } V^\mu + A^\mu) \quad (17.1.22)$$

where  $V^\mu$  and  $A^\mu$  are linear combinations of the octets of vector currents  $V_j^\mu$  and axial-vector currents  $A_j^\mu$ . The matrix elements of the latter are all expressed in terms of just two unknown constants usually labelled  $F$  and  $D$  (as explained in Appendix 3) which thus measure the contribution of the axial-vector part of the hadronic current relative to the vector part.

For example in  $n \rightarrow p + e^- + \bar{\nu}_e$ , comparing with (1.2.6) one finds

$$G_A/G_V = F + D \quad (17.1.23)$$

[For details of  $SU(3)_F$  assignments needed to evaluate the matrix elements, see Bailin (1982) Chapter 4. Note that the convention for the signs of  $F, D$  used in experimental papers, and which we are following, is opposite to that of Bailin.]

The analysis of the hyperon decays yields

$$0.61 \leq F/D \leq 0.64. \quad (17.1.24)$$

Now consider the eighth quark axial-vector current

$$\bar{\psi} \left( \frac{\lambda^8}{2} \right) \gamma^\mu \gamma_5 \psi = \frac{1}{2\sqrt{3}} \left\{ J_u^{5\mu} + J_d^{5\mu} - 2J_s^{5\mu} \right\}. \quad (17.1.25)$$

Its protonic matrix elements, via (16.9.45), (16.9.49) and (17.1.19) can be expressed in terms of  $\frac{1}{2\sqrt{3}}[\Delta_u + \Delta_d - 2\Delta_s]$ . Comparison with the  $SU(3)_F$  decomposition eventually leads to

$$\Delta_u + \Delta_d - 2\Delta_s = 3F - D = 0.68 \pm 0.08. \quad (17.1.26)$$

We are now able to solve for the individual  $\Delta_f$  to get:

$$\left. \begin{aligned} \Delta_u &= 0.74 \pm 0.08, \\ \Delta_d &= -0.51 \pm 0.08, \\ \Delta_s &= -0.23 \pm 0.08. \end{aligned} \right\} \quad (17.1.27)$$

There are two surprises. Firstly the size of  $\Delta_s$ . Intuitively, since strange quarks are part of the sea in a proton, one might have expected the  $s, \bar{s}$  to be more or less unpolarized. The large value of  $\Delta_s$  was unexpected. Secondly, the sum

$$\Delta_u + \Delta_d + \Delta_s = 0.00 \pm 0.24 \quad (17.1.28)$$

is consistent with zero, whereas in the simple parton model it ought to equal unity, as we shall now argue. [Note that inclusion of the SLAC data changes the above values slightly. Also there are QCD corrections to (17.1.1) but these too have only a small effect on the quoted values (see Leader and Anselmino, 1988).]

Consider a proton moving along  $OZ$  with helicity  $+\frac{1}{2}$ . It has  $J_Z = \frac{1}{2}$ . If a constituent with position vector  $\mathbf{r}$  relative to the CM of the proton is moving with momentum  $x\mathbf{P}$ , i.e. also along  $OZ$ , as is usually assumed in the simple parton model, then since  $\mathbf{L} = \mathbf{r} \times x\mathbf{P}$  has no component along  $OZ$ , its total  $z$ -component of angular momentum is just its helicity. Thus we expect to have

$$J_Z = \frac{1}{2} = \sum_j \int_0^1 dx \left[ \left( \frac{1}{2} \right) f_j^P(x) + \left( -\frac{1}{2} \right) f_j^A(x) \right] \quad (17.1.29)$$

which upon using (16.8.10) becomes

$$\int_0^1 dx [\Delta u(x) + \Delta d(x) + \Delta s(x) + \Delta \bar{u}(x) + \Delta \bar{d}(x) + \Delta \bar{s}(x)] = 1$$

or

$$\Delta_u + \Delta_d + \Delta_s = 1 \quad (17.1.30)$$

in contradiction with (17.1.28).

However there are two reasons why this result should not be taken literally.

1. We have already seen that gluons carry a large proportion of the linear momentum of the nucleon. They could equally well contribute significantly to the angular momentum.
2. As discussed in the Appendix to Chapter 16 we should allow the quarks to have some intrinsic transverse momentum inside the nucleon. In particular putting for the quark momentum

$$\kappa = (\kappa_T, xP)$$

estimates indicate (see Section 17.4.2) that  $\langle \kappa_T^2 \rangle$  could be as large as  $0.6 \text{ (GeV}/c)^2$ . Then the quark transverse motion will contribute

$$|L_Z| = |(\mathbf{r} \times \boldsymbol{\kappa})_Z| = r_T \kappa_T$$

where  $r_T$  is a measure of the transverse size of the nucleon, say 1 fm. So the contribution to  $L_Z$  from a given constituent could be of order  $800 \text{ MeV}f/c \approx 4\hbar$ ! Of course upon summing over constituents or integrating  $\kappa_T$  the result might average to zero, but it is important to appreciate that with such an intrinsic  $\kappa_T$  one can easily build up significant angular momentum, on the scale of  $\hbar$ .

In summary (17.1.30) should be replaced by the correct *angular momentum sum rule*

$$\langle S_Z \rangle_{\text{quarks}} + \langle S_Z \rangle_{\text{gluons}} + \langle L_Z \rangle = \frac{1}{2} \quad (17.1.31)$$

where

$$\langle S_Z \rangle_{\text{quarks}} = \frac{1}{2}(\Delta_u + \Delta_d + \Delta_s). \quad (17.1.32)$$

The above clearly indicates that the failure of (17.1.30), which was referred to as the ‘spin crisis’, is not really in fundamental contradiction with anything. But it is a little disconcerting to discover that the proton spin is almost entirely orbital or gluonic, especially if we recall that static models of the hadrons in their ground state have the quarks in relative  $\ell = 0$  *s*-states, have no gluons and have the hadron spin built entirely

from the quark spins! However, one can equally argue that it is quite misleading to equate *constituent quarks* with *partonic quarks*.

Although the subject is too technical to discuss in detail, we simply note that the analogue of the evolution equations of Sections 22.2 and 23.4 for the polarized parton number densities implies that the polarized gluon density  $\Delta G(x, Q^2)$  must grow with  $Q^2$ . So perhaps a large gluonic contribution to (17.1.31) is not as odd as it seems at first sight.

### 17.1.3 The nuclear EMC effect

Nothing in the developments that led to the formulae of Chapters 15–16 limited their application to specific targets. Thus, the same formalism applies where the target is not a hadron but a nucleus. What came as a great surprise, therefore, was the discovery of new effects that one encounters when dealing with such a case. The first presentation of the EMC effect came at the 1982 High Energy Physics Conference in Paris and the data (EMC, 1983) were published soon after. There are at least two reasons why it attracted so much attention. On the one hand, it made quite obvious that a nucleus with atomic weight  $A$  is not just a collection of  $A$  nucleons (actually not a novelty to nuclear physicists); on the other hand, it gave the first direct glimpse of internal (quark) degrees of freedom at work in nuclei.

At the above conference, the pessimistic statement was made that ‘we can hardly think of any mechanism which could produce such an effect’. One year later there were 120 theoretical papers purporting to explain the effect. Ten years (and several thousand papers) later, the main impact has probably been to arouse the interest of particle physicists in nuclear physics and of nuclear experts in particle physics.

Concisely, what has come to be known as the EMC effect is simply the statement that nucleons bound in nuclear matter behave differently from free nucleons in deep inelastic scattering. More precisely, the nucleon scaling functions appear to have a different  $x$  dependence when measured for free nucleons or for nucleons bound in nuclei. The deviation of the nuclear scaling functions from the free nucleon case increases with the atomic number  $A$  while remaining qualitatively similar for all nuclei. A broad variety of theoretical explanations have been offered ranging from QCD mechanisms to conventional nuclear physics phenomena. Now, the dust is slowly settling, and it appears possible to take stock of the situation.

On the experimental side, the issue raised by the SLAC data of 1984 which challenged the EMC findings at small  $x$  has been largely settled by the results presented to the 1986 Berkeley conference by the EMC and by the BCDMS collaborations. These dedicated experiments (Norton, 1986; Voss, 1986) have shown that the truth lies in between the original EMC

points and the SLAC data but somewhat closer to the latter. This is in line with what had already been suggested by the BCDMS collaboration some time earlier (BCDMS, 1985). The low  $x$  EMC data fall very close to the lower limit of the 7% systematic uncertainty already quoted in the original paper (EMC, 1983). The latest data raise still other problems in the very small  $x$  domain ( $x \leq 0.05$ –0.1) where the experimental analysis is the hardest to perform and the theoretical investigation the most subject to many complications.

On the theoretical side, an overabundance of mechanisms has been advocated to explain the data and this makes the whole matter somewhat inconclusive. The present prevailing theoretical attitude can be summarized by saying that in the very small  $x$  region ( $x \leq 0.1$ ) a number of non-perturbative effects (shadowing, sea quarks and gluons) dominate; in the intermediate  $x$  domain ( $0.2 \leq x \leq 0.8$ ), the EMC effect can reasonably well be attributed to a combination of nuclear binding and Fermi motion in a nuclear physics approach, and/or, in a parton–QCD approach, to a partial quark deconfinement within the hadronic boundary which affects the basic properties of the hadrons. A nucleon bound in a nucleus appears somewhat larger and somewhat less massive than a free nucleon.

For a detailed review see Barone and Predazzi (1987) and Sloan *et al.* (1988) where complete references can be found.

The details of the mechanisms suggested by the various authors vary considerably, from an excess of pions or  $\Delta$ -isobars to assuming the existence of multi-nucleon bags within the nucleus, from scaling (either in  $Q^2$  or in  $x$ ) properties to introducing multi-partonic clusters, from empirical models where one gives the bound nucleon effective properties quite different from those of free nucleons to standard nuclear binding, from kinematical to relativistic effects, from evidence of diquarks to phase transitions and so on. The trouble is that often these various mechanisms overlap in their effects and that different mechanisms may be at work in different  $x$  regions.

The qualitative trend abstracted from the data is summarized in Fig. 17.8 where the ratio

$$\rho_A(x, Q^2) = F_2^A(x, Q^2)/F_2^N(x, Q^2). \quad (17.1.33)$$

is shown. Compilations of the most recent data (Arneodo, 1994) for light nuclei and for heavy nuclei are shown in Fig. 17.9 and 17.10 respectively. We shall confine ourselves to a few critical points.

(a) *Shadowing* Especially for heavy nuclei, the very low  $x$  region is dominated by shadowing, i.e. by the fact that the cross-section of a nuclear process is experimentally smaller than  $A$  times the cross-section

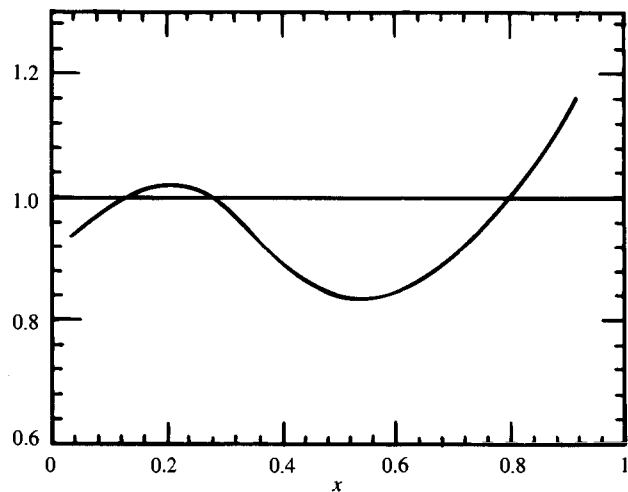


Fig. 17.8. The qualitative behaviour of  $\rho_A(x)$  defined in (17.1.33).

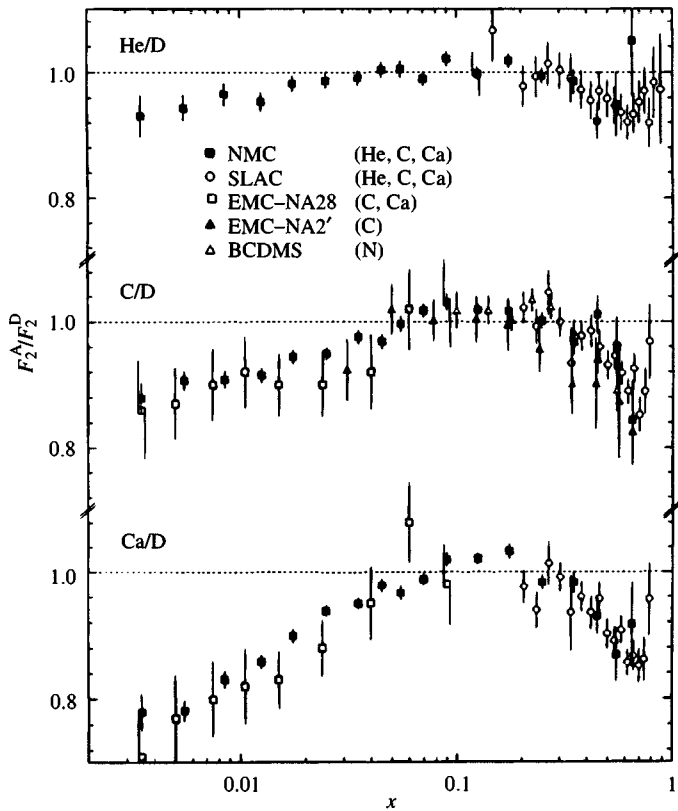


Fig. 17.9. Experimental data on  $\rho_A(x)$  for light nuclei.

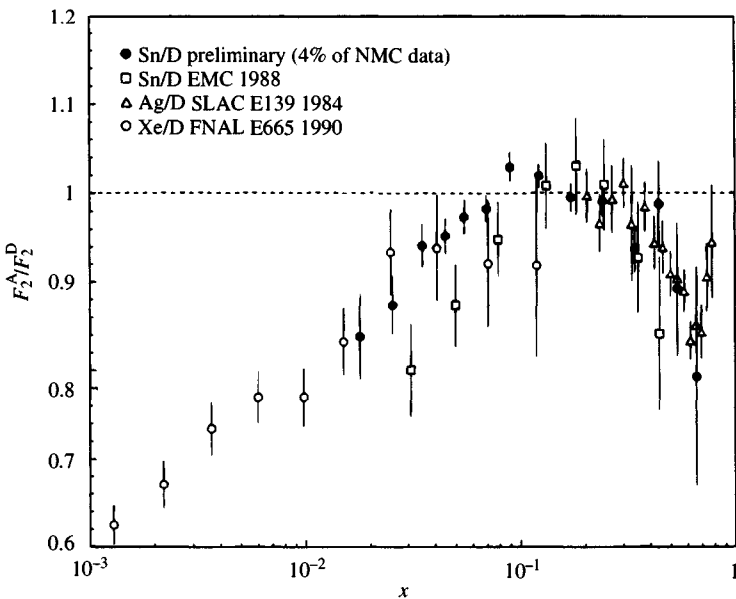


Fig. 17.10. Experimental data on  $\rho_A(x)$  for heavy nuclei.

for a single nucleon. Shadowing in pseudo-elastic reactions was anticipated on theoretical grounds by the vector meson dominance model (VDM) (Stodolski, 1967) and found experimentally in photoproduction experiments. The main motivation and ideas are very simple; things become much more complicated when one probes deeper into the subject (see Covolan and Predazzi, 1991, and Nikolaev and Zakharov, 1991).

The term *shadowing*, adopted from optical terminology, refers to the situation wherein the inner constituents of a composite target are screened from the impinging probe by the outer constituents. Implicit in this picture is the idea that the inner constituents will become more and more visible to the probe the more penetrating the latter is. With virtual photons, this is expected to occur with increasing  $Q^2$ , as will be explained presently. A nucleus, from the point of view of the photon has a two-fold structure. It is an ensemble of nucleons which are themselves made of partons. Complications arise. For example, it was anticipated long ago (Nikolaev and Zakharov, 1975) that a mechanism of fusion of partons from different nucleons within the nucleus could lead to a persistence of shadowing even at large  $Q^2$ : the effect of shadowing on each parton decreases with  $Q^2$ , but the number of soft partons increases sharply with  $Q^2$ . This could not be tested until quite recently, and the data of Fig. 17.10 do seem to support such a conclusion. (As already mentioned, the *very* low  $x$  domain is still rather poorly understood.)

The VMD picture which anticipated the experimental finding of shadowing is very simple: real photons have a hadronic cross-section of  $\sim 150 \mu\text{b}$  corresponding to a mean free path in nuclear matter of about 500 fm, i.e. much larger than any nuclear radius. As a consequence, all the nucleons in a nucleus, even the innermost ones and those at the back of the nucleus, should, in principle, have the same probability of interacting with the incoming photon. The nuclear cross-section, in this case, should be the sum of all individual single nuclear cross-sections. As it turns out, the experiments show that the nuclear cross-sections are much smaller than  $A$  times the nucleon cross-section. The VMD mechanism explains this by postulating that vector mesons (like  $\rho, \omega, \phi$  etc.) ‘mediate’ the photon–hadron interaction. The physical photon is visualized as a superposition of a bare photon and of a hadronic component made up of states with the same quantum numbers as the photon, i.e. vector mesons.

The VMD is then generalized to include contributions from heavy vector meson resonances, as well as from the continuum (as evidenced in  $e^+e^-$  scattering). In this picture, shadowing results from the interplay of three characteristic lengths:

1. the *coherence length*, i.e. the distance which the physical photon travels in its hadronic mode. From the uncertainty principle, in the rest frame of the target nucleus, this distance is

$$d \sim \frac{1}{\Delta E} \simeq \frac{2\nu}{Q^2 + m_v^2} \quad (17.1.34)$$

( $\Delta E$  is the difference between the vector meson energy  $[\nu^2 + m_v^2 + Q^2]^{1/2}$  and the photon energy  $\nu$  which is assumed to be large);

2. the *mean free path*, i.e. the mean distance travelled by the hadronic state without being absorbed by the nuclear medium. As an order of magnitude

$$\lambda \simeq \frac{1}{n\sigma_{vN}} \quad (17.1.35)$$

where  $n$  is the nuclear density and  $\sigma_{vN}$  the vector meson–nucleon cross-section;

3. the *nuclear radius*

$$R_A = r_0 A^{1/3} \quad \text{with } r_0 \sim 1.12 \text{ fm.} \quad (17.1.36)$$

The necessary conditions for shadowing to take place are then

$$\lambda \leq d \quad (17.1.37)$$

and

$$\lambda \leq R. \quad (17.1.38)$$

While condition (17.1.38) is essentially geometrical, condition (17.1.37) is most easily satisfied as  $\nu$  increases, or rather the larger  $\nu$  is compared with  $Q^2$ . This is why shadowing is relevant in the deep inelastic regime at small  $x$ . From the arguments given above, shadowing would be expected to disappear as  $Q^2$  increases relative to  $\nu$ . As already mentioned, arguments based on parton fusion alter this conclusion. Present data (Fig. 17.10) seem to support the latter argument.

(b) *Antishadowing* Also important is the prediction (Nikolaev and Zakharov, 1975) of *antishadowing* on the basis of the momentum conservation sum rule

$$\int_0^1 F_2^A(x, Q^2) dx = Z \int_0^1 F_2^p(x, Q^2) dx + (A - Z) \int_0^1 F_2^n(x, Q^2) dx \quad (17.1.39)$$

where A, p, n refer to the nucleus, protons and neutrons respectively.

Antishadowing (somewhat of a misnomer since it has nothing to do with the geometric concept of shadowing) denotes the enhancement that must occur at larger  $x$  to compensate for the shadowing depletion that occurs towards  $x = 0$  if (17.1.39) is to hold (see Figs. 17.10).

Experimentally, the case of antishadowing is not so clear cut (see Figs. 17.9 and 17.10).

(c) *Fermi motion* The large  $x$  behaviour of  $\rho_A(x)$  is quite well understood in terms of the nuclear Fermi motion. This is a well-known effect in nuclear physics and, basically, takes into account that the nucleons are moving inside a nucleus and thus have a spread of possible momenta. In the limiting case one nucleon could possibly carry all the momentum of the nucleus! The Bjorken variable, even for a nuclear target, is still defined by  $x = Q^2/2m_N\nu$ . If we consider  $x_A = Q^2/2M_A\nu$  where  $M_A$  is the mass of the nucleus, then we should have  $0 \leq x_A \leq 1$ . It follows that the permitted range for  $x$  is

$$0 \leq x \leq \frac{M_A}{m_N} \sim A. \quad (17.1.40)$$

The basic formula to take Fermi motion into account can be derived along lines very similar to those followed in the appendix to Chapter 16 [see eqn (16.9.19)]. The difference, of course, is that now  $\mathcal{P}$  represents the momentum distribution of a nucleon in the nucleus. The following convolution formula emerges either using the techniques of the operator product expansion, or more simply, by considering the kinematics of Fig. 17.11 which shows a nucleus of atomic number  $A$  in a reference frame in which it is moving very fast with momentum  $P$  along  $OZ$ . A nucleon  $i$  inside the nucleus has  $z$ -component of momentum  $p_z = zP/A$  and a parton,

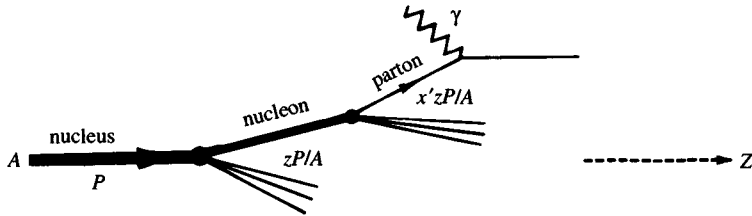


Fig. 17.11. Kinematics for interaction of a photon with a parton emanating from a nucleon which is in motion inside a nucleus.

with momentum fraction  $x'$  inside the nucleon, interacts with the photon. Analogous to the arguments leading to (16.1.4) one finds

$$F_2^A(x, Q^2) = \int_x^A dz \phi_{i/A}(z) F_2^i\left(\frac{x}{z}, Q^2\right) \quad (17.1.41)$$

where  $F_2^A$  is the scaling function of the nucleus and  $F_2^i$  that of nucleon  $i$  (in fact, the same convolution will result no matter what sort of nuclear constituent  $i$  is, i.e. a nucleon, a multi-nuclear bag, a cluster of partons or any other kind of constituent). In the simplest picture  $\phi_{i/A}(z)$  is related to the momentum space wave function  $\phi_{i/A}(\vec{p})$  of  $i$  in  $A$  via

$$\phi_{i/A}(z) = \int d^3p |\phi_{i/A}(\vec{p})|^2 \delta(z - Ap_z/P). \quad (17.1.42)$$

The normalization of the probability amplitude for an individual nucleon gives (baryon number conservation)

$$\int_0^A \phi_{i/A}(z) dz = 1. \quad (17.1.43)$$

Because the nuclear scaling function does not vanish at  $x = 1$  [see (17.1.40)] while the free nucleon scaling function does, we expect that the ratio  $\rho_A(x, Q^2)$  goes to infinity at  $x = 1$  as indeed the data in Fig. 17.10 suggests.

(d) *Concluding remarks on the EMC effect* As we have seen, we move from shadowing in the low  $x$  domain to antishadowing at intermediate  $x$ , to Fermi motion effects near  $x = 1$ ; thus, by continuity, a minimum is expected at some  $x$  value between the antishadowing maximum and the point  $x = 1$ . This is indeed borne out by the data. That the minimum deepens with increasing  $A$ , as seen by comparing Fig. 17.9 and Fig. 17.10, has been interpreted as an effect of nuclear binding (see, e.g., Kryzywicki, 1985, and references therein), but relativistic effects are also important. We draw the reader's attention to new experimental analyses

by the NMC which are attempting to study the dependence not just on  $A$  but separately upon the nuclear density and the nuclear radius.

#### 17.1.4 Experimental status of the scaling functions

As mentioned earlier, one of the most convincing pieces of evidence in favour of QCD is the small breaking of Bjorken scaling which will be treated in detail in Chapters 22 and 23. Given that this breaking is only of a few per cent, one must clearly rely upon a very high level of experimental accuracy. Thus, the finding of an apparently serious  $x$ -dependent disagreement (Withlow, 1990) in the measurements of the proton scaling function  $F_2$  from the EMC (1985) and the BCDMS collaborations (BCDMS, 1989) was quite disturbing. The data concerning this disagreement are shown in Fig. 17.12 which includes SLAC data. It has been demonstrated that these data are extremely sensitive to the value of  $R = \sigma_L/\sigma_T$  (usually a theoretical input) used in the experimental analysis and that reasonable consistency is obtained between different sets of data if (i) the same input for  $R$  is used and (ii) some small relative normalization shifts within the quoted uncertainties are applied (Bazizi *et al.*, 1990). The value of  $R$  used is taken from QCD calculations (Gluck and Reya, 1978; Altarelli and Martinelli, 1978) [see (23.8.13) and (23.8.14)]. Fig. 17.13 shows the data of Fig. 17.12 re-analysed in this way. The agreement is now quite reasonable.

Fig. 17.14 shows the excellent agreement between the slopes  $dF_2/d\ln Q^2$  as a function of  $x$  for the BCDMS and the EMC data compared with the QCD prediction. A more detailed discussion is given in Section 23.9.

The same authors also compare the EMC data re-analysed as above, with the preliminary data from the NMC (NMC, 1990). Again the agreement is fair. Finally, Fig. 17.15 shows the ratio  $F_2^n/F_2^p$  as function of  $x$  from the EMC (1987) and BCDMS (1990). The agreement is reasonable.

## 17.2 Neutrino cross-sections in the quark–parton model for $Q^2 \ll M_Z^2$

In Chapters 15 and 16 we developed the theory of deep inelastic scattering from a very general point of view, using the general structure of the cross-section in terms of the three scaling functions  $F_j(x)$ . From their experimental behaviour we were led to the quark–parton picture in which a virtual photon,  $W^\pm$  or  $Z^0$  emitted at the lepton vertex interacts with a quark or antiquark in the target hadron. At the level of the simple

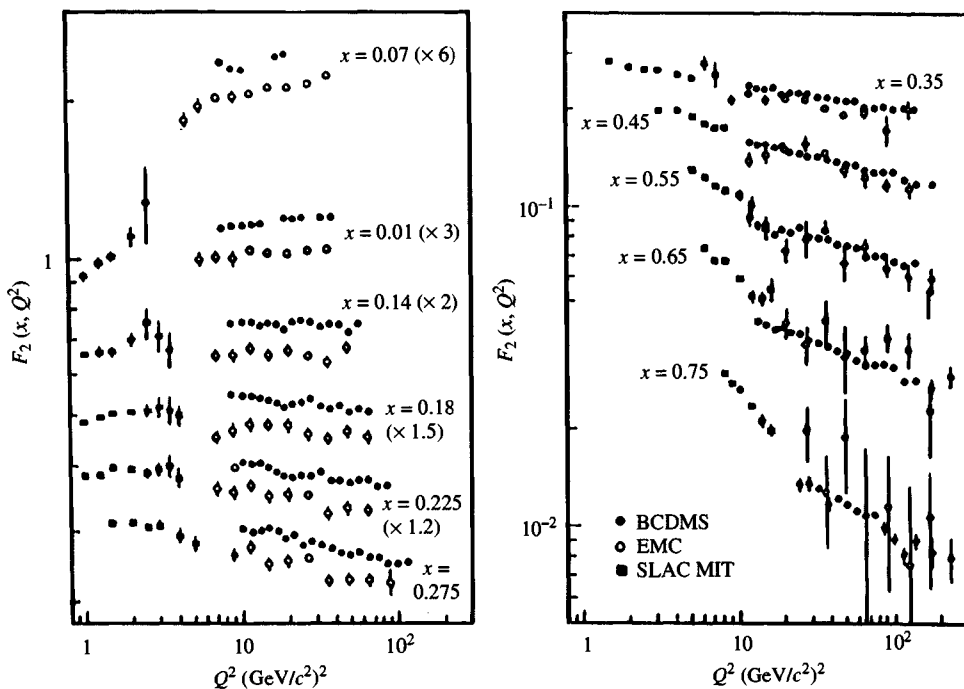


Fig. 17.12. Data on  $F_2(x, Q^2)$  for various  $x$  bins as function of  $Q^2$  (BCDMS, EMC and SLAC MIT).

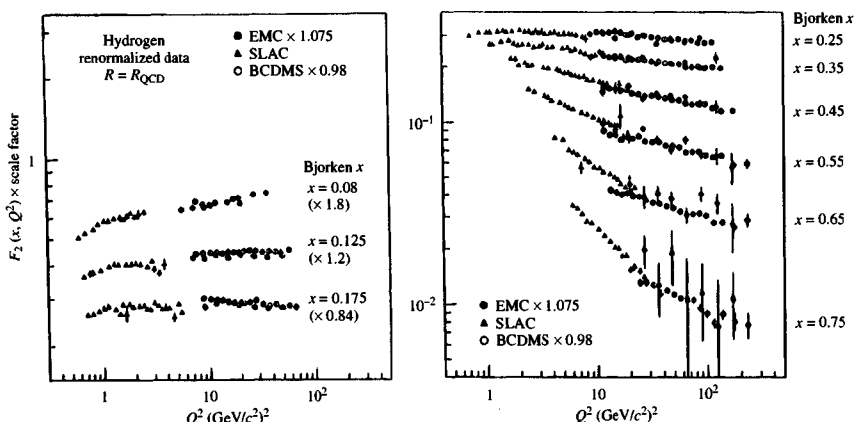


Fig. 17.13. The data of Fig. 17.12 as re-analysed using the same values of  $R$  for each experiment and with small normalization shifts as indicated.

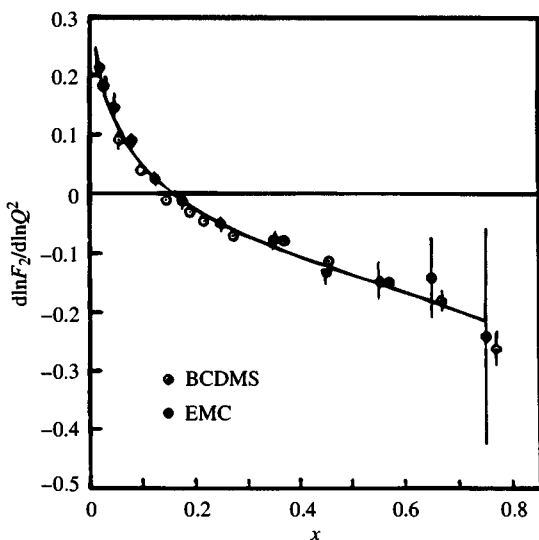


Fig. 17.14. The measured slopes  $d \ln F_2 / d \ln Q^2$  as a function of  $x$ . The smooth curve represents the behaviour expected from QCD in leading order with  $\Lambda_{LO} = 230$  MeV.

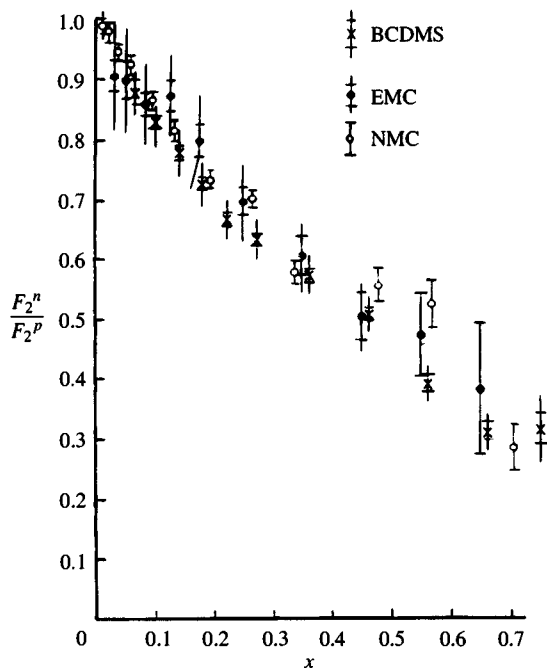


Fig. 17.15. Ratio  $F_2^n / F_2^p$ . Inner errors are statistical, outer systematic and statistical combined.

quark-parton model the hadron is just a ‘mini-accelerator’ providing a certain number density  $q_j(x)$  of type  $j$  quarks with momentum fraction in the range  $x \rightarrow x + dx$ . Binding energy and other strong interaction effects are ignored at this level. Later, when we come to consider QCD, we shall see that perfect Bjorken scaling is modified and the  $F_j(x)$  depend weakly on  $Q^2$ . For the purposes of the QCD analysis it will be best to work in terms of the  $F_j(x)$ , but here, once we accept the above picture of the interaction, it is physically more transparent to jettison the  $F_j(x)$  and look at the cross-section expressed directly in terms of the parton densities.

Once we assume that we are dealing with lepton scattering on point-like spin-half objects, we expect, on the basis of our results for  $\nu e \rightarrow \nu e$  and  $\bar{\nu} e \rightarrow \bar{\nu} e$  [see Section 5.1 and (5.1.26 and 29)] to find that our angular distribution is a sum of two terms, with the characteristic structure of the scattering off left-handed and right-handed objects. So for neutrino reactions we expect ‘1’ from  $\nu L \rightarrow \nu L$  and ‘ $(1 - y)^2$ ’ from  $\nu R \rightarrow \nu R$  and vice versa for antineutrino reactions. [For electromagnetic reactions we would expect ‘1’ + ‘ $(1 - y)^2$ ’.]

We now substitute the various formulae for the  $F_j(x)$  (16.4.26–30) into the cross-section expressions (15.5.7), and ignoring the term  $xy m_N^2/s$ , obtain for CC reactions initiated by a  $\nu$  or  $\bar{\nu}^*$ :

$$\begin{aligned} \frac{d^2\sigma_{CC}^{\nu p}}{dxdy} &= 2\pi sx \left( \frac{\alpha}{2\sin^2\theta_W M_W^2} \right)^2 \left( \frac{M_W^2}{M_W^2 + Q^2} \right)^2 \\ &\quad \times \left\{ D(x, Q^2) + (1 - y)^2 \bar{U}(x, Q^2) \right\}, \end{aligned} \quad (17.2.1)$$

$$\begin{aligned} \frac{d^2\sigma_{CC}^{\bar{\nu} p}}{dxdy} &= 2\pi sx \left( \frac{\alpha}{2\sin^2\theta_W M_W^2} \right)^2 \left( \frac{M_W^2}{M_W^2 + Q^2} \right)^2 \\ &\quad \times \left\{ \bar{D}(x, Q^2) + (1 - y)^2 U(x, Q^2) \right\} \end{aligned} \quad (17.2.2)$$

where we have introduced the shorthand

$$\begin{aligned} U(x, Q^2) &\equiv U[u] \quad \equiv u(x)(|V_{ud}|^2 + |V_{us}|^2) \\ &\quad + (\xi_b/x)u(\xi_b)|V_{ub}|^2\theta(x_b - x) \\ &\approx u(x) \\ D(x, Q^2) &\equiv D[d, s] \quad \equiv d(x)|V_{ud}|^2 + (\xi_c/x)d(\xi_c)|V_{cd}|^2\theta(x_c - x) \\ &\quad + s(x)|V_{us}|^2 + (\xi_c/x)s(\xi_c)|V_{cs}|^2\theta(x_c - x) \\ &\approx d(x) \end{aligned} \quad (17.2.3)$$

---

\* CC reactions initiated by charged leptons are dealt with in Section 16.6.

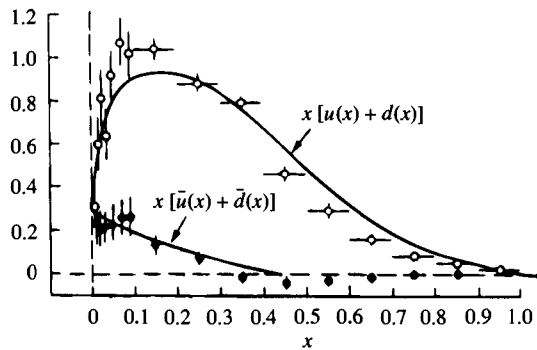


Fig. 17.16. Quark and antiquark distributions determined from low energy charged current reactions. (From Cabibbo, 1976.)

We see that for  $y$  large,  $y \approx 1$ , the  $x$  dependence in neutrino and anti-neutrino reactions determines the quark and antiquark distribution respectively.

For an isoscalar target  $N_0$  the cross-section *per nucleon* is:

$$\begin{aligned} \frac{d^2\sigma_{CC}^{eN_0}}{dxdy} &= \pi sx \left( \frac{\alpha}{2\sin^2\theta_W M_W^2} \right)^2 \left( \frac{M_W^2}{M_W^2 + Q^2} \right)^2 \\ &\quad \times \left\{ D_0(x, Q^2) + (1-y)^2 \bar{U}_0(x, Q^2) \right\} \\ \frac{d^2\sigma_{CC}^{\bar{e}N_0}}{dxdy} &= \pi sx \left( \frac{\alpha}{2\sin^2\theta_W M_W^2} \right)^2 \left( \frac{M_W^2}{M_W^2 + Q^2} \right)^2 \\ &\quad \times \left\{ \bar{D}_0(x, Q^2) + (1-y)^2 U_0(x, Q^2) \right\} \end{aligned} \quad (17.2.4)$$

where

$$\begin{aligned} U_0 &= U[u] + U[u \rightarrow d] \\ D_0 &= D[d, s] + D[d \rightarrow u, s]. \end{aligned} \quad (17.2.5)$$

From these we learn principally about the sea quark combination  $\bar{u} + \bar{d}$ , but once the KM matrix elements are known one can also get information on  $s(x)$  especially if one studies semi-inclusive charm production (see Section 18.2).

Fig. 17.16 shows quark and antiquark distributions determined in this way from low energy CC data using the approximations  $U \approx u, D \approx d$ . There is clear confirmation of the increase in the relative importance of the sea at small  $x$ .

As a measure of the contribution of the various sea components com-

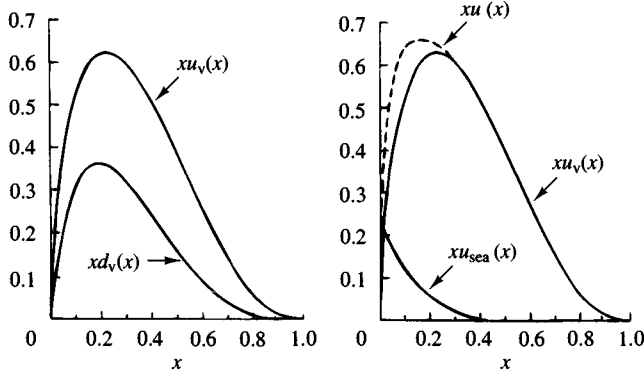


Fig. 17.17. Typical shapes for parton distributions compatible with deep inelastic data. (After Buras, 1977.)

pared with the dominant valence contribution in nucleons, let us define

$$\eta_j \equiv \frac{\int_0^1 x q_j(x) dx}{\int_0^1 x [u_V(x) + d_V(x)] dx}. \quad (17.2.6)$$

Analyses of CC reactions typically give values like

$$\begin{aligned} \eta_{\bar{u}} + \eta_{\bar{d}} &\approx 18\text{--}20\% \\ 2\eta_s &\approx 0.44(\eta_{\bar{u}} + \eta_{\bar{d}}). \end{aligned} \quad (17.2.7)$$

Several fits have been made to the data from proton and ‘neutron’ targets to try to determine the shape of the individual parton distribution functions and to distinguish between the sea and valence contributions. Typical shapes are shown in Fig. 17.17 wherein was used  $u(x) = u_V(x) + u_{\text{sea}}(x)$  and  $u_{\text{sea}}(x) = d_{\text{sea}}(x)$  etc. The importance of the sea at small  $x$  only is clearly shown.

Let us now turn to NC reactions. In Section 10.1 we discussed certain NC results which did not depend upon our detailed picture of hadrons. We now look at more specific predictions that follow in the quark–parton model. Thus substituting (16.4.41–43) into (15.5.9) yields

$$\begin{aligned} \frac{d^2\sigma_{\text{NC}}^{\nu p}}{dxdy} &= 2\pi sx \left( \frac{\alpha}{2\sin^2\theta_W \cos^2\theta_W M_Z^2} \right)^2 \left( \frac{M_Z^2}{M_Z^2 + Q^2} \right)^2 \\ &\times \left\{ (g_L^u)^2 u(x) + (g_L^d)^2 [d(x) + s(x)] \right. \\ &+ (g_R^u)^2 \bar{u}(x) + (g_R^d)^2 [\bar{d}(x) + \bar{s}(x)] \\ &+ (1-y)^2 [(g_R^u)^2 u(x) + (g_R^d)^2 [d(x) + s(x)] \\ &\left. + (g_L^u)^2 \bar{u}(x) + (g_L^d)^2 [\bar{d}(x) + \bar{s}(x)]] \right\} \end{aligned} \quad (17.2.8)$$

where we have used R and L couplings for flavour  $f$ ,

$$g_L^f \equiv \frac{1}{2}(g_V^f + g_A^f) \quad g_R^f \equiv \frac{1}{2}(g_V^f - g_A^f) \quad (17.2.9)$$

with, as usual,

$$g_V^u = \frac{1}{2} - \frac{4}{3} \sin^2 \theta_W, \quad g_V^d = -\frac{1}{2} + \frac{2}{3} \sin^2 \theta_W, \quad g_A^u = \frac{1}{2}, \quad g_A^d = -\frac{1}{2}. \quad (17.2.10)$$

For antineutrino interactions simply make the substitution

$$g_L^f \rightarrow g_R^f \quad g_R^f \rightarrow g_L^f \quad (17.2.11)$$

in (17.2.8).

There is no simple relation between the proton or neutron NC and CC cross-sections, (17.2.8) and (17.2.1). However if we consider an isoscalar target  $N_0$  we get some interesting connections between the two types of cross-section. In the region  $Q^2 \ll M_Z^2$  or  $M_W^2$  we may, to a high degree of accuracy, take

$$\frac{M_W^2}{M_W^2 + Q^2} = \frac{M_Z^2}{M_Z^2 + Q^2} = 1. \quad (17.2.12)$$

If we restrict ourselves to values of  $x$  where the sea contribution is negligible, and if we ignore the difference between  $D(x, Q^2)$ ,  $U(x, Q^2)$  and  $d(x)$ ,  $u(x)$ , we find

$$\left. \begin{aligned} \frac{d\sigma_{NC}^{\nu N_0}}{dx} &\approx \rho_0^2 \left( \frac{1}{2} - \sin^2 \theta_W + \frac{20}{27} \sin^4 \theta_W \right) \frac{d\sigma_{CC}^{\nu N_0}}{dx} \\ \frac{d\sigma_{NC}^{\bar{\nu} N_0}}{dx} &\approx \rho_0^2 \left( \frac{1}{2} - \sin^2 \theta_W + \frac{20}{9} \sin^4 \theta_W \right) \frac{d\sigma_{CC}^{\bar{\nu} N_0}}{dx} \end{aligned} \right\} [\text{sea} = 0] \quad (17.2.13)$$

where, as in Section 5.2,

$$\rho_0 = \frac{M_W^2}{\cos^2 \theta_W M_Z^2} \quad (17.2.14)$$

and  $\rho_0 = 1$  in the SM, i.e. with minimal Higgs mechanism, and where we have used

$$\begin{aligned} (g_R^u)^2 + (g_R^d)^2 &= \frac{5}{9} \sin^4 \theta_W, \\ (g_L^u)^2 + (g_L^d)^2 &= \frac{1}{2} - \sin^2 \theta_W + \frac{5}{9} \sin^4 \theta_W. \end{aligned} \quad (17.2.15)$$

Sometimes an integrated form of (17.2.13) is used for the total cross-sections, but it cannot be accurate to better than about 10%. A more reliable connection, which does not neglect the  $\bar{u}$ ,  $\bar{d}$  sea contribution, follows from (17.2.4 and 1). One finds, with the approximations  $D \approx d$ ,  $U \approx$

$u, s(x) \approx 0$ :

$$\begin{aligned} \frac{1}{\rho_0^2} \frac{d^2\sigma_{NC}^{\nu N_0}}{dxdy} &\approx [(g_L^u)^2 + (g_L^d)^2] \frac{d^2\sigma_{CC}^{\nu N_0}}{dxdy} + [(g_R^u)^2 + (g_R^d)^2] \frac{d^2\sigma_{CC}^{\bar{\nu} N_0}}{dxdy}, \\ \frac{1}{\rho_0^2} \frac{d^2\sigma_{NC}^{\bar{\nu} N_0}}{dxdy} &\approx [(g_R^u)^2 + (g_R^d)^2] \frac{d^2\sigma_{CC}^{\nu N_0}}{dxdy} + [(g_L^u)^2 + (g_L^d)^2] \frac{d^2\sigma_{CC}^{\bar{\nu} N_0}}{dxdy}. \end{aligned} \quad (17.2.16)$$

It is easy to check that these reproduce the famous result of Paschos and Wolfenstein (10.1.22) when  $\rho_0 = 1$ .

Integrating (17.2.16) we have

$$\begin{aligned} \frac{1}{\rho_0^2} \sigma_{NC}^{\nu N_0} &\approx (\frac{1}{2} - \sin^2 \theta_W + \frac{5}{9} \sin^4 \theta_W) \sigma_{CC}^{\nu N_0} + \frac{5}{9} \sin^4 \theta_W \sigma_{CC}^{\bar{\nu} N_0}, \\ \frac{1}{\rho_0^2} \sigma_{NC}^{\bar{\nu} N_0} &\approx \frac{5}{9} \sin^4 \theta_W \sigma_{CC}^{\nu N_0} + (\frac{1}{2} - \sin^2 \theta_W + \frac{5}{9} \sin^4 \theta_W) \sigma_{CC}^{\bar{\nu} N_0}. \end{aligned} \quad (17.2.17)$$

Introducing, as in Section 10.1,

$$\begin{aligned} R_\nu &\equiv \sigma_{NC}^{\nu N_0} / \sigma_{CC}^{\nu N_0}, & R_{\bar{\nu}} &\equiv \sigma_{NC}^{\bar{\nu} N_0} / \sigma_{CC}^{\bar{\nu} N_0}, \\ r &\equiv \sigma_{CC}^{\bar{\nu} N_0} / \sigma_{CC}^{\nu N_0} \end{aligned} \quad (17.2.18)$$

one has

$$\frac{1}{\rho_0^2} R_\nu \approx \frac{1}{2} - \sin^2 \theta_W + \frac{5}{9} \sin^4 \theta_W (1 + r), \quad (17.2.19)$$

$$\frac{1}{\rho_0^2} R_{\bar{\nu}} \approx \frac{1}{2} - \sin^2 \theta_W + \frac{5}{9} \sin^4 \theta_W (1 + 1/r). \quad (17.2.20)$$

These equations can be used to obtain a measurement of  $\rho_0$  and  $\sin^2 \theta_W$ .  $R^\nu$  and  $R^{\bar{\nu}}$  can be determined very accurately since they involve comparing CC and NC reactions in the *same*  $\nu$  or  $\bar{\nu}$  beam.  $r$  is less accurately known since one has to compare CC reactions induced by  $\nu$  and  $\bar{\nu}$ , so that the relative beam intensity is required. But the term involving  $r$  is multiplied by  $\frac{5}{9} \sin^4 \theta_W \approx 0.035$  thus reducing the uncertainty caused by  $r$ . Recent determinations of  $R^\nu$ ,  $R^{\bar{\nu}}$  and  $r$  are given in Table 17.1. They were obtained using the CERN 160 GeV narrow band  $\nu$  and  $\bar{\nu}$  beam on an iron target.

Since  $R_\nu$  is more accurately known than  $R_{\bar{\nu}}$  let us use (17.2.19) with  $\rho_0 = 1$  to measure  $\sin^2 \theta_W$ . One finds with the CDHSW data,  $\sin^2 \theta_W = 0.236$ . But given the accuracy of the data, the approximate formulae (17.2.16, 17, 19, 20) are inadequate. Thus in obtaining a value of  $\sin^2 \theta_W$  corrections are made to account for the strange quark contribution, for the KM matrix, for the charm threshold, for the fact that the iron nucleus is not perfectly isoscalar, and for higher order corrections to the SM. Many of these corrections turn out to have opposite signs and the net result is

Experiment	$R_\nu$	$R_{\bar{\nu}}$	$r$
CDHSW			
$M_x > 10 \text{ GeV}/c^2$	$0.3072 \pm 0.0033$	$0.382 \pm 0.016$	$0.393 \pm 0.014$
CHARM			
$M_x > 4 \text{ GeV}/c^2$	$0.3093 \pm 0.0031$	$0.390 \pm 0.014$	$0.456 \pm 0.011$
CHARM			
$M_x > 9 \text{ GeV}/c^2$	$0.3052 \pm 0.0033$	$0.397 \pm 0.015$	$0.429 \pm 0.010$

Table 17.1. Recent experimental data on NC/CC and  $\bar{\nu}/\nu$  cross-section ratios on iron. Data are: CDHSW (1990a) and CHARM (1987).

a correction of 1–2%. The results are

$$\begin{aligned} \text{CDHSW} : \sin^2 \theta_W &= 0.228 \pm 0.005 \text{ (exp.)} \pm 0.005 \text{ (theory)}, \\ \text{CHARM} : \sin^2 \theta_W &= 0.236 \pm 0.005 \text{ (exp.)} \pm 0.005 \text{ (theory)} \end{aligned} \quad (17.2.21)$$

in beautiful agreement with the value deduced from  $M_W$  and  $M_Z$  in Section 7.7.

If we do not insist on  $\rho_0 = 1$  then from (17.2.19,20) one obtains

$$\begin{aligned} \text{CDHSW} : \rho_0 &= 0.991 \pm 0.020 \text{ (exp.)} \pm 0.004 \text{ (theory)}, \\ \text{CHARM} : \rho_0 &= 0.990 \pm 0.009 \text{ (exp.)} \pm 0.005 \text{ (theory)} \end{aligned} \quad (17.2.22)$$

perfectly compatible with the SM result.

Finally integrating (17.2.1, 2 and 8) over  $x$  and comparing NC and CC reactions for experimental accuracy, we note that for any target N the ratio of the  $y$  distributions have the form

$$\begin{aligned} \frac{d\sigma_{\text{NC}}^{\nu N}/dy}{d\sigma_{\text{CC}}^{\nu N}/dy} &= \frac{1 + \alpha(1 - y)^2}{F_L + F_R(1 - y)^2}, \\ \frac{d\sigma_{\text{CC}}^{\bar{\nu} N}/dy}{d\sigma_{\text{NC}}^{\bar{\nu} N}/dy} &= \frac{\alpha + (1 - y)^2}{\bar{F}_R + \bar{F}_L(1 - y)^2}. \end{aligned} \quad (17.2.23)$$

We shall not clutter the page with the formulae for the coefficients  $\alpha, F, \bar{F}$ , which depend on  $\sin^2 \theta_W$  and on integrals over the parton distribution of the form  $\int_0^1 x q_j(x) dx$ . They can be read off trivially from (17.2.1, 2 and 8). From analyses of this type one gets a quantitative feeling for the strange sea contribution. For  $\eta_s$  [see (17.2.6)] one finds

$$\eta_s \approx 3\text{--}5\%. \quad (17.2.24)$$

(The reader is warned that in some literature  $\eta_s$  is defined a factor of 2 larger than ours is.) This estimate is supported by data on charm production in deep inelastic neutrino scattering where the dominant transition is  $s \rightarrow c$  (see Section 18.2).

To summarize, for  $Q^2 \ll M_W^2$ , there is generally good agreement between the quark–parton model cross-sections and experiment. Much is learned about the quark number densities but the difficulty of working with neutrino beams means that detailed  $x$  distributions are still rather imprecise. It is important and interesting to use the quark distributions in studying other physical processes.

### 17.3 Cross-sections in the quark–parton model for $Q^2$ comparable with $M_Z^2$

There are, of course, no experiments yet in this regime but with HERA in operation there is much interest in the quark–parton predictions.

As explained in Section 16.5 the formulae for the scaling functions simplify since thresholds are irrelevant (except for top, the effect of which is quite negligible). Consequently the cross-section formulae also simplify. Substituting (16.5.4 and 5) into (15.5.8) we have for CC reactions initiated by  $e^\mp$ :

$$\begin{aligned}\frac{d^2\sigma_{CC}^{e^-}}{dxdy} &= \frac{\pi\alpha^2 sx}{4\sin^4\theta_W(Q^2 + M_W^2)^2} \left\{ u(x) + (1-y)^2[\bar{d}(x) + \bar{s}(x)] \right\}, \\ \frac{d^2\sigma_{CC}^{e^+}}{dxdy} &= \frac{\pi\alpha^2 sx}{4\sin^4\theta_W(Q^2 + M_W^2)^2} \left\{ \bar{u}(x) + (1-y)^2[d(x) + s(x)] \right\}.\end{aligned}\tag{17.3.1}$$

For NC reactions we substitute (16.4.9–11) and (16.4.41–43) into (15.5.10), average over the initial lepton helicity and utilize (15.5.12) for the anti-lepton case. Thus for unpolarized NC reactions initiated by  $e^\mp$  we find:

$$\begin{aligned}\frac{d^2\sigma_{NC}(e^\mp)}{dxdy} &= \frac{4\pi\alpha^2 s}{Q^4} \left\{ xy^2 F_1^{NC}(x, Q^2) + (1-y)F_2^{NC}(x, Q^2) \right. \\ &\quad \left. \pm x \left( y - \frac{y^2}{2} \right) F_3^{NC}(x, Q^2) \right\}\end{aligned}\tag{17.3.2}$$

where

$$\begin{aligned}F_1^{NC}(x, Q^2) &= \frac{1}{2} \sum_{j=u,d,s} [q_j(x) + \bar{q}_j(x)] \left[ Q_j^2 - 2Q_j v_e v_j \chi(Q^2) \right. \\ &\quad \left. + (v_e^2 + a_e^2)(v_j^2 + a_j^2) \chi^2(Q^2) \right],\end{aligned}\tag{17.3.3}$$

$$F_2^{NC} = 2x F_1^{NC}\tag{17.3.4}$$

and  $F_3$  is given in terms of *valence* contributions only

$$F_3^{\text{NC}}(x, Q^2) = -2\chi(Q^2) \sum_{j=u,d} q_j v(x) [Q_j a_e a_j - 2v_e v_j a_e a_j \chi(Q^2)]. \quad (17.3.5)$$

In the above

$$\chi(Q^2) = \frac{Q^2}{Q^2 + M_Z^2} \quad (17.3.6)$$

and the  $v_e, v_j, a_e, a_j$  are defined in (5.1.4,5).

We stress that in this region of very large  $Q^2$  it is essential to take into account the QCD effects which induce the replacement

$$q_j(x) \rightarrow q_j(x, Q^2) \quad (17.3.7)$$

and to allow for  $c\bar{c}$  and  $b\bar{b}$  production via the mechanism in Fig. 16.10.

It will be extremely exciting to see whether the model continues to be successful in the new kinematic regime opened up at HERA.

#### 17.4 Application of the parton model to related processes

We mentioned in the Appendix to Chapter 16 that a phase factor  $e^{iq^* \cdot x}$  typically plays an important rôle when attempting to transfer a momentum  $q^*$  to a quantum mechanical system.

We can see this a little more directly in the case of deep inelastic scattering if we start with the expression (a sum over initial spins is implied)

$$\begin{aligned} W^{\alpha\beta}(N) &= \frac{1}{2} \sum_X \langle P | J^\alpha(0) | X \rangle \langle X | J^\beta(0) | P \rangle \\ &\times (2\pi)^3 \delta^4(P_X - P - q^*) \end{aligned} \quad (17.4.1)$$

and use a trick that will allow us to carry out the sum over the states  $|X\rangle$ . We put

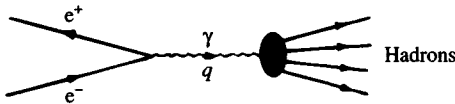
$$(2\pi)^3 \delta^4(P_X - P - q^*) = \frac{1}{2\pi} \int d^4 z e^{iz \cdot (P_X - P - q^*)} \quad (17.4.2)$$

and we use the fact that translations in space-time are generated by the operators  $\hat{P}^\mu$  corresponding to energy and momentum. Thus

$$J^\beta(z) = e^{i\hat{P} \cdot z} J^\beta(0) e^{-i\hat{P} \cdot z} \quad (17.4.3)$$

so that

$$\begin{aligned} \langle X | J^\beta(0) | P \rangle &= \langle X | e^{-i\hat{P} \cdot z} J^\beta(z) e^{i\hat{P} \cdot z} | P \rangle \\ &= e^{iz \cdot (P - P_X)} \langle X | J^\beta(z) | P \rangle \end{aligned} \quad (17.4.4)$$

Fig. 17.18. Feynman diagram for  $e^+e^- \rightarrow \text{hadrons}$ .

since  $|P\rangle$  and  $|X\rangle$  are eigenstates of energy and momentum. Putting (17.4.4) and (17.4.2) into (17.4.1) yields

$$W^{\alpha\beta}(N) = \frac{1}{4\pi} \int d^4z e^{-iz\cdot q^*} \langle P | J^\alpha(0) J^\beta(z) | P \rangle, \quad (17.4.5)$$

where we have carried out the sum now over *all* states  $|X\rangle$ , i.e. no longer constrained by the  $\delta$ -function, and used completeness

$$\sum_X |X\rangle \langle X| = 1.$$

Eqn (17.4.5), which is exact, shows clearly the emergence of the above mentioned phase factor. We shall use (17.4.5) as our guide in looking at other processes to which the parton model may be applicable.

#### 17.4.1 $e^+e^-$ annihilation into hadrons

We have several times used the famous result (9.5.23)

$$R = \frac{\sigma(e^+e^- \rightarrow \text{hadrons})}{\sigma(e^+e^- \rightarrow \mu^+\mu^-)_{\text{QED}}} = \sum_{\substack{\text{flavour} \\ \text{and colours}}} Q_j^2 \quad (17.4.6)$$

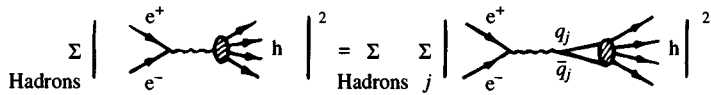
for energies where the  $Z^0$  contribution is negligible. Indeed this relation has played an important rôle in pinpointing the existence of new quarks and the new heavy lepton  $\tau$ , and we turn now to consider its derivation in the parton model.

The process  $e^+e^- \rightarrow \text{hadrons}$  is described by Fig. 17.18 which is very similar to the deep inelastic diagram (Fig. 15.4 looked at sideways) except for the fact that the initial nucleon state is missing in Fig. 17.18 and that the photon is now time-like.

One can thus see by analogy with (17.4.5) that the cross-section for  $e^+e^- \rightarrow \text{hadrons}$  in the CM system is governed by

$$\frac{1}{4\pi} \int d^4z e^{-iz\cdot q} \langle 0 | J_\alpha^{\text{em}}(0) J_\beta^{\text{em}}(z) | 0 \rangle, \quad (17.4.7)$$

where  $q$  is now the photon momentum in the CM. The same sort of analysis as in the Appendix to Chapter 16 will show that the relevant interaction times are very short, as the CM energy (i.e.  $q_0$ )  $\rightarrow \infty$ . We can

Fig. 17.19. Quark model picture of  $e^+e^- \rightarrow \text{hadrons}$ .

therefore go through all the impulse approximation steps used previously, but now using as final states  $q\bar{q}$  pairs, and again supposing that at high enough energies, i.e.  $q^2 \gg m_N^2$ , there is unit probability for the quark-antiquark pair to convert to hadrons. One thereby gets the pictorial equation Fig. 17.19 where the sum is over different flavours and colours, and which when all the details are included yields

$$\sigma(e^+e^- \rightarrow \gamma \rightarrow \text{hadrons}) \stackrel{q^2 \rightarrow \infty}{=} \frac{4\pi\alpha^2}{3q^2} \sum_{\substack{\text{flavours} \\ \text{and colours}}} Q_j^2 \quad (17.4.8)$$

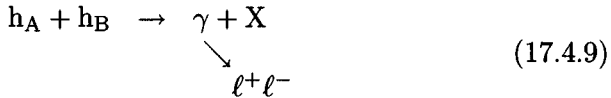
which gives (17.4.6) immediately.

Note that compared with the deep inelastic case there is no probability function in (17.4.8) for finding the parton. This is because we have a transition from the vacuum state and not from a nucleon. Note also that it is the probability of the transition from the  $q\bar{q}$  normalized singlet colour state to the hadrons that has been taken to be unity.

The elementary result (17.4.6) will be modified by QCD effects which we shall take up in Section 22.1.

#### 17.4.2 The Drell-Yan process

The reaction



where  $h_A$  and  $h_B$  are hadrons, and where the invariant mass  $m$  of the lepton-antilepton pair is large compared with  $m_N$ , has become known as the Drell-Yan process (Drell and Yan, 1971). The reaction is shown diagrammatically in Fig. 17.20 where it is assumed that the  $\ell^+\ell^-$  mass is well below  $M_Z$ . When LHC or SSC are functioning it will be possible to study ultra-high  $\ell^+\ell^-$  masses, in which case  $Z^0$  exchange must also be taken into account.

There is again a similarity with the deep inelastic process, except that we now begin with a state of two hadrons, and the photon is time-like.

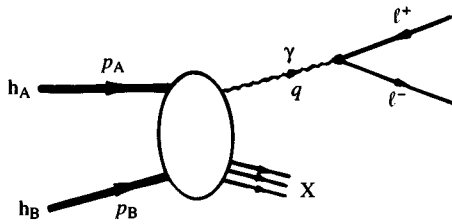


Fig. 17.20. Feynman diagram for Drell-Yan process  $h_A + h_B \rightarrow \ell^+ \ell^- X$ .

The cross-section is by analogy controlled by the tensor

$$W_{\mu\nu}^{D-Y} = \frac{1}{4\pi} \sum_X \langle h_A h_B | J_\mu^{\text{em}}(0) | X \rangle \langle X | J_\nu^{\text{em}}(0) | h_A h_B \rangle_{\text{IN}} \times (2\pi)^4 \delta^4(p_X - p_A - p_B - q), \quad (17.4.10)$$

which, as in (17.4.7), can be written as

$$= \frac{1}{4\pi} \int d^4z e^{-iq \cdot z} \langle h_A h_B | J_\mu^{\text{em}}(0) J_\nu^{\text{em}}(z) | h_A h_B \rangle_{\text{IN}}. \quad (17.4.11)$$

Compared with the previous cases there is an added element here which arises in the formal derivation of (17.4.10) and (17.4.11) using the LSZ reduction formalism of field theory [see, for example, Gasiorowicz (1967)], and which is beyond the scope of this book. Namely the two-hadron state has to be specified as a so-called ‘IN’ state. Luckily, for our needs this is irrelevant, and it will be permissible to think of  $|h_A h_B\rangle_{\text{IN}}$  as simply a state of two *free* hadrons. For those who are *au fait* with such concepts, it is to be noted that the  $J_\alpha^{\text{em}}$  are the em currents in the Heisenberg picture.

We wish now to see if there is a kinematic region where the impulse approximation will be valid. Since there are two nucleons involved we shall wish to treat them symmetrically so the obvious ‘infinite momentum’ frame is the CM as  $s = (p_A + p_B)^2 \rightarrow \infty$ .

In the CM we have, as  $s \rightarrow \infty$ ,

$$p_A = (P, 0, 0, P), \quad p_B = (P, 0, 0, -P). \quad (17.4.12)$$

The mass  $m$  of the lepton-antilepton pair is simply given by

$$m^2 = q^2 \quad (17.4.13)$$

and we consider a regime where

$$\tau \equiv \frac{m^2}{s} = \frac{q^2}{s} = \frac{q^2}{4P^2} \quad (17.4.14)$$

is *fixed* as  $P \rightarrow \infty$ . This implies that

$$q^2 = q_0^2 - |\mathbf{q}|^2 = (q_0 - |\mathbf{q}|)(q_0 + |\mathbf{q}|) = 0(P^2). \quad (17.4.15)$$

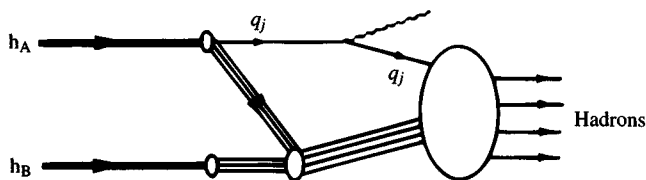


Fig. 17.21. Diagram for Drell-Yan process in which the virtual parton is far off its mass shell.

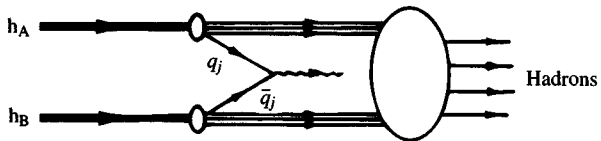


Fig. 17.22. Diagram for Drell-Yan process in which the virtual parton can be close to its mass shell.

By energy conservation

$$q_0 < 2P$$

and, the photon, being time-like,

$$q_0 > |\mathbf{q}|.$$

It then follows from (17.4.15) that both  $q_0 - |\mathbf{q}|$  and  $q_0 + |\mathbf{q}|$  must be of the order of  $P$  as  $P \rightarrow \infty$ . An analysis of the phase factor in (17.4.11) like that carried out in the Appendix to Chapter 16, shows that the important times and distances are

$$t \sim z \sim \frac{1}{P} \quad (17.4.16)$$

so we may proceed to apply the parton picture.

Note the difference *vis-à-vis* the deep inelastic case. There one had  $t - z \sim 1/P$  but  $t$  and  $z$  individually could be large. Here we have both  $t$  and  $z$  of the order of  $1/P$ .

There are now, in principle, two basic types of diagram (Figs. 17.21 and 17.22).

The parton process involved in Fig. 17.21 looks very similar to the deep inelastic process (see Fig. 16.1) but the crucial difference is that the photon is time-like here, which implies that the struck parton is very far off its mass shell after emitting the massive photon; so the amplitude from this diagram should be drastically suppressed and will be ignored.

In Fig. 17.22, on the other hand, the quark  $q_j$  and the antiquark  $\bar{q}_j$  that annihilate to produce the photon, can actually be on their mass shells.

Assuming, as usual, incoherence and unit probability for quarks to turn into hadrons at high energies, the result for the cross-section can be written down intuitively by visualizing the collision in the CM. There, the hadrons can be regarded as a source of quarks  $q_j$  and antiquarks  $\bar{q}_j$  which, if their transverse momentum is limited, collide essentially head-on and annihilate,

$$q_j + \bar{q}_j \rightarrow \gamma \rightarrow \ell^+ \ell^-.$$

The cross-section to produce  $\ell^+ \ell^-$  will then be given by

$$\begin{aligned} \sigma(h_A h_B \rightarrow \ell^+ \ell^- X) &= \sum_j \sigma(q_j \bar{q}_j \rightarrow \ell^+ \ell^-) \\ &\quad \times (\text{flux of } q_j \text{ and } \bar{q}_j \text{ provided by } h_A, h_B). \end{aligned} \quad (17.4.17)$$

For the required annihilation cross-section one has at high  $q^2$ , where any masses involved in the flux factor become irrelevant,

$$\sigma(q_j \bar{q}_j \rightarrow \gamma \rightarrow \ell^+ \ell^-) = \sigma(\ell^+ \ell^- \rightarrow \gamma \rightarrow q_j \bar{q}_j) \quad (17.4.18)$$

so that from (17.4.8)

$$\sigma(q_j \bar{q}_j \rightarrow \gamma \rightarrow \ell^+ \ell^-) \stackrel{q^2 \rightarrow \infty}{=} \frac{4\pi\alpha^2}{3q^2} Q_j^2. \quad (17.4.19)$$

To compute the flux of  $q_j, \bar{q}_j$  provided by the hadrons, let us denote the momenta of  $q_j, \bar{q}_j$  in the CM by

$$\begin{aligned} p(q_j) &= \left( \sqrt{(x'_A P)^2 + \kappa^2 + \mu_j^2}, \kappa, x'_A P \right) \\ &\approx \left( x'_A P + \frac{\mu_j^2 + \kappa^2}{2x'_A P}, \kappa, x'_A P \right) \end{aligned} \quad (17.4.20)$$

and

$$\begin{aligned} p(\bar{q}_j) &= \left( \sqrt{(x'_B P)^2 + \bar{\kappa}^2 + \mu_j^2}, \bar{\kappa}, -x'_B P \right) \\ &\approx \left( x'_B P + \frac{\mu_j^2 + \bar{\kappa}^2}{2x'_B P}, \bar{\kappa}, -x'_B P \right), \end{aligned}$$

where  $\kappa$  and  $\bar{\kappa}$  are perpendicular to the collision axis, and assume, as usual, that  $\kappa, \bar{\kappa}$  are limited and that  $x'_A P, x'_B P \gg$  an effective mass of order  $\sqrt{\mu_j^2 + \kappa^2}$ .

Since the relative velocity involved in the collision is essentially the velocity of light, the flux from partons whose  $Z$  component of momentum

lies between  $x'_A P$  and  $(x'_A + dx'_A)P$  and between  $-x'_B P$  and  $-(x'_B + dx'_B)P$  is

$$\left( \begin{array}{l} \text{Flux factor for} \\ \text{given colour and} \\ \text{flavour} \end{array} \right) = \frac{1}{9} [q_j^A(x'_A)\bar{q}_j^B(x'_B) + \bar{q}_j^A(x'_A)q_j^B(x'_B)]dx'_A dx'_B, \quad (17.4.21)$$

where  $q_j^A(x'_A)dx'_A$  is the number of flavour  $j$  quarks in hadron  $h_A$  with momentum fraction  $x'_A$  as seen in the CM, and  $\bar{q}_j^B(x'_B)$  refers similarly to antiquarks.

The factor  $\frac{1}{9}$  occurs because on average only  $\frac{1}{3}$  of the quarks of a given flavour  $j$  in each hadron will have the particular colour necessary for the annihilation of identical colours to take place.

Since energy and momentum are conserved in the  $q\bar{q} \rightarrow \ell^+ \ell^-$  process, we have for the components of the momentum of the lepton pair in the overall CM

$$\left. \begin{aligned} q_T &= \kappa + \bar{\kappa}, \\ q_z &= (x'_A - x'_B)P, \\ q_0 &\simeq (x'_A + x'_B)P + \frac{\mu_j^2 + \kappa^2}{2x'_A P} + \frac{\mu_j^2 + \bar{\kappa}^2}{2x'_B P}. \end{aligned} \right\} \quad (17.4.22)$$

Very simple and elegant results emerge if we assume that we are at such high energies that we can completely ignore the parton masses and perpendicular momenta. Let us therefore begin by doing this.

Once we drop the terms involving  $\mu_j^2$ ,  $\kappa^2$  and  $\bar{\kappa}^2$ , the possible values of  $x'_A, x'_B$  for a given  $q_0, q_z$  are fixed. If we define

$$x_A \equiv \frac{1}{2P}(q_0 + q_z), \quad x_B \equiv \frac{1}{2P}(q_0 - q_z), \quad (17.4.23)$$

then only constituents with  $x'_A = x_A, x'_B = x_B$  can contribute. Putting all this information into (17.4.17) yields

$$\left. \begin{aligned} \frac{d^2\sigma}{dx_A dx_B} &= \frac{4\pi\alpha^2}{3q^2} \frac{1}{9} \sum_{\substack{\text{flavours} \\ \text{and colours}}} Q_j^2 [q_j^A(x_A)\bar{q}_j^B(x_B) + \bar{q}_j^A(x_A)q_j^B(x_B)] \\ &= \frac{4\pi\alpha^2}{3q^2} \frac{1}{3} \sum_{\substack{\text{flavours} \\ \text{only}}} Q_j^2 [q_j^A(x_A)\bar{q}_j^B(x_B) + \bar{q}_j^A(x_A)q_j^B(x_B)]. \end{aligned} \right\} \quad (17.4.24)$$

Experimentally the cross-section is usually given into a range of  $q^2 = m^2$  and a range of longitudinal momentum fractions denoted by  $\xi$

$$\xi \equiv \frac{q_z}{P} = x_A - x_B. \quad (17.4.25)$$

Since

$$\begin{aligned} q^2 &= (q_0 - q_z)(q_0 + q_z) - \mathbf{q}_T^2 \\ &= 4x_A x_B P^2 - \mathbf{q}_T^2 \\ &\simeq 4x_A x_B P^2 = x_A x_B s \end{aligned} \quad (17.4.26)$$

one has the Jacobian

$$\frac{\partial(q^2, \xi)}{\partial(x_A, x_B)} = s(x_A + x_B)$$

so that

$$\frac{d^2\sigma}{dq^2 d\xi} = \frac{4\pi\alpha^2}{9q^2 s} \sum_{\text{flavours}} Q_j^2 \frac{q_j^A(x_A)\bar{q}_j^B(x_B) + \bar{q}_j^A(x_A)q_j^B(x_B)}{x_A + x_B}. \quad (17.4.27)$$

It is customary to rewrite this in the form

$$\begin{aligned} s^2 \frac{d^2\sigma}{dq^2 d\xi} &= \frac{4\pi\alpha^2}{9\tau^2} \sum_{\text{flavours}} Q_j^2 \frac{x_A x_B}{x_A + x_B} \\ &\times [q_j^A(x_A)\bar{q}_j^B(x_B) + \bar{q}_j^A(x_A)q_j^B(x_B)], \end{aligned} \quad (17.4.28)$$

where we have used  $\tau \approx x_A x_B$  as follows from (17.4.14 and 26). The values of  $x_A, x_B$  are of course fixed by  $\tau, \xi$ :

$$\left. \begin{aligned} x_A &\simeq \frac{1}{2}(\sqrt{4\tau^2 + \xi^2} + \xi), \\ x_B &\simeq \frac{1}{2}(\sqrt{4\tau^2 + \xi^2} - \xi). \end{aligned} \right\} \quad (17.4.29)$$

If we consider reactions initiated in pp collisions we recognize in (17.4.28) the distributions  $xq_j(x), x\bar{q}_j(x)$  that appeared in the formulae for the deep inelastic structure function  $F_2(x)$  [see (16.1.7)]. If these are known from the study of deep inelastic scattering, then the Drell-Yan cross-section is completely determined. There are difficulties, however, that we shall discuss later.

Notice that if we look at pairs produced with  $\xi = 0$  we have  $x_A = x_B = \tau$  and

$$sq^2 \frac{d^2\sigma}{dq^2 d\xi} \Big|_{\xi=0} = \frac{2\pi\alpha^2}{9} \sum_{\text{flavours}} Q_j^2 [q_j^A(\sqrt{\tau})\bar{q}_j^B(\sqrt{\tau}) + \bar{q}_j^A(\sqrt{\tau})q_j^B(\sqrt{\tau})] \quad (17.4.30)$$

so that we measure the product of distribution functions at  $x = \sqrt{\tau}$  directly.

If we integrate (17.4.28) over  $\xi$  we are left with the ‘scaling’ result

$$s^2 \frac{d\sigma}{dq^2} = F(\tau) \quad (17.4.31)$$

or, equivalently,

$$m^3 \frac{d\sigma}{dm} = 2\tau^2 F(\tau). \quad (17.4.32)$$

The right-hand sides depend upon the single variable  $\tau = q^2/s$ , while, in principle, the left-hand sides could depend upon both  $s$  and  $q^2$ . It should be noticed that on dimensional grounds the right-hand sides must depend only on dimensionless combinations of kinematical variables. If we are in a region where all masses are negligible,  $q^2/s$  is the only option available.

Equations (17.4.31) and (17.4.32) are often recast into the form

$$\frac{d\sigma}{dm^2}(h_A + h_B \rightarrow \ell^+ \ell^- X) = \frac{4\pi\alpha^2}{9m^4} \sum_{\text{flavours}} Q_j^2 \mathcal{L}_{jj}^{AB}(\tau), \quad (17.4.33)$$

where the ‘luminosity’, for flavours  $i, j$ ,

$$\begin{aligned} \mathcal{L}_{ij}^{AB}(\tau) &\equiv \int dx'_A dx'_B x'_A x'_B [q_i^A(x'_A) \bar{q}_j^B(x'_B) + \bar{q}_j^A(x'_A) q_i^B(x'_B)] \\ &\times \delta(x'_A x'_B - \tau) \end{aligned} \quad (17.4.34)$$

describes the rôle of the hadrons in supplying the quarks for the reaction. Let us now see to what extent the experimental situation supports this picture.

In comparing with experiment we must be careful to look only at kinematic regions in which our assumptions are justified. Keeping  $\tau$  fixed is not enough. We have assumed  $x'_A P, x'_B P$  large, (say compared with  $m_N$ ) so we should exclude *at least* the regions  $0 \leq x_A \leq m_N/P, 0 \leq x_B \leq m_N/P$ . A measurement at constant  $\tau$  corresponds to being on a hyperbola  $x_A = \tau/x_B$  (see Fig. 17.23) and as  $\xi$  varies we move along the hyperbola. To test scaling (17.4.31, 32) we must ensure that the hyperbola lies outside the shaded regions in Fig. 17.23. This corresponds to demanding  $\tau > \tau_s$  where  $\tau_s \equiv m_N/P = 2m_N/\sqrt{s}$ , which in terms of  $q^2$  means  $q^2 > q_s^2 \equiv 2m_N\sqrt{s}$ .

The approximate minimum safe values of  $\tau$  and  $q^2$  for some typical energies are shown in Table 17.2.

To test the detailed predictions (17.4.28) in proton–proton collisions is difficult since one requires the distribution function for antiquarks inside nucleons. These, it will be recalled, are important only at small  $x$  in deep inelastic scattering and, consequently, are difficult to determine accurately. On the other hand, in  $p\bar{p}$  collisions there is a strong source of antiquarks in the  $\bar{p}$  and one would take  $\bar{q}_j^{\bar{p}}(x) = q_j^p(x)$  so this will be an ideal reaction for testing the model.

Since mesons are principally made up of  $q\bar{q}$ , they too will be a strong source of  $\bar{q}$ , and it has indeed been found that the lepton pair produc-

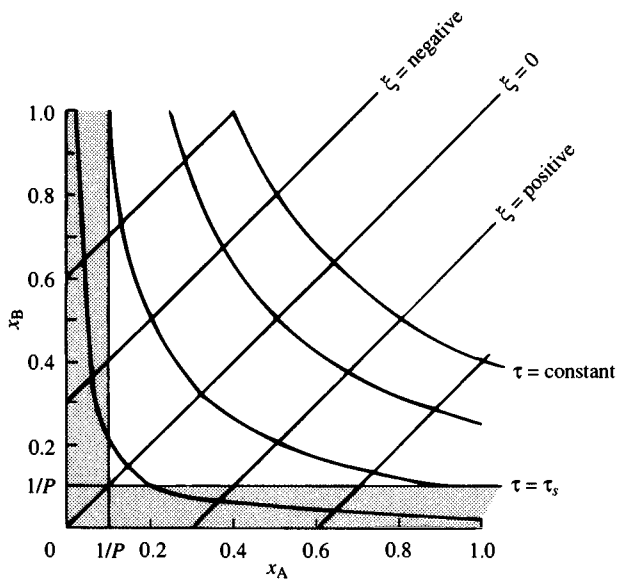


Fig. 17.23. Correspondence between variables  $(\xi, \tau)$  and the parton momentum fractions  $(x_A, x_B)$ .

Fixed target $p_L$ (GeV/c)	$\sqrt{s}$ (GeV)	$\tau_s$	$q_s^2$ (GeV/c) $^2$
30	7.5	0.27	15
50	9.7	0.21	19
200	19	0.11	38
300	24	0.08	48
400	27	0.07	54
800	39	0.05	78
	546	0.004	1092
	1800	0.001	3600

Table 17.2. Minimum safe values of  $\tau$  and  $q^2$  for application of the parton model in Drell-Yan reactions.

tion rate in  $\pi p$  collisions is *much greater* than in  $pp$ , as can be seen in Fig. 17.24. This is one of the most striking confirmations of the whole physical picture. Also shown are results obtained using an antiproton beam on a platinum target. There is a clear indication that the  $\bar{p}N$  cross-section is much bigger than the  $pN$  one.

In addition, because of the electromagnetic nature of the Drell-Yan process, one will expect quite different rates for  $\pi^\pm$  induced reactions.

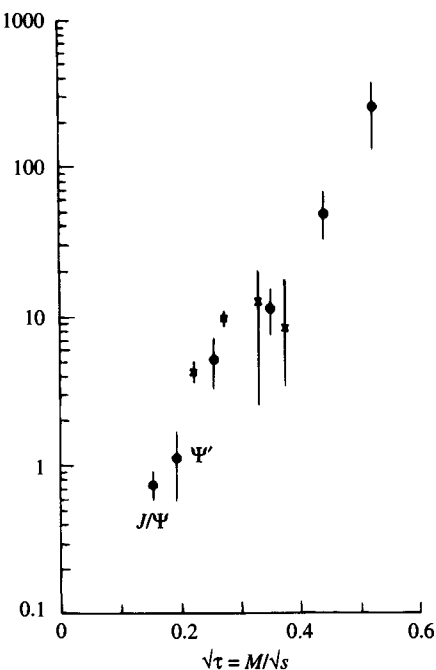


Fig. 17.24. Ratios of  $\pi^- N$  to  $pN$  (●) and  $\bar{p}N$  to  $pN$  (✕) data for the Drell-Yan process as function of  $\tau$ . [Data taken from Anderson *et al.* (1979), Hogan *et al.*, (1979) and Badier *et al.* (1979).]

Thus with  $\pi^+ \approx u\bar{d}$ ,  $\pi^- \approx d\bar{u}$ , and  $p \approx uud$  one will expect approximately to have [see (17.4.27)]

$$\frac{\sigma(\pi^+ p \rightarrow \mu^+ \mu^- X)}{\sigma(\pi^- p \rightarrow \mu^+ \mu^- X)} \simeq \frac{Q_{\bar{d}}^2}{2Q_{\bar{u}}^2} = \frac{1}{8}$$

and for isoscalar targets,

$$\frac{\sigma(\pi^+ N_0 \rightarrow \mu^+ \mu^- X)}{\sigma(\pi^- N_0 \rightarrow \mu^+ \mu^- X)} \simeq \frac{1}{4}.$$

Both these remarkable results are closely reproduced by the data.

All this is a nice confirmation of the general picture. If the parton distribution functions in the nucleon are assumed known from deep inelastic scattering, one can use the Drell-Yan process to learn about the  $q$  and  $\bar{q}$  distributions inside the meson: information which otherwise would be very difficult to come by.

In attempting a quantitative comparison with experiment, there is another point to note. The model describes what is often referred to as ‘the continuum’ production of lepton pairs, i.e. lepton pairs which are *not* the

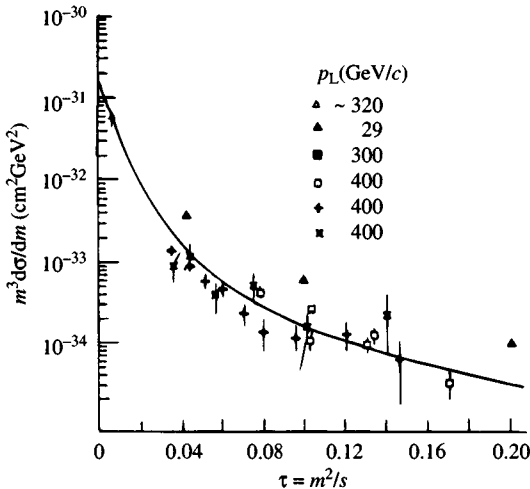


Fig. 17.25. Differential cross-section  $m^3 d\sigma/dm$  vs  $\tau$  for  $pp \rightarrow \mu^+ \mu^-$  at various laboratory momenta. (From Ellis, 1977.)

decay product of some  $J = 1$  meson resonance such as  $J/\Psi$  or  $\Upsilon$ . For data with  $m$  near the mass of such a resonance, it is essential to first subtract out those events in which it is believed that the leptons originate in the resonance.

In Fig. 17.25 is shown  $m^3 d\sigma/dm$  plotted against  $\tau$  for  $pp$  collisions. Most of the experimental points are at  $p_L \sim 300\text{--}400 \text{ GeV}/c$ , and cluster together fairly well. The points at  $p_L = 29 \text{ GeV}/c$  lie higher than these, suggesting that there is some  $s$  dependence. The curve is a theoretical calculation using parton distribution functions that yield a reasonable fit to the deep inelastic data. The general agreement between theory and the higher energy experiments is not bad.

It could be that scaling only sets in at energies somewhat higher than  $p_L = 29 \text{ GeV}/c$ . On the other hand, from Table 17.2 we see that at this energy  $\tau_s \simeq 0.3$  so all the  $29 \text{ GeV}/c$  points in Fig. 17.25 are way below the safe region in  $\tau$ . In fact, many of the points at  $300 \text{ GeV}/c$  and  $400 \text{ GeV}/c$  are also at values of  $\tau$  below  $\tau_s$ . So perhaps it is best not to draw any firm conclusions from these data.

In Figs. 17.26 and 17.27, data at  $p_L = 200 \text{ GeV}/c$ ,  $300 \text{ GeV}/c$  and  $400 \text{ GeV}/c$  are plotted, first vs  $m$  and then vs  $\tau$ . This time most of the points occur at safe values of  $\tau$ . The plot vs  $m$  shows a strong dependence on  $s$  whereas the plot vs  $\tau$  shows little or no dependence on  $s$ . Thus scaling seems to hold in support of the result (17.4.31).

Two other features of the data seem to support the physical picture:

1. The dependence of the cross-section on the  $A$ -value for various nuclei

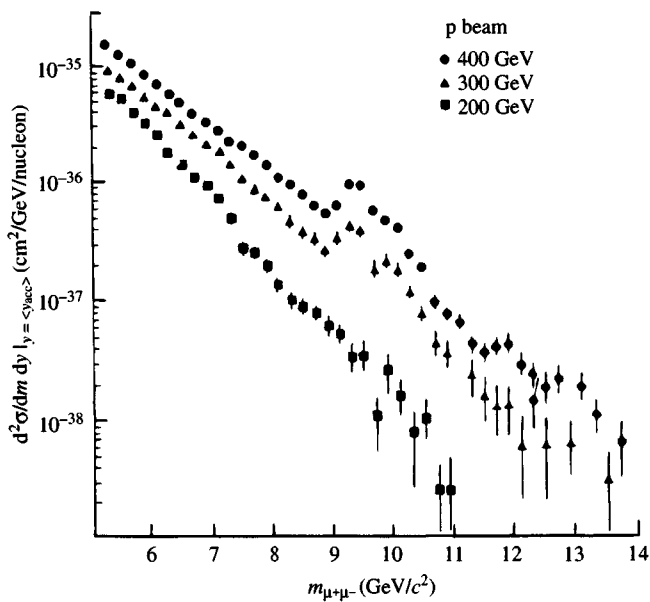


Fig. 17.26. Data on  $pp \rightarrow \mu^+\mu^-X$  at various energies plotted against  $m$ , the mass of the lepton pair. (From Vannucci, 1978.)

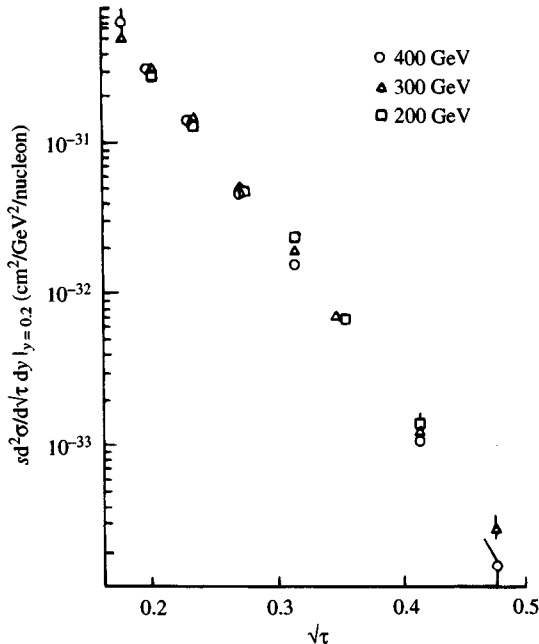


Fig. 17.27. Scaling shown by same data as in Fig. 17.26 when plotted against  $m^2/s$ . (From Vannucci, 1978.)

$m = \text{mass of lepton pair (GeV}/c^2)$	$\langle q_T \rangle (\text{GeV}/c)$
$4.5 < m < 5.5$	$1.59 \pm 0.16$
$5.5 < m < 6.5$	$1.69 \pm 0.34$
$6.5 < m < 8$	$1.32 \pm 0.24$
$8 < m < 11$	$1.64 \pm 0.52$

Table 17.3. Mean  $q_T$  of lepton pairs for several mass ranges.

(Be, Cu, Pt) goes like  $A^\alpha$  with  $\alpha$  very close to one ( $\alpha = 1.02 \pm 0.2$ ) which is what is expected since one is adding up over all the quarks inside the nucleus. Most data are on heavy nuclei, so the extraction of the cross-section *per nucleon* requires a good knowledge of  $\alpha$ . An early experiment had found  $\alpha \approx 1.12$  and consequently a smaller cross-section per nucleon than more recent experiments have yielded. New data using a hydrogen target are in good agreement with the nucleon data extracted using  $\alpha = 1$ . The situation is quite bizarre since the nucleon cross-section extracted with the presumably incorrect value of  $\alpha$  is in excellent quantitative agreement with the simple parton model prediction, whereas the newer data give a cross-section per nucleon which is a factor 1.5–2 larger than the theoretical prediction, and which might therefore have challenged the factor of  $\frac{1}{3}$  in (17.4.24) that arises from colour. But, *mirabile dictum*, calculations of the QCD corrections, which were expected to be small, have produced a factor of the order of 2! This extraordinary situation will be discussed in Section 23.11.

2. The angular distribution of, say, the  $\mu^+$  in the  $\mu^+ \mu^-$  CM system is in fair agreement with the  $1 + \cos^2 \theta$  distribution expected for a photon dominated process [see (8.3.4)].

In the above treatment we have neglected the parton momenta  $\kappa$  and  $\bar{\kappa}$  so that our lepton pair is produced with  $q_T = 0$ . In fact experiments indicate a surprisingly large value for  $\langle q_T \rangle$  in the production of pairs with a given mass, as shown in Table 17.3.

If both  $\kappa$  and  $\bar{\kappa}$  had a Gaussian probability distribution, say like  $e^{-\lambda \kappa^2}$ , then from (17.4.22) we would find that the  $q_T$  dependence is  $e^{-(\lambda/2)q_T^2}$ , implying that

$$\langle q_T \rangle = \sqrt{2} \langle \kappa \rangle. \quad (17.4.35)$$

Although we have no reason to believe that the distribution *is* Gaussian, (17.4.35) is likely to yield a reasonable estimate for  $\langle \kappa \rangle$ . The result for  $\langle \kappa \rangle$  is then surprisingly big, larger than 1 GeV/c! We shall see later that

there are QCD diagrams which yield muon pairs with large  $q_T$ . Thus it would be misleading to try to attribute the experimental  $q_T$  behaviour to a purely intrinsic  $\kappa_T$  distribution of the partons.

When the QCD effects are taken into account it is found that the data require intrinsic transverse momenta of order  $\langle \kappa_T^2 \rangle \approx 0.6(\text{GeV}/c)^2$ .

### 17.4.3 Production of heavy mesons by Drell-Yan mechanism

We have mentioned that the Drell-Yan analysis above refers to the continuum production of lepton-antilepton pairs, and that any events where the lepton pair originates from a heavy meson resonance should be subtracted out before comparing theory and experiment. We now consider lepton pair production via a resonance. In fact, we have already studied this question in Section 5.3.1 in connection with the production and detection of  $W^\pm$  and  $Z^0$  in  $p\bar{p}$  collisions, but we then neglected all details of the parton model.

Consider therefore the process

$$h_A + h_B \rightarrow V + X \quad \begin{matrix} \searrow \\ \ell^+ \ell^- \end{matrix} \quad (17.4.36)$$

where  $V$  is *any* neutral heavy vector meson whose coupling to quarks and leptons is some mixture of vector and axial-vector.

Suppose the interaction part of the Lagrangian is

$$\begin{aligned} \mathcal{L}_{\text{INT}} = & V^\mu \left[ \sum_j \bar{q}_j (\lambda_V^j \gamma_\mu - \lambda_A^j \gamma_\mu \gamma_5) q_j \right. \\ & \left. + \sum_\ell \bar{\ell} (\lambda_V^\ell \gamma_\mu - \lambda_A^\ell \gamma_\mu \gamma_5) \ell \right], \end{aligned} \quad (17.4.37)$$

where the sums run over all quarks and all leptons that couple to  $V$ .

Then the cross-section can easily be seen to be obtainable from (17.4.33) by the following substitutions:

$$\begin{aligned} 16\pi^2 \alpha^2 Q_j^2 \equiv [e^2][e^2 Q_j^2] \rightarrow & [(\lambda_V^j)^2 + (\lambda_A^j)^2][(\lambda_V^\ell)^2 + (\lambda_A^\ell)^2], \\ \frac{1}{m^4} \rightarrow & \frac{1}{(m^2 - M_V^2)^2 + M_V^2 \Gamma_V^2}, \end{aligned} \quad \left. \right\} \quad (17.4.38)$$

where  $M_V, \Gamma_V$  are the mass and full width of the  $V$  meson. There are no cross-terms in (17.4.38) because there is no vector–axial-vector interference in the total cross-section.

In Section 5.3.1 we derived a formula for the width of the  $W^+$  meson using the couplings appropriate to the WS theory. It is simple to see that

with the general couplings allowed in (17.4.37), and with the assumption that most of the decay is into light particles [see discussion after (5.3.15)], the formula (5.3.11) will be modified to

$$\Gamma_V \simeq \frac{M_V}{12\pi} \left\{ \sum_j \left[ (\lambda_V^j)^2 + (\lambda_A^j)^2 \right] + \sum_\ell \left[ (\lambda_V^\ell)^2 + (\lambda_A^\ell)^2 \right] \right\}, \quad (17.4.39)$$

the sum running over all quarks and leptons whose masses are much smaller than  $M_V$ .

If we are interested in the production cross-section for the vector mesons ( $W$  or  $Z^0$ ) we can treat them as elementary particles, ignoring their width, and replace eqn (17.4.19) by the cross-section for  $q_i + \bar{q}_j \rightarrow V$  (averaged over colour)

$$\hat{\sigma}(q_i \bar{q}_j \rightarrow V) = \frac{\pi}{3} \left[ (\lambda_V^j)^2 + (\lambda_A^j)^2 \right] \delta(q^2 - M_V^2). \quad (17.4.40)$$

The calculation leading to (17.4.40) is the same as that for  $\Gamma_V$ , aside from phase-space factors.

For the case of  $W$  and  $Z^0$  this becomes (see Section 9.6)

$$\hat{\sigma}(q_i \bar{q}_j \rightarrow W) = \frac{\pi}{3} \sqrt{2} G M_W^2 |V_{ij}|^2 \delta(q^2 - M_W^2) \quad (17.4.41)$$

where  $V_{ij}$  is the relevant KM matrix element, and [see eqns (5.1.4,5)]

$$\hat{\sigma}(q_j \bar{q}_j \rightarrow Z^0) = \frac{\pi}{3} \sqrt{2} G M_Z^2 \left[ (g_V^j)^2 + (g_A^j)^2 \right] \delta(q^2 - M_Z^2). \quad (17.4.42)$$

With the obvious changes implied by using (17.4.40) instead of (17.4.19), and bearing in mind that (17.4.40) includes a colour average, from (17.4.24) we obtain

$$\sigma^W(s) = \frac{\pi}{3} \sqrt{2} G \sum_{\substack{\text{flavours} \\ i,j}} |V_{ij}|^2 \mathcal{L}_{ij}^{AB}(\tau_W) \quad (17.4.43)$$

where  $\tau_W = M_W^2/s$  and the luminosity  $\mathcal{L}_{ij}$  was defined in (17.4.34). Similarly

$$\sigma^Z(s) = \frac{\pi}{3} \sqrt{2} G \sum_j \left[ (g_V^j)^2 + (g_A^j)^2 \right] \mathcal{L}_{jj}^{AB}(\tau_Z) \quad (17.4.44)$$

where  $\tau_Z = M_Z^2/s$ .

These expressions are the basis for the calculated cross-sections shown in Figs. 5.4 and 5.5. Note that (17.4.43) differs from the crude estimate (5.3.14) only by the KM matrix elements, which are not important, and by the luminosity factor  $\mathcal{L}$  which does have a significant effect on the cross-section, especially at very high energies, as was explained in the discussion following Figs. 5.4 and 5.5.

**Note added in proof: polarized deep inelastic scattering**

In Sections 15.6, 16.8 and 17.1.2 we emphasized the consequences of the European Muon Collaboration's (EMC) unexpected results in an experiment in 1987 on polarized deep inelastic lepton–hadron scattering, and we stressed the importance of testing the Bjorken sum rule by comparing neutron and proton data.

A recent experiment (1994) by the Spin Muon Collaboration (SMC) at CERN has confirmed the EMC results; and measurements using a deuterium target, by the SMC, and using a  ${}^3\text{He}$  target, by the E142 collaboration at SLAC, are consistent with the Bjorken sum rule when allowance is made for the different  $Q^2$ -values in the experiments. A complete survey is given in M. Anselmino, A. V. Efremov and E. Leader (1995), ‘The theory and phenomenology of polarized deep inelastic scattering’, to appear in *Physics Reports*.

# Appendix 1

## Elements of field theory

The aim of this appendix is to illustrate a few of the techniques of perturbative field theory and to explain the derivation of some of the results that have been quoted in the text. (For the notational conventions see after the Preface.)

### A1.1 Fields and creation operators

We consider first the expansion of a free field operator in terms of creation and annihilation operators. For a real scalar field describing quanta of mass  $\mu$  we write

$$\phi(x, t) = \int \frac{d^3 k}{(2\pi)^3 2\omega} [a(\mathbf{k}) e^{-ik \cdot x} + a^\dagger(\mathbf{k}) e^{ik \cdot x}], \quad (\text{A1.1.1})$$

where  $k_0 \equiv \omega = +\sqrt{\mathbf{k}^2 + \mu^2}$ .

The equal time commutation relations (20.2.5,6) then lead to

$$\begin{aligned} [a(\mathbf{k}), a(\mathbf{k}')] &= [a^\dagger(\mathbf{k}), a^\dagger(\mathbf{k}')] = 0 \\ [a(\mathbf{k}), a^\dagger(\mathbf{k}')] &= (2\pi)^3 2\omega \delta(\mathbf{k} - \mathbf{k}'), \end{aligned} \quad (\text{A1.1.2})$$

showing that  $a$  and  $a^\dagger$  are respectively destruction and creation operators.

The vacuum state  $|0\rangle$  is normalized to one:

$$\langle 0|0\rangle = 1 \quad (\text{A1.1.3})$$

and the one-particle states are defined by

$$|\mathbf{k}\rangle \equiv a^\dagger(\mathbf{k})|0\rangle. \quad (\text{A1.1.4})$$

From (A1.1.2) follows

$$\langle \mathbf{k}|\mathbf{k}'\rangle = (2\pi)^3 2\omega \delta(\mathbf{k} - \mathbf{k}') \quad (\text{A1.1.5})$$

and the very useful and simple result

$$\langle 0|\phi(x)|\mathbf{k}\rangle = e^{-ik \cdot x}. \quad (\text{A1.1.6})$$

For *free fields* (A1.1.2) and (A1.1.1) allow the calculation of the commutator of  $\phi(x), \phi^\dagger(y)$  for *arbitrary* times:

$$[\phi(x), \phi^\dagger(y)] = i\Delta(x - y; \mu), \quad (\text{A1.1.7})$$

where the singular function  $\Delta$  is given by

$$\Delta(x; \mu) \equiv -\frac{i}{(2\pi)^3} \int d^4k \delta(k^2 - \mu^2) \epsilon(k_0) e^{-ik \cdot x}, \quad (\text{A1.1.8})$$

and the step function  $\epsilon$  is defined by

$$\epsilon(k_0) = \pm 1 \text{ for } k_0 \gtrless 0. \quad (\text{A1.1.9})$$

It should be noted that the fields satisfy *local commutativity* or *microscopic causality*, i.e.

$$[\phi(x), \phi^\dagger(y)] = 0 \quad \text{if } (x - y)^2 < 0. \quad (\text{A1.1.10})$$

For free fields the vacuum expectation value of the *time ordered product* of two bosonic fields is

$$\begin{aligned} \langle 0|T[\phi(x)\phi^\dagger(y)]|0\rangle &\equiv \theta(x_0 - y_0)\langle 0|\phi(x)\phi^\dagger(y)|0\rangle \\ &\quad + \theta(y_0 - x_0)\langle 0|\phi^\dagger(y)\phi(x)|0\rangle \\ &= \Delta_F(x - y), \end{aligned} \quad (\text{A1.1.11})$$

where

$$\begin{aligned} \theta(x_0) &= 1 \text{ if } x_0 > 0 \\ &= 0 \text{ if } x_0 < 0 \end{aligned} \quad (\text{A1.1.12})$$

and  $\Delta_F$  is the causal or Feynman propagator function:

$$\Delta_F(x; \mu) \equiv \frac{i}{(2\pi)^4} \int d^4k \frac{e^{-ik \cdot x}}{k^2 - \mu^2 + i\epsilon}. \quad (\text{A1.1.13})$$

$\Delta_F$  is a Green's function for the Klein-Gordon equation, i.e. it satisfies

$$(\square_x + \mu^2)\Delta_F(x - y; \mu) = -\delta^4(x - y). \quad (\text{A1.1.14})$$

For a simple product of fields it is easy to see the existence of a singularity as the space-time points approach each other. One has

$$\langle 0|\phi(x)\phi(y)|0\rangle = \int \frac{d^3k}{(2\pi)^3 2\omega} e^{-ik \cdot (x-y)} \quad (\text{A1.1.15})$$

so that

$$\langle 0|\phi(x)\phi(x)|0\rangle = \int \frac{d^3k}{(2\pi)^3 2\omega} = \infty. \quad (\text{A1.1.16})$$

Using (A1.1.1) and (A1.1.2) it is a straightforward matter to examine the behaviour of any kind of product, either as  $x \rightarrow y$  or as  $(x - y)^2 \rightarrow 0$ , for free fields. This is the basis of the Wilson expansion.

For spinor fields of mass  $m$  we use

$$\begin{aligned} \psi(x) = \sum_{\text{spin projection}} \int & \frac{d^3 p}{(2\pi)^3 2E} [a_r(\mathbf{p}) u_r(\mathbf{p}) e^{-ip \cdot x} \\ & + b_r^\dagger(\mathbf{p}) v_r(\mathbf{p}) e^{ip \cdot x}], \end{aligned} \quad (\text{A1.1.17})$$

the spinors being normalized so that

$$u_r^\dagger(\mathbf{p}) u_{r'}(\mathbf{p}) = v_r^\dagger(\mathbf{p}) v_{r'}(\mathbf{p}) = 2E \delta_{rr'}, \quad (\text{A1.1.18})$$

where  $E \equiv +\sqrt{\mathbf{p}^2 + m^2}$ .

The canonical anticommutation relations lead to

$$\{b_r(\mathbf{p}), b_{r'}^\dagger(\mathbf{p})\} = \{a_r(\mathbf{p}), a_{r'}^\dagger(\mathbf{p})\} = (2\pi)^3 2E \delta_{rr'} \delta^3(\mathbf{p} - \mathbf{p}'), \quad (\text{A1.1.19})$$

all other anticommutators vanishing. It can be shown that  $a_r^\dagger(\mathbf{p})$  creates positive energy particles with momentum  $\mathbf{p}$  and spin projection  $r$ , whereas  $b_r(\mathbf{p})$  creates negative energy particles with momentum  $-\mathbf{p}$  and spin projection  $-r$ , the latter being interpreted as the destruction of a positive energy particle of opposite charge, of momentum  $\mathbf{p}$  and spin projection  $r$ .

The states for a single *particle* are defined by

$$|\mathbf{p}, r\rangle \equiv a_r^\dagger(\mathbf{p}) |0\rangle \quad (\text{A1.1.20})$$

and for *antiparticles* by

$$|\overline{\mathbf{p}}, \overline{r}\rangle \equiv b_r^\dagger(\mathbf{p}) |0\rangle. \quad (\text{A1.1.21})$$

From (A1.1.19) the normalization is then

$$\langle \mathbf{p}', r' | \mathbf{p}, r \rangle = \langle \overline{\mathbf{p}'}, \overline{r'} | \overline{\mathbf{p}}, \overline{r} \rangle = (2\pi)^3 2E \delta_{rr'} \delta^3(\mathbf{p}' - \mathbf{p}). \quad (\text{A1.1.22})$$

From (A1.1.17) one then deduces the simple results

$$\begin{aligned} \langle 0 | \psi(x) | \mathbf{p}, r \rangle &= u_r(\mathbf{p}) e^{-ip \cdot x} \\ \langle \mathbf{p}, r | \bar{\psi}(x) | 0 \rangle &= \bar{u}_r(\mathbf{p}) e^{ip \cdot x} \\ \langle 0 | \bar{\psi}(x) | \overline{\mathbf{p}}, \overline{r} \rangle &= \bar{v}_r(\mathbf{p}) e^{-ip \cdot x} \\ \langle \overline{\mathbf{p}}, \overline{r} | \psi(x) | 0 \rangle &= v_r(\mathbf{p}) e^{ip \cdot x} \end{aligned} \quad (\text{A1.1.23})$$

For a detailed exposition the reader is referred to Bjorken and Drell (1965). Note that, with our normalization, eqn (B.1) of their Appendix B holds for *all* particles irrespective of spin or mass. Care must be taken to use  $\Lambda_\pm = m \pm \not{p}$  instead of their eqn (A.3).

For hermitian spin 1 vector fields we use generically

$$A_\mu(x) = \sum_{\lambda} \int \frac{d^3k}{(2\pi)^3 2E} \{ \epsilon_\mu(\mathbf{k}, \lambda) a_\lambda(\mathbf{k}) e^{-ik \cdot x} + \epsilon_\mu^*(\mathbf{k}, \lambda) a_\lambda^\dagger(\mathbf{k}) e^{ik \cdot x} \} \quad (\text{A1.1.24})$$

where  $\lambda$  = helicity and  $\epsilon_\mu$  the polarization vector.

One has for fixed  $\mathbf{k}$  and  $\lambda$

$$k_\mu \epsilon^\mu(\mathbf{k}, \lambda) = 0, \quad \epsilon_\mu^*(\mathbf{k}, \lambda) \epsilon^\mu(\mathbf{k}, \lambda) = -1 \quad (\text{A1.1.25})$$

and for *massive* vector mesons of mass  $m$

$$\sum_{\lambda=1,0,-1} \epsilon_\mu^*(\mathbf{k}, \lambda) \epsilon_\nu(\mathbf{k}, \lambda) = -g_{\mu\nu} + k_\mu k_\nu / m^2. \quad (\text{A1.1.26})$$

The analogous result for physical photons and ‘physical’ gluons is

$$\sum_{\lambda=\pm 1} \epsilon_\mu^*(\mathbf{k}, \lambda) \epsilon_\nu(\mathbf{k}, \lambda) = -g_{\mu\nu} + \frac{k_\mu n_\nu + k_\nu n_\mu}{\mathbf{k} \cdot \mathbf{n}} - \frac{k_\mu k_\nu}{(\mathbf{k} \cdot \mathbf{n})^2} \quad (\text{A1.1.27})$$

where  $n$  is the unit time-like vector  $n^\mu = (1, 0, 0, 0)$ .

There are several cases of the use of (A1.1.24):

(a) for *photons* the sum over  $\lambda$  involves  $\lambda = \pm 1$  only.

(b) for *gluons*  $\lambda = \pm 1$  and in addition

$$A_\mu \rightarrow A_\mu^b, \quad a_\lambda(\mathbf{k}) \rightarrow a_\lambda^b(\mathbf{k})$$

where  $b$  is the colour label.

(c) for *W bosons*  $\lambda = 1, 0, -1$  and

$$A_\mu \rightarrow W_\mu^j, \quad j = 1, 2, 3.$$

Recall that the physical  $W_\mu$  are given by (Section 4.2)

$$W_\mu^\pm = \frac{1}{\sqrt{2}} (W_\mu^1 \mp i W_\mu^2)$$

The commutation relations for photons and gluons are discussed in Section 21.2. For massive vector mesons see Gasiorowicz (1976), Chapter 3.

The analogue of (A1.1.23) is

$$\langle 0 | A_\mu(x) | \mathbf{k}, \lambda \rangle = \epsilon_\mu(\mathbf{k}, \lambda) e^{-ik \cdot x}, \quad \langle \mathbf{k}, \lambda | A_\mu(x) | 0 \rangle = \epsilon_\mu^*(\mathbf{k}, \lambda) e^{ik \cdot x} \quad (\text{A1.1.28})$$

## A1.2 Parity, charge conjugation and G-parity

### A1.2.1 Parity

For the fields we have been considering the parity operator  $\mathcal{P}$  has the following effect:

$$\mathcal{P}\phi(\mathbf{x}, t)\mathcal{P}^{-1} = \pm\phi(-\mathbf{x}, t) \quad \text{for scalar/pseudo-scalar fields, (A1.2.1)}$$

$$\mathcal{P}\psi(\mathbf{x}, t)\mathcal{P}^{-1} = \gamma_0\psi(-\mathbf{x}, t), \quad (\text{A1.2.2})$$

$$\mathcal{P}A_j(\mathbf{x}, t)\mathcal{P}^{-1} = -A_j(-\mathbf{x}, t) \quad j = 1, 2, 3 \quad \left. \right\} \text{ for photon or (A1.2.3)}$$

$$\mathcal{P}A_0(\mathbf{x}, t)\mathcal{P}^{-1} = A_0(-\mathbf{x}, t) \quad \left. \right\} \text{ gluon fields (A1.2.4)}$$

It follows that  $\bar{\psi}\gamma_\mu\psi$  is a vector, whereas  $\bar{\psi}\gamma_\mu\gamma_5\psi$  is a pseudo-vector, i.e. if

$$\begin{aligned} V_\mu(\mathbf{x}, t) &\equiv \bar{\psi}(\mathbf{x}, t)\gamma_\mu\psi(\mathbf{x}, t) \\ A_\mu(\mathbf{x}, t) &\equiv \bar{\psi}(\mathbf{x}, t)\gamma_\mu\gamma_5\psi(\mathbf{x}, t), \end{aligned} \quad \left. \right\} \quad (\text{A1.2.5})$$

then

$$\begin{aligned} \mathcal{P}V_j(\mathbf{x}, t)\mathcal{P}^{-1} &= -V_j(-\mathbf{x}, t) \quad j = 1, 2, 3 \\ \mathcal{P}V_0(\mathbf{x}, t)\mathcal{P}^{-1} &= V_0(-\mathbf{x}, t), \end{aligned} \quad \left. \right\} \quad (\text{A1.2.6})$$

whereas

$$\begin{aligned} \mathcal{P}A_j(\mathbf{x}, t)\mathcal{P}^{-1} &= A_j(-\mathbf{x}, t) \quad j = 1, 2, 3 \\ \mathcal{P}A_0(\mathbf{x}, t)\mathcal{P}^{-1} &= -A_0(-\mathbf{x}, t). \end{aligned} \quad \left. \right\} \quad (\text{A1.2.7})$$

### A1.2.2 Charge conjugation

The charge conjugation operator  $\mathcal{C}$  has the following effect:

$$\mathcal{C}A_\mu(\mathbf{x}, t)\mathcal{C}^{-1} = -A_\mu(\mathbf{x}, t) \quad \text{for photons.} \quad (\text{A1.2.8})$$

Thus an  $n$ -photon state is an eigenstate of  $\mathcal{C}$  with eigenvalue  $(-1)^n$ , known as the charge parity.

For the neutral  $\pi^0$  field one has

$$\mathcal{C}\phi^{(0)}(\mathbf{x})\mathcal{C}^{-1} = \phi^{(0)}(\mathbf{x}), \quad (\text{A1.2.9})$$

whereas for the charged fields

$$\mathcal{C}\phi(\mathbf{x})\mathcal{C}^{-1} = \phi^\dagger(\mathbf{x}), \quad \mathcal{C}\phi^\dagger(\mathbf{x})\mathcal{C}^{-1} = \phi(\mathbf{x}). \quad (\text{A1.2.10})$$

In terms of Hermitian fields  $\phi_{1,2}(x)$

$$\left. \begin{aligned} \phi(x) &= \frac{1}{\sqrt{2}}(\phi_1 + i\phi_2) \\ \phi^\dagger(x) &= \frac{1}{\sqrt{2}}(\phi_1 - i\phi_2) \end{aligned} \right\} \quad (\text{A1.2.11})$$

$$\mathcal{C}\phi_1(x)\mathcal{C}^{-1} = \phi_1(x), \quad \mathcal{C}\phi_2(x)\mathcal{C}^{-1} = -\phi_2(x), \quad (\text{A1.2.12})$$

so that  $\mathcal{C}$  causes a reflection in the 1–3 plane of isospace. It can be seen that only an electrically neutral state, and in particular only a state with equal numbers of  $\pi^+$  and  $\pi^-$ , can be an eigenstate of  $\mathcal{C}$ .

For spinors, if  $\alpha, \beta$  label spin indices,

$$\left. \begin{aligned} \mathcal{C}\psi_\alpha(x)\mathcal{C}^{-1} &= (C\gamma^0)_{\alpha\beta}\psi_\beta^\dagger(x) \\ \mathcal{C}\bar{\psi}_\alpha(x)\mathcal{C}^{-1} &= -\psi_\beta(x)(C^{-1})_{\beta\alpha}, \end{aligned} \right\} \quad (\text{A1.2.13})$$

where  $C$  is a  $4 \times 4$  matrix

$$C = i\gamma^2\gamma^0 = -C^{-1} = -C^T, \quad (\text{A1.2.14})$$

which has the property of taking the transpose of the  $\gamma$  matrices

$$C\gamma_\mu C^{-1} = -\gamma_\mu^T. \quad (\text{A1.2.15})$$

From (A1.2.13) and (A1.1.17) follows

$$\mathcal{C}b(\mathbf{p}, r)\mathcal{C}^{-1} = a(\mathbf{p}, r), \quad \mathcal{C}a^\dagger(\mathbf{p}, r)\mathcal{C}^{-1} = b^\dagger(\mathbf{p}, r), \quad (\text{A1.2.16})$$

so that  $\mathcal{C}$  has the effect of interchanging particles and antiparticles.

It follows that the vector current built from coloured quarks (Section 21.3) behaves under charge conjugation as follows:

$$\begin{aligned} \mathcal{C}\bar{\psi}_i\gamma^\mu\left(\frac{1}{2}\lambda^a\right)_{ij}\psi_j\mathcal{C}^{-1} &= (\mathcal{C}\bar{\psi}_i\mathcal{C}^{-1})\gamma^\mu\left(\frac{1}{2}\lambda^a\right)_{ij}(\mathcal{C}\psi_j\mathcal{C}^{-1}) \\ &= -\psi_{i,\beta}(C^{-1})_{\beta\alpha}\gamma_{\alpha\delta}^\mu\left(\frac{1}{2}\lambda^a\right)_{ij}(C\gamma^0)_{\delta\rho}\psi_{j,\rho}^\dagger \\ &= \psi_{i,\beta}(\gamma^{\mu T})_{\beta\sigma}\left(\frac{1}{2}\lambda^a\right)_{ij}\gamma_{\sigma\rho}^0\psi_{j,\rho}^\dagger \end{aligned}$$

by (A1.2.15)

$$= -\bar{\psi}_j\gamma^\mu\left(\frac{1}{2}\lambda^a\right)_{ij}\psi_i, \quad (\text{A1.2.17})$$

where the minus sign comes from the fact that  $\psi_i, \bar{\psi}_j$  anticommute.

For leptons, with no colour,  $\frac{1}{2}\lambda^a$  is replaced by the unit matrix in the vector current, and one has

$$\mathcal{C}\bar{\psi}\gamma^\mu\psi\mathcal{C}^{-1} = -\bar{\psi}\gamma^\mu\psi, \quad (\text{A1.2.18})$$

which, with (A1.2.8), shows that the electromagnetic coupling of photons and leptons is invariant under charge conjugation.

In order to make the coupling of gluons to coloured quarks invariant under charge conjugation, from (A1.2.17) we have to demand that

$$\mathcal{C} \left( \frac{1}{2} \lambda^a \right)_{ij} \mathbf{A}_\mu^a \mathcal{C}^{-1} = - \left( \frac{1}{2} \lambda^a \right)_{ji} \mathbf{A}_\mu^a. \quad (\text{A1.2.19})$$

For a state of a fermion and its antiparticle with orbital angular momentum  $l$  and total spin  $S$  one has

$$\mathcal{C}|l, S\rangle = (-1)^{l+S}|l, S\rangle. \quad (\text{A1.2.20})$$

It follows from this that the  ${}^3S_1$  state of positronium decays into three photons whereas the  ${}^1S_0$  state decays into two photons.

The situation is more complicated for  $q\bar{q} \rightarrow$  gluons as a consequence of the more involved rule (A1.2.19), and was discussed in Section 11.6.

The consequences of CPT invariance on the structure of matrix elements is discussed in Appendix 6.

### A1.2.3 G-parity

This is the combined operation of charge conjugation and a rotation of  $\pi$  about the ‘2’ axis of isospace:

$$G \equiv \mathcal{C} e^{i\pi T_2}, \quad (\text{A1.2.21})$$

where  $T_2$  is the generator of rotations about the ‘2’ axis.

The useful point is that, unlike  $\mathcal{C}$ , charged states can be eigenstates of  $G$ . For example, for pions

$$G\phi_i G^{-1} = -\phi_i, \quad (\text{A1.2.22})$$

where  $i$  is the isospin label.

Thus the  $G$ -parity of an  $n$ -pion state is  $(-1)^n$ , and this leads to various selection rules for hadronic reactions.

For further details consult Gasiorowicz (1976), Chapters 16, 17 and 30.

## A1.3 The S-matrix

The  $S$ -matrix in perturbation theory is given as follows.

The Hamiltonian in the so-called ‘interaction picture’ is first split into a free field part and an interaction (perturbative) part

$$H = H_0 + H_I. \quad (\text{A1.3.1})$$

Then, short circuiting an involved and subtle argument, if  $H_I$  is considered as made up of an expression involving free field operators, the

*S*-operator is given by

$$\begin{aligned} S &= 1 - i \int_{-\infty}^{\infty} dt_1 H_I(t_1) + \frac{(-i)^2}{2!} \int_{-\infty}^{\infty} dt_1 dt_2 T[H_I(t_1) H_I(t_2)] + \dots \\ &= \sum_{n=0}^{\infty} \frac{(-i)^n}{n!} \int_{-\infty}^{\infty} dt_1 \cdots dt_n T[H_I(t_1) \cdots H_I(t_n)]. \end{aligned} \quad (\text{A1.3.2})$$

When one substitutes the actual form of  $H_I$  for a particular theory one has in (A1.3.2) a perturbative expansion for  $S$ . It is then not difficult to read off the rules for a diagrammatic representation of the perturbation series. The subtlety in a gauge theory is the problem of finding  $H$ . The Lagrangian contains redundant variables which have to be constrained by gauge fixing terms, and one is then dealing with the quantum version of a dynamical system subject to holonomic constraints—a non-trivial matter. It is partly for this reason that the Feynman integral approach is preferred for those theories.

Since the Hamiltonian is the space integral of the Hamiltonian density

$$H_I(t) = \int d^3x \mathcal{H}_I(t, x) \quad (\text{A1.3.3})$$

the expression for  $S$  is often written in the form

$$S = \sum_{n=0}^{\infty} \frac{(-i)^n}{n!} \int d^4x_1 d^4x_2 \cdots d^4x_n T[\mathcal{H}_I(x_1) \mathcal{H}_I(x_2) \cdots \mathcal{H}_I(x_n)] \quad (\text{A1.3.4})$$

known as the Dyson perturbative expansion.

# Appendix 2

## Feynman rules for QED, QCD and the SM

We give here, without derivation, the rules for calculating (up to a sign) what is known as the Feynman amplitude  $\mathcal{M}$  in QED, QCD and the SM. We illustrate with a few topical examples. A detailed treatment can be found in Bjorken and Drell (1965) and in Cutler and Sivers (1978).

### A2.1 Relation between $S$ -matrix and Feynman amplitude

The rules for calculating the Feynman amplitude  $\mathcal{M}$  are essentially universal and irrespective of the normalization convention for the states.

Clearly, however, the matrix elements  $\langle f|S|i\rangle$  of the  $S$ -operator depend upon the normalization convention, so the relationship between  $\langle f|S|i\rangle$  and  $\mathcal{M}$  will be convention dependent.

With our relativistically invariant normalization

$$\langle \mathbf{p}'|\mathbf{p}\rangle = (2\pi)^3 2E \delta^3(\mathbf{p}' - \mathbf{p}) \quad (\text{A2.1.1})$$

for all particles, one has the simple result

$$\langle f|S|i\rangle = \langle f|i\rangle + (2\pi)^4 \delta^4(P_f - P_i) \mathcal{M}. \quad (\text{A2.1.2})$$

Often it is useful to use other normalization conventions. To read off the analogue of (A2.1.2) it is simplest to avoid the complications of ‘continuum normalization’ and Dirac  $\delta$ -function by quantizing the system in a finite volume  $V$ . The key connection is the equivalence

$$(2\pi)^3 \delta^3(\mathbf{p}' - \mathbf{p}) \longleftrightarrow V \delta_{\mathbf{p}'\mathbf{p}} \quad (\text{A2.1.3})$$

so that our normalization corresponds to

$$\langle \mathbf{p}'|\mathbf{p}\rangle = V 2E \delta_{\mathbf{p}'\mathbf{p}} \quad \text{or} \quad \langle \mathbf{p}|\mathbf{p}\rangle = V 2E. \quad (\text{A2.1.4})$$

If we prefer to utilize states normalized to unity in the volume  $V$ , i.e.

$\langle \mathbf{p} | \mathbf{p} \rangle = 1$ , then we will have

$$S_{f_i} = \delta_{f_i} + (2\pi)^4 \delta^4(P_f - P_i) \prod_{\substack{\text{all} \\ \text{particles } j}} \left( \frac{1}{V2E_j} \right)^{\frac{1}{2}} \mathcal{M}. \quad (\text{A2.1.5})$$

As a consequence of our normalization convention  $u^\dagger u = v^\dagger v = 2E$  for spinors (see the notational conventions) the cross-section for any process  $1 + 2 \rightarrow 3 + 4 + \dots + n$  is expressed in terms of  $\mathcal{M}$  by formula (B.1) of Appendix B of Bjorken and Drell (1964), for all particles, *mesons* or *baryons*

$$\begin{aligned} d\sigma = & \frac{1}{|\mathbf{v}_1 - \mathbf{v}_2|} \frac{1}{2E_1} \frac{1}{2E_2} \overline{|\mathcal{M}|^2} \frac{d^3 \mathbf{p}_3}{(2\pi)^3 2E_3} \dots \frac{d^3 \mathbf{p}_n}{(2\pi)^3 2E_n} \times \\ & \times (2\pi)^4 \delta^4(p_3 + p_4 + \dots + p_n - p_1 - p_2) \end{aligned} \quad (\text{A2.1.6})$$

where  $\mathbf{v}_1$  and  $\mathbf{v}_2$  are the velocities of the beam and target particles in a reference frame where their collision is collinear.

In (A2.1.6)  $\overline{|\mathcal{M}|^2}$  is the modulus squared of the Feynman amplitude summed over final spins and colours and averaged over initial spins and colours.

For the differential decay rate of a particle of mass  $M$  in its rest frame, where its 4-momentum is  $p = (M, 0, 0, 0)$ ,

$$\begin{aligned} d\Gamma = & \frac{1}{2M} \overline{|\mathcal{M}|^2} \frac{d^3 \mathbf{p}_1}{(2\pi)^3 2E_1} \dots \frac{d^3 \mathbf{p}_n}{(2\pi)^3 2E_n} \times \\ & \times (2\pi)^4 \delta^4(p - p_1 - p_2 - \dots - p_n) \end{aligned} \quad (\text{A2.1.7})$$

Note that in both (A2.1.6 and 7) care must be exercised when dealing with identical particles. When integrating over phase space, if there are  $n_j$  particles of type  $j$  in the final state then one must include a factor  $1/(n_j!)$ .

Many useful formulae needed in doing the spin sums implied in  $\overline{|\mathcal{M}|^2}$ , especially the traces of products of Dirac matrices, can be found in Bjorken and Drell (1964) Appendix A and Section 7.2.

## A2.2 QCD and QED

In this section: Greek indices are Lorentz tensor indices;  $a, b, c, d$  are gluon colour indices;  $l, j$  are quark colour indices;  $k, p, q, r$  label 4-momenta. The  $f_{abc}$  and the matrices  $t^a$  are discussed in Section 21.3. No flavour indices are shown; all vertices are diagonal in flavour. The strong interaction coupling constant is  $g$ , and is related to the  $\alpha_s$  used throughout the book by  $\alpha_s = g^2/4\pi$ .  $Q_f$  is the electric charge of fermion  $f$  in units of  $e$ .

The rules are given for two classes of gauges:

- the *covariant* gauges labelled by ‘ $a$ ’, as discussed in Section 21.2 ( $a = 1$  is the Feynman gauge;  $a = 0$  the Landau gauge) in which the subsidiary condition, at least at the classical level, is  $\partial^\mu A_\mu^c = 0$  for all values of the colour label  $c$ , and the gauge fixing term in the Lagrangian is  $(-1/2a)\Sigma_c(\partial^\mu A_\mu^c)^2$ .
- an *axial* gauge, one of a family again labelled by ‘ $a$ ’, in which the subsidiary condition is  $n^\mu A_\mu^c = 0$  for all  $c$ , where  $n^\mu$  is a fixed space-like or null 4-vector, and where the gauge fixing term in the Lagrangian is  $(-1/2a)\Sigma_c(n^\mu A_\mu^c)^2$ .

We allow the quarks to have a mass parameter  $m$  which should be put to zero when working with massless quarks.

(a) *The propagators*

$$\text{lepton} \xrightarrow[p]{} \frac{i(p+m)}{p^2 - m^2 + i\epsilon} \quad (\text{A2.2.1})$$

$$\text{quark } j \xrightarrow[p]{} l \delta_{jl} \frac{i(p+m)}{p^2 - m^2 + i\epsilon} \quad (\text{A2.2.2})$$

In the above the arrow indicates the flow of fermion number and  $p$  is the 4-momentum in that direction. (Note:  $j, l$  are quark colour labels,  $b, c$  gluon and ghost colour labels.)

$$\text{gluon } b, \beta \xrightarrow[k]{\text{wavy line}} c, \gamma \quad \delta_{bc} \frac{i}{k^2 + i\epsilon} \times \begin{cases} \text{Covariant gauges:} \\ \left[ -g_{\beta\gamma} + (1-a) \frac{k_\beta k_\gamma}{k^2 + i\epsilon} \right] \quad (\text{A2.2.3}) \end{cases}$$

$$\text{Axial gauges with } a=0: \quad \left[ -g_{\beta\gamma} + \frac{n_\beta k_\gamma + n_\gamma k_\beta}{n \cdot k} - \frac{n^2 k_b k_\gamma}{(n \cdot k)^2} \right] \quad (\text{A2.2.4})$$

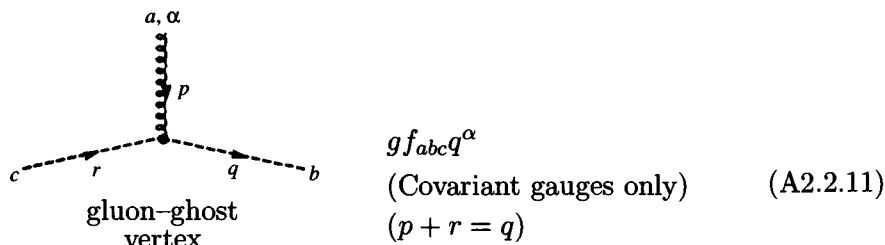
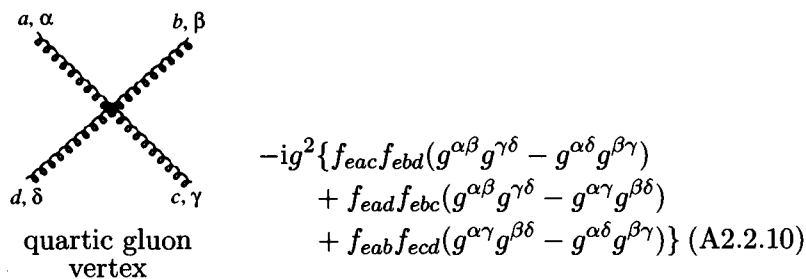
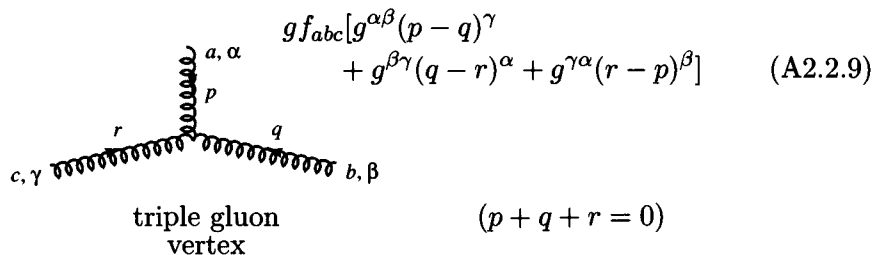
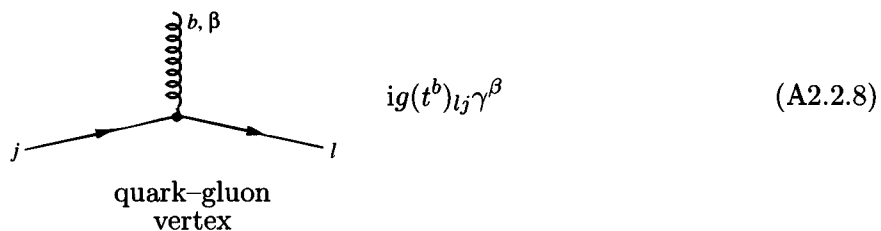
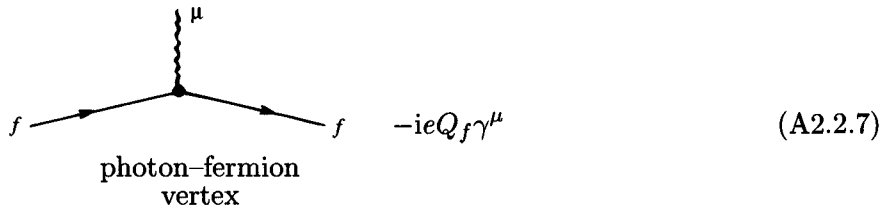
Note that in the above axial gauges the propagator is orthogonal to  $n^\beta$ ; and is orthogonal to  $k^\beta$  when  $k^2 = 0$ .

$$\text{photon } \alpha \xrightarrow[k]{\text{wavy line}} \beta \quad i \frac{-g_{\alpha\beta}}{k^2 + i\epsilon} \quad (\text{A2.2.5})$$

$$\text{ghost } b \xrightarrow[p]{} c \quad \delta_{bc} \frac{i}{p^2 + i\epsilon} \quad (\text{Covariant gauges only})$$

$$(\text{A2.2.6})$$

## (b) The vertices



Note that the ghosts are scalar fields, but a factor  $(-1)$  must be included for each closed loop, as is the case for fermions. Note also that the sign of  $\mathcal{M}$ , if it is important, has to be determined by comparing the order of the fermion operators in the diagram with their order in the expression for the  $S$ -operator.

### A2.3 The SM

In this section: Greek indices are Lorentz indices;  $i, j$  label generations.

$u_i = (u, c, t)$ ,  $d_j = (d, s, b)$ ;  $V_{ij}$  are the Kobayashi–Maskawa matrix elements [see eqns (9.2.6 and 7)].

For the  $W^\pm$  and  $Z^0$  propagator ( $M = M_W$  or  $M_Z$ ):

$$\frac{\alpha}{k} \text{~~~~~} \beta = \frac{i[-g_{\alpha\beta} + k_\alpha k_\beta/M^2]}{k^2 - M^2 + i\epsilon} \quad (\text{A2.3.1})$$

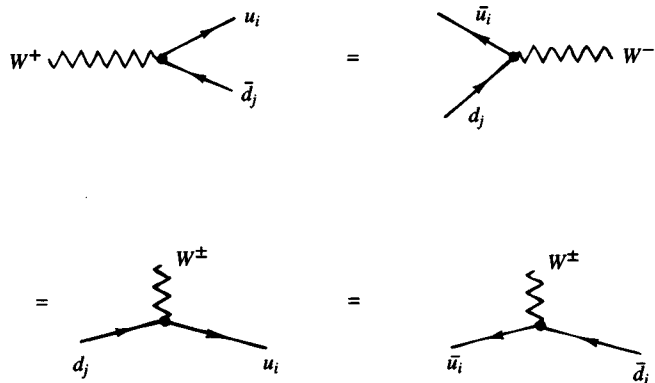
For the vertices (all results are independent of colour):

#### 1 Charged weak hadronic interactions.

Let us introduce generation labels  $i, j = 1, 2, 3$  such that

$$(u_1, u_2, u_3) \equiv (u, c, t) \quad \text{and} \quad (d_1, d_2, d_3) \equiv (d, s, b)$$

then from (9.3.8), (9.3.10) and (9.2.1) one deduces



$$= -\frac{ie}{2\sqrt{2}\sin\theta_W} V_{ij} \gamma^\mu (1 - \gamma_5) \quad (\text{A2.3.2})$$

$$\begin{aligned}
 & \text{W- vertex with } d_j \text{ and } \bar{u}_i \quad = \quad \bar{d}_j \rightarrow \text{W+ vertex with } u_i \\
 & \text{W± vertex with } u_i \text{ and } d_j \quad = \quad \bar{d}_j \rightarrow \text{W± vertex with } \bar{u}_i \\
 & = -\frac{ie}{2\sqrt{2}\sin\theta_W} V_{ij}^* \gamma^\mu (1 - \gamma_5) \quad (\text{A2.3.3})
 \end{aligned}$$

By convention all the topologically similar vertices are given the same sign in the Feynman rules. The overall sign of a diagram has to be determined by comparing the order of the fermion operator in the diagram with their normal order in the  $S$  operator.

## 2 Neutral weak hadronic interactions.

From (9.3.1), (9.3.2) and (9.3.3) we get, with  $q_j = u_j$  or  $d_j$ ,

$$\begin{aligned}
 & \text{Z0 vertex with } q_j \text{ and } \bar{q}_j \quad = \quad \bar{q}_j \rightarrow \text{Z0 vertex with } q_j \\
 & \text{Z0 vertex with } q_j \text{ and } q_j \quad = \quad \bar{q}_j \rightarrow \text{Z0 vertex with } \bar{q}_j \\
 & = ie\gamma^\mu (v_j - a_j\gamma_5) \quad (\text{A2.3.4})
 \end{aligned}$$

where

$$\begin{aligned}
 v_j &= \frac{I_3^{jL} - 2Q_j \sin^2\theta_W}{2\sin\theta_W \cos\theta_W} & a_j &= \frac{I_3^{jL}}{2\sin\theta_W \cos\theta_W} \\
 &\equiv \frac{g_V^j}{2\sin\theta_W \cos\theta_W} & &\equiv \frac{g_A^j}{2\sin\theta_W \cos\theta_W} \\
 & & & \quad (\text{A2.3.5})
 \end{aligned}$$

where  $I_3^{jL}$  is the third component of weak isospin of the left-handed part of the quark  $j$ , i.e.  $I_3^{jL} = \frac{1}{2}$  for  $u, c, t$ ;  $= -\frac{1}{2}$  for  $d, s, b$ . Concerning overall signs see comment in (1) above.

3 Higgs coupling to quarks.

$$\begin{aligned}
 & \text{H} \xrightarrow{\text{---}} q_j \quad \bar{q}_j \\
 & = \\
 & \text{H} \xrightarrow{\text{---}} q_j \quad q_j \\
 & = \\
 & \text{H} \xrightarrow{\text{---}} \bar{q}_j \quad \bar{q}_j
 \end{aligned}$$

$$= i \frac{\sqrt{\pi\alpha}}{\sin\theta_W} \left( \frac{m_j}{M_W} \right) I \quad (\text{A2.3.6})$$

where  $m_j$  is the mass of quark  $j$  and  $I$  is the unit  $4 \times 4$  matrix. Concerning overall signs see comment in (1) above.

## A2.4 Some examples of Feynman amplitudes

A full and detailed calculation of a reaction rate, starting from a Feynman amplitude, is given in Section 8.6.

Here, for pedagogical reasons, we give a few examples of partonic Feynman diagrams and their corresponding amplitudes. As usual for any  $2 \rightarrow 2$  partonic process

$$A(p_1) + B(p_2) \rightarrow C(p_3) + D(p_4) \quad (\text{A2.4.1})$$

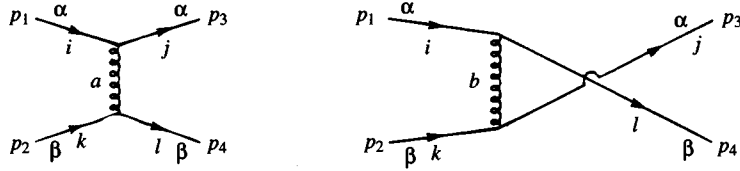
we define the partonic version of the Mandelstam variables:

$$\begin{aligned}
 \hat{s} &= (p_1 + p_2)^2 \\
 \hat{t} &= (p_1 - p_3)^2 \\
 \hat{u} &= (p_1 - p_4)^2.
 \end{aligned} \quad (\text{A2.4.2})$$

1 Quark-quark scattering.

$$q_\alpha(p_1) + q_\beta(p_2) \rightarrow q_\alpha(p_3) + q_\beta(p_4) \quad (\text{A2.4.3})$$

where  $\alpha, \beta$  are flavour labels. The two lowest order diagrams are



where  $i, j, k, l$  label quark colours and  $a, b$  the gluon colours. Note that since a gluon is flavour-blind the  $u$ -channel diagrams only contributes if  $\alpha = \beta$ , i.e. scattering of quarks of the same flavour.

Choosing the Feynman gauge  $a = 1$  in (A2.2.3) and using (A2.2.7) one reads off (the  $i\epsilon$  may be put to zero here):

$$\begin{aligned} \mathcal{M}_{(t)}(q_\alpha^i q_\beta^k \rightarrow q_\alpha^j q_\beta^l) &= \left[ \bar{u}_\beta(p_4) ig(t^b)_{lk} \gamma^\mu u_\beta(p_2) \right] \frac{-ig_{\mu\nu}}{\hat{t}} \times \\ &\quad \times \left[ \bar{u}_\alpha(p_3) ig(t^b)_{ji} \gamma^\nu u_\alpha(p_1) \right] \\ &= i \frac{g^2}{\hat{t}} (t^b_{lk} t^b_{ji}) \left[ \bar{u}_\beta(p_4) \gamma_\mu u_\beta(p_2) \right] \times \\ &\quad \times \left[ \bar{u}_\alpha(p_3) \gamma^\mu u_\alpha(p_1) \right], \end{aligned} \quad (\text{A2.4.4})$$

$$\begin{aligned} \mathcal{M}_{(u)}(q_\alpha^i q_\beta^k \rightarrow q_\alpha^j q_\beta^l) &= (-1) \delta_{\alpha\beta} \left[ \bar{u}_\alpha(p_3) ig(t^b)_{jk} \gamma^\mu u_\beta(p_2) \right] \times \\ &\quad \times \left( \frac{-ig_{\mu\nu}}{\hat{u}} \right) \left[ \bar{u}_\beta(p_4) ig(t^b)_{li} \gamma^\nu u_\alpha(p_1) \right] \\ &= (-1) \delta_{\alpha\beta} i \frac{g^2}{\hat{u}} (t^b_{jk} t^b_{li}) \left[ \bar{u}_\alpha(p_3) \gamma_\mu u_\beta(p_2) \right] \times \\ &\quad \times \left[ \bar{u}_\beta(p_4) \gamma^\mu u_\alpha(p_1) \right]. \end{aligned} \quad (\text{A2.4.5})$$

The factor  $(-1)$  in (A2.4.5) does not come from the Feynman rules. It comes from comparing the order of the fermion operators underlying the two diagrams. Symbolically we have:

$$\begin{aligned} \mathcal{M}_{(t)} : & (\bar{\psi}_3 \psi_1) (\bar{\psi}_4 \psi_2) \\ \mathcal{M}_{(u)} : & (\bar{\psi}_4 \psi_1) (\bar{\psi}_3 \psi_2). \end{aligned} \quad (\text{A2.4.6})$$

To rearrange the operators in  $\mathcal{M}_{(u)}$  into the order occurring in  $\mathcal{M}_{(t)}$  requires three interchanges (i.e. an odd number); hence the relative  $(-1)$ .

In the above the colour  $b$  is, of course, summed over. Rules for doing colour sums are given in Section A2.5. To calculate the unpolarized cross-section involves forming

$$|\mathcal{M}|^2 \equiv |\mathcal{M}_{(t)} + \mathcal{M}_{(u)}|^2 \quad (\text{A2.4.7})$$

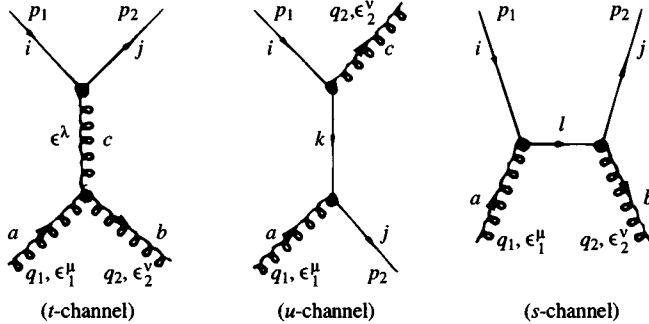
summing over final spins and colours, averaging over initial colours and spins.

## 2 Quark-gluon scattering.

There are three diagrams for

$$q(p_1) + G_a(q_1) \rightarrow q(p_2) + G_b(q_2) \quad (\text{A2.4.8})$$

The amplitude does not depend on the quark flavour so it is not indicated. (Of course initial and final quarks have the same flavour.)



Here

$$\hat{s} = (p_1 + q_1)^2, \quad \hat{t} = (p_1 - p_2)^2, \quad \hat{u} = (p_1 - q_2)^2. \quad (\text{A2.4.9})$$

We shall only deal with the  $t$ -channel amplitude. From (A2.2.3) in Feynman gauge ( $a = 1$ ) and using (A2.2.8 and 9) we get

$$\begin{aligned} \mathcal{M}_{(t)}(q_i G_a \rightarrow q_j G_b) &= \left[ \epsilon_\sigma^*(q_2) g f_{cba} C^{\mu\rho\sigma} \epsilon_\rho(q_1) \right] \times \\ &\quad \times \left( \frac{-ig_{\mu\nu}}{\hat{t}} \right) [\bar{u}(p_2) i g(t^c)_{ji} \gamma^\nu u(p_1)] \\ &= \frac{g^2}{\hat{t}} (f_{cba} t^c_{ji}) \left[ \epsilon_\sigma^*(q_2) C^{\mu\rho\sigma} \epsilon_\rho(q_1) \right] \times \\ &\quad \times [\bar{u}(p_2) \gamma_\mu u(p_1)] \end{aligned} \quad (\text{A2.4.10})$$

where

$$\begin{aligned} C^{\mu\rho\sigma} &= g^{\mu\rho} (p_1 - p_2 + q_2)^\sigma + g^{\rho\sigma} (-q_2 - q_1)^\mu + \\ &\quad + g^{\sigma\mu} (q_1 - p_1 + p_2)^\rho. \end{aligned} \quad (\text{A2.4.11})$$

## A2.5 Colour sums

We list here some identities, generalized to  $SU(N)$  where appropriate, which are useful in performing the sums over initial and final colour states. The summation convention is assumed throughout this discussion.

The  $qqG$  vertex involves a factor of  $t^a$ :

$$t^a \equiv \frac{1}{2}\lambda^a \quad (\text{A2.5.1})$$

where the  $SU(3)$  matrices  $\lambda^a$  are those introduced by Gell-Mann. The commutation relations for the  $t^a$  are given by the structure constants of the group,

$$[t^a, t^b] = if_{abc}t^c \quad (\text{A2.5.2})$$

$$[t^a, t^b] = \frac{1}{N}\delta_{ab}I_{(N)} + d_{abc}t^c, \quad (\text{A2.5.3})$$

where  $I_{(N)}$  is the  $N$ -dimensional unit matrix. The  $f_{abc}$  are antisymmetric and the  $d_{abc}$  symmetric under the interchange of any two indices. In  $SU(2)$ , the quantities analogous to  $(t^a, f_{abc}, d_{abc})$  are  $(\sigma^a/2, \epsilon_{abc}, 0)$ . Some useful identities involving the matrices  $t^a$  are

$$\left. \begin{aligned} t^a t^b &= \frac{1}{2} \left[ \frac{1}{N} \delta_{ab} I_{(N)} + (d_{abc} + if_{abc}) t^c \right], \\ t_{ij}^a t_{kl}^a &= \frac{1}{2} \left[ \delta_{il} \delta_{jk} - \frac{1}{N} \delta_{ij} \delta_{kl} \right], \\ \text{Tr } t^a &= 0, \\ \text{Tr}(t^a t^b) &= \frac{1}{2} \delta_{ab}, \\ \text{Tr}(t^a t^b t^c) &= \frac{1}{4} (d_{abc} + if_{abc}), \\ \text{Tr}(t^a t^b t^a t^c) &= -\frac{1}{4N} \delta_{bc}. \end{aligned} \right\} \quad (\text{A2.5.4})$$

It is sometimes profitable to define the  $(N^2 - 1)$ -dimensional matrices  $F_a$  and  $D_a$ ;

$$\left. \begin{aligned} (F_a)_{bc} &= -if_{abc}, \\ (D_a)_{bc} &= d_{abc}. \end{aligned} \right\} \quad (\text{A2.5.5})$$

The Jacobi identities are

$$\left. \begin{aligned} f_{abe}f_{ecd} + f_{cbe}f_{aed} + f_{dbe}f_{ace} &= 0, \\ f_{abe}d_{ecd} + f_{cbe}d_{aed} + f_{dbe}d_{ace} &= 0, \end{aligned} \right\} \quad (\text{A2.5.6})$$

or, equivalently,

$$\left. \begin{aligned} [F_a, F_b] &= if_{abc}F_c \\ [F_a, D_b] &= if_{abc}D_c. \end{aligned} \right\} \quad (\text{A2.5.7})$$

A generalization of the  $SU(2)$  relation

$$\epsilon_{ijm}\epsilon_{klm} = \delta_{ik}\delta_{jl} - \delta_{il}\delta_{jk} \quad (\text{A2.5.8})$$

is

$$f_{abe} f_{cde} = \frac{2}{N} (\delta_{ac}\delta_{bd} - \delta_{ad}\delta_{bc}) + (d_{ace}d_{bde} - d_{bce}d_{ade}). \quad (\text{A2.5.9})$$

Some further identities, written in both notations, are

$$\left. \begin{aligned} f_{abb} &= 0, & \text{Tr } \mathbf{F}_a &= 0, \\ d_{abb} &= 0, & \text{Tr } \mathbf{D}_a &= 0, \\ f_{acd} f_{bcd} &= N\delta_{ab}, & \text{Tr}(\mathbf{F}_a \mathbf{F}_b) &= N\delta_{ab} \\ && \mathbf{F}_a \mathbf{F}_a &= N\mathbf{I}_{(2N-1)} \\ f_{acd} d_{bcd} &= 0, & \text{Tr}(\mathbf{F}_a \mathbf{D}_b) &= 0 \\ && \mathbf{F}_a \mathbf{D}_a &= 0 \\ d_{acd} d_{bcd} &= \frac{N^2 - 4}{N} \delta_{ab}, & \text{Tr}(\mathbf{D}_a \mathbf{D}_b) &= \frac{N^2 - 4}{N} \delta_{ab}, \\ && \mathbf{D}_a \mathbf{D}_a &= \frac{N^2 - 4}{N} \mathbf{I}_{(2N-1)}. \end{aligned} \right\} \quad (\text{A2.5.10})$$

Specializing to the matrix notation, one has

$$\left. \begin{aligned} \text{Tr}(\mathbf{F}_a \mathbf{F}_b \mathbf{F}_c) &= i \frac{N}{2} f_{abc}, \\ \text{Tr}(\mathbf{D}_a \mathbf{F}_b \mathbf{F}_c) &= \frac{N}{2} d_{abc}, \\ \text{Tr}(\mathbf{D}_a \mathbf{D}_b \mathbf{F}_c) &= i \frac{N^2 - 4}{2N} f_{abc}, \\ \text{Tr}(\mathbf{D}_a \mathbf{D}_b \mathbf{D}_c) &= \frac{N^2 - 12}{2N} d_{abc}. \end{aligned} \right\} \quad (\text{A2.5.11})$$

The above relations can be used to show

$$\text{Tr}(\mathbf{F}_a \mathbf{F}_b \mathbf{F}_a \mathbf{F}_c) = \frac{N^2}{2} \delta_{bc}. \quad (\text{A2.5.12})$$

We now illustrate the use of these relations by calculating some colour sums representative of those required in Section A2.4.

Consider the  $|\mathcal{M}_{(t)}|^2$  term for  $qq \rightarrow qq$  in (A2.4.4).  $\overline{|\mathcal{M}_{(t)}|^2}$  will involve a colour factor

$$\frac{1}{3} \sum_i \frac{1}{3} \sum_k \sum_{j,l} (t_{lk}^b t_{ji}^b) (t_{lk}^a t_{ji}^a)^*$$

which, since the  $t^a$  are Hermitian,

$$\begin{aligned} &= \frac{1}{9} \sum_{i,j,k,l} (t_{lk}^b t_{kl}^a) (t_{ji}^b t_{ij}^a) \\ &= \frac{1}{9} \text{Tr} (\mathbf{t}^b \mathbf{t}^a) \text{Tr} (\mathbf{t}^b \mathbf{t}^a) \\ &= \frac{1}{9} \left( \frac{1}{2} \delta_{ab} \right) \left( \frac{1}{2} \delta_{ab} \right) = \frac{2}{9} \end{aligned} \quad (\text{A2.5.13})$$

where we have used (A2.5.4) and the fact that  $a, b = 1, 2, \dots, 8$ .

As a final example consider  $|\mathcal{M}_{(t)}|^2$  in  $qG_a \rightarrow qG_b$  in (A2.4.10).  $|\mathcal{M}_{(t)}|^2$  will involve a colour factor

$$\begin{aligned} &\frac{1}{8} \sum_a \frac{1}{3} \sum_i \sum_{b,j} (f_{cba} t_{ji}^c) (f_{dba} t_{ji}^d)^* \\ &= \frac{1}{24} \sum_{abij} f_{cba} f_{dba} t_{ji}^c t_{ij}^d \\ &= \frac{1}{24} \sum_{a,b} f_{cba} f_{dba} \text{Tr} (\mathbf{t}^c \mathbf{t}^d) \\ &= \frac{1}{24} (N \delta_{cd}) \left( \frac{1}{2} \delta_{cd} \right) = \frac{1}{2} \end{aligned} \quad (\text{A2.5.14})$$

where we have used (A2.5.10) with  $N = 3$ , and (A2.5.4).

## A2.6 The Gell-Mann $SU(3)$ matrices

The Hermitian generators of  $SU(3)$  are represented by the matrices  $\lambda^a/2$  ( $a = 1, \dots, 8$ ) where the  $\lambda^a$  are the Gell-Mann matrices which are the analogue for  $SU(3)$  of the Pauli matrices for  $SU(2)$ . We list some of their properties.

They satisfy the commutation relations

$$\left[ \frac{\lambda^a}{2}, \frac{\lambda^b}{2} \right] = i \sum_c f_{abc} \frac{\lambda^c}{2} \quad (\text{A2.6.1})$$

$a, b, c = 1, 2, \dots, 8$ .

The same commutation rules are obeyed by the  $n^2 - 1$  generators of any  $SU(n)$  group where, however,  $a, b, c = 1, 2, \dots, n^2 - 1$ .

The ‘structure constants’ of the group  $f_{abc}$  are antisymmetric with respect to interchange of any two indices. The non-zero constants are given in Table A2.1.

The anticommutation rules for the  $SU(3)$  matrices are also useful:

$$\{\lambda^a, \lambda^b\} \equiv \lambda^a \lambda^b + \lambda^b \lambda^a = 2 \sum_c d_{abc} \lambda^c + \frac{4}{3} \delta_{ab} \quad (\text{A2.6.2})$$

where the coefficients  $d_{abc}$ , symmetric under permutation of any two indices, are given in Table A2.2.

$abc$	$f_{abc}$	$abc$	$f_{abc}$
123	1	345	$1/2$
147	$1/2$	367	$-1/2$
156	$-1/2$	458	$\sqrt{3}/2$
246	$1/2$	678	$\sqrt{3}/2$
257	$1/2$		

Table A2.1. Non-zero  $f_{abc}$  for  $SU(3)$ .

$abc$	$d_{abc}$	$abc$	$d_{abc}$
118	$1/\sqrt{3}$	355	$1/2$
146	$1/2$	366	$-1/2$
157	$1/2$	377	$-1/2$
228	$1/\sqrt{3}$	448	$-1/2\sqrt{3}$
247	$-1/2$	558	$-1/2\sqrt{3}$
256	$1/2$	668	$-1/2\sqrt{3}$
338	$1/\sqrt{3}$	778	$-1/2\sqrt{3}$
344	$1/2$	888	$-1/\sqrt{3}$

Table A2.2. Non-zero  $d_{abc}$ .

From the fact that the  $\lambda$ s are traceless matrices, using (A2.6.1 and 2) one gets

$$\text{Tr}(\lambda^a \lambda^b) = 2\delta_{ab} \quad (\text{A2.6.3})$$

$$\text{Tr}(\lambda^a [\lambda^b, \lambda^c]) = 4if_{abc} \quad (\text{A2.6.4})$$

$$\text{Tr}(\lambda^a \{\lambda^b, \lambda^c\}) = 4d_{abc} \quad (\text{A2.6.5})$$

## A2.7 The Fierz reshuffle theorem

It sometimes happens, when dealing with the matrix element corresponding to a Feynman diagram involving spin  $\frac{1}{2}$  particles, that it is convenient to rearrange the order of the spinors compared with the order they acquire directly from the Feynman diagram. An example of this occurred in Section 5.1 where it was helpful to go from the form (5.1.17) to (5.1.18).

In general, let  $\Gamma^i (i = 1, \dots, 16)$  stand for any one of the independent combinations of unit matrix and  $\gamma$  matrices:  $I, \gamma^\mu, \sigma^{\mu\nu} = \frac{1}{2}i[\gamma^\mu, \gamma^\nu]$  with  $\mu > \nu, i\gamma^\mu \gamma_5, \gamma_5$ .

Let  $\Gamma_i$  stand for the above set of matrices with their Lorentz indices

lowered where relevant, i.e.  $\Gamma_i$  contains for example  $\gamma_\mu$  whereas  $\Gamma^i$  contains  $\gamma^\mu$  etc.

As a result of the algebraic properties of the set  $\Gamma^i$  it can be shown that

$$\frac{1}{4} \sum_i (\Gamma_i)_{\alpha\beta} (\Gamma^i)_{\gamma\delta} = \delta_{\alpha\delta} \delta_{\beta\gamma}. \quad (\text{A2.7.1})$$

If now **A** and **B** are any  $4 \times 4$  matrices, then on multiplying (A2.7.1) by  $A_{\rho\alpha} B_{\nu\gamma}$  we obtain

$$\begin{aligned} \frac{1}{4} \sum_i A_{\rho\alpha} (\Gamma_i)_{\alpha\beta} B_{\nu\gamma} (\Gamma^i)_{\gamma\delta} &= A_{\rho\delta} B_{\nu\beta} \\ A_{\rho\delta} B_{\nu\beta} &= \frac{1}{4} \sum_i (\mathbf{A}\Gamma_i)_{\rho\beta} (\mathbf{B}\Gamma^i)_{\nu\delta}. \end{aligned} \quad (\text{A2.7.2})$$

Since the 16  $\Gamma^i$  are a complete set of  $4 \times 4$  matrices, each product  $\mathbf{A}\Gamma_i$  etc. will reduce to a sum of  $\Gamma_i$ .

After some labour one can obtain the following relation

$$\begin{aligned} [\gamma^\mu (1 - \gamma_5)]_{\rho\delta} [\gamma_\mu (1 - \gamma_5)]_{\nu\beta} \\ = -[\gamma^\mu (1 - \gamma_5)]_{\rho\beta} [\gamma_\mu (1 - \gamma_5)]_{\nu\delta}, \end{aligned} \quad (\text{A2.7.3})$$

which when sandwiched between spinors leads from (5.1.17) to (5.1.18).

Clearly, analogous relations can be worked out for any product of the  $\Gamma$  matrices. Results may be found in Section 2.2B of Marshak, Riazuddin and Ryan (1969).

## A2.8 Dimension of matrix elements

A knowledge of the physical dimensions of a matrix element is often very useful in assessing its possible kinematical behaviour.

For cross-sections and differential cross-sections the dimension counting is trivial: (we are using  $\hbar = c = 1$  natural units)

$$\begin{aligned} [\sigma] &= [\text{AREA}] = [\text{MASS}]^{-2} \\ \left[ \frac{d\sigma}{d\Omega} \right] &= [\text{MASS}]^{-2} \\ \left[ \frac{d\sigma}{dt} \right] &= [\text{MASS}]^{-4}. \end{aligned}$$

For a Feynman amplitude, as computed directly from a Feynman diagram *but without any spinors for the external lines*, one has the following dimensional factors:

Internal boson, photon, gluon line:  $[\text{MASS}]^{-2}$

Internal fermion line:  $[\text{MASS}]^{-1}$

Integration over four-momentum of *each* loop:  $[\text{MASS}]^4$

The dimensions of Green's functions were discussed in Section 20.6.

## Appendix 3

### Conserved vector currents and their charges

In Section 2.3.1 we showed how the invariance of a Lagrangian under an infinitesimal global gauge transformation

$$\delta\phi_j(x) = -i\theta q_j \phi_j(x) \quad (\text{not summed}) \quad (\text{A3.1})$$

led to the existence of a vector current  $J^\mu(x)$ , the Noether current, which is conserved

$$\partial_\mu J^\mu = 0 \quad (\text{A3.2})$$

and a ‘charge operator’

$$\hat{Q} = \int d^3x J_0(x, t) \quad (\text{A3.3})$$

which is independent of time. We also mentioned that the  $q_j$  are the ‘charges’, i.e. the eigenvalues of  $\hat{Q}$ . Moreover it can be shown that  $\hat{Q}$  is the generator of the transformations (A3.1), i.e.

$$\phi'_j = e^{i\theta\hat{Q}} \phi_j e^{-i\theta\hat{Q}} \quad (\text{A3.4})$$

and

$$[\hat{Q}, \phi_j] = -q_j \phi_j \quad (\text{not summed}). \quad (\text{A3.5})$$

If the  $q_j$  are the *electric* charges of the particles then  $J^\mu$  is the electromagnetic current.

In the more general, non-Abelian case (2.3.22), where  $\phi$  is a column vector composed of  $n$  fields, and where

$$\delta\phi = -i\mathbf{L} \cdot \boldsymbol{\theta}\phi = -iL^j \cdot \theta_j \phi \quad (\text{A3.6})$$

with the  $L^j$  ( $j = 1, \dots, N$ ) being  $n \times n$  matrices representing the  $N$  group generators  $T_j$  and satisfying the group commutation relations (2.3.21), one finds a set of  $N$  conserved Noether currents

$$J_j^\mu = -i \frac{\delta\mathcal{L}}{\delta(\partial_\mu\phi_r)} L_{rs}^j \phi_s \quad (\text{A3.7})$$

and one has a set of  $N$  ‘charge operators’

$$\hat{Q}_j = \int d^3x J_0^j(x, t) \quad (\text{A3.8})$$

which are independent of time.

Moreover one can show that the  $\hat{Q}_j$  are the generators of the transformations (A3.6).

Thus

$$\hat{Q}_j = T_j \quad (\text{A3.9})$$

and the eigenvalues of the  $\hat{Q}_j$  are the eigenvalues of the group generators. Also one has, analogous to (A3.5),

$$[T_j, \phi_r] = -L_{rs}^j \phi_s \quad (\text{A3.10})$$

As an example consider the group of isospin rotations,  $SU(2)$ . In this case the  $L^j$  ( $j = 1, 2, 3$ ) are the isospin matrices; for example, for an isospin-half field they are  $\tau/2$  where the  $\tau$  are the Pauli matrices, and the diagonal charge  $\hat{Q}_3$  is  $T_3$ , the operator whose eigenvalues are the third components of isospin.

In electroweak theory the matrix elements of conserved vector currents taken between hadronic states are of great importance.

Consider now the matrix elements of such a set of  $J_j^\mu(x)$  and their associated ‘charge operators’  $\hat{Q}_j$ . We shall study matrix elements between sets of states of definite momentum  $\mathbf{P}$  which transform under the action of the group generators as

$$T_j |P, \rho\rangle = M_{\rho' \rho}^j |P, \rho'\rangle \quad (\rho = 1, \dots, n) \quad (\text{A3.11})$$

where the  $M^j$  are an  $n$ -dimensional representation of the  $T_j$ . For example for the group of isospin rotations and for a set of isodoublet states (A3.11) would read

$$T |P; I = \frac{1}{2}, I_3\rangle = (\frac{\tau}{2})_{I'_3 I_3} |P; I = \frac{1}{2}, I'_3\rangle. \quad (\text{A3.12})$$

We shall now prove the remarkable result that

$$\langle P; \rho' | J_j^\mu(0) | P; \rho \rangle = 2M_{\rho' \rho}^j P^\mu \quad (\text{A3.13})$$

i.e. the matrix elements are known *exactly* without any dynamical calculation.

On grounds of Lorentz invariance we can write

$$\langle P; \rho' | J_j^\mu(0) | P; \rho \rangle = 2a_{\rho' \rho}^j P^\mu \quad (\text{A3.14})$$

where the  $a_{\rho' \rho}^j$  are scalars (numbers). So we must show that

$$a_{\rho' \rho}^j = M_{\rho' \rho}^j \quad (\text{A3.15})$$

Consider, using (A3.9) and (A3.11),

$$\begin{aligned}\langle \mathbf{P}'; \rho' | \hat{Q}_j | \mathbf{P}; \rho \rangle &= M_{\rho'' \rho}^j \langle \mathbf{P}'; \rho' | \mathbf{P}; \rho'' \rangle \\ &= M_{\rho' \rho}^j (2\pi)^3 2P_0 \delta^3(\mathbf{P}' - \mathbf{P}).\end{aligned}\quad (\text{A3.16})$$

From the definition of  $\hat{Q}_j$  the left-hand side equals

$$\begin{aligned}&\int d^3x \langle \mathbf{P}'; \rho' | J_j^0(x, 0) | \mathbf{P}, \rho \rangle \\ &= \int d^3x e^{i\mathbf{x} \cdot (\mathbf{P} - \mathbf{P}')} \langle \mathbf{P}'; \rho' | J_j^0(0) | \mathbf{P}, \rho \rangle\end{aligned}\quad (\text{A3.17})$$

where we have used the translation property

$$e^{i\hat{P} \cdot x} \hat{O}(0) e^{-i\hat{P} \cdot x} = \hat{O}(x). \quad (\text{A3.18})$$

Thus, by (A3.14), the right-hand side of eqn (A3.17) becomes

$$\begin{aligned}&(2\pi)^3 \delta^3(\mathbf{P}' - \mathbf{P}) \langle \mathbf{P}; \rho' | J_j^0(0) | \mathbf{P}, \rho \rangle \\ &= (2\pi)^3 \delta^3(\mathbf{P}' - \mathbf{P}) 2a_{\rho' \rho}^j P^0.\end{aligned}\quad (\text{A3.19})$$

Comparing (A3.19) with (A3.16) yields the desired result (A3.15).

As an example, if  $J_j^\mu$  is the electromagnetic current and  $q$  the charge of the hadron, then from (A3.13),

$$\langle \mathbf{P}; q | J_{\text{em}}^\mu(0) | \mathbf{P}; q \rangle = 2qP^\mu. \quad (\text{A3.20})$$

For  $\mu = 0$  this simply states that the expectation value of the charge density (in units of  $e$ ) at the origin is  $2P^0q$  for a plane wave. The factor  $2P^0$  reflects the relativistic normalization of the states.

Similarly, if  $J_j^\mu$  are the isotopic spin currents

$$\langle \mathbf{P}; I, I'_3 | J_j^\mu(0) | \mathbf{P}; I, I_3 \rangle = 2(I_j)_{I'_3 I_3} P^\mu \quad (\text{A3.21})$$

where the  $(2I + 1) \times (2I + 1)$  matrices  $I_j$  represent the isospin generators for isospin  $I$ .

If we take the isospin raising current  $J_+^\mu = J_1^\mu + iJ_2^\mu$ , the associated ‘charge operator’ is now the isospin raising operator  $T_+$  (see Section 1.3) whose effect on a state of definite isospin is given in (1.3.15). From the above one deduces

$$\langle \mathbf{P}; I, I_3 + 1 | J_+^\mu(0) | \mathbf{P}; I, I_3 \rangle = \sqrt{(I - I_3)(I + I_3 + 1)} 2P^\mu \quad (\text{A3.22})$$

It is important to appreciate the miraculous power of (A3.13). The currents could be made of quark and gluon fields so that all the complications of the strong interactions intervene in relating them dynamically to the hadron states. Nonetheless if the group of transformations is a symmetry group of the physical hadrons we are able to get an exact result for

the hadronic matrix elements of the currents! Such considerations were extensively utilized in the appendix to Chapter 16 (Section 16.9).

It is also important to separate the dynamical properties from the group theoretical properties. An example from  $SU(3)$  will illustrate this very well. Let  $V_j^\mu$  ( $j = 1, \dots, 8$ ) be any set of currents or operators which transform as an octet under  $SU(3)$ , i.e.

$$[T_i, V_j^\mu] = if_{ijk}V_k^\mu \quad (\text{A3.23})$$

where the  $f_{ijk}$  are the  $SU(3)$  structure constants defined in Appendix 2. From this alone follows a ‘Wigner–Eckart’ theorem which for the baryon octet  $|\mathbf{P}; i\rangle$  ( $i = 1, \dots, 8$ ) reads

$$\langle \mathbf{P}; i | V_j^\mu | \mathbf{P}; k \rangle = 2P^\mu \{if_{ijk}F_V + d_{ijk}D_V\} \quad (\text{A3.24})$$

where the group constants  $d_{ijk}$  are defined in Appendix 2.6 and  $F_V$  and  $D_V$  are *unknown* constants. Eqn (A3.24) is itself miraculous —  $8^3$  matrix elements are expressed in terms of two numbers,  $F_V$  and  $D_V$ . But the values of  $F_V$  and  $D_V$  depend upon the detailed dynamics. Only if the  $V_j^\mu$  form a set of *conserved* currents can we deduce that  $F_V = 1$ ,  $D_V = 0$ .

If we consider non-diagonal matrix elements of vector currents between a spin-half baryon octet the most general form allowed by Lorentz invariance and parity conservation is

$$\begin{aligned} \langle \mathbf{P}'; i | V_j^\mu | \mathbf{P}; k \rangle = & \bar{u}(\mathbf{P}') \{ G_{ijk}^1(q^2) \gamma^\mu + G_{ijk}^2(q^2) \sigma^{\mu\nu} q_\nu \\ & + G_{ijk}^3(q^2) q^\mu \} u(\mathbf{P}) \end{aligned} \quad (\text{A3.25})$$

where the  $G$ s are form factors depending on the momentum transfer.

Now because for  $\mathbf{P}' = \mathbf{P}$ ,

$$\bar{u}(\mathbf{P}) \gamma^\mu u(\mathbf{P}) = 2P^\mu \quad (\text{A3.26})$$

when we let  $q^2 \rightarrow 0$  we find, via (A3.24),

$$G_{ijk}^1(0) = if_{ijk}F_V + d_{ijk}D_V. \quad (\text{A3.27})$$

If the vector currents are *conserved* we find in addition, via (1.1.4), for all  $q^2$

$$G_{ijk}^3(q^2) = 0 \quad (\text{A3.28})$$

and by (A3.13)

$$F_V = 1, \quad D_V = 0. \quad (\text{A3.29})$$

For any octet of *axial-vector* currents  $A_j^\mu$  with matrix elements taken between a spin-half baryon octet whose polarization is specified by the covariant spin vector  $S^\mu$ , one has an expression analogous to (A3.24):

$$\langle \mathbf{P}, \mathbf{S}; i | A_j^\mu | \mathbf{P}, \mathbf{S}; k \rangle = 2m_B S^\mu \{if_{ijk}F_A + d_{ijk}D_A\} \quad (\text{A3.30})$$

with  $F_A$ ,  $D_A$  unknown constants, and  $m_B$  the baryon mass. The Lorentz structure arises from the fact that

$$\bar{u}(\mathbf{P}, \mathbf{s})\gamma^\mu\gamma_5 u(\mathbf{P}, \mathbf{s}) = 2m_B S^\mu. \quad (\text{A3.31})$$

The above type of matrix element occurs in the analysis of hyperon  $\beta$ -decay, where, if  $SU(3)_F$  invariance holds, each transition amplitude is expressed in the form

$$(KM \text{ matrix element}) \times (V^\mu + A^\mu) \quad (\text{A3.32})$$

the vector and axial-vector currents being certain linear combinations of the octet members  $V_j^\mu$  and  $A_j^\mu$ . In this way *all* hyperon  $\beta$ -decays are described in terms of a  $KM$  matrix element and two constants  $F_A$  and  $D_A$ . Details may be found in Chapter 4 of Bailin (1982).

## References

- Abarbanel, H. D. I., Goldberger, M. L. and Treiman, S. B. (1969). *Phys. Rev. Lett.* **22**, 500.
- Abe, K. (1991). In *Proceedings of the 25th International Conference on High Energy Physics*, Singapore, 1990, eds. K. K. Phua and Y. Yamaguchi, p. 33. Singapore: World Scientific.
- Abers, E. S. and Lee, B. W. (1973). *Phys. Rep.* **9C**, no. 1.
- Abrams, G. S. et al. (1975). *Phys. Rev. Lett.* **36**, 291.
- Adler, S. L. (1969). *Phys. Rev.* **177**, 2426.
- Ahrens, L. A. et al. (1987). *Phys. Rev.* **35**, 785.
- ALEPH (1991): Decamp, D. et al., *Phys. Lett.* **B258**, 236.
- Algard, M. J. et al. (1978). *Phys. Rev. Lett.* **41**, 70.
- Allaby, J. V. et al. (1987). *Z. Phys.* **C36**, 611.
- Allen, R. C. et al. (1985). *Phys. Rev. Lett.* **55**, 2401.
- Allen, R. C. et al. (1990). *Phys. Rev. Lett.* **64**, 1330.
- Altarelli, G. (1989). *Ann. Rev. Nucl. Part. Sci.* **39**, 357.
- Altarelli, G. and Martinelli, G. (1978). *Phys. Lett.* **76B**, 89.
- Altarelli, G. et al. (1985). *Z. Phys.* **C27**, 617.
- Altarelli, G., et al. (1988). *Nucl. Phys.* **B308**, 724.
- Altarelli, G., Kleiss, R. and Verzegnassi, C., editors (1989). *Z Physics at LEP1*. CERN 89-08.
- Amaldi, U. (1990). In *Techniques and Concepts of High Energy Physics V*, ed. T. Ferbel, Plenum Press Series 8, 204.
- Anderson, K. J. et al. (1979). *Phys. Rev. Lett.* **42**, 944.
- Angelini, C. et al. (1979). *Phys. Lett.* **84B**, 151.
- Anselmino, M. (1979). *Phys. Rev.* **D19**, 2803.
- Anselmino, M. and Leader, E. (1992). *Phys. Lett.* **B293**, 216.
- Anselmino, M., Lichtenberg, D. B. and Predazzi, E. (1990a). *Z. Phys.* **C48**, 605.
- Anselmino, M., Caruso, F., Leader, E. and Soares, J. (1990b). *Z. Phys.* **C48**, 689.
- Applequist, T., Barnett, R. M. and Lane, K. (1978). *Ann. Rev. Nucl. Part. Sci.* **28**, 387.

- ARGUS (1987a): Albrecht, H. *et al.*, *Phys. Lett.* **B185**, 218; **B197**, 452; **B199**, 451.  
ARGUS (1987b): Albrecht, H. *et al.*, *Phys. Lett.* **B192**, 245.  
ARGUS (1990): Albrecht, H. *et al.*, *Phys. Lett.* **B246**, 278 and **B250**, 164.  
Arneodo, M. (1994). *Phys. Rep.* **240**, 301.  
Ashman, J. *et al.* (1988). *Phys. Lett.* **B206**, 364.  
Atwood, W. B. *et al.* (1975). *Phys. Rev.* **D12**, 1884.  
Aubert, J. J. *et al.* (1974). *Phys. Rev. Lett.* **33**, 1404.  
Augustin, J. E. *et al.* (1974). *Phys. Rev. Lett.* **33**, 1406.  
Bacci, C. *et al.* (1974). *Phys. Rev. Lett.* **33**, 1408.  
Bacino, W. *et al.* (1978). *Phys. Rev. Lett.* **41**, 13.  
Badier, J. *et al.* (1979). *Phys. Lett.* **89B**, 144.  
Baglin, C. *et al.* (1987). *Nucl. Phys.* **B286**, 592.  
Bailin, D. (1982). *Weak Interactions*, 2nd edn. Sussex University Press.  
Baltay, C. (1978). In *Proceedings of the 19th International Conference on High Energy Physics*, Tokyo, 1978, ed. G. Takeda, p. 882. Tokyo: Physical Society of Japan.  
Barber, D. P. *et al.* (1979). *Phys. Rev. Lett.* **43**, 1915.  
Barkov, L. M. and Zolotorev, M. S. (1980). *Sov. Phys. JETP* **52**, 360.  
Barone, V. and Predazzi, E. (1987). *Ann. de Physique Fr.* **12**, 525.  
Barone, V. *et al.* (1991). *Phys. Lett.* **B268**, 279.  
Basdevant, J. L., Bediaga, I. and Predazzi, E. (1987). *Nucl. Phys.* **B294**, 1054.  
Basdevant, J. L., Martin, A. and Richard, J. M. (1990). *Nucl. Phys.* **B343**, 60, 69.  
Baum, G. *et al.* (1983). *Phys. Rev. Lett.* **51**, 1135.  
Bazizi, K., Wimpenny, S. J. and Sloan, T. (1990). Contributed paper to the *25th International Conference on High Energy Physics*, Singapore, 1990. CERN-PRE 90-175.  
BCDMS (1985): Bari, G. *et al.*, *Phys. Lett.* **B163**, 282; see also Voss, R., talk at the *11th International Conference on Neutrino Physics and Astrophysics*, Dortmund, 1984.  
BCDMS (1987): Benvenuti, A. C. *et al.*, *Phys. Lett.* **B195**, 91.  
BCDMS (1989): Benvenuti, A. C. *et al.*, *Phys. Lett.* **B223**, 485.  
BCDMS (1990): Benvenuti, A. C. *et al.*, *Phys. Lett.* **B237**, 599.  
Bediaga, I., Correa, A. and Predazzi, E. (1988). *Phys. Lett.* **215B**, 166.  
Bediaga, I. *et al.* (1985). *Nuovo Cim. Lett.* **42**, 92.  
Beeneker, W., Kuijff, H. van Neerven, W. L. and Smith J. (1989). *Phys. Rev.* **D40**, 54.  
Behrends, R. E., Finkelstein, R. J. and Sirlin, A. (1956). *Phys. Rev.* **101**, 866.  
Berends, F. A. and Kleiss, R. (1985). *Nucl. Phys.* **B260**, 32.  
Berends, F. A. , Burgers, G. J. H. and van Neerven, W. L. (1987). *Phys. Lett.* **185B**, 395; (1988a). *Nucl. Phys.* **B297**, 429; *Nucl. Phys.* **B304**, 92.  
Berends, F. A. *et al.* (1988b). *Nucl. Phys.* **B301**, 583.  
Berestetskii, V. B., Lifshitz, E. M. and Pitaevskii, L. P. (1971). *Relativistic Quantum Theory*, section 41. Pergamon Press.

- Berger, Ch. *et al.* (1980). Test of QED in the reactions  $e^+e^- \rightarrow e^+e^-$  and  $e^+e^- \rightarrow \mu^+\mu^-$  at CM energies from 9.4 to 31.6 GeV. DESY preprint 80/01.
- Berkelman, K. (1986). *Rep. Prog. Phys.* **49**, 1.
- Bernardini, M. *et al.* (1973). *Nuovo Cim.* **17A**, 383.
- Birich, G. N. *et al.* (1984). *Sov. Phys. JETP* **60**, 442.
- Bjorken, J. D. (1966). *Phys. Rev.* **148**, 1467.
- Bjorken, J. D. (1969). *Phys. Rev.* **179**, 1547.
- Bjorken, J. D. (1971). *Phys. Rev.* **D1**, 1376.
- Bjorken, J. D. (1977). In *Proceedings of the 1976 SLAC Summer Institute on Particle Physics*, Stanford, 1977, ed. M. C. Zipf, p. 1. Stanford: SLAC.
- Bjorken, J. D. and Drell, S. C. (1964). *Relativistic Quantum Mechanics*. New York: McGraw-Hill.
- Bjorken, J. D. and Drell, S. C. (1965). *Relativistic Quantum Fields*. New York: McGraw-Hill.
- Bjorken, J. D. and Glashow, S. L. (1964). *Phys. Lett.* **11**, 255.
- Blatt, J. M. and Weisskopf, V. F. (1979). *Theoretical Nuclear Physics*. New York: Springer-Verlag.
- Blondel, A. (1990). In *Proceedings of the 1989 IUCF Topical Conference*, Spencer, Indiana, 1989, eds. J. Sowinski and S. E. Vigdor. Teaneck, New Jersey: World Scientific.
- Blondel, A. *et al.* (1989). *Z. Phys.* **C45**, 361.
- Bloom, E. D. (1982). *J. de Phys.* **C3**, 407.
- Bloom, E. D. (1985). *Proc. Aspen Winter Conf.*, Aspen, Colorado, 1985 and SLAC-Pub. 3573.
- Bloom, E. D. and Peck, C. W. (1983) *Ann. Rev. Nucl. Part. Sci.* **33**, 143.
- Bolton, R. D. *et al.* (1988). *Phys. Rev.* **D38**, 2077.
- Bouchiat, M. A., Guena, J., Hunter, L., and Pottier, L. (1984). *Phys. Lett.* **117B**, 358 and **134B**, 493.
- Bouchiat, M. A., Guena, J., Pottier, L. and Hunter L. (1986). *J. Physique* **47**, 1709.
- Bourrely, C., Leader, E. and Soffer, J. (1980). *Phys. Rep.* **59**, no. 2.
- Boyarski, A. M. *et al.* (1975). *Phys. Rev. Lett.* **34**, 1357.
- Braaten, E. (1989a). *Phys. Rev.* **D39**, 1458.
- Braaten, E. (1989b). In *Proceedings of the Tau-Charm Factory Workshop*, Stanford 1989, ed. Lydia Beers, p. 408. SLAC-343.
- Brandelik, R. *et al.* (1979). DESY Report 79/74.
- Brandt, S. and Dahmen, H. D. (1979). *Z. Phys.* **C1**, 61.
- Brodsky, S. J., Lepage, G. P. and Tuan, S. F. (1987). *Phys. Rev. Lett.* **59**, 621.
- Budny, R. (1973). *Phys. Lett.* **45B**, 340.
- Buras, A. J. (1977). *Nucl. Phys.* **B125**, 125.
- Burchell, M. (1992). In *Proc. 12th Int. Conf. on Physics in Collision*, Boulder, Colorado, 1992.
- Cabibbo, N. (1963). *Phys. Rev. Lett.* **10**, 531.
- Cabibbo, N. (1976). The Physics Interests of a 10 TeV Proton Synchrotron, p. 99. CERN Ed. 76-12.

- Caffo, M. et al. (1989). In *Z Physics at LEP1*, eds. G. Altarelli, R. Kleiss and C. Verzegnassi, Vol. 1, p. 171. CERN 89-08.
- Cahn, R. N. and Gilman, F. J. (1978). *Phys. Rev.* **D17**, 1313.
- Carimalo, C. (1987). *Int. J. Mod. Phys.* **A2**, 249.
- Catani, S. (1992). In *QCD at 200 TeV*, eds. L. Cifarelli and Yu. L. Dokshitzer, p. 21. New York: Plenum.
- CCFR (1990a): Leung, W. C. et al., in *Proceedings of the 25th Rencontre de Moriond (Hadronic Interactions)* Gif-sur-Yvette: Editions Frontières.
- CCFR (1990b): Foudas, C. et al., *Phys. Rev. Lett.* **64**, 1207.
- CDF (1989a): Abe, F. et al., *Phys. Rev. Lett.* **63**, 1447.
- CDF (1989b): Huth, J. In *Proceedings of the Workshop on Calorimetry for the SSC*, Tuscaloosa, Alabama, 1989. Fermilab-Conf. 89/117-E.
- CDHSW (1990): Blondel, A. et al., *Z. Phys.* **C45**, 361.
- CDHSW (1991): Berge, J. P. et al., *Z. Phys.* **C49**, 187.
- Chanowitz, M. S. (1987). *Proc. Second Int. Conf. on Hadron Spectroscopy*, KEK, Tsukuba, Japan.
- CHARM (1987): Allaby, J. V. et al., *Z. Phys.* **C36**, 611.
- CHARM (1989): Dorenbosch, J. et al., *Z. Phys.* **C41**, 567.
- CHARM II (1991): Geigerat, D. et al., *Phys. Lett.* **B259**, 499.
- CLEO (1980): Andrew, D. et al., *Phys. Rev. Lett.* **45**, 452.
- CLEO (1987): Bebek, C. et al., *Phys. Rev.* **D36**, 1289.
- CLEO (1989): Artuso, M. et al., *Phys. Rev. Lett.* **62**, 2233.
- Close, F. E. (1973). *Partons and Quarks*. Daresbury Lecture Note Series No. 12, Daresbury Laboratory, Warrington.
- Close, F. E. (1979). *An Introduction to Quarks and Partons*. London: Academic.
- Condon, E. U. and Shortley, G. H. (1963). *The Theory of Atomic Spectra*. Cambridge: Cambridge University Press.
- Consoli, M. et al. (1989). In *Z Physics at LEP1*, eds. G. Altarelli, R. Kleiss and C. Verzegnassi. Vol. 1, p. 7. CERN 89-08.
- Covolan, R. and Predazzi, E. (1991). In *Hadronic Physics with Multi-GeV electrons*, eds. B. Desplanques and D. Goutte, p. 199. New York: Nova Scientia.
- Creutz, M. (1983). *Quarks, Gluons and Lattices*. Cambridge: Cambridge University Press.
- Creutz, M., Jacobs, L. and Rebbi, C. (1983). *Phys. Rep.* **95**, 201.
- CUSB II (1990): Lee-Franzini, J. et al., *Phys. Rev. Lett.* **65**, 2947.
- Cutler, R. and Sivers, D. (1978). *Phys. Rev.* **D17**, 196.
- DASP (1977). Brandelik, R. et al., *Phys. Lett.* **70B**, 125, 132.
- Dawson, S., Ellis, R. K. and Nason, P. (1988). *Nucl. Phys.* **B303**, 607.
- Dawson, S., Ellis, R. K. and Nason, P. (1989a). *Nucl. Phys.* **B327**, 49.
- Dawson, S., Ellis, R. K. and Nason, P. (1990). *Nucl. Phys.* **B335**, 260.
- Dawson, S. et al. (1989b). *The Higgs Hunter's Guide*, SC/PP-89/13.
- de Groot, J. G. H. et al. (1979). *Z. Phys.* **1C**, 143.
- DELPHI (1990): Abreu, P. et al., *Phys. Lett.* **B242**, 536.
- Derbenev, Ya. S. et al. (1978). *Part. Accel.* **8**, 115.

- de Rujula, A., Georgi, H. and Glashow, S. L. (1975). *Phys. Rev.* **D12**, 147.
- Diemoz, M. et al. (1988). *Z. Phys.* **C39**, 21.
- Dittmar, M. (1990). In *Proceedings of the 2nd International Conference on Medium and High Energy Physics*, Taiwan, 1990. CERN preprint-PPE/90-106.
- Drell, S. D. and Hearn, A. (1966). *Phys. Rev. Lett.* **16**, 908.
- Drell, S. D. and Yan, T. M. (1971). *Ann. Phys.* **66**, 555.
- Dydak, F. (1978). In *Proceedings of the 17th Internationale Universitätswochen für Kernphysik*, Schladming, Austria, 1978. Vienna: Springer-Verlag.
- Dydak, F. (1991). In *Proceedings of the 25th International High Energy Conference*, Singapore, 1990, Vol. 1, p. 3. Singapore: World Scientific.
- Eichten, E. and Gottfried, K. (1976). *Phys. Lett.* **66B**, 286.
- Eichten, E. et al. (1975). *Phys. Rev. Lett.* **34**, 369.
- Eichten, E. et al. (1978). *Phys. Rev.* **D17**, 3090.
- Eichten, E. et al. (1980). *Phys. Rev.* **D21**, 203.
- Eichten, E. et al. (1984). *Rev. Mod. Phys.* **56**, 579.
- Eichten, E. et al. (1986). *Rev. Mod. Phys.* **58**, 1065.
- Eigen, G. et al. (1982). *Phys. Rev. Lett.* **49**, 1616.
- Einstein, A., Podolski, B. and Rosen, N. (1935). *Phys. Rev.* **47**, 777.
- Ellis, J. (1977). In *Weak and Electromagnetic Interactions at High Energies*, Les Houches Summer School 1976, Session XXIX, ed. R. Bailin and C. H. Llewellyn-Smith, p. 1. Amsterdam: North Holland.
- Ellis, J. and Fogli, G. L. (1990). *Phys. Lett.* **B249**, 543.
- Ellis, J., Gaillard, M. K. and Nanopoulos, D. V. (1976). *Nucl. Phys.* **B106**, 292.
- Ellis, N. and Kernan, A. (1990). *Phys. Rep.* **195**, 23.
- Epele, L. N. et al. (1994). *Z. Phys.* **C64**, 285.
- EMC (1983): Aubert, J. J. et al., *Phys. Lett.* **123B**, 275.
- EMC (1985): Aubert, J. J. et al., *Nucl. Phys.* **B259**, 189.
- EMC (1986): Aubert, J. J. et al., *Nucl. Phys.* **B272**, 158.
- EMC (1987): Aubert, J. J. et al., *Nucl. Phys.* **B293**, 740.
- Feldman, G. J. (1977). In *Proceedings of the Summer Institute on Particle Physics*, p. 241. SLAC Publication 204.
- Feldman, G. J. et al. (1976). *Phys. Lett.* **63B**, 466.
- Feltesse, J. (1987). In *Proceedings of the HERA Workshop*, Hamburg, 1987, ed. R. D. Peccei, p. 33. Hamburg: DESY.
- Fermi, E. and Yang, C. N. (1949). *Phys. Rev.* **76**, 1739.
- Fetscher, W., Gerber, H-J. and Johnson, K. F. (1986). *Phys. Lett.* **B173**, 102.
- Feynman, R. P. (1969). In *Proceedings of the 3rd Topical Conference on High Energy Collisions of Hadrons*, Stonybrook, NY, 1969, ed. C. N. Yang et al., p. 237. New York: Gordon and Breach.
- Feynman, R. P. (1972). *Photon-Hadron Interactions*, section 33. Reading, MA: W. Benjamin.
- Feynman, R. P. and Gell-Mann, M. (1958). *Phys. Rev.* **109**, 193.
- Flügge, G. (1978). In *Proceedings of the 19th International Conference on High Energy Physics*, Tokyo, 1978, ed. G. Takeda, p. 793. Tokyo: Physical Society of Japan.

- Franzini, P. (1981). In *Proceedings of the International Conference on High Energy Physics*, Lisbon, 1981, eds. G. Dias de Deus and J. Soffer, p. 76. European Physical Society.
- Franzini, P. J. et al. (1989). In *Z Physics at LEP1*, eds. G. Altarelli, R. Kleiss and C. Verzegnassi, Vol. 2, p. 59. CERN 89-08.
- Freund P. G. O. and Nambu, Y. (1975). *Phys. Rev. Lett.* **34**, 1645.
- Fulton, R. et al. (1990). *Phys. Rev. Lett.* **64**, 16.
- Gabathuler, E. (1979). In *Proceedings of the EPS Conference on High Energy Physics*, Geneva, 1979, p. 695. Geneva: CERN Scientific Information Service.
- Gambino, P. (1990). Dissertation, University of Torino (unpublished).
- Gasiorowicz, S. (1967). *Elementary Particle Physics*. New York: Wiley.
- Gell-Mann, M. (1958). *Phys. Rev.* **111**, 362.
- Gell-Mann, M. (1962). *Phys. Rev.* **125**, 1067.
- Gell-Mann, M. (1964). *Phys. Lett.* **8**, 214.
- Georgi, H. and Glashow, S. L. (1972). *Phys. Rev. Lett.* **28**, 1494.
- Gerasimov, S. (1966). *Sov. J. Nucl. Phys.* **2**, 930.
- Gerber, H. J. (1987). In *Proceedings of the Europhysics Conference on High Energy Physics*, Uppsala, Sweden, eds. S. Kullander and R. Salmeron, Vol. II, p. 937. European Physical Society.
- Gilman, F. J. (1967). *Phys. Rev.* **167**, 1365.
- Gittelman, B. (1991). In *Proceedings of the 25th International High Energy Conference*, Singapore, 1990, eds. K. K. Phua and Y. Yamaguchi, p. 227. Singapore: World Scientific.
- Glashow, S. L. (1961). *Nucl. Phys.* **22**, 579.
- Glashow, S. L., Iliopoulos, J. and Maiani, L. (1970). *Phys. Rev. D* **2**, 1285.
- Glover, E. W. N. et al. (1989). In *Z Physics at LEP1*, eds. G. Altarelli, R. Kleiss and C. Verzegnassi, Vol. 2, p. 1. CERN 89-08.
- Gluck, M. and E. Reya (1978). *Nucl. Phys.* **B145**, 24.
- Godfrey, S. and Isgur, N. (1985). *Phys. Rev. D* **32**, 189.
- Goldberger, M. L. and Watson, K. M. (1964). *Collision Theory*, John Wiley and Sons.
- Goldhaber, G. (1976). In *Proceedings of the Summer Institute on Particle Physics*, p. 379. SLAC Publication 198.
- Goldhaber, G. et al. (1976). *Phys. Rev. Lett.* **37**, 255.
- Goldstone, J. (1961). *Nuovo Cim.* **19**, 15.
- Goldstone, J., Salam, A. and Weinberg, S. (1962). *Phys. Rev.*, **127**, 965.
- Green, M. and Schwarz, J. (1984). *Phys. Lett. B* **149**, 117.
- Greenberg, O. W. (1964). *Phys. Rev. Lett.* **13**, 598.
- Gromes, D. J. (1977). *Nucl. Phys.* **B131**, 80.
- Gross, D. J. et al. (1985). *Phys. Rev. Lett.* **54**, 502.
- Grosse, H. (1977). *Phys. Lett.* **68B**, 343.
- Gupta, S. N., Radford, S. and Repko, W. (1984). *Phys. Rev. D* **30**, 2425.
- Gursey, F. and Radicati, L. A. (1964). *Phys. Rev. Lett.* **13**, 1973.
- Haber, H. E. and Kane, G. (1985). *Phys. Rep.* **B117**, 75.
- Halzen, F. and Morris, D. A. (1991). *Particle World* **2**, 10.
- Han, K. et al. (1982). *Phys. Rev. Lett.* **49**, 1612.

- Han, M. Y. and Nambu, Y. (1965). *Phys. Rev.* **139B**, 1006.
- Hand, L. N. (1963). *Phys. Rev.* **129**, 1834.
- Hara, Y. (1964). *Phys. Rev.* **B134**, 701.
- Heimann, R. L. (1973). *Nucl. Phys.* **B64**, 429.
- Henley, E. M. and Wilets, L. (1976). *Phys. Rev.* **A14**, 1411.
- Herb, S. et al. (1977). *Phys. Rev. Lett.* **39**, 252.
- Heusch, C. (1989). In *Proceedings of the Tau-Charm Factory Workshop*, Stanford 1989, ed. Lydia Beers, p. 528. SLAC-343.
- Hey, A. J. G. (1974). In *Proceedings of the 9th Rencontre de Moriond*, ed. J. Tran Thanh Van, Lab. de Phys. Th. et Part. El., Bat. 211, 91405 Orsay, France.
- Hey, A. J. G. and Mandula, J. E. (1972). *Phys. Rev.* **D5**, 2610.
- Higgs, P. W. (1964a). *Phys. Lett.* **12**, 132.
- Higgs, P. W. (1964b). *Phys. Rev. Lett.* **13**, 508.
- Higgs, P. W. (1966). *Phys. Rev.* **145**, 1156.
- Hofstadter, R. (1957). *Ann. Rev. Nucl. Sci.* **7**, 231.
- Hogan, G. E. et al. (1979). *Phys. Rev. Lett.* **42**, 948.
- Hollik, W. F. L. (1990a). *Fortsch. Phys.* **38**, 165.
- Hollik, W. (1990b). In *Lectures of the CERN-JINR School of Physics*, Egmond aan-Zee, Nederlands, 1989. Geneva: CERN Scientific Information Service.
- Hollister, J. H. et al. (1981). *Phys. Rev. Lett.* **46**, 643.
- Iizuka, J. (1966). *Suppl. Progr. Theor. Phys.* **37-38**, 21.
- Isgur, N. and Wise, M. B. (1989). *Phys. Lett.* **B232**, 113.
- Isgur, N. and Wise, M. B. (1990). *Phys. Lett.* **B237**, 527.
- Itzykson, C. and Zuber, J-B. (1980). *Quantum Field Theory*. New York: McGraw-Hill.
- Jackson, J. D. (1963). *Elementary Particles and Field Theory*, ed. K. W. Ford, p. 354, Brandeis Summer Institute 1962. New York: Benjamin.
- Jacob, M. and Wu, T. T. (1987). *Phys. Lett.* **B197**, 253.
- Jadach, S. et al. (1989). In *Z Physics at LEP1*, eds. G. Altarelli, R. Kleiss and C. Verzegnassi, Vol. 1, p. 235. CERN 89-08.
- Jauch, J. M and Rohrlich, F. (1955). *The Theory of Photons and Electrons*. Reading, MA: Addison Wesley.
- Jean-Marie, B. et al. (1976). *Phys. Rev. Lett.* **36**, 291.
- Jona-Lasinio, G. and Nambu, Y. (1961a). *Phys. Rev.* **122**, 345.
- Jona-Lasinio, G. and Nambu, Y. (1961b). *Phys. Rev.* **124**, 246.
- Kamon, T. (1989). In *Proceedings of the 8th Topical Workshop on  $\bar{p}p$  Collider Physics*, Castiglione della Pescaia, Italy, 1989.
- Kinoshita, T. (1978). In *Proceedings of the 19th International Conference on High Energy Physics*, Tokyo, 1978, ed. G. Takeda, p. 591. Tokyo: Physical Society of Japan.
- Kinoshita, T. and Sirlin, A. (1959). *Phys. Rev.* **113**, 1652.
- Kobayashi, M. and Maskawa, T. (1973). *Prog. Theor. Phys.* **49**, 652.
- Köpke, L. and Wermes, N. (1989). *Phys. Rep.* **174**, 67.
- Krammer, M. and Kraseman, H. (1979). *Acta Physica Austriaca*, Suppl. XXI, 259.

- Kryzywicki, A. (1985). *Nucl. Phys.* **A446**, 135.
- Kühn, J. H. (1991). In *Proceedings of the 25th International Conference on High Energy Physics*, Singapore, 1990, eds. K. K. Phua and Y. Yamaguchi, p. 1169. Singapore: World Scientific.
- Kühn, J. H. and Wagner, F. (1984). *Nucl. Phys.* **B236**, 16.
- Kühn, J. H. and Zerwas, P. M. (1990). In *Z Physics at LEP1*, eds. G. Altarelli, R. Kleiss and C. Verzegnassi, Vol. 1, p. 267. CERN 89-08.
- Kwong, W. and Rosner, J. L. (1988). *Phys. Rev.* **D38**, 279.
- Kwong, W., Quigg, Ch. and Rosner, J. L. (1987). *Ann. Rev. Nucl. Part.* **37**, 325.
- L3 (1990a): Adeva, B. et al., *Phys. Lett.* **B250**, 199.
- L3 (1990b): Adeva, B. et al., *Phys. Lett.* **B247**, 473.
- L3 (1990c): Adeva, B. et al., *Phys. Lett.* **B248**, 225.
- L3 (1991): Adeva, B. et al., *Phys. Lett.* **B252**, 703.
- Landau, L. D. (1948). *Sov. Phys. Dok.* **60**, 207.
- Landau, L. D. and Lifshitz, E. M. (1977). *Quantum Mechanics*, p. 509. Pergamon Press.
- Langacker, P. (1989). In *Proceedings of the 24th International Conference on High Energy Physics*, Munich, 1988, eds. R. Kotthaus and J. H. Kühn, p. 190. Berlin: Springer Verlag.
- Leader, E. (1968). *Phys. Rev.* **166**, 1599.
- Leader, E. and Anselmino, M. (1988). *Z. Phys.* **C41**, 239.
- Lederman, L. M. (1978). In *Proceedings of the 19th International Conference on High Energy Physics*, Tokyo, 1978, ed. G. Takeda, p. 706. Tokyo: Physical Society of Japan.
- Lee, T. D. and Wu, C. S. (1965). *Ann. Rev. Nucl. Sci.*, **15**, 381.
- Lichtenberg, D. B. (1978). *Unitary Symmetry and Elementary Particles*, 2nd edn. New York: Academic Press.
- Lichtenberg, D. B. (1987). *Int. J. Mod. Phys.* **A2**, 1669.
- Lichtenberg, D. B., Predazzi, E. and Rossetti, C. (1988). *Z. Phys.* **C40**, 357.
- Lichtenberg, D. B. et al. (1989). *Z. Phys.* **C41**, 615; (1990) *Z. Phys.* **C46**, 75.
- Linde, A. (1976). *Sov. Phys. JETP Lett.* **23**, 64.
- Lindner, M. (1986). *Z. Phys.* **C31**, 295.
- Lovelock, D. M. J. (1985). *Phys. Rev. Lett.* **54**, 377.
- Lüscher, M., Szymanzik, K. and Weisz, P. (1980). *Nucl. Phys.* **B173**, 365.
- Macpherson, M. J. D. et al. (1987). *Europhysics Letters* **4**, 811.
- Macpherson, M. J. D. et al. (1991). *Phys. Rev. Lett.* **67**, 2784.
- Maiani, L. (1991). *Helv. Phys. Acta* **64**, 853.
- Marciano, W. (1979). *Phys. Rev.* **D20**, 274.
- Marciano, W. J. (1989). *Nucl. Phys.* **B** (Proc. Suppl.) **11**, 5.
- Marciano, W. J. and Sirlin, A. (1988). *Phys. Rev. Lett.* **61**, 1815.
- Marshak, R. E., Riazuddin and Ryan, C. P. (1969). *Theory of Weak Interactions in Particle Physics*. New York: Wiley-Interscience.
- Martin, A. (1977). *Phys. Lett.* **67B**, 330.
- Martin, A. D., Roberts, R. G. and Stirling, W. J. (1988). *Phys. Lett.* **B206**, 327.

- Martin, A. D., Roberts, R. G. and Stirling, W. J. (1989). *Mod. Phys. Lett.* **A4**, 1135; *Phys. Lett.* **B228**, 149.
- Matsuura, T. and van Neerven, W. L. (1988). *Z. Phys.* **C38**, 623.
- Matsuura, T., van der Marck, S. C. and van Neerven, W. L. (1988). *Phys. Lett.* **B211**, 171.
- Matsuura, T., van der Marck, S. C. and van Neerven, W. L. (1989). *Nucl. Phys.* **B319**, 570.
- Merzbacher, E. (1962). *Quantum Mechanics*. New York: Wiley.
- Morrison, R. J. (1990). *Nucl. Phys.* **B** (Proc. Suppl.) **16**, 108.
- Mulvey, J. (1987). In *Proceedings of the Workshop on Physics at Future Accelerators*, La Thuile and Geneva, 1987. CERN 87-07.
- Nachtmann, O. (1976). In *Proceedings of the 11th Moriond Meeting*, ed. J. Tran Thanh Van, p. 17. Ed. Frontières.
- Narison, S. and Pich, A. (1988). *Phys. Lett.* **B211**, 183.
- Navikov, V. A. et al. (1978). *Phys. Rep.* **41C**, 1.
- Neubert, M. (1992). In *Proceedings of the International Conference on B-Factories*, Stanford, California. SLAC-PUB-5842.
- Nicrosini, O. and Trentadue, L. (1987). *Phys. Lett.* **16B**, 551.
- Nicrosini, O. and Trentadue, L. (1988). *Z. Phys.* **C39**, 479.
- Nikolaev, N. N. and Zakharov, B. G. (1975). *Phys. Lett.* **B55**, 397; *Sov. J. Nucl. Phys.* **21**, 227.
- Nikolaev, N. N. and Zakharov, B. G. (1991). *Z. Phys.* **C49**, 607.
- NMC (1990): see C. Peroni, in *Proceedings of the Fermilab Workshop on Structure Functions*, Fermilab, Batavia, 1990. See also Windmolders, R., in *Proceedings of the 12th International Conference on Particles and Nuclei (PANIC 90)*, Cambridge MA, and *Phys. Rev. Lett.* **66** (1991) 2712.
- Noecker, M. C., Masterton, P. B. and Witman, C. (1988). *Phys. Rev. Lett.* **61**, 310.
- Norton, P. R. (1986). Contributed paper to the *23rd International Conference on High Energy Physics*, Berkeley, 1986.
- Okubo, S. (1963). *Phys. Lett.* **5**, 165.
- Okun, L. (1991). In *Proceedings of the 25th International Conference on High Energy Physics*, Singapore, 1990, eds. K. K. Phua and Y. Yamaguchi, Vol. 1, p. 319. Singapore: World Scientific.
- OPAL (1990): Akrawy, M. Z., *Phys. Lett.* **B241**, 133.
- Panofsky, W. K. H. (1968). In *Proceedings of the 14th International Conference on High Energy Physics*, Vienna, p. 23. Geneva: CERN Scientific Information Service.
- Pantaleone, J., Tye, S-H. H. and Ng, Y. I. (1986). *Phys. Rev.* **D33**, 777.
- Particle Data Group (1992). *Phys. Rev.* **D45**, N. 11, Part II.
- Partridge, R. et al. (1980). *Phys. Rev. Lett.* **45**, 1150.
- Paschos, E. A. and Türke, U. (1988). *Phys. Rep.* **178**, 145.
- Paschos, E. A. and Wolfenstein, L. (1973). *Phys. Rev.* **D7**, 91.
- Passarino, G. and Veltman, M. (1990). *Phys. Lett.* **B237**, 537.
- Peccei, R. D. (1988). Editor, *Proceedings of the 1987 HERA Workshop*, DESY publication.

- Perl, M. L. (1978). *Nature* **275**, 273.
- Perl, M. L. et al. (1975). *Phys. Rev. Lett.* **35**, 1489.
- Perl, M. L. et al. (1976). *Phys. Rev. Lett.* **38**, 117.
- Perl, M. L. et al. (1977). *Phys. Lett.* **70B**, 487.
- Peskin, M. E. (1990). Theory of precision electroweak measurements.  
SLAC-Pub. 5210.
- Pich, A. (1989). In *Proceedings of the Tau-Charm Factory Workshop*, Stanford 1989, ed. Lydia Beers, p. 416. SLAC-343.
- PLUTO (1977): Burmester, J. et al., *Phys. Lett.* **68B**, 297, 301.
- Preparata, G., Ratcliffe, P. G. and Soffer, J. (1990). *Phys. Rev.* **D42**, 930.
- Prescott C. Y. et al. (1978). *Phys. Lett.* **77B**, 347.
- Quigg, C. (1977). *Rev. Mod. Phys.* **14**, 297.
- Quigg, C. and Rosner, J. L. (1977a). *Phys. Lett.* **71B**, 153.
- Quigg, C. and Rosner, J. L. (1977b). *Phys. Lett.* **72B**, 462.
- Raab, J. R. et al. (1988). *Phys. Rev.* **D37**, 391.
- Rabi, S., West, G. B. and Hoffman, C. M. (1989). *Phys. Rev.* **D39**, 828.
- Rapidis, P. et al. (1977). *Phys. Rev. Lett.* **39**, 526.
- Ramond, P. (1981). *Field Theory: A Modern Primer*, Reading, MA:  
Benjamin/Cummings.
- Rebbi, C. (1983). *Lattice Gauge Theories and Monte Carlo Simulations*.  
Singapore: World Scientific.
- Reinders, L. J., Rubinstein, H. and Azachi, S. Y. (1985). *Phys. Rep.* **127**, 1.
- Richardson, J. (1979). *Phys. Rev.* **82B**, 282.
- Richter, B. (1976). In *Physics with Very High Energy e<sup>+</sup>e<sup>-</sup> Colliding Beams*, p. 237. CERN Report 76-18.
- Ross, D. A. and Veltman, M. (1975). *Nucl. Phys.* **B95**, 135.
- Sakita, B. (1964). *Phys. Rev.* **136B**, 1756.
- Sakurai, J. J. (1967). *Advanced Quantum Mechanics*, Addison-Wesley.
- Sakurai, J. J. (1978). *Schwinger Symposium*, p. 300.
- Salam, A. (1968). In *Elementary Particle Physics*, ed. N. Svartholm, p. 367.  
Stockholm: Almqvist and Wiksell.
- Sandars, P. G. H. (1989). In *Physics of Highly-ionized Atoms* (NATO ASI Series), ed. R. Marrus. New York: Plenum.
- Schindler, R. H. (1986). In *Proc. SLAC Summer Institute*, p. 239. Stanford:  
SLAC.
- Schopper, H. S. (1977). DESY Report 77/79.
- Schröder, H. (1989). In *Proceedings of the 24th International Conference on High Energy Physics*, München, 1988, eds. R. Kotthaus and J. H. Kühn, p. 73. Berlin: Springer Verlag.
- Sciulli, F. (1986). In *Proceedings of the International Symposium on Lepton and Photon Interactions at High Energies*, Kyoto 1985, eds. M. Konuma and K. Takakashi. Kyoto: Kyoto University.
- Shifman, M. A., Vainshtein, A. I. and Zakharov, V. I. (1978). *Nucl. Phys.* **B147**, 385, 448, 519.
- Sirlin, A. (1980). *Phys. Rev.* **D22**, 971.
- SLAC E140 (1988): Dasu, S. et al., *Phys. Rev. Lett.* **41**, 1061.

- SLAC (1989): Whitlow, L. W. *et al.*, in *Proceedings of the International Symposium on Lepton and Photon Interactions*, Stanford, ed. M. Riordan. Teaneck, New Jersey: World Scientific.
- SLAC-343 (1989). Proceedings of the tau-charm factory workshop, Stanford, 1989.
- Sloan, T., Smadja, G. and Voss, R. (1988). *Phys. Rep.* **162**, 45.
- Stack, J. (1984). *Phys. Rev.* **D29**, 1213.
- Steinberger, J. (1949). *Phys. Rev.* **76**, 1180.
- Stirling, W. J. and Wu, T. T. (1984). *Phys. Rep.* **107**, 59.
- Stodolski, L. (1967). *Phys. Rev. Lett.* **18**, 135.
- Struminsky, B. V. (1965). Dubna Preprint P-1939.
- Susskind, L. (1977). *Phys. Rev.* **D16**, 1519.
- Takahashi, Y. (1957). *Nuovo Cim.* **6**, 370.
- Taylor, J. C. (1976). *Gauge Theories of Weak Interactions*. Cambridge: Cambridge University Press.
- Taylor, J. D. *et al.* (1987). *J. Phys.* **B20**, 5423.
- Tenchini, R. (1990). In *Proceedings of the 18th Annual SLAC Summer Institute on Particle Physics*. University of Pisa Preprint INFN PI/AE 90/10.
- 'tHooft, G. and Veltman, M. (1974). Diagrammer. In *Particle Interactions at Very High Energies*, Pt B, ed. F. Halzen, D. Speiser and J. Weyers. New York: Plenum Press.
- Thresher, J. J. (1989). In *Proceedings of the 24th International Conference on High Energy Physics*, Munich, 1988, eds. R Kotthaus and J. H. Kühn, p. 387. Berlin: Springer Verlag.
- Tixier, M. H. (1988). In *Proceedings of the Conference on Microphysical Reality and Quantum Formalism*, eds. A. Van der Merwe *et al.*, p. 361. Kluwer Academic Publishers.
- Törnquist, N. A. (1981). *Found. Phys.* **11**, 171.
- Trippé, T. G. *et al.* (1977). *Phys. Lett.* **68B**, 1. [Addendum *Phys. Lett.* (1978), **B75**, 1.]
- UA1 (1983): Arnison, G. *et al.*, *Phys. Lett.* **B122**, 103.
- UA2 (1983): Banner, M. *et al.*, *Phys. Lett.* **B122**, 476.
- UA5 (1983): Alguard, K. *et al.*, *Phys. Lett.* **B121**, 209.
- UA5 (1984): Alner, G. J. *et al.*, *Phys. Lett.* **B138**, 304.
- Van der Bij, J. J. and Hoogeveen, F. (1987). *Nucl. Phys.* **B283**, 477.
- Van der Meer, S. (1981). *IEEE Trans, Nucl. Sci.* **28**, 1994.
- Van Nieuwenhuizen, P. (1981). *Phys. Rep.* **68**, 191.
- Vannucci, F. (1978). Contribution to the Karlsruhe Summer Institute, Karlsruhe, Germany.
- Van Royen, R. and Weisskopff, V. F. (1967a). *Nuovo Cimento* **50**, 617; (1967b) *erratum Nuovo Cimento* **51**, 583.
- Veltman, M. (1977). *Nucl. Phys.* **B123**, 89.
- Vilain, P. (1990). *14th International Conference on Neutrino Physics and Astrophysics*, Geneva. CERN Scientific Information Service.
- Voss, R. (1986). Contributed paper to the *23rd International Conference on High Energy Physics*, Berkeley, 1986.

- WA25 (1985): Allasia, D. *et al.*, *Z. Phys.* **C28**, 321.  
Wegner, F. J. (1971). *J. Math. Phys.* **12**, 2259.  
Ward, J. C. (1950). *Phys. Rev.* **78**, 1824.  
Weinberg, S. (1967). *Phys. Lett.* **12**, 132.  
Weinberg, S. (1976a). *Phys. Rev. Lett.* **36**, 294.  
Weinberg, S. (1976b). *Phys. Rev.* **D13**, 974.  
Wess, J. and Zumino, B. (1974). *Nucl. Phys.* **B70**, 39.  
Wiik, B. H. and Wolf, G. (1978). *A review of e<sup>+</sup>e<sup>-</sup> interactions*, DESY Preprint 78/23.  
Winter, K. (1978). In *Proceedings of the 1978 International School of Subnuclear Physics 'Ettore Majorana'*, ed. A. Zichichi. New York: Plenum Press.  
Withlow, L. C. (1990). Ph.D. thesis and SLAC rep. 357 and references therein.  
Wolf, G. (1979). In *Proceedings of the EPS International Conference on High Energy Physics*, Geneva, 1979, p. 220. Geneva, CERN Scientific Information Service.  
Wu, C. S. and Moskowski, S. A. (1966). *Beta Decay*. New York: Wiley.  
Yang, C. N. (1950). *Phys. Rev.* **77**, 242.  
Yang, C. N. and Mills, R. L. (1954). *Phys. Rev.* **96**, 191.  
Zholentz, A. A. *et al.* (1980). *Phys. Lett.* **B96**, 214.  
Zichichi, A. (1977). In *Proceedings of the 1975 International School of Subnuclear Physics 'Ettore Majorana'*, ed. A. Zichichi, part B, p. 741. New York: Plenum Press.  
Zumerle, G. (1992). In *Proceedings of the 12th Conference on Physics in Collision*, Boulder, Colorado, 1992.  
Zweig, G. (1964). Unpublished. CERN Preprints, Th 401, 412.

# Analytic subject index for vols. 1 and 2

Bold numbers refer to major references, for example definitions

- abelian gauge symmetries *see* gauge symmetry      evidence for 1.360  
absorptive part of transition amplitude 2.33–34, 2.383      antishadowing 1.414  
acoplanarity 2.254, 2.266      Applequist–Carrazone theorem 2.122  
Action 1.29      asymmetries and polarization at the  $Z^\circ$  1.149  
    Euclidean 2.327, 2.396      asymptotic freedom 2.81  
    Lattice QCD, for 2.305      scaling, and 2.81  
active flavours 2.123      Lattice QCD, in 2.304  
ADA storage ring 1.119      away jet 2.221  
Ademollo–Gatto theorem 2.3      axial anomaly *see* anomalies  
Adler sum rule 1.401, 2.146, 2.154      axial gauges 2.114  
AEEC 2.281      axions 2.332, 2.341  
Altarelli–Parisi equations 2.148, 2.185       $A_1, A_2$  asymmetry parameters for  
    summary of 2.186       $\gamma N \rightarrow \gamma N$  1.346–349, 1.381,  
angular momentum sum rule 1.408      1.405  
angular ordering 2.275, 2.285       $A_{\parallel}$  longitudinal asymmetry in  
anomalies      polarized DIS 1.348  
    axial isosinglet current 2.330       $A_{\perp}$  transverse asymmetry in  
    baryon number axial current 2.341      polarized DIS 1.350  
    baryon number vector current 2.334       $\alpha$ , fine structure constant in QED  
    lepton number vector current 2.334      1.57  
    *see also* triangle anomaly      effective or running 1.57  
anomalous dimensions **2.83**, 2.142       $\alpha_s$ , fine structure constant for QCD  
anomalous magnetic moment of nucleon 1.321      1.207, 1.260  
anticommutators 1.445, 2.353      effective or running **2.79**  
anti-linear (anti-unitary) operators 2.384      formula to lowest order 2.84  
antipartons **1.359**      formula to next to leading order  
  2.124–126, 2.269  
experimental determination  
     $J/\Psi$  decay 1.260  
jet production in  $e^+e^-$  collisions  
  2.258, 2.265, 2.282

- jet production in hadronic reactions 2.239
- $\Upsilon$  decay 1.260
- vector quarkonium states 1.260
- $\alpha_1, \alpha_2, \alpha_3$  couplings in GUT 2.343
- $a_e, a_f, a_l$  neutral weak axial vector coupling constants 1.68
- bare coupling constant 2.54
- bare field 2.54
- bare mass 2.54
- baryon non-conservation *see*  $B$ -violation
- baryon number current
  - anomaly in 2.341
  - axial vector 2.341
- $B^0 - \bar{B}^0$  mixing 1.297, 2.19
  - dynamics of 2.45
  - incoherent production, in 2.20
  - $\Upsilon(4S)$  decay, in 2.20
- $B^0 - \bar{B}^0$  CP-violation 2.48
  - $B^0 \rightarrow \psi K_S$  2.51
- binomial distribution, negative **2.297**
- Bhabha scattering 1.126
- Bjorken limit **1.338**, 2.138
- Bjorken scaling **1.336**, 1.348, 2.138
  - see also* DIS
- Bjorken sum rule 1.347, 1.349
  - parton model, in 1.406
- Bjorken  $x$  **1.338**
- $B_K$  in  $K^0 - \bar{K}^0$  CP-violation 2.39
  - Lattice QCD, in 2.305
- $B-L$  symmetry (baryon-lepton) **2.339**
- Bloch states **2.314**, 2.319, 2.328
- $B$  mesons *see* bottom mesons
- Bott theorem 2.324
- bottom mesons
  - decays 1.290
  - $\bar{B}^0 \rightarrow D^{+*} l^- \bar{\nu}$  1.291
  - lifetime, theory of 1.285, 1.291
- bottom particles
  - discovery of 1.270, 1.273
  - lifetime 1.299
- bottom production
  - at LEP 1.295
  - cross-section 1.294
  - forward-backward asymmetry 1.298
  - threshold in DIS 1.369
  - bottom quark 1.157, 1.160
  - charge of 1.273, 1.279
  - lifetime of 1.285
  - transitions in standard model 1.270
- broken symmetries *see* spontaneous symmetry breaking
- $B$ -violation (baryon number)
  - GUT, in 2.342
  - SM, in 2.332, 2.336
    - $qq \rightarrow 7\bar{q} + 3\bar{l}$  2.336
    - $qq \rightarrow 7\bar{q} + 3\bar{l} + n$  gauge bosons 2.337; perturbative corrections 2.337; unitarity bound 2.337
    - $\sigma_{tot}$  for, 2.338
- $\beta$ -decay 1.6–7, 2.12
  - hyperons, of 2.2
  - kaons, of 2.2
  - neutrinoless 2.345
  - pions, of 1.14
  - quark picture of 1.12
- $\beta$ -function
  - $b, b'$  in QCD 2.120
    - see also* renormalization group
  - $\beta$  parameter (Lattice QCD) 2.305
  - $b, b'$  (QCD  $\beta$ -function) 2.120
- Cabibbo allowed reactions 1.10, 1.270, 1.283
- Cabibbo angle 1.10, 1.270, 1.283
- Cabibbo forbidden reactions 1.10, 1.270, 1.283
- Cabibbo theory 1.10–13
- Callan–Gross relation 1.355
- Callan–Symanzik equation 1.355, 1.393, 2.146, 2.154
- canonical quantization 2.55
- causality 1.444, 2.352
- charge conjugation 1.447, 2.357
  - invariance 1.465, 2.373

- charge operator of conserved current 1.466, 2.374  
 charge raising operator 1.18  
 charged current (CC) reactions 1.332  
*see also* DIS  
 charged weak hadronic interaction 1.177  
 charged weak leptonic interaction 1.67  
 charm 1.270  
   detection of 1.270, 1.276  
   discovery and basic properties 1.270  
   production  
     at LEP 1.295  
     cross-section 1.294  
      $Z^0$  decay, in 1.295–297  
 charm baryons 1.272–279  
   mass relations 1.272, 1.282  
 charm mesons 1.272–277  
   decay, theory of 1.283  
   detection of 1.272, 1.276  
   hadronic decays 1.287  
   leptonic decays 1.286  
   lifetimes 1.284  
   mass relations 1.282  
   semi-leptonic decays 1.279, 1.287  
 charm quark 1.157  
   charge of 1.280  
   decay of 1.282  
   threshold in DIS 1.369  
   transitions in SM 1.270, 1.282  
 charmonium 1.202, 1.241  
   decay into gluons 1.213–218  
   decay selection rules 1.216  
   *see also* narrow vector resonances  
 chiral charge 2.330  
 chiral symmetry 1.10, 2.106  
   Lattice QCD, in 2.305  
    $\theta$ -vacuum non-invariance 2.329  
    $U(1)$  problem 2.328, 2.340  
 CLIC  $e^+e^-$  collider 1.154  
 cluster fragmentation 2.277  
 coefficient function (Wilson expansion) 2.136  
 coherence length (DIS) 1.413  
 collinear singularities 2.171–180  
 colour 1.4, 1.166  
    $e^+e^- \rightarrow$  hadrons, in 1.274  
    $\pi^0 \rightarrow 2\gamma$ , in 1.168  
   QCD, in 2.105  
   triangle anomaly, in 1.170  
 colour charge 2.109, 2.322  
 colour charge density 2.322  
 colour-electric, magnetic fields 2.321  
 colour sums 1.459, 2.367  
 commutation relations 1.443, 2.351  
   canonical 1.5  
   generators of gauge transformations, for 1.34–35  
    $\phi^4$  theory, in 2.54  
 compositeness 2.347  
 Compton scattering 1.459, 2.61, 2.367, 2.390–394  
   gauge invariance, in 2.109  
   gluons, of 1.459, 2.390–392  
 confinement 2.98, 2.309  
 conjugate momentum 2.55  
 continuum limit (Lattice QCD) 2.305, 2.307  
 convolution theorem (Mellin transforms) 2.148  
 correlation functions 2.302  
 Coulomb gauge 2.102  
 counter terms (renormalization) 2.60  
 counting rules 2.230  
 coupling constants  
   Fermi  $G$  1.6, 1.56–58, 1.108, 1.110, 1.115  
   QCD, in, *see*  $\alpha_s$   
   QED, in, *see*  $\alpha$   
   SM, in  
     data from LEP 1.133  
      $g$ ,  $g'$  1.52;  $e$ , relation to 1.53;  $G$ , relation to 1.56  
      $G$ , relation to SM parameters;  
       lowest order, in 1.57–58, 1.108; radiative corrections to 1.108; beyond lowest order 1.109–110  
     Higgs-fermion 1.90  
     Higgs-lepton 1.61

- Higgs- $W$ ,  $Z^0$  1.92
- lepton axial vector 1.68
- lepton vector 1.68
- neutral weak 1.68
- coupling of fields *see* Lagrangian density
- covariant derivative
  - non-Abelian theories, in 1.35–37
  - QED, in 1.32
  - QCD, in 2.105
- covariant gauges 2.103, 2.114
- covariant spin vector 1.343
  - partons, for 1.394
- CPT invariance *see* TCP invariance
- CP-violation 1.162, 2.12
  - $B^0$ - $\bar{B}^0$  system, in 2.19, 2.48
  - $D^0$ - $\bar{D}^0$  system, in 2.19
  - dynamics of 2.32
  - formalism, general 2.15, 2.23
  - $K^0$ - $\bar{K}^0$  system, in 2.18, 2.23
  - practical aspects 2.17
  - QCD, in 2.319, 2.329, 2.341
- creation operators 1.1, 1.4, 1.443, 2.351
- current conservation
  - gauge transformations, and 1.31
  - matrix elements, with *see* current matrix elements
- operator product expansion, in 2.135
- QCD, in 2.108
- QED, in 1.2, 2.109–110
- current correlation function 2.302
- current-current form of weak interactions 1.6
  - effective Hamiltonian, and 2.381
- current matrix elements
  - axial vector octet 1.468, 2.376
  - conserved currents, for 1.465, 2.373
    - electromagnetic 1.467, 2.375
    - $F$  and  $D$  parameters 1.406–407, 1.468, 2.376
    - general symmetry group 1.467, 2.375
    - isospin 1.467, 2.375
  - isospin raising operator 1.467, 2.375
  - $SU(3)$  octet 1.468, 2.376
  - quark–parton model for 1.393
  - vector octet 1.468, 2.376
- currents
  - anomalous 2.330, 2.334, 2.341
  - conserved
    - matrix elements *see* current matrix elements
    - associated charge 1.31, 1.465, 2.373; group generators, relation to 1.466, 2.372
  - electromagnetic 1.2
    - quarks, of 1.163
  - $K_\mu$  (QCD) 2.326
  - QCD 2.106
    - Noether currents 2.109
    - non-gauge invariance of 2.109
  - weak 1.6
    - axial vector 1.10; partially conserved (PCAC) 1.11
    - charged quark, coupled to  $W$  1.164
    - conserved vector current (CVC) 1.8
  - $F$  and  $D$  parameters 1.406–407, 1.468, 2.376
  - hadronic matrix elements of 1.8;
    - see also* current matrix elements
  - neutral bounds on 1.187;
    - Cabibbo theory, in 1.11; evidence for 1.184; leptonic, coupled to  $Z^0$  1.60; quark, coupled to  $Z^0$  1.163
  - nucleon vector 1.8
  - octet of conserved vector 1.10
  - strangeness changing hadronic 1.10, 1.202
  - $SU(3)_F$ ; hadronic 1.11; matrix elements of 1.468, 2.376; quark fields, in terms of 1.12
  - $V-A$  structure of 1.7

- cut-off parameter (field theory) 2.57,  
     2.62  
 CVC *see* currents  
 $c_A, c_V$  neutral weak couplings 1.71,  
     1.75  
 $C_A$  (QCD) xxvi, 2.119  
 $C_F$  (QCD) xxvi, 2.130  
 $C_2(G)$  (QCD) xxvi, 2.119  
 $C_2(R)$  (QCD) xxvi, 2.130  
 $\Xi_c$  charm baryon 1.275
- $D$  and  $F$  in current matrix elements  
     1.11, 1.407, 1.468, 2.376  
 $D^0$ - $\bar{D}^0$  mixing 2.19  
 $d$ -dimensional integrals *see*  
     dimensional regularization  
 $D$  mesons 1.271–277  
     detection of 1.272, 1.276  
     hadronic decays 1.287  
     leptonic decays 1.286  
     lifetimes, of 1.284  
     mass relations 1.282  
     semi-leptonic decays 1.279, 1.287  
 decay rate in terms of Feynman  
     amplitude 1.452, 2.360  
 decoupling theorem for heavy quarks  
     2.122  
 degenerate vacuum  
     classical field theory, in 2.318  
     double-well potential, in 2.314  
     QCD, in *see* vacuum, QCD, in  
     SM, in *see* vacuum, SM, in  
 diffraction dissociation 2.295  
 dimensional regularization 2.63, 2.71  
      $d$ -dimensional integrals 2.86  
         convergence of 2.87  
         divergence and analytic  
           continuation 2.87  
         examples of 2.91  
         MS and  $\overline{\text{MS}}$  schemes 2.96  
         regularization, in 2.89  
 $\phi^4$ -theory, in 2.93–99  
 dimensions  
     matrix elements, of 1.464, 2.372  
     operators, of 2.136, 2.302  
     physical, in natural units 1.5
- dipole moment of neutron, electric  
     2.341  
 diquarks 2.232  
 Dirac form factors 1.322  
 Dirac matrices *see*  $\gamma$ -matrices  
 Dirac operator (Lattice QCD) 2.306  
 DIS **1.324**  
     Altarelli, Parisi, Gribov, Lipatov  
         equations 2.148  
     distribution functions *see* partons,  
         distribution functions  
 electromagnetic interactions **1.325**  
     Bjorken limit 1.338  
     cross-section for 1.325–328,  
         1.339; scaling functions  $F_j$ ,  
         in terms of 1.339  
     hadronic tensor for 1.325–327,  
         1.386; relation to  $\gamma N \rightarrow \gamma N$   
         1.329–330  
     leptonic tensor for 1.312, 1.325  
     one photon exchange, test for  
         1.325  
 $R$  ratio of longitudinal to  
     transverse cross-sections  
     1.331, 1.337, 1.346, 1.355,  
     1.400, 1.427  
 scaling behaviour 1.336–338  
 scaling functions  $F_j$  1.338, 1.355,  
     1.416, 2.184, 2.195–205; *see*  
         also scaling functions  
 structure functions  $W_j$  1.328;  
     data on 1.364;  $\gamma N$   
     cross-section, relation to  
         1.330, 1.345; moments of  
         2.140, 2.148  
 EMC effect 1.409  
 $F_L$  longitudinal scaling function  
     2.198  
 HERA collider, role of 1.340–342  
 $lh \rightarrow lCX$ , semi-inclusive 2.227  
 $lN \rightarrow lX$   
      $Q^2 \approx M_W^2$  in CC reactions;  
         cross-sections for 1.425;  
         scaling functions for 1.375  
 $Q^2 \ll M_Z^2$ , for *see* DIS,  
     electromagnetic interactions

- $Q^2 \approx M_Z^2$  in NC reactions; cross-section for 1.341, 1.425;  $\gamma$ - $Z^0$  interference 1.341; hadronic tensor for 1.341; scaling functions for 1.341, 1.374
- moments of scaling functions 2.140
- $Q^2$ -dependence of; higher order, in 2.151;  $\Lambda$  parameter (QCD) 2.153; leading order, in 2.148; renormalization scheme dependence 2.153
- momentum carried by partons 2.188
- neutrino induced reactions **1.331**
- $\nu N \rightarrow l^- X$  (CC reactions) 1.331; cross-sections for 1.332–335, 1.339, 1.419; scaling functions, in terms of 1.339; hadronic tensor for 1.332 (charm threshold, below 1.332); leptonic tensor for 1.332–333; NC reactions, relation to 1.423–424; scaling functions  $F_j$  1.338, 1.371, 2.141, 2.147, 2.195–205 (*see also* scaling functions); structure functions  $W_j$  for 1.335 (moments of 1.140, 1.148;  $WN \rightarrow WN$ , relation to 1.339)
  - $\nu N \rightarrow \nu N$  (NC reactions) **1.331**; CC reactions, relation to 1.423–424; cross-sections for 1.333–334, 1.340, 1.416–422 (scaling functions, in terms of 1.340); hadronic tensor for 1.333; leptonic tensor for 1.333; scaling functions  $F_j$  1.339, 1.361 (*see also* scaling functions); structure functions  $W_j$  for 1.335 (moments of 2.140, 2.148;  $Z^0 N \rightarrow Z^0 N$ , relation to 1.340)
- nuclear effects **1.409**
- antishadowing 1.414
- coherence length 1.413
- experimental 1.416
- Fermi motion 1.414
- mean free path 1.413
- nuclear radius 1.413
- scaling functions, convolution formula 1.415
- shadowing 1.412
- vector meson dominance 1.413
- operator product expansion **2.135**
- parton model, in **1.353**
- antipartons 1.359
  - Callan–Gross relation 1.355, 1.366, 1.383, 2.146, 2.154
  - experimental tests **1.396**
  - Fermi motion 1.354, 1.382, 1.414
  - Gottfried sum rule 1.363, 1.402
  - impulse approximation, as 1.396
  - neutrino cross-sections in 1.356–358
  - partons as quarks 1.361
  - polarized DIS, in 1.378;  $A_1$ ,  $\gamma N$  asymmetry 1.381; Bjorken sum rule 1.379, 1.406; quark distributions, polarized 1.379, 1.406; scaling functions 1.378
  - quark-parton, detailed 1.364; bottom production, threshold for 1.369; charm production, threshold for 1.369; gluons, evidence for 1.377; Nachtmann inequality 1.367; parton distributions (*see* partons, distribution functions); scaling functions 1.366, 1.371–375
  - $r$ , ratio of  $\bar{\nu}$  to  $\nu$  cross-sections 1.359
  - scaling functions  $F_j$  1.355–357
  - structure functions  $W_j$  1.354–356
- parton model with transverse motion 1.384–386
- current matrix elements in 1.393

- hadronic tensor 1.389
- scaling functions 1.389
- polarization effects **1.342**, 1.378
  - $A_{\parallel}$  longitudinal asymmetry 1.348
  - $A_{\perp}$  transverse asymmetry 1.350
  - Bjorken sum rule 1.347, 1.349, 1.379, 1.406
  - cross-sections 1.345–346
  - Drell, Hearn, Gerasimov sum rule 1.347
  - hadronic tensor 1.344
  - Hey, Mandula sum rule 1.350
  - leptonic tensor 1.344
  - parton model for 1.378, 1.393
  - scaling functions  $g_1, g_2$  1.348
  - spin crisis 1.405
  - structure functions  $G_j$  1.344; polarized  $\gamma N$  cross-section, relation to 1.346
- QCD, in 2.155, 2.163, 2.183
  - data, comparison with 2.202
  - evolution equations 2.186
  - $F_L$  longitudinal scaling function 2.198
  - heavy quark production 2.201
  - momentum carried by partons 2.188
  - scaling functions; leading logarithmic approximation 2.174, 2.185; beyond LLA 2.195; renormalization scheme dependence 2.181, 2.196
  - small- $x$  behaviour 2.189
  - spin-dependent parton distributions 2.187
  - $x \rightarrow 1$  behaviour 2.192
- renormalization group analysis 2.131, 2.142
- scale breaking 2.140
- scaling 1.336, 1.348, 2.138
- scaling functions
  - see* DIS, electromagnetic interactions; neutrino induced reactions; parton
- model for; polarization effects
  - see also* scaling functions in DIS
- small- $x$  behaviour 1.375, 1.402, 2.138
- spin crisis 1.405
- sum rules
  - Adler **1.401**, 2.146, 2.154
  - angular momentum 1.407
  - Bjorken 1.347–349, 1.379, 1.406
  - Drell, Hearn, Gerasimov 1.347
  - experimental tests 1.401
  - Gottfried 1.363, 1.402, 2.154
  - Gross, Llewellyn-Smith 1.401, 2.146, 2.154
  - Hey, Mandula 1.350
  - Llewellyn-Smith 1.401, 1.403
  - momentum 1.377
  - $x \rightarrow 1$  behaviour 2.191
- dispersive part of transition
  - amplitude 2.33–34, 2.383
- distributions of partons *see* partons, distribution functions
- DORIS storage ring 1.118
- double  $\beta$ -decay 1.7
- Drell, Hearn, Gerasimov sum rule 1.347
- Drell–Yan reaction 1.429
  - colour, rôle of 1.432
  - cross-section 1.431
  - data 1.435, 2.216
  - high mass,  $m \approx M_Z$  2.216
  - nucleii, in 1.439
  - parton model for 1.429
    - applicability conditions 1.434
  - $p_T$  distribution 2.213
- QCD-improved parton model for 2.209
  - data, comparison with 2.216
  - scaling 1.434
  - vector meson production 1.440, 2.210
- dual field tensor
  - QED, in 2.319
  - QCD, in 2.321
- $\delta$ , phase angle in KM matrix **1.163**

- $B^0-\bar{B}^0$  mixing, in 2.46  
 $K^0-\bar{K}^0$  CP-violation, from 2.27,  
   2.39  
 $\delta_0, \delta_2, \pi\pi$  phase-shifts 2.23  
 $\Delta I = \frac{1}{2}$  rule in non-leptonic  $K$ -decay  
   2.26  
 $\Delta r$  parameter in radiative corrections  
   to SM 1.109  
 $\Delta S = \Delta Q$  rule for semileptonic  
   decays 1.14  
 $\Delta(x)$  singular function 1.464, 2.352  
 $d_{abc}$  in  $SU(3)$  1.460–463, 2.370–373
- EEC energy correlations 2.280  
 effective coupling *see* running  
   coupling  
 effective Hamiltonians 2.378  
   current-current interaction,  
     relation to 2.381  
 elastic scattering, hadronic 2.289  
   differential cross-section 2.292  
   Odderon 2.293  
    $\rho$ , real to imaginary ratio 2.289,  
     2.293  
    $\sigma_{\text{el}}/\sigma_{\text{tot}}$  2.291  
 electromagnetic current *see* currents  
 electron–neutrino scattering 1.69–76  
 electron-number 1.7  
 electron self-energy 2.56  
 EMC effect 1.409  
 energy flow 2.280  
 energy–energy correlations (EEC)  
   2.280  
 Euclidean action in QCD 2.327,  
   2.396  
 Euclidean space conventions  
   2.395–396  
 Euclidean time 2.309, 2.316, 2.395  
 Euler–Lagrange equations 2.29, 2.54  
 event generators 2.270  
 evolution equations 2.148, 2.185  
   summary of 2.186  
 exclusive reactions *see* elastic  
   scattering; large  $p_T$  reactions  
 $E_{S_p}$  (sphaleron energy) 2.336  
 $\epsilon(x)$  step function 1.464, 2.352
- $\epsilon, \epsilon'$  in  $K^0-\bar{K}^0$  CP-violation  
 CP-violating Hamiltonian, relation  
   to 2.28  
 definitions 2.26  
 estimate in SM 2.35–40  
 numerical values 2.27–28  
 Wu–Yang convention 2.28–29
- $e^+e^-$   
 colliders 1.118  
   ADA 1.119  
   CLIC 1.154  
   LEP 1.122  
   SLC 1.125  
   TRISTAN 1.121  
   luminosity 1.120  
   polarization 1.120, 1.123  
   storage rings 1.118
- $e^+e^-$  reactions  
   Bhabha scattering 1.126  
    $e^+e^- \rightarrow f\bar{f}$ ; and the SM 1.132  
     angular distribution 1.134, 2.255  
     asymmetry at  $Z^0$  1.149  
     Breit–Wigner form 1.137, 1.140  
     cross-section, total 1.129, 1.136  
     helicity amplitudes 1.137  
     polarized beams, with 1.151  
     polarization of  $f$  in SM 1.153  
      $\sigma_L, \sigma_T$  2.256  
     vector and axial couplings at  $Z^0$   
       1.150  
    $e^+e^- \rightarrow$  hadrons  
     colour, rôle of 1.174  
     energy–energy correlations 2.280  
     energy flow 2.280  
     multiplicity 2.277  
     *see also* Monte Carlo for  
        $e^+e^- \rightarrow$  hadrons;  $R$
- $e^+e^- \rightarrow hX$  2.255  
   angular distribution 2.255  
   polarized beams, with 2.258  
    $\sigma_L, \sigma_T$  2.256  
    $e^+e^- \rightarrow \mu^+\mu^-$  1.126, 1.129  
     angular distribution 1.129  
     forward–backward asymmetry  
       1.138

- $e^+e^- \rightarrow$  Jets *see jets in  $e^+e^-$  physics*
- $e^+e^- \rightarrow \pi^+\pi^-$  2.257
- $e^+e^- \rightarrow q\bar{q}$  2.255
- $e^+e^- \rightarrow 2\gamma$  1.126
- $e^+e^- \rightarrow \tau^+\tau^-$  1.143–147
- $e^+e^- \rightarrow X$  1.134  
parton model for 1.426
- energies  $\ll M_Z$ , at 1.126
- LEP data 1.133
- Möller scattering 1.128
- QED, tests of 1.130
- $R, \sigma(e^+e^- \rightarrow X)/\sigma(e^+e^- \rightarrow \mu^+\mu^-)_{\text{QED}}$  1.122, 1.175, 1.205, 1.222, 1.239, 1.273, 1.300, 1.427, 2.128, 2.131–133, 2.262
- SM, in 1.132
- $e\mu \rightarrow e\mu$  **1.317**  
Mott cross-section 1.320
- $e\mu \rightarrow eX$  1.329
- $eN \rightarrow eX$  *see* DIS
- $ep \rightarrow ep$  1.321–324  
electromagnetic form factors 1.322  
dipole form 1.323  
parton model, in 2.229
- $e$ -nucleus scattering 1.189  
parity violating asymmetry 1.191
- $e\nu_e, e\bar{\nu}_e$  elastic scattering 1.69–74
- $e\nu_\mu, e\bar{\nu}_\mu$  elastic scattering 1.74–77
- $F$  in matrix elements of  $SU(3)$   
currents 1.407, 1.468, 2.376
- factorization scale 2.181
- fastest apparent convergence method 2.133
- Fermi–Breit interaction 1.249
- Fermi coupling constant **1.6**  
numerical value 1.58
- Fermi Lagrangian **1.6**  
QED, in 2.103
- Fermi motion  
parton model, in 1.354, 1.382, 1.414
- Fermi theory **1.6**  
problems with 1.23
- Feynman amplitude  
cross-section, in terms of 1.472, 2.360
- decay rate, in terms of 1.472, 2.360
- operator form of 2.35, 2.378–381
- $S$ -matrix, relation to 1.451, 2.359  
*see also* Feynman rules
- Feynman gauge 2.104, 2.114
- Feynman path integrals 2.305  
double-well potential, in 2.315
- Feynman propagator 1.444, 2.352
- Feynman rules  
QCD 1.452, 2.114, 2.360  
QED 1.452, 2.360  
quark–gluon scattering 1.459, 2.367  
quark–quark scattering 1.458, 2.366  
SM 1.455–457, 2.363–365
- field operators 1.1, 1.443, 2.351  
photon 1.2, 1.446, 2.354  
scalar 1.443, 2.351  
spinor 1.445, 2.353  
spin 1 1.446, 2.354
- field tensors ( $F_{\mu\nu}, G_{\mu\nu}$ ) 1.37, 2.99, 2.105  
dual  
QCD, in 2.321  
QED, in 2.319  
QCD, for 2.104  
equations of motion 2.321  
fields, in terms of 2.321  
QED, for 1.33, 2.99  
fields, in terms of 2.319
- $W$  boson, for 1.37
- Fierz reshuffle theorem 1.463, 2.371
- fine structure constant 1.57  
effective or running 1.57, 1.106
- flavour 1.160  
classification of hadrons 1.209  
 $n_f$ , number of flavours 2.120  
 $n_f^*$ , number of active flavours 2.123
- form factors, elastic, of nucleon **1.321**
- Dirac 1.322
- parton model, in 2.229

- Sachs 1.322
- forward-backward asymmetry in
  - $e^+e^-$  1.138, 1.149
  - at  $Z^0$  1.149
- fragmentation functions 2.208, 2.221, 2.225
- Froissart bound 2.290
- $F_L$ , longitudinal scaling function 2.198
- $f_{abc}$  structure constants xxvi, 1.460–463, 2.105, 2.368–371
- $f_\pi$ ,  $f_K$ ,  $f_D$ , pseudoscalar meson decay constants 1.286
- Lattice QCD, in 2.312
- CP-violation, rôle in 2.38
- gauges
  - axial 2.114
  - Coulomb 1.38, 2.101
  - covariant 2.103, 2.114
  - Feynman 2.104, 2.114
  - Landau 2.104, 2.114, 2.117
  - Lorentz 2.99
  - $R$ -gauge 1.47
  - unitary 1.47
- gauge boson *see* gauge symmetry
- gauge fixing parameter
  - Landau gauge, in 2.117
  - QCD, in 2.114
  - QED, in 2.100
  - renormalization of 2.117
- gauge fields *see* gauge symmetry;
  - gluons; pure gauges
- gauge freedom 1.38, 2.99
- gauge invariance
  - 1st kind, of 1.30
  - 2nd kind, of 1.32
  - Feynman diagrams, of 2.102
  - $\epsilon^\mu(K) \rightarrow \epsilon^\mu(K) + ck^\mu$  in QED 2.109, in QCD 2.111
- see also* gauge symmetry
- gauge symmetry
  - Abelian global 1.30
  - Abelian local 1.31
  - charge conservation, and 1.30
  - charge operator, in 1.31
- conserved currents, in 1.31
- covariant derivative
  - non-Abelian theories, in 1.35–37
  - QED, in 1.32
- gauge bosons  $W$  and  $Z^0$  1.49–51
  - coupling to Higgs boson 1.52, 1.62
  - coupling to leptons 1.55
  - discovery of 1.63–65
  - self-coupling 1.55
  - see also* gluons
- gauge fields: photon 1.32
  - see also* gluons
- Noether's theorem 1.31
- non-Abelian global 1.33
- non-Abelian local 1.35
- transformation of fields 1.32
- transformation of quark fields 1.161, 2.108
  - see also* gauge transformation of fields
- gauge transformations of fields
  - Abelian, global 1.30
  - Abelian, local 1.32
  - large gauge transformations 2.325
  - non-Abelian global 1.34
  - non-Abelian local 1.35
  - photon field 1.32
  - QED, in 2.99
  - quarks 1.161, 2.108
  - vacuum in QCD, rôle in 2.321
  - vacuum in QED, rôle in 2.319
  - $W$  field 1.36
  - $W$  field tensor 1.37, 2.99, 2.105
- gauge theories
  - non-perturbative 2.301
  - see also* QCD; QED
- gauginos 2.347
- Gauss' law 2.100
- Gell-Mann matrices 1.460–462, 2.368–370
- Gell-Mann, Nishijima formula 1.160
- ghosts
  - propagator for 2.115
  - QCD, in 2.113
  - QED, in 2.104

- Gilman convention for virtual photon flux 1.330
- GIM mechanism 1.159, 1.164
- global gauge symmetry *see* gauge symmetry
- glueballs **1.264**  
  data on 1.266  
  Lattice QCD, in 2.310  
  production rate, theoretical 1.264  
  quantum numbers of 1.265  
  QCD sum rules, in 2.304
- gluinos 2.347
- gluons **1.4**  
  covariant derivative for 2.105  
  DIS, rôle in 1.377  
  field tensor for 2.105  
  gauge transformation of 2.108  
  number density, polarized 1.409  
  number density, unpolarized 2.150,  
    2.191  
  *see also* partons, distribution functions  
  propagator for 2.115  
  self-coupling 1.4, 1.55, 2.108, 2.115  
  spin of 2.265, 2.287  
  2G colour singlet state 1.217  
  3G colour singlet state 1.217
- gluon reactions  
   $GG \rightarrow GG$   
   $GG \rightarrow q\bar{q}$   
   $G\gamma \rightarrow q\bar{q}$  *see* parton–parton reactions
- Goldstone bosons 1.40, 1.44
- Goldstone theorem 1.40, 1.44
- Gottfried sum rule 1.363, 1.402,  
  2.154
- grand unification 2.339, 2.342
- grand unification mass (scale) 2.343
- Grassmann variables 2.306
- Green's functions **2.66**, 1.444, 2.352  
  operator product expansion, in  
    1.142
- Gribov, Lipatov equation 2.148
- Gribov, Levin, Ryskin equation 2.190
- Gross, Llewellyn-Smith sum rule  
  1.401, 2.146, 2.154
- group generators and charges 1.465,  
  2.373
- $G_A$ , axial coupling constant 1.8–10
- $G_V$ , vector coupling constant 1.8–10
- $G$ -parity 1.449, 2.357
- GUT 2.339, 2.342  
  evolution of couplings 2.343  
  Weinberg angle, in 2.44  
    *see also*  $SU(5)$
- $\gamma$ -function *see* renormalization group
- $\gamma$ -matrices xxiv  
   $d$ -dimensions, in 2.65  
  traces of 1.452, 2.360
- ' $\gamma$ ', virtual photon  
  flux of 1.330  
  polarization vector for 1.330  
   $\gamma$ – $Z^0$  interference in DIS 1.341,  
    1.374
- $\gamma$ -reactions  
   $\gamma\gamma \rightarrow q\bar{q}$   
   $\gamma q \rightarrow \gamma q$   
   $\gamma G \rightarrow q\bar{q}$  *see* parton–parton reactions  
  ' $\gamma$ '  $N \rightarrow$  ' $\gamma$ '  $N$   
   $A_1, A_2$  asymmetry parameters  
    1.346–349, 1.381, 1.405  
  DIS, relation to 1.330  
  longitudinal cross-section 1.330  
   $R, \sigma_L/\sigma_T$  1.331  
  transverse cross-section 1.330  
   $g_A^e, g_A^f, g_A^l$  neutral weak axial vector coupling constants 1.68, 1.141,  
    1.150  
   $g_V^e, g_V^f, g_V^l$  neutral weak vector coupling constants 1.68, 1.141,  
    1.150
- Hand convention for virtual photon flux 1.330
- heavy flavours 1.269  
  production of 1.295  
  spectroscopy of 1.269
- heavy lepton 1.29, 1.50, 1.300  
  helicity  
    conservation 1.17

- conservation rule in large  $p_T$ 
  - reactions 2.230
- fermions, of 1.16
- matrix elements for particles and antiparticles 1.17
- HERA ep collider 1.340–342
- Hey, Mandula sum rule 1.350
- hidden charm *see* narrow vector resonances; quarkonium
- hierarchy problem 2.344, 2.349
- Higg's boson 1.45, 1.51, 1.90
  - coupling to fermions 1.61, 1.90
    - to gauge bosons 1.51, 1.62
    - to leptons 1.61–62
    - to  $W$  and  $Z^0$  1.91
  - isospin 1.8
    - matrix elements, relations between 1.19, 1.467, 2.375
  - nucleon doublet 1.8
  - rotations 1.18
  - weak interactions, structure of 1.19
- Higg's decays in SM 1.91
  - to  $f\bar{f}$  1.92
  - to gluons 1.93
  - to photons 1.92
  - to  $W$  and  $Z^0$  1.91
- Higg's lifetime in SM 1.93
- Higg's mass
  - limits on 1.97
  - theoretical constraints on 1.97
- Higg's mechanism **1.45**
  - minimal version 1.51, 1.54
- Higg's phenomenon 1.40
- Higg's production in SM 1.95
  - $Z^0 \rightarrow H f\bar{f}$  1.95
  - $Z^0 \rightarrow H\gamma$  1.96
  - $Z^0 \rightarrow H\mu^+\mu^-$  1.97
- Higg's vacuum expectation value, numerical 1.57–58
- Higgsinos 2.347
- homotopy class 2.325
- hybrids **1.264**
  - data 1.266
  - production rate, theoretical 1.264
  - quantum numbers 1.265
- hyperon  $\beta$ -decay 1.469, 2.4, 2.377
- impulse approximation (partons) 1.382
- inclusive reactions *see* large  $p_T$  reactions
- indefinite metric in QED 2.104
- inelastic electron–nucleon scattering
  - see* DIS
- inelastic neutrino–nucleon scattering
  - see* DIS
- infinite momentum frame 1.377, 1.383
- intermediate vector boson 1.23
- inverse  $\mu$ -decay 1.76
- instantons 2.301, 2.312, 2.341
  - QCD, in 2.318, 2.326
  - CP-violation, rôle in 2.328
    - functional form 2.328
  - Quantum Mechanics, in 2.312
  - SM, in 2.332
- interaction picture 1.449, 2.357
- isospin 1.8
- Jacobi identity 1.460, 2.368
- jet algorithms 2.282
- jet finders 2.282
- $J/\psi$  *see* narrow vector resonance
- jets in  $e^+e^-$  physics 2.253, 2.255
  - acoplanarity 2.254
  - angular ordering 2.275, 2.285
  - cross-sections 2.283
    - $\alpha_s$ , implications for 2.283
  - four-jet events 2.262
  - gluon jets 2.265, 2.268
  - gluon, spin of 2.265, 2.287
    - non-Abelian coupling of 2.288
  - independent fragmentation 2.285
  - infrared divergences 2.25, 2.282
  - jet axis 2.260
  - jet broadening 2.255, 2.263
  - jet definition 2.282
  - jet finders 2.282
  - mean  $p_T$  in a jet 2.266
  - multiplets 2.262
  - oblateness 2.269
  - particle flow patterns 2.285

- QCD, tests of 2.268, 2.285  
 $R$ , expression to  $O(\alpha_s^3)$  2.263  
 SPEAR, at 2.258  
 sphericity 2.254, 2.259  
 spheroicity 2.254  
 spin of quarks 2.260  
 three-jet events 2.262, 2.265,  
     2.282, 2.285  
 thrust 2.254  
 jets in hadronic reactions 2.219  
     away jet 2.221  
     beam jet 2.220, 2.233  
     evidence for 2.233  
     inclusive  $A + B \rightarrow \text{jet} + X$  2.234  
         data 2.238  
         jet axis 2.234  
     jet fragmentation 2.249  
     jet/ $\pi^0$  ratio 2.237  
     leading particle effect 2.233  
     multijets 2.249  
      $O(\alpha_s^3)$  calculation of production  
         2.250  
     target jet 2.220, 2.233  
     thrust 2.36  
     towards jet 2.21  
     transverse momentum to jet axis  
         2.239  
     trigger 2.221  
     trigger bias 2.234  
     two-jet production 2.239; angular  
         distribution 2.241;  
          $Q^2$ -evolution 2.242
- Kaluza–Klein 2.349  
 $K^0$ – $\bar{K}^0$  CP-violation *see*  
     CP-violation  
 $K^0$ – $\bar{K}^0$  mixing, introductory 1.165  
     detailed phenomenology 2.23  
     general 2.19  
     mass difference 2.14–18, 2.30
- $K$ -factor  
     Drell–Yan, in 2.212  
     jet production, in 2.249
- $K^\mu$  current in QCD 2.326  
 KNO scaling 2.297  
 $K^0$  reactions
- $K^0 \rightarrow \pi l \nu$  1.288, 2.17  
 $K^0 \rightarrow 2\pi, 3\pi$  2.18, 2.23  
 Klein–Gordon equation 2.54  
 Kobayashi–Maskawa matrix 1.161,  
     2.1  
 $B^0$ – $\bar{B}^0$  CP-violation, in 2.48  
 $B^0$ – $\bar{B}^0$  mixing, in 2.46  
 $\beta$ -decay, rôle in 2.2  
 charm decay, in 1.270, 1.285  
 CP-violation, in 2.37, 2.40  
 determination of 2.1  
     phase  $\delta$  2.38  
     phase of  $V_{td}$  2.49, 2.52  
     phase of  $V_{ts}$  2.49  
          $|V_{ud}|$  2.4  
          $|V_{us}|$  2.4  
          $|V_{ub}|$  2.5, 2.7–8  
          $|V_{cb}|$  2.6–7  
          $|V_{cd}|$  2.9–10  
          $|V_{cs}|$  2.9–10  
          $|V_{td}|$  2.10  
          $|V_{ts}|$  2.10  
 DIS, in 1.371, 2.8  
 numerical values, summary 2.11  
 quark masses, rôle in 1.179  
 Kogut–Susskind action 2.305  
 Kogut–Susskind ghost 2.332  
 $\chi$  in  $B^0$ – $\bar{B}^0$  mixing 2.22, 2.47  
 $\chi_b$  states 1.236–238, 1.253  
 $\chi_c$  states 1.220–221, 1.253
- Lagrangian density 1.2  
 charged weak leptonic interactions  
     1.67  
 current–current form of hadronic  
     weak interactions 1.158–9  
 Fermi, QED 2.104  
     generalised, QED 2.105  
 Fermi, weak interaction 1.6  
 Feynman diagram vertices, for, in  
     QCD, QED 1.452–5  
 Feynman diagram vertices, for, in  
     SM 1.69, 1.455–7  
 gauge boson–lepton coupling 1.56  
 gauge boson self-coupling 1.56  
 Higgs–gauge boson coupling 1.54

- Higgs-lepton coupling, for 1.62  
 intermediate vector boson weak interactions 1.24  
 local gauge theory, in 1.38  
 $\mathcal{L}_\theta$  in QCD 2.329  
 neutral weak leptonic interactions 1.67  
 quark-Higgs coupling, for 1.180  
 quark-W coupling, for 1.164, 1.177  
 quark-Z<sup>0</sup> coupling, for 1.163, 1.177–8  
 QCD, for 2.106  
 QED, for 1.2, 2.100  
 $\phi^4$ -field theory, for 2.54  
 Landau gauge 2.104, 2.117  
 large gauge transformations 2.325  
 large  $p_T$  reactions  
   exclusive 2.228  
     counting rules 2.230  
     diquarks 2.231  
     elastic form factors 2.229  
     fixed angle scattering 2.230  
     helicity conservation rule 2.230–231  
     parton model for 2.228  
   hadronic, jets 2.219  
   inclusive 2.225  
     parton model for 2.256  
 jets  
   evidence for 2.233  
   inclusive  $A + B \rightarrow \text{jet} + X$  2.234; fragmentation 2.249  
   multijets 2.249;  $\alpha_s$  from 2.249  
 $O(\alpha_s^3)$  calculation for jet production 2.250  
   transverse momentum relative to jet axis 2.239  
 jet/ $\pi^0$  ratio 2.237  
 $pp \rightarrow \pi^0 X$  2.233  
 prompt photons 2.245  
 QCD interpretation 2.232  
 scaling 2.223  
 semi-inclusive 2.227  
 two-jet production 2.239  
   angular distribution 2.241  
   parton model for 2.241
- $Q^2$ -evolution 2.242  
 $\gamma/\pi^0$  ratio 2.247  
*see also* DIS; jets in e<sup>+</sup>e<sup>−</sup>; jets in hadronic reactions  
 Lattice QCD 2.304  
   action for 2.305  
   asymptotic freedom 2.309  
    $B_K$  parameter, from 2.312  
    $\beta$ -parameter, in 2.305  
   confining phase 2.309  
   continuum limit 2.306–307  
   Dirac operator 2.306  
   Euclidean time, in 2.309  
    $f_\pi, f_D, f_K$  parameters, from 2.312  
   glueball masses, from 2.310  
   hadron masses, from 2.310  
   mass calculation 2.309  
   operators, choice of 2.309  
   potential,  $q\bar{q}$ , from 2.311  
   quenched approximation 2.306  
   semi-leptonic decays, from 2.312  
   string tension 2.310  
   Wilson loop factor 2.306  
    $\Lambda$ -parameter, in 2.308  
   lattice regularization 2.65–66  
 leading logarithmic approximation (LLA)  
   beyond the LLA 2.195  
   QCD, in 2.132, 2.174, 2.184  
 leading particle effect 2.233  
 left-handed fermions 1.16  
   lepton doublet 1.56–7  
   quark doublets 1.161  
 LEP e<sup>+</sup>e<sup>−</sup> collider 1.121  
   polarization in 1.123  
 lepton  
   couplings *see* coupling constants;  
     Lagrangian density  
   heavy 1.28  
   propagator 2.114  
   *see also*  $\tau$ -lepton  
 lepton non-conservation *see*  $L$ -violation  
 lepton number  
   conservation 1.7  
   violation *see*  $L$ -violation

- leptonic reactions
  - inverse  $\mu$ -decay 1.76
  - $\mu$ -decay 1.57
  - $\nu_e e$  and  $\bar{\nu}_e e$  elastic scattering 1.69
  - $\nu_\mu e$  and  $\bar{\nu}_\mu e$  elastic scattering 1.74
  - purely leptonic reactions 1.67
  - see also*  $e^+e^-$  reactions
- light cone components 1.164
- LHC  $pp$  collider 1.77, 1.121
- Llewellyn-Smith relation 1.403
- local gauge invariance *see* gauge symmetry
- longitudinal cross-section for photon 1.330
- longitudinal scaling function  $F_L$  2.198–199
- Lorentz condition 2.99
- low  $p_T$  reactions **2.289**
  - diffraction dissociation 2.295
  - triple Pomeron mechanism 2.296
- inclusive reactions 2.295
- multiplicity
  - average 2.296
  - distribution 2.297
  - KNO scaling 2.297
  - negative binomial distribution 2.297
  - small- $x$  physics, link with 2.298–299
- see also* elastic scattering, hadronic luminosity in  $e^+e^-$  colliders 1.120
- luminosity in parton model 1.434
- Lund model 2.276
- $L$ -violation (lepton number)
  - GUT, in 2.344
  - SM, in 2.332, 2.336–338
    - $\sigma_{\text{tot}}$  for  $L$ -violation 2.338
    - $qq \rightarrow 7\bar{q} + 3l$  2.336
    - $qq \rightarrow 7\bar{q} + 3l + n$  gauge bosons 2.337; perturbative corrections 2.338; unitarity bound 2.338
- $\Lambda$  parameter in QCD 2.125–127, 2.203–204, 2.242, 2.287, 2.308
- $\Lambda_c$  charm baryon 1.272
- magnetic moment, anomalous 1.321
- Mandelstam variables 2.226
- mass generation *see* spontaneous mass generation
- mass singularity 2.173, 2.177, 2.182
- Maxwell equations 2.99, 2.319–320
- Mellin transform 2.148
  - convolution theorem, for 2.149
- method of fastest apparent convergence 2.133
- Metropolis algorithm 2.306
- Michel parameter 1.21
- $\tau$ -decay, in 1.312
- microscopic causality 1.444
- minimal coupling in QED 1.32
- minimal Higgs mechanism 1.54
  - radiative corrections to, tests of 1.114
  - test of, in  $\nu_\mu e$  scattering 1.76
  - tests at LEP 1.146
- minimal standard model 1.51
- minimal  $SU(5)$  2.342
- minimum sensitivity, principle of 2.133
- mixing **2.12**
  - $B^0 - \bar{B}^0$  system, in 1.97–98, 2.19
    - data for 2.47–48
    - dynamics of 2.46
  - $D^0 - \bar{D}^0$  system 2.19
  - general formalism 2.12
  - $K^0 - \bar{K}^0$  system 2.18
    - dynamics of 2.32
    - practical aspects of 2.17
- Møller scattering 1.128
- momentum carried by parton 2.189
- momentum conservation
  - DIS sum rule 1.377
  - nucleii, in 1.414
- momentum operators 1.3
- Monte Carlo for  $e^+e^- \rightarrow$  hadrons 2.270
  - cross-section estimates 2.271
  - energy-energy correlations 2.280
  - event generators 2.272
  - event shape parameters 2.278
  - hadronization phase 2.276

- cluster fragmentation 2.277
- Lund model for 2.276
- string fragmentation 2.276
- HERWIG** 2.275
  - infrared problems 2.273–274
  - jet cross-sections 2.282
  - JETSET** 2.276
  - perturbative phase 2.273
    - angular ordering 2.275
    - matrix element approach 2.274
    - parton shower approach 2.274
  - QCD, in 2.272
- Monte Carlo in Lattice QCD 2.306
- Mott cross-section 1.320
- MPS *see* renormalization schemes
- MS,  $\overline{\text{MS}}$  *see* renormalization schemes
- muon–electron universality 1.20
- muon number conservation 1.8–9
- $\mu$ -decay 1.57
- $\mu$  lifetime
  - electroweak radiative corrections to 1.107
  - lowest order, in 1.57
  - QED radiative corrections to 1.57
  - tests of corrections, experimental 1.112
- $\mu N \rightarrow \mu X$  *see* DIS
- $m_H$  (Higgs mass) 1.54
  - limits on 1.97
  - relation to Higgs width 1.91, 1.92
- $m_t$  (top mass)
  - CP-violation, rôle in 2.37, 2.45
  - $m_H$ , connection with, 1.98
  - muon lifetime, rôle in 1.109
  - note added in proof xxix
  - value, from LEP data 1.146
- Nachtmann inequality 1.367
- Nachtmann moments 2.148
- narrow vector resonances **1.202**
  - $J/\Psi$  discovery 1.204
    - decay;  $\alpha_s$  determination 1.219;
      - baryonic 1.232; leptons, into 1.220; mesons, into 1.218 (OZI rule 1.213)
    - mass determination 1.224
  - properties 1.213, 1.225
  - quantum numbers 1.228, 1.232
  - spectroscopy, experimental 1.219, 1.221
  - widths 1.220, 1.225, 1.254
- $\Psi'$  states 1.222
- $\Psi'$  (3685) 1.222
  - properties 1.225
  - $\Psi' \rightarrow \rho\pi$  puzzle 1.267
- $\Upsilon$  discovery 1.234
  - decay;  $\alpha_s$  determination 1.261; leptons, into 1.262; photons and gluons, into 1.261; theoretical 1.254
  - family 1.236, 1.238
  - mass differences 1.237
- negative binomial distribution 2.297
- neutral current (NC) interactions 1.332
  - see also* DIS
- neutral currents
  - evidence for 1.184
  - see also* currents
- neutral weak hadronic interactions 1.177
- neutral weak leptonic interactions 1.67
- neutrino
  - masses 2.346
  - narrow-band beams 1.397
  - number of species
    - LEP data 1.147
    - $\bar{p}p$  collision data 1.87
    - wide-band beams 1.397
  - neutrino oscillations 2.339, 2.344–346
  - neutrino reactions
    - $\nu_e e$ ,  $\bar{\nu}_e e$  elastic scattering in SM 1.69
      - in old  $V-A$  theory 1.74
    - $\nu_\mu e$ ,  $\bar{\nu}_\mu e$  elastic scattering 1.74
      - comparison with  $\nu_e e$  and  $\bar{\nu}_e e$  1.75
  - $\nu N \rightarrow \nu X$  1.182–184, 1.331
    - cross-sections in parton model 1.357
  - see also* DIS

- $\nu p \rightarrow \nu p$  1.184  
 neutrinoless  $\beta$ -decay 2.345  
 neutron–antineutron oscillations  
     2.344, 2.387  
 neutron electric dipole moment 2.341  
 Noether currents 1.31  
     chiral  $U(1)$  transformation for  
         2.331  
     QCD, in 2.107  
 Noether theorem 1.31  
 non-Abelian gauge theories *see* QCD;  
     Standard Model  
 non-Abelian gauge transformations  
     1.35  
 non-singlet distributions 2.186  
 non-singlet operators 2.140  
 nuclear effects in DIS 1.409  
     experimental data on 1.411–412  
     *see also* DIS  
 $\nu_\tau$  (tau neutrino) 1.302, **1.312**  
     helicity of 1.315  
 $n_f$ , number of flavours 2.119  
 $n_f^*$ , number of active flavours 2.123  
 oblateness 2.267, 2.279  
 Odderon 2.293  
 old fashioned perturbation theory  
     2.383  
 one particle irreducibility 2.170  
 Operator Product Expansion 2.136  
 optical rotation in atoms  
     experimental 1.199–200  
     theoretical 1.193  
 optical theorem 1.329  
 orbital angular momentum of partons  
     1.407  
 ortholepton hypothesis 1.302  
 OZI rule 1.213  
     QCD, in 1.217  
 paralepton hypothesis 1.302  
 parity 1.447, 2.355  
 parity invariance 2.385  
 parity violation  
     asymmetry in  $e^-$ –nucleus  
         scattering 1.189  
 QCD, in 2.341  
      $\tau$ -decay, in 1.315  
     SM, in 1.61, 1.193  
 particle flow patterns 2.278  
 partons **1.352**  
     antipartons **1.359**  
         evidence for 1.363  
         distribution functions 1.362  
     Bjorken scaling, with 1.355–356  
     covariant spin vector for 1.394  
     distribution functions 1.354, 2.180  
         data on, 1.420–421, 2.151–152,  
             2.193, 2.206–207, 2.244–245  
     non-singlet **2.186**  
     polarized 1.379, 1.405  
      $Q^2$ -dependence 2.148, 2.180;  
         gluons, of 2.193;  
         interpretation of 2.182;  
         models for 2.148; sea quarks  
             of 2.152; valence quarks, of  
             2.151  
     QCD field theoretic definition of  
         2.166; beyond the LLA  
         2.195; evolution equations  
         2.186; evolution, non-linear  
         2.190–192;  $Q^2$ -dependence  
         2.180; renormalization  
         scheme dependence 2.196;  
         small- $x$  behaviour 2.189;  
         spin-dependent distributions  
             2.187  
     singlet **2.186**  
     small- $x$  behaviour 1.375; Regge  
         theory, link with 1.375  
         summary of 2.200  
     fusion (recombination) 2.191  
     gluons, evidence for 1.377  
     orbital angular momentum, of  
         1.407  
     ‘+’ formalism for integrals 2.187  
     quarks, as 1.361  
     quark–parton model 1.364  
     recombination (fusion) 2.191  
     splitting functions 2.179–187  
     structure functions of  
         electromagnetic interactions  
             1.353

- general  $V-A$  interaction 1.356  
 spin  $\frac{1}{2}$ , evidence for 1.356, 2.260  
*see also* DIS
- partonic cross-sections  
 angular distribution, graphical  
   2.240, 2.242  
*see also* parton–parton reactions
- parton model **1.316**, 1.352  
 field theory, in 2.155, 2.163, 2.168,  
   2.206  
 collinear singularities 2.171,  
   2.177  
 factorization scale 2.181  
 fragmentation functions 2.208  
 large  $p_T$  reactions 2.206  
 leading logarithmic structure  
   2.174  
 $Q^2$ -dependent distribution  
   functions 2.208
- Pomeron, of 2.296  
*see also* DIS; Drell–Yan; partons;  
    $W$  production
- parton–parton reactions  
 cross-sections in  
   angular distributions, graphical  
     2.240, 2.242  
   at  $90^\circ$  2.391  
 $qq \rightarrow qq$  2.387–388, 2.391  
 $q\bar{q} \rightarrow q\bar{q}$  2.387–388, 2.391  
 $q\bar{q} \rightarrow q\bar{q}$  2.388, 2.391  
 $q\bar{q} \rightarrow GG$  2.389, 2.391  
 $GG \rightarrow q\bar{q}$  2.389  
 $qG \rightarrow qG$  2.390–391  
 $\bar{q}G \rightarrow \bar{q}G$  2.390–391  
 $GG \rightarrow GG$  2.390–391  
 $q\bar{q} \rightarrow G\gamma$  2.392  
 $G\gamma \rightarrow q\bar{q}$  2.392  
 $qG \rightarrow q\gamma$  2.392  
 $\bar{q}G \rightarrow \bar{q}\gamma$  2.392  
 $q\gamma \rightarrow qG$  2.393  
 $\bar{q}\gamma \rightarrow \bar{q}G$  2.393  
 $q\bar{q} \rightarrow \gamma\gamma$  2.393  
 $\gamma\gamma \rightarrow q\bar{q}$  2.394  
 $q\gamma \rightarrow q\gamma$  2.394  
 $\bar{q}\gamma \rightarrow \bar{q}\gamma$  2.394  
 $qq \rightarrow qq$  2.222, 2.240
- colour sum 1.461, 2.369  
 cross-sections 2.387–388, 2.391  
 Feynman amplitude calculation  
   1.458, 2.366
- $qG \rightarrow qG$   
 colour sum 1.462, 2.370  
 cross-section 2.390–391  
 Feynman amplitude calculation  
   1.459, 2.366
- Paschos–Wolfenstein relation 1.188,  
   1.423
- path integrals *see* Feynman path  
   integral
- Pauli–Villars cut-off 2.62
- Peccei–Quinn symmetry 2.332
- penguin diagrams 2.41
- perturbation theory, old fashioned  
   2.383
- PETRA storage ring 1.118
- photinos 2.347
- photon field 1.2
- photon propagator  
   Coulomb gauge, in 2.102  
   covariant gauge, in 2.102, 2.104
- pion decay 1.14  
 $\pi^0 \rightarrow 2\gamma$  1.168  
 $\pi \rightarrow l\nu$  1.286
- polarization  
 $e^+e^-$  colliders, in 1.121  
 $e^+e^- \rightarrow f\bar{f}$  with polarized beams  
   1.149  
   polarization of  $f$  1.153  
 $e^+e^- \rightarrow hX$  with polarized beams  
   2.258  
 $e^+e^- \rightarrow \tau^+\tau^-$   
   polarization of  $\tau$  1.154
- inelastic lepton–nucleon scattering,  
   in 1.342, 1.378
- LEP, at 1.123
- $Z^0$ , measurements at 1.149
- polarization vector 1.446, 2.354  
 massive vector mesons, for 1.330  
 virtual  $\gamma$ , for 1.330
- polarized deep inelastic scattering  
**1.342**, 1.378, 1.406

- polarized scaling functions *see* scaling functions
- polarized structure functions 1.344, 1.378
- Pomeranchuk theorem 2.290
- Pomeron
  - operator product expansion, in 2.141
  - partonic structure of 2.296
  - QCD interpretation of 2.299
  - small- $x$  scaling functions, link with 1.375
  - triple Pomeron mechanism 2.296
- potential,  $q\bar{q}$  *see* quarkonium
- $pp \rightarrow pp$  at large  $p_T$  2.230–233
- principle of minimum sensitivity 2.133
- prompt photons 2.245
- proton decay 2.339, 2.344
- proton lifetime 2.339, 2.344
- propagators
  - gluon 1.453, 2.115, 2.361
  - ghost 1.453, 2.115, 2.361
  - lepton 1.453, 2.114, 2.361
  - photon 1.453, 2.102, 2.104, 2.361
  - quark 1.453, 2.114, 2.361
  - $W$  and  $Z^0$  1.455, 2.363
- pure gauges
  - QCD, in 2.323
  - classes of 2.324–325
  - QED, in 2.320
  - $SU(2)$  colour theory, in 2.324
    - classification of 2.325
    - homotopy classes 2.325
    - $\theta$ -vacuum 2.326
    - winding number 2.325
- purely leptonic reactions *see* leptonic reactions
- $\pi\pi$  phase shifts in  $K^0-\bar{K}^0$ 
  - CP-violation 2.23–24
- $\Psi'$  (3685) *see* narrow vector resonances
- QCD **1.4, 2.97**; qualitative features 1.206
- Applequist–Carrazone theorem 2.122
- charmonium decay, in 2.302
- chiral symmetry 2.106
- colour 2.105
- colour charge 2.109, 2.322
- Compton scattering with gluons 2.111
- covariant derivatives 2.105
- current conservation 2.107
- decoupling theorem for heavy quarks 2.122
- deep inelastic scattering *see* DIS, QCD
- degenerate vacuum 2.318
- detailed theory 2.104
- Drell–Yan reactions 2.209
  - $p_T$  distributions 2.213
- equations of motion 2.106, 2.321
- Feynman rules 1.452–455, 2.114, 2.360
- field energy 2.322
- field tensor  $G_{\mu\nu}^a$  2.105
- flavour symmetry 2.106
- $\gamma/\pi^0$  ratio 2.247
- gauge transformations 2.109, 2.322
- generators of  $SU(3)_C$  2.105
- ghosts 2.113
- heavy quarks 2.121
- jet production in  $e^+e^-$  collisions 2.262
  - $\alpha_s$ , implications for 2.282
  - gluons; non-Abelian coupling 2.288; spin of 2.287
  - tests of 2.268, 2.283
- jet production in hadronic reactions
  - $\alpha_s$  evaluation 2.249
  - data 2.237
  - multiplets 2.249
  - $O(\alpha_s^3)$  calculation 2.250
  - $Q^2$ -evolution 2.242
  - Lagrangian 2.106
  - $\Lambda$  parameter 2.125
  - renormalization scheme dependence 2.127

- large  $p_T$  exclusive reactions 2.228
- large  $p_T$  inclusive reactions 2.225
- Monte Carlo formulation 2.270
- multiplicity in  $e^+e^-$  collisions
  - 2.277
- Noether currents 2.107
- parton model *see* DIS; parton model; partons, distributions; QCD
  - large  $p_T$  reactions 2.206
- Pomeron, in 2.296
- prompt photon production 2.245
- QED, differences with 2.107
  - $\epsilon_\mu(k) \rightarrow \epsilon_\mu(k) + ck_\mu$  2.109
  - non-conservation of quark current 2.107
  - non-gauge invariance of currents 2.108
  - self-coupling of gluons 2.107
- quark fields 2.105
- quark masses 2.106
- renormalization group 2.116, 2.121
- renormalization point, choice of 2.133
- $\tau$ -decay, test in 1.311
- vertices 1.4, 1.454, 2.362
- $W$  and  $Z^0$  production 2.216
  - data, comparison with 2.216–219
- $p_T$  distributions 2.217
- QCD sum rules 2.302
  - current correlation functions 2.302
  - glueballs 2.304
  - meson spectroscopy 2.304
- QCD vacuum *see* vacuum, QCD in QED
  - Coulomb gauge 2.101
  - detailed theory 2.98
  - $\epsilon_\mu(k) \rightarrow \epsilon_\mu(k) + ck_\mu$ , invariance under 2.109
  - Feynman gauge 2.104
  - field energy 2.320
  - field tensor  $F_{\mu\nu}$  2.99
  - gauge transformations 2.99, 2.320
  - Gauss' law 2.100
  - ghosts 2.104
  - Lagrangian 1.2
- generalized Fermi 2.103
- Landau gauge 2.104
- Lorentz condition 2.99
- Maxwell equations 2.99, 2.319
- propagators
  - Coulomb 2.102
  - covariant 2.102, 2.104
  - transverse 2.102
- quantization
  - difficulties with 2.100
  - transverse modes, of 2.101
  - subsidiary condition 2.103
- $q\bar{q}$  potential *see* quarkonium
  - Lattice QCD, in 2.311
- quark content of hadrons 1.210–212
- quark distributions *see* partons, distribution functions
- quark fields
  - covariant derivative for 2.105
  - gauge transformation in QCD 1.161, 2.108
  - QCD, in 2.106
- quark fusion (recombination) 2.191
- quark-lepton parallelism 1.208
- quark-lepton universality 1.157
- quark masses
  - constituent 1.174, 1.209, 2.106
  - current 2.106
  - KM matrix, and 1.179
  - QCD, in 2.106
- quark mixing 1.160 *see also* Kobayashi–Maskawa matrix
- quark number densities *see* partons, distribution functions
- quark phase convention in CP-violation 2.29
- quark propagator 1.453, 2.114, 2.361
- quark–quark reactions *see* parton–parton reactions
- quark recombination 2.191
- quark spin 1.356, 2.260
- quark statistics 1.166
- quarkonium 1.240
  - $J/\Psi$  decay
  - $\alpha_s$  determination 1.260
  - leptons, into 1.262

- photons and gluons, into 1.259
- theoretical 1.254
- positronium analogy 1.241
- $q\bar{q}$  potential 1.242
  - data, conditions from 1.246–248
  - effective strength 1.245
  - Fermi–Breit interaction 1.249
  - flavour independence 1.244
  - QCD, relation to 1.242–245
  - spin dependence 1.248
  - spin–orbit interaction 1.249
  - spin–spin interaction 1.249
  - tensor interaction 1.249
- spectroscopy, theoretical 1.247
  - data, comparison with 1.249
- $\Upsilon$  decay
  - $\alpha_s$  determination 1.261
  - leptons, into 1.262
  - photons and gluons, into 1.261
  - theoretical 1.260
- quarks **1.4**
  - couplings
    - gluons and photons, to 1.454, 2.362
    - $Z^0$  and  $W$ , to 1.163, 1.177–178, 1.455–456, 2.363–364
    - quantum numbers of 1.12, 1.160
  - quenched approximation 2.306
- $R$  in  $B^0$ – $\bar{B}^0$  mixing 2.20
- $R$ ,  $\sigma(e^+e^- \rightarrow X)/\sigma(e^+e^- \rightarrow \mu^+\mu^-)_{\text{QED}}$ 
  - bottom threshold region, in 1.239
  - charm region, in 1.300
  - charm threshold region, in 1.222
  - data
    - below 35 GeV 1.205
    - 10–60 GeV 1.124
  - parton model, in 1.427
- QCD
  - $O(\alpha_s^2)$  calculation 2.132
  - $O(\alpha_s^3)$  calculation 2.263
  - quark charge, rôle in 1.209
  - renormalization group analysis 2.128
  - $Z^0$  exchange, with 2.134
- radiative corrections to SM 1.101
  - problems with 1.112
- $R$ -gauge 1.47
- Regge behaviour of scaling functions 1.375
- Regge theory 2.289, 2.141
- regularization **2.53**
  - cut-off procedures 2.62
  - dimensional 2.63, 2.71
    - see also* dimensional regularization
  - lattice 2.304
  - Pauli–Villars 2.62
- renormalizability of gauge theories 1.47
- renormalization **1.103, 2.53**
  - counter terms in 2.60
  - Wilson expansion operators, of 2.142
    - see also* renormalization schemes
- renormalization group **2.53, 2.61, 2.73**
  - $\beta$ -function, for
    - dimensional regularization, in 2.75, 2.78
    - mass independent schemes, in 2.75
    - momentum point subtraction (MPS) schemes, in 2.74
    - QCD, for 2.78, 2.83–85, 2.117, 2.119–120
    - QED, for 2.78
    - $\phi^4$  theory, in 2.76–78
    - scheme dependence of 2.85
  - Callan–Symanzik equation 2.74
  - detailed treatment 2.73
  - DIS, in 2.135
    - conserved currents 2.143
    - moments of structure functions 2.142, 2.144
  - parton model, relation to 2.145
  - scale breaking 2.145
  - Wilson coefficient functions 2.142;  $Q^2$ -dependence 2.144
  - Wilson expansion operators, renormalization of 2.142

- $e^+e^- \rightarrow$  hadrons, in 2.128  
 leading logarithmic approximation (LLA) 2.132  
 $R$  to 4<sup>th</sup> order, calculation 2.132–134  
 renormalization point, choice of 2.133  
 $Z^0$  exchange, inclusion of 2.134  
 equations 2.74, 2.117, 2.143  
 $\gamma$ -function, in mass independent schemes, in 2.75  
 momentum point subtraction schemes (MPS), in 2.75  
 QCD, in 2.117–120  
 QCD, in 2.97, **2.116**  
 qualitative treatment 2.61  
 renormalization point 2.67  
 choice of 2.133  
 renormalization schemes 2.60  
 choice of 2.66  
 DIS scheme 2.196  
 example in  $\phi^4$  theory 2.76, 2.93  
 lattice 2.65  
 mass-independent 2.75  
 MS, minimal subtraction 2.72–75, 2.96, 2.125  
 $\overline{\text{MS}}$ , modified minimal subtraction 2.72–75, 2.96, 2.125  
 MPS, momentum point subtraction 2.67, 2.93  
 on-shell or physical 2.61  
 parton distributions, rôle in 2.195–202  
 QCD, in 2.117–118  
 renormalized fields 2.58  
 renormalized mass, choice of 2.156  
 renormalized parameters **2.58**  
 dimensional regularization, in 2.63  
 momentum point subtraction, in 2.67  
 renormalized vertex  
 $\phi^4$  theory by dimensional regularization  
 MS and  $\overline{\text{MS}}$  schemes, in 2.96  
 MPS scheme, in 2.93  
 MS and  $\overline{\text{MS}}$  schemes, in 2.71  
 MPS scheme, in 2.70  
 right-handed fermions 1.16  
 Rosenbluth formula 1.323  
 running coupling 1.106, **2.79–80**, 2.269  
 number of active flavours, rôle of 2.124  
 QCD, in lowest order 2.84, 2.120  
 next-to-leading order 2.126  
 recommended form 2.126, 2.269  
 renormalization scheme dependence 2.127  
 $R$ , ratio of longitudinal to transverse cross-sections for virtual photon-nucleon scattering 1.331, 1.337, 1.355, 1.400, 2.199  
 $R_\nu, R_{\bar{\nu}}$  1.184, 1.423  
 $\rho$ , ratio of real to imaginary parts of amplitude 2.289, 2.293  
 $\rho_0 = M_W^2 / (M_Z^2 \cos^2 \theta_W)$  1.76, 1.423  
 $r$ , ratio of CC antineutrino to neutrino cross-sections 1.188, 1.359, 1.423  
 $r$  in  $B^0-\bar{B}^0$  mixing 2.19, 2.46  
 $r$  in  $D^0-\bar{D}^0$  mixing 2.19  
 Sachs form factors 1.322  
 St Augustine 2.273  
 scale breaking  
 deep inelastic scattering, in 2.145  
 QCD, in 2.83  
 scaling  
 asymptotic freedom, relation to 2.83  
 deep inelastic lepton–hadron scattering, in **1.335**, 2.146  
 Green’s functions 2.83  
 large  $p_T$  hadronic reactions, in 2.221  
 scaling functions in DIS  
 Altarelli, Parisi, Gribov, Lipatov equations for 2.148

- data on  
 $F_2(x)$  from eD and  $\nu$ Fe scattering 1.404  
 $F_2(x)$  from  $\mu$ Fe and  $\nu$ Fe scattering 1.405  
 $F_2(x, Q^2)$  electromagnetic 1.417, 2.205  
 $F_2(x)$  from neutrino interactions 2.243  
 $F_2(x)$  bottom and charm production effects 2.201  
 $F_2^p/F_2^n$  1.367, 1.418, 2.202  
 $F_2^A/F_2^D$  1.411  
 $dF_2^p/d\ln Q^2$  1.418, 2.203–204  
 $xF_3(x)$  2.147, 2.243  
 $F_L$ , longitudinal 2.198  
jet production, data on 2.245  
moments of *see* DIS, moments  
moments, in terms of 2.148  
nucleii, in 1.409–416  
parton model, in 1.355–357  
detailed quark–parton model, in;  
  charged current reactions for  $Q^2 \ll M_W^2$  1.368;  
  charged current reactions for  $Q^2 \approx M_W^2$  1.374;  
  electromagnetic reactions 1.366; neutral current reactions for  $Q^2 \ll M_Z^2$  1.373; neutral current reactions for  $Q^2 \approx M_Z^2$  1.374  
polarized  $g_j(x)$  1.348, 1.379  
soft hadronic physics *see* low  $p_T$  reactions  
spin-dependent scaling functions 1.348  
spin structure of weak interactions 1.16  
QCD, in  
  beyond the LLA 2.195  
  data, comparison with 2.202  
  heavy quark production effects 2.201  
leading logarithmic approximation (LLA) 2.186  
renormalization scheme  
  dependence 2.196  
small  $x$  behaviour 1.375, 1.404, 2.299  
splitting functions for 2.149, 2.179, 2.187  
conservation laws 2.188  
detailed formulae 2.187  
unpolarized  $F_j(x)$  1.339  
sea quarks **1.363**, 1.365, 1.376, 2.152  
self-coupling  
  electroweak gauge bosons 1.55  
  non-Abelian gauge fields 1.37  
self-energy of electron 2.56  
MPS scheme, in 2.68  
semi-leptonic reactions  
  data and Weinberg angle 1.189  
  inclusive  $\nu N \rightarrow \nu X$  1.182  
  Lattice QCD, in 2.312  
  neutral currents  
    bound on cross-section for 1.187  
    evidence for 1.184  
    relation to charged current reactions 1.187  
 $\nu p \rightarrow \nu p$  1.184  
optical rotation in atoms 1.193  
parity violation in  $e^-$ -nucleus scattering 1.189  
SM, in 1.182  
shadowing 1.410  
singlet distributions 2.186  
singlet operators 2.140  
SLC  $e^+e^-$  collider 1.125–127  
sleptons 2.347  
small gauge transformations 2.325  
S-matrix 1.449, 2.357, 2.384  
  Dyson expansion for 1.150  
  Feynman amplitude, relation to 1.451, 2.359  
  T-matrix, relation to 2.384  
SPEAR  $e^+e^-$  collider 1.118  
sphaleron 2.332, 2.336  
 $E_{S_p}$  (energy) of 2.336  
sphericity 2.254, 2.261, 2.278  
spherocity 2.254, 2.278  
spin crisis in parton model 1.405

- spin vector 1.343
- spontaneous mass generation 1.46
- spontaneous symmetry breaking
  - 1.40**
  - field theory, in 1.41
  - global invariance, in 1.41
- SppS* collider 1.77, 1.117
- SSC pp collider xxx, 1.78, 1.121
- Standard Model **1.50**
  - beyond the 1.114, 2.339
  - criticism of 2.340
  - minimal version 1.114
  - number of parameters 2.342
  - parity violation 1.196
  - parameter values at  $Z^0$  1.142
  - radiative corrections to 1.101
  - test of in lowest order 1.67
- step function  $\epsilon(x)$  1.444
- string fragmentation 2.276
- string tension 2.310
- strong CP-violation 2.319, 2.329,
  - 2.342**
- strangeness changing currents *see* currents
- strangeness changing reactions 1.14
- structure constants of gauge group
  - 1.34
- SU(3)*, properties of 1.460,
  - 2.368–369
- structure function of muon 1.329
- structure functions
  - operator product expansion, in 2.137
  - parton model, in 1.354, 1.388
    - see also* DIS
- subsidiary condition in QED 2.103
- subtraction point in renormalization
  - 2.67
- sum rules *see* DIS, sum rules; QCD
  - sum rules
- supergravity 2.339, 2.347
- superstring theories 2.339
- supersymmetry 2.339, 2.347
- SUSY 2.339, 2.347
  - couplings, evolution of 2.349
  - generators of 2.348
- mass scale 2.350
- unification scale 2.350
- SU(3)<sub>F</sub>* invariance 1.10
  - particle assignments 1.209
  - quark content of hadrons 1.209
- SU(3)<sub>C</sub>* 2.105
- SU(5)* 2.242, 2.339
  - proton lifetime 2.344
  - running coupling 2.343
  - Weinberg angle 2.344
- symmetry breaking *see* spontaneous symmetry breaking
- $S^2, S^3$  (topological manifolds) 2.320
- $\sigma_L, \sigma_T$  in  $e^+e^- \rightarrow hX$  2.256
  - in  $e^+e^- \rightarrow f\bar{f}$  2.257
- $\sigma_{\text{tot}}$  in hadronic reactions 2.289
- $\Sigma_C$  charm baryon 1.277, 1.279
  - mass relations 1.282
- T*, transition operator (*T*-matrix)
  - 2.382**
  - absorptive part of 2.33, 2.383
  - dispersive part of 2.33, 2.383
  - perturbative expansion 2.382
  - S*-operator, relation to 2.382
  - tau-electron universality 1.21
  - tau lepton *see*  $\tau$ -lepton
  - TCP invariance 2.384
  - $K^0-\bar{K}^0$  system, in 2.385
  - $m_{\bar{p}}/m_p$  2.385
- Tevatron  $p\bar{p}$  collider 1.77
- Thomson cross-section 2.62
- thrust **2.236**, 2.254, 2.278
- time ordered product 1.444, 2.352
- time reversal invariance 2.384
- threshold corrections for charm and bottom 1.369
- top quark xix, 1.160
- topological charge 2.318, 2.341
- total hadronic cross-sections 2.289
- towards jet 2.221
- translation operators 1.3
- transverse cross-section in  $\gamma N$  1.330
- transverse motion in parton model
  - 1.386
- triangle anomaly

- colour, relevance to 1.70
- dimensional regularization, in 2.65
- $\pi^0 \rightarrow 2\gamma$  1.70
  - see also* anomalies
- trigger bias 2.234
- trigger jet 2.221
- triple Pomeron mechanism 2.296
- TRISTAN  $e^+e^-$  collider 1.121
- tunneling
  - double-well potential, in 2.314
  - QCD, in 2.326
- twist 2.136
- $T$ , time ordered product 1.444, 2.352
- $T$ , in QCD xxvi, 2.119–120
- $T(R)$  in QCD xxvi, 2.119
- $\tau$ -lepton 1.300
  - decays
    - leptonic 1.310
    - Michel parameter 1.312
    - parity violation 1.314
    - QCD, tests of 1.311
    - semi-leptonic 1.310
    - $V-A$  structure 1.313
  - discovery of 1.301
  - lifetime 1.306
  - mass 1.304
  - point-like structure 1.308
  - polarization in  $e^+e^- \rightarrow \tau^+\tau^-$  1.154
  - properties, table of 1.303
  - rare decays 1.314
  - spin 1.307
  - $\tau-e-\mu$  universality 1.309
- $\tau$ -neutrino 1.302, 1.312
  - helicity of 1.312
  - mass of 1.314
- $\theta$ , TCP operator 2.384
- $\theta_C$  *see* Cabibbo angle
- $\theta$  problem 2.329–332, 2.340, 2.349
- $\theta$ -vacuum
  - periodic potential in QM 2.314
  - QCD, in 2.318, 2.326
    - axions 2.332
    - chiral non-invariance 2.331
    - mass generation 2.331
    - Peccei–Quinn symmetry 2.332
  - problems with 2.331
  - strong CP-violation 2.329
  - $U(1)$  problem resolution 2.329
  - value of  $\theta$  2.331
- $\theta_W$  *see* Weinberg angle
- $\theta(x)$  step function 1.444, 2.352
  - integral representation for 2.382
- $t^a$ -matrices, properties of 1.460, 2.368
- $U(1)$  problem 2.329, 2.340
  - resolution of 2.331
- unitary bound
  - Fermi theory, violation in 1.24
  - longitudinally polarized vector boson production, in 1.26
  - vector meson exchange, in 1.24
- unitary gauge 1.47
- universality of weak interactions
  - 1.13, 1.20
  - $\mu-e$  1.21
  - quark–lepton 1.157
  - $\tau-e$  1.21
- UNK pp collider 1.78
- $\Upsilon$  (*upsilon*) *see* narrow vector resonances
- $V-A$  structure of weak interactions 1.7
  - tests of, in leptonic reactions 1.21
- vacuum
  - QCD, in 2.318, 2.326, 2.341
  - QED, in 2.319
  - Quantum Mechanics, in 2.312
    - double-well potential 2.314
    - periodic potential 2.313
  - SM, in 2.333
    - baryon number 2.335
    - lepton number 2.335
    - sphaleron 2.336;  $E_{Sp}$  2.336
    - see also*  $\theta$ -vacuum
  - vacuum expectation value
    - fields, of 2.313
    - Higgs field, of 1.42, 1.52, 1.58
  - valence quarks **1.362**, 1.366, 2.151
  - Van Royen, Weisskopf formula 1.256

- vector boson 1.24
  - longitudinally polarized, difficulties with 1.26
  - mass of charged 1.27
  - neutral, need for 1.29
  - production in Drell–Yan reactions 1.440
- vector meson dominance 1.412
- vector potential 1.2
- vertices in field theory 1.454–457, 2.56–73, 2.362–365
  - Feynman rules for
    - $B$  and  $L$  violating 2.337
    - gluon–ghost 2.116
    - quark–gluon 2.115
    - quartic gluon 2.116
    - SM, in 1.69
    - triple gluon 2.115
    - $\phi^4$ -theory, in 2.57–59
  - summary of 1.454–457, 2.362–365
- virtual photons *see ‘ $\gamma$*
- $v_e, v_f, v_l$  neutral weak vector coupling constants 1.68
- Ward–Takahashi identity
  - axial identity 1.171
  - QED, in 1.3
- $W$ -boson
  - couplings
    - see* coupling constants; Lagrangian density
  - decay, in SM 1.78
  - discovery 1.63
  - mass 1.57–58
    - $\bar{p}p$  collisions, from 1.82
    - $Z^0$  mass, relation to 1.58
  - polarization vector for 1.330
  - production
    - $B$  and  $L$  violating reactions, in 2.332
      - parton model, in 1.440
      - $\bar{p}p$  collisions, in 1.78, 1.82
    - QCD, in 2.216
    - SM, in 1.79
    - theory comparison with 2.217
- transverse momentum distribution 2.217
- width and lifetime
  - $\bar{p}p$  collision data on 1.82–87
  - SM, in 1.79
  - see also* gauge symmetry
- weak currents *see* currents
- weak hypercharge 1.60, 1.161
- weak interactions
  - Cabibbo theory 1.10
  - $\Delta S = \Delta Q$  rule 1.15
  - historical introduction 1.6
  - intermediate vector boson 1.23
  - isospin structure 1.18
  - $\mu$ –e universality 1.21
  - spin structure 1.16
  - $\tau$ –e universality 1.21
  - universality 1.13, 1.20
  - $V$ – $A$  structure 1.7, 1.20
  - see also* Standard Model
- weak isospin 1.13, 1.60, 1.161
- weak magnetism 1.14
- Weinberg angle 1.52
  - GUT, in 2.344
  - hadronic reactions, from 1.77
  - LEP data, from 1.145
  - lowest order SM 1.105
  - semi-inclusive  $\nu N$  data, from 1.189
  - summary of data 1.88
  - value, numerical 1.58
- Wigner, Eckhart theorem 1.19, 2.376
- Wilson action 2.305
- Wilson coefficient functions 2.136
- Wilson loop factor 2.306
- Wilson operator product expansion 2.135
- winding number 2.318, 2.325, 2.333, 2.341
- winos 2.347
- Wu–Yang convention in CP-violation 2.29
- $x$  Bjorken 1.338
- $x$  in  $D^0$ – $\bar{D}^0$  mixing 2.19
- $x_d, x_s$  in  $B^0$ – $\bar{B}^0$  mixing 2.46–48
- $y$  in  $D^0$ – $\bar{D}^0$  mixing 2.19

- Yang–Mills theories 1.35  
*see* QCD; Standard Model
- $\eta_c$  (2980) 1.219, 1.253
- $\eta'_c$  (3592) 1.219
- $\eta_{+-}, \eta_{00}$  in  $K^0-\bar{K}^0$  CP-violation 2.23–28
- $Z^0$ -boson
- couplings
  - see also* coupling constants; Lagrangian density
  - discovery of 1.63
  - mass
  - LEP data, for 1.134
  - $\bar{p}p$  collision data, from 1.82
  - $W$  mass, relation to 1.54, 1.58
  - polarization vector, for 1.330
  - production
  - $B$  and  $L$  violating reactions, in 2.337
  - parton model for 1.440
  - $\bar{p}p$  collision data on 1.82
  - QCD, in 2.216
- theory, comparison with 2.217
- transverse momentum distributions 2.217
- widths
- LEP data, on 1.134
  - $\bar{p}p$  collision data, from 1.82
  - QCD effects on 2.269
  - SM, in 1.144
  - $Z^0 \rightarrow f\bar{f}$  partial width in SM 1.144
  - see also* gauge symmetry
- $Z_g$  coupling constant renormalization parameter 2.58
- MPS scheme, in 2.67–71, 2.76
- MS,  $\overline{\text{MS}}$  schemes, in 2.71–73, 2.77
- $Z_m$  mass renormalization parameter 2.58
- MPS scheme, in 2.67–71
  - MS,  $\overline{\text{MS}}$  schemes, in 2.71–73
- $Z_\phi$  field renormalization parameter 2.58
- MPS scheme, in 2.67–71
  - MS,  $\overline{\text{MS}}$  schemes, in 2.71–73
- zinos 2.347